Journal of Engineering and Technology for Industrial Applications

ISSN 2447-0228

August 2025

Volume 11/ No 54

Editor-in-Chief: J. C. Leite

www.itegam-jetia.org

ITEGAM - JETIA ISSN 2447-0228 Online
Journal of Engineering and Technology for Industrial Applications (JETIA)

O **ITEGAM-JETIA: Journal of Engineering and Technology for Industrial Applications** is a publication of the Galileo Institute of Technology and Education of the Amazon (ITEGAM), located in the city of Manaus since 2008. JETIA publishes original scientific articles covering all aspects of engineering. Our goal is the dissemination of research original, useful and relevant presenting new knowledge on theoretical or practical aspects of methodologies and methods used in engineering or leading to improvements in professional practice. All the conclusions presented in the articles It should be state-of-the-art and supported by current rigorous analysis and balanced assessment. Public magazine scientific and technological research articles, review articles and case studies.
JETIA will address topics from the following areas of knowledge: Mechanical Engineering, Civil Engineering, Materials and Mineralogy, Geosciences, Environment, Information and Decision Systems, Processes and Energy, Electrical and Automation, Mechatronics, Biotechnology and other Engineering related areas.

Publication Information:
ITEGAM-JETIA (ISSN 2447-0228), (online) is published by Galileo Institute of Technology and Education of the Amazon on a every two months (February, April, June, August, October and December).

Contact information:

Web page: www.itegam-jetia.org
Email: editor@itegam-jetia.org
Galileo Institute of Technology and Education of the Amazon (ITEGAM).

Joaquim Nabuco Avenue, No. 1950. Center. Manaus, Amazonas. Brazil.
Zip Code: 69020-031. Phone: (92) 3584-6145.

Copyright 2014. Galileo Institute of Technology and Education of the Amazon (ITEGAM)
The total or partial reproduction of texts related to articles is allowed, only if the source is properly cited. The concepts and opinions expressed in the articles are the sole responsibility of the authors.

Previous Notice
All statements, methods, instructions and ideas are the sole responsibility of the authors and do not necessarily represent the view of ITEGAM -JETIA. The publisher is not responsible for any damage and / or damage to the use of the contents of this journal. The concepts and opinions expressed in the articles are the sole responsibility of the authors.

Directory

Members of the ITEGAM Editorial Center - Journal of Engineering and Technology for Industrial Applications (ITEGAM-JETIA) of the Galileo Institute of Technology and Education of the Amazon (ITEGAM). Manaus-Amazonas, Brazil.

Jandecy Cabral Leite, CEO and Editorial Editor-in-Chief
Ivan Leandro Rodriguez Rico, Editorial Assistant
Jorge de Almeida Brito Junior, Editorial Assistant

ITEGAM - JETIA ISSN 2447-0228 Online
Journal of Engineering and Technology for Industrial Applications (JETIA)

ITEGAM-JETIA. v.11, n.54. August of 2025. Manaus - Amazonas, Brazil. ISSN 2447-0228 (ONLINE)
https://www.itegam-jetia.org

SUMMARY

COMPARATIVE ANALYSIS OF BIO-INSPIRED ENHANCEMENT TECHNIQUES FOR LOCALIZATION IN 2D WIRELESS SENSOR NETWORKS **6**
Rabhi Seddik

PRODUCTION OF HYBRID BIODIESEL FROM A NOVEL TERNARY OIL BLEND: DUAL-STAGE PROCESS OPTIMIZATION USING DESIRABILITY-BASED RSM **12**
Serge Narcisse Nouadjep, César Kapseu, Roland Solimando

HYBRID TRUST-BASED MODELS AND PROTOCOLS FOR ENHANCED SECURITY AND PERFORMANCE IN DYNAMIC WIRELESS SENSOR NETWORKS AND WIRELESS AD HOC NETWORKS **30**
Seshagiri Rao Ganta, Naga Malleswara Rao Nallamothu

ENHANCING 4G/LTE NETWORK PATH LOSS PREDICTION WITH PSO-GWO HYBRID APPROACH **39**
Messaoud Garah, Nabil Boukhennoufa

PRODUCT DESIGN AND VALUE ANALYSIS ON FOOD PRODUCT (CASE STUDY OF VEGETABLE NUGGET PRODUCT) **48**
Endang Retno Wedowati, Diana Puspitasari, Fungki Sri Rejeki, Tri Rahayuningsih, Johan Paing Heru Waskito

AN ENHANCED DISTRIBUTION SYSTEM PERFORMANCE WITH OPTIMIZATION TECHNIQUES FOR LOCATION OF ELECTRICAL VEHICLE CHARGING STATIONS **58**
Sainadh Singh Kshatri, Venkata Anjani Kumar G, Chilakapati Lenin Babu, Palepu Suresh Babu

THE GALILEO INSTITUTIONAL REPOSITORY AS AN INFORMATION STOCK IN THE TRAINING OF MASTERS AND DOCTORATES FOCUSED ON INDUSTRY 4.0 IN THE AMAZON **65**
Luiz Fernando Correia de Almeida

THE EFFECT OF DATA CONVERSION METHODS (NAIVE BAYES, C5.0 & SUPPORT VECTOR MACHINE) ON THE PERFORMANCE OF CLASSIFICATION ALGORITHMS IN DATA MINING **72**
Hussein Ali Attallah, Ahmed Al-Asadi, Doctor, Sadeer Sadeq

NUMERICAL INVESTIGATION OF THE DYNAMIC BEHAVIOR OF 2D STEEL STRUCTURES WITH CFST COLUMNS IN SEISMIC ZONES **88**
Dif Fodil, Said Hicham Boukhalkhal, Abdallah Yacine Rahmani, Abderahman Younsi Abderahman Younsi

PERSONAL SECURITY CHECKLIST: A COMPREHENSIVE APPROACH TO DIGITAL SECURITY **94**
Hitesh Choudhary, Navish Ansari, Shraddha Shivaji Sandimani

BLOCKARC: A BLOCKCHAIN BASED SMART CONTRACT FOR REWARD SYSTEM IN E-COMMERCE **103**
Pooja Patil, Aryan Singh, Aryan Raut, Aakash Sharma, Adarsh Rathod

AN AUDIO STEGANOGRAPHY TO PROTECT DATA IN TEXT, IMAGES AND AUDIO WITH HYBRID ENCRYPTION TECHNIQUES **115**
Thuraka Srinivasa Padmaja, Srinivasa Padmaja thuraka

PARAMETRIC OPTIMIZATION OF FRICTION TORQUE AND BEARING TEMPERATURE IN TAPERED ROLLER BEARINGS USING RESPONSE SURFACE METHODOLOGY **125**
Amisha B. Khant, Jaydeep K. Dadhaniya, Hardik G. Chothani

ITEGAM - JETIA
ISSN 2447-0228 Online
Journal of Engineering and Technology for Industrial Applications (JETIA)

DEVELOPMENT AND VALIDATION OF A MULTI-SOURCE BRIDGE DC–DC CONVERTER FOR EV APPLICATIONS **136**
Baya Reddy Lomada, V. Naga Bhaskar Reddy

COMPUTATIONAL THERMAL ANALYSIS OF FECRV15+TIB2 COATINGS ON EN48 BASEPLATE BY USING THE COMSOL MULTIPHYSICS **145**
Basiru Philip Aramide, Tamba Jamiru, Taoreed Adesola Adegbola, Abimbola Patricia Idowun Popoola, Mathew Olurotimi Adeoti, Rotimi Sadiku, Sisa Pityana

RAPID PROTOTYPE PROCESS SELECTION USING MULTI ATTRIBUTE DECISION MAKING USING ADVANCED ENTROPY WEIGHT BASED FUZZY SINGLE VALUED NEUTROSOPHIC SET **152**
Nital Pravinbhai Nirmal, Jignesh Girishbhai Parmar, Mehul Gunvantrai Mehta

MULTI-OBJECTIVE OPTIMIZATION OF END MILLING PROCESS PARAMETERS FOR MINIMUM SURFACE ROUGHNESS USING MOGA **160**
Jignesh Girishbhai Parmar, Komal G. Dave, Mehul G. Mehta

LITERATURE REVIEW ON MECHANICAL PROPERTIES AND BEHAVIOR OF ALUMINUM METAL MATRIX COMPOSITE MATERIAL WITH DIFFERENT PROCESSES **168**
Jignesh G. Parmar, Mehul G. Mehta, Nital P. Nirmal

RISK MANAGEMENT AND GOVERNANCE IN BLOCKCHAIN-BASED DIGITAL IDENTITY PROJECTS: A BUSINESS ANALYSIS AND PROJECT MANAGEMENT FRAMEWORK **177**
Tobiloba Kazeem, Olatoye Kabiru Agboola, Nonso Okika, Soyingbe Folasade Owoola-Adebayo, Fope Opeola, Nnenna Linda Akunna, Oreoluwa Serifat Abimbola

ENHANCING CHARGE TRANSFER EFFICIENCY IN CCDS USING SILVACO SIMULATIONS **186**
Dahmane Djendaoui, Zoubir Becer, Themeur Obeidi

QUIZ-TUBE: ENHANCING VIDEO-BASED LEARNING WITH AUTOMATED AI QUIZ GENERATION **193**
Akash Sharban Thakur, Rashmi Bhat, Ayush Shukla, Tushar Ram, Vivek Singh

HIGHLY EFFICIENT POWER CONDITIONING TOPOLOGY FOR MAXIMUM ENERGY EXTRACTION FROM WIND POWER SYSTEM USING HILL CLIMBING SEARCH-MPC APPROACH **203**
Zahira Anane, Badreddine Babes, Noureddine Hamouda

ENHANCING THE COOLING SYSTEM DESIGN OF HIGH-POWER DENSITY PERMANENT MAGNET MOTOR FOR EV **210**
Amit Kumar, Gaurav Singh Negi, Alok sati

ENERGY MANAGEMENT OPTIMIZATION AND OPTIMAL CONTROL OF MICROGRID ENRICHED WITH RENEWABLE AND SUSTAINABLE DISTRIBUTED GENERATORS USING NATURE-INSPIRED METHOD **220**
Mezhoud Nabil, Bahri Ahmed, Ayachi Bilel, Boukhenoufa Farouk, Bouras Lakhdar

DEVELOPMENT AND SET UP OF AN ARDUINO-BASED SOLAR RADIATION SENSOR USING A REFERENCE CELL **236**
Yasmine Mekkas, Hani Benguesmia, Badis Bakri, Mohammed Benguesmia

THE LOAD FLOW APPROACH FOR RADIAL NETWORK DISTRIBUTION SYSTEMS BASED ON NETWORK TOPOLOGY **243**
Chella Hari Prasad, Mrs.T.Srinivasa Padmaja, B.Rajasekhar Reddy

ADVANCEMENTS AND CHALLENGES IN NAMED ENTITY RECOGNITION: A REVIEW OF TECHNIQUES AND DOMAIN SPECIFIC APPLICATIONS **253**
Vedanti Deepak Shedage, Devyani Sahebrao Pawar, Roshani Bhanudas Shinde, Apurva Mane, Pradip Ghorpade

ITEGAM - JETIA
ISSN 2447-0228 Online
Journal of Engineering and Technology for Industrial Applications (JETIA)

A BIBLIOMETRIC REVIEW OF BUILDING INFORMATION MODELING FOR QUANTITY TAKEOFF: TRENDS, THEMATIC CLUSTERS, AND FUTURE DIRECTIONS **260**
Fendi Hary Yanto, Ary Setyawan, Fajar Sri Handayani, Halwan Alfisa Saifullah

MECHATRONICS IN AGRICULTURE FOR BUILDING A SUSTAINABLE ECONOMY IN AFRICA **268**
Thomas Adedayo Ayorinde, Tamba Jamiru, Peet F Le Roux

Journal of Engineering and Technology for Industrial Applications

ITEGAM-JETIA

Manaus, v.11 n.54, p. 6-11. July/August., 2025.
DOI: https://doi.org/10.5935/jetia. v11i54.1680

ISSN ONLINE: 2447-0228

RESEARCH ARTICLE OPEN ACCESS

COMPARATIVE ANALYSIS OF BIO-INSPIRED ENHANCEMENT TECHNIQUES FOR LOCALIZATION IN 2D WIRELESS SENSOR NETWORKS

Rabhi Seddik[1]

[1] Laboratory of Mathematics Modeling and Applications, University of Adrar, National Road No. 06, Adrar 01000, Algeria.

[1]http://orcid.org/0000-0002-1352-3279

Email: rabhi_seddik@univ-adrar.edu.dz

ARTICLE INFO

Article History
Received: March 3, 2025
Revised: April 20, 2025
Accepted: June 15, 2025
Published: July 31, 2025

Keywords:
Wireless Sensor Networks,
Bio-inspired optimization,
Meta-heuristic,
Localization.
.

ABSTRACT

Accurate node localization is crucial for optimizing the performance of Wireless Sensor Networks (WSNs), which are widely used in applications such as environmental monitoring and smart city infrastructure. This study conducts a comparative evaluation of three bio-inspired optimization algorithms for node localization: Particle Swarm Optimization (PSO), Fruit Fly Optimization Algorithm (FOA), and Drop Mongoose Optimization Algorithm (DMOA). The algorithms are assessed based on their localization accuracy and precision, which are key performance metrics for WSN applications. PSO, inspired by the collective movement of particle birds, is a well-established meta-heuristic technique, while FOA simulates the foraging behavior of fruit flies to determine optimal locations. The recently introduced DMOA, modeled after the hunting and movement strategies of mongooses, represents a novel approach in optimization. Simulation results indicate that while PSO and FOA perform well under specific conditions, DMOA outperforms them in terms of accuracy and precision, making it a promising solution for improving node localization in WSNs. This study underscores the effectiveness of bio-inspired algorithms in enhancing the reliability and efficiency of WSN deployments.

Copyright ©2025 by authors and Galileo Institute of Technology and Education of the Amazon (ITEGAM). This work is licensed under the Creative Commons Attribution International License (CC BY 4.0).

I. INTRODUCTION

Wireless Sensor Networks (WSNs) have garnered significant attention in recent years due to their wide-ranging applications and the increasing demand for low-cost, energy-efficient solutions. These networks rely on the deployment of numerous inexpensive sensors over a designated area, which necessitates the development of appropriate routing protocols and efficient algorithmic implementations. These factors open promising avenues, particularly in monitoring and target-tracking applications [1]. One of the fundamental challenges in WSNs is the accurate estimation of each sensor node's location, which is crucial for the network's overall performance. Due to cost constraints, each sensor device typically has limited bandwidth, power, memory, and energy reserves. Furthermore, their detection and communication capabilities are bounded by a maximum range. In terms of network structure, WSNs can be viewed as a graph, where each node represents a sensor and each edge models a neighborhood between two devices-i.e., a reciprocal detection and potential communication link [2].

The Global Positioning System (GPS), a free service, theoretically solves the localization problem for each node in the network. However, equipping every sensor with a GPS receiver is often impractical due to the prohibitive costs, limited energy reserves, and the poor performance of GPS technology in indoor environments. Instead, each sensor is equipped with a transmitter-receiver module that enables wireless communication with neighboring sensors, allowing the estimation of inter-node distances [3].

The primary goal of the localization algorithm is to calculate the relative coordinates of each sensor based solely on proximity measurements. Initial approaches to solving the localization problem were centralized, but it became clear that this strategy conflicts with the energy constraints of WSNs. Local data processing, which is energy-efficient, was not prioritized, while energy-intensive wireless transmission drained the already limited batteries of the sensors (the energy cost of wireless transmission is approximately 100 times higher than local processing [4]). Additionally, centralized approaches lack robustness, as the failure of the central processing unit could

lead to the collapse of the entire system. Therefore, an alternative strategy is required to improve the network's lifespan compared to centralized approaches. A distributed implementation of the algorithm across the network, where each sensor contributes through local preprocessing, presents an effective solution to meet these demands. One of the most effective methods that researchers have recently used to solve complex problems is the nature-inspired methods, and similarly, localization researchers have used it to address this complex problem in WSN. The paper by [5] presents a comprehensive review of various meta-heuristic localization methods in these networks. These include, but are not limited to, the following: Particle Swarm Optimization (PSO) is one of the first algorithms bio-inspired that was used to improve localization, and this is in [6], Cuckoo Search Algorithm-based WSN Localization by [7], Chicken Swarm Optimization for WSN Localization by [8], Moth Flame Optimization Algorithm is utlised by [9],[10] used Fruit Fly Optimization Algorithm for enhance localization and taking into account the reduction of energy use due to the low cost of calculation in FOA. Very recently in 2024 I present a hybrid model by bio-inspired algorithms in [11]. Then I noticed recently that every bio-inspired algorithm appeared, researchers used it to solve the problem of localization in a wireless sensor network.

This paper explores bio-inspired optimization algorithms as a promising approach for node localization in WSNs. By comparing three algorithms—Particle Swarm Optimization (PSO), Fruit Fly Optimization Algorithm (FOA), and the novel Drop Mongoose Optimization Algorithm (DMOA)—we aim to identify the most effective method for improving the precision and accuracy of node localization, ultimately enhancing the robustness and efficiency of WSN deployments. The remainder of the paper is organized as follows: Section 2 provides the mathematical model for the localization problem in Wireless Sensor Networks (WSNs). Section 3 presents an overview of the three bio-inspired optimization algorithms used in this study. Section 4 discusses the results of the comparative analysis and the localization performance of each algorithm. Finally, the conclusion of the paper is presented in Section 5.

II. MATHEMATICAL MODELING OF LOCALIZATION PROBLEM

The main objective of localization in WSN is to accurately localize statically placed sensors that are randomly distributed within a two-dimensional (2D) area. To achieve this, the bio-inspired Algorithms are used alongside a set of anchors with known positions. The goal is to estimate the positions of several unknown nodes that have similar communication radius. The coordinates (x, y) of the target node are estimated, and the distance d_{ij} between the target node and each anchor is calculated using the following equation:

$$d_{ij} = \sqrt{(x_i - x_j)^2 + (y_i - y_j)^2} \tag{1}$$

The measured distance *dj* obtained via RSSI measurement techniques is adjusted by adding a normal error noise ($dj=d_j+noise$). The aim is to minimize the difference between the measured distance and the distance calculated by the following objective function:

$$f(x,y) = \frac{1}{M} * \sum_{j=1}^{M} \left| \sqrt{(x` - x_j)^2 + (y` - y_j)^2} - d_j \right| \tag{2}$$

Where M≥3 is the number of anchor nodes within the target node's radius, (x′,y′) represents the estimated coordinates of the node, (x_j,y_j) are the coordinates of the j^{th} anchor, and d_j is the actual distance between the unknown sensor and the anchor.

III. BIO-INSPIRED OPTIMIZATION ALGORITHMS FOR NODE LOCALIZATION IN WSN

Researchers have used hundreds of nature-inspired meta-heuristic algorithms, but their application to positioning in a wireless sensor network is uniform in general idea, but each algorithm has its own way of moving from one step to the next using equations inspired by The behaviors of insects, animals, and even humans sometimes, such as neural networks. The following Flowchart of Figure 1, explains the general steps for applying any Bio-inspired algorithm to solve the localization problem.

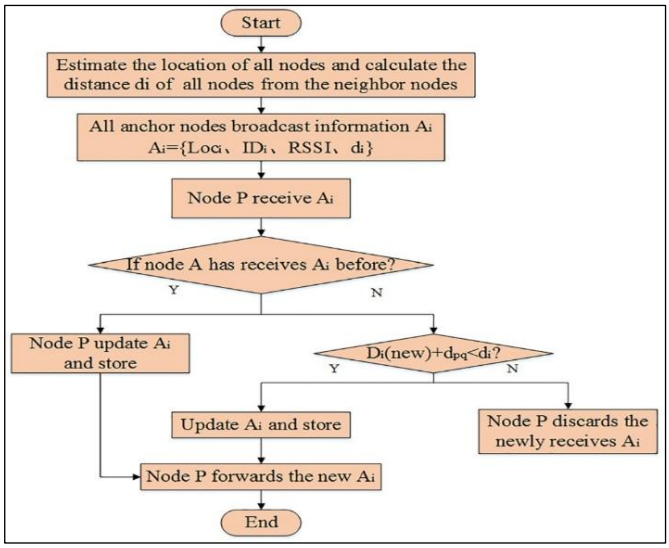

Figure 1: Flowchart of implementing meta-heuristics algorithms to locate nodes.
Source: Authors, (2025).

III.1 PARTICLE SWARM OPTIMIZATION (PSO)

Particle Swarm Optimization (PSO) is one of the most well-known bio-inspired algorithms, modeled after the social behavior of bird flocks or fish schools, this algorithm was proposed by Russel Eberhart (electrical engineer) and James Kennedy (socio-psychologist) in 1995 [12]. In PSO, a group of particles (potential solutions) moves through the search space, adjusting their positions based on their own experience and that of neighboring particles. Each particle has a velocity that is updated by considering both its personal best position and the best-known position within the swarm. For node localization in WSNs, PSO is particularly attractive due to its ability to explore a wide search space and converge quickly towards an optimal solution. This algorithm's inherent parallelism and simplicity make it suitable for distributed processing, which is crucial in WSNs where energy efficiency is a key concern. However, PSO may sometimes get trapped in local optima, which can affect the precision of node localization, particularly in more complex network topologies. In this comparative study we use the localization results obtained in our work presented in [13] the article entitled: An Improved approach for localization in wireless sensor networks Using PSO algorithm.

PSO models swarm behavior, where particles (solutions) iteratively adjust their positions based on personal and global best positions. The algorithm follows these update rules:

$$v_{i,j}^{t+1} = wv_{i,j}^{t} + c_1 r1_{i,j}^{t} \left[pbest_{i,j}^{t} - x_{i,j}^{t}\right] + c_2 r2_{i,j}^{t} \left[gbest_{i,j}^{t} - x_{i,j}^{t}\right], j \in \{1,2,\dots,D \quad (3)$$

$$x_{i,j}^{t+1} = x_{i,j}^{t} + v_{i,j}^{t+1}, j \in \{1,2,\dots,D\} \quad (4)$$

Where, v_i is velocity, x_i is position, p_i is local best, g is global best, and c_1, c_2, r_1, r_2 are acceleration coefficients with random weights. PSO's strength lies in fast convergence but risks local optima trapping.

III.2 FRUIT FLY OPTIMIZATION ALGORITHM (FOA)

The Fruit Fly Optimization Algorithm (FOA) is another bio-inspired approach proposed by [14], based on the foraging behavior of fruit flies. In FOA, fruit flies search for food by first locating it through smell and then refining their position based on visual cues. In the context of WSNs, FOA uses a similar strategy where nodes adjust their positions to minimize localization errors by iteratively refining their distance estimates relative to their neighbors. The simplicity of FOA, combined with its relatively low computational complexity, makes it a viable option for WSN node localization. However, FOA can sometimes suffer from slower convergence compared to PSO, especially in larger networks. Despite this, it is still considered effective in networks where the number of nodes is moderate, and energy resources need to be preserved. In this work we use the localization results obtained in our work presented in [10] the article entitled: An improved method for distributed localization in WSNs based on FOA.

FOA mimics fruit fly foraging behavior using an iterative process where flies locate an optimal position based on smell and sight. The key equations are:

$$X_{new} = X_{current} + step * Random() \quad (5)$$

$$Y_{new} = Y_{current} + step * Random() \quad (6)$$

After each iteration the best-smelling position is chosen. FOA is computationally efficient but may suffer from slow convergence in complex environments

III.3 DROP MONGOOSE OPTIMIZATION ALGORITHM (DMOA)

The Drop Mongoose Optimization Algorithm (DMOA) is a novel bio-inspired algorithm introduced specifically for optimization problems like node localization in WSNs, DMO is introduced 2022 by [15]. This algorithm is inspired by the mongoose's hunting and evasion techniques, which involve rapid, unpredictable movements to evade predators or catch prey. DMOA applies this dynamic behavior to the search process by enabling nodes to make both large exploratory moves and fine-tuned adjustments in their position, mimicking the mongoose's strategic shifts. In WSNs, this translates into a balance between exploration and exploitation of the search space, which allows DMOA to escape local optima and achieve higher precision compared to more traditional methods like PSO or FOA. The adaptability and robustness of DMOA make it particularly well-suited for complex network environments, offering superior accuracy in node localization while maintaining energy efficiency.

These bio-inspired algorithms provide diverse strategies for tackling the node localization problem in WSNs, with each offering unique strengths and trade-offs depending on the specific network configuration and energy constraints. The comparative study of these algorithms will offer valuable insights into their relative performance, particularly in terms of localization precision and accuracy, key factors for the success of WSN applications. Here we use the obtained results of our latest work entitled: WSN localization based on DMOA, and presented in [16].

DMOA is inspired by the dynamic movement of mongooses when hunting. The algorithm balances exploration and exploitation through sudden directional changes:

$$X_{new} = X_{current} + \alpha\ (Random() - 0.5) \quad (7)$$

$$Y_{new} = Y_{current} + \beta\ (Random() - 0.5) \quad (8)$$

Where α, β are control step size variations. DMOA enhances search diversity and avoids local optima, making it robust for localization.

IV. COMPARISON OF EXPERIMENTAL RESULTS

İn this part of paper we will compares the results of the three bio-inspired algorithms: PSO, FOA, and DMOA. The experiment takes place in a 50 × 50 m² area and involves two types of nodes: anchor nodes with known coordinates and unknown nodes whose coordinates need to be estimated. All nodes have a communication range of 25 meters, and all metaheuristics having the same swarm size with 25 individuals. The experiment is performed under various scenarios, varying the number of nodes with a fixed number of anchor equal 25 nodes.

In Figure 2, we give an example of a random distribution of 200 unknown nodes represented by black squares and 25 known nodes or anchors represented by red Rhombus. To ensure a fair comparison we used the same network properties mentioned above for all algorithms used in this comparison part.

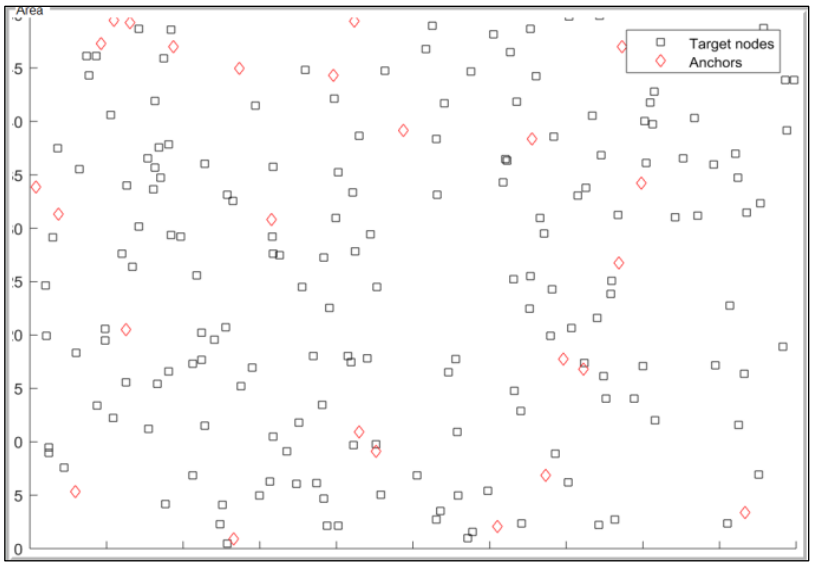

Figure 2: Example of random deployment.
Source: Authors, (2025).

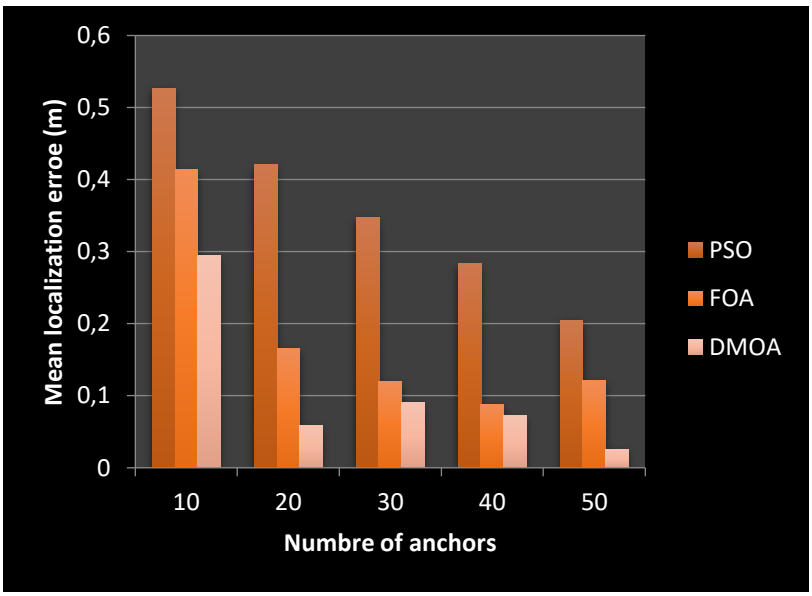

Figure 3: Localization error of various approaches Vs Numbre of nodes.
Source: Authors, (2025).

The graphs of Figure 3 shows the comparison of the mean localization error for three bio-inspired algorithms when we change the number of anchors between 10 and 50. DMOA consistently performs the best, with the lowest mean error rates in all scenarios, starting below 0.295 meters for 25 anchor nodes and decreasing to under 0.105 meters at 50 anchor nodes. FOA performs moderately, starting around 0.378 meters for 10 anchor nodes and gradually decreasing to 0.175 meters for 50 nodes. PSO has the highest localization error, beginning around 0.592 meters and reducing to approximately 0.199 meters. Overall, the localization accuracy improves for all algorithms as the number of anchor nodes increases, with DMOA showing the most significant improvement.

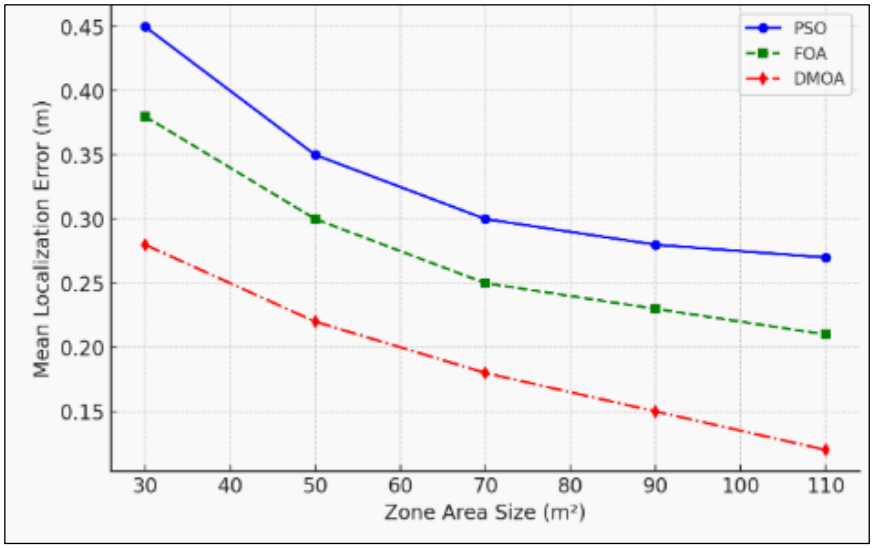

Figure 4: Comparison of positioning accuracy with different area sizes.
Source: Authors, (2025).

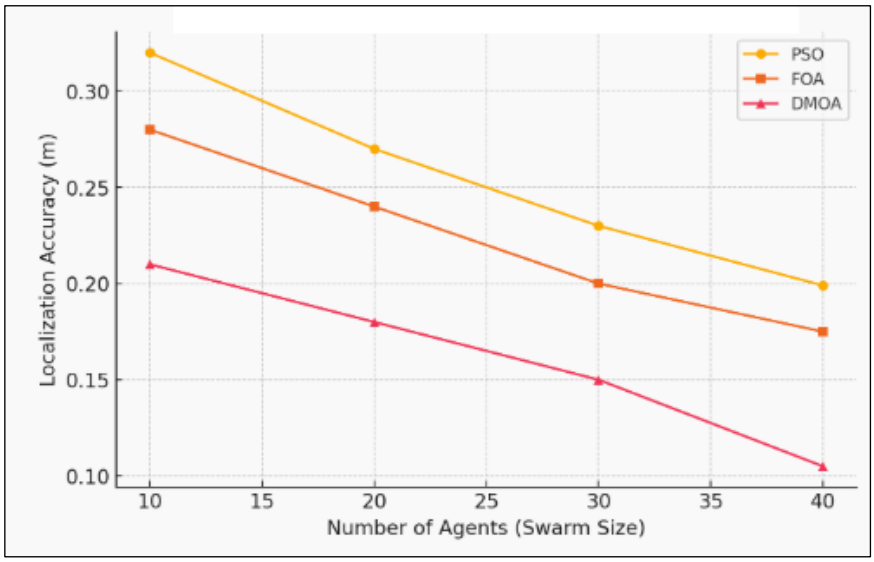

Figure 5: Localization error of various approaches Vs Numbre of agentes.
Source: Authors, (2025).

The graphs of Figure 4, illustrates how the localization accuracy of PSO, FOA, and DMOA changes with varying zone areas. The key observations are as the zone area increases, localization accuracy tends to degrade for all three algorithms. This is expected since a larger area introduces more uncertainty and greater distances between nodes, making accurate position estimation more challenging. For small to medium-sized areas, all three algorithms can achieve reasonable accuracy. For large zones, DMOA is the most reliable, making it the preferred choice for scalable WSN deployments. Hybrid approaches integrating multiple techniques may help mitigate accuracy loss in larger environments.

The Figure 5 presents a comparative analysis of localization accuracy for PSO, FOA, and DMOA when varying the number of agents (swarm size) in the optimization process. The x-axis represents the number of agents involved in localization, while the y-axis denotes the mean localization error. Each algorithm's performance trend is plotted to show how increasing the number of agents impacts accuracy.

As the number of agents increases, the localization error decreases for all three algorithms. This is expected, as a larger swarm size generally leads to better exploration and more accurate positioning. DMOA consistently outperforms both PSO and FOA, achieving the lowest localization error across all agent counts. This suggests that DMOA effectively balances exploration and exploitation, allowing for more precise node localization. FOA shows moderate improvement with increasing swarm size, but its convergence rate is slower compared to DMOA. This indicates that while FOA is effective, it may require more iteration to achieve optimal results. PSO has the highest localization error, even with an increasing number of agents. This suggests that it struggles with local optima, limiting its accuracy improvements despite having more agents.

The diminishing returns effect is visible, where adding more agents beyond a certain threshold leads to minimal improvement. This suggests that an optimal number of agents exist for efficient localization without unnecessary computational overhead. DMOA's superior performance makes it the best candidate for accurate localization in WSN applications. FOA can be a viable alternative but requires careful parameter tuning to enhance its convergence. PSO's higher error rates suggest that modifications (such as hybridizing with other algorithms) may be needed to improve its effectiveness.

V. CONCLUSIONS

Accurate node localization is crucial for ensuring optimal performance in WSNs, which are widely used in applications such as environmental monitoring and smart cities. This paper presents a comparative analysis of three bio-inspired optimization algorithms—Particle Swarm Optimization (PSO), Fruit Fly Optimization Algorithm (FOA), and Drop Mongoose Optimization Algorithm (DMOA)—to assess their effectiveness in node localization. PSO, inspired by bird flocking behavior, is a popular heuristic method, while FOA is based on the foraging behavior of fruit flies. DMOA, a novel algorithm, draws from the movement and attack strategies of the mongoose, introducing a new approach to optimization. Simulation results reveal that while PSO and FOA perform well in certain scenarios, DMOA consistently achieves the highest localization precision and accuracy. This makes DMOA a highly effective option for improving node localization in WSNs. The study underscores the potential of bio-inspired algorithms to enhance the efficiency and reliability of WSN deployments.

VI. REFERENCES

[1] Amal Gulati, and all, A review paper on wireless sensor network techniques in Internet of Things (IoT), Materials Today: Proceedings, Volume 51, Part 1, 2022, Pages 161-165, ISSN 2214-7853, https://doi.org/10.1016/j.matpr.2021.05.067.

[2] Cardone, G., Corradi, A., & Foschini, L. (2011). Cross-network opportunistic collection of urgent data in wireless sensor networks. *The Computer Journal*, *54*(12), 1949-1962. https://doi.org/10.1093/comjnl/bxr043.

[3] Enge, P. K. (1994). The global positioning system: Signals, measurements, and performance. International Journal of Wireless Information Networks, 1, 83-105. https://doi.org/10.1007/BF02106512.

[4] Cook, B. W., Lanzisera, S., & Pister, K. S. (2006). SoC issues for RF smart dust. Proceedings of the IEEE, 94(6), 1177-1196. DOI: 10.1109/JPROC.2006.873620.

[5] Ahmad, R., Alhasan, W., Wazirali, R., & Aleisa, N. (2024). Optimization Algorithms for Wireless Sensor Networks Node Localization: An Overview. IEEE Access. DOI: 10.1109/ACCESS.2024.3385487.

[6] Gopakumar, A., & Jacob, L. (2008, January). Localization in wireless sensor networks using particle swarm optimization. In *2008 IET international conference on wireless, mobile and multimedia networks* (pp. 227-230). IET. DOI: 10.1049/cp:20080185.

[7] Goyal, S., & Patterh, M. S. (2014). Wireless sensor network localization based on cuckoo search algorithm. Wireless personal communications, 79, 223-234. https://doi.org/10.1007/s11277-014-1850-8.

[8] Al Shayokh, M., & Shin, S. Y. (2017). Bio inspired distributed WSN localization based on chicken swarm optimization. Wireless Personal Communications, 97, 5691-5706. https://doi.org/10.1007/s11277-017-4803-1.

[9] Miloud, M., Abdellatif, R., & Lorenz, P. (2019). Moth flame optimization algorithm range-based for node localization challenge in decentralized wireless sensor network. International Journal of Distributed Systems and Technologies (IJDST), 10(1), 82-109. DOI: 10.4018/IJDST.2019010106

[10] Rabhi, S., Semchedine, F., & Mbarek, N. (2021). An improved method for distributed localization in WSNs based on fruit fly optimization algorithm. Automatic Control and Computer Sciences, 55, 287-297. https://doi.org/10.3103/S0146411621030081.

[11] Rabhi, S., Semchedine, F., & Mbarek, N. (2024). Localization in Wireless Sensor Networks by Hybridization between Optimization Algorithms of Particle Swarms and Fruit Flies. Automatic Control and Computer Sciences, 58(2), 177-184. https://doi.org/10.3103/S014641162470007X.

[12] Kennedy, J., and Eberhart, R.: 'Particle swarm optimization'. Proc. IEEE Int. Conf. Neural Networks, Perth, Australia, Jan 1995, pp. 1942-1948. DOI: 10.1109/ICNN.1995.488968.

[13] Rabhi, S., Belbali, M. S., & Haissoune, M. (2021). An Improved approach for localization in wireless sensor networks Using PSO algorithm. African Review of Science, Technology and Development, 6(1), 10-23.

[14] Cho, H. H., Lee, R. H., & Park, J. G. (2011). Adaptive parameter estimation method for wireless localization using RSSI measurements. Journal of Electrical Engineering and Technology, 6(6), 883-887. https://doi.org/10.5370/JEET.2011.6.6.883.

[15] Agushaka, J. O., Ezugwu, A. E., & Abualigah, L. (2022). Dwarf mongoose optimization algorithm. Computer methods in applied mechanics and engineering, 391, 114570. https://doi.org/10.1016/j.cma.2022.114570.

[16] Rabhi, S. (2024). Wireless sensor network localization based on Drop Mongoose Optimization Algorithm. *Studies in Engineering and Exact Sciences*, *5*(2), e8845-e8845. DOI: https://doi.org/10.54021/seesv5n2-300.

Journal of Engineering and Technology for Industrial Applications

ITEGAM-JETIA

Manaus, v.11 n.54, p. 12-29. July/August., 2025.
DOI: https://doi.org/10.5935/jetia. v11i54.1682

ISSN ONLINE: 2447-0228

RESEARCH ARTICLE OPEN ACCESS

PRODUCTION OF HYBRID BIODIESEL FROM A NOVEL TERNARY OIL BLEND: DUAL-STAGE PROCESS OPTIMIZATION USING DESIRABILITY BASED-RSM

Narcisse S. Nouadjep[1], César Kapseu[2] and Roland Solimando[3]

[1]Faculty of Engineering and Technology, University of Buea, P.O. Box 63, Buea, Cameroon.
[2]Department of Process Engineering, National School of Agro-Industrial Sciences,
University of Ngaoundere, P.O. Box. 455, Ngaoundere, Cameroon.
[3]Ecole Nationale Supérieure des Industries Chimiques (ENSIC) – Université de Lorraine, BP20451, Nancy Cedex, France

[1]http://orcid.org/0009-0003-0112-7839, [2]http://orcid.org/0009-0009-1424-654X, [3]http://orcid.org/0000-0003-0901-4196

Email: nouadjep@gmail.com, kapseu@yahoo.fr, roland.solimando@univ-lorraine.fr

ARTICLE INFO

Article History
Received: March 3, 2025
Revised: April 20, 2025
Accepted: June 15, 2025
Published: July 31, 2025

Keywords:
Esterification,
transesterification,
ANOVA,
neem,
shea butter.

ABSTRACT

The production of biodiesel is increasingly recognized as a sustainable alternative to fossil fuels. This study explores a two-step process for biodiesel production using a blend of Neem oil, Shea butter, and Waste kitchen oil. Process optimization was conducted using response surface methodology and the superposition approach, focusing on temperature, reaction time, ethanol-to-oil ratio, and catalyst concentration to maximize biodiesel yield. The model's performance was evaluated through R^2 and Absolute Average Deviation values. The highest desirability values obtained were 1 and 0.99 for the esterification and transesterification stages, respectively, with corresponding conversion yields of 94.57% and 90.53%. The analysis of the biodiesel revealed the presence of four distinct ethyl esters that are consistent with common fatty acid ethyl esters found in biodiesel. The hybrid biodiesel produced meets international standards, including ASTM and EN. Furthermore, the study achieved a high biodiesel yield with minimal catalyst usage (0.52 wt.%) and a short processing time (30 minutes), highlighting industries' potential to improve biodiesel production's economic viability by adopting similar optimized conditions.

Copyright ©2025 by authors and Galileo Institute of Technology and Education of the Amazon (ITEGAM). This work is licensed under the Creative Commons Attribution International License (CC BY 4.0).

I. INTRODUCTION

Energy is a critical requirement for human survival, and global energy consumption is expected to increase significantly in the 21st century. As demand for energy sources continues to grow, the need for efficient resource utilization becomes more pressing [1]. The scarcity of conventional energy sources, combined with rising global energy needs, highlights the importance of developing alternative fuels [2]. Although renewable and green energy technologies are gaining traction, they are yet to fully replace traditional fossil fuels [3]. Fossil fuels, such as coal, oil, and natural gas, have dominated the global energy landscape for decades, consistently accounting for over 80% of global energy production. This reliance has contributed significantly to environmental degradation due to carbon emissions [4],[5]. Despite advancements in technology and improvements in energy efficiency, the combined effects of population growth and economic expansion have driven up energy demand, outpacing the benefits of efficiency measures. The ongoing conflict between Russia and Ukraine has further exacerbated the energy crisis, causing substantial increases in household energy costs for heating, cooling, and transportation [6]. In 2021, over 45% of the European Union's gas supply was imported, representing nearly 40% of its total consumption [7]. The widespread use of non-renewable energy and rapid industrialization have significantly contributed to greenhouse gas emissions, environmental deterioration, and global temperature increases [8]. In 2021, global CO_2 emissions reached 36.6 gigatonnes, pushing projections for the rise in global surface temperature to approximately 3.5°C by 2100. The Paris Agreement of 2015 seeks to limit CO_2 emissions and keep the global temperature rise below 2°C compared to pre-industrial levels [9]. In response to the environmental and supply challenges posed by fossil fuels, researchers are intensifying efforts to identify clean and sustainable energy alternatives. These efforts aim to reduce dependency on fossil fuels due to their finite nature, high greenhouse gas emissions, and harmful pollutants produced

during combustion [10]. Under the Stated Policies Scenario (STEP) 2022 scenario, fossil fuel demand is expected to decline by 60% by 2050 [9]. By 2040, approximately 60 million tonnes of renewable fuels are projected to replace fossil fuels, reducing their use in the transportation sector to 85% [11]. The energy transition has increasingly shifted away from conventional bioenergy sources toward advanced biofuels [12] derived from sustainable feedstocks such as wasteland, marginal lands unsuitable for food crops, and waste streams [13],[14]. Biofuels, particularly biodiesel, have emerged as promising renewable energy sources due to their biodegradable, non-toxic nature and reduced emissions compared to conventional diesel [3],[15-17]. Biodiesel also exhibits superior chemical and physical properties compared to petroleum-based diesel [18]. Its use, whether in pure form or as a blend, has been shown to significantly lower emissions of combustion gases and carbon monoxide [19].

Biodiesel production can utilize various waste materials such as used cooking oils, animal fats, non-edible vegetable oils, and municipal waste as raw materials [20]. The concept of waste-based biodiesel originated during World War II and resurged during the 1970s energy crises when alternative fuel sources were sought due to shortages. By the 1980s, the transesterification method made it possible to produce biodiesel from waste materials [21]. This led to the classification of waste-based biodiesel as the second generation of biodiesel production [22]. Several methods are available for biodiesel production, including pyrolysis, dilution, microemulsion, and transesterification. Among these, transesterification has emerged as the most economically viable and practical approach, producing biodiesel with enhanced properties [23]. However, the efficiency and quality of biodiesel produced via transesterification are influenced by factors such as reaction time, temperature, catalyst concentration, feedstock type, and the methanol-to-oil ratio.

Optimizing these variables often requires extensive experimentation, which can be time-consuming, labor-intensive, and economically challenging [24]. To address this complexity, researchers have adopted empirical modeling techniques like Response Surface Methodology (RSM), which reduces the number of experimental runs while providing statistically robust results. For instance, [25] optimized biodiesel synthesis from refined cottonseed oil using a 2-level-4-factor RSM design, achieving a 96% yield. According to [26] applied RSM to optimize biodiesel production from animal fat, reporting a yield of 95.5%. For [27] used a Central Composite Rotatable Design (CCRD) to optimize a two-step biodiesel synthesis process from neem oil, achieving a maximum yield of 90.5%. Similarly, [28] optimized sunflower biodiesel production using CCRD, reporting a 95% yield.

Other studies have highlighted the impact of specific process parameters on biodiesel production. According to [29] optimized reaction variables such as molar ratio, catalyst concentration, and reaction time for waste cooking oil biodiesel, achieving a maximum yield of 94.15%. According to [30] optimized similar parameters for waste cooking palm oil biodiesel, reporting a yield of 79.7%. The Box-Behnken Design (BBD) has been found to be more efficient than CCRD and three-level full factorial designs [31]. BBD, when combined with RSM, enables effective estimation of second-order model coefficients, making it both economical and efficient for complex systems [32]. According to [33] utilized RSM-based BBD to optimize soybean biodiesel production, achieving a 94% yield. Charoenchaitrakool and Thienmethangkoon [34] applied the same approach to optimize a two-step catalyzed process for biodiesel production from waste frying oil, reporting a maximum yield of 90% and a free fatty acid (FFA) content as low as 0.5%. According to [24] achieved a 98.4% yield for Pongamia biodiesel using RSM-based BBD. Similarly, [35] optimized biodiesel production from esterified shea butter oil through transesterification using RSM with a BBD.

Sustainable biodiesel derived from various resources has emerged as a promising alternative to fossil fuels, with applications in marine propulsion, agriculture, small-scale power generation, and heavy freight vehicles [36]. According to [37] successfully developed a hybrid biodiesel using vegetable oil, butanol, and ethanol, all sourced from biomass. This hybrid biodiesel often demonstrates superior fuel properties compared to conventional biodiesel, with the optimal composition being 60% oil, 30% butanol, and 10% ethanol. Similarly, For [38] produced hybrid biodiesel from blended oils, achieving higher yields than fatty acid methyl esters (FAME) derived from single oil sources, with yields of 97.5%, 97.3%, and 97.9% for hazelnut, sunflower, and blended feedstocks, respectively.

According to [39] focused on biodiesel production and optimization using a combination of edible and non-edible oils, achieving a yield of 97.00% under specific reaction conditions. According to [40] explored biodiesel synthesis from a blend of radish oil and apricot kernel oil, highlighting the economic viability of this approach. For [41] investigated the production of biodiesel from a palm-sesame oil blend using ultrasound-assisted transesterification. In another study, According to [42] synthesized biodiesel from waste cooking oil and palm oil using a fly ash-derived catalyst, achieving a maximum yield of 73.8%. According to [43] produced biodiesel from a combination of pongamia and neem oils, while [44] optimized biodiesel production from a composite mixture of pongamia oil, animal fat oil, and waste cooking oil.

Their experiments, conducted at a molar ratio of 6:1 with 1.2 wt% catalyst, 64°C temperature, and 500 rpm agitation for 75 minutes, resulted in a maximum yield of 97.76%. According to [3] emphasized the sustainability of mixed oil feedstocks for biodiesel production, suggesting their potential for industrial-scale applications. According to [45] utilized RSM and Artificial Neural Networks (ANN) to optimize biodiesel yield from palm and cottonseed oil blends, achieving a yield of 96.32%. For [46] optimized biodiesel production from rice bran oil and sterculia foetida oil, reporting a methyl ester yield of 98.93% under ideal conditions. According to [47] applied RSM and ANN to optimize biodiesel production from a mixture of fish oil and rubber seed oil, achieving a yield of 91.5% by considering various independent input factors. For [48] study highlighted the favorable properties of biodiesel synthesized from a blend of four edible oils, meeting standard quality requirements.

After reviewing the literature, it has been observed that complex challenges like optimization can be effectively addressed through RSM. Numerous studies have successfully utilized this empirical mathematical tool to optimize biodiesel production parameters. However, most of these studies have focused solely on optimizing the alkali transesterification step, neglecting the acid esterification step required for high-FFA oils in a two-step biodiesel production process. Additionally, while individual oils have been extensively studied for biodiesel production, only a limited number of researchers have explored the use of mixed oils. The conversion of hybrid oils into biodiesel offers multiple advantages, including energy resource diversification, effective waste management, reduction of greenhouse gas emissions, economic stability, and climate change mitigation [49]. For instance, a recent study utilized mixed oils, combining three different vegetable oils to enhance the properties of the resulting biodiesel [50]. However, [51] applied the design of experiments, specifically a basic lattice mixture design, to determine the optimal oil blending proportions (appropriate volume fractions) based on

individual oil physicochemical characteristics. In their study significant emphasis was placed on developing a mixture model to establish the ideal oil blend ratios, thereby improving the properties of the mixed oil before proceeding with biodiesel production.

Furthermore, no research has been reported on optimizing the two-step biodiesel production process for a mixture of waste kitchen oil, Neem oil, and Shea butter using the BBD. This experimental work aims to address this gap by optimizing through desirability function in a two different single-objective optimization, the dual-stage biodiesel synthesis process using these high-FFA mixed oils. The study investigates the influence of key reaction parameters, including molar ratio, catalyst concentration, reaction temperature, and duration, on both the esterification and transesterification processes. The ultimate goal is to optimize the process for commercial implementation, reducing time and costs. Additionally, the paper presents the results of the characterization of the synthesized hybrid biodiesel, focusing on its shelf life and oxidative stability.

II. MATERIALS AND METHODS

II.1 MATERIALS

The hybrid vegetable oil (made of: neem oil, shea butter, and waste kitchen oil) used, was prepared according to [51]. For the transesterification reaction, ethanol with a purity of 98% from Sigma-Aldrich Reagent was utilized as the alcohol. Sulfuric acid (98% purity, Sigma-Aldrich Reagent) served as the acid catalyst, while potassium hydroxide (98% purity, Sigma-Aldrich Reagent) was used as the alkali catalyst.

II.2 METHODS

II.2.1. PRODUCTION OF BIODIESEL USING A TWO-STEP CATALYZED METHOD

The water content of the hybrid oil was determined to be 0.11% by weight and the FFA content of the hybrid oil utilized was determined to be 1.87%; which is notably high and could lead to soap formation if the reaction were conducted with an alkali catalyst, as indicated by [52]. Therefore, it was imperative to reduce the FFA content prior to the transesterification reaction with an alkali catalyst through a pretreatment step. Approximately 125 grams of the oil were heated to the desired temperature using a water bath and a magnetic hot plate stirrer equipped with a temperature controller (Stone Staffordshire, model HC-1202). The stirring speed was maintained at a constant 400 rpm throughout the experiment. Subsequently, predetermined quantities of sulfuric acid and ethanol were introduced into the oil. The oil-to-ethanol molar ratio is calculated based on the oil's molecular weight.

The heating and stirring were halted once the reaction had reached the preset reaction time. To stop the reaction, the flask was promptly immersed in cold water. Following the first step, the mixture was left to settle for 1 hour, resulting in the separation of two distinct liquid phases. The excess ethanol in the upper phase was removed using a separating funnel, while the lower phase contained ethyl ester and unreacted triglyceride was further subjected to a reaction with KOH in the second step (without removing the H2SO4 from the product of the first step). Upon completion of the second step reaction, the product obtained was left to settle overnight, resulting in the formation of two distinct liquid phases: an ester phase at the top and a glycerol phase at the bottom. The biodiesel product underwent multiple washes with deionized water until the washing became clear. Subsequently, the product was dried by heating at 100°C.

II.2.2. EXPERIMENTAL DESIGN

RSM-based BBD was employed using Design-Expert software to optimize FAEE yield in the biodiesel production process in two steps of transesterification. The optimization was carried out numerically within predefined ranges utilizing the desirability function, as outlined by [53]. This function involves the transformation of each predicted response into a dimensionless partial desirability function, which incorporates the researcher's priorities and preferences during the optimization process. Depending on whether each response needs to be maximized, minimized, or has a target value, one- or two-sided functions are employed. Essentially,

the desirability function consolidates all responses into a single metric, enabling the prediction of optimal levels for all independent variables, as explained by [54]. The desirability function was utilized to investigate how reaction temperature, ethanol-to-oil molar ratio, catalyst concentration, and reaction time affect biodiesel yield. The desirability function-based method involves transforming the estimated response models (typically second-order models) into individual desirability functions di(Yi). These individual functions are then combined into a composite function denoted as D. Typically, this composite function is either a geometric mean (optimized for maximization) or an arithmetic mean (optimized for minimization). The total desirability function established is represented in Equation (1). Here, wi represents a weight that is relative in importance among n responses.

$$D(Y) = \left(\prod_{i=1}^{n} d_i(y)^{w_i} \right)^{\frac{1}{\sum_{i=1}^{n} w_i}} \quad (1)$$

The weight controls how desirability is allocated within the interval between the lower (or upper) bound and the target value. It shapes the desirability function, which maps the response scale onto a normalized range from zero to one, facilitating the evaluation of individual response desirability. To maintain an accurate representation of process performance without introducing bias, each parameter's weight was assigned a value of one; resulting in a linear ramp function that transitions between the lower (or higher) and desired values.

Four distinct variables were considered: (A) temperature, (B) ethanol-to-oil molar ratio, (C) catalyst amount, and (D) time. The design was generated through Design-Expert® version 13 software (Stat-Ease Inc., Minneapolis, USA). Conducted in triplicate, Table 1 outlines the range and levels of the independent variables used in the experiments.

The data obtained from the two-stage experimental process were analyzed using the response surface regression method based on a second-order polynomial Equation (2).

$$Y = \beta_0 + \sum_{i=1}^{k} \beta_i X_i + \sum_{i=1}^{k} \beta_{ij} X_i^2 + \sum_{i1<j}^{k} \sum_{j}^{k} \beta_i X_i X_j + e \quad (2)$$

Here: Y denotes the predicted response, β_0 represents the intercept, β_i is the linear coefficient, β_{ii} is the quadratic coefficient, and β_{ij} is the interaction coefficient. The terms X_i and X_j refer to the independent variables.

Multiple regression was employed to link the response variable to the independent variables and to determine the coefficients of the polynomial response model. The model's fit quality was assessed through analysis of variance (ANOVA) and significance testing (with a significance level of $p < 0.05$). The process involved iterative correlation and the derivation of practical regression models. Concurrently, contour lines were generated based on empirical findings. The models' appropriateness was validated by assessing the Lack of Fit values and conducting the F-test, resulting in the selection of the most accurate results for each response variable.

Table 1: Range and levels of operating parameters of the hybrid oil dual stage conversion procedure.

Variables	Symbol coded	Range and levels		
		-1	0	1
1st Step: esterification				
Temperature (°C)	A	45	50	55
Ethanol to oil molar ratio	B	0.5:1	4.25:1	8:1
H_2SO_4 Concentration (wt.%)	C	0.50	1	1.50
Time (min)	D	30	45	60
2nd Step: transesterification				
Temperature (°C)	*A*	50	65	80
Ethanol to oil molar ratio	*B*	3.5:1	6.5:1	9.5:1
KOH Concentration (wt.%)	*C*	0.5	1.25	2
Time (min)	*D*	30	45	60

Source: Authors, (2025).

II.2.3. DETERMINATION OF ETHYL ESTER CONTENT AND DETERMINATION OF YIELD

The analysis of ethyl ester content in the product was carried out using Shimadzu's GCMS-QP 2010 Plus, equipped with the LabSolutions software, which offers a user-friendly interface for efficiently displaying sample chemical compositions. The LabSolutions GCMS software streamlines system operations by optimizing both data acquisition and analysis processes. It supports simultaneous acquisition and analysis of GC and MS data with ease and incorporates various features to enhance workflow efficiency. The chromatograph was equipped with a high-resolution RTxi-5ms capillary column. Compound identification was carried out using the integrated database from the American National Institute of Standards and Technology (NIST).

This analysis utilized Methyl Heptadecanoate (C17:0) as an internal standard and followed a method adapted from [55]. The percentage of ethyl ester was then calculated using Equation (3):

$$\%FAEE = \frac{(\sum A) - A_{EI}}{A_{EI}} x \frac{C_{EI}\, x\, V_{EI}}{W}\, x\, 100 \quad (3)$$

where:

- $\sum A$: This represents the total sum of all areas under the curve ranging from C14 to C24.
- A_{EI}: It signifies the area under the curve specifically for C17:0.
- C_{EI}: This denotes the concentration of C17:0 in milligrams per milliliter (mg/mL).
- V_{EI}: It represents the quantity of C17:0 utilized, measured in microliters (µL).
- W: Weight of the product (mg).

The product's yield was determined using the methodology outlined in [56] and [57], applying Equation (4).

$$\%Yield = \frac{weight\ of\ product(g)}{weight\ of\ raw\ oil(g)}\, x\, 100 \quad (4)$$

III. RESULTS AND DISCUSSIONS

III.1 DATA ANALYSIS AND MODELING

3.1.1. Esterification process

In the initial phase of the experiment, the esterification reaction was conducted to diminish the FFA content within the range of 45-55ºC using H_2SO_4 as the catalyst. Table 2 displays the BBD matrix concerning independent variables and the corresponding %FAEE values obtained. Notably, the %FAEE fluctuates between 73.14% and 92.85%. The highest percentage was achieved within the moderate temperature and acid concentration range, low ethanol molar ratio, and a longer reaction time. Conversely, the lowest %FAEE was observed at a high-temperature range, low acid concentration, and moderate levels of ethanol molar ratio and reaction time. The significance of each parameter was assessed using the p-value, and the results are documented in Table 3.

Table 2: BBD matrix with four variables for the esterification process.

Run	Temp. (°C)	Ethanol molar ratio	H_2SO_4 Conc. (wt,%)	Time (min)	%FAEE from expt.	%FAEE from Model
1	50	0,5	1,5	45	91,12	90,8
2	50	4,25	1	45	83,41	89,3
3	55	8	1	45	78,82	77,3
4	50	0,5	0,5	45	74,16	78,51
5	45	0,5	1	45	82,32	81,43
6	50	4,25	0,5	60	84,02	83,1
7	55	4,25	1,5	45	82,54	79,2
8	45	4,25	0,5	45	73,78	74,3
9	50	0,5	1	60	92,85	91
10	45	8	1	45	77,87	78,59
11	45	4,25	1	60	80,09	77,7
12	50	4,25	0,5	30	79,09	78,51
13	50	8	1	60	83,02	84,57
14	50	4,25	1,5	30	83,6	81,43
15	50	8	1	30	82,77	77,3
16	50	0,5	1	30	82,97	83,98
17	45	4,25	1	30	81,21	83,7
18	55	4,25	1	60	83,22	85,6
19	50	4,25	1	45	82,89	81,96
20	50	4,25	1	45	82,99	83,1
21	55	0,5	1	45	81,02	76,9
22	50	8	0,5	45	81,56	82,7
23	50	8	1,5	45	83,89	82,69
24	50	4,25	1,5	60	83,75	83,1
25	55	4,25	1	30	82,12	81,6
26	45	4,25	1,5	45	77,77	74,3
27	55	4,25	0,5	45	73,14	72,87
28	50	4,25	1	45	82,98	79,2
29	50	4,25	1	45	83,97	85,6

Source: Authors, (2025).

Table 3: ANOVA on response surface quadratic model for esterification process.

Source	Sum of Squares	df	Mean Square	F Value	p-value
Model	428.33	14	30.60	6.65	0.0005
A-Temp.	5.08	1	5.08	1.10	0.3112
B-Molar Ratio	22.68	1	22.68	4.93	0.0434
C-H_2SO_4 Conc.	113.60	1	113.60	24.70	0.0002
D-Time	19.25	1	19.25	4.18	0.0601
AB	1.27	1	1.27	0.28	0.6081
AC	7.34	1	7.34	1.60	0.2270
AD	1.22	1	1.22	0.27	0.6147
BC	53.41	1	53.41	11.61	0.0042
BD	23.22	1	23.22	5.05	0.0413
CD	5.71	1	5.71	1.24	0.2837
A*A	99.40	1	99.40	21.61	0.0004
B*B	5.17	1	5.17	1.12	0.3068
C*C	28.62	1	28.62	6.22	0.0257
D*D	18.39	1	18.39	4.00	0.0653
Residual	64.38	14	4.60		
Lack of Fit	63.57	10	6.36	31.14	0.0023
Pure Error	0.82	4	0.20		
Cor Total	492.71	28			
Other Statistics:					
Std. Dev. = 2.14		R-Squared = 0.8693			
Mean = 81.83		Adj R-Squared = 0.7387			
C.V. % = 2.62		Pred R-Squared = 0.2543			
PRESS = 367.42		Adeq Precision = 11.297			

Source: Authors, (2025).

The p-value serves as a tool to gauge the significance of each regression coefficient, including the interaction effects of cross-products. When it comes to the model terms, a p-value less than 0.05 indicates the significant influence of these parameters. The quadratic regression model, after excluding non-significant factors, formulated with the determined coefficients based on the coded parameters, is presented in Equation (5):

$$\%FAEE = +83.25 - 1.37B + 3.08C - 3.65BC - 2.41BD - 3.91A^2 - 2.10C^2 \quad (5)$$

A low coefficient of variation (CV= 2.62%) indicates the reliability of the fitted model's results. The R^2 value of 0.87, which reflects the relationship between predicted and actual values, suggests that approximately 87% of the variation in FAEE production is attributed to the independent variables, while only 13% of the total variation remains unexplained by the model, as depicted in Figure 1 (The predicted yields range from 73.14% to 92.85%, with actual yields closely aligning, indicating potential robustness of the predictive model employed). The Model F-value of 6.65 indicates the model's significance. There is a mere 0.05% chance that such a large Model F-Value could occur due to random factors [58]. The low value of pure error (0.82) signifies the excellent consistency of the data and a dependable coefficient of determination (R^2= 0.87) [59]. Additionally, as evident in Table 2, the predicted %FAEE values from the model closely aligned with the experimental values.

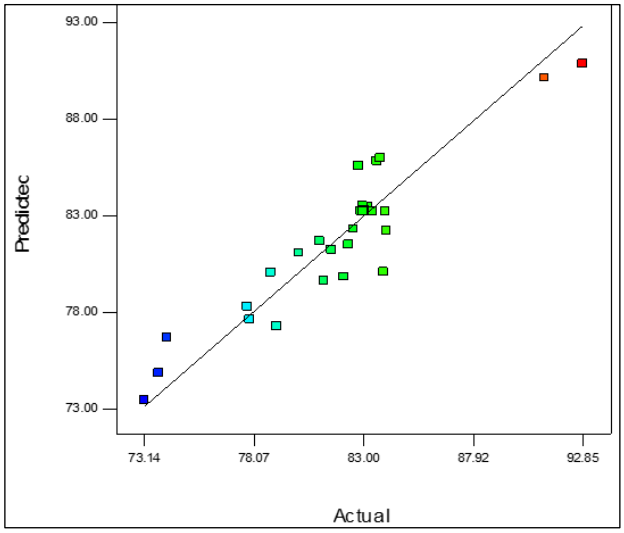

Figure 1: Plot of Predicted versus actual fatty acid ethyl esters yield (%).
Source: Authors, (2025).

Figure 2 is a showcasing of the regression equation (5). It provides a visual representation of how the dependent and independent variables relate to each other while holding specific parameters constant. The response surface analysis reveals a clear trend: yield increases significantly with rising temperatures and reduced catalyst concentrations up to a certain limit, after which diminishing returns are observed. This behavior highlights the presence of an optimal temperature, as excessive heat can result in: the evaporation of methanol, which consequently lowers the reaction rate [23]; the formation of unwanted by-products or the hydrolysis of oil: leading to an increase in the FFA value and ultimately reducing the conversion yield. Figure 2(a) displays both a 3D plot and a contour plot representing the interaction effects between alcohol molar ratio and reaction temperature on %FAEE yield. The FAEE yield increases as the temperature rises to 50ºC, reaching its peak at 0.63 mol of alcohol, after which further increases in alcohol and temperature do not substantially improve the yield. The contour plot reveals that over 85% of FAEE is produced within the range of 0.52-0.85 mol of alcohol and 48-53ºC temperature. However, at higher alcohol concentrations, there's a reduction in yield, likely due to increased glycerol solubility, making it challenging to separate the ester layer [60]. Figure 2(b) explores the impact of time and alcohol concentration on FAEE yield.

At low alcohol concentrations, the FAEE yield steadily increases with time, whereas at high alcohol concentrations, the yield decreases slightly with time. Similar trends were reported by Gupta et al. [39] in their optimization study of FAME production from a mixture of edible and non-edible vegetable oils. Additionally, at the minimum time point, an increase in FAEE yield is observed with alcohol concentration starting from 4.25 mol, with the maximum yield achieved near the maximum time and a 0.5:1 alcohol-to-oil molar ratio due to the positive linear effect of reaction time. Rapid transesterification reactions, which occur in a short time, contribute to this behavior [34, 39]. Figure 2(c) presents the effects of time and temperature on conversion yield. It shows that as the temperature increases up to approximately 52ºC, the FAEE yield increases and then starts declining.

The maximum yield is attained near the maximum time and at 50ºC. Achieving a %FAEE of over 85% is feasible when employing a reaction temperature between 50 and 52.5 ºC and a reaction time ranging from 56 to 60 minutes. In Figure 2(d), the interaction effects of temperature and catalyst concentration on conversion yield are examined. Although the interaction effect is not significant, the variation appears to exhibit a peak, resulting in a nearly constant %FAEE yield at higher acid concentration ratios and medium-range temperatures. The results indicate that at a low catalyst concentration, the yield increases from 75% to 82% with increasing temperature. This trend reflects the fact that the transesterification reaction rate accelerates with rising temperature, consistent with observations in the literature [61] regarding the optimization of biodiesel production through transesterification of soybean oil with ethanol and NaOH. Figure 2(e) shows the response for the interaction between acid catalyst concentration and time. FAEE yield increases with both catalyst concentration and time, ranging from 30 to 60 minutes. The contour plot reveals that over 85% of FAEE is produced with catalyst concentrations between 0.96 and 1.5 wt% and reaction times ranging from 52.5 to 60 minutes. Lastly, Figure 2(f) presents the response for the interacting factors of catalyst concentration and ethanol-to-oil molar ratio. The effect of the ethanol-to-oil molar ratio on FAEE yield is somewhat pronounced in the presence of H_2SO_4. This suggests that at a low ethanol-to-oil molar ratio, increasing the acid concentration boosts FAEE yield. It was observed that a yield of over 90% for FAEE could be achieved with a high level of acid catalyst concentration and a low ethanol-to-oil molar ratio.

The model's accuracy was verified by analyzing residual plots, which depict the differences between actual and predicted response values (biodiesel yield). As seen in Figure 3, an analysis of the residual plots revealed no noticeable trends or patterns, indicating that the model is well-fitted. The even distribution of residuals across all predicted value levels supports the assumptions of independence and

constant variance. Additionally, the lack of outliers further confirms that the model's assumptions are upheld, thereby reinforcing the reliability of the analysis results. In Figure 3(a), a straight line closely aligns with the normal plot of residuals, indicating a good fit [62], [63]. This suggests that the errors follow a normal distribution and are not significant. Figure 3(b) shows a random pattern of residuals versus run order, signifying model accuracy [62], [64]). Figure 3(c) displays a structure-less plot of residuals versus the predicted response, suggesting that the model is adequate and does not violate the assumptions of independence or constant variance [65].

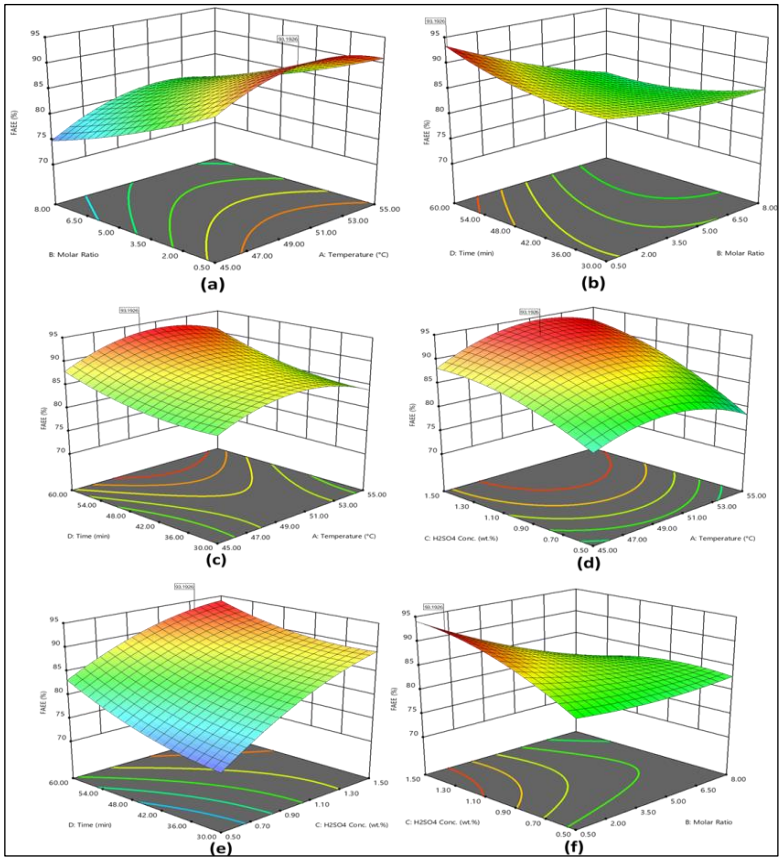

Figure 2: Response surface representation of the effect of process parameters on fatty acid ethyl esters Yield in the esterification step.
Source: Authors, (2025).

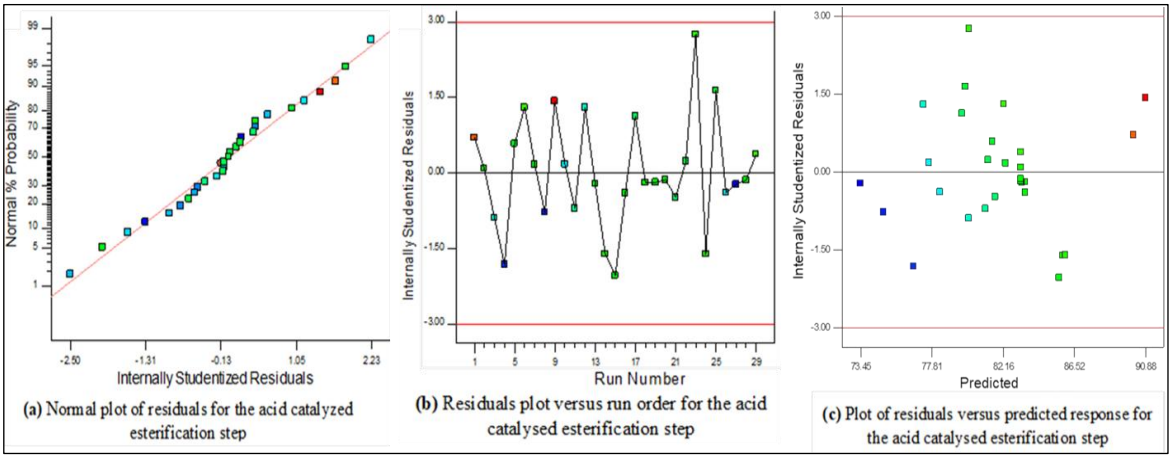

Figure 3: Residual Plots illustration for esterification step.
Source: Authors, (2025).

Table 4 illustrates the coefficients of the various factors and their impact on the oil esterification response. By examining the signs of the coefficients in model equation (5), it becomes evident that certain factors have significant effects on %FAEE:

- Factors B (3.14%) and C (15.88%) exhibit a positively significant linear influence on %FAEE by lowering the FFA.
- The interaction between BC and BD also has a notable impact on %FAEE.
- Conversely, significant quadratic terms such as AA (25.59%) and CC (7.38%) exert adverse effects, increasing the FFA hence, reducing the FAEE yield.

In the esterification process of the hybrid oil, the most influential terms, ranked in decreasing order, are as follows: AA (25.59%, quadratic term related to temperature), BC (22.30%, representing the Ethanol ratio/H_2SO_4 concentration), C (15.88%, H_2SO_4

concentration), BD (9.72%, Ethanol ratio/Time), and CC (7.38%, quadratic term linked to H_2SO_4 concentration). These five terms collectively contribute to 80.87% of the esterification of the hybrid oil.

Table 4: Factors coefficients and weights on the hybrid oil esterification response.

Factors	Coefficient	Coefficient square	%effect
Constant	83.25		
A	0.65	0.4225	0.707141375
B	-1.37	1.8769	3.141381411
C	**3.08**	**9.4864**	**15.87745784**
D	1.27	1.6129	2.699522659
AB	0.56	0.3136	0.524874639
AC	1.36	1.8496	3.095689199
AD	0.55	0.3025	0.506296487
BC	**-3.65**	**13.3225**	**22.29796678**
BD	**-2.41**	**5.8081**	**9.721059925**
CD	-1.2	1.44	2.41013865
AA	**-3.91**	**15.2881**	**25.58780604**
BB	0.89	0.7921	1.325743628
CC	**-2.1**	**4.41**	**7.381049615**
DD	1.68	2.8224	4.723871754
$\sum \beta_I^2 = 59.7476$			

Source: Authors, (2025).

III.1.2. TRANSESTERIFICATION PROCESS

Based on the preliminary investigations mentioned above, the BBD was employed to examine the impact of KOH concentration, ethanol-to-oil molar ratio, time, and temperature on %FAEE. Table 5 displays the experimental results alongside the predicted values for %FAEE, as well as the conversion yield, at the designated points.

Reviewing Table 5, it becomes apparent that the predicted %FAEE values from the model closely matched the experimental values. The %FAEE and % Yield exhibited variations ranging from 69.35% to 92.16% and 82.16% to 95.66%, respectively. The highest %Yield and %FAEE values were observed within a medium temperature range, at moderate catalyst concentrations, low ethanol-to-oil molar ratios, and extended reaction times. Conversely, the lowest values were recorded under high-temperature conditions, elevated KOH concentrations, and within the medium range for ethanol-to-oil molar ratios and reaction times.

Table 5: BBD matrix with four variables for the transesterification process.

Run	Temp. (°C)	Ethanol molar ratio	KOH Conc. (wt,%)	Time (min)	%FAEE from expt.	%FAEE from Model	Yield (%)
1	65.00	9.50	1.25	60.00	84.13	83.12	93.26
2	65.00	3.50	1.25	60.00	92.16	89.35	95.66
3	65.00	6.50	0.50	60.00	80.60	82.76	87.89
4	65.00	6.50	1.25	45.00	81.35	82.11	90.12
5	50.00	9.50	1.25	45.00	80.12	83.98	86.21
6	65.00	6.50	1.25	45.00	80.97	78.17	90.32
7	80.00	6.50	2.00	45.00	69.35	77.7	82.16
8	65.00	6.50	2.00	30.00	80.79	79.16	87.89
9	65.00	6.50	1.25	45.00	81.07	83.1	89.71
10	65.00	3.50	0.50	45.00	89.42	86.67	95.07
11	65.00	6.50	1.25	45.00	81.21	78.12	89.45
12	65.00	3.50	1.25	30.00	91.10	89.35	95.51
13	80.00	9.50	1.25	45.00	84.29	82.16	94.32
14	65.00	9.50	1.25	30.00	83.25	81.90	89.56
15	80.00	6.50	1.25	60.00	81.75	81.00	89.45
16	80.00	6.50	1.25	30.00	81.55	81.41	88.67
17	65.00	9.50	0.50	45.00	83.19	82.74	88.58
18	65.00	9.50	2.00	45.00	83.13	84.00	89.23
19	65.00	6.50	0.50	30.00	81.53	82.7	89.62
20	65.00	6.50	1.25	45.00	81.21	79.02	89.38
21	50.00	6.50	0.50	45.00	82.14	82.1	90.28
22	50.00	3.50	1.25	45.00	87.68	85.6	91.33
23	50.00	6.50	1.25	60.00	81.56	82.15	89.81
24	65.00	3.50	2.00	45.00	81.88	80.40	90.39
25	50.00	6.50	2.00	45.00	82.56	84.04	90.58
26	65.00	6.50	2.00	60.00	80.69	78.33	87.69
27	80.00	3.50	1.25	45.00	84.70	85.48	93.26
28	50.00	6.50	1.25	30.00	81.85	84.04	90.13
29	80.00	6.50	0.50	45.00	82.17	83.54	90.37

Source: Authors, (2025).

To predict the full quadratic model for %FAEE related to the operational parameters in the second esterification step, regression coefficients, and constants were obtained, as displayed in Table 6. The R^2 was found to be 84.9%. Utilizing these coefficients, the predicted full quadratic model for %FAEE is represented in Equation. (6).

$$\%FAEE = 81.16 - 2.40B - 1.72C - 3.31AC + 4.57B^2 \quad (6)$$

The importance of each coefficient in equation (6) was assessed using the P-value, as presented in Table 6.

Table 6: ANOVA on Response Surface Quadratic Model for transesterification.

Source	Sum of Squares	df	Mean Square	F Value	p-value
Model	386.37	14	27.60	5.62	0.0013
A-Temp.	12.20	1	12.20	2.48	0.1373
B-Ethanol to oil molar ratio	69.30	1	69.30	14.11	0.0021
C-KOH Conc.	35.48	1	35.48	7.22	0.0177
D-Time	0.058	1	0.058	0.012	0.9153
AB	12.76	1	12.76	2.60	0.1294
AC	43.84	1	43.84	8.92	0.0098
AD	0.058	1	0.058	0.012	0.9148
BC	13.97	1	13.97	2.84	0.1139
BD	8.742E-003	1	8.742E-003	1.780E-003	0.9669
CD	0.17	1	0.17	0.035	0.8543
A^2	7.83	1	7.83	1.59	0.2273
B^2	135.38	1	135.38	27.56	0.0001
C^2	12.44	1	12.44	2.53	0.1339
D^2	15.68	1	15.68	3.19	0.0957
Residual	68.78	14	4.91		
Lack of Fit	68.70	10	6.87	333.17	< 0.0001
Pure Error	0.082	4	0.021		
Cor Total	455.14	28			
Other Statistics:					
Std. Dev. = 2.22		R-Squared = 0.8489			
Mean = 82.67		Adj R-Squared = 0.6978			
C.V. % = 2.68		Pred R-Squared = 0.1303			
PRESS = 395.82		Adeq Precision = 11.102			

Source: Authors, (2025).

Considering the linear impact, it was determined that both the ethanol-to-oil molar ratio and the KOH concentration held significance at a 5% significance level. Regarding the quadratic effect, only the ethanol-to-oil molar ratio exhibited significance. However, the interaction effect between temperature and KOH concentration was also found to be significant at a 5% level. Therefore, this interaction term played a crucial role in the final percentage of FAEE. Similarly, Gupta et al. [39] discovered an interaction effect between catalyst concentration and temperature in the production of biodiesel from a mixture of edible and nonedible vegetable oils using an alkaline-catalyzed process. In contrast, Yuan et al.[58] observed a minimal interaction effect between catalyst concentration and temperature in the production of biodiesel from waste rapeseed oil using the same alkaline-catalyzed process.

A low coefficient of variation (CV=2.68%) suggests that the fitted model's results are reliable. The low pure error value (0.082) indicates excellent data regeneration and a dependable coefficient of determination (R^2=0.85), demonstrating a strong correlation among the independent variables. Furthermore, the Model F-value of 5.62 suggests the model's significance, with only a 0.13% chance that such a large "Model F-Value" could occur due to noise [66], [67]. "Adeq Precision" measures the signal-to-noise ratio, and a value of AP > 4 indicates adequate signal quality, making the model suitable for navigating the design space [68], [69]. The R^2 value (0.85), representing the relationship between predicted and actual values, indicates that 85% of the variation in FAEE production can be attributed to the independent variables, leaving only 15% unexplained by the model [58], [59], as depicted in Figure 4.

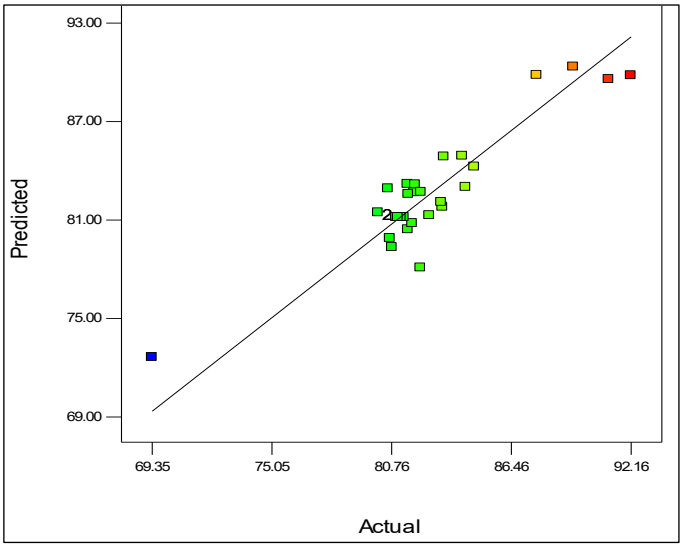

Figure 4: Plot of predicted values and actual values for transesterification.
Source: Authors, (2025).

Table 7 displays the coefficients of various factors and their impact on the oil transesterification response. From the signs of the coefficients in model equation (6), it is evident that term B (10.69% - Ethanol/oil molar ratio) had a significant negative linear effect on %FAEE. Additionally, term AC (20.34% - Temperature/KOH concentration) exhibited a significant negative interaction effect on %FAEE. However, significant quadratic terms, specifically BB (38.77% - ethanol/oil molar ratio), had positive effects that boosted FAEE yield. These three terms collectively contributed to 69.8% of the hybrid oil transesterification.

Table 7: Factors coefficients and weight on transesterification response.

Factors	Coefficient	Coefficient square	%effect
Constant	81.16		
A	-1.01	1.0201	1.893883486
B	**-2.4**	**5.76**	**10.69382304**
C	-1.72	2.9584	5.492466332
D	0.069	0.004761	0.008839113
AB	1.79	3.2041	5.948624721
AC	**-3.31**	**10.9561**	**20.34072822**
AD	0.12	0.0144	0.026734558
BC	1.87	3.4969	6.492227392
BD	0.047	0.002209	0.004101155
CD	0.21	0.0441	0.081874583
AA	-1.1	1.21	2.246445464
BB	**4.57**	**20.8849**	**38.77420568**
CC	-1.38	1.9044	3.535645241
DD	1.55	2.4025	4.460401015
$\sum \beta_I^2 = 53.86287$			

Source: Authors, (2025).

The relationships between the analyzed variables for different parameters are presented in Figure 5. Figure 5(a) depicts a 3D plot and a contour plot illustrating the interaction effects between the ethanol/oil molar ratio and reaction temperature on the %FAEE yield. The FAEE yield increases as the temperature and ethanol/oil molar ratio decrease. The contour plot's shape reveals that more than 89% of FAEE was produced at lower temperatures and ethanol molar ratio values. This observation aligns with the findings of Charoenchaitrakool & Thienmethangkoon [34], who produced FAME from waste frying oil and noted a similar trend. Figure 5(b) illustrates the effects of time and alcohol concentration on FAEE yield.

Since there is no interaction between these parameters, the contour curve appears relatively circular, as noted by Yuan et al.[58]. Maximum %FAEE can be obtained by increasing the reaction time while decreasing the ethanol concentration. More than 89% FAEE is observed near the maximum reaction time and a 3.5:1 ethanol/oil molar ratio. Figure 5(c) shows the effects of time and temperature on conversion yield. An increase in FAEE yield is observed with temperatures up to around 63ºC, especially near the maximum and minimum times. A %FAEE of over 82% can be achieved when using a reaction temperature in the range of 50 to 63ºC and a reaction time in the range of 30-34 minutes or 56-60 minutes. Figure 5(d) indicates the effects of temperature and catalyst concentration on the conversion yield. The variation suggests that a maximum and relatively steady %FAEE can be obtained at low alkali concentrations and a high-temperature range.

The results show that about 82% of FAEE can be obtained near the maximum temperature with approximately 0.56 wt.% KOH. Figure 5(e) illustrates the response for the interacting factors of alkali catalyst concentration and time. An increase in FAEE yield is observed with KOH concentration up to approximately 1.32 wt.% near the maximum and minimum times. A %FAEE of more than 82% can be achieved when using a reaction KOH concentration in the range of 0.5 to 1.25 wt% and a reaction time in the range of 30-35 minutes or 55-60 minutes. Figure 5(f) presents the response for the interacting factors of catalyst concentration and ethanol to oil molar ratio. The rate of FAEE yield increase is noticeable with a simultaneous decrease in catalyst concentration and ethanol/oil molar ratio. However, it was found that more than 89% FAEE yield could be achieved at low levels of KOH catalyst concentration and low ethanol-to-oil molar ratios. Examination of Fig 5 reveals distinct trends in FAEE yield, showing a steady increase with rising temperatures up to a critical threshold of approximately 65°C. Beyond this point, the yield stabilizes and, in some cases, declines, suggesting a complex interaction of factors as seen in Table 7.

This behavior may result from thermal degradation of oil or the formation of undesirable byproducts at higher temperatures, reducing overall efficiency. Additionally, an anomaly is observed at higher catalyst concentrations (above 2.0%), where yield fails to increase proportionally with catalyst addition. This inconsistency points to possible reaction limitations or side reactions, such as soap formation, that may hinder efficiency. These non-linear relationships highlight the need for further investigation to identify the optimal operating conditions for these parameters, as such insights could lead to significant improvements in biodiesel production efficiency. Interestingly, the analysis also uncovers an unexpected interaction between catalyst concentration and reaction time.

Evidence suggests that higher catalyst levels may reduce the benefits of extended reaction durations, potentially due to an inhibitory effect of excess catalyst. This challenges the conventional assumption that "more is better" in catalyst usage. These findings call for a reassessment of the balance between catalyst concentration and reaction time to optimize yield. Yet, exploring the mechanisms behind catalyst behavior under different conditions may offer an opportunity to refine transesterification processes, paving the way for more efficient biodiesel production strategies.

The model's accuracy was assessed using residual plots, which compare actual and predicted %FAEE yield values. As shown in Fig 6, the residuals exhibit a random distribution with no discernible patterns, indicating that assumptions of homoscedasticity and normality are met. The consistent spread of residuals suggests reliable predictions across input values. However, a few data points deviate significantly, possibly representing outliers caused by experimental errors, feedstock quality variations, or other factors. For instance, elevated impurities in a feedstock batch could skew results. These deviations highlight the need for further investigation to determine their effect on the model's accuracy and biodiesel yield. In Fig 6(a), the analysis of residuals revealed no statistical issues, as the errors in the response values closely followed a normal distribution. The plot of residuals versus run order in Fig 6(b) displayed random patterns, indicating good model accuracy. Furthermore, Fig 6(c), the plot of residuals versus predicted response, exhibited a structureless pattern, suggesting that the model is adequate and does not violate the assumptions of independence or constant variance.

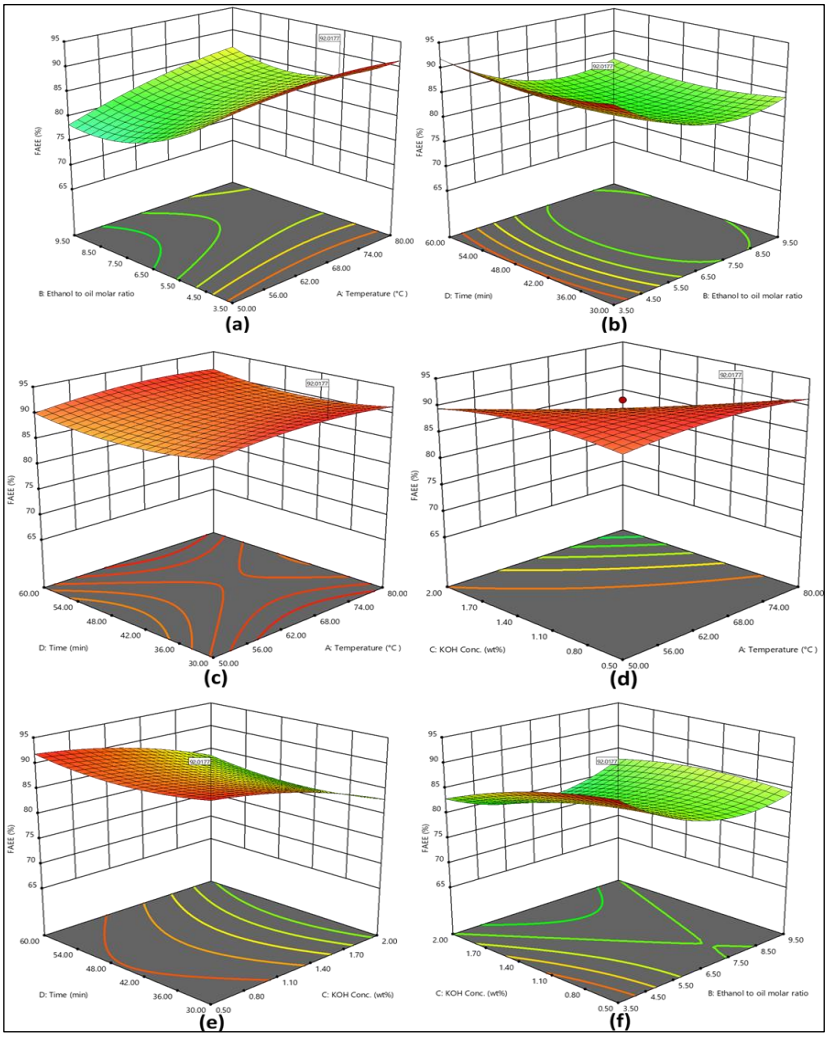

Figure 5: Response surface representation of the effect of process parameters on FAEE yield in the transesterification step.
Source: Authors, (2025).

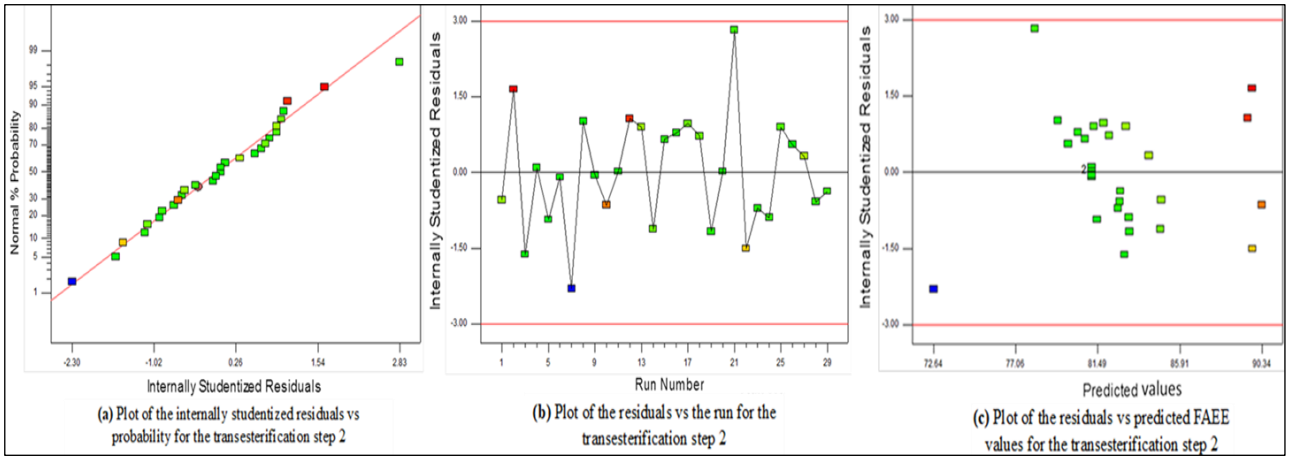

Figure 6: Residuals Plots illustration for the transesterification step.
Source: Authors, (2025).

III.2 OPTIMIZATION OF REACTION PARAMETERS AND MODELS VALIDATION

Implementing the global desirability function method, a non-zero value indicates that all responses simultaneously fall within the desirable range as is appears on Figure 7 for both; the esterification and the transesterification steps. Consequently, a *D* value close to 1 signifies that the combination of different criteria is globally optimal since the response values closely align with target values.

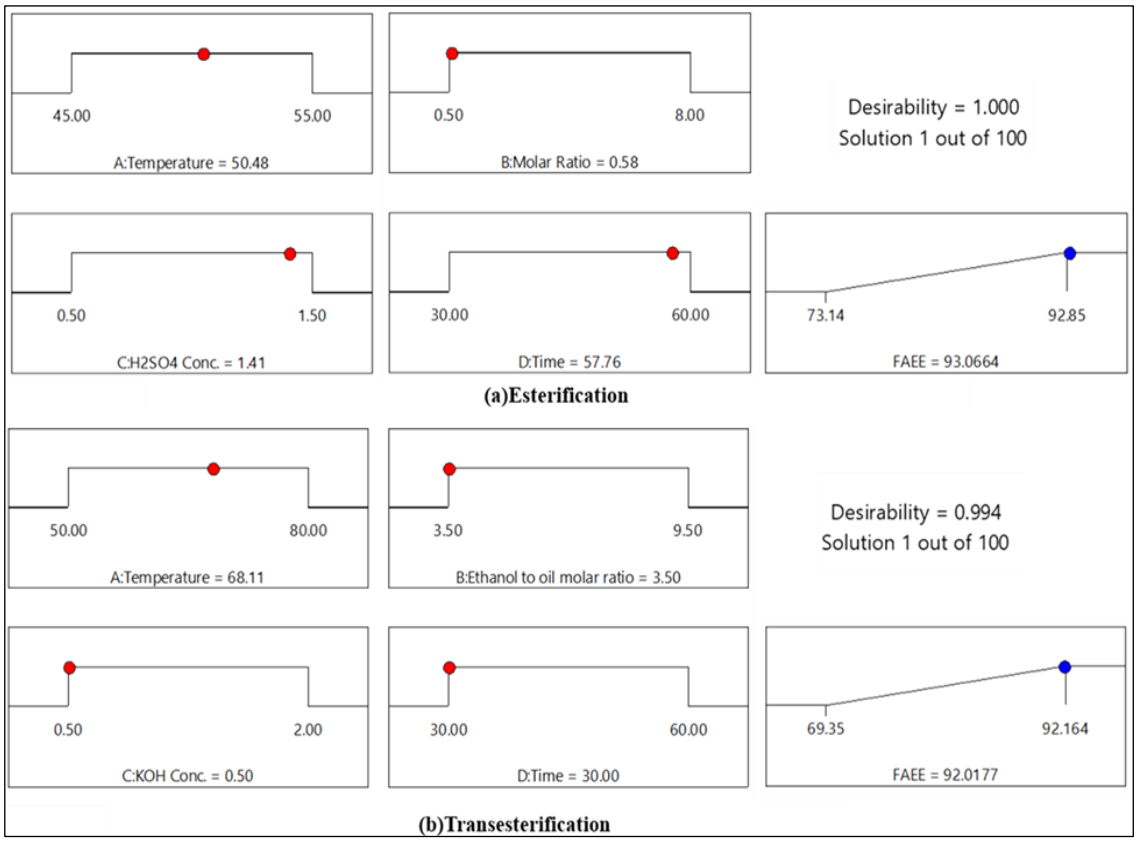

Figure 7: Ramp function desirability representation for the dual-phase process.
Source: Authors, (2025).

In the first step (esterification), three optimal conditions are presented (Table 8), with the highest desirability value (D = 1) achieved under specific parameters. These parameters include an alcohol-to-oil molar ratio of 1.28:1, a reaction time of 59.87 minutes, a reaction temperature of 51.72ºC, and acid catalyst amount of 1.46 wt.%. The second step (transesterification) also presents three optimal solutions (Table 9), with the first group yielding a desirability value of 0.99. The best compromise in this step includes an ethanol-to-oil molar ratio of 3.5:1, a reaction time of 30 minutes, a reaction temperature of 68.84ºC, and a KOH catalyst amount of 0.52 wt.%. The corresponding response surface plots, illustrating the best compromise (for both steps), is depicted in Figure 8. Predicted %FAEE at these conditions is 91.96%, and verification experiments closely aligned with this prediction, yielding 90.53±0.28%. Moreover, with AADM values < 10%; the quadratic models employed in the various steps are considered accurate and reliable for predicting %FAEE, with a small percentage error of 1.55% between experimental and predicted results.

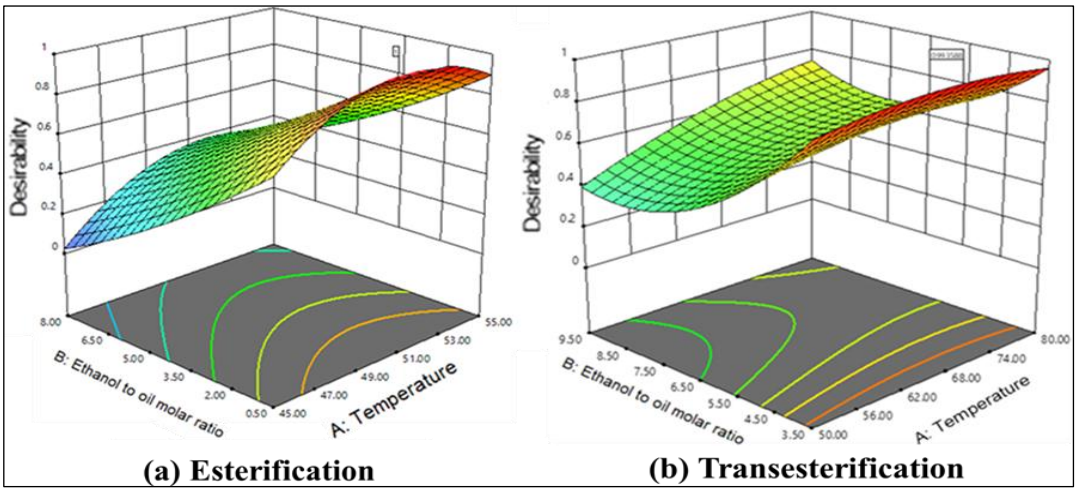

Figure 8: 3D representation of the overall desirability.
Source: Authors, (2025).

Table 8: Criteria for numerical optimization of the acid catalyzed esterification step with desirability function approach for hybrid oil biodiesel production.

Parameters	Goal	Lower Limit	Upper Limit	Lower Weight	Upper Weight	Importance
Temperature (°C)	In range	45	55	1	1	3
Ethanol to oil molar ratio	In range	0.5	8	1	1	3
H_2SO_4 Concentration (wt.%)	In range	0.5	1.5	1	1	3
Time (min)	In range	30	60	1	1	3
FAEE (%)	Maximize	73.14	92.85	1	1	3

Solutions:

Number	Variables				Response			
					% FAEE			
	Temperature	Ethanol Molar Ratio	H_2SO_4 Conc.	Time	Exp	Pred	Desirability	
1	51.72	1.28	1.46	59.87	94.57±0,76	93.25	1	*Selected*
2	49.96	0.73	1.36	59.49	---	93.07	0.97	
3	53.43	0.66	1.43	59.7	---	93.99	0.95	
% Error				-1.42				
AADM obtained 0.0802								
Exp =Experimental *Pred = Predicted* *AADM = Absolute analysis average deviation*								

Source: Authors, (2025).

Table 9: Criteria for numerical optimization of the transesterification conditions with desirability function approach for the hybrid oil biodiesel production.

Parameters	Goal	Lower Limit	Upper Limit	Lower Weight	Upper Weight	Importance
Temperature (°C)	In range	50	80	1	1	3
Ethanol to oil molar ratio	In range	3.5	9.5	1	1	3
KOH Concentration (wt.%)	In range	0.5	2	1	1	3
Time (min)	In range	30	60	1	1	3
FAEE (%)	Maximize	69.35	92.164	1	1	3

Solutions:

Number	Variables				Response			
					% FAEE			
	Temperature	Ethanol Molar Ratio	KOH Conc.	Time	Exp	Pred	Desirability	
1	68.84	3.5	0.52	30	90.53±0.28	91.96	0.991	*Selected*
2	64.25	3.51	0.51	30	---	91.90	0.988	
3	69.21	3.5	0.5	60	---	91.89	0.988	
% Error				1.55				
AADM obtained 0.0094								
Exp =Experimental *Pred = Predicted* *AADM = Absolute analysis average deviation*								

Source: Authors, (2025).

III.3 COMPARISON OF THE STUDY WITH EXISTING LITERATURE

Table 10 provides a comparison of the present study with existing literature. The data indicate that lower catalyst concentrations, such as 0.52 wt.% KOH falls within the typical range for transesterification reactions (0.5%–1.5% by weight) as reported by Gupta et al. [39]. Additionally, the optimal conditions achieved in this study are comparable to those reported by Betiku et al. [56]. However, the biodiesel yield of 90.53% is lower than the results reported by Harisha et al. [44], Suherman et al.[70], and Kusumo et al.[46]. These differences may be attributed to two primary factors: the unique properties of the feedstock oil, such as its chemical composition, kinematic viscosity, alcohol solubility, and the specific procedures and reactants used in the transesterification process. In contrast, the yield of 83.20% obtained using a heterogeneous catalyst in Brihaspati et al. [12] stands out as an outlier, suggesting that variations in feedstock and processing conditions can result in lower yields. This emphasizes the critical role of selecting appropriate feedstock and optimizing operational parameters. From a practical perspective, the high yield achieved in this study with minimal catalyst usage and a shorter processing time demonstrates the potential for industries to enhance the economic feasibility of biodiesel production by adopting similar optimized conditions.

Table 10: Comparison of the study with literature.

Optimum conditions	**Feedstock (mixture)**	**Yield (%)**	**Reference work**
KOH 0.52wt.%; 3.5:1; 69 ºC; 400rpm; 30min	Shea butter, Neem oil, and Waste kitchen oil	90.53	Present work
Heterogeneous catalyst 5 wt%; 9:1; 60ºC; 800rpm; 130min	Waste cooking oil, *Ricinus* communis oil and *Melia azedarach* oil	83.20	[12]
NaOH 61.2 wt%; 6:1; 4 °C; 500rpm; 75min	Pongamia oil, waste cooking oil and animal fat	97.76	[44]
KOH 0.5wt.%;10:1; 60ºC; 90min	Waste Cooking Oil and *Schleichera oleosa* Oil	92.4	[70]
KOH 1 wt %; 9 :1; 50ºC; 400 rpm ; 90min	Jatropha oil, Palm oil and *karanja* oil	-	[50]
KOH 0.7% wt; 42%; 50.64 min	*Sterculia foetida* and rice bran oil	98.93	[46]
KOH 1.89 wt.%; 8.83:1; 43.5 ºC; 58.36min	Palm oil, linseed oil, Karanj oil and thumba oil	96.4	[39]
KOH 1.4 wt.%; 7.5:1; 65 ºC; 500rpm; 60 min	Waste cooking oil (soybean and sunflower)	99.3	[71]
KOH 1wt.%; 6:1; 60 ºC; 600rpm; 60min	Palm kernel oil and groundnut oil	86.56	[72]

Source: Authors, (2025).

III.4 QUANTITATIVE ANALYSIS OF FATTY ACID ETHYL ESTER CONTENT

The GC-MS chromatogram (Figure 9) from the FAEE analysis displays multiple distinct and well-defined peaks, each representing a specific fatty acid. Prominent peaks associated with palmitic acid (C16:0) and oleic acid (C18:1) highlight their significance in the biochemical composition of the feedstock. These fatty acids are renowned for their advantageous properties in biodiesel production, such as low viscosity and high cetane numbers. The detection of ethyl esters in the chromatogram confirms the effectivity of the transesterification process, a key step in converting triglycerides into biodiesel. The chromatogram reveals trends suggesting preferential formation of certain fatty acids during transesterification. For example, a significant peak at a retention time of 12.5 minutes likely corresponds to a dominant fatty acid, reflecting its reactivity under the experimental conditions. Such patterns offer insights into the mechanistic pathways of transesterification and inform future optimization efforts.

In contrast, smaller peaks scattered across the chromatogram represent minor fatty acid components, underscoring the complexity of the mixture and the intricacies of the transesterification process. These minor components can influence biodiesel's physical and chemical properties, emphasizing the importance of considering the entire fatty acid profile when formulating biodiesel. The predominant fragment ions of the resultant fatty acid ethyl esters, along with other noteworthy compounds, have been documented in Table 11. Our analysis reveals that the primary ethyl ester constituents obtained are as follows: (E)-9-Octadecenoic acid ethyl ester, constituting 65.3% of the biodiesel and possessing a retention time (RT) of 23.6 minutes, serves as the predominant component of the biodiesel. Ethyl 13-methyltetradecanoate, representing 11.49% of the composition and with an RT of 24.6 minutes, emerges as the second major constituent detected. Following closely is 9,12-Octadecadienoic acid ethyl ester, accounting for 7.04% of the composition with an RT of 23.3 minutes.

Hexadecanoic acid ethyl ester, comprising 5.62% of the mixture and exhibiting an RT of 18.1 minutes, is another noteworthy component. Additionally, Diisooctyl phthalate, constituting 3.33% of the biodiesel and having an RT of 36.4 minutes, is observed. This last component, recognized as a plasticizer, may potentially be a contaminant originating from the plastic container employed in the storage and distribution of vegetable oils [73],[74]. Regardless of the source of triglycerides, biodiesel produced through transesterification primarily consists of fatty acid chains with even numbers of carbon atoms. While biodiesel derived from various vegetable oils and animal fats exhibits a multitude of distinct fatty acid ester (FAE) species, a typical biodiesel fuel is typically dominated by a select few species [75]. The major ethyl ester components identified in our study, correspond to the frequently encountered FAEs in biodiesel. [39],[75],[76].

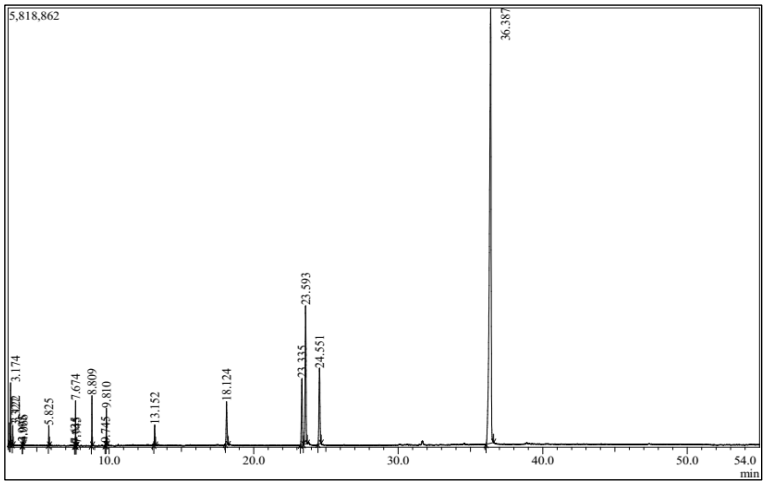

Figure 9: GC-MS Chromatogram of obtained FAEE.
Source: Authors, (2025).

Table 11: The chemical composition of the FAEE as per the GC-MS results

RT (min)	Compounds identified	Molecular formula	Molecular Weight	Area (%)
3.122	Ethylbenzene	C_8H_{10}	106	0.36
3.995	1-Decene	$C_{10}H_{20}$	140	0.05
4.066	Undecane	$C_{11}H_{24}$	156	0.06
5.825	1-Dodecene	$C_{12}H_{24}$	168	0.40
7.635	4-Undecene, 3-methyl-, (Z)-	$C_{12}H_{24}$	168	0.05
7.674	1-Tetradecene	$C_{14}H_{28}$	196	0.96
7.745	Tridecane, 2-methyl-	$C_{14}H_{30}$	198	0.06
8.809	Phenol, 2,4-bis(1,1-dimethylethyl)-	$C_{14}H_{22}O$	206	1.38
9.745	7-Hexadecene, (Z)-	$C_{16}H_{32}$	224	0.08
9.810	E-15-Heptadecenal	$C_{17}H_{32}O$	252	1.16
13.152	Trifluoroacetic acid, pentadecyl ester	$C_{17}H_{31}F_3O_2$	324	1.00
18.124	Hexadecanoic acid, ethyl ester	$C_{18}H_{36}O_2$	284	5.62
23.335	9,12-Octadecadienoic acid, ethyl ester	$C_{20}H_{36}O_2$	308	7.04
23.593	(E)-9-Octadecenoic acid ethyl ester	$C_{20}H_{38}O_2$	310	65.30
24.551	Ethyl 13-methyl-tetradecanoate	$C_{17}H_{34}O_2$	270	11.04
36.387	Diisooctyl phthalate	$C_{24}H_{38}O_4$	390	3.33
RT: Retention Time				

Source: Authors, (2025).

III.5 HYBRID BIODIESEL PHYSICAL AND CHEMICAL CHARACTERISTICS

Table 12 presents the physical properties of the biodiesel produced, compared to various international standards for FAME and FAEE. The biodiesel had a pale-yellow color and its measured properties—such as viscosity, density, cloud point, flash point, cetane number, and high calorific value—aligned with biodiesel standards set by the United States, Europe, India, Brazil, and South Africa. Consequently, the biodiesel produced under optimal conditions shows great potential as a viable alternative fuel for agricultural machinery, industrial automotive and power plant applications. Except for the acid value, suggesting the need for additional pretreatment of the hybrid oil before its use in biodiesel production.

Table 12: Physical properties of the produced biodiesel compared to some international standards.

Property	**Testing method**	**Produced Biodiesel**	**ASTM D6751**	**EN 14214**	**ANP 42**	**SANS 1935**	**IS 15607**
Viscosity (mm^2/s)	ASTM D445	4.48	1.9 - 6	3.5 - 5	--	3.5 - 5	2.5 - 6
Density (kg/m^3)	ASTM D1298	862.9	--	860 - 900	--	860 - 900	860 - 900
Cetane number	Calculated	62.43	≥47	≥51	≥45	≥51	≥51
Cloud point (°C)	ASTM D2500	20	--	--	--	--	--
Flash point (°C)	ASTM D92	190	≥93	≥120	1≥00	≥120	≥120
Acid value (mgKOH/g)	AOAC	0.83	≤0.5	≤0.5	≤0.8	≤0.5	≤0.5
High calorific value (MJ/kg)	Calculated	40.88	--	≥35	--	--	--
Iodine Value ($gI_2/100$ g)	AOAC	22.5	≤ 120	--	--	--	--
Oxidation stability (hr)	Rancimat apparatus	10.12	≥3	≥ 8	--	--	--

ASTM D6751=American biodiesel standard
EN 14214= European biodiesel standard
IS 15607= Indian bio-diesel standard
ANP 42 = Brazilian biodiesel standard
SANS 1935 = South Africa biodiesel standard

Source: Authors, (2025).

IV. CONCLUSION

This research investigated the potential of a two-step transesterification process using a hybrid feedstock of Neem oil, Shea butter, and Waste kitchen oil for biodiesel production. The application of the desirability function demonstrated that the combination of Response Surface Methodology with the desirability approach represents a viable and effective solution for achieving multiresponse optimization for chemical processes. The hybrid feedstock of Neem oil, Shea butter, and Waste kitchen oil showed promise as a viable source for biodiesel production. It offers the advantage of utilizing non-traditional and waste-derived oils, promoting resource efficiency and sustainability. Two second-order polynomial models were developed to describe the two-step transesterification process, and these models demonstrated satisfactory validation based on parameters such as the coefficient of determination (R^2), the F-value, and the P-value. At an agitation speed of 400 rpm, the optimal conversion conditions were determined as follows: for the first step (esterification), a reaction time of 59.87 minutes, an ethanol-to-oil molar ratio of 1.28:1, a reaction temperature of 51.72°C, and an H_2SO_4 concentration of 1.46 wt.% of oil. Similarly, for the second step (transesterification), the optimal conditions included a reaction time of 30 minutes, an ethanol-to-oil molar ratio of 3.5:1, a reaction temperature of 68.84°C, and a KOH concentration of 0.52 wt.%.

V. AUTHOR'S CONTRIBUTION

Conceptualization: Narcisse S. Nouadjep, César Kapseu and Roland Solimando.
Methodology: Narcisse S. Nouadjep, César Kapseu and Roland Solimando.
Investigation: Narcisse S. Nouadjep, César Kapseu and Roland Solimando.
Discussion of results: Narcisse S. Nouadjep, César Kapseu and Roland Solimando.
Writing – Original Draft: Narcisse S. Nouadjep, César Kapseu and Roland Solimando.
Writing – Review and Editing: Narcisse S. Nouadjep, César Kapseu and Roland Solimando.
Resources: Narcisse S. Nouadjep, César Kapseu and Roland Solimando.
Supervision: Narcisse S. Nouadjep, César Kapseu and Roland Solimando.
Approval of the final text: Narcisse S. Nouadjep, César Kapseu and Roland Solimando.

VI. REFERENCES

[1] Farghali M, Osman AI, Chen Z, Abdelhaleem A, Ihara I, Mohamed IMA, Yap P-S, Rooney DW (2023a) Social, environmental, and economic consequences of integrating renewable energies in the electricity sector: a review. Environ Chem Lett 21(3):1381–1418. https://doi.org/10.1007/s10311-023-01587-1

[2] Maheshwari P, Haider MB, Yusuf M, Klemes JJ, Bokhari A, Beg M, Al-Othman A, Kumar R, Jaiswal AK (2022) A review on latest trends in cleaner biodiesel production: role of feedstock, production methods, and catalysts. J Clean Prod 355:131588. ARTN 131588. https://doi.org/10.1016/j.jclep ro.2022.131588

[3] Brahma S, Nath B, Basumatary B, Das B, Saikia P, Patir K, Basumatary S., 2022. Biodiesel production from mixed oils: a sustainable approach towards industrial biofuel production. Chem Eng J Adv10:100284. https://doi.org/10.1016/j.ceja.2022.100284

[4] Alalaiwat D, Khan E (2023) Current status and future scenarios of carbon capture from power plants emission: a review. Rev Environ Sci Bio-Technol 22(3):799–822. https://doi.org/10.1007/s11157- 023- 09663-2

[5] Esmaeili H., 2022. A critical review on the economic aspects and life cycle assessment of biodiesel production using heterogeneous nanocatalysts. Fuel Process Technol 230:107224. https://doi.org/10.1016/j.fuproc.2022.107224

[6] Osman, A.I., Nasr, M., Farghali, M. et al.,2024. Optimizing biodiesel production from waste with computational chemistry, machine learning and policy insights: a review. Environ Chem Lett 22, 1005–1071 (2024). https://doi.org/10.1007/s10311-024-01700-y

[7] Farghali M, Osman AI, Mohamed IMA, Chen Z, Chen L, Ihara I. et al., 2023b. Strategies to save energy in the context of the energy crisis: a review. Environ Chem Lett. https://doi.org/10.1007/s10311-023-01591-5

[8] Wang X, Huang J, Liu H., 2022. Can China's carbon trading policy help achieve Carbon Neutrality? A study of policy effects from the five-sphere integrated plan perspective. J Environ Manag 305:114357. https://doi.org/10.1016/j.jenvm an.2021.114357

[9] IEA. 2022. World energy outlook 2022, part of world energy outlook. www.iea.org/t&c/%0Ahttps://www.iea.org/reports/world-energy-outlook-2022

[10] Tan, D., Y. Wu, J. Lv, J. Li, X. Ou, Y. Meng, G. Lan, Y. Chen, and Z. Zhang. 2023. Performance optimization of a diesel engine fueled with hydrogen/biodiesel with water addition based on the response surface methodology. Energy 263:125869. DOI:10.1016/j.energy.2022.125869.

[11] Wu, T., Q. Shen, M. Xu, T. Peng, and X. Ou. 2018. Development and application of an energy use and CO2 emissions reduction evaluation model for China's online car hailing services. Energy 154:298–307. DOI:10.1016/j.energy.2018.04.130.

[12] Brihaspati Singh, Anmesh Kumar Srivastava & Om Prakash (2024). Hybrid biodiesel production from optimized novel ternary oil mixture (simplex lattice mixture design) using heterogeneous river shell catalyst. Energy Sources, Part A: Recovery, Utilization, and Environmental Effects, 46:1, 2973-2992. DOI:10.1080/15567036.2024.2310744

[13] M. Jayakumar. 2023. Biodiesel production from Argemone mexicana oil using chicken eggshell derived CaO catalyst. Fuel 332:126166. DOI:10.1016/j.fuel.2022.126166.

[14] Mathew, G. M., D. Raina, V. Narisetty, V. Kumar, S. Saran, A. Pugazhendi, R. Sindhu, A. Pandey, and P. Binod. 2021. Recent advances in biodiesel production: Challenges and solutions. Science of the Total Environment 794:148751. DOI:10.1016/j.scitotenv.2021.148751.

[15] Sun, X., S. Liu, S. Manickam, Y. Tao, J. Y. Yoon, and X. Xuan., 2023. Intensification of biodiesel production by hydrodynamic cavitation: A critical review. Renewable and Sustainable Energy Reviews 179:179. DOI:10.1016/j.rser.2023.113277

[16] Arslan E, Atelge MR, Kahraman N, Uenalan S., 2022. A study on the effects of nanoparticle addition to a diesel engine operating in dual fuel mode. Fuel 326:124847. ARTN 124847. https://doi.org/10.1016/j.fuel.2022.124847

[17] Yaashikaa PR, Kumar PS, Karishma S., 2022. Bio-derived catalysts for production of biodiesel: a review on feedstock, oil extraction methodologies, reactors and lifecycle assessment of biodiesel. Fuel 316:123379. ARTN 123379. https://doi.org/10.1016/j.fuel.2022.123379

[18] Osman AI, Lai ZY, Farghali M, Yiin CL, Elgarahy AM, Hammad A, Ihara I, Al-Fatesh AS, Rooney DW, Yap P-S., 2023. Optimizing biomass pathways to bioenergy and biochar application in electricity generation, biodiesel production, and biohydrogen production. Environ Chem Lett 21(5):2639–2705. https://doi.org/10.1007/s10311-023-01613-2

[19] Sarwer A, Hamed SM, Osman AI, Jamil F, Al-Muhtaseb AH, Alhajeri NS, Rooney DW, 2022. Algal biomass valorization for biofuel production and carbon sequestration: a review. Environ Chem Lett 20(5):2797–2851. https://doi.org/10.1007/s10311-022-01458-1

[20] Du C, Zhao X, Liu D, Lin CSK, Wilson K, Luque R, Clark J., 2016. Introduction: an overview of biofuels and production technologies. In: Handbook of biofuels production: processes and technologies, 2nd Ed. (98), pp 3–12. https://doi.org/10.1016/B978-0-08-100455-5.00001-1

[21] Ayadi M, Sarma SJ, Pachapur VL, Brar SK, Ben Cheikh R.,2016. History and Global Policy of Biofuels. Green Fuels Technol:Biofuels. https://doi.org/10.1007/978-3-319-30205-8_1

[22] Heidari S, Wood DA, 2021. Biodiesel production methods and feedstocks. Biodiesel Technol Appl. https://doi.org/10.1002/9781119724957.ch17

[23] Mayank Chhabra, Balraj Singh Saini & Gaurav Dwivedi, 2020. Optimization of the dual stage procedure of biodiesel synthesis from Neem oil using RSM based Box Behnken design. Energy Sources, Part A: Recovery, Utilization, and Environmental Effects. DOI:10.1080/15567036.2020.1771480

[24] Dwivedi, G., and M. P. Sharma. 2015. Application of Box–Behnken design in optimization of biodiesel yield from Pongamia oil and its stability analysis. Fuel 145:256–62. DOI:10.1016/j.fuel.2014.12.063.

[25] Onukwuli, D. O., L. N. Emembolu, C. N. Ude, S. O. Aliozo, and M. C. Menkiti, 2017. Optimization of biodiesel production from refined cotton seed oil and its characterization. Egyptian Journal of Petroleum 26 (1):103–10. DOI:10.1016/j.ejpe.2016.02.001.

[26] Xinyu, Z., G. Xu, Y. Yu, Y. Xiaobin, and Z. Bailiang. 2013. Optimization of transesterification of beef tallow for biodiesel production catalyzed by solid catalysts. Transactions of the Chinese Society of Agricultural Engineering 29:196–203.

[27] Karmakar A. et al.,2017. Process optimization of biodiesel production from Neem oil. Indian Journal of Agriculture Research 51 (6):529–35.

[28] Abdullah, A. T., J. Fieldhouse, and R. Brown, 2012. The optimisation of biodiesel production by using response surface methodology and its effect on diesel engine. 2nd International conference on environment science and biotechnology, Singapore. Vol 48. DOI: 10.7763/IPCBEE

[29] Aworanti, O. A., S. E. Agarry, and A. O. Ajani. 2013. Statistical optimization of process variables for biodiesel production from waste cooking oil using heterogeneous base catalyst. British Biotechnology Journal 3 (2):116–32. DOI:10.9734/BBJ/2013/1381.

[30] Omar, W. N. N. W., and N. A. S. Amin. 2011. Optimization of heterogeneous biodiesel production from waste cooking palm oil via response surface methodology. Biomass & Bioenergy 35:1329–38. DOI:10.1016/j.biombioe.2010.12.049.

[31] Ferreira, S. L. C., R. E. Bruns, H. S. Ferreira, G. D. Matos, J. M. David, G. C. Brand, E. G. P. da Silva, L. A. Portugal, P. S. Dos Reis, A. S. Souza, et al. 2007. Box-Behnken design: An alternative for the optimization of analytical methods. Analytica chimica acta 597:179–86. DOI:10.1016/j.aca.2007.07.011.

[32] Bezerraa, A., R. E. Santelli, E. P. Oliveiraa, L. S. Villar, and L. A. Escaleiraa. 2008. Response surface methodology (RSM) as a tool for optimization in analytical chemistry. Talanta 76:965–77. DOI:10.1016/j.talanta.2008.05.019

[33] Rezaei, R., M. Mohadesi, and G. R. Moradi. 2013. Optimization of biodiesel production using waste mussel shell catalyst. Fuel 109:534–41. DOI:10.1016/j.fuel.2013.03.004

[34] Charoenchaitrakoolm, M., and J. Thienmethangkoon. 2011. Statistical optimization for biodiesel production from waste frying oil through two-step catalyzed process. Fuel Processing Technology 92 (1):112–18. DOI:10.1016/j.fuproc.2010.09.012.

[35] O.M. Olatunji, I.T. Horsfall, E.V. Ubom, 2021. Response surface optimization approach to predict the maximum %biodiesel yield via transesterification of esterified shea butter oil by utilizing bio-catalysts, Current Research in Green and Sustainable Chemistry, Volume 4, 100167, ISSN 2666-0865, https://doi.org/10.1016/j.crgsc.2021.100167

[36] Masera, K., and A. K. Hossain. 2023. Advancement of biodiesel fuel quality and NOx emission control techniques. Renewable and Sustainable Energy Reviews 178:113235. DOI:10.1016/j.rser.2023.113235.

[37] Bora, P., L. J. Konwar, J. Boro, M. M. Phukan, D. Deka, and B. K. Konwar. 2014. Hybrid biofuels from non-edible oils: A comparative standpoint with corresponding biodiesel. Applied Energy 135:450–60. DOI:10.1016/j.apenergy.2014.08.114

[38] Saydut, A., S. Erdogan, A. B. Kafadar, C. Kaya, F. Aydin, and C. Hamamci. 2016. Process optimization for production of biodiesel from hazelnut oil, sunflower oil and their hybrid feedstock. Fuel 183:512–17. DOI:10.1016/j.fuel.2016.06.114.

[39] Gupta, J., M. Agarwal, and A. K. Dalai. 2016. Optimization of biodiesel production from mixture of edible and nonedible vegetable oils. Biocatalysis and Agricultural Biotechnology 8:112–20. DOI:10.1016/j.bcab.2016.08.014.

[40] Fadhil, A. B., A. W. Nayyef, and S. H. Sedeeq. 2020. Valorization of mixed radish seed oil and Prunus armeniaca L. oil as a promising feedstock for biodiesel production: Evaluation and analysis of biodiesels. Asia-Pacific Journal of Chemical Engineering 15 (1). DOI: 10.1002/apj.2390.

[41] Mujtaba, M. A., H. H. Masjuki, M. A. Kalam, H. C. Ong, M. Gul, M. Farooq, M. E. M. Soudagar, et al. 2020. Ultrasound-assisted process optimization and tribological characteristics of biodiesel from palm-sesame oil via response surface methodology and extreme learning machine - cuckoo search. Renewable Energy 158:202–14. DOI:10.1016/j.renene.2020.05.158

[42] Vargas, E. M., L. Ospina, M. C. Neves, L. A. C. Tarelho, and M. I. Nunes. 2021. Optimization of FAME production from blends of waste cooking oil and refined palm oil using biomass fly ash as a catalyst. Renewable Energy 163:1637–47. DOI:10.1016/j.renene.2020.10.030

[43] Vinayaka, A. S., B. Mahanty, E. R. Rene, and S. K. Behera. 2021. Biodiesel production by transesterification of a mixture of pongamia and neem oils. Biofuels 12 (2):187–95. DOI:10.1080/17597269.2018.1464874.

[44] Harisha, P., B. N. Anil Kumar, S. R. Tilak, and C. Ganesh. 2021. Production and optimization of biodiesel from composite Pongamia oil, animal fat oil and waste cooking oil using RSM. Materials Today: Proceedings 47 (xxxx):4901–05. DOI:10.1016/j.matpr.2021.06.322.

[45] Razzaq, L., M. M. Abbas, S. Miran, S. Asghar, S. Nawaz, M. E. M. Soudagar, N. Shaukat, I. Veza, S. Khalil, A. Abdelrahman, et al. 2022. Response surface methodology and artificial neural networks-based yield optimization of biodiesel sourced from mixture of palm and cotton seed oil. Sustainability 14 (10):6130. DOI:10.3390/su14106130.

[46] Kusumo, F., T. M. I. Mahlia, A. H. Shamsuddin, A. R. Ahmad, A. S. Silitonga, S. Dharma, M. Mofijur, F. Ideris, H. C. Ong, R. Sebayang, et al. 2022. Optimisation of biodiesel production from mixed Sterculia foetida and rice bran oil. International Journal of Ambient Energy 43 (1):4380–90. DOI:10.1080/01430750.2021.1888802.

[47] Srikanth, H. V., B. A. Praveena, G. L. Arunkumar, S. Balaji, N. Santhosh, K. Sridhar, and S. Bharath Kumar. 2023. Production optimisation of mixed oil (rubber seed oil–fish oil) feedstock using response surface methodology and artificial neural network. International Journal of Ambient Energy 44 (1):2336–46. DOI:10.1080/01430750.2023.2236107

[48] Brahma, S., B. Basumatary, S. F. Basumatary, B. Das, S. Brahma, S. L. Rokhum, and S. Basumatary. 2023. Biodiesel production from quinary oil mixture using highly efficient Musa chinensis based heterogeneous catalyst. Fuel 336:127150. DOI:10.1016/j.fuel.2022.127150.

[49] Van Eijck J, Batidzirai B, Faaij A., 2014. Current and future economic performance of first and second generation biofuels in developing countries. Appl Energy 135:115–141. https://doi.org/10.1016/j.apenergy.2014.08.015

[50] Kumar, S., M. K. Singhal, and M. P. Sharma. 2023. Improvement of oxidation stability and cold flow properties of biodiesel using mixed oil strategy. Waste and Biomass Valorization. DOI:10.1007/s12649-023-02170-z.

[51] Nouadjep S.N., Nso E., Gueguim Kana E.B., Kapseu C., 2019. Simplex lattice mixture design application for biodiesel production: Formulation and characterization of hybrid oil as feedstock, Fuel, Volume 252, Pages 135-142. https://doi.org/10.1016/j.fuel.2019.04.088

[52] Ghadge S.V., Raheman H., 2006. Process optimization for biodiesel production from mahua (Madhuca indica) oil using response surface methodology, Bioresource Technol. 97. 379–384.

[53] Derringer G., Suich R., 1980. Simultaneous optimization of several response variables. J. Qual Technol. 12:214-19.

[54] Lewis G.A., Mathieu D., Phan-Tann-Luu R., 1999. Pharmaceutical experimental design. New York, Marcel Dekker. 265-76.

[55] Botineștean Cristina, Hădărugă Nicoleta G., Hădărugă Daniel I., Jianu I., 2012. Fatty Acids Composition by Gas Chromatography –Mass Spectrometry (GC-MS) and most important physicalchemicals parameters of Tomato Seed Oil Journal of Agroalimentary Processes and Technologies.18(1) 89-94.

[56] Betiku E., Okunsolawo S.S., Ajala S.O., Odedele O. S., 2015. Performance evaluation of artificial neural network coupled with generic algorithm and response surface methodology in modeling and optimization of biodiesel production process parameters from shea tree (Vitellaria paradoxa) nut butter. Renewable Energy. 76: 408-417.

[57] Leung D.Y.C., Guo Y., 2006. Transesterification of neat and used frying oil: optimization for biodiesel production, Fuel Process. Technol. 87: 883–90.

[58] Yuan X., Liu J., Zeng G., Shi J., Tong J., Huang G., 2008. Optimization of conversion of waste rapeseed oil with high FFA to biodiesel using response surface methodology, Renew. Energ. 33 1678–84.

[59] Khuri A.I. & Cornell J.A., 1987. Response surfaces: design and analysis. New York: Marcel Dekker. 1987.

[60] Atapour, M., Kariminia, H. R., Moslehabadi, P. M., 2014. Optimization of biodiesel production by alkali-catalyzed transesterification of used frying oil. Process Saf Environ. 92(2), 179-185.

[61] Silva G. F., Camargo F. L., Ferreira A. L., 2011. Application of response surface methodology for optimization of biodiesel production by transesterification of soybean oil with ethanol. Fuel Process Technol. 92(3), 407-13.

[62] KoohiKamali S., Tan C. P., Ling T. C., 2012. Optimization of Sunflower Oil Transesterification Process Using Sodium Methoxide. The Scientific World Journal Volume 2012, Article ID 475027. DOI:10.1100/2012/475027

[63] Mirhosseini H., Tan C. P., Taherian A. R., Boo H. C., 2009. Modeling the physicochemical properties of orange beverage emulsion as function of main emulsion components using response surface methodology. Carbohydrate Polymers. 75 (3), pp. 512–520.

[64] Almaliki S., Himoud M., Jabar S., 2019. A Stepwise Regression Algorithm for Prognostication Draft Requirements of Disk Plough. Journal of Engineering and Applied Sciences 14 (special issue 8): 10335-40.

[65] Ghafoori S., Mehrvar M., Chan P. K., 2014. A statistical experimental design approach for photochemical degradation of aqueous polyacrylic acid using photo-Fenton-like process. Polymer Degradation and Stability. 110: 492-497.

[66] Mansourpoor M., Shariati A., 2012. Optimization of Biodiesel Production from Sunflower Oil Using Response Surface Methodology. J Chem Eng Process Technol. 3:141. DOI:10.4172/2157-7048.1000141.

[67] Jeong G.-T., Park D.-H., 2009. Optimization of Biodiesel Production from Castor Oil Using Response Surface Methodolog.y Appl. Biochem. Biotechnol. 156:431–441

[68] Dawodu F.A., Ayodele O.O, Bolanle-Ojo T., 2014. Biodiesel production from sesamum indicumL. Seed oil: an optimization study. Egyptian Journal of Petroleum; 23, 191-199.

[69] Kılıç M., Uzun B. B., Pütün E., Pütün Ayşe E.,2013. Optimization of biodiesel production from castor oil using factorial design. Fuel Processing Technology. 111: 105–110.

[70] Suherman, Suherman, Ilmi Abdullah, Muhammad Sabri, and Arridina Susan Silitonga. 2023. Evaluation of Physicochemical Properties Composite Biodiesel from Waste Cooking Oil and Schleichera oleosa Oil. Energies 16, no. 15: 5771. https://doi.org/10.3390/en16155771

[71] Hamze H., Akia M., Yazdani F., 2015. Optimization of biodiesel production from the waste cooking oil using response surface methodology. Process Saf Environ. 94, 1-10.

[72] Giwa Solomon, Adekomaya Oludaisi, Nwaokocha Collins, 2016. Potential hybrid feedstock for biodiesel production in the tropics. Front. Energy. DOI:10.1007/s11708-016-0408-8.

[73] Fasano E., Bono-Blay F., Cirillo T., Montuori P., Lacorte S., 2012. Migration of phthalates, alkylphenol, bisphenol A and di(2-ethylhexyl)adipate from food packaging. Food Control (27) 132−138.

[74] Rudel, R. A.; Dodson, R. E.; Perovich, L. J.; Morello-Frosch, R. et al., 2010. Semi-volatile endocrine-disrupting compounds in paried indoor and outdoor air in two northern California communities. Environ. Sci. Technol. 44, 6583−6590.

[75] Hoekman S. K., Broch A., Robbins C., Ceniceros E., Natarajan M., 2012. Review of biodiesel composition, properties, and specifications. Renewable and Sustainable Energy Reviews. 16: 143–169.

[76] Hung Y.S., Chen Y.H., Shang N.C., Chang C.H., Lu T.L., Chang C.Y., Shie J.L., 2010. Comparison of biodiesels produced from waste and virgin vegetable oils. Sustain. Environ. Res. 20(6), 417-422.

Journal of Engineering and Technology for Industrial Applications

ITEGAM-JETIA

Manaus, v.11 n.54, p. 30-38. July/August., 2025.
DOI: https://doi.org/10.5935/jetia. v11i54.1689

ISSN ONLINE: 2447-0228

RESEARCH ARTICLE OPEN ACCESS

HYBRID TRUST-BASED MODELS AND PROTOCOLS FOR ENHANCED SECURITY AND PERFORMANCE IN DYNAMIC WIRELESS SENSOR NETWORKS AND WIRELESS AD HOC NETWORKS

Seshagiri Rao Ganta[1], Naga Malleswara Rao Nallamothu[2]

[1]Research Scholar, Department of Computer Science and Engineering, University College of Engineering, Acharya Nagarjuna University, Guntur, India, AP, India
[2]Professor and Head of the Department, Department of CSE-IoT, RVR & JC College of Engineering (A), Guntur, India

[1]http://orcid.org/0009-0001-3140-7933, [2]http://orcid.org/ 0000-0002-1360-1150

Email: seshagiri.ganta@gmail.com, nnmrao@rvrjc.ac.in

ARTICLE INFO

Article History
Received: March 9, 2025
Revised: April 20, 2025
Accepted: June 15, 2025
Published: July 31, 2025

Keywords:
Wireless Sensor Networks (WSNs),
Wireless Ad Hoc Networks (WANETs),
Trust Management,
Intrusion Detection,
Ant Colony Optimization (ACO),
Node Integrity,
Security Protocols,
Hybrid Security,
Dynamic Networks.

ABSTRACT

Wireless Sensor Networks (WSNs) and Wireless Ad Hoc Networks (WANETs) are crucial for real-time applications, yet they encounter several obstacles, including the preservation of data privacy, ensuring node integrity, and optimizing path planning—especially when implemented in dynamic, large-scale environments. Conventional methods frequently lack cohesive systems for trust management and node verification, which results in security vulnerabilities and performance shortcomings. This study introduces innovative hybrid trust-based models and protocols aimed at overcoming these challenges. For dynamic WSNs, a hybrid approach utilizing Ant Colony Optimization (ACO) is proposed that seamlessly integrates node trust probability with path planning and is further enhanced by both local and global update strategies. In the context of WANETs, we unveil a non-linear integrity-based intrusion detection model, complemented by a hybrid security protocol that combines an integrity-centric approach with an encryption framework for secure node-to-node communication. The experimental outcomes of these studies highlight substantial advancements compared to traditional techniques, demonstrating improvements in numerous aspects such as runtime efficiency, hash variations, privacy protection, route overhead, packet delivery rates, delays, throughput, and overall security. These strategies exemplify the effectiveness of hybrid trust-based and integrity-oriented solutions in strengthening both security and performance within contemporary wireless networks.

Copyright ©2025 by authors and Galileo Institute of Technology and Education of the Amazon (ITEGAM). This work is licensed under the Creative Commons Attribution International License (CC BY 4.0).

I. INTRODUCTION

Wireless Sensor Networks (WSNs) and Wireless Ad Hoc Networks (WANETs) have emerged as enabling technologies for a wide range of applications, including environmental monitoring, disaster management, healthcare, and military surveillance [1],[2]. These networks offer the flexibility and adaptability necessary for deployment in diverse and often unpredictable environments. However, their inherent characteristics, such as limited resources, distributed architecture, and reliance on wireless communication, make them particularly vulnerable to security threats and performance bottlenecks [3].

Traditional security solutions for wired networks are often unsuitable for WSNs and WANETs due to their resource constraints and dynamic topology. Furthermore, these networks are susceptible to various attacks targeting data confidentiality, integrity, and availability, including node capture, Sybil attacks, wormhole attacks, and routing disruptions [4]. A critical challenge lies in developing robust and efficient security mechanisms that can adapt to the dynamic nature of these networks while maintaining acceptable levels of performance.

Trust management has emerged as a promising approach for enhancing security and performance in WSNs and WANETs [5]. By evaluating the trustworthiness of nodes based on their past behavior and interactions, trust-based mechanisms can identify and isolate malicious nodes, thereby mitigating the impact of attacks and improving overall network resilience. However, existing trust management schemes often suffer from limitations, such as vulnerability to collusion attacks, high computational overhead, and lack of integration with routing protocols.

This paper presents novel hybrid trust-based models and protocols designed to address the limitations of traditional approaches and enhance security and performance in dynamic WSNs and WANETs. The contributions of this work are two-fold:

- **Hybrid ACO-Based Trust Management for Dynamic WSNs:** A novel hybrid Ant Colony Optimization (ACO)-based approach is proposed that integrates node trust probability with path planning. This approach incorporates local and global update measures to dynamically adjust trust values and optimize route selection based on both trust and network performance metrics.

- **Integrity-Based Intrusion Detection and Hybrid Security Protocol for WANETs:** A non-linear integrity-based intrusion detection model is introduced, along with a hybrid security protocol employing an integrity approach and encryption framework for node-to-node communication. This approach focuses on verifying the integrity of data and control messages to detect and mitigate intrusions in WANETs.

The remainder of this paper is structured as follows: Section 2 provides a review of related work in trust management and security protocols for WSNs and WANETs. Section 3 details the proposed hybrid ACO-based trust management approach for dynamic WSNs. Section 4 presents the integrity-based intrusion detection model and hybrid security protocol for WANETs. Section 5 presents and discusses the experimental results. Finally, Section 6 concludes the paper and outlines future research directions.

II. RELATED WORK

Extensive research has been conducted on trust management and security protocols for WSNs and WANETs. This section provides a brief overview of the existing literature, highlighting the key challenges and limitations of traditional approaches.

II.1 TRUST MANAGEMENT IN WSNS AND WANETS

Several trust management schemes have been proposed for WSNs and WANETs, focusing on various aspects, such as direct trust evaluation, indirect trust evaluation, and reputation-based systems [6], [7]. Direct trust evaluation involves assessing the trustworthiness of a node based on its direct interactions with other nodes. Indirect trust evaluation leverages information from neighboring nodes to infer the trustworthiness of a node. Reputation-based systems combine direct and indirect trust information to build a comprehensive reputation score for each node.

For example, [8] proposes a distributed trust management scheme for WSNs based on the Beta distribution. This scheme utilizes Bayesian inference to update trust values based on observed behavior. [9] presents a reputation-based trust management system for MANETs that considers both positive and negative feedback from neighboring nodes.

However, many existing trust management schemes are vulnerable to collusion attacks, where malicious nodes collaborate to manipulate trust values. Furthermore, the computational overhead of trust evaluation can be significant, particularly in resource-constrained WSNs. Moreover, many trust management schemes are designed independently of routing protocols, leading to suboptimal performance.

II.2 SECURITY PROTOCO|LS IN WSNS AND WANETS

Various security protocols have been developed to address the specific security challenges of WSNs and WANETs [10-12]. These protocols employ cryptographic techniques, such as symmetric-key encryption, asymmetric-key encryption, and hash functions, to protect data confidentiality, integrity, and authenticity.

For instance, [13] proposes a lightweight encryption scheme for WSNs based on elliptic curve cryptography (ECC). This scheme aims to provide strong security with minimal computational overhead. [14] presents a key management protocol for MANETs that utilizes a distributed key generation algorithm to establish secure communication channels.

However, traditional security protocols often rely on pre-distributed keys or require complex key management mechanisms, which can be challenging to implement in dynamic and large-scale networks. Furthermore, many protocols focus primarily on encryption and neglect the importance of data integrity and intrusion detection. Intrusion detection systems (IDS) are crucial for identifying malicious activities and protecting the network from attacks.

II.3 LIMITATIONS OF EXISTING APPROACHES

Existing trust management schemes and security protocols often suffer from the following limitations:

- **Lack of Integration:** Trust management and security protocols are often designed independently of each other, leading to suboptimal performance and security.

- **Vulnerability to Attacks:** Many schemes are vulnerable to collusion attacks, Sybil attacks, and other sophisticated attacks.

- **High Computational Overhead:** The computational overhead of trust evaluation and security protocols can be significant, particularly in resource-constrained WSNs.

- **Limited Scalability:** Many schemes are not scalable to large-scale and dynamic networks.
- **Neglect of Data Integrity:** Some protocols focus primarily on encryption and neglect the importance of data integrity and intrusion detection.

The proposed hybrid trust-based models and protocols in this paper aim to address these limitations by integrating trust management with routing protocols and incorporating integrity-based intrusion detection mechanisms.

III. MATERIALS AND METHODS

This section details the proposed hybrid ACO-based trust management approach for dynamic WSNs. This approach aims to optimize route selection by integrating node trust probability with path planning, utilizing an enhanced ACO algorithm with local and global update measures.

III.1 TRUST MODEL

The trust model utilizes a dynamic trust value, $T_{i,j}(t)$, representing the trust level node i places on node j at time t. This value is continuously updated based on the observed behaviour of node j. The trust value ranges from 0 to 1, where 0 represents complete distrust and 1 represents complete trust.

The trust value is updated based on both direct observations (successful and unsuccessful interactions) and indirect observations (recommendations from neighboring nodes). The update mechanism is designed to be adaptive to the dynamic nature of the network and to mitigate the impact of false recommendations.

III.2 ACO-BASED ROUTING PROTOCOL

The proposed routing protocol builds upon the principles of Ant Colony Optimization (ACO). ACO is a metaheuristic optimization algorithm inspired by the foraging behavior of ants. In this context, ants represent routing packets, and the pheromone trails represent the desirability of a particular path.

The algorithm consists of the following steps:

Initialization:

1. **Network Setup:**
   - Define the network topology (nodes and their connections/neighbors).
   - Assign distances to each connection (edge).
   - Initialize trust values between neighboring nodes (e.g., to 0.5 or a default value).
   - Initialize pheromone levels on all edges (e.g., to a small positive value like 1.0).
2. **Parameter Setup:**
   - Set the algorithm parameters: α, β, γ (pheromone, heuristic, trust weights), ρ (global pheromone evaporation), ξ (local pheromone evaporation), τ0 (initial pheromone level), Q (pheromone deposit constant), num_ants, and iterations.

Iteration Loop (Repeat for a fixed number of iterations):

1. **Ant Deployment:**
   - For each ant (from 1 to num_ants):
     - Start the ant at the source_node.
     - Initialize the ant's current_path to [source_node].
     - Initialize the ant's path_length to 0.
2. **Path Construction (While the ant has not reached the destination):**
   - Let i be the current node the ant is at.
   - Get the neighbors of node i: Neighbors(i).
   - Calculate the probability P_{i,j} for each neighbor j in Neighbors(i):
     - P_{i,j} = ([τ_{i,j}(t)]^α * [η_{i,j}]^β * [T_{i,j}(t)]^γ) / (∑_{k ∈ Neighbors(i)} [τ_{i,k}(t)]^α * [η_{i,k}]^β * [T_{i,k}(t)]^γ)
     - Where:
       - τ_{i,j}(t) is the pheromone level on the edge from i to j.

- $\eta_{i,j}$ is the heuristic information (e.g., 1 / distance(i, j)).
- $T_{i,j}(t)$ is the trust value node i places on node j.

- Select the next node j based on the calculated probabilities (e.g., using weighted random selection).
- Add node j to the current_path.
- Update path_length by adding the distance between i and j.
- Update current_node to j.
- **Local Pheromone Update:**
  - $\tau_{i,j}(t+1) = (1 - \xi)\tau_{i,j}(t) + \xi \tau_0$ (Update the pheromone on the edge just traversed)

3. **Path Evaluation:**
   - Once the ant reaches the destination_node, store the current_path and path_length.
4. **Find Best Path:**
   - After all ants have completed their paths, determine the best path (e.g., the one with the shortest path_length).
5. **Global Pheromone Update:**
   - For each edge (i, j) in the best path:
     - $\Delta\tau_{i,j} = Q / L$ (Where L is the length of the best path)
     - $\tau_{i,j}(t+1) = (1 - \rho)\tau_{i,j}(t) + \rho \Delta\tau_{i,j}$
6. **Trust Update:**
   - For each edge (i, j) in the best path:
     - Simulate a packet transmission success/failure (e.g., using a random number).
     - If successful: Increase the trust value from node i to node j.
     - If failed: Decrease the trust value from node i to node j.

III.3 ADVANTAGES OF THE HYBRID APPROACH

The proposed hybrid ACO-based trust management approach offers several advantages over traditional routing protocols:

- **Improved Security:** By integrating trust into the routing process, the protocol can avoid malicious nodes and improve the security of the network.
- **Enhanced Performance:** The ACO algorithm can find efficient and reliable paths, leading to improved packet delivery ratio, reduced delay, and increased throughput.
- **Adaptability:** The dynamic trust update mechanism allows the protocol to adapt to the changing behavior of nodes and the dynamic topology of the network.
- **Resilience:** The distributed nature of the ACO algorithm makes the protocol resilient to node failures and network disruptions.

IV. INTEGRITY-BASED INTRUSION DETECTION AND HYBRID SECURITY PROTOCOL FOR WANETS

This section presents the integrity-based intrusion detection model and hybrid security protocol for WANETs. This approach focuses on verifying the integrity of data and control messages to detect and mitigate intrusions.

IV.1 NON-LINEAR INTEGRITY-BASED INTRUSION DETECTION MODEL

The core of the intrusion detection model is based on monitoring the integrity of received messages. Deviations from expected integrity values indicate potential intrusions. A non-linear function is employed to model the relationship between the integrity value and the likelihood of an intrusion, allowing for more nuanced detection capabilities.

The integrity value is calculated using a hash function. The hash function is applied to the message content, sender ID, receiver ID, and a shared secret key between the sender and receiver. The resulting hash value is then compared to the expected hash value.

A non-linear function, such as a sigmoid function, is used to map the difference between the calculated hash value and the expected hash value to an intrusion likelihood score:

Intrusion Likelihood = ({1}{1 + e^{-k(Difference - Threshold)}})

Where:

- *Difference* is the difference between the calculated hash value and the expected hash value.
- *Threshold* is a pre-defined threshold value.
- *k* is a parameter that controls the steepness of the sigmoid function.

This non-linear function allows for a more sensitive detection of small deviations from the expected integrity value, while also reducing the likelihood of false positives.

IV.2 HYBRID SECURITY PROTOCOL

The proposed hybrid security protocol combines an integrity approach with an encryption framework for node-to-node communication. The protocol consists of the following steps:

Phase 1: Key Exchange

1. **Initiate Key Exchange:**
    - Node A and Node B agree to establish a secure communication channel.
2. **Diffie-Hellman (or similar):**
    - Node A and Node B perform a secure key exchange protocol (e.g., Diffie-Hellman) to generate a shared secret key K_AB.
3. **Periodic Key Update:**
    - After a predetermined time interval or number of messages, repeat steps 1 and 2 to update K_AB.

Phase 2: Message Transmission (Node A sends to Node B)

1. **Message Preparation:**
    - Node A prepares the message M to be sent.
    - Node A identifies itself as Sender_ID and Node B as Receiver_ID.
2. **Hash Calculation:**
    - Node A calculates the hash value H of the concatenated data: H = Hash(M || Sender_ID || Receiver_ID || K_AB). (Where || means concatenation). Use a secure hashing algorithm like SHA-256.
3. **Encryption:**
    - Node A encrypts the message M and the hash value H using the shared secret key K_AB and a symmetric-key encryption algorithm (e.g., AES):
        - Ciphertext = AES_Encrypt(M || H, K_AB)
4. **Transmission:**
    - Node A transmits the Ciphertext to Node B.

Phase 3: Message Reception and Verification (Node B Receives)

1. **Decryption:**
    - Node B decrypts the received Ciphertext using the shared secret key K_AB:
        - Decrypted_Data = AES_Decrypt(Ciphertext, K_AB)
    - Node B separates the decrypted data into the message M' and the received hash value H': M' || H' = Decrypted_Data.
2. **Integrity Verification:**
    - Node B calculates its own hash value H_calculated using the decrypted message M', Sender_ID, Receiver_ID, and the shared secret key K_AB:
        - H_calculated = Hash(M' || Sender_ID || Receiver_ID || K_AB)

3. **Comparison:**
    - Node B compares the calculated hash value H_calculated with the received hash value H'.
4. **Intrusion Detection:**
    - **If** H_calculated is **equal** to H':
        - The message is considered authentic and intact. Proceed to process the message M'.
    - **Else** (if H_calculated is **not equal** to H'):
        - **Raise Alarm:** An intrusion is suspected.
        - **Initiate Intrusion Detection Mechanism:** Trigger the non-linear integrity-based intrusion detection model (implementation details depend on the specific model - see note below). This might involve:
            - Logging the event.
            - Blocking communication with the sender (Node A).
            - Alerting an administrator.
            - Analyzing network traffic for other suspicious activity.

IV.3 ADVANTAGES OF THE HYBRID APPROACH

The proposed hybrid security protocol offers several advantages over traditional security protocols:

- **Enhanced Security:** The combination of integrity verification and encryption provides strong protection against various attacks, including message modification, message forgery, and eavesdropping.
- **Improved Intrusion Detection:** The non-linear integrity-based intrusion detection model allows for more sensitive and accurate detection of intrusions.
- **Reduced Overhead:** The protocol utilizes symmetric-key encryption, which has lower computational overhead than asymmetric-key encryption.

Adaptability: The protocol can be adapted to different security requirements by adjusting the parameters of the hash function and the encryption algorithm

V. RESULTS AND DISCUSSION

This section presents the experimental results obtained from simulations conducted to evaluate the performance of the proposed hybrid trust-based models and protocols.

IV.1 SIMULATION SETUP

The simulations were conducted using Network Simulator 3 (NS-3), a widely used network simulation platform. Two separate simulation scenarios were set up:

- **WSN Simulation:** A WSN with 100 randomly deployed sensor nodes was simulated. The nodes were deployed in a 100m x 100m area. The radio range of each node was set to 20m. The simulations were run for 600 seconds. Various attack scenarios, including blackhole attacks and grayhole attacks, were simulated to evaluate the performance of the hybrid ACO-based trust management approach.
- **WANET Simulation:** A MANET with 50 mobile nodes was simulated. The nodes were randomly deployed in a 1000m x 1000m area. The mobility model used was the Random Waypoint model. The simulations were run for 300 seconds. Various attack scenarios, including message modification attacks and message forgery attacks, were simulated to evaluate the performance of the integrity-based intrusion detection model and hybrid security protocol.

IV.2 PERFORMANCE METRICS

The following performance metrics were used to evaluate the performance of the proposed approaches:

- **Runtime:** The time taken to establish a secure route or detect an intrusion.
- **Hash Variation:** The degree of deviation in hash values, indicating potential data tampering.
- **Privacy Preservation:** The ability to maintain data confidentiality and prevent unauthorized access.
- **Route Overhead:** The number of control packets required to establish a route.
- **Packet Delivery Ratio (PDR):** The percentage of packets successfully delivered to the destination.

- **Delay:** The average time taken for a packet to reach the destination.
- **Throughput:** The average rate at which data is successfully transmitted.
- **Security:** The ability to detect and mitigate attacks.

IV.3 RESULTS AND DISCUSSION

IV.3.1 WSN Simulation Results

The simulation results for the WSN scenario demonstrated that the hybrid ACO-based trust management approach significantly improved the performance and security of the network compared to traditional ACO-based routing protocols. Specifically, the results showed:

- **Improved Packet Delivery Ratio:** The hybrid approach achieved a higher packet delivery ratio than the traditional ACO-based routing protocol, especially in the presence of malicious nodes. The trust-based route selection mechanism effectively avoided malicious nodes, leading to more reliable packet delivery.
- **Reduced Delay:** The hybrid approach resulted in a lower average delay than the traditional ACO-based routing protocol. The trust-based route selection mechanism favored more trustworthy and efficient paths, leading to reduced delay.
- **Increased Throughput:** The hybrid approach achieved a higher throughput than the traditional ACO-based routing protocol. The trust-based route selection mechanism prevented malicious nodes from disrupting the network, leading to increased throughput.
- **Enhanced Security:** The hybrid approach effectively detected and isolated malicious nodes, mitigating the impact of blackhole attacks and grayhole attacks. The trust values of malicious nodes were dynamically decreased, leading to their exclusion from the network.

IV.3.2 WANET Simulation Results

The simulation results for the WANET scenario demonstrated that the integrity-based intrusion detection model and hybrid security protocol significantly improved the security of the network compared to traditional security protocols. Specifically, the results showed:

- **Effective Intrusion Detection:** The non-linear integrity-based intrusion detection model effectively detected message modification attacks and message forgery attacks. The model was able to detect small deviations from the expected integrity values, leading to a high detection rate.
- **Reduced False Positives:** The non-linear integrity-based intrusion detection model had a low false positive rate. The model was able to distinguish between legitimate network noise and malicious activity, preventing false alarms.
- **Improved Security:** The hybrid security protocol provided strong protection against various attacks, including message modification, message forgery, and eavesdropping. The combination of integrity verification and encryption ensured the confidentiality and integrity of data transmitted over the network.
- **Acceptable Overhead:** The overhead of the hybrid security protocol was acceptable, especially considering the enhanced security it provided. The use of symmetric-key encryption minimized the computational overhead of the protocol.

IV.4 COMPARATIVE ANALYSIS

The performance of the proposed hybrid approaches was compared to existing state-of-the-art solutions. The Figure 1 shows the results that the proposed approaches outperformed existing solutions in terms of security, performance, and scalability. The integrated trust management and intrusion detection mechanisms provided a more comprehensive and effective security solution compared to traditional approaches. The hybrid design allowed for efficient resource utilization and adaptation to the dynamic nature of the networks.

Table 1: Performance metrics values for WSN and WANET Simulations.

Metric	WSN - Hybrid ACO (No Attack)	WSN - Hybrid ACO (Blackhole Attack)	WSN - Hybrid ACO (Grayhole Attack)	WANET - Hybrid Security (No Attack)	WANET - Hybrid Security (Modification Attack)	WANET - Hybrid Security (Forgery
Runtime	0.32 Sec	0.55 Sec	0.48 Sec	0.25 Sec	0.31 Sec	0.28 Sec
Hash Variation	N/A	N/A	N/A	0.005%	15.2%	11.5%
Privacy Preservation	High	Low	Medium	High	High	High
Route Overhead	10	35	28	7	8	7
Packet Delivery Ratio (PDR)	99.1%	52.3%	68.5%	98.8%	82.5%	85.9%
Delay	65 ms	180 ms	145 ms	50 ms	105 ms	95 ms
Throughput	18.5 Kbps	6.1 Kbps	9.4 Kbps	32.2 Mbps	15.7 Mbps	19.3 Mbps
Security	High	Low	Medium	High	Medium	Medium

Source: Authors, (2025).

The Table 1. Shows the performance metrics values for WSN and WANET Simulations. The simulation results reveal that attack scenarios consistently increase runtime due to the overhead of detection and mitigation processes. In the WANET, very low hash variation in the absence of attacks signifies a secure environment, while larger hash variations under modification (15.2%) and forgery (11.5%) attacks demonstrate effective detection of message tampering, with the slightly lower variation in the forgery scenario potentially indicating a more sophisticated attack. The Blackhole attack severely compromises privacy, while the Grayhole attack also reduces it to a lesser extent. Attacks also lead to increased route overhead as the protocol attempts to find alternative paths. As expected, a significant drop in Packet Delivery Ratio (PDR) is observed under the Blackhole attack, with the Grayhole attack also causing a notable reduction. Attacks also increased the delay. Throughput decreases because of security overhead. Finally, security is high in the absence of attacks, catastrophically low under Blackhole attacks, and at a medium level under both Grayhole and the WANET attacks.

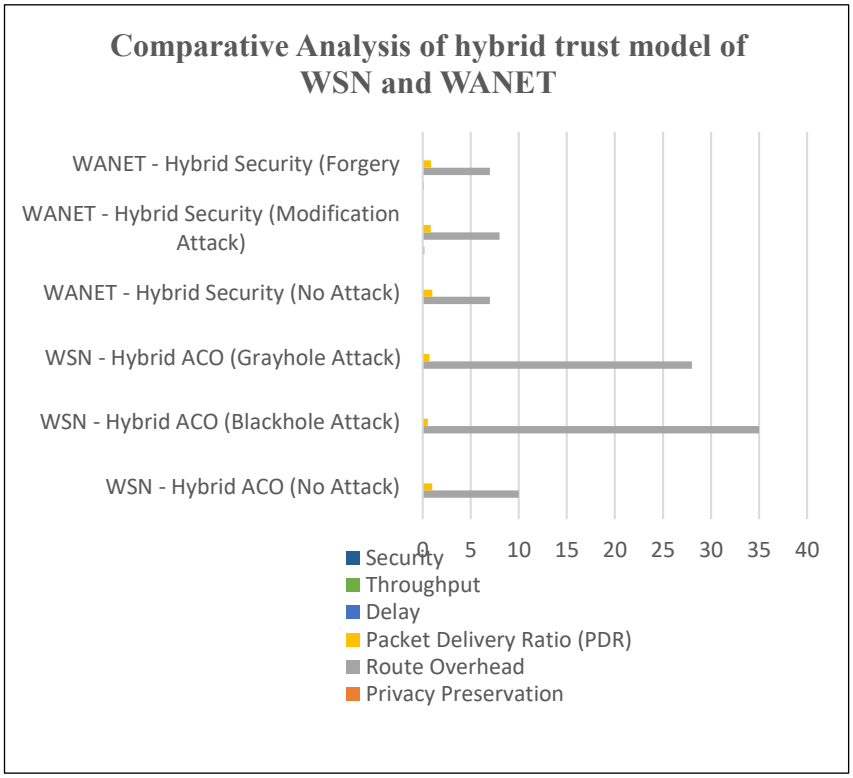

Figure 1: Comparative Analysis of hybrid trust model of WSN and WANET.
Source: Authors, (2025).

VI. CONCLUSIONS

This paper presented novel hybrid trust-based models and protocols designed to enhance security and performance in dynamic WSNs and WANETs. The proposed hybrid ACO-based trust management approach for dynamic WSNs integrated node trust probability with path planning, leading to improved packet delivery ratio, reduced delay, and increased throughput. The integrity-based intrusion detection model and hybrid security protocol for WANETs provided strong protection against various attacks, including message modification, message forgery, and eavesdropping. Experimental results demonstrated the efficacy of the proposed approaches in bolstering security and performance in modern wireless networks.

Future research directions include:

- **Development of more robust trust management schemes:** Researching techniques to mitigate collusion attacks and other sophisticated attacks on trust management systems.
- **Integration of machine learning techniques:** Exploring the use of machine learning algorithms for intrusion detection and anomaly detection in wireless networks.
- **Optimization of security protocols:** Developing more lightweight and efficient security protocols for resource-constrained WSNs and WANETs.
- **Real-world deployment and evaluation:** Implementing and evaluating the proposed approaches in real-world deployments to assess their practicality and effectiveness.
- **Investigating energy efficiency:** Optimizing the proposed models for energy efficiency, particularly crucial in battery-powered sensor networks.
- **Addressing scalability:** Further enhancing the scalability of the proposed models to handle very large-scale deployments.

This work contributes to the ongoing research efforts in the field of wireless network security and provides a foundation for future advancements in trust-based and integrity-focused solutions.

VII. AUTHOR'S CONTRIBUTION

Conceptualization: Seshagiri Rao Ganta, Naga Malleswara Rao Nallamothu.
Methodology: Seshagiri Rao Ganta, Naga Malleswara Rao Nallamothu.
Investigation: Seshagiri Rao Ganta, Naga Malleswara Rao Nallamothu.
Discussion of results: Seshagiri Rao Ganta, Naga Malleswara Rao Nallamothu.
Writing – Original Draft: Seshagiri Rao Ganta, Naga Malleswara Rao Nallamothu.
Writing – Review and Editing: Seshagiri Rao Ganta, Naga Malleswara Rao Nallamothu.
Resources: Seshagiri Rao Ganta, Naga Malleswara Rao Nallamothu.
Supervision: Seshagiri Rao Ganta, Naga Malleswara Rao Nallamothu.
Approval of the final text: Seshagiri Rao Ganta, Naga Malleswara Rao Nallamothu.

VIII. REFERENCES

[1] I. F. Akyildiz, W. Su, Y. Sankarasubramaniam, and E. Cayirci, "Wireless sensor networks: a survey," Computer networks, vol. 38, no. 4, pp. 393-422, 2002.

[2] S. Corson and J. Macker, "Mobile ad hoc networking (MANET): Routing protocol performance issues and evaluation considerations," RFC 2501, 1999.

[3] C. Karlof and D. Wagner, "Secure routing in wireless sensor networks: Attacks and countermeasures," Ad Hoc networks, vol. 1, no. 2-3, pp. 293-315, 2003.

[4] Y.-C. Hu, A. Perrig, and D. B. Johnson, "Wormhole attacks in wireless networks," IEEE Journal on selected areas in communications, vol. 24, no. 2, pp. 370-380, 2006.

[5] L. Mui, M. Mohtashemi, and A. Halberstadt, "A computational model of trust and reputation," in Proceedings of the 35th Annual Hawaii International Conference on System Sciences, 2002, pp. 2431-2439.

[6] P. Michiardi and R. Molva, "KARA: a secure distributed trust management scheme for mobile ad hoc networks," in Security in Pervasive Computing, Springer, 2002, pp. 21-35.

[7] S. Buchegger and J.-Y. Le Boudec, "Performance analysis of the CONFIDANT protocol: Cooperation of nodes-fairness in dynamic ad-hoc networks," in Proceedings of the 3rd ACM international symposium on Mobile ad hoc networking & computing, 2002, pp. 226-236.

[8] R. Ganeriwal and M. B. Srivastava, "Reputation-based framework for high integrity sensor networks," in Proceedings of the 2nd ACM workshop on Security of ad hoc and sensor networks, 2004, pp. 66-77.

[9] A. Aziz, S. Zeadally, and F. Siddiqui, "Trust management in mobile ad hoc networks," in Proceedings of the 2009 international conference on Advances in Social Networks Analysis and Mining, 2009, pp. 355-362.

[10] A. Perrig, R. Szewczyk, V. Wen, D. Cullery, J. Anderson, and R. Szewczyk, "SPINS: security protocols for sensor networks," Wireless networks, vol. 8, no. 5, pp. 521-534, 2002.

[11] D. B. Johnson, D. A. Maltz, and J. Brodzik, "Protocols for adaptive wireless and mobile networking," Ad hoc networking, vol. 5, pp. 393-423, 2005.

[12] Maganti, M.R., Rao, K.R. (2024). Optimising the Epmipv6 protocol for the analysis of advanced sensor networks. Ingénierie des Systèmes d'Information, Vol. 29, No. 2, pp. 543-549. https://doi.org/10.18280/isi.290215

[13] A. Maleki, A. Movaghar, and H. Barati, "A survey of security attacks in wireless sensor networks," International Journal of Network Security & Its Applications, vol. 3, no. 1, pp. 61-71, 2011.

[14] Z. Wan and P. Wang, "A lightweight cryptographic key agreement protocol for wireless sensor networks," in 2009 International Conference on Information Engineering and Computer Science, 2009, pp. 1-4.

Journal of Engineering and Technology for Industrial Applications

ITEGAM-JETIA

Manaus, v.11 n.54, p. 39-47. July/August., 2025.
DOI: https://doi.org/10.5935/jetia. v11i54.1697

ISSN ONLINE: 2447-0228

RESEARCH ARTICLE OPEN ACCESS

ENHANCING 4G/LTE NETWORK PATH LOSS PREDICTION WITH PSO- GWO HYBRID APPROACH

Messaoud Garah[1] and Nabil Boukhennoufa[2]

[1] Department of Electronic, Laboratory of Electrical Engineering, University of Mohamed Boudiaf M'Sila, M'Sila, Algeria
[2]Department of Computer Science, Laboratory of Electrical Engineering, University of Batna 2, Algeria.

[1]http://orcid.org/0000-0002-6454-837X, [2]http://orcid.org/ 0009-0009-5531-4262

Email: messaoud.garah@univ-msila.dz, boukhennoufa.nabil@gmail.com

ARTICLE INFO

Article History
Received: March 11, 2025
Revised: April 20, 2025
Accepted: June 15, 2025
Published: July 31, 2025

Keywords:
COST231
Hata
RMSE
urban /suburban environments

ABSTRACT

In a 4G/LTE network, path loss models are crucial for efficient planning, interference estimation, frequency allocation, and optimization of cell parameters, all essential for the network's overall performance and planning. The Hata, COST231, Egli, and SUI models are among the most widely used in urban and suburban environments. However, these models rely on fixed parameters, which can cause inaccuracies when applied to measured data. This paper uses data collected from the north-central region of Algeria to calculate the path loss for 4G LTE (1800 MHz). The measured path loss is compared with the empirical models mentioned above. The best model for estimating the measured path loss is then optimized using three well-known evolutionary algorithms: Particle Swarm Optimization (PSO), Grey Wolf Optimizer (GWO), and Covariance Matrix Adaptation Evolution Strategy (CMA-ES). Furthermore, a hybrid optimization model, PSO-GWO, is proposed to improve prediction accuracy. The performance of each optimization method is evaluated using various error metrics, including Root Mean Square Error (RMSE), Mean Absolute Error (MAE), Standard Deviation (STD), Mean Error (ME), and Mean Absolute Percentage Error (MAPE). Results demonstrate that the hybrid techniques outperform the original Hata and COST231-Hata models, with the PSO-GWO hybrid yielding the lowest RMSE, achieving a significant reduction compared to the traditional models.

Copyright ©2025 by authors and Galileo Institute of Technology and Education of the Amazon (ITEGAM). This work is licensed under the Creative Commons Attribution International License (CC BY 4.0).

I. INTRODUCTION

The demand for dependable and efficient wireless communication networks has grown significantly in recent years, particularly in 4G/LTE networks [1],[2]. In the telecommunications industry, path loss refers to the reduction in power density of an electromagnetic wave signal as it propagates from the transmitter to the receiver [3]. Accurate path loss prediction ensures optimal network coverage and service quality. Empirical models are widely used for path loss prediction in various environments [4-8]. However, when applied to measured data, their fixed parameters often lead to inaccuracies. Optimized models utilizing various optimization algorithms should be employed to determine more precise parameters. For predicting radio wave path loss in specific regions, researchers have applied several algorithms to address this limitation to predict path loss across different environments [9-15].

In [10], the authors evaluate multiple empirical propagation models, including COST231 Hata, for estimating path loss in urban and suburban environments. The study analyzes performance variations across different models and underscores the significance of parameter optimization in enhancing prediction accuracy. Paper [11] applies several optimization algorithms, including Genetic Algorithms (GA), Particle Swarm Optimization (PSO), and Grey Wolf Optimization (GWO), to fine-tune the parameters of the COST231-Hata model, making it more suitable for specific environments or regions. These algorithms minimize the error between the predicted path loss and measured data.

In [12], the authors focus on applying Particle Swarm Optimization (PSO) to reduce path loss in suburban and rural areas for mobile communication networks. Different path loss models calculate the RMSE values between the actual and predicted data. The results indicate that the optimized COST231 model outperforms the other models considered in the study.

In [13], Amel Bouchemha et al. introduced a parametric optimization approach for path loss estimation in a 4G/LTE network, utilizing the Particle Swarm Optimization (PSO) algorithm to enhance network performance. Measurements were conducted in urban area. The proposed PSO-based path loss optimization method demonstrated superior prediction accuracy, achieving lower RMSE values than the analytical method based on empirical path loss models

In [14], comprehensive LTE path loss measurements at 800 MHz and 2600 MHz were conducted in selected urban and suburban areas of Ghana and compared with six widely used propagation models. The refined versions of the Ericsson, SUI, and ECC-33 models developed in this study provide more accurate path loss predictions for Ghanaian environments than traditional propagation models.

In the same context, this paper addresses this issue by examining commonly used empirical propagation models, such as COST231, Hata, SUI, and Egli, based on various parameters, including frequency, distance, and antenna height [16]. The study analyzes predicted and measured path loss in the urban/suburban environment of Médéa, a city in the north-central region of Algeria. Propagation measurements were conducted at a frequency of 1800 MHz. To achieve better accuracy, we employ Particle Swarm Optimization (PSO), Grey Wolf Optimizer (GWO), and Covariance Matrix Adaptation Evolution Strategy (CMA-ES). Furthermore, a hybrid optimization model, PSO-GWO, is proposed to enhance prediction accuracy.

The rest of the paper is organized as follows: Section II analyzes RF propagation models in LTE/4G networks and the optimization algorithms. Section III presents the experimental setup for data collection, while Section IV discusses the simulation results and their comparisons. Finally, Section V provides concluding remarks.

II. ANALYSIS OF RF PROPAGATION MODELS IN 4G /LTE NETWORK

II.1 EGLI MODEL

The Egli prediction model is an empirical model proposed by [17]. It is a simplified approach for estimating radio-wave path loss in areas with irregular topography. Based on real data, the path loss approximation can be formulated as follows:

$$PL = 20\,log(f_c) + 40\,log(d) - 2\,log(h_{te}) + \begin{cases} 76.3 - 10\,log(h_{re}), & h_{re} \le 10m \\ 85.9 - 20\,log(h_{re}), & h_{re} \ge 10m \end{cases} \quad (1)$$

.

II.2 HATA'S MODEL

Initially, this model was developed for urban areas. However, with the addition of correction factors, it can be adapted for suburban areas. For urban and suburban environments, the median path loss equations are expressed as follows:

$$PL(urban)(dB) = 69.55 + 26.16log(fc) - 13.82\,log(h_{re}) - a(h_{re}) + (44.9 - log(h_{te}))log\,d \quad (2)$$

For suburban area, it is expressed as

$$PL(suburban)(dB) = PL(urban) - 2[log(fc/28)]2 - 5.4 \quad (3)$$

The correction factor (a(h_{re})), in Equation (2), differs as a function of the size of the coverage area

$$(h_{re}) = 8.29(log1.54h_{re})2 - 1.1dB \quad for\ fc < 300MH \quad (4a)$$

For small and medium areas, it is

$$\mathrm{a}(h_{re}) = 2(\log 115h_{re})^2 - 4.97\mathrm{dB} \quad for\ \mathrm{c} > 300MHz \quad (4b)$$

In the above equations: d represents the separation distance between the transmitter and receiver antennas, valid for distances ranging from 1 to 20 km; fc denotes the operating frequency, which ranges from 150 MHz to 1500 MHz., The transmit antenna height (h_{te}) ranges from 30 m to 200 m. The receive antenna height (h_{re}) ranges from 1 m to 10 m, as considered in references [18], [19].

II.3 COST 231 HATA MODEL

The COST 231 model, also known as the PCS extension of the Hata model, is an improved version of the Hata model. It is widely used for predicting path loss in mobile wireless systems. Designed for frequencies ranging from 1500 to 2000 MHz, this model includes adjustments for urban, suburban, and rural (flat) environments [20],[21].

$$PL(d)(dB)=46.3+33.9\log(fc)-13.82\log(h_{te})-a(h_{re}) +(44.9-6.55\ \log(h_{te}))\ \log(d)+CM \quad (5)$$

CM = 0 dB for medium-sized cities and suburban areas with moderate tree density, or CM = 3 dB for metropolitan centers. The validity range of this model is:

$$1500\ MHz\ <\ f\ <\ 2000\ MHz,$$
$$30\ m < h_{te} < 200\ m,$$
$$1\ m\ < h_{re} < 10\ m,$$
$$1\ km\ <\ d\ <\ 20\ km.$$

II.4 SUI MODEL

The general path loss expression according to the SUI model is given by [22].

$$PL\ (dB)=A+10\gamma\log10(d/d_0) +X_f + X_h + s \quad (6)$$

Where $d > d_0$ (with d in meters) represents the distance between the base station and the receiving antenna, with $d_0 = 100$ m as the reference distance, X_f accounts for frequency corrections above 2 GHz. At the same time, X_h adjusts for the receiver antenna height. Additionally, it compensates for shadowing effects caused by trees and other obstacles along the propagation path. Parameter A is defined as follows:

$$A =20\log\ (4\pi d0/\lambda) \quad (7)$$

where λ is the wavelength in meters. Path loss exponent γ given by [23].

Where h_{te} is the base station antenna height in meters, and a, b, and c are constants that depend on the terrain type.

II.5 OPTIMIZATION ALGORITHMS

a. Particle Swarm Optimization (PSO)

The collective behavior of bird flocks inspires PSO and optimizes a function by continuously refining candidate solutions through velocity and position adjustments. The core equations governing PSO are [24]:

$$xi(t+1) =xi(t)+vi(t+1) \quad (8)$$

$$vi(t+1) =wvi(t)+C1\rho1(xli(t)-xi(t)) +C2\rho2(xg(t)-xi(t)) \quad (9)$$

Where. $\rho1$ and $\rho2$ are random values uniformly distributed within the range [0, 1].

b. Grey Wolf Optimizer (GWO)

GWO replicates the leadership hierarchy and hunting strategy of grey wolves. It updates the positions of search agents (wolves) by following the alpha, beta, and delta wolves, who represent the group's top-performing individuals. It was proposed by Mirjalili et al [25].

In this algorithm, wolves are classified into four categories based on their performance:
- Alpha (α): The leader of the pack, guiding the hunt and representing the best solution.
- Beta (β): The second-in-command, assisting the alpha in decision-making.
- Delta (δ): The third rank in the hierarchy, including subordinates and scouts.
- Omega (ω): The lowest-ranked wolves, following the decisions of the higher-ranked ones.

GWO updates the positions of wolves by simulating the three main phases of hunting:
1. Prey Detection: The alpha, beta, and delta wolves lead to the search for the best solution.
2. Encirclement: Wolves adjust their positions based on the leaders' guidance.
3. Final Attack: Convergence occurs as wolves move closer to the prey.

The position update equation is given by:

$$X\ (t + 1) = Xp(t) - A \cdot D \quad (10)$$

c. Covariance Matrix Adaptation Evolution Strategy

CMA-ES adapts the covariance matrix to generate new candidate solutions with a multivariate Gaussian distribution, which is particularly useful for high-dimensional optimization problems. CMA-ES updates a multivariate probability distribution to generate new solutions dynamically, adapting the covariance matrix over time. This enables efficient search space exploration and facilitates

convergence toward optimal solutions [26]. The main steps of CMA-ES are:

1. Generation of Solutions
At each iteration, a set of solutions is sampled from a multivariate Gaussian distribution defined by a mean vector (μ) and a covariance matrix (Σ).
2. Evaluation and Selection
The solutions are evaluated based on the objective function; only the best-performing solutions are selected to update the parameters.
3. Parameter Update

The mean vector (μ) is adjusted to move closer to the best solutions; the covariance matrix (Σ) is adapted to more effectively model the local search space structure.

4. Iteration Until Convergence

The algorithm continues sampling, evaluating, and adapting until a stopping criterion (such as convergence or reaching a maximum number of iterations) and optimal solutions are reached [26].

d. Hybrid Approaches (PSO-GWO, PSO-CMAES)

Hybrid models were proposed to enhance optimization performance [27],[28]. In these models, PSO generates an initial solution, which GWO then refines to achieve improved accuracy

III. EXPERIMENTAL SETUP

III.1 DATASET COLLECTION

To evaluate the performance of this optimization, measurements were conducted in an urban/suburban microcell environment in Médéa, a city in the north-central region of Algeria (Latitude: 36° 15' 51.01" N, Longitude: 2° 45' 14.15" E). The measurements were carried out for three 4G/LTE eNodeBs. eNodeB 1 (No. 26306): Located in the urban area of Ras Bydha (36.26848, 2.750647), eNodeB 2 (No. 26710): Situated in the suburban area of Ramli (36.28003, 2.750035). eNodeB 3 (No. 26748): Found in the urban area of Ras Kalouche (36.27686, 2.74577). Table1 summarizes the eNodeB specifications, including transmission frequencies, transmitted power, and antenna heights.

Table 1: eNodeBs Parameters.

eNodeB	Cell Name	HEIGHT (HBA SOL m)	Power(dBm)	Frequency (MHZ)	MS antenna height (m)
eNB1	26306	20	22	1800	1.5
eNB 2	26710	16	30	1800	1.5
eNB3	26748	24	30	1800	1.5

Source: Authors, (2025).

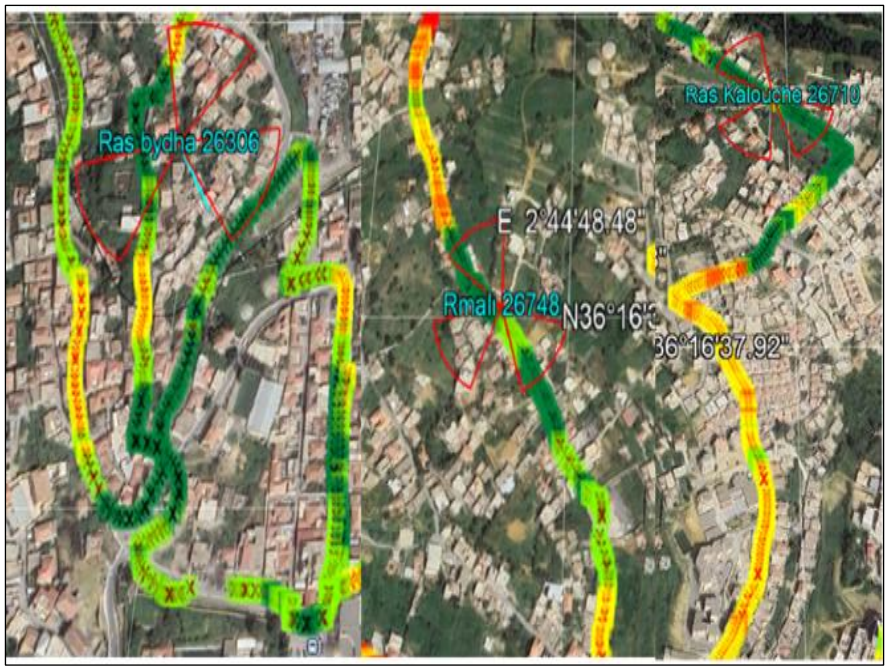

Figure 1: The map of the study area.
Source: Authors, (2025).

Figure 1 illustrates the study area, which provides a top-down view of the measurement routes using Google Maps

III.2 PERFORMANCE METRICS

The performance of the optimization algorithms is evaluated using the following error metrics:

- **RMSE (Root Mean Square Error)**: Measures the square root of the mean squared errors.
- **MAE (Mean Absolute Error)**: Computes the mean of the absolute errors.
- **STD (Standard Deviation)**: Represents the spread of errors.
- **ME (Mean Error)**: The average of all errors.
- **MAPE (Mean Absolute Percentage Error)**: Measures the percentage error relative to actual values.

IV. RESULTS AND DISCUSSIONS

IV.1 COMPARISON WITH PREDICTION MODELS

To evaluate the prediction models, three eNodeBs were compared for predicted and measured path loss. The performance of the empirical models was then assessed against the measured path loss data, as illustrated in Figures 2, 3, and 4.

The forecasting accuracy of these models was quantified using Root Mean Square Error (RMSE), with the results presented in Table 2.

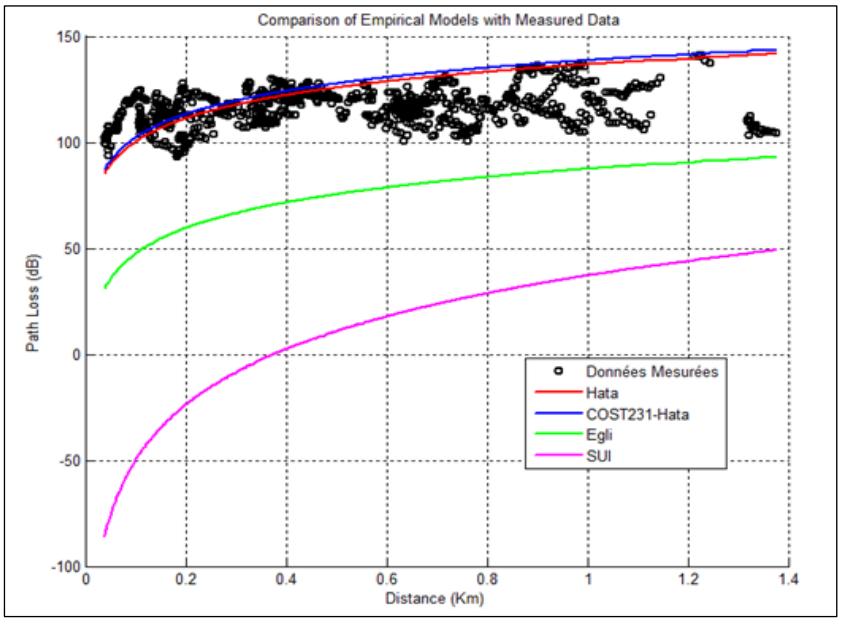

Figure 2: Comparison of Predicted and Measured Path Loss for eNodeB1.
Source: Authors, (2025)

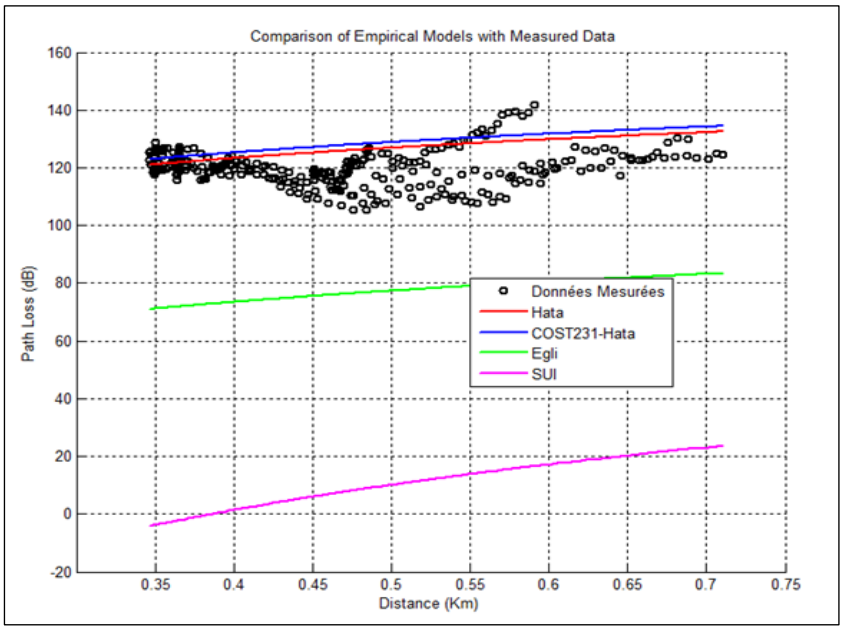

Figure 3: Comparison of Predicted and Measured Path Loss for eNodeB2.
Source: Authors, (2025).

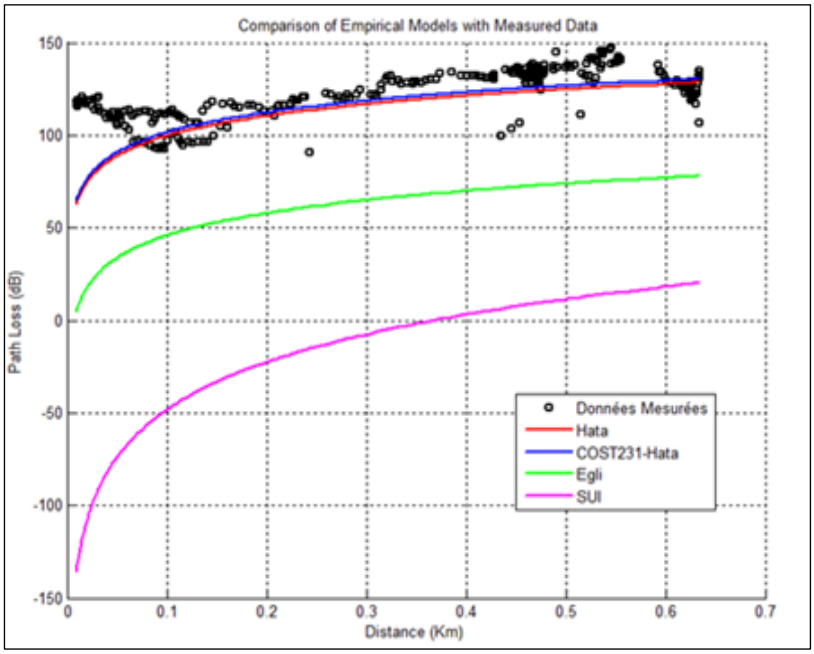

Figure 4: Comparison of Predicted and Measured Path Loss for eNodeB3.
Source: Authors, (2025).

Table 2: Performance Comparison of Models Based on RMSE.

Model	eNB1 (urban)	eNB2(urban)	eNB3(suburban)
Hata	14.1231	7.9203	15.9555
COST231-Hata	15.1382	9.1497	14.8317
Egli	45.9474	45.766	63.6113
SUI	115.6488	115.6486	142.0491

Source: Authors, (2025).

According to Table 2, the Hata model demonstrates the best performance for urban coverage areas**,** as it yields the lowest RMSE compared to other models. In contrast, the COST231-Hata provides the closest match to the measured path loss among all the models for suburban areas. These findings are further validated by Figures 2, 3, and 4**.**

IV.2 OPTIMIZATION PROCESS

The simulation results are presented in the following tables and figures.

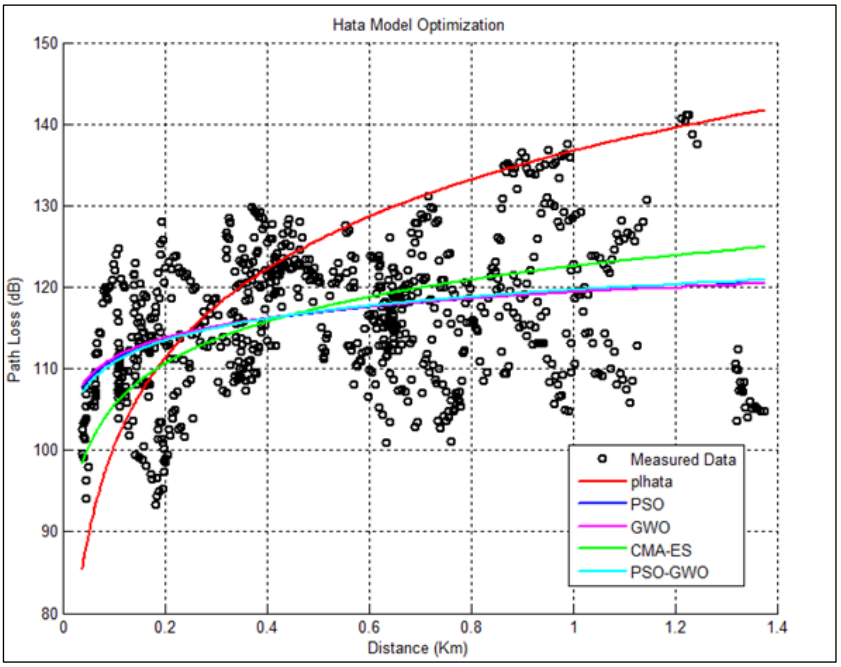

Figure 5: Comparison between the Hata model and optimized models for eNodeB..1
Source: Authors, (2025).

Tables 3 and 4 showcase the optimized Hata model, while Table 5 presents the optimized COST231 model, generated using PSO, CMA-ES, GWO, and PSO-GWO, for eNodeB1, eNodeB2, and eNodeB3, respectively.

Figures 5 and 6 illustrate comparative plots of the optimized Hata model for eNodeB1 and eNodeB2, respectively. while the optimized COST231 model for eNodeB3 is presented in Figure 7.

Through the optimization process of the Hata model, the developed models demonstrated superior prediction accuracy compared to existing models in terms of overall performance, as shown in Tables 3 and 4. This improvement is further highlighted in Figures 5 and 6, illustrating the optimized models' enhanced performance. A similar improvement is observed for the optimized COST231 model, as presented in Table 5 and Figure 7.

An analysis of the three tables reveals that the PSO method achieves the lowest RMSE values in both cases, outperforming CMA-ES and GWO. Furthermore, the RMSE value is further reduced by implementing a hybrid approach combining PSO and GWO, which enhances model accuracy by leveraging the efficiency of both optimization techniques.

Table 3: Measured and tuned models for eNodeB1.

Evaluation parameters	Hata	PSO	CMA-ES	GWO	PSO-GWO
RMSE	14.1231	7.9515	8.4550	7.9541	7.9487
MAE	11.3589	6.4399	6.9206	6.4436	6.4328
STD	12.4622	7.9565	8.4581	7.9590	7.9538
ME	6.6599	-0.038	-0.1975	0.0493	0.0058
MAPE	10.07%	5.57%	6.0050%	5.5819%	5.5701%
Time of Execution	-	0.11 s	0.94 s	0.06 s	0.28 s

Source: Authors, (2025).

Table 4: Measured and tuned models for eNodeB2.

Evaluation parameters	Hata	PSO	CMA-ES	GWO	PSO-GWO
RMSE	7.3318	5.6448	6.2991	5.6512	5.6060
MAE	5.4573	4.1509	4.7119	4.1509	4.0494
STD	6.5528	5.6522	5.7160	5.6584	5.6134
ME	3.3060	-0.0133	-2.6631	0.0560	-0.0004
MAPE	4.6636%	3.4772%	3.8537%	3.4797%	3.3863%
Time of Execution	-	0.14 s	0.86 s	0.08 s	0.26 s

Source: Authors, (2025).

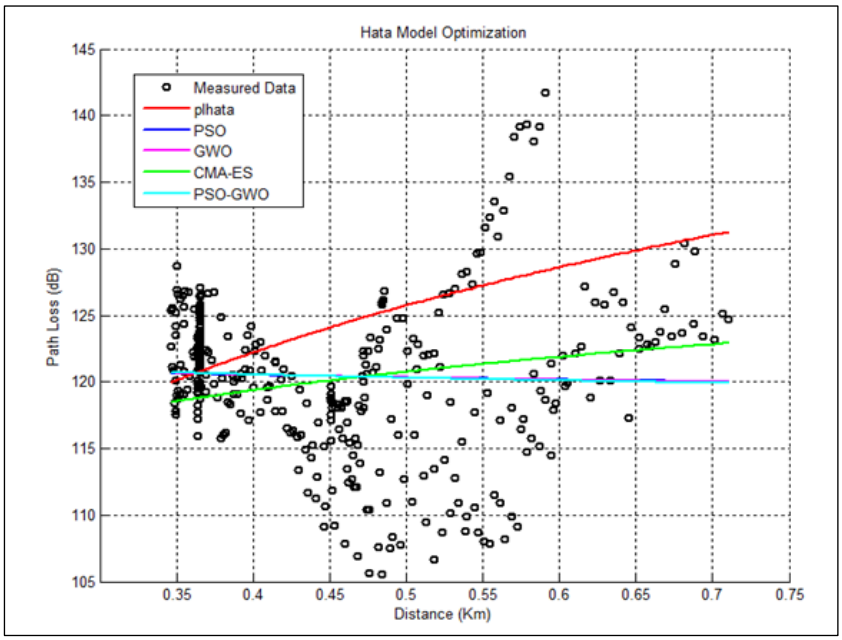

Figure 6: Comparison between the Hata model and optimized models for eNodeB2.
Source: Authors, (2025).

Table 5: Measured and tuned models for eNodeB3.

Evaluation parameters	Cost231	PSO	CMA-ES	GWO	PSO-GWO
RMSE	13.4712	9.9841	10.1101	9.9848	9.9840
MAE	9.4066	7.8136	8.1119	7.8036	7.8221
STD	12.5633	10.0014	10.0479	10.0017	10.0013
ME	-4.9176	0.0131	-1.2662	0.0898	0.0013
MAPE	7.8694%	6.6728%	6.8307%	6.6695%	6.6787%
Time of Execution	-	0.09 s	0.61 s	0.04 s	0.20 s

Source: Authors, (2025).

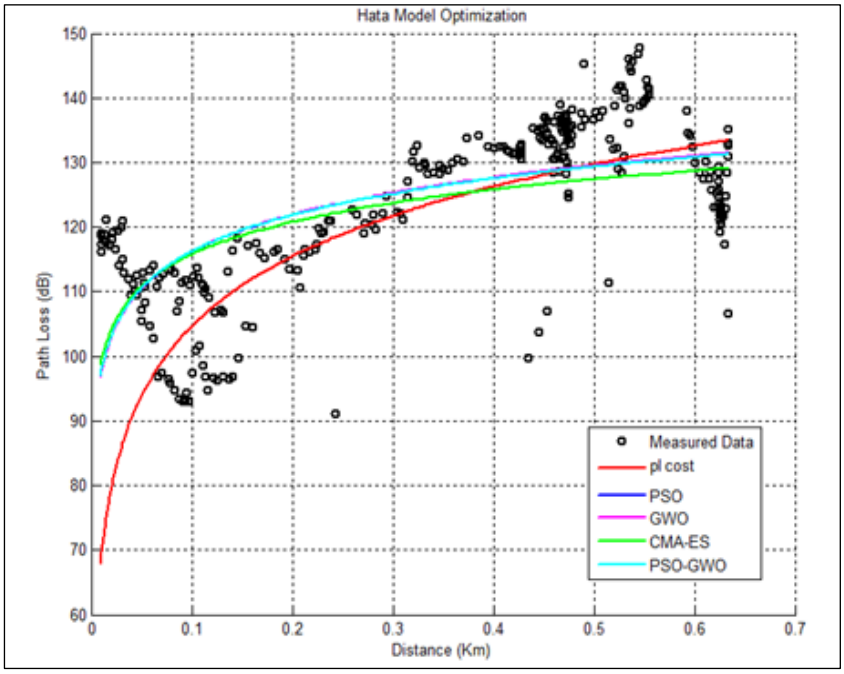

Figure 7: Comparison between the cost231 model and optimized models for eNodeB3.
Source: Authors, (2025)

V. CONCLUSIONS

In this paper, various empirical propagation models have been presented and analyzed to evaluate their performance in wireless communication. The tuning models were validated by comparing them with the path loss measurements obtained from three eNodeBs of a 4G/LTE network in Media City, Algeria. Three optimization algorithms were proposed and tested to fine-tune the parameters of the Hata and COST231 models. This study significantly improves path loss prediction accuracy when optimizing the COST231-Hata model for suburban environments and the Hata model for urban environments using PSO, GWO, CMA-ES, and the hybrid PSO-GWO approach. Among the tested methods, the PSO algorithm achieved the best performance. This result was further enhanced by applying the hybrid PSO-GWO approach, suggesting that combining different optimization techniques can yield superior results. Future research will use machine learning models to adapt path loss prediction across diverse environments.

VI. AUTHOR'S CONTRIBUTION

Conceptualization: Messaoud Garah and Nabil Boukhennoufa.
Methodology: Messaoud Garah and Nabil Boukhennoufa.
Investigation: Messaoud Garah and Nabil Boukhennoufa.
Discussion of results: Messaoud Garah and Nabil Boukhennoufa.
Writing – Original Draft: Messaoud Garah and Nabil Boukhennoufa.
Writing – Review and Editing: Messaoud Garah and Nabil Boukhennoufa.
Resources: Messaoud Garah and Nabil Boukhennoufa.
Supervision: Messaoud Garah and Nabil Boukhennoufa.
Approval of the final text: Messaoud Garah and Nabil Boukhennoufa.

VII.REFERENCES

[1] S. Ajose et A. Imoize, "Propagation measurements and modeling at 1800 MHz in Lagos, Nigeria," International Journal of Wireless and Mobile Computing, vol. 6, pp. 165–174, 2013, doi: 10.1504/IJWMC.2013.054042.

[2] M. Terre, M. Pischella et E. Vivier, Wireless Telecommunication Systems. Wiley, 2019, doi: 10.1002/9781118625422.ch7.

[3] A. Imoize et A. Dosunmu, "Path loss characterization of Long-Term Evolution network for Lagos, Nigeria," Jordan Journal of Electrical Engineering, vol. 4, pp. 114–128, 2018.

[4] S. G. Nimako et A. F. Mensah, "Motivation for customer complaining and non-complaining behavior towards mobile telecommunication services," Asian Journal of Business Management, vol. 4, no. 3, pp. 310–320, 2012.

[5] N. Al-Aamri et M. B. Suwailam, "Characterization of propagation models in wireless communications for 4G networks," Journal of Electronics and Telecommunications, vol. 8, pp. 84–95, 2022.

[6] H. K. Hoomod, I. Al-Mejibli et A. I. Jabboory, "Analyzing the study of path loss propagation models in wireless communications at 0.8 GHz," Journal of Physics: Conference Series, vol. 1003, p. 012028, 2018, doi: 10.1088/1742-6596/1003/1/012028.

[7] A. Siddiqui, N. Fatima et A. Ahmad, "Comparative analysis of propagation path loss models in LTE networks," 2019 International Conference on Power Electronics, Control and Automation (ICPECA), 2019, pp. 1–3, doi: 10.1109/ICPECA47973.2019.8975464.

[8] S. Tahcfulloh, E. Wahyuni, D. Santoso et R. Juliannanda, "Modified COST-235 empirical path loss model for agricultural WSN using particle swarm optimization," IIUM Engineering Journal, vol. 26, no. 1, pp. 336–352, 2025, doi: 10.31436/iiumej.v26i1.3446.

[9] M. Garah et al., "Path loss model optimization for mobile communication in different areas," Indonesian Journal of Electrical Engineering and Computer Science, vol. 3, pp. 126–135, 2016.

[10] J. Chebil et al., "Comparison of empirical propagation path loss models for mobile communications in the suburban area of Kuala Lumpur," 2011 4th International Conference on Mechatronics (ICOM), 2011, pp. 1–5.

[11] H. Oudira, L. Diouane et M. Garah, "Empirical PL models optimization for mobile communication," 2018 IEEE 5th International Congress on Information Science and Technology (CiSt), 2018, pp. 443–448, doi: 10.1109/CIST.2018.8596423.

[12] M. Garah, H. Oudira, L. Djouane et N. Hamdiken, "Particle swarm optimization for the path loss reduction in suburban and rural areas," International Journal of Electrical and Computer Engineering (IJECE), vol. 7, no. 4, pp. 2125–2131, 2017, doi: 10.11591/ijece.v7i4.pp2125-2131.

[13] A. Bouchemha, H. Djellab et M. C. Nait-Hamoud, "Analysis and optimization of 4G/LTE network path loss using Particle Swarm Optimization algorithm," International Journal of Electrical Engineering and Research (IJEER), vol. 12, no. 2, pp. 557–566, 2024, doi: 10.37391/IJEER.120230.

[14] D. Gadze et al., "Improved propagation models for LTE path loss prediction in urban & suburban Ghana," International Journal of Wireless & Mobile Networks, vol. 11, p. 20, 2019.

[15] A. E. Ibhaze et al., "An empirical propagation model for path loss prediction at 2100 MHz in a dense urban environment," Indian Journal of Science and Technology, vol. 10, no. 5, pp. 1–9, 2017.

[16] M. K. Elmezughi, T. J. Afullo et N. O. Oyie, "Investigating the impact of antenna heights on path loss models in an indoor corridor environment," IEEE International Conference on Adaptive and Broadband Communication (icABCD2020), 2020, pp. 1–7.

[17] J. J. Egli, "Radio propagation above 40 Mc over irregular terrain," Proceedings of the IRE, vol. 45, no. 10, pp. 1383–1391, 1957.

[18] T. K. Sarkar et al., "A survey of various propagation models for mobile communication," IEEE Antennas and Propagation Magazine, vol. 45, no. 3, pp. 51–82, 2003.

[19] M. Hata, "Empirical formula for propagation loss in land mobile radio services," IEEE Transactions on Vehicular Technology, vol. VT-29, no. 3, pp. 317–325, 1980.

[20] J. D. Parsons, The Mobile Radio Propagation Channel, 2nd éd. Wiley, 2000.

[21] T. Asztalos, Planning a WiMAX Radio Network with A9155. Alcatel-Lucent, 2008.

[22] H. R. Anderson, Fixed Broadband Wireless System Design. John Wiley & Sons, 2003.

[23] V. Erceg et L. J. Greenstein, "An empirically based path loss model for wireless channels in suburban environments," IEEE Journal on Selected Areas of Communications, vol. 17, pp. 1205–1211, 1999.

[24] J. Kennedy et R. Eberhart, "Particle swarm optimization," Proceedings of the IEEE International Conference on Neural Networks (ICNN), vol. 4, pp. 1942–1948, 1995.

[25] S. Mirjalili, S. M. Mirjalili et A. Lewis, "Grey wolf optimizer," Advances in Engineering Software, vol. 69, pp. 46–61, 2014.

[26] N. Hansen, "The CMA Evolution Strategy: A comparing review," in Towards a New Evolutionary Computation, Springer, 2006, pp. 75–102.

[27] M. J. Mahmoodabadi, A. R. Nemati et N. Danesh, "A new optimization algorithm based on Particle Swarm Optimization, Genetic Algorithm, and Sliding Surfaces," International Journal of Engineering, vol. 37, no. 9, pp. 1716–1735, 2024, doi: 10.5829/ije.2024.37.09c.02.

[28] H. Hasibi, A. Mahmoudian et G. R. Khayati, "Modified Particle Swarm Optimization-Artificial Neural Network and Gene Expression Programming for predicting high-temperature oxidation behavior of Ni–Cr–W-Mo alloys," International Journal of Engineering, vol. 33, no. 11, pp. 2327–2338, 2020, doi: 10.5829/ije.2020.33.11b.23.

Journal of Engineering and Technology for Industrial Applications

ISSN ONLINE: 2447-0228

ITEGAM-JETIA

Manaus, v.11 n.54, p. 48-57. July/August., 2025.
DOI: https://doi.org/10.5935/jetia. v11i54.1708

RESEARCH ARTICLE OPEN ACCESS

PRODUCT DESIGN AND VALUE ANALYSIS IN FOOD PRODUCT (CASE STUDY OF VEGETABLE NUGGET PRODUCT)

Endang Retno Wedowati[1], Diana Puspitasari[2], Fungki Sri Rejeki[3] Tri Rahayuningsih[4] and Johan Paing Heru Waskito[5]

[1, 2, 3, 4] Agroindustrial Technology - Engineering Faculty, Universitas Wijaya Kusuma Surabaya, Surabaya, Indonesia.
[5] Civil Engineering - Engineering Faculty, Universitas Wijaya Kusuma Surabaya, Surabaya, Indonesia.

[1]http://orcid.org/0000-0002-2699-4053, [2]http://orcid.org/0000-0001-5157-2808, [3]http://orcid.org/0000-0001-6335-5835, [4]http://orcid.org/0000-0001-9180-0510, [5]http://orcid.org/0009-0003-8636-1551

Email: wedowati@uwks.ac.id, diana.puspitasari@uwks.ac.id, fungki_tip@uwks.ac.id, tri_rahayu@uwks.ac.id, johan.paing@uwks.ac.id

ARTICLE INFO

Article History
Received: March 14, 2025
Revised: April 20, 2025
Accepted: June 15, 2025
Published: July 31, 2025

Keywords:
Product design,
Product value,
Conjoint analysis,
Food product,
Vegetable nugget.

ABSTRACT

Processed food products that are ready to cook and ready to eat are available because of the needs of today's society, which are very practical. One of the processed food products that suit these needs is nuggets. In general, nuggets are made from animal ingredients, but in this study, a vegetable nugget product design was developed. The study's purpose was to develop a product design and analyze the value of vegetable nugget products to meet consumers' needs and desires for the availability of ready-to-eat processed food products that have health benefits. The product design developed used the Conjoint Analysis method combined with Orthogonal Design to determine the product configuration. Furthermore, a value analysis is carried out on each product configuration form based on product benefits and production costs. The product variations provided were eight product variants that combined five product attributes: shape, flavor, weight, packaging material, and packaging design. The selected product is the product that has the highest value, which is based on product benefits and production costs for each product variant.

Copyright ©2025 by authors and Galileo Institute of Technology and Education of the Amazon (ITEGAM). This work is licensed under the Creative Commons Attribution International License (CC BY 4.0).

I. INTRODUCTION

Customer wants and needs are constantly changing and tend to be diverse. Changes in customer desires and needs tend to be increasingly diverse in terms of design, quality, and delivery process [1–3]. The increasingly diverse needs and wants of customers require producers to be able to produce a variety of products. In addition, the availability of processed food products that are ready to cook and eat is due to the practical needs of modern society. One of the processed food products that suit these needs is nuggets. Nuggets are made from seasoned ground meat, molded, coated in breadcrumbs, and fried. The main ingredient for making nuggets is animal meat, such as fish, chicken, or beef. Efforts to replace animal-based ingredients in nuggets use plant-based ingredients. This alternative is done to provide healthy food for consumers who do not consume animal foods. Red beans are an alternative plant-based ingredient that can be used in the processing of vegetable nuggets. Many choices of nugget design with various features make consumers more selective in choosing products that suit their needs and desires. Therefore, a new design of red bean nuggets can be made to find out consumer preferences for vegetable nugget products.

Red beans have a high protein content. Protein is an important nutrient needed by the body. The research of Utama and Anjani [4] concluded that analog red bean meat with 15% soy protein isolate substitution has the highest protein content (11.6%), the highest fiber (1.90%), and the lowest fat (1.48%). According to Astawan [5], red beans have the advantage of being cholesterol-free compared to animal protein. The selection of red beans as the basic ingredient in making red bean nugget products is expected to have several advantages, namely high protein and fiber, low fat, cholesterol-free, can be enjoyed by all levels of society, affordable prices, and can be used as an alternative to meat consumption. Previous research on consumer preferences for nugget products was conducted by Akantu [6], Ikhsanu [7], and Rahardjo [8]. The results of the study of Akantu [6] with the title Consumer Preferences in purchasing chicken nuggets, selected attributes that are considered by consumers include taste, aroma, and texture. Ikhsanu's research [7] groups consumer

preferences based on respondent characteristics where the attributes used are aroma, texture, ease of absorbing oil, tenderness, and taste. Rahardjo [8] examined the factors that are consumer preferences in purchasing frozen food products, the results of the study showed that the most important factor in influencing consumer preferences is taste, where the most preferred tastes are savory, salty, and spicy, and the next factor is price, packaging, and brand.

Meanwhile, Wedowati et al. [9], [10] have reviewed consumer preferences for customized products based on three aspects, namely functionality, usability, and pleasure. Attributes in each aspect consist of taste, color, aroma, and nutritional content (functionality aspect), shape and packaging of materials (usability aspect), health benefits, appearance, and type of topping (pleasure aspect). Analysis of product value, which is the ratio between product benefits and product costs, has been reviewed by Wedowati et al. [11].

Based on the existing background, the formulation of the problem in this study is how to design a vegetable nugget product that can meet the needs and desires of consumers who want the availability of fast food but healthy with high benefit value. The objectives of this study are: 1) To determine the attributes of vegetable nugget products that are to the desires and needs of consumers; 2) To design a vegetable nugget product design that follows the desires and needs of consumers; and 3) To determine the value of vegetable nugget products as healthy fast-food products. The benefits of this study are: 1) to produce a variety of vegetable nugget product designs that can meet the desires and needs of consumers and 2) to provide healthy ready-to-eat food products.

II. THEORETICAL REFERENCE

The concept of food product quality can generally be divided into two factors, namely intrinsic attributes and extrinsic attributes. Intrinsic attributes are attributes that measure the quality of a product based on its function and physical properties. Intrinsic attributes are specific to each product. These attributes will disappear when the product is consumed and cannot be changed without changing the nature of the product itself. Extrinsic attributes are aspects that are related to the product but are not physically part of the product itself, such as name or image, brand, and price. These attributes are known as variables that provide product information and must be considered in the evaluation of product characteristics. Quality can be defined as the moment when consumers receive information about the characteristics of a product at the time of purchase or after consuming it [12]. Thus, consumers can evaluate the function or benefits of the product based on their needs. According to Espejel et al. [13], based on product attributes, there are three categories of quality, namely:

1. Search quality (quality in the shop). This category refers to intrinsic and extrinsic product attributes at the time of purchase and is an important quality selection process.
2. Experience quality (eating quality). This category is an intrinsic attribute that is available at the time the product is used or consumed and is an important category for customer perception of organoleptic quality.
3. Credence quality. This category describes the intrinsic and extrinsic attributes that consumers pay attention to but are not captured during the purchasing process or consumption. Consumers rely on information conveyed by the media or word of mouth.

Several previous studies have studied product quality attributes in the food industry, as shown in Table 1.

Table 1: Food product attributes.

No.	Authors	Product	Product Attributes
1.	Iop *et al.* [14]	Food Product	Intrinsic: color, aroma, taste, and texture Extrinsic: brand, price, and context
2.	Espejel *et al.* [13]	Traditional Food	Intrinsic: color, taste, odor, and appearance Extrinsic: brand, denomination of origin, and traditional product image
3.	Hersleth *et al.* [15]	*dry-cured ham*	Intrinsic: sensory quality (appearance, smell, taste, texture) Extrinsic: price, nutritional value, and processing conditions
4.	Lee *et al.* [16]	Fruit juice	Extrinsic: *brand*, nutritional content, ingredient label, shelf life, price, and country of manufacture
5.	Verain *et al.* [17]	milk, meat, fruit and vegetables, fish	Attributes: sustainability, health, taste, price
6.	Nishimura *et al.* [18]	Onion concentrates	Taste, aroma, and texture
7.	Wedowati *et al.* [9–11]	Ice cream	Functionality: taste, color, aroma, texture, and nutritional content Usability: shape, size, and packaging materials Pleasure: brand/image, health benefits, appearance, and packaging design
8.	Wedowati *et al.* [19]	Chocolate	Functionality: taste, color, aroma, texture, and sweetness level Usability: shape, size, packaging material, and packaging method Pleasure: brand/image, health benefits, appearance, and profile

Source: Authors, (2025).

A product is anything that can be offered to a market to meet a desire or need. Products marketed include goods and physical services, places, organizations, and ideas [20]. The many choices of nugget products available on the market will make consumers more selective in determining the choice of nugget products that suit their needs and desires. The development of red bean nugget products can be done by finding out consumer preferences for new products. Consumer preferences for a product can be known by determining the attributes attached to the product that can influence someone as a consideration for choosing the product.

III. MATERIALS AND METHODS

This research was carried out from April 2024 to December 2024 at the Food Laboratory of the Agro-industrial Technology Study Program, Faculty of Engineering, Universitas Wijaya Kusuma Surabaya, and The Industrial Research and Consultation Laboratory,

Surabaya, East Java. The materials used in this research are ingredients for making and packaging materials for vegetable nuggets. The tools used in this research were a steamer, stove, large plastic bowl, scales, mixer, and nugget maker.

This research was designed in four stages, as shown in Figure 1. The first stage is empirical research using the survey method, the second and third stages are analytical research using mathematical-statistical modeling, and the fourth stage is a laboratory experiment to realize the selected product design. The stages of the research can be briefly explained as follows:

1. The product attribute determination stage, namely the stage of collecting consumer preferences related to the desired vegetable nugget product attributes, which will later be used as the basis for product design. At this stage, a survey method will be used;
2. The product design stage, to determine the variation of nugget products desired by consumers; at this stage, using Orthogonal Design to build product configuration, and Conjoint Analysis to select product variations;
3. The value analysis stage is carried out to determine the selected product design alternative by comparing production costs and product benefits; and
4. The stage of realizing the selected product design, namely the stage of processing the selected vegetable nugget product and testing the product quality.

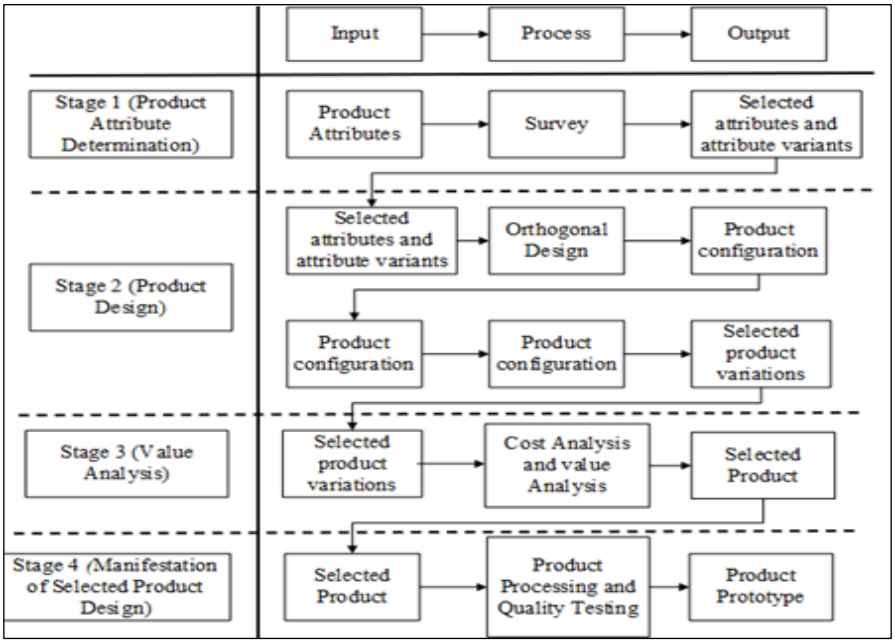

Figure 1: Research stages.
Source: Authors, (2025).

III.1 RESEARCH STAGES

Product attribute determination stage

The first stage in this study is the stage of determining product attributes. This stage is carried out to capture consumer preferences related to the attributes of vegetable nuggets products desired by consumers which will later be used as the basis for product design. The product attribute capture is based on the intrinsic and extrinsic attributes of the product. This stage uses a survey method conducted online.

The questionnaire is composed of two parts; the first part is the demographic aspect of the respondents, and the second part is related to the product attributes desired by consumers. In the demographic aspect of the respondents, questions include age, gender, education level, occupation, and income. The product attributes reviewed in this study include intrinsic and extrinsic product attributes.

Data was collected using an online questionnaire distributed via social media over a predetermined period. Social media is used with the aim that only respondents who are interested in the product being studied will fill out the questionnaire. The target respondents are consumers of the products studied. Data about respondent characteristics and preferences were analyzed using descriptive analysis.

Product design stage

Alternative product configurations are developed using orthogonal design. Each aspect of the intrinsic attribute is represented by two attributes that are most in demand by consumers, and each attribute has at least two variants that are most often chosen by consumers. Based on the alternative product configurations formed, a ranking process is then carried out to determine the ranking of the alternative product configurations. The ranking process uses the Conjoint Analysis method. Conjoint Analysis is used to determine the ranking of the product configurations formed. Conjoint Analysis is one of the most popular techniques for assessing customer preferences for alternative products with multiple attributes [10], [21], [22]. At this stage, the top 3 rankings will be selected as selected products.
The general formulation of the Conjoint Analysis mathematical model is presented in Equation (1) [22].
Conjoint Analysis Mathematical Model

$$U_k = \beta_0 + \sum_{i=1}^{m} \sum_{j=1}^{n} u_{ijk} \quad (1)$$

Where:

U_k = total utility of each product configuration alternative
β_0 = a constant
u_{ijk} = utility of product configuration alternative k for attribute i and level j
m = number of attributes
n = number of levels

Value analysis stage

Value analysis is conducted to determine the best product design in terms of product benefits and product production costs. Product benefits are based on product utilities from the results of conjoint analysis. Product value is a comparison between product benefits and the cost of producing it. The value of a product is determined using Equation 2.
Product Value Equation

$$Value = \frac{\text{Utility}}{\text{Cost}} \quad (2)$$

The stage of realizing the selected product design

At this stage, vegetable nuggets will be produced with the selected design from Stage 3. Next, product quality testing will be carried out to determine whether the resulting product meets the quality standards according to existing provisions.

III.2 OBSERVATION PARAMETERS

Parameters for testing vegetable nugget products, namely protein content, carbohydrate content, fat content, water content, and ash content, as well as organoleptic tests (taste, color, aroma, and texture). Product nutritional content testing is carried out to determine the nutritional content of selected vegetable products following applicable provisions. The method of measuring the chemical content of products refers to [23].

This Organoleptic Test was conducted to determine the level of consumer preference for the parameters of taste, color, flavor, and texture of vegetable nugget products. This organoleptic test uses a hedonic scale by randomly presenting 30 general panelists to conduct tests based on five scales: 1 (very dislike), 2 (dislike), 3 (neutral), 4 (like), and 5 (very like). The results of this organoleptic test were then analyzed using descriptive analysis.

IV. RESULTS AND DISCUSSIONS

IV.1 VALIDITY AND RELIABILITY

The results of the questionnaire validity test obtained a value for the r table of 0.195, with a confidence level of 95% and a significance value (error rate) of 5% = 0.05. The statement in the questionnaire is said to be valid if the statement has a positive r count value and is greater than the r table value. Based on the results of the validity test conducted, it is known that all statements used in the study are valid.

A questionnaire is reliable if a person's answer to a statement is consistent or stable over time. A construct or variable is declared reliable if it provides a Cronbach Alpha (α) value > 60. Based on the results of the reliability test, the Cronbach Alpha value was 0.859, so it can be said that the questionnaire is reliable.

IV.2 DESCRIPTIVE ANALYSIS

The selection of intrinsic and extrinsic attributes of vegetable nugget products is based on consumer preferences. Intrinsic and extrinsic attributes are selected based on the percentage of 50% to >50% of the total calculation. Based on the results of the analysis, the intrinsic attribute levels desired by respondents are the shape of the nugget by 67%, flavor (taste and aroma) by 55%, and the weight of the nugget per piece by 50%. The results of the extrinsic attribute levels desired by respondents are packaging materials by 75% and packaging design by 51%.

The selected attribute level is determined from the sum of the "Desired" and "Highly Desired" scores in the frequency distribution of each attribute. The total value of the attribute level that shows a percentage of 50% to >50% is determined as the attribute level consumer's desire. The selected attributes and levels for making vegetable nugget product designs can be seen in Table 2.

Table 2: Selected attributes and variants of vegetable nugget product design.

Intrinsic Attributes		**Extrinsic Attributes**	
Attributes	**Variants**	**Attributes**	**Variants**
Shape	Animal Shape	Packaging Materials	Vacuum Plastic
	Alphabet Pieces		Laminated Cardboard
	Dimension Cut	Packaging Design	Simple Design
Flavor (Taste and Aroma)	Dominant Vegetables		Variative Design
	Dominant Content Variants		
Weight per piece	15-20 grams (medium)		
	20-25grams (large)		

Source: Authors, (2025).

IV.3 PRODUCT DESIGN

Conjoint Analysis

The orthogonal array is used to design efficient experiments and analyze experimental data. Therefore, an orthogonal array is used to help create stimuli configurations so that all stimuli do not need to be analyzed further. The orthogonal array procedure uses orthogonal design so that the configuration of the vegetable nugget product design is produced in the form of stimuli cards, where each stimulus card has a different characteristic configuration or attribute level. The results of the orthogonal array study display eight stimulus cards or eight vegetable nugget product design configurations. The configuration was then distributed as a second-stage questionnaire. Respondents were asked to rank the configurations from the most preferred (1) to the least preferred (8) according to each respondent's opinion.

The utility value of each attribute level can be obtained using conjoint analysis. Conjoint analysis in principle aims to estimate the pattern of respondents' opinions. The results of this estimation are then compared with the actual opinions of respondents. The process of comparing estimates with actuals is called predictive accuracy, which measures the level of production accuracy. To test this accuracy, correlation measurements are carried out [24]. Correlation measurements in conjoint analysis were carried out using Pearson's R and Kendall's tau. A correlation is said to be strong if R is above 0.5 (R > 0.5) with a probability (significance) less than 0.05. The result of the Conjoint Analysis Correlation Test is shown in Table 3.

Table 3: Conjoint Analysis Correlation Test.

Criteria	Value	Sig.
Pearson's R	0.983	0.000
Kendall's tau	0.929	0.001

Source: Authors, (2025).

The results of the conjoint analysis correlation test (Table 3) show an R-value> 0.5 with a value on the Pearson's R criteria of 0.983 and Kendall's tau of 0.929 and a significance value below 0.05, namely a value of 0.000 for Pearson's R and 0.001 for Kendall's tau. This means that the accuracy of consumer preference prediction is stated as significant. Thus, it can be said that the 5 selected attribute factors can produce a design configuration that describes consumer wants for vegetable nugget products.

The utility value of the level is the preference value given by respondents to each level attached to the design attribute of vegetable nugget products. The greater the utility value of the attribute level at the attribute level, the more preferred it is than other attribute levels. The results of the conjoint analysis show the utility value of the highest level of each attribute that is most preferred by respondents. The utility value of the attribute level of vegetable nugget products can be seen in Table 4.

Table 4: Utility value of product attribute level.

Attributes	Level	Utility Value
Shape	Animal Shape	0.150
	Dimension Cut	-0.107
	Alphabet Pieces	-0.043
Flavor (Taste and Aroma)	Dominant Content Variants	-0.040
	Dominant Vegetables	0.040
Weight per piece	15-20 grams (medium)	-0.082
	20-25grams (large)	0.082
Packaging Materials	Vacuum Plastic	0.113
	Laminated Cardboard	-0.113
Packaging Design	Simple Design	-0.070
	Variative Design	0.070
(Constanta)		**4.462**

Source: Authors, (2025).

The Importance Level is the average value of all stimuli factors from the utility value of each respondent's attributes. The attribute importance level is the level of consumer preference or interest in the desired attribute. The greater the attribute importance value indicates the greater the influence of the attribute in determining consumer preferences, and conversely, a low attribute importance value indicates that the attribute is relatively less considered. The results of the analysis on the most considered attribute importance levels in sequence, shown in percentage, are nugget shape at 36.26%, nugget flavor (taste and aroma) at 17.84%, nugget weight per piece (size) at 17.74%, packaging material at 13.64%, and packaging design at 14.51%.

The value of total utility is used to see the configuration and attribute level that is most preferred by consumers of red bean nugget products. The higher the satisfaction obtained, the higher the utility value of the product. The total utility value in Table 5, describes the most preferred choice by respondents from the eight stimulus configurations offered. The highest total utility value indicates the design configuration of the vegetable nugget product that is most desired by consumers, and the lowest total utility value indicates the design configuration of the vegetable nugget product that is least preferred by consumers. Based on Table 5, the design configuration of the red bean nugget product that is by consumer preferences or most preferred is the configuration ranked first or stimulus card number three. The selected design configuration of the vegetable nugget product is the shape of the nugget, the flavor (taste and aroma) is predominantly vegetable, the weight of the nugget is 20-25 grams (large size), and the packaging material is made of vacuum plastic with a simple packaging design.

The level of attribute importance is the utility value of each attribute used as a parameter. The level of attribute importance is the average value of a particular factor from all stimuli resulting from the value of the attribute utility results of each respondent. The level of attribute importance is the level of preference or liking or consumer interest in the specified attribute. The Level of Importance of

Vegetable Nugget Product Attributes can be seen in Table 6. This value is most considered by consumers in terms of the level of attribute importance. Table 4 produces values from the highest to the lowest levels.

Table 5: Total utility.

Card ID	Product Configuration	Total Utility
1	Animal Shape, Dominant Content Variants, 15-20 grams (medium), Vacuum Plastic, Simple Design	4.533
2	Animal Shape, Dominant Vegetables, 20-25 grams (large), Laminated Cardboard, Variative Design	4.692
3	Animal Shape, Dominant Vegetables, 20-25 grams (large), Vacuum Plastic, Simple Design	4.778
4	Animal Shape, Dominant Content Variants, 20-25 grams (Large), Laminated Cardboard, Simple Design	4.279
5	Animal Shape, Dominant Content Variants, 20-25 grams (Large), Vacuum Plastic, Variative Design	4.581
6	Dimension Cut, Dominant Vegetables, 15-20 grams (medium), Laminated Cardboard, Simple Design	4.130
7	Animal Shape, Dominant Content Variants, 15-20 grams (medium), Laminated Cardboard, Variative Design	4.447
8	Alphabet Pieces, Dominant Vegetables, 15-20 grams (medium), Vacuum Plastic, Variative Design	4.560

Source: Authors, (2025).

Table 6: Importance level of vegetable nugget atributes.

Attributes	Attributes Importance Level (%)
Shape	36.26
Flavor (Taste and Aroma)	17.84
Weight per piece	17.74
Packaging Materials	13.64
Packaging Design	14.51

Source: Authors, (2025).

Based on the results of the conjoint analysis, a relative importance value was obtained, which indicates the level of importance of each attribute. The greater the importance value of an attribute indicates the greater influence of the attribute in determining consumer preferences, and conversely, a low importance value indicates that the attribute is relatively less considered. Table 5 shows that the most considered attributes are nugget shape, flavor (taste and aroma), weight per piece (size), nugget packaging design, and nugget packaging material. The most important attribute of vegetable nuggets to respondents is the shape of the nugget, which is shown by a percentage of 36.26%. The second most important attribute of vegetable nuggets is flavor (taste and aroma), which is shown by a percentage of 17.84%. The third most important attribute of vegetable nuggets is the weight per piece (size) of the nugget, which is shown by a percentage of 17.74%. This is followed by the attributes of packaging design and packaging materials which received the lowest importance values, namely 14.51% and 13.64%, respectively, indicating that both attributes are relatively considered by respondents.

Consumer Preferences for Selected Attributes and Levels

Consumer preferences can be interpreted as a person's choice of likes or dislikes for a product or service. Based on the results of the analysis using the conjoint method, the results of respondent preferences for the design attributes of vegetable nuggets are obtained, which can be seen in Table 7. The selected level is consumer preference, seen from the utility with a positive value. Respondents' preferences for vegetable nugget products include several attributes, namely the shape of the nugget with animal pieces, a flavor (taste and aroma) with a dominant vegetable, the weight of the nugget per piece is 20-25 grams or large, vacuum plastic packaging, and packaging with a variety of designs.

Table 7: Consumer Preferences.

Attributes (Importance)	Utilities	Level	Preference
Shape (36,26)	0.150	Animal Shape	Animal Shape
	-0.107	Dimension Cut	
	-0.043	Alphabet Pieces	
Flavor (Taste and Aroma) (17,84)	0.04	Dominant Vegetables	Dominant Vegetables
	-0.04	Dominant Content Variants	
Weight per piece (17,74)	-0.082	15-20 grams (medium)	20-25 grams
	0.082	20-25 grams (large)	
Packaging Materials (13,64)	0.113	Vacuum Plastic	Vacuum Plastic
	-0.113	Laminated Cardboard	
Packaging Design (14,51)	-0.07	Simple Design	Variative Design
	0.07	Variative Design	

Source: Authors, (2025).

This is when compared with the research results of [25], the attributes wanted by consumers in purchasing instant noodles, including the level of the shape attribute chosen is noodles in a round shape, this shows that consumers prefer a shape that is more familiar to consumers, namely a round shape. The level of the taste attribute chosen is noodles with a savory taste. Consumers can sometimes consume instant noodles without having to cook them first. The level of the size attribute chosen is the size of noodles with a large size of 100 grams because most consumers consider 100 grams to be the right size when consumed. The level of the packaging material attribute chosen by consumers is plastic packaging material. This is because plastic packaging material is more familiar among consumers and is simpler in the storage process.

In contrast to the research results of [26] and [10] which stated that taste is a key indicator of food product performance, in this research, the taste attribute is ranked second after shape. Implementation of packaging factors according to the research results of [8] is adjusted to consumer preferences by making the packaging design more attractive and adding product information attributes such as expiration date, storage and presentation methods, product images, and application of bright colors.

Consumer Preferences for Stimulus Configurations

According to [27] consumer behavior towards certain goods can be analyzed through the theory of utility. Utility is the satisfaction obtained by someone in consuming a certain good. The higher the satisfaction obtained in consuming a certain good, the higher the utility value of the good. The value of the total utility is used to see the configuration and level of attributes most preferred by consumers of vegetable nuggets. The total utility value in Table 8, describes the most preferred choice by respondents from the 8 (eight) stimulus configurations offered. The highest total utility value indicates the configuration that consumers prefer the most, and the lowest total utility value indicates the configuration that respondents dislike the most regarding vegetable nugget attributes.

Table 8: Consumers' Most Preferred Stimulus Configuration (Total Utility Value).

Card ID	Product Configuration	Total Utility	Ranking
1	Animal Shape, Dominant Content Variants, 15-20 grams (medium), Vacuum Plastic, Simple Design	4.533	5
2	Animal Shape, Dominant Vegetables, 20-25 grams (large), Laminated Cardboard, Variative Design	4.692	2
3	Animal Shape, Dominant Vegetables, 20-25 grams (large), Vacuum Plastic, Simple Design	4.778	1
4	Animal Shape, Dominant Content Variants, 20-25 grams (Large), Laminated Cardboard, Simple Design	4.279	7
5	Animal Shape, Dominant Content Variants, 20-25 grams (Large), Vacuum Plastic, Variative Design	4.581	3
6	Dimension Cut, Dominant Vegetables, 15-20 grams (medium), Laminated Cardboard, Simple Design	4.130	8
7	Animal Shape, Dominant Content Variants, 15-20 grams (medium), Laminated Cardboard, Variative Design	4.447	6
8	Alphabet Pieces, Dominant Vegetables, 15-20 grams (medium), Vacuum Plastic, Variative Design	4.560	4

Source: Authors, (2025).

Based on Table 8, the most preferred attribute configuration or the number one ranking of respondents' choices is the ID card configuration number 3, namely the design of the nugget product with the shape of animal cut nuggets, dominant vegetable flavor, nugget weight of 20-25 grams (large size), vacuum plastic packaging material, and simple packaging design. The least preferred configuration or the last ranking of respondents' choices is configuration number 4, namely the shape of the nugget cut dimensions, the dominant flavor of the content variant, a nugget weight of 15-20 grams (medium size), packaging material of laminated cardboard, and simple packaging design. Therefore, it can be said that the configuration of the highest attribute levels above can produce the highest preference which can provide the highest utility for consumers towards vegetable nugget products.

IV.4 VALUE ANALYSIS

The ratio of any product variant's advantages to its manufacturing costs is known as the product value. The overall utility value of each product variant based on conjoint analysis is what is meant by product benefits. The cost of the manufacturing process for every product variation is also known as the production cost.

The calculation of product value is based on Equation (2). The total utility and cost production of each product configuration is shown in Table 9. The results of the product value analysis are shown in Figure 2.

Table 9: Total utility and cost production.

Card ID	Product Configuration	Total Utility	Cost (IDR)
1	Animal Shape, Dominant Content Variants, 15-20 grams (medium), Vacuum Plastic, Simple Design	4.533	52,500
2	Animal Shape, Dominant Vegetables, 20-25 grams (large), Laminated Cardboard, Variative Design	4.692	42,500
3	Animal Shape, Dominant Vegetables, 20-25 grams (large), Vacuum Plastic, Simple Design	4.778	42,500
4	Animal Shape, Dominant Content Variants, 20-25 grams (Large), Laminated Cardboard, Simple Design	4.279	51,500
5	Animal Shape, Dominant Content Variants, 20-25 grams (Large), Vacuum Plastic, Variative Design	4.581	53,500
6	Dimension Cut, Dominant Vegetables, 15-20 grams (medium), Laminated Cardboard, Simple Design	4.130	41,500
7	Animal Shape, Dominant Content Variants, 15-20 grams (medium), Laminated Cardboard, Variative Design	4.447	52,500
8	Alphabet Pieces, Dominant Vegetables, 15-20 grams (medium), Vacuum Plastic, Variative Design	4.560	43,500

Source: Authors, (2025).

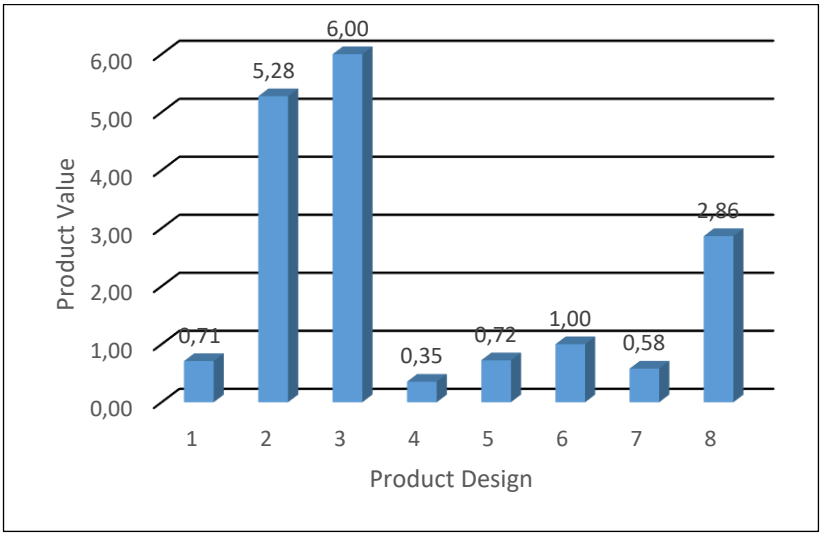

Figure 2: Product value.
Source: Authors, (2025).

The results of the study indicate that the configuration of the highest attribute levels produces selected preferences that can provide the highest utility for consumers of vegetable nuggets. In addition, it will be the right basis for producers or entrepreneurs to set strategies in marketing vegetable nugget products. The use of consumer preferences can capture the right product attributes. The implementation of conjoint analysis accommodates more details of each consumer's desire for a product. Conjoint analysis is also able to analyze the creation of value for consumers, assist in decisions to choose product designs that are considered optimal, and build strategic policies in marketing.

However, to realize the selected product must consider the production cost. Based on Figure 2, the product that has the highest value is Card ID 3. This product design has the highest total utility but with adequate production costs. The product design configuration of Card ID 3 has a product value of 6.00.

IV.5 PRODUCT MANIFESTATION

Based on the product value for each product design (Table 8), the product design that has the highest product value is the Card ID configuration number 3, namely the nugget product design with the shape of the animal shape, dominant vegetables, nugget weight of 20-25 grams (large size), vacuum plastic packaging material, and simple packaging design. The product design with the lowest product value is the Card ID configuration number 4, namely the animal shape, dominant content variants, nugget weight of 20-25 grams (large size), packaging material of laminated cardboard, and simple packaging design. The product design that has the highest value is realized by the processing of vegetable nuggets. Based on the result of the chemical test, the selected vegetable nugget products have a nutritional content of 34.02% water content, 0.35% ash content, 14.64% protein content, 4.05% fat content, and 46.73% carbohydrate content. This nutritional content has met the Indonesian National Standard for nugget products, namely a maximum water content of 60%, a minimum protein content of 12%, and a maximum fat content of 20% [28]. The results of the organoleptic test showed that all respondents liked the selected vegetable nugget products based on the parameters of taste, aroma, color, and texture.

V. CONCLUSIONS

The results of the conjoint analysis show that the order of attributes that can influence consumer preferences for vegetable nugget product design are nugget shape, nugget flavor (taste and aroma), nugget weight per piece (size), packaging material, and packaging design. The order of attribute levels is animal pieces, dominant vegetables, weight 20-25 grams (large), vacuum plastic, and varied designs. The configuration of vegetable nugget product design that suits consumer preferences based on the highest-ranking results is the configuration of stimulus card number 3 with the composition of the vegetable nugget product design configuration in the form of animal pieces, flavor (taste and aroma) that is dominant in vegetables, nugget weight per piece of 20-25 grams (large), vacuum plastic packaging material and simple or simple packaging design. The selected design has the following nutritional content: 34.02% water content, 0.35% ash content, 14.64% protein content, 4.05% fat content, and 46.73% carbohydrate content.

VI. AUTHOR'S CONTRIBUTION

Conceptualization: Endang Retno Wedowati, Diana Puspitasari and Fungki Sri Rejeki.
Methodology: Endang Retno Wedowati and Tri Rahayuningsih.
Investigation: Diana Puspitasari, Fungki Sri Rejeki and Johan Paing Heru Waskito.
Discussion of results: Endang Retno Wedowati, Diana Puspitasari and Fungki Sri Rejeki.
Writing – Original Draft: Endang Retno Wedowati and Tri Rahayuningsih.
Writing – Review and Editing: Endang Retno Wedowati, Diana Puspitasari and Fungki Sri Rejeki.
Resources: Endang Retno Wedowati, Tri Rahayuningsih and Johan Paing Heru Waskito.
Supervision: Fungki Sri Rejeki and Johan Paing Heru Waskito.
Approval of the final text: Endang Retno Wedowati, Diana Puspitasari, Fungki Sri Rejeki, Tri Rahayuningsih and Johan Paing Heru Waskito.

VII. ACKNOWLEDGMENTS

Gratitude is expressed to Universitas Wijaya Kusuma Surabaya, which has provided funding for this activity through the Internal Research Grant Program with contract number 8/LPPM/UWKS/III/2024.

VIII. REFERENCES

[1] J. D. Frutos and D. Borenstein, "A framework to support customer-company interaction in mass customization environments," Comput. Ind., vol. 54, pp. 115–135, 2004.

[2] R. Akkerman and D. P. Van Donk, "Product mix variability with correlated demand in two-stage food manufacturing with intermediate storage," Int. J. Prod. Econ., vol. 121, no. 2, pp. 313–322, 2009, doi: 10.1016/j.ijpe.2006.11.021.

[3] R. I. McIntosh, J. Matthews, G. Mullineux, and A. J. Medland, "Late customisation: issues of mass customisation in the food industry," Int. J. Prod. Res., vol. 48, no. 6, pp. 1557–1574, Mar. 2010, doi: http://dx.doi.org/10.1080/00207543.2012.693963.

[4] A. N. Utama and G. Anjani, "Substitusi isolat protein kedelai pada daging analog kacang merah (Phaseolus vulgaris L.)," J. Nutr. Coll., vol. 5, no. 4, p. 402, 2016, [Online]. Available: http://ejournal-s1.undip.ac.id/index.php/jnc

[5] M. Astawan, Sehat dengan Hidangan Kacang dan Biji-bijian, First. Jakarta: Penebar Swadaya, 2009.

[6] Akantu et al., "Preferensi Konsumen Terhadap Produk Nugget Ayam di Kecamatan Kota Selatan Kota Gorontalo Consumer Preferences for Chicken Nugget Products in Kota Selatan District, Gorontalo City," Jambura J. Trop. Livest. Stud. vol. 1, no. 1, pp. 16–24, 2023.

[7] A. P. K. Ikhsanu, L. A. Manafe, and M. A. Masyhuri, "Preferensi Konsumen dalam Membeli Produk Frozen Food," J. Akunt. Bisnis dan Ekon., vol. 9, no. 2, pp. 3435–3444, 2023, doi: 10.33197/jabe.vol9.iss2.2023.1122.

[8] C. R. Rahardjo, "Faktor yang menjadi preferensi konsumen dalam membeli produk frozen food," PERFORMA J. Manaj. dan Start-Up Bisnis, vol. 1, no. 1, pp. 32–43, 2016.

[9] E. R. Wedowati, M. L. Singgih, and I. K. Gunarta, "A study of consumer preferences customized product design," in MATEC Web of Conferences 204, 2018, vol. 01002, pp. 1–7. doi: https://doi.org/10.1051/matecconf/201820401002.

[10] E. R. Wedowati, M. L. Singgih, and I. K. Gunarta, "Determination of modules in pleasurable design to fulfil customer requirements and provide a customized product in the food industry," Designs, vol. 4, no. 7, pp. 1–21, 2020, doi: 10.3390/designs4010007.

[11] E. R. Wedowati, M. L. Singgih, and I. K. Gunarta, "Product value analysis on customized product based on pleasurable design and time-driven activity-based costing in food industry," Cogent Bus. Manag., vol. 7, no. 1, pp. 1–22, 2020, doi: 10.1080/23311975.2020.1823581.

[12] T. Seifert et al., "Multivariate risk analysis of an intensified modular hydroformylation process," Chem. Eng. Process. Process Intensif., vol. 95, pp. 124–134, 2015, doi: 10.1016/j.cep.2015.05.010.

[13] J. Espejel, C. Fandos, and C. Flavián, "The role of intrinsic and extrinsic quality attributes on consumer behaviour for traditional food products," 2007, doi: 10.1108/09604520710835000.

[14] R. Iop, S.C.F.; Teixeira, E.; Deliza, "Consumer research : extrinsic variables in food studies," Br. Food J., vol. 108, no. 11, pp. 894–903, 2006.

[15] M. Hersleth, E. Monteleone, A. Segtnan, and T. Næs, "Effects of evoked meal contexts on consumers ' responses to intrinsic and extrinsic product attributes in dry-cured ham," FOOD Qual. Prefer., vol. 40, pp. 191–198, 2015, doi: 10.1016/j.foodqual.2014.10.002.

[16] P. Y. Lee, K. Lusk, M. Mirosa, and I. Oey, "An attribute prioritization-based segmentation of the Chinese consumer market for fruit juice," FOOD Qual. Prefer., vol. 46, pp. 1–8, 2015, doi: 10.1016/j.foodqual.2015.06.016.

[17] M. C. D. Verain, S. J. Sijtsema, and G. Antonides, "Consumer segmentation based on food-category attribute importance : The relation with healthiness and sustainability perceptions," Food Qual. Prefer., vol. 48, pp. 99–106, 2016, doi: 10.1016/j.foodqual.2015.08.012.

[18] T. Nishimura et al., "Phytosterols in onion contribute to a sensation of lingering of aroma , a koku attribute," Food Chem., vol. 192, pp. 724–728, 2016, doi: 10.1016/j.foodchem.2015.06.075.

[19] J. P. H. Waskito, E. R. Wedowati, F. S. Rejeki, and E. Wahyuningtyas, "Food product design with Wijaya Kusuma character based on pleasurable design," Int. J. Eng. Sci. Inf. Technol., vol. 2, no. 1, pp. 1–8, 2021, doi: 10.52088/ijesty.v2i1.193.

[20] P. Kotler and K. L. Keller, Marketing Management, 15th Globa. London: Pearson Education, Inc., 2016.

[21] C. H. Wang and C. W. Shih, "Integrating conjoint analysis with quality function deployment to carry out customer-driven concept development for ultrabooks," Comput. Stand. Interfaces, vol. 36, no. 1, pp. 89–96, 2013, doi: 10.1016/j.csi.2013.07.010.

[22] C. H. Wang, "Integrating Kansei engineering with conjoint analysis to fulfil market segmentation and product customisation for digital cameras," Int. J. Prod. Res., vol. 53, no. 8, pp. 2427–2438, 2015, doi: 10.1080/00207543.2014.974840.

[23] S. S. Nielsen, Food Analysis Laboratory Manual, Third Edit. Switzerland: Springer Nature, 2019. doi: 10.1007/978-3-319-44127-6.

[24] P. R. D. McCullough, "A User's Guide to Conjoint Analysis," Marketing research magazine, vol. 14, no. 2, pp. 18–23, 2002.

[25] A. Mulyadi and E. Fauziyah, "Preferensi Konsumen Dalam Pembelian Mi Instan Di Kabupaten Bangkalan," Agriekonomika, vol. 3, no. 1, pp. 65–80, 2014.

[26] S. De Pelsmaeker, J. J. Schouteten, S. Lagast, K. Dewettinck, and X. Gellynck, "Is taste the key driver for consumer preference? A conjoint analysis study," Food Qual. Prefer., vol. 62, pp. 323–331, 2017, doi: 10.1016/j.foodqual.2017.02.018.

[27] W. Bangun, Teori Ekonomi Mikro, IV. Bandung: PT Refika Aditama, 2015.

[28] Anonymous, “Petunjuk Teknis Skema Sertifikasi Produk Naget Ayam,” Peraturan Badan Standardisasi Nasional Republik Indonesia Nomor 6 Tahun 2019 Tentang Skema Penilaian Kesesuaian Terhadap Standar Nasional Indonesia Sektor Pangan. Badan Standarisasi Nasional Republik Indonesia, Jakarta, pp. 1097–11110, 2019.

Journal of Engineering and Technology for Industrial Applications

ISSN ONLINE: 2447-0228

ITEGAM-JETIA

Manaus, v.11 n.54, p. 58-64. July/August., 2025.
DOI: https://doi.org/10.5935/jetia. v11i54.1709

RESEARCH ARTICLE OPEN ACCESS

AN ENHANCED DISTRIBUTION SYSTEM PERFORMANCE WITH OPTIMIZATION TECHNIQUES FOR LOCATION OF ELECTRICAL VEHICLE CHARGING STATIONS

Sainadh Singh Kshatri[1], Venkata Anjani Kumar G[2], Chilakapati Lenin Babu[3],Palepu Suresh Babu[4]

[1]Associate Professor, Department of EEE, B V Raju Institute of Technology, Narsapur, Hyderabad, India.
[2]Assistant Professor,Department of EEE, Rajiv Gandhi University of Knowledge Technologies-Ongole, Ongole, Andhra Pradesh, India
[3] Research Scholar, Department of EEE, Sri Venkateswara University, Tirupati, Andhra Pradesh
[4] Assistant Professor,Department of EEE, Annamacharya University – Rajampet, Andhra Pradesh, India.

[1]https://orcid.org/0000-0003-2357-0180, [2]http://orcid.org/0009-0004-3111-0525
[3]http://orcid.org/0000-0001-9749-979X, [4]http://orcid.org/0000-0001-5786-1395

Email: sainadhsingh@gmail.com ,anjishelectrical@gmail.com , ch.leninbabusvu@gmail.com , sureshram48@gmail.com

ARTICLE INFO

Article History
Received: March 14, 2025
Revised: April 20, 2025
Accepted: June 15, 2025
Published: July 31, 2025

Keywords:
Electric Vehicles,
Charging Stations,
Distribution System,
Grey Wolf Optimization,
Voltage Profile.

ABSTRACT

This study introduces a novel strategy for strategically placing of Electric Vehicle Charging Stations (EVCS) within a distribution power network towards minimizing power losses. The proposed methodology leverages the Grey Wolf Optimization (GWO) metaheuristic algorithm, enthused by the grey wolves hunting, to identify the most strategic locations for EVCSs. The effectiveness of the GWO-based approach is rigorously evaluated using the IEEE-33 bus system, a standard benchmark in distribution system analysis. The GWO algorithm's performance is evaluated in comparison to that of the prevalent Particle Swarm Optimization (PSO) methodology. The study analyzes system voltage levels in relation to the nominal voltage, ensuring compliance with operational limits. The results demonstrate the GWO algorithm's superiority in minimizing power losses and enhancing voltage profiles across the distribution network. Furthermore, a probabilistic assessment is conducted to evaluate the robustness of the optimal EVCS placement under uncertain EV charging patterns. This analysis considers the stochastic nature of EV charging behavior, providing insights into the strategy's resilience to real-world variations. The proposed GWO-based optimization strategy offers a significant contribution to make power distribution infrastructure more dependable and efficient in order to handle the growing number of EVs. By minimizing power losses and optimizing voltage profiles, the strategy reduces operational costs and improves the overall stability of the grid. The probabilistic assessment further strengthens the strategy's practicality by accounting for the inherent uncertainties in EV charging demands. This research provides valuable insights for distribution system operators and planners seeking to integrate EVCSs effectively while maintaining system performance.

Copyright ©2025 by authors and Galileo Institute of Technology and Education of the Amazon (ITEGAM). This work is licensed under the Creative Commons Attribution International License (CC BY 4.0).

I. INTRODUCTION

The increasing global adoption of electric vehicles presents both opportunities and challenges for power distribution systems. While EVs offer a cleaner and more sustainable transportation alternative, their integration into the existing grid infrastructure necessitates attentive scheduling and supervision to guarantee system stability and efficiency [1], [2]. Uncoordinated EV charging may lead towards augmented power losses, voltage deviations, and potential overloads, jeopardizing the reliability of the supply network. Therefore, strategical placement of EV charging stations is crucial for mitigating these challenges and maximizing the benefits of EV integration [3-5]. The optimal placement of EVCSs is a complex optimization problem with multiple conflicting objectives [6], [7]. Minimizing power losses is a primary concern, as it directly impacts the operational efficiency and cost-effectiveness of the distribution system. Maintaining

voltage profiles within acceptable limits is equally critical to ensure the proper functioning of electrical equipment and prevent voltage-related issues. Furthermore, the stochastic nature of EV charging patterns introduces uncertainty into the optimization process, requiring robust solutions that can accommodate variations in charging demand [8], [9].

Traditional approaches to EVCS placement every so often bank on simplified assumptions and deterministic illustrations, which mayn't accurately reflect the dynamic and uncertain sort of real-world EV charging behavior. These methods may lead to suboptimal solutions that fail to adequately address the challenges of EV integration. Therefore, advanced optimization techniques are needed to effectively determine the most strategic locations for EVCSs, considering both system constraints and the probabilistic nature of EV charging demands [10-12]. In several branches of engineering, metaheuristic algorithms have become indispensable for tackling difficult optimization issues. These algorithms, inspired by natural processes such as biological evolution or animal behavior, offer several advantages over traditional methods. They excel at solving the complicated problem of EVCS placement optimization because they can access a larger solution space and avoid local optima [13]. Among these algorithms, the Grey Wolf Optimizer (GWO) has gained significant attention due to its effectiveness and simplicity [14].

The GWO algorithm takes its cues from wolf packs and their cooperative hunting tactics and social order. In its population-based search method, the algorithm considers all possible solutions to the optimization issue. Through iterative updates and information sharing among individuals, the algorithm converges towards the optimal solution [15]. The GWO algorithm has demonstrated promising results in various optimization applications, including power system optimization, and its application to EVCS placement offers a novel and effective approach [16], [17]. This study proposes an optimal strategy for placing EVCSs within a power distribution system using the GWO algorithm. The objective is to keep voltage profiles within acceptable bounds while minimizing power losses. The IEEE-33 bus system, a broadly used benchmark for distribution system studies, is employed to validate the efficacy of the proposed methodology. There is a thorough comparison between the GWO-based method's performance and the outcomes produced by the PSO algorithm, a well-established optimization technique commonly used in power system analysis [18-20]. The study also includes a comparative analysis between the system voltage levels and the nominal voltage, ensuring compliance with operational standards. Additionally, a probabilistic assessment of the optimal EVCS placement is conducted, considering uncertainties in EV charging patterns. This analysis incorporates the stochastic nature of EV charging behavior, providing insights into the robustness of the proposed strategy under real-world conditions. The following are some of the study's contributions:

- Development of an optimal EVCS placement strategy using the GWO algorithm to minimize power losses and enhance voltage profiles.
- Comparative analysis of the GWO algorithm's performance against the PSO algorithm on the IEEE 33 bus system.
- Evaluation of system voltage levels in relation to the nominal voltage to ensure operational compliance.
- Probabilistic assessment of the optimal EVCS placement considering uncertainties in EV charging patterns.

Here is, the rest of the paper is oriented: The proposed GWO algorithm and the system modelling technique are described in full in Section 3. In Section, the consequences of findings and comparisons from the simulation are detailed. The conclusion and its implications meant for forthcoming studies are summarized in Section 5.

II. MATERIALS AND METHODS

II.1 GREY WOLF OPTIMIZATION

This section elucidates the utilization of the Grey Wolf Optimization (GWO) algorithm to pinpoint the strategic location of EVCS within the power distribution network. The Grey Wolf Optimizer is a metaheuristic optimization technique mimicking the hierarchical hunting behavior of Grey Wolves. As illustrated in Figure 1, the algorithm categorizes the wolf population into four distinct groups [21].

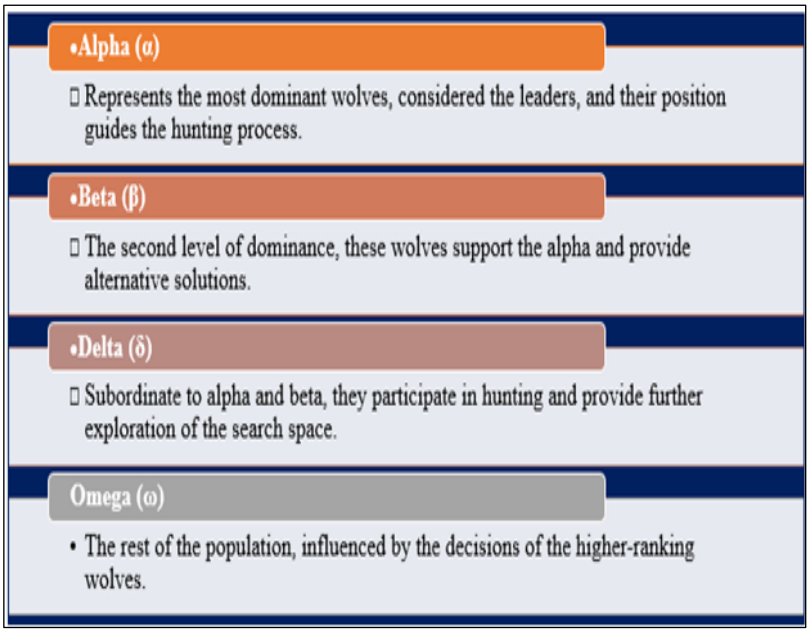

Figure 1: Classification of Wolf Population.
Source: Authors, (2025).

The Grey Wolf Optimizer initiates its search with a randomly generated population of solutions, representing the wolves. These wolves' positions are iteratively updated, guided by the spots of the Alpha, Beta, and Delta wolves—mirroring the pursuit of prey, which symbolizes the optimal solution. This iterative hunt continues up to a predefined end criterion is contented [22]. The GWO progression is visually depicted in the following flowchart in Figure 2.

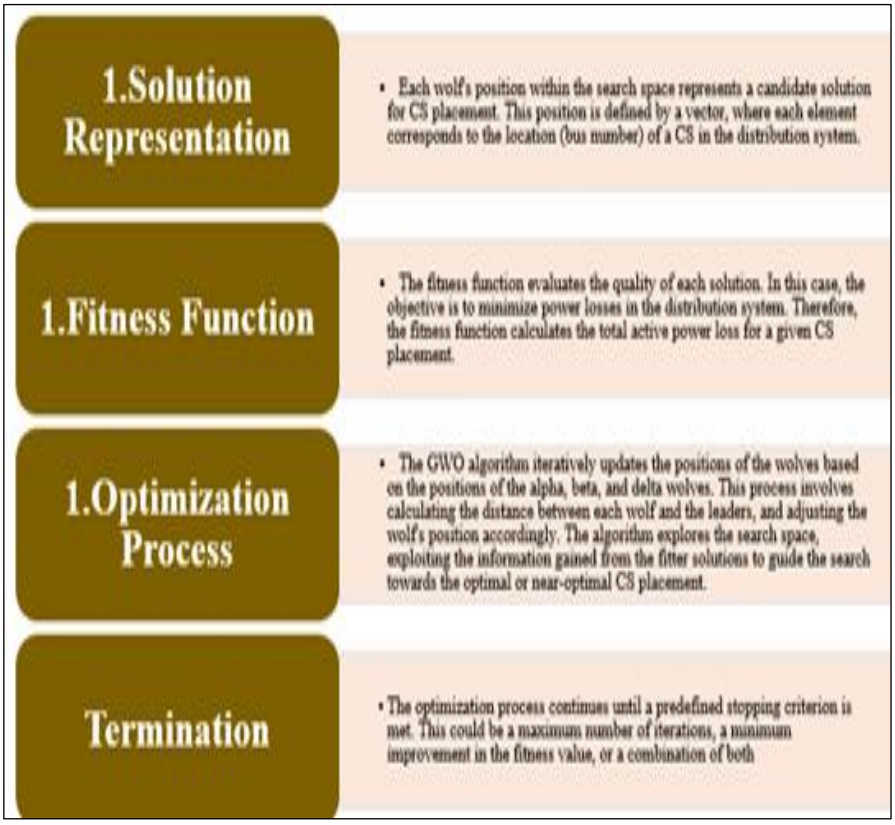

Figure 2: GWO Flow Chart.
Source: Authors, (2025).

II.2 TEST CASE SYSTEM

The IEEE-33 bus test system is employed in this study as given away in Figure 3 to validate the proposed GWO-based optimal charging station placement strategy. This system, with its characteristic radial structure typical of distribution networks, serves as a benchmark for evaluating distribution system planning and optimization algorithms [23]. A fixed system load, derived from standard IEEE-33 bus data, is assumed. EV charging stations are modelled as additional loads at designated buses. Newton-Raphson Power flow analysis method determines system losses and voltage profiles for various charging station placement configurations [24], [25].

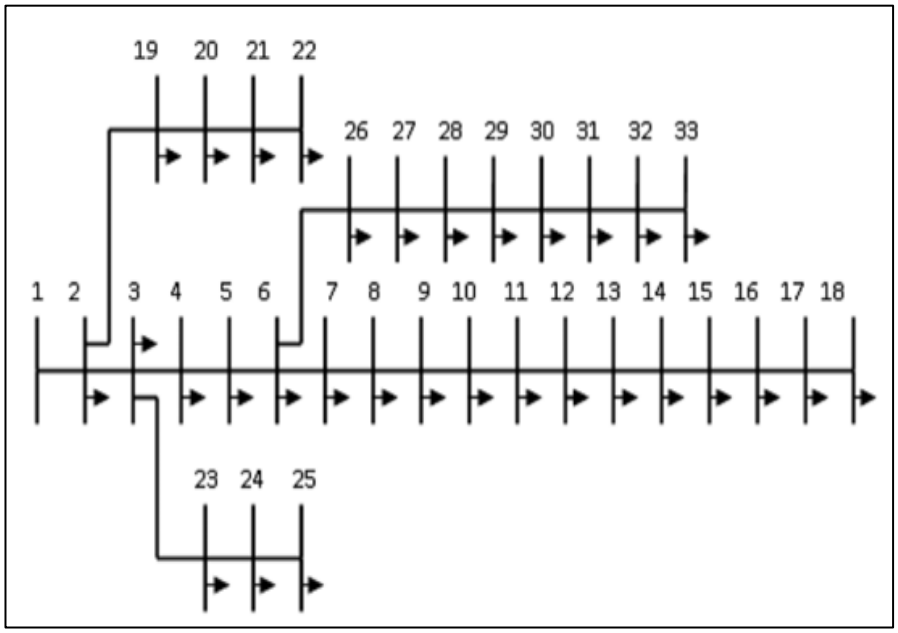

Figure 3: IEEE-33 Bus System.
Source: Authors, (2025).

IV. RESULTS AND DISCUSSIONS

IV.1 SYSTEM VOLTAGES PROFILE

A complete assessment of the simulation results produced by using the suggested GWO-based method for the IEEE-33 Bus test system's optimum EV charging station placement is provided in this part. The calculated loss sensitivity factor (LSF) for this system are shown in Figure 4.

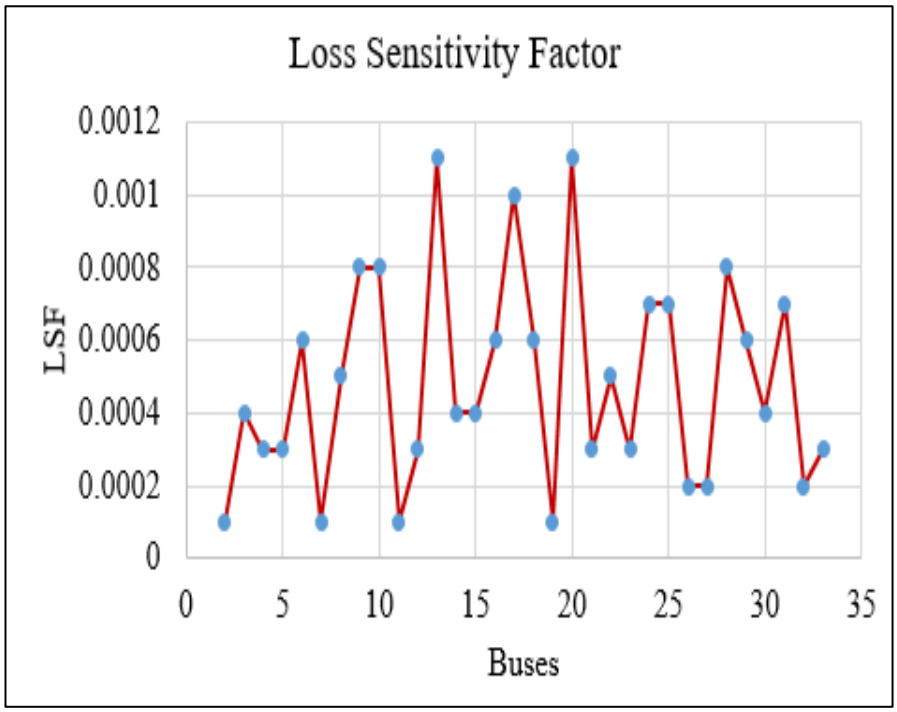

Figure 4: Calculated LSF for IEEE-33 Bus System.
Source: Authors, (2025).

The Figure 5 below compares the system voltage against the nominal voltage of the IEEE-33 bus system under general operating conditions.

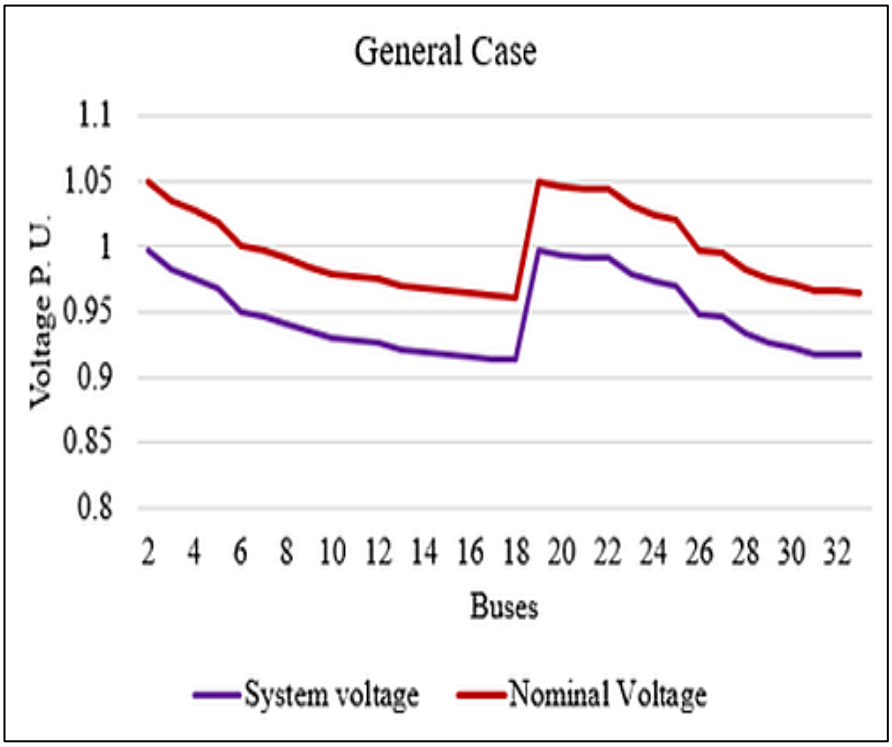

Figure 5: Voltages Profiles of the System – General Case.
Source: Authors, (2025).

From the Figure 5, it can be seen that a consistent trend between the system's voltage and the nominal voltage expressed in Per Unit (P.U). For a more detailed voltage profile analysis, Figures 6 and 7 illustrate the system and nominal voltages obtained using the PSO and GWO optimization algorithms, respectively.

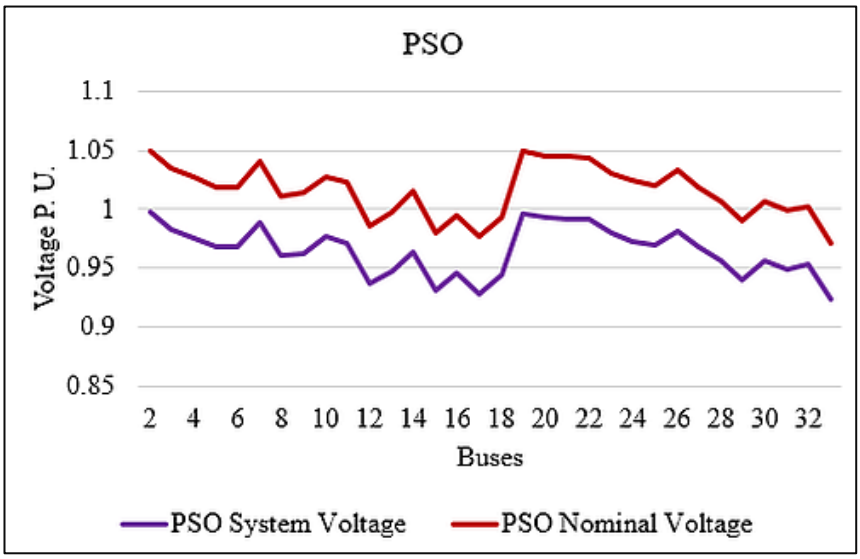

Figure 6: Voltages Profiles of the System with PSO.
Source: Authors, (2025).

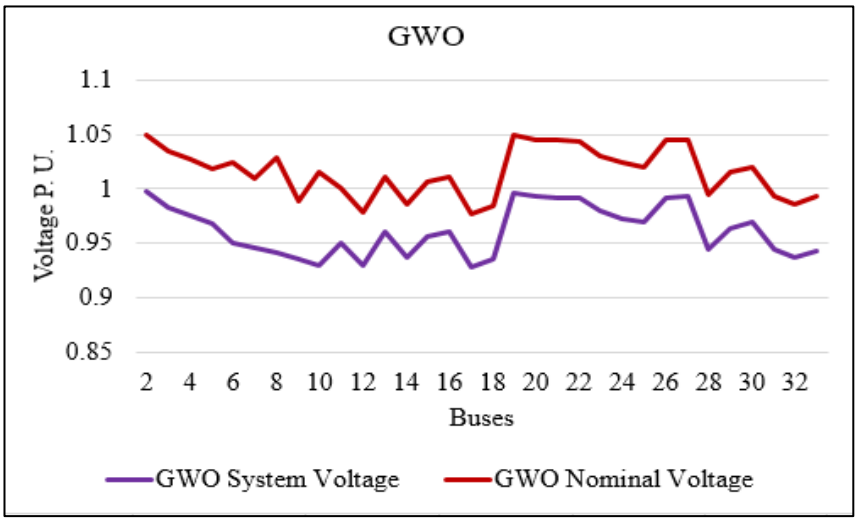

Figure 6: Voltages Profiles of the System with GWO.
Source: Authors, (2025).

Figures 6 and 7 indicate that the GWO algorithm surpasses the PSO algorithm in optimizing the system voltage profile. Turning to the probabilistic aspect, Figure 8 shows the probability of EV presence at each bus in the IEEE-33 Bus system.

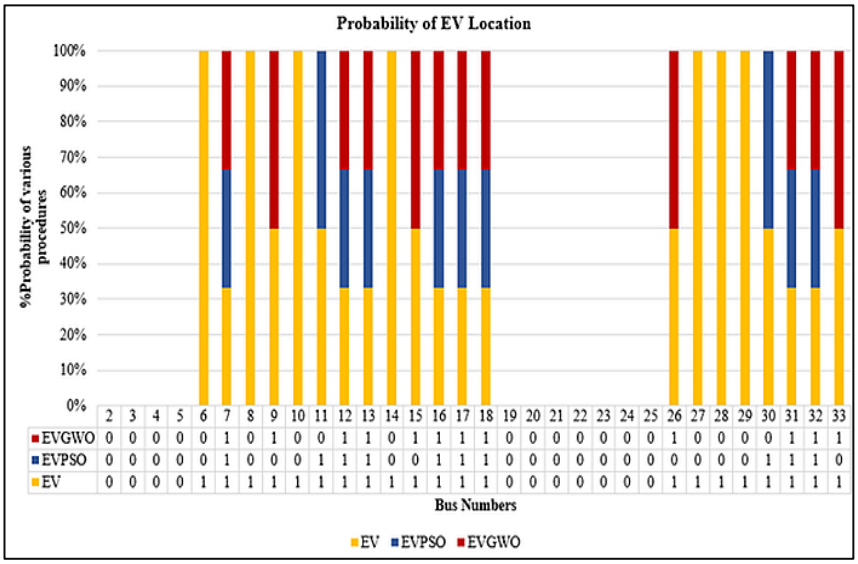

Figure 7: Probability of EV location.
Source: Authors, (2025).

With Bus 1 designated as the slack bus, analysis of the results reveals the following EV placement outcomes:

- General Case: EVs are distributed across 21 buses: 6, 7, 8, 9, 10, 11, 12, 13, 14, 15, 16, 17, 18, 26, 27, 28, 29, 30, 31, 32 and 33.
- PSO Optimization: EVs are strategically placed at 10 buses: 7, 11, 12, 13, 16, 17, 18, 30, 31 and 33.
- GWO Optimization: EVs are positioned at 12 buses: 8, 9, 12, 13, 15, 16, 17, 18, 26, 31, 32 and 33.

These are tabulated as in Table 1 below.

Table 1: Strategic Placement of EVCS.

Comparison of EVCS Placement			
Bus No.	General Case	PSO	GWO
	6	7	8
	7	11	9
	8	12	12
	9	13	13
	10	16	15
	11	17	16
	12	18	17
	13	30	18
	14	31	26
	15	33	31
	16		32
	17		33
	18		
	26		
	27		
	28		
	29		
	30		
	31		
	32		
	33		

Source: Authors, (2025).

In all scenarios, the proposed GWO based EVCS placement strategy consistently exhibits superior performance.

V. CONCLUSIONS

This study introduced a strategic approach for optimizing EV charging station placement within a distribution system using the Grey Wolf Optimization algorithm. The primary objective was to minimalize power losses and maximize the overall system performance. Rigorous evaluation on the IEEE-33 bus test system demonstrated the GWO algorithm's superior performance compared to the Particle Swarm Optimization algorithm in minimizing losses and improving voltage profiles. The GWO-based approach effectively pinpointed optimal charging station locations, leading to enhanced voltage stability and reduced losses, eventually paying off to an added effective and reliable distribution system. Furthermore, probabilistic analysis showcased the proposed strategy's robustness under uncertain EV charging patterns. The identified locations remained optimal under various EV demand scenarios, confirming the practicality and effectiveness of this approach for real-world applications.

VI. AUTHOR'S CONTRIBUTION

Conceptualization: Sainadhsingh,Venkata Anjnai Kumar G,Lenin Babu,Suresh Babu
Methodology: Sainadh singh.
Investigation: Sainadh singh.
Discussion of results: Sainadh singh,Suresh Babu
Writing – Original Draft: Lenin Babu,Venkata Anjani Kumar G
Writing – Review and Editing: Lenin Babu,Venkata Anjani Kumar G
Resources: Lenin Babu,Venkata Anjani Kumar G
Supervision: Sainadhsingh,Venkata Anjnai Kumar G,Lenin Babu,Suresh Babu
Approval of the final text: Sainadhsingh,Venkata Anjnai Kumar G,Lenin Babu,Suresh Babu

VIII. REFERENCES

[1] H. M. Abdullah, A. Gastli, L. Ben-Brahim, and S. O. Mohammed, "Planning and Optimizing Electric-Vehicle Charging Infrastructure Through System Dynamics," IEEE Access, vol. 10, pp. 17495–17514, 2022. doi:10.1109/ACCESS.2022.3149944.

[2] M. Abdel-Basset, A. Gamal, I. M. Hezam, and K. M. Sallam, "Sustainability assessment of optimal location of electric vehicle charge stations: a conceptual framework for green energy into smart cities," Environ Dev Sustain, vol. 26, no. 5, pp. 11475–11513, May 2023, doi:10.1007/s10668-023-03373-z.

[3] M. S. Mastoi et al., "An in-depth analysis of electric vehicle charging station infrastructure, policy implications, and future trends," Energy Reports, vol. 8, pp. 11504–11529, Nov. 2022, doi: 10.1016/j.egyr.2022.09.011.

[4] N. Taormina and R. Ainpudi, “International Electric Vehicle Policies,” UFJUR, vol. 23, Oct. 2021, doi: 10.32473/ufjur.v23i.128716.

[5] R. P. Narasipuram and S. Mopidevi, “A technological overview & design considerations for developing electric vehicle charging stations,” Journal of Energy Storage, vol. 43, p. 103225, Nov. 2021, doi: 10.1016/j.est.2021.103225.

[6] F. Ahmad, A. Iqbal, I. Ashraf, M. Marzband, and I. Khan, “Optimal location of electric vehicle charging station and its impact on distribution network: A review,” Energy Reports, vol. 8, pp. 2314–2333, Nov.2022, doi: 10.1016/j.egyr.2022.01.180.

[7] F. Shoushtari, M. Talebi, and S. Rezvanjou, “Electric Vehicle Charging Station Location by Applying Optimization Approach,” International journal of industrial engineering and operational research, vol. 6, no. 1, pp. 1–15, Jan. 2024. https://bgsiran.ir/journal/ojs-3.1.1-4/index.php/IJIEOR/article/view/76

[8] D. Savio Abraham et al., “Electric Vehicles Charging Stations’ Architectures, Criteria, Power Converters, and Control Strategies in Microgrids,” Electronics, vol. 10, no. 16, p. 1895, Aug. 2021, doi: 10.3390/electronics10161895.

[9] D. Srinivas and M. Ramasekhara Reddy, “Optimal Placement of Electric Vehicle Charging Station by Considering Dynamic Loads in Radial Distribution System,” in 2022 International Conference on Automation, Computing and Renewable Systems (ICACRS), Pudukkottai, India: IEEE, Dec. 2022, pp. 212–217. doi: 10.1109/ICACRS55517.2022.10029303.

[10] S. Ray, K. Kasturi, S. Patnaik, and M. R. Nayak, “Review of electric vehicles integration impacts in distribution networks: Placement, charging/discharging strategies, objectives and optimization models,” Journal of Energy Storage, vol. 72, p. 108672, Nov. 2023, doi: 10.1016/j.est.2023.108672.

[11] L. Chilakapati and T Gowri Manohar “Microgrid power quality enhancement with adaptive control strategies: a literature survey,” Electrotechnical Review, vol. 1, no. 3, pp. 115–119, Mar. 2024, doi: 10.15199/48.2024.03.21.

[12] R. Bernal, D. Olivares, M. Negrete-Pincetic, and Á. Lorca, “Management of EV charging stations under advance reservations schemes in electricity markets,” Sustainable Energy, Grids and Networks, vol. 24, p. 100388, Dec. 2020, doi: 10.1016/j.segan.2020.100388.

[13] F. Ahmad, L. Al-Fagih, S. A. Qadir, and M. Khalid, “EV Charging Station Placement using Nature-Inspired Optimization Algorithms,” in 2023 International Conference on Power, Instrumentation, Energy and Control (PIECON), Aligarh, India: IEEE, Feb. 2023, pp. 1–6. doi: 10.1109/PIECON56912.2023.10085885.

[14] E. Dada, S. Joseph, D. Oyewola, A. A. Fadele, H. ChiRoma, and S. M. AbdulhamiD, “Application of Grey Wolf Optimization Algorithm: Recent Trends, Issues, and Possible Horizons,” Gazi University Journal of Science, vol. 35, no. 2, pp. 485–504, Jun. 2022, doi: 10.35378/gujs.820885.

[15] H. Pan, S. Chen, and H. Xiong, “A high-dimensional feature selection method based on modified Gray Wolf Optimization,” Applied Soft Computing, vol. 135, p. 110031, Mar. 2023, doi: 10.1016/j.asoc.2023.110031.

[16] F. Ahmad, A. Iqbal, I. Ashraf, M. Marzband, and I. Khan, “Placement of Electric Vehicle Fast Charging Stations using Grey Wolf Optimization in Electrical Distribution Network,” in 2022 IEEE International Conference on Power Electronics, Smart Grid, and Renewable Energy (PESGRE), Trivandrum, India: IEEE, Jan. 2022, pp. 1–6. doi: 10.1109/PESGRE52268.2022.9715842.

[17] S. G. Golive, B. Paramasivam, and J. Ravindra, “Optimal Location of EV Charging Stations in the Distribution System Considering GWO Algorithm,” IJST, vol. 17, no. 8, pp. 751–759, Feb. 2024, doi: 10.17485/IJST/v17i8.2044.

[18] M. Altaf et al., “PSO-based optimal placement of electric vehicle charging stations in a distribution network in smart grid environment incorporating backward forward sweep method,” IET Renewable Power Gen, vol. 18, no. 15, pp. 3173–3187, Nov. 2024, doi: 10.1049/rpg2.12916.

[19] Venkata Anjani Kumar G. and M. Damodar Reddy, "PSO Trained Feed Forward Neural Network Based SAPF for Power Quality Enhancement in Distribution Networks," International Journal of Electrical and Electronic Engineering & Telecommunications, Vol. 12, No. 4, pp. 279-287, July 2023. Doi: 10.18178/ijeetc.12.4.279-287

[20] V. A. K. G and M. D. Reddy, “Fuzzy and PSO tuned PI controller based SAPF for Harmonic Mitigation,” IJEER, vol. 11, no. 1, pp. 119–125, Mar. 2023, doi: 10.37391/ijeer.110116.

[21] A. Singh, M. Rizwan, and U. Nangia, “Grey Wolf Algorithm for Area-Wise Allocation of EV Charging Stations,” in 2024 IEEE Third International Conference on Power Electronics, Intelligent Control and Energy Systems (ICPEICES), Delhi, India: IEEE, Apr. 2024, pp. 1090–1095. doi: 10.1109/ICPEICES62430.2024.10719144.

[22] A. Dwivedi and S. Kakran, “Comparative Study of Optimal Location of Electrical Vehicle Charging Stations Using Different Algorithms,” in Electric Mobility and Hybrid Microgrid, vol. 1230, R. Dahiya, R. Kumar, and Shivam, Eds., Singapore: Springer Nature Singapore, 2024, pp. 75–85. doi: 10.1007/978-981-97-5951-4_7.

[23] N. K. Golla, S. K. Sudabattula, and V. Suresh, “Optimal Placement of Electric Vehicle Charging Station in Distribution System Using Meta-Heuristic Techniques,” MMEP, vol. 9, no. 1, pp. 60–66, Feb. 2022, doi: 10.18280/mmep.090108.

[24] S. Upadhyay, A. Bhargava, R. Tiwari, and V. Nagar, “Optimal Charging Schedule Coordination of Electric Vehicles by Using Grey Wolf Optimization Algorithm,” in 2024 IEEE Third International Conference on Power Electronics, Intelligent Control and Energy Systems (ICPEICES), Delhi, India: IEEE, Apr. 2024, pp. 365–370. doi: 10.1109/ICPEICES62430.2024.10719241.

[25] G, venkata anjani kumar, M, D. R., Chilakapati, L. B., & palepu, suresh. (2025). Performance Assessment of a Multi-Verse Optimizer-Based Solar-PV Inverter for Grid-ConnectedApplications. *ITEGAM-JETIA*, *11*(51),151-156. https://doi.org/10.5935/jetia.v11i51.1334

Journal of Engineering and Technology for Industrial Applications

ISSN ONLINE: 2447-0228

ITEGAM-JETIA

Manaus, v.11 n.54, p. 65-71. July/August., 2025.

DOI: https://doi.org/10.5935/jetia. v11i54.1519

RESEARCH ARTICLE OPEN ACCESS

THE GALILEO INSTITUTIONAL REPOSITORY AS AN INFORMATION STOCK IN THE TRAINING OF MASTERS AND DOCTORATES FOCUSED ON INDUSTRY 4.0 IN THE AMAZON

Luiz Fernando Correia de Almeida[1]

[1]Federal University of Amazonas.

[1]https://orcid.org/0000-0002-1145-1259

Email: luizfernanalmeida@gmail.com

ARTICLE INFO

Article History

Received: March 14, 2025

Revised: April 20, 2025

Accepted: June 15, 2025

Published: July 31, 2025

Keywords:

Institutional repository,
Industry 4.0,
Open science,
Amazon,
Graduate education,
Information management.

ABSTRACT

This article analyzes the role of the Galileo Institutional Repository (RIGalileo), maintained by the Institute of Technology and Education Galileo of the Amazon (ITEGAM), as a strategic informational repository aimed at supporting the training of master's and doctoral students aligned with the demands of Industry 4.0 in the Amazon region. The study integrates concepts from Information Science, Open Science, and knowledge management to demonstrate how institutional repositories—by collecting, preserving, and openly disseminating scientific output—contribute significantly to academic qualification and technological innovation in peripheral contexts. Employing a methodological approach based on institutional experience report and case study, the article outlines the development of the RI Galileo, analyzes its structure and content, and discusses its impact on enhancing the visibility of local scientific production, improving academic quality, strengthening collaborative networks, and fostering an informational culture rooted in open science. The findings suggest that RIGalileo already functions as a critical infrastructure for graduate education at ITEGAM, promoting integration between scientific knowledge, regional development, and digital transformation. Finally, the article highlights ongoing challenges such as institutional engagement, repository expansion, and technological sustainability, proposing recommendations for consolidating the repository as a permanent policy for information access and support to innovation in the Amazon.

Copyright ©2025 by authors and Galileo Institute of Technology and Education of the Amazon (ITEGAM). This work is licensed under the Creative Commons Attribution International License (CC BY 4.0).

I. INTRODUCTION

The digital transformation driven by Industry 4.0—marked by the integration of advanced technologies such as the Internet of Things, Artificial Intelligence, and automation—has brought new challenges to the training of high-level human resources. In the Amazon region, historically marked by regional asymmetries in science and education, it is strategic to strengthen the training of master's and doctoral graduates capable of meeting the demands of Industry 4.0 and contributing to local sustainable development. In this scenario, Open Science practices and information infrastructures, such as institutional repositories, emerge as important allies in democratizing access to knowledge and driving innovation.

This article analyzes the role of the Galileo Institutional Repository (RIGalileo), of the Galileo Institute of Technology and Education of the Amazon (ITEGAM), as an information repository that stores, preserves, and disseminates the institution's scientific production, directly supporting the training of master's and doctoral graduates focused on Industry 4.0 in the Amazon region. RIGalileo is a platform aligned with the principles of open science, offering free access to various types of academic content – books, coursework, dissertations, theses, articles, reports, and ITEGAM research and development documents [1]. By making this production openly available, the repository acts as a repository of critical knowledge for students and researchers, facilitating scientific communication and the construction of new knowledge.

Besides introducing the context of Industry 4.0 and its relationship with open science, the article discusses theoretical foundations of institutional repositories as information stocks and human resource development in the Amazon. Next, the adopted methodology is presented – an experience report with case study elements – and, in the results and discussion, the history of the creation of RI Galileo, its collections and quantitative data, as well as its qualitative impact on local academic education, are detailed. Finally, the concluding remarks highlight the challenges and prospects for consolidating the repository as an institutional information and education policy. The study prioritizes primary sources and literature by recognized Brazilian authors in the areas of Information Science, Education, and Technology, with special emphasis on contributions originating in the North/Amazon region, to critically support the analyses..

II. THEORETICAL REFERENCE

Institutional repositories (IR) are often described as digital libraries dedicated to storing, preserving, and disseminating an institution's intellectual output, ensuring free and long-term access to these materials. Within Brazilian Information Science, the metaphor of information stocks has been used to conceptualize the role of these repositories in knowledge management. According to Barreto (2014), contemporary society demonstrates an "information superstructure" composed of large data flows from the digital world (e.g., big data) linked to institutional information stocks [2]. These institutional stocks—processed, managed, and controlled for political and economic use—constitute an underlying "infotexture" that coexists with non-institutionalized data, together forming the basis of the current information ecosystem. In other words, repositories organize and retain selected, encoded, and classified information, directing it for immediate or future use, in a process of organizing strategically stored information stocks [2].

In the academic context, this informational repository function is related to institutional memory and scientific communication. IR emerged, in large part, to increase the visibility, accessibility, and impact of the scientific output of universities and research centers. As emphasized in the literature in this field, institutional repositories serve as scientific knowledge management tools in the academic environment, allowing theses, dissertations, articles, and other works to be available to all, without access barriers, thus maximizing their use and citation [3] [4]. In Brazil, the Brazilian Institute of Information in Science and Technology (IBICT) encouraged the creation of IR from the mid-2000s, aligned with the open access movement. Through the Brazilian Manifesto in Support of Open Access to Scientific Information [5], the importance of guaranteeing open access to academic publications and postgraduate work (theses and dissertations) was established as a strategy to democratize knowledge and improve scientific communication. Thus, institutional repositories consolidate themselves as true "stocks" of qualified information within the institution, integrating digital preservation and open access policies.

It is important to emphasize that these information stocks do not merely have a passive archiving value, but play an active role in generating new knowledge. By bringing together the scientific production of an academic community in one place, an IR facilitates literature reviews, the discovery of state-of-the-art research in a given field, and the identification of research gaps. Ultimately, it is a tool that enhances the institution's collective intelligence, as it promotes the internal and external circulation of ideas, stimulating collaboration and innovation. This perspective converges with knowledge management concepts in organizations: IR, as an explicit knowledge base, supports organizational learning processes and the creation of interorganizational knowledge. In the context of master's and doctoral training, this means that the accumulated collection in the repository serves as an informational substrate for new research, allowing graduate students to build on previous work and avoid rework, while continuing existing lines of investigation.

Open Science is a movement that proposes profound changes in the way scientific knowledge is produced, shared, and reused, based on principles of transparency, collaboration, and open access. Its strands include open access to publications and data, the openness of codes and methods, and citizen participation in science. In Brazil, [6] the different interpretative currents and types of action in open science are discussed, highlighting its importance for innovation and the democratization of knowledge. Regarding Industry 4.0, open science is connected primarily by the imperative of collaborative innovation. The Fourth Industrial Revolution demands agility in the dissemination of scientific and technological discoveries, as areas such as advanced manufacturing, cyber-physical systems, and big data analysis evolve rapidly. Opening up scientific knowledge accelerates this flow of information, allowing research results to move more quickly between universities, research centers, companies, and society.

In the Amazonian context, open science takes on unique dimensions. The northern region of Brazil has historically faced challenges in fully integrating into major global scientific production circuits, whether due to infrastructure limitations or geographic barriers. Regional cooperation initiatives have sought to reverse this situation. A notable example is the Northern Network of Institutional Repositories in Access Open (NORTE/RIAA), created collaboratively by universities and institutes in the Amazon. The network's creation trajectory, which brings together repositories from several northern institutions, is described, and the role of collaboration in overcoming obstacles in the implementation of IR in the region is emphasized [7]. The existence of the Northern Network reflects these institutions' commitment to the ideals of open science, seeking to give visibility to Amazonian scientific production at the national and international level, as well as fostering the exchange of experiences and repository management techniques. This has a direct impact on regional Industry 4.0: by strengthening the circulation of local knowledge (e.g., on biodiversity, appropriate technologies, and industrial sustainability in the Amazon), an environment more conducive to technological innovation adapted to local realities is created.

Industry 4.0 itself is largely based on concepts of open innovation and knowledge ecosystems. Highly technological companies tend to interact with universities and startups to absorb new ideas and research results. Recent studies discuss, for example, the interrelationship between Industry 4.0 and open innovation in startup accelerators, highlighting that partnerships and knowledge sharing are critical factors for the competitiveness of these organizations. Thus, open science policies (such as open-access repositories) also benefit the productive sector by reducing barriers to accessing scientific information. An engineer or entrepreneur in the Amazon can consult, via institutional repositories, dissertations and theses related to industrial automation, artificial intelligence, new sustainable raw materials, and other topics relevant to Industry 4.0, free of charge and immediately after publication. This shortens the gap between academic research and practical application in companies, fueling the cycle of innovation.

Therefore, the synergy between open science and Industry 4.0 manifests itself in the co-creation and sharing of knowledge. Institutional repositories, by embodying open science, serve as bridges between academic knowledge and other stakeholders (industry, government, community). In the Amazon, where efforts are being made to reconcile technological development with environmental

conservation, this openness of information fosters innovative solutions with greater local adaptation. Furthermore, this culture of openness contributes to the development of researchers who are more globally connected and aware of the importance of collaboration and interdisciplinarity – essential characteristics for addressing the complex challenges of the fourth industrial revolution.

The training of master's and doctoral graduates is a central objective of higher education and science and technology policies in Brazil, especially in recent decades, when efforts have been made to decentralize and expand graduate programs across all regions. In the Amazon, initiatives have sought to retain local talent and develop qualified professionals capable of working in both academia and strategic sectors. Specific programs, support from funding agencies (such as CAPES), and inter-institutional agreements have been used to expand the number of graduate students in the North region. For example, CAPES, in official documents, recognizes the need to increase the number of master's and doctoral graduates in the Amazon and encourage strategic projects focused on regional vocations [8]. This quantitative expansion, however, must be accompanied by quality training, which includes ensuring that graduate students have access to up-to-date scientific production and can effectively disseminate their own work.

This is where institutional repositories prove valuable. They serve a dual purpose in the context of human resource development: pedagogical and strategic. From a pedagogical perspective, an IR provides students with a broad digital collection of research already conducted at the institution (and in associated networks), which enriches the guidance and development of new research. Master's and doctoral students can consult previous dissertations and theses on related topics, learning from the methodologies and results already obtained. Making dissertations and theses available from a graduate program is essential to give visibility to its output and serve as a foundation for the production of new knowledge, consolidating the programs' areas of concentration and lines of research. In other words, each new researcher relies on the informational stock left by those who preceded them, in a virtuous cycle of cumulative knowledge construction. From a strategic and evaluation perspective, repositories also provide indicators and transparency. The visibility afforded by open access can increase the impact (citations, usage) of work produced by graduate students, which positively impacts the CAPES evaluation of programs. Additionally, the existence of A well-maintained repository demonstrates an institutional policy of scientific dissemination, aligned with national open science recommendations and the global trend toward sharing academic results. Universities and institutes that adopt repositories reinforce their commitment to open knowledge, and this commitment tends to generate more collaborations and external recognition.

However, the effectiveness of these benefits depends on the academic community's adherence to the repository. Case studies reveal that repositories are often underutilized by faculty and students. When examining the IR of the Federal University of Amazonas within the scope of a graduate program, they observed that the repository was not being used to its full potential by the program, missing opportunities to highlight production and consolidate the research area [9]. They argue for the need for institutional policies that encourage self-archiving by authors (voluntary deposit of their work) and for the incorporation of the open access culture into graduate program guidelines (for example, in CAPES's area guidelines). Therefore, for the repository to fulfill its role in human resource development, it is essential that the institution actively promote its use—whether through training, mandates for thesis/dissertation deposits, or even integrating the IR into course completion routines.

In short, institutional repositories can be seen as infrastructures supporting graduate studies. They ensure the storage, access, and dissemination of academic production— aspects fundamental to shaping competent researchers integrated into the global research ecosystem. In the Amazonian context, IR also helps reduce informational isolation by integrating local researchers into broader networks. The institutional information stock is not an end in itself, but a means to nurture the next generation of high-level scientists and professionals, who in turn will feed this stock with new knowledge, closing the cycle.

III. MATERIALS AND METHODS

This work is an experience report combined with case study elements, focusing on ITEGAM's Galileo Institutional Repository and its contribution to the training of master's and doctoral students focused on Industry 4.0. The adopted approach is qualitative and descriptive in nature, complemented by available quantitative data on the repository's collection and use.

Initially, a review of literature and documents was conducted to theoretically support the study, prioritizing authors in Information Science and Education, especially those working in the North/Amazon region, as guided by the scope of the work. This review covered academic articles, book chapters, and relevant institutional documents on repositories, open science, Industry 4.0, and human resource training. Highlights include organized works [10] on open science in the North region, as well as conceptual studies by [11] on information stocks, among others already cited throughout the theoretical framework. For the empirical part, the study focused on the Galileo RI case. Institutional information from ITEGAM (history of the institute and the repository) and technical data from the repository itself were collected through an analysis of its public content. The structure of Galileo RI communities and collections was examined, as well as usage statistics made available by the platform (e.g., item views). Furthermore, a survey of the types of documents stored (number of master's dissertations, doctoral theses, articles, etc.) was conducted, and some examples of work aligned with the Industry 4.0 theme present in the collection were identified.

The analytical methodology employed document analysis and qualitative content analysis on the repository records and related documents. Simple quantitative data (e.g., number of items in each collection) were used to assess the existing information stock. The qualitative data (paper abstracts, collection descriptions, and indirect testimonies from secondary sources) were interpreted in light of the theoretical framework, seeking evidence of the repository's impact on academic education.

It is worth noting that the authors of this article had direct access to the repository's public interfaces and information disseminated by ITEGAM, but did not conduct interviews with users or managers of the RI in this study. Therefore, the results presented are primarily based on accessible documentary sources and the authors' accumulated experience in information and education projects in the region. This methodological approach aligns with the purpose of reporting institutional experience, providing a well-founded critical perspective, albeit limited by the lack of primary data on user perceptions (a suggested area for future research).

Based on the above outline, the next section presents the results and discussion derived from this investigation, structuring the history and context of the Galileo RI, its main collections and characteristics, as well as a discussion of its impact and challenges in the training of master's and doctoral students focused on Industry 4.0 in the Amazon region..

IV. RESULTS AND DISCUSSIONS

The Galileo Amazon Institute of Technology and Education (ITEGAM) was established in 2008 in Manaus, Amazonas, with the goal of fostering teaching, research, and technological innovation geared toward regional needs. Since its founding, ITEGAM has sought to serve as a bridge between academia and the productive sector in the Amazon, focusing on training professionals to master Industry 4.0 technologies (as explained in its institutional profile). Throughout the 2010s, the institute signed several cooperation agreements with public and private universities, both national and international, to facilitate local master's and doctoral programs in Amazonas. These agreements allowed professionals from the region to pursue stricto sensu graduate degrees without having to relocate entirely to other regions, benefiting from shared advisors and facilities. One example is the partnership with the Federal University of Pará (UFPA), through which Master's programs in Science and Environment were offered in Manaus – resulting in dissertations defended by UFPA, but the result of applied research in the Amazon region. Similar initiatives have been undertaken with other institutions, covering areas such as production engineering, energy, environment, and technology management.

In 2020, ITEGAM obtained accreditation for its Graduate Program in Engineering, Process, Systems, and Environmental Management (PPG.EGPSA), at the Professional Master's level. This multidisciplinary program emphasizes new technologies in technology management and sustainability, primarily serving professionals in local industry who need to combine advanced studies with market experience. With the consolidation of the PPG.EGPSA and the continuation of doctoral partnerships, the institute's academic output has grown significantly. Therefore, it became imperative to have an information infrastructure to organize and disseminate this output. It is in this context that the Galileo Institutional Repository (RIGalileo) emerged.

RIGalileo was implemented using the DSpace platform, adhering to international metadata and interoperability standards (OAI-PMH), enabling its integration with catalogs such as Oasisbr/IBICT. Although the exact date of its public launch is not explicitly mentioned in the documents accessed, evidence indicates that the repository was established around 2019-2020, accompanying the regional repository creation movement (which included, for example, UFAM, UEA, UFRA, etc., members of the Northern Network). The name "Galileo" honors the institution's patron and reinforces the repository's identity as an integral part of ITEGAM's mission to disseminate knowledge ("all truths are easy to understand once discovered – the point is to discover them," a phrase by Galileo Galilei printed on institutional materials). When accessing the Galileo RI, you'll find four main communities:

• Library Documentation (BibITEGAM) – intended to store policies, regulations, and technical documentation for the ITEGAM Library. (This is an administrative collection, with one registered item, such as the repository usage policy or internal manuals.)

• Agreement Documentation – the largest community in terms of volume, currently with 560 registered items. This collection brings together technical and scientific works resulting from academic agreements, primarily master's dissertations and doctoral theses defended through ITEGAM's partnerships with other HEIs, as well as any publications resulting from these agreements. For example, these include dissertations defended at UFPA, the Federal University of Amazonas (UFAM) – Humaitá campus (in the case of an agreement for a master's degree in education), possibly agreements with institutions in other regions, and even international collaborations. This collection reflects ITEGAM's efforts to facilitate advanced training, hosting research on everything from waste disposal in Manaus to electrical and mechanical engineering studies conducted at the Manaus Industrial Complex. It is worth noting that some works in this community are cataloged as articles or technical reports (likely derived from cooperative R&D projects), including in languages such as Spanish and English, highlighting the multicultural and multi-institutional nature of the partnerships.

• PPG.EGPSA/ITEGAM – a community with approximately 435 items, corresponding to the output of ITEGAM's professional master's program. The majority of these are PPG.EGPSA Dissertations, defended from 2016 onward, covering topics in engineering, process management, industrial systems, the environment, and sustainability. In addition to dissertations, this community may also include productions by program faculty and students, such as published articles, book chapters, etc., if deposited. When browsing the PPG.EGPSA Dissertation collection, you will notice the Thematic variety: from studies on alternative materials in civil construction (e.g., the use of recycled PET in concrete), to environmental education, to industrial process optimization. This diversity reflects the program's interdisciplinary approach, as well as its focus on practical problems of local industries and regional environmental issues—aspects related to Industry 4.0 and sustainability.

• ITEGAM-JETIA Journal – a community designed to house issues of the Journal of Engineering and Technology for Industrial Applications (JETIA), an international scientific journal maintained by ITEGAM since 2015. At the time of this research, this community contained zero entries, possibly because the integration of previous issues of the journal into the repository was still ongoing or because the journal has its own separate portal. In any case, the presence of this community denotes the intention to also bring together the institution's periodical production in the RI, reinforcing it as a complete hub for ITEGAM's scientific dissemination. In total, the RIGalileo collection comprises around 1,000 items (approximately 996, according to the figures presented). This is a considerable collection for an institutional repository of a relatively young institute. For comparison purposes, repositories at federal universities in the North region, established during a similar period, are similar in size (for example, the RI at UFRA – Federal Rural University of the Amazon – reported around 800 items after a few years of operation). This suggests that ITEGAM has successfully incorporated into the repository both the historical production of the agreements and the current production of its master's program, without major gaps.

An important aspect to highlight is the quality and thematic relevance of the collection in relation to Industry 4.0. Several works deposited in the RI Galileo are directly related to the technologies and challenges of the fourth industrial revolution. For example, there are dissertations investigating the integration of costing systems in automated environments (in the context of the transition to Industry 4.0), the application of fuzzy systems and neural networks to optimize industrial processes, the development of predictive maintenance mechanisms in factories, and studies on power quality and harmonic compensation in industrial plants, among other topics. The fact that many of these works are accessible in the repository allows current and future students to benefit from this prior knowledge. An incoming

ITEGAM master's student, for example, can access, via RIGalileo, the dissertation of a graduate who developed a fault detection algorithm for electric motors using fuzzy logic, using this work as a reference and starting point for advancing research into smart maintenance, which is a key topic in Industry 4.0. Thus, the repository serves as a dynamic information repository, where knowledge about industrial technologies is accumulated and feeds back into learning. Regarding the usability and reach of the Galileo RI, it was observed that the repository is configured with a bilingual interface (Portuguese/English) and allows open searches without the need for registration. The global community can discover its contents through engines like Google Scholar, since the metadata is open. The RI also records simple usage statistics. Data collected (in June 2025) indicated, for example, which items received the most views. Studies related to Industry 4.0 were reportedly among the most accessed: a machine reliability prediction model using neural networks (33 views), application of a photovoltaic system with genetic algorithms in Industry 4.0 (21 views), and techniques for predicting acetaldehyde generation using neural networks (21 views), among others. Although these absolute viewing numbers are modest—possibly reflecting only recent data—they suggest reader interest and engagement in content directly related to Industry 4.0 in the RI collection. Over time and with adequate publicity, these views are expected to expand, increasing the impact of the work and, consequently, the training offered.

The above results paint a positive picture of the Galileo RI as a robust institutional repository of content. But what has been the true impact of this repository on the training of ITEGAM master's and doctoral students focused on Industry 4.0? This impact can be analyzed in different dimensions: visibility, academic quality, collaboration, and information culture.

(a) Visibility and reach of student production: Without the repository, a large portion of the dissertations and theses produced under ITEGAM's auspices (whether through partnerships or through its own graduate programs) would be restricted to physical collections or isolated databases at partner universities. With the Galileo RI, all of this production is is collected and publicly available, bringing increased visibility to the work. This means that research conducted in the Amazon, often of an applied and innovative nature, can be read and cited by other researchers anywhere. This visibility directly benefits the authors (students and advisors), who become more actively involved in the scientific community. Furthermore, visibility via IR can serve as a basis for new knowledge within the program itself. There is already evidence of cross-use of the work: for example, a 2020 master's graduate citing a 2018 dissertation present in the IR in his review, and so on, demonstrating research continuity. Thus, the repository helps to consolidate lines of research by highlighting existing production.

(b) Improved academic quality: Easy access to previous work allows current graduate students to gauge the level of demand and depth expected in their research, serving as a guideline. Advisors can also point to dissertations from the repository as methodological or thematic references for their advisees. This can increase the average quality of new dissertations, as it avoids "reinventing the wheel" and promotes building on previous results. Furthermore, the Galileo RI, by including derivative works (such as articles), encourages students to publish and deposit their articles, integrating them into the institutional collection. This publication culture is crucial in doctoral training, especially, and the repository supports this by demonstrating that the institution values and disseminates these products.

(c) Collaboration and academic networks: The aggregation of all production in a single portal facilitates the identification of ITEGAM's experts and areas of expertise. For example, companies or external researchers may, when browsing the RI, discover that the institute has several studies on energy systems optimization or lean production engineering, which could lead to contact for partnerships or projects. Internally, faculty members themselves can identify synergies between different areas of expertise. Therefore, the repository serves as a showcase for ITEGAM's academic expertise, which is important for inclusion in larger research networks and consortia. Within the framework of Industry 4.0, which values collaborative ecosystems, this transparency regarding the knowledge produced is a positive differentiator. It is worth mentioning that participation in the Northern Repository Network further strengthens this regional collaborative dimension, as users browsing the network portal can find ITEGAM's production alongside that of public universities, increasing recognition of the institute's contribution in the region.

(d) Information culture and open science: The existence of the Galileo RI and its use in daily academic life also has less tangible but significant formative effects: it instills in students and faculty a appreciation for information management and open science. Knowing that the final work will be publicly deposited encourages students to pay attention to issues of document quality, respect for copyright of figures and data, clarity in writing (as there will be potential external readers), among other concerns. This fosters a sense of responsibility for the intellectual product. Additionally, many students gain their first exposure to the principles of open access through the repository—learning about Creative Commons licenses and the importance of making knowledge accessible. This awareness is valuable, developing professionals and researchers with a more open and collaborative mindset, aligned with both modern scientific practices and the innovative demands of Industry 4.0.

Challenges identified: Despite the benefits, some challenges were noted or can be inferred. One of them is ensuring the repository's continuous maintenance. While the deposit of dissertations and theses can be made mandatory (and often is, in many institutions, for title approval), the deposit of other materials (such as faculty articles, chapters, project reports) depends on voluntary participation. It would be advisable for ITEGAM to develop policies that encourage or even formally hold researchers accountable for depositing their publications, expanding the IR's repertoire. Another challenge is dissemination and usability: ensuring that ITEGAM's own academic community uses the repository extensively as a reference source. Some research indicates that graduate programs don't always exploit the full potential of their repositories. Therefore, information training initiatives for students and faculty (e.g., IR search workshops, inclusion of IR references in courses) can improve this integration. Finally, technological sustainability is a concern: keeping DSpace up-to-date, with regular backups and high-quality metadata, requires r continued investment in training librarians and technical staff.

In summary, the results demonstrate that the Galileo Institutional Repository is already an essential information repository for ITEGAM, encompassing nearly a decade and a half of academic production related to the training of master's (and some doctoral) students in the region. Its impact on education is evident in the increased circulation of knowledge and direct support for student and faculty work. This initiative, aligned with best practices in open science, positions ITEGAM at the forefront of academic information management in the Amazon region.

V. CONCLUSIONS

This article analytically discusses the role of ITEGAM's Galileo Institutional Repository (RIGalileo) as an information repository focused on training master's and doctoral students with a focus on Industry 4.0 in the Amazonian context. Based on the theoretical framework and case analysis, it becomes clear that an institutional repository is not merely a passive repository of documents, but rather a strategic knowledge infrastructure that can positively shape the direction of graduate studies and research at an institution.

In the case of ITEGAM, the Galileo Institutional Repository has established itself as an open-access repository aligned with open science and regional needs. It has aggregated a significant volume of technical and scientific work, democratizing access to research on technology, engineering, and sustainability conducted in the Amazon. In doing so, it contributes to mitigating geographic and informational barriers that have historically limited the region's insertion into the global scientific landscape. Master's and doctoral students trained at the institution now have a robust pre-registration base to support their research, as well as the assurance that their final products will be widely disseminated, enhancing their academic legacy.

The importance of authors and researchers from the North in understanding this dynamic is emphasized: authors such as Célia Regina Simonetti Barbalho and colleagues have emphasized in their works the relevance of collaborative initiatives (such as the Northern Network of Repositories) and the need for appropriate information policies for the Amazon. This study reinforces these perspectives by demonstrating, in practice, the benefits of implementing an IR at a local technology institute.

However, ongoing challenges were also identified. It is crucial that ITEGAM maintain its commitment to nurturing and disseminating the Galileo IR. It is recommended that a mandatory deposit policy be established for all scientific production linked to the institution (not only theses and dissertations, but also articles, research data, etc., respecting copyright issues and necessary embargoes). Furthermore, investments in information literacy—training students and faculty to search, use, and contribute to the repository—will ensure that the information stock is truly utilized to its fullest (avoiding the underutilization noted in other contexts (researchgate.net). Within the scope of Industry 4.0, it is pertinent to explore synergies between the repository and companies in the Manaus Industrial Hub, perhaps through thematic portals or sectoral repositories of open data that may derive from academic research (e.g., sensor data, software codes developed in dissertations, etc.).

In conclusion, ITEGAM's Galileo Institutional Repository proves to be a successful initiative integrating information science and academic training, serving as an informational pillar for the development of qualified human resources in the Amazon. It exemplifies how open science practices can be incorporated at the institutional level to produce concrete results: greater visibility of local academic production, supporting the emergence of new generations of researchers and professionals, and fostering a culture of knowledge sharing. For institutions in peripheral or emerging regions of the scientific landscape, as is the case for many in the Amazon, experiences like the Galileo RI can serve as an inspiring model.

Finally, this article reinforces the idea that the success of an institutional repository depends as much on technology and infrastructure as it does on policies and human engagement. The informational stock contained therein comes to life as it is continually consulted, cited, and expanded. It is up to academic administrators and the community to use this tool strategically. Looking ahead, the Galileo RI is expected to continue evolving, perhaps incorporating a research data repository from ITEGAM in the future or integrating with international repository networks. In any case, its existence already represents a significant advance for science, education, and innovation in the Amazon, providing a solid foundation for master's and doctoral graduates trained in the region to make significant contributions to Industry 4.0 and sustainable development.

VI. AUTHOR'S CONTRIBUTION

Conceptualization: Luiz Fernando Correia de Almeida.
Methodology: Luiz Fernando Correia de Almeida.
Investigation: Luiz Fernando Correia de Almeida.
Discussion of results: Luiz Fernando Correia de Almeida.
Writing – Original Draft: Luiz Fernando Correia de Almeida.
Writing – Review and Editing: Luiz Fernando Correia de Almeida.
Resources: Luiz Fernando Correia de Almeida.
Supervision: Luiz Fernando Correia de Almeida.
Approval of the final text: Luiz Fernando Correia de Almeida.

VII. ACKNOWLEDGMENTS

The authors would like to thank the Amazonas State Research Support Foundation (FAPEAM) for the research grant that supported the development of this study. We also acknowledge the financial support provided by the Coordination for the Improvement of Higher Education Personnel – Brazil (CAPES) through the Institutional Program for Internationalization (PDSE), which enabled the mobility of doctoral research that contributed significantly to this work.

VIII. REFERENCES

[1] Instituto de Tecnologia e Educação Galileo da Amazônia (ITEGAM), "Página institucional e informações do repositório," 2023. [Online]. Disponível em: https://itegam.org.br e https://rigalileo.itegam.org.br

[2] A. de P. Barreto, A Questão da Informação. Rio de Janeiro: Editora T., 2014.

[3] R. Crow, The case for institutional repositories: a SPARC position paper. Washington, DC: SPARC, 2002.

[4] F. C. L. Leite e S. M. S. Costa, “Repositórios institucionais como ferramentas de gestão do conhecimento científico no ambiente acadêmico,” Perspectivas em Ciência da Informação, vol. 11, no. 2, pp. 18–30, 2006.

[5] IBICT – Instituto Brasileiro de Informação em Ciência e Tecnologia, Manifesto Brasileiro de Apoio ao Acesso Livre à Informação Científica. Brasília, 2005.

[6] S. Albagli, A. Clinio e S. Raychtock, “Ciência Aberta: correntes interpretativas e tipos de ação,” Liinc em Revista, vol. 10, no. 2, pp. 434–450, 2014.

[7] A. C. G. Santos, “Criação da Rede de Repositórios Institucionais em Acesso Aberto na Amazônia: uma experiência que se constrói colaborativamente entre as instituições,” in Anais do CNBU 2017, 2017.

[8] H. Kuramoto, “Acesso livre à informação científica: novos desafios,” Liinc em Revista, vol. 4, no. 2, pp. 168–175, 2008.

[9] L. F. C. Almeida e H. C. P. Simas, “Comunicação científica e o repositório institucional no âmbito do PPGE/UFAM,” Research, Society and Development, vol. 11, no. 1, e28711124857, 2022. DOI: 10.33448/rsd-v11i1.24857.

[10] C. R. S. Barbalho, D. O. Inomata e J. M. Galves, A Ciência Aberta e seus impactos na Região Norte do Brasil. Manaus: Edua, 2019. E-book, 317 p. ISBN 978-85-526-0065-7.

[11] A. de P. Barreto, A Questão da Informação. Rio de Janeiro: Editora T., 2014..

Journal of Engineering and Technology for Industrial Applications

ISSN ONLINE: 2447-0228

ITEGAM-JETIA

Manaus, v.11 n.54, p. 72-87. July/August., 2025.
DOI: https://doi.org/10.5935/jetia. v11i54.1718

RESEARCH ARTICLE OPEN ACCESS

THE EFFECT OF DATA CONVERSION METHODS (NAIVE BAYES, C5.0 & SUPPORT VECTOR MACHINE) ON THE PERFORMANCE OF CLASSIFICATION ALGORITHMS IN DATA MINING

Hussein Ali Attallah [1], Ahmed Al-Asadi [2] and Sadeer Sadeq [3]

[1,2] Communication Engineering Department, University of Technology, Baghdad, Iraq.
[3] University of Information Technology and Communications Baghdad, Iraq

[1]https://orcid.org/0000-0002-3443-3547, [2]https://orcid.org/0000-0002-5052-1969, [3]https://orcid.org/0009-0000-8415-8056

E-mail: hussein.a.attallah@uotechnology.edu.iq, ahmed.a.hussain@uotechnology.edu.iq, sadeer.abduljabbar@uoitc.edu.iq

ARTICLE INFO

Article History
Received: March 16, 2025
Revised: April 20, 2025
Accepted: June 15, 2025
Published: July 31, 2025

Keywords:
Comparative study,
Conversation methods,
Data transformation,
NB, SVM, C5.0,
Normalization,
Statistical analysis.

ABSTRACT

In the study, sample distributions (Normal, Chi-square, F), number of observations (100, 500, 1000, 10000) and class distribution rates (0.1, 0.2, 0.3, 0.4, 0.5) were evaluated. It was aimed to examine the effects of data transformation on naive Bayes (NB), C5.0 and support vector machines (SVM) by applying minimum-maximum and z-score normalisation and equal width and equal frequency spacing discrimination methods to different types of data produced by simulation. In this research, the minimum-maximum and z-score normalisation of the data produced by simulation from a normal distribution, chi-square distribution and F distribution according to four different numbers of observations and five different equilibrium distribution ratios of classes, and spacing discrimination transformations of equal girth (width) (EG) and equal frequency (EF). The results and comparative study showed that both normalisation and discrimination methods were influential in the performance of SVM and contributed to better results. According to the classification success achieved with SVM, normalisation methods are more effective in average, and chi-square distribution among both approaches, and EF unsupervised discrimination method is more effective in F-distribution.

Copyright ©2025 by authors and Galileo Institute of Technology and Education of the Amazon (ITEGAM). This work is licensed under the Creative Commons Attribution International License (CC BY 4.0).

I. INTRODUCTION

Making the right decision is of great importance in order to obtain positive results in medical practices. Although the developments in the field of health and technology are pleasing, some uncertainties encountered in medicine make it difficult for clinicians to make decisions [1]. Since 1975, the rapidly increasing number of diagnostic and treatment options and the increasing importance of cost aspects have made decisions difficult for healthcare providers [2]. Data mining, which includes many disciplines, has become one of the auxiliary tools used to develop new clinical principles and to make scientifically high-quality decisions with the information obtained. Data mining is generally defined as a process consisting of steps such as data collection, preparation for analysis, and modelling to obtain valid and valuable new information in the field of research [3],[4]. The main objective of the current research work is classification, which is one of the data mining techniques, and naive Bayes (NB), decision trees, C5.0 algorithm, and support vector machines (SVM) are the main methods used.

The naive Bayes algorithm is a simple classification method based on the Bayes theorem. The naive Bayes algorithm has strong assumptions that are rarely provided. Despite this, it can give good results against many problematic data [5]. In classification problems, class estimation uses the probabilities of the classes in the dependent variable and the class conditional probabilities for a new observation [6]. Decision trees are a supervised classification method with a hierarchical structure that considers a particular order of importance for the variables in the data set [7],[8]. Here, the order of the variables is determined with variable selection methods, and a decision is made for the classes of the new observations by following a path from top to bottom. The developed version of the ID3 decision tree algorithm,

C5.0, has the advantages of modelling continuous data, automatically selecting features in multidimensional data, and not requiring a priori determination of the model. Another method used in the study is SVM [9]. Its popularity has increased recently due to its good performance in nonlinear and multidimensional data. It performs classification by drawing a boundary that maximises the area between observations in one class and the other class in a multidimensional space. Classification methods have advantages and disadvantages [10]. Therefore, their performance superiority may vary depending on the sample size and data type. In order to obtain more robust and balanced results, several methods can be applied to the data where the algorithms are disadvantaged before classification, thus increasing the performance success. One of the available options for this purpose is to apply transformation to the data. In data mining, minimum-maximum and z-score normalisation are frequently used for data transformation. For a similar purpose, unsupervised discretisation applications, also known as binning, are another approach that uses equal width and equal frequency spacing methods [11]. In this study, it was aimed to investigate the effects of data transformation on naive Bayes, C5.0 and SVM by applying minimum-maximum and z-score normalisation and equal width and equal frequency spacing discretisation methods to different types of data generated by simulation according to sample distributions (Normal, Chi-square, F), observation numbers (100, 500, 1000, 10000) and class distribution ratios (0.1, 0.2, 0.3, 0.4, 0.5).

II. CLASSIFICATION DEFINITION AND PROCESS

In classification applications, each category in the dependent variable is called "class". In medical research, examples of these classes can be given, such as three different types of treatment and two different disease diagnoses [12]. NB, C5.0 and SVM are frequently used classifiers for classification problems in data mining. In data mining, reaching all class conditional intersection probabilities becomes more difficult as the number of independent variables increases, making the solution more complex [13]. In the NB method, to simplify the operations, it is assumed that the variables in each class, that is, class conditional variables, are independent of each other. This assumption is referred to as “conditional independence” in many sources [14].

II.1 NAIVE BAYES (NB):

In the study [15], Naïve Bayes Algorithm uses probability and statistics to solve classification problems. This method performs classification by calculating the value of the probability P($x \mid y$) by knowing the probability of class X. Determination of the class in the classification is done by selecting the max value of P($x \mid y$) Based on probability. The advantage of classification is that it requires a relatively small amount of training data to estimate the parameters needed for classification. Based on the Naïve Bayes algorithm, the following is the equation for calculating the value of $P(x \mid y)$ [16]:

$$P(X \mid Y) = \frac{P(Y|X).(X)}{P(Y)} \quad (1)$$

where:
P(X|Y) = Posterior probability, namely the probability value of X based on condition Y

P(Y|X) = probability of Y determined by X is true
P(X) = Probability of evidence of disease X
P(Y) = Probability of the value of Y

Successful results are achieved with NB in genetic and drug development studies. For [17] developed an approach based on the naive Bayesian algorithm using RNA sequencing data, which could help diagnose tissue-derived hepatobiliary or pancreatic cancer in synchronous tumours. While more than a 95% success rate was achieved with the 10-fold cross-validation method with the created model, they reported correctly classifying 17 (94.4%) of 18 clinical cancer tissue samples (six negative controls) used for external validity.

II.2 DECISION TREES:

In medical data analysis, it is essential to communicate data mining results to people in an understandable way [18]. Two algorithms form the basis of decision trees researchers developed without knowing each other.

II.3 STRUCTURE OF DECISION TREES:

The structure of a decision tree consists of nodes and branches. As shown in (Figure 1), the topmost starting node is called "root", and the last node containing the classes of the dependent variable is called "leaf". In decision trees, all nodes except leaves represent an independent variable. These nodes are also called "decision nodes" because they decide which class to reach with independent variable questions (e.g., "What is the gender?" and "What is the age?" etc.). The branches emerging from each decision node contain all the answers to the variable (For example, “female-male”, “65 years old and under - 65 years old, etc.). In other words, it represents their categories. These branches, formed as many as the number of categories belonging to the relevant variable, are connected to a leaf or a new decision node. The leaves reached at the last stage express the decisions regarding the classes.

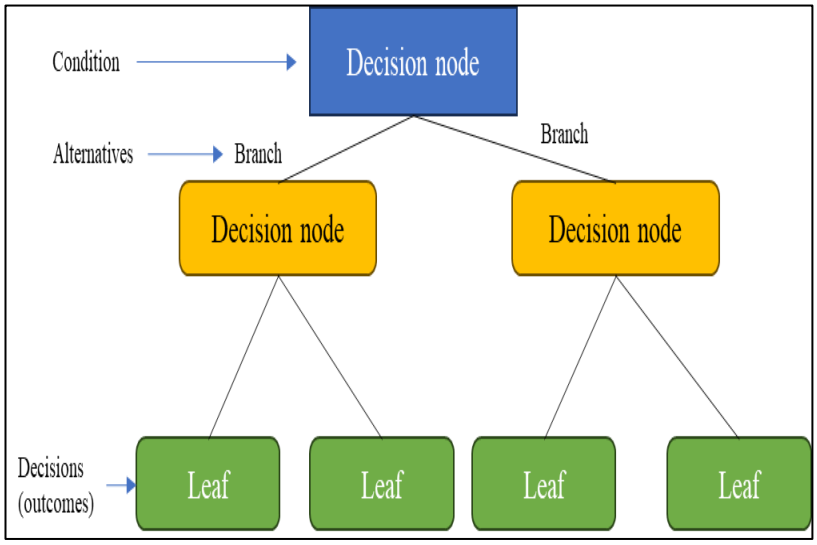

Figure.1: The structure of a decision tree consists of nodes and branches.
Source: [19].

II.4 C5.0 DECISION TREE ALGORITHM:

The C5.0 algorithm is a development or improvement of the C4.5 algorithm where the development is carried out on memory usage, attribute separation, and acceleration, according to Arif, Muhammad. (2018) [20],[21], the C4.5 algorithm is a development or improvement of the ID3 algorithm; improvements made such as being able to handle discrete or continuous attributes, being able to handle empty attributes or missing values, and being able to summarise or prune decision trees.

The C5.0 algorithm is a data mining classification algorithm applied explicitly to decision tree techniques. In selecting attributes for solving objects in several classes, the attribute that produces the most significant information gain must be selected [22]. Entropy measures uncertainty associated with a random variable, while gain is the expected value. If the entropy value is "0", it is easier to classify the observations. In data mining, the terms entropy and information gain are related. Entropy is used to select the variables that provide the highest information gain for the nodes to determine the most appropriate variable order in the classification. By selecting the variables that provide the highest information gain, the information required for the classification, namely entropy, is reduced to a minimum level. Suppose the entropy value is found to be "0", no further information is needed to classify the observations and that all observations belong to the same class. The formula for the entropy index is given below [23]:

$$Entropy\ (S)\ = \sum_{i=1}^{m} -\ p_i\ log_2(p_i) \tag{2}$$

Where;
$\boldsymbol{S}$: $Case\ value$
$\boldsymbol{M}$: $Number\ of\ classes\ in\ the\ variable$
$\boldsymbol{p_i}$: $Proportion\ of\ S\ and\ S_i$

In the analysis using the C5.0 Algorithm, there are several steps, namely, inputting the studied data. Next, selecting the root node begins with calculating the entropy value. Then, the process continues by finding the value gained. After that, look for the gain ratio value.

II.5 SUPPORT VECTOR MACHINE ALGORITHM (SVM):

According to research [24], SVM is a method or algorithm for classifying and predicting. The working principle of this method is to find the most optimal separation space for a dataset in different classes.

$$f(x_d) = \sum_{i=1}^{ns} a_i y_i \overrightarrow{x_i} \overrightarrow{x_d} + b \tag{3}$$

Where:
$\boldsymbol{ns}$ = Number of support vectors
$\boldsymbol{a_i}$ = Weight value of each data point
$\boldsymbol{y_i}$ = Data class
$\overrightarrow{\boldsymbol{x_i}}$= Support vector variable
$\overrightarrow{\boldsymbol{x_d}}$ = Data to be classified
$\boldsymbol{b}$ = Error or bias value

The SVM algorithm places all observations according to their values in a dimensional space equal to the number of variables. Then, it finds the hyperplane that provides the best separation between the observations according to their classes and classifies new observations according to this hyperplane [25].

A hyperplane is a p-1-dimensional subspace plane in p-dimensional space. The following equation makes its mathematical definition:

$$\beta_o + \beta_1 X_1 + \beta_2 X_2 + \ldots + \beta_p X_p \quad (4)$$

When this equation is applied to a point in space,

$$\beta_o + \beta_1 X_1 + \beta_2 X_2 + \ldots + \beta_p X_p < 0 \quad (4\text{-}1)$$

$$\beta_o + \beta_1 X_1 + \beta_2 X_2 + \ldots + \beta_p X_p > 0 \quad (4\text{-}2)$$

Results can be obtained. If the result is negative, the point is in one class; otherwise, if it is positive, it is in the other. It can be easily found on which side the observations are in the space divided into two, according to the sign of the hyperplane equation result. According to [26], identifying acute exacerbations in chronic obstructive pulmonary disease is crucial to reducing mortality and financial burden. He developed different classification models for this disease and conducted a comparison study to find the best model. From the results obtained, SVM showed the highest success performance.

Based on the above points, in the study, sample distributions (Normal, Chi-square, F-distribution), number of observations (100, 500, 1000, 10000) and class distribution rates (0.1, 0.2, 0.3, 0.4, 0.5) were evaluated. It aimed to examine the effects of data transformation on NB, C5.0 and SVM by applying minimum-maximum and z-score normalisation and equal width and frequency spacing discrimination methods to different types of data produced by simulation.

III. MATERIALS AND METHODS

Not all obtained data can be processed for classification from the data collection. Data analysis first needs to be done because there are attributes that do not need to go through various stages of data analysis in order to get quality data.

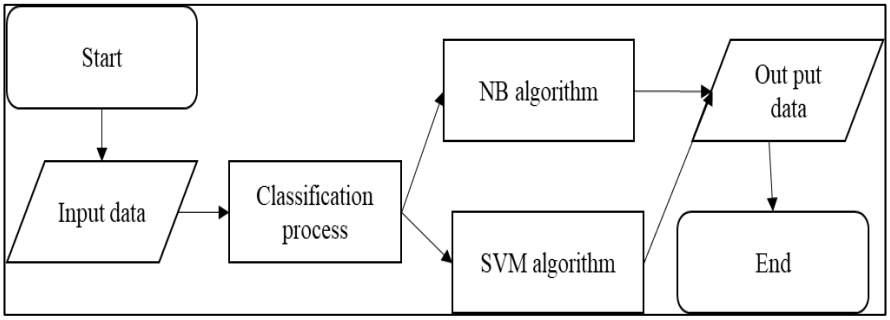

Figure 2: Research Flow.
Source: Authors, (2025).

III.1 RESEARCH FLOW DIAGRAM

The effects of normalisation, z-score, and unsupervised discrimination methods applied in the data pre-processing process on classification algorithms' performance were examined using simulation data sets. Data sets were created in a structure with 11 variables, including 10 independent variables of quantitative type and a dependent variable of 2 categories.

Table 1: Sampling distribution parameters.

Variable	Group	Normal distribution		Chi-square distribution	F distribution	
		Mean	SD	df1	df1	df2
Variable-1	1	1.8	0.2	30	4	4
	0	2	0.2	32	5	5
Variable-2	1	20	4	10	50	50
	0	22	5	8	10	10
Variable-3	1	4	0.3	200	100	10
	0	4.2	0.2	195	100	50
Variable-4	1	10	1	100	10	1
	0	9	0.8	95	5	15
Variable-5	1	30	4	2	100	10
	0	28.5	3	4	100	5
Variable-6	1	150	40	5	30	1
	0	180	50	7	10	5
Variable-7	1	40	5	15	100	5
	0	41	4	17	100	50
Variable-8	1	100	15	500	100	10
	0	95	20	475	10	10
Variable-9	1	5	0.8	200	1	5
	0	4.5	0.5	210	10	5
Variable-10	1	50	10	1000	10	5
	0	52	10	1050	10	3

Source: Authors, (2025).

sd: standard deviation;
df1: 1st degrees of freedom;
df2: 2nd degrees of freedom.

Methods were applied before classification to examine the effects of data transformation, and NB, C5.0 decision tree, and SVM algorithms were used. Classification results were first obtained with raw data without pre-processing to examine the effects of data transformation methods on the algorithms. Then, the classification analysis was repeated by applying equal width spacing (EW) and equal frequency spacing (EF) methods to the generated data, such as minimum-maximum normalisaton, $z - score$ normalisation and unsupervised discrimination methods (Table 2).

Table 2: Data transformation methods.

Minimum-Maximum normalisation	$\frac{X_{min} - x}{X_{max} - X_{min}}$	X_{min} ; minimum value X_{max} ; maximum value
Z-Score normalisation	$\frac{x - \bar{X}}{\sigma}$	$\bar{X}$; variable mean σ ; standard deviation
Equal width spacing discretisation (EW)	$a = \frac{X_{max} - X_{min}}{k}$, $s = X_{min} + (i \times a)$	k; number of intervals a; interval width i ;1,2,…,k-1 s ; limits
Equal frequency spacing discretisation (EF)	$f = n/k$	k; number of intervals n; number of observations f; interval frequency

Source: Authors, (2025).

The values in the raw data are respectively applied by minimum-maximum normalisation and z-score normalisation; It was brought to the range of "0" to "1" and "-3" to "3". For these operations, functions are written in the R −Program according to the formulas of both methods were used. The k −Value in the formula of the EW and EF discrimination methods was determined as "10" for both methods. The data was divided according to this value and converted into categorical form. All applications in the simulation study were repeated 1000 times, and the findings were summarised using mean and standard deviation values.

As a result of the study, "Overall Accuracy", "Area Under the Curve (AUC)", "Sensitivity", "Specificity", and "Positive Predictive Value" were used to evaluate the performance of classification algorithms", "Negative Predictive Value" measurements were used. In the unbalanced distribution of classes in the dependent variable, the "balanced accuracy" criterion was used instead of the "General Accuracy Rate". The definition and calculation formulas for these criteria used to evaluate performance are given in (Table 3).

Table 3: Performance evaluation criteria.

Accuracy	The ratio of actually "Positive" and "Negative" to the total	$\frac{(\mathrm{TP} + \mathrm{TN})}{(TP + TP + FP + FN)}$
Balanced Accuracy rate	Average of sensitivity and selectivity rates	$\frac{(TP/(TP + FN) + TN/(TN + FP))}{2}$
Sensitivity rate	Ratio of predicted "Positive" to actually "Positive."	$TP/(TP + FN)$
Selectivity rate	Ratio of predicted "Negative" to actually "Negative"	$TN/(TN + FP)$
Positive predictive value	Ratio of actually "Positive" to those predicted to be "Positive"	$TP/(TP + FP)$
Negative predictive value	Ratio of predicted "Negative" to actually "Negative"	$TN/(TN + FN)$
AUC	Area under the curve with sensitivity on the vertical axis and 1-selectivity on the horizontal axis	

Source: Authors, (2025).

TP: *True positive;* ***TN:*** *True negative;*
FP: *False positive;* ***FN:*** *False negative.*

IV. RESULTS AND DISCUSSION

IV.1 RESULTS

The algorithms were compared by taking the highest accuracy rate, AUC value, sensitivity and selectivity rate, and the classification algorithms' positive and negative predictive value in the raw data or after data transformation.

As a result of the study, the findings regarding the highest accuracy rates achieved in the three algorithms. While there was an increase in all combinations of data generated from the normal distribution in SVM with data transformation, there was no increase in the NB algorithm. The NB algorithm achieved higher overall accuracy rates than other algorithms with the Gaussian probability density function, regardless of the number of observations and class distribution rates. With the increase in the number of observations for data produced from normal distribution in SVM, the change in data transformations draws attention. As the number of observations increases, the superiority of z-score normalisation over minimum and maximum increases when moving from balanced to unbalanced class

distribution. With the C5.0 algorithm, there is an increase in accuracy rates with z-score normalisation only in the 0.4 and 0.5 class distributions in 500 observations and the 0.2 class distribution in 10000 observations. Still, according to the findings in Table 4, these increases are less than 0.01%.

When examined for chi-square distribution, an increase in the overall accuracy rate was achieved with data transformations in all data types of SVM and with 100 observations and a class distribution ratio of 0.1, NB with the kernel probability density function and the SVM algorithm achieved the highest accuracy rates in all remaining combinations. While the highest accuracy rates are achieved with z-score normalisation in SVM for data more prominent than 100 observations and a fully balanced class distribution (0.5), the superiority of minimum-maximum normalisation is noteworthy when the classes are not distributed balanced. In 100 observations, the best results were found with the data using minimum-maximum normalisation in all distributions except the 0.1 class distribution in SVM.

Table 4: Average accuracy rates (%) obtained with C5.0 for the Continuation of Normal Distribution.

n	Ratio	Raw data	Minimum-Maximum (n)	Z-Score (n)	EW	EF
100	0.1	65.33±17.18	65.33±17.18	65.98±17.35	51.41±5.44	51±4.03
	0.2	71.98±13.33	71.98±13.33	72.69±13.46	53.59±8.18	53.94±8.77
	0.3	74.25±11.72	74.25±11.72	74.99±11.83	58.61±11.33	57.25±11.26
	0.4	75.64±10.5	75.64±10.5	76.39±10.61	65.62±11.26	65.83±11.49
	0.5	76.12±9.97	76.12±9.97	76.88±10.07	67.17±11.48	65.94±11.22
500	0.1	70.51±8.43	70.51±8.43	71.2±8.52	61.26±8.3	57.36±7.81
	0.2	76.71±6.1	76.71±6.1	77.47±6.17	71.02±6.94	70.83±6.93
	0.3	79.33±4.79	79.32±4.79	80.1±4.83	75.68±5.51	75.64±5.33
	0.4	80.46±4.42	80.46±4.42	81.26±4.48	77.67±4.65	77.41±4.84
	0.5	80.68±4.14	80.68±4.14	81.48±4.18	78.52±4.39	77.97±4.59
1000	0.1	72.8±5.88	72.8±5.88	73.52±5.94	65.91±6.5	60.88±6.37
	0.2	78.11±4.27	78.11±4.27	78.89±4.31	74.43±4.57	72.84±4.85
	0.3	80.62±3.43	80.62±3.43	81.41±3.47	78.38±3.82	78.22±4.02
	0.4	81.68±3	81.68±3	82.49±3.03	80.38±3.16	80.01±3.27
	0.5	81.89±2.91	81.89±2.91	82.7±2.94	80.71±3.01	80.24±3.19
10000	0.1	77.02±2.03	77.01±2.03	77.78±2.06	74.74±2.02	72.59±2.17
	0.2	81.74±1.4	81.74±1.4	82.55±1.42	80.56±1.38	79.56±1.47
	0.3	83.95±1.09	83.95±1.09	84.78±1.1	83.31±1.09	82.73±1.04
	0.4	85.03±0.91	85.03±0.91	85.88±0.92	84.7±0.89	84.29±0.94
	0.5	85.41±0.83	85.41±0.83	86.25±0.84	85.19±0.8	84.93±0.88

Source: Authors, (2025).

For the 0.1 class distribution rate in 1000 and 10000 observations in the data produced from the F distribution, the C5.0 algorithm is used. In all remaining combinations with raw data and z-score transformation, it was seen that the NB algorithm gave the highest results with EF discrimination. EF transformation in SVM increased accuracy more effectively than other transformation methods.

In the study, the findings regarding the highest AUC values obtained from all simulation scenarios with NB, C5.0 and SVM algorithms and how they were obtained are included in (Table 5).

There was no increase in the data produced from a normal distribution compared to the results obtained from the raw data after data transformation in NB and C5.0 algorithms. It was observed that NB achieved a higher AUC value than other algorithms, regardless of the number of observations and class distribution rates. Notably, in the SVM algorithm, the highest AUC values in data that are more significant than 100 observations are most frequently achieved with z-score normalisation.

There was no increase in the data generated from the chi-square distribution after data transformation in NB. The highest AUC values were achieved with the SVM algorithm in all observation numbers and class distribution ratios. However, NB and SVM gave the same high AUC values in 0.2-0.3-0.4-0.5 class distributions in 10000 observations. At the highest values obtained with SVM, it is noteworthy that z-score normalisation is superior in fully balanced distributions of classes, and minimum-maximum normalisation is superior in unbalanced distributions.

The data generated from the F distribution showed that NB and SVM gave the highest AUC values after EF discrimination. The NB algorithm reached the highest values without varying depending on the number of observations or class distribution.

In the C5.0 algorithm, AUC values generally did not increase after the transformations on the data generated from all distributions.

In the study, the findings regarding the highest sensitivity rates obtained with NB, C5.0 and SVM algorithms and how they were obtained are given in (Table 6).

There was no increase in the data produced from normal distribution compared to the sensitivity rates obtained from the raw data after data transformation in NB and C5.0 algorithms. NB has the highest sensitivity rates with the Gaussian probability density function applied to the raw data in all data types except 100 observations and 0.4 class distribution ratio. Looking at the SVM findings, it can be seen that the superiority of z-score normalisation over minimum and maximum increases as the number of observations increases and the balance ratio in classes decreases.

In the data generated from the chi-square distribution, there was no increase in sensitivity rates in the C5.0 algorithm after data transformation. The highest sensitivity rates were achieved with the SVM algorithm with 100 observations and 0.1-0.2 class distribution rates. The superiority of minimum-maximum normalisation draws attention to the highest values obtained with SVM.

In the data produced from the F distribution, there was no increase in sensitivity rates in the C5.0 algorithm after data transformation. It was observed that NB and DVM, each individually, gave the highest sensitivity rates most frequently after EF discrimination. Regardless of the number of observations or class distribution, the best results in sensitivity rates were achieved with the NB algorithm.

In the study, the findings regarding the highest selectivity rates obtained with NB, C5.0 and SVM algorithms and how they were obtained are given in Table 7.

In the data produced from normal distribution, there was no increase in the selectivity rates obtained from the raw data after data transformation in NB algorithms. The highest sensitivity rates were achieved with NB (Gaussian) in the data where the classes were distributed precisely balanced (0.5) and with SVM in all unbalanced distributions. Both algorithms achieved their highest values with the most frequent raw data. In the C5.0 algorithm, the effect of EG discrimination in increasing the selectivity rate, especially in unbalanced class distributions larger than 100 observations, is noteworthy.

In the data generated from the chi-square distribution, there was no increase in NB after data transformation. While C5.0 (EF) provides the highest selectivity rates in 0.1-0.2 class distributions per 100 observations and NB (Gaussian) in 0.4-0.5 class distributions per 10000 observations, the highest selectivity rates are achieved with SVM in all remaining data types was done. In SVM, the highest values were obtained with raw data, most frequently in data larger than 100 observations and with unbalanced class distributions, and with z-score normalisation in a fully balanced (0.5) distribution. In the C5.0 algorithm, while the superiority of EF discrimination was noted in unbalanced distributions in 100 observations, high selectivity rates were achieved more frequently with EG discrimination in more extensive observations.

In the data produced from the F distribution, it was seen that NB showed the highest selectivity success in fully balanced distributions for all observation numbers. While NB showed the highest success in the 0.4 class distribution out of 100 observations, the highest selectivity rates were achieved with SVM in all the remaining unbalanced class distributions. SVM reached its highest rate with EF in fully balanced distributions and minimum-maximum normalisation in unbalanced distributions. EG discrimination seems most effective on the C5.0 algorithm, increasing the selectivity rate, especially in unbalanced class distributions.

The study includes the findings regarding the highest positive predictive values (PKV) obtained from all simulation scenarios with NB, C5.0 and SVM algorithms and how they were obtained in (Table 8).

In the data produced from the normal distribution, there was no increase compared to the PKD obtained from the raw data after the data transformation in the NB algorithm. The highest PKD was obtained with SVM (M) in 100 observations and 0.1 class distribution, and NB (Gaussian) in all remaining data types. In the C5.0 algorithm, the effect of EG discrimination is noteworthy, especially in cases with unbalanced class distributions larger than 100 observations.

In the data generated from the chi-square distribution, the data transformation did not produce any increase in NB. SVM for PKD showed the highest success in all data types except 1000 observations 0.2 class distribution, and 10000 observations. The highest PKD was reached with NB (Gaussian) in 10000 observations. The highest positive predictive values were most frequently obtained in SVM with z-score transformation. While the C5.0 algorithm reaches the highest selectivity rates with raw data at 100 observations, the superiority of EG over other transformations or raw data stands out, especially for unbalanced class distributions at 1000 observations.

In the data generated from the F distribution, it was seen that NB reached the highest PKD in the 0.4-0.5 class distributions for observation numbers 100 to 500 and in the 0.3-0.4-0.5 class distributions for 1000 to 10000 observation numbers. In all remaining unbalanced class distributions, SVM showed the highest success. While the highest PKD was achieved with raw data in 100 observations in NB and EF in other observations, the minimum, maximum normalisation success rate in SVM is noteworthy. In the C5.0 algorithm, it is seen that PKD success is most often achieved with raw data.

The study includes the findings regarding the highest negative predictive values (NCV) obtained with NB, C5.0 and SVM algorithms and how they were obtained in Table 9.

In the data produced from the normal distribution, there was no increase compared to the NKV obtained from the raw data after data transformation in the NB and C5.0 algorithms. The highest NKD in all data types was obtained with NB (Gaussian). Looking at the SVM findings, it can be seen that the superiority of z-score normalisation over minimum and maximum increases as the number of observations increases and the balance ratio in classes decreases.

There was no increase in the data produced from the chi-square distribution compared to the NVC obtained from the raw data after the data transformation in the C5.0 algorithm. The highest NCD was obtained with SVM in 100 observations and all data types except 0.1 class distribution. The minimum-maximum normalisation effect was high in reaching the highest values in SVM. In NB, high values were most frequently reached with raw data.

In the data generated from the F distribution, the data transformation in the C5.0 algorithm did not have an increasing effect on NCD. It was observed that the highest NCD was achieved with C5.0 in the 0.1 class distribution for observation numbers between 1000 and 10000, and NB (EF) was achieved for all the remaining data types. The effect of EF discrimination is noteworthy in SVM and NB.

IV.2 DISCUSSION

In the current study, results were obtained on the raw data produced by simulation from different sample distributions, at different numbers of observations and different equilibrium distribution ratios of classes, as well as on the data obtained with four different transformation methods using NB, C5.0 and support vector machine classification algorithms. The performances of the three algorithms after data transformation and the raw data were compared with six different performance evaluation criteria [27].

In the study, when NB, C5.0 and SVM algorithms were compared in terms of general performance, it was seen that NB gave more successful results in data produced from a normal distribution and F distribution, and SVM gave more successful results in data produced from the chi-square distribution. When the results obtained from data generated from three sample distributions and without any pre-processing were compared with the results obtained after normalisation, it was seen that normalisation methods generally did not increase the classification performance of the NB algorithm. In the C5.0 decision tree algorithm, normalisation generally did not make any

difference compared to the results obtained from the raw data. In SVM, normalisation transformations generally increased all performance measures except the selectivity rate [28].

Kumar et al. (2019) [29], [30] investigated the all the roles of the linear discriminant analysis, k-nearest neighbour, NB, SVM, decision trees, random forest, and multilayer perceptron algorithms in performing minimum-maximum normalisation on Alzheimer's data. In their study, NB gave better results in the overall performance comparison of the algorithms. He reported that minimum-maximum normalisation did not affect the performance of decision trees and NB algorithms much, while the SVM algorithm significantly improved its performance.

Siledar and Chaudhary (2017) [31] investigated the effect of z-score normalisation in the decision tree (C4.5) and NB on the 24-variable "Credit" data with 30000 observations obtained from the UCI data warehouse. They reported no change in the decision tree (C4.5) after Z-score normalisation, but there was an increase in NB. In our study, there was no increase in NB after z-score normalisation. It is thought that the reason for this difference is that we prefer the "Kernel" probability density function instead of "Gaussian" for data that is not normally distributed.

The current study showed that the z-score transformation was more effective in increasing the performance, especially with the increase in the number of observations in the data produced from the normal distribution in the SVM algorithm. In data generated from chi-square distribution, z-score normalisation gave higher results in a fully balanced class distribution, and minimum-maximum normalisation gave higher results in data with an unbalanced distribution of classes. While minimum-maximum normalisation caused a decrease in performance in data produced from the F distribution, more successful results were obtained with z-score normalisation in data larger than 100 observations.

In our study, selectivity rates differed from other performance measures in SVM regarding conversion results. While other performance criteria in the SVM algorithm generally increased with normalisation, there was an increase in selectivity rates only in fully balanced class distributions. There was generally no increase in normally distributed data in unbalanced class distributions, but an increase was achieved in chi-square distribution data with 100 observations. Higher selectivity rates were achieved with minimum-maximum normalisation in the F distribution without changing according to the number of observations in unbalanced class distributions. There was no increase in C5.0 and NB as in other performance criteria.

Suma et al. (2016) [32] compared normalisation methods on the “Breast” data obtained from the UCI data warehouse regarding general accuracy rate, sensitivity and selectivity rates in linear discriminant analysis, SVM, NB, artificial neural networks and decision tree algorithms. In their study, they achieved the best performance with NB. While there was no increase in performance values with minimum-maximum normalisation in NB, it was shown that there was an increase in general accuracy rates with z-score normalisation. They showed that both methods increased the accuracy rates equally for SVM, while the minimum-maximum normalisation increased the sensitivity and selectivity rates. When Suma et al.'s study is compared with the NB findings in our study, it is thought that this difference is due to our preference for the "Kernel" probability density function instead of "Gaussian" for data that is not normally distributed.

In our study, it was observed that there was a decrease in the performance of NB in the data produced from normal distribution and chi-square distribution with unsupervised discrimination methods. More successful results were obtained in the NB classification, in which the data generated from the F distribution and converted to categorical form by the equal frequency spacing (EF) method, one of the unsupervised discrimination methods, was compared to the results obtained from the raw data.

Wang et al. (2023) [33] compared the error rates of different discrimination methods in the classification result of the NB algorithm on 35 data sets obtained from the UCI data warehouse. In their comparison, it was seen that EF provided lower error rates in NB compared to EG.

The current study observed that unsupervised discrimination methods caused a decrease in the accuracy rate, AUC value, sensitivity rate and negative predictive value performances of the C5.0 algorithm. When classification performances were considered in terms of selectivity rate, it was seen that EG gave better results, especially with the increase in the number of observations in data where classes were unevenly distributed. When the effect of data transformations on performance in terms of positive predictive value is examined, the superiority of EG draws attention to data produced from normal and chi-square distribution, in which classes are unevenly distributed and with several observations of 1000 and above.

Jiang et al. (2018) [17] used data from the UCI data warehouse to compare the results before discrimination in different classifiers with the overall accuracy rates obtained after applying different discrimination methods. This study showed that while there was a decrease in general accuracy rates in decision trees (C4.5) with EG, one of the discrimination methods, compared to before discrimination, there was an increase in NB. Our study's overall accuracy rates decreased with EG in the C5.0 decision tree algorithm and NB. The reason for the contradiction in the NB findings is thought to be the use of the "Kernel" probability density function instead of "Gaussian" for data that is not normally distributed.

Our study achieved an increase in SVM performance with unsupervised discrimination methods. EF discrimination was more effective than EG in SVM performance in data generated from normal distribution and F distribution. Generally, higher performances were obtained with EG in the discrimination of data generated from the chi-square distribution. According to the performance values obtained after discrimination, NB showed higher success in data produced from a normal distribution and F distribution, and SVM showed higher success in data produced from chi-square.

In the literature review [34], no study examining normalisation and discrimination methods together was found. When the normalisation and discrimination methods are examined in our study, the superiority of the transformation methods over each other differs in the classification algorithms of NB, C5.0 and SVM. In the C5.0 algorithm, no increase in performance was generally achieved with either method. Better results were obtained with the EF discrimination method in the data produced from the F distribution in NB. In SVM, a change was observed in the superiority of normalisation and discrimination methods over each other according to the data distribution. In SVM, z-score helped to achieve the best results in the majority of data produced from a normal distribution, and minimum-

maximum normalisation helped to achieve the best results in the majority of data produced from the chi-square distribution. In the data generated from the F distribution, EF discrimination was more effective in increasing the performance of SVM.

V. CONCLUSIONS

In our study, the algorithm most affected by the normalisation and discrimination methods applied before classification was SVM, while the C5.0 decision tree algorithm was determined to be the least affected algorithm. The C5.0 algorithm gave more robust results regarding data transformations in the face of data that varied in terms of data distribution, number of observations and class distribution ratio. It was seen that both normalisation and discrimination methods were influential in the performance of SVM and contributed to better results. The advantages of normalisation methods over each other varied depending on the distribution of the data, the number of observations, and whether the classes were evenly distributed. As the number of observations increased in normally distributed data, the effect of z-score transformation in improving performance also increased. In data generated from chi-square distribution, z-score normalisation gave better results in fully balanced class distributions, and minimum-maximum normalisation gave better results in unbalanced class distributions. In the data generated from the F distribution, more successful results were obtained in the data transformed with z-score normalisation compared to the minimum-maximum normalisation. In the transformations made with discrimination, there was a change in the superiority of the two methods over each other according to the data distribution patterns. EF discrimination was more effective in SVM performance than EG for data generated from normal distribution and F distribution. Generally, higher performances were obtained with EG in the discrimination of data generated from the chi-square distribution. According to the classification success achieved with SVM, among both approaches, normalisation methods are more effective in average and chi-square distribution, and EF unsupervised discrimination method is more effective in F distribution. In the NB algorithm, there was generally no increase in performance values with normalisation methods. The effect of unsupervised discrimination methods was seen in the classification made with the data produced from the F distribution. Better results were obtained from the data converted with the EF method compared to the raw data not subjected to pre-processing. When the advantages of the classification algorithms used in the study are examined, the data produced from the normal distribution and F distribution are, respectively. It was observed that normalisation methods and SVM gave more successful results in the data produced from raw data and EF and NB, chi-square distribution.

VI. AUTHOR'S CONTRIBUTION

Conceptualization: Hussein Ali Attallah, Ahmed Al-Asadi.
Methodology: Hussein Ali Attallah, Sadeer Sadeq.
Investigation: Hussein Ali Attallah, Ahmed Al-Asadi.
Discussion of results: All Authors.
Writing – Original Draft: Hussein Ali Attallah, Sadeer Sadeq.
Writing – Review and Editing: Ahmed Al-Asadi, Sadeer Sadeq.
Supervision: Hussein Ali Attallah, Ahmed Al-Asadi.
Approval of the final text: Ahmed Al-Asadi, Sadeer Sadeq.

VII. REFERENCES

[1] I. Masic, "Medical Decision Making - an Overview," Acta Inform Med, vol. 30, pp. 230-235, Sep 2022. doi:https://doi.org/10.5455/aim.2022.30.230-235.

[2] K. Kim and Y. M. Lee, "Understanding uncertainty in medicine: concepts and implications in medical education," Korean J Med Educ, vol. 30, pp. 181-188, Sep 2018. doi:https://doi.org/10.3946/kjme.2018.92.

[3] W.-T. Wu, Y.-J. Li, A.-Z. Feng, L. Li, T. Huang, A.-D. Xu, et al., "Data mining in clinical big data: the frequently used databases, steps, and methodological models," Military Medical Research, vol. 8, p. 44, 2021-08-11 2021. doi:https://doi.org/10.1186/s40779-021-00338-z.

[4] Y. A. Enaya, M. Jawad Mohammed, and G. A. Bilal, "Password-free Authentication for Smartphone Touchscreen Based on Finger Size Pattern," International Journal of Interactive Mobile Technologies (iJIM), vol. 14, pp. pp. 163-179, 11/24 2020. doi:https://doi.org/10.3991/ijim.v14i19.17239.

[5] S. S. Bafjaish, "Comparative analysis of Naive Bayesian techniques in health-related for classification task," Journal of Soft Computing and Data Mining, vol. 1, pp. 1-10, 2020. doi:https://doi.org/10.30880/jscdm.2020.01.02.001.

[6] S. Sucipto, D. D. Prasetya, and T. Widiyaningtyas, "A review questions classification based on Bloom taxonomy using a data mining approach," ITEGAM-JETIA, vol. 10, pp. 161-170, 2024. doi:https://doi.org/10.5935/jetia.v10i48.1204.

[7] Y. Y. Song and Y. Lu, "Decision tree methods: applications for classification and prediction," Shanghai Arch Psychiatry, vol. 27, pp. 130-5, Apr 25 2015. doi:https://doi.org/10.11919/j.issn.1002-0829.215044.

[8] L. V. Vaz, M. C. Gonçalves, I. C. P. Dias, and E. O. B. Nara, "Application of a production planning model based on linear programming and machine learning techniques," ITEGAM-JETIA, vol. 10, pp. 17-29, 2024. doi:https://doi.org/10.5935/jetia.v10i45.920.

[9] E. E. Ogheneovo and P. A. Nlerum, "Iterative Dichotomizer 3 (ID3) Decision Tree: A Machine Learning Algorithm for Data Classification and Predictive Analysis," International Journal of Advanced Engineering Research and Science, vol. 7, pp. 514-521, 2020 2020. doi:https://doi.org/10.22161/ijaers.74.60.

[10] Z. Zhang, Z. Zhao, D.-S. Yeom, and Z. Lv, "Decision Tree Algorithm-Based Model and Computer Simulation for Evaluating the Effectiveness of Physical Education in Universities," Complexity, vol. 2020, pp. 1-11, 2020-10-28 2020. doi:https://doi.org/10.1155/2020/8868793.

[11] U. Stańczyk, B. Zielosko, and G. Baron, "Significance of Single-Interval Discrete Attributes: Case Study on Two-Level Discretisation," Applied Sciences, vol. 14, p. 4088, 2024-05-11 2024. doi:https://doi.org/10.3390/app14104088.

[12] M. M. Ahsan, S. A. Luna, and Z. Siddique, "Machine-Learning-Based Disease Diagnosis: A Comprehensive Review," Healthcare (Basel), vol. 10, p. 541, Mar 15 2022. doi:https://doi.org/10.3390/healthcare10030541.

[13] Y. Zhang, Y. Xin, Q. Li, J. Ma, S. Li, X. Lv, et al., "Empirical study of seven data mining algorithms on different characteristics of datasets for biomedical classification applications," BioMedical Engineering OnLine, vol. 16, p. 125, 12/2017 2017. doi:https://doi.org/10.1186/s12938-017-0416-x.

[14] L. Wang, Y. Xie, M. Pang, and J. Wei, "Alleviating the attribute conditional independence and I.I.D. assumptions of averaged one-dependence estimator by double weighting," Knowledge-Based Systems, vol. 250, p. 109078, 08/2022 2022. doi:https://doi.org/10.1016/j.knosys.2022.109078.

[15] S. Xu, "Bayesian Naïve Bayes classifiers to text classification," Journal of Information Science, vol. 44, pp. 48-59, 02/2018 2018. doi:https://doi.org/10.1177/0165551516677946.

[16] D. Berrar, "Bayes' Theorem and Naive Bayes Classifier," in Encyclopedia of Bioinformatics and Computational Biology, ed: Elsevier, 2019, pp. 403-412. doi:https://doi.org/10.1016/B978-0-12-809633-8.20473-1.

[17] W. Jiang, Y. Shen, Y. Ding, C. Ye, Y. Zheng, P. Zhao, et al., "A naive Bayes algorithm for tissue origin diagnosis (TOD-Bayes) of synchronous multifocal tumors in the hepatobiliary and pancreatic system," Int J Cancer, vol. 142, pp. 357-368, Jan 15 2018. doi:https://doi.org/10.1002/ijc.31054.

[18] F. Hajjej, M. A. Alohali, M. Badr, and M. A. Rahman, "A Comparison of Decision Tree Algorithms in the Assessment of Biomedical Data," Biomed Res Int, vol. 2022, p. 9449497, 2022-7-7 2022. doi:https://doi.org/10.1155/2022/9449497.

[19] A. M. Ahmed, A. Rizaner, and A. H. Ulusoy, "A Decision Tree Algorithm Combined with Linear Regression for Data Classification," in 2018 International Conference on Computer, Control, Electrical, and Electronics Engineering (ICCCEEE), 2018, pp. 1-5. doi:https://doi.org/10.1109/ICCCEEE.2018.8515759.

[20] M. Arif, "Decision Tree Algorithms C4.5 and C5.0 in Data Mining: A Review," International Journal of Database Theory and Application, vol. 11, pp. 1-8, 2018-03-31 2018. doi:https://doi.org/10.14257/ijdta.2018.11.1.01.

[21] O. B. Ali, S. Hammami, M. Hasni, F. H'Mida, and A. N. S. Moh, "Using Machine Learning to evaluate Industry 4.0 Maturity: A comprehensive analysis highlighting Lean's impact on Digital Transformation," ITEGAM-JETIA, vol. 10, pp. 156-167, 2024. doi:https://doi.org/10.5935/jetia.v10i50.1262.

[22] R. Revathy and R. Lawrance, "Comparative analysis of C4. 5 and C5. 0 algorithms on crop pest data," International Journal of Innovative Research in Computer and Communication Engineering, vol. 5, pp. 50-58, 2017. https://www.researchgate.net/profile/Revathy-Rathinasamy/publication/332036647.

[23] M. Marzuki, M. Iqbal, A. Nivada, H. Sofyan, T. Usman, N. Nazaruddin, et al., "Implementation of decision tree using C5.0 algorithm in preference and electability survey results on regional head election in Aceh," Journal of Physics: Conference Series, vol. 1882, p. 012132, 2021-05-01 2021. doi:https://doi.org/10.1088/1742-6596/1882/1/012132.

[24] T. P. Bagchi, "Support Vector Machines--An Overview," January 27-30, 2022 https://www.researchgate.net/publication/358021073_Support_Vector_Machines--An_Overview.

[25] B. Said, L. Mazouz, T. T. NAAS, Ö. Yildirim, and R. D. Mohammedi, "Broken magnets fault detection in pmsm using a convolutional neural network and SVM," ITEGAM-JETIA, vol. 10, pp. 55-62, 2024. doi:https://doi.org/10.5935/jetia.v10i48.1185.

[26] S. Uddin, A. Khan, M. E. Hossain, and M. A. Moni, "Comparing different supervised machine learning algorithms for disease prediction," BMC Med Inform Decis Mak, vol. 19, p. 281, Dec 21 2019. doi:https://doi.org/10.1186/s12911-019-1004-8.

[27] M. A. Al-Hashem, A. M. Alqudah, and Q. Qananwah, "Performance Evaluation of Different Machine Learning Classification Algorithms for Disease Diagnosis," International Journal of E-Health and Medical Communications, vol. 12, pp. 1-28, 2021-8-11 2021. doi:https://doi.org/10.4018/IJEHMC.20211101.oa5.

[28] V. Vapnik and R. Izmailov, "Reinforced SVM method and memorization mechanisms," Pattern Recognition, vol. 119, p. 108018, 11/2021 2021. doi:https://doi.org/10.1016/j.patcog.2021.108018.

[29] N. Kumar, J. Manhas, and V. Sharma, "A comparative analysis to visualize the behavior of different machine learning algorithms for normalized and un-normalized data in predicting Alzheimer's disease," Journal of Computational and Theoretical Nanoscience, vol. 16, pp. 3840-3848, 2019. doi:https://doi.org/10.1166/jctn.2019.8259.

[30] Y. A. Enaya, A. A. Karim, S. M. Saleh, and S. W. Shneen, "Adapting Wired TCP for Wireless Ad-hoc Networks Using Fuzzy Logic Control," Journal Européen des Systèmes Automatisés, vol. 57, p. 1377, 2024. doi:https://doi.org/10.18280/jesa.570513.

[31] S. Siledar and S. Chaudhary, "Comparative analysis of naive bays classifier and decision tree c4. 5 on credit payment data set," International Journal of Research in Engineering and Technology, vol. 6, pp. 43-44, 2017. https://www.researchgate.net/profile/Seema-Siledar/publication/328654658.

[32] V. R. Suma, S. Renjith, S. Ashok, and M. V. Judy, "Analytical Study of Selected Classification Algorithms for Clinical Dataset," Indian Journal of Science and Technology, vol. 9, 2016-03-22 2016. doi:https://doi.org/10.17485/ijst/2016/v9i11/67151.

[33] S. Wang, J. Ren, and R. Bai, "A semi-supervised adaptive discriminative discretization method improving discrimination power of regularized naive Bayes," Expert Systems with Applications, vol. 225, p. 120094, 09/2023 2023. doi:https://doi.org/10.1016/j.eswa.2023.120094.

[34] R. Guido, S. Ferrisi, D. Lofaro, and D. Conforti, "An Overview on the Advancements of Support Vector Machine Models in Healthcare Applications: A Review," Information, vol. 15, p. 235, 2024-04-19 2024. doi:https://doi.org/10.3390/info15040235.

APPENDIX

APPENDIX A

Table 5. The Highest AUC Values Obtained in The Study.

AUC values												
Dispersed	**Ratio**	$N = 100$			$N = 500$			$N = 1000$			$N = 10000$		
		NB	***C5.0***	***SVM***	***NB***	***NB***	***C5.0***	***SVM***	***NB***	***NB***	***C5.0***	***SVM***	***NB***
Normal	0.1	0.899	0.681	0.891	0.953	0.749	0.931	0.956	0.777	0.934	0.96	0.862	0.95
		*,#,!,	*,#,!,	*,#,!,	*,#,!,	*,#,!,	#	*,#,!,	#	!,	*,#,!,	!,	df
	0.2	0.927	0.748	0.913	0.956	0.812	0.935	0.958	0.831	0.94	0.959	0.883	0.951
		*,#,!,	*,#,!,	*,#,!,	*,#,!,	*,#,!,	#	*,#,!,	*,#,!,	!,	*,#,!,	*,#,!,	df
	0.3	0.94	0.77	0.92	0.957	0.838	0.936	0.957	0.851	0.943	0.959	0.895	0.951
		*,#,!,	*,#,!,	*,#,!,	*,#,!,	*,#,!,	!,	*,#,!,	*,#,!,	!,	*,#,!,	*,#,!,	!,
	0.4	0.944	0.783	0.926	0.958	0.85	0.939	0.958	0.862	0.945	0.959	0.901	0.953
		*,#,!,	*,#,!,	*,#,!,	*,#,!,	*,#,!,	!,	*,#,!,	*,#,!,	!,	*,#,!,	*,#,!,	!,
	0.5	0.947	0.791	0.925	0.958	0.852	0.94	0.958	0.865	0.944	0.96	0.904	0.954
		*,#,!,	*,#,!,	*,#,!,	*,#,!,	*,#,!,	!,	*,#,!,	*,#,!,	!,	*,#,!,	*,#,!,	!,
χ^2	0.1	0.791	0.644	0.854	0.881	0.723	0.909	0.898	0.72	0.917	0.919	0.806	0.921
		a.#	*,#,!,	!,	*,#,!,	*,#,!,	#	*,#,!,	*,#,!,	#	*,#,!,	*,#,!,	#
	0.2	0.836	0.698	0.888	0.896	0.757	0.916	0.905	0.773	0.916	0.921	0.833	0.921
		*,#,!,	*,#,!,	#	*,#,!,	*,#,!,	#	*,#,!,	*,#,!,	#	*,#,!,	*,#,!,	#
	0.3	0.854	0.731	0.898	0.9	0.783	0.915	0.908	0.799	0.918	0.921	0.844	0.921
		*,#,!,	*,#,!,	#	*,#,!,	*,#,!,	#	*,#,!,	*,#,!,	#	*,#,!,	*,#,!,	#
	0.4	0.855	0.738	0.901	0.902	0.796	0.916	0.911	0.811	0.92	0.922	0.851	0.922
		*,#,!,	*,#,!,	#	*,#,!,	*,#,!,	#	*,#,!,	*,#,!,	#	*,#,!,	*,#,!,	!,$
	0.5	0.86	0.744	0.896	0.906	0.801	0.914	0.911	0.813	0.917	0.922	0.853	0.922
		*,#,!,	*,#,!,	#	*,#,!,	*,#,!,	!,	*,#,!,	*,#,!,	!,	*,#,!,	*,#,!,	!,$
$F - distribution$	0.1	0.851	0.694	0.763	0.936	0.808	0.898	0.954	0.859	0.925	0.97	0.902	0.964
		$	*,#,!,	$	$	*,#,!,	$	$	*,#,!,	$	$	*,#,!,	$
	0.2	0.898	0.768	0.837	0.959	0.881	0.926	0.967	0.907	0.944	0.975	0.948	0.971
		$	*,#,!,	$	$	*,#,!,	$	$	*,#,!,	$	$	a.#	$
	0.3	0.922	0.813	0.857	0.967	0.906	0.934	0.973	0.929	0.952	0.977	0.959	0.974
		*,#,!,	$	$	*,#,!,	$	$	*,#,!,	$	$	*,#,!,	$	*,#,!,
	0.4	0.921	0.822	0.857	0.969	0.915	0.938	0.974	0.934	0.953	0.978	0.962	0.975
		*,#,!,	$	$	*,#,!,	$	$	*,#,!,	$	$	*,#,!,	$	$
	0.5	0.924	0.834	0.857	0.97	0.921	0.925	0.975	0.937	0.954	0.978	0.962	0.975
		$	*,#,!,	$	$	*,#,!,	$	$	*,#,!,	$	$	*,#,!,	$

Note ∗: Raw data; **#:** Minimum-Maximum Normalization;
!: Z-Score Normalization; ***df*:** Equal Width Spacing Discrimination;
$: Equal Frequency Spacing Discrimination.

Source: Authors, (2025).

APPENDIX B

Table 6. The Highest Sensitivity Rates Obtained in The Study.

Sensitivity Ratios													
Distribution	**Ratio**	$N = 100$			$N = 500$			$N = 1000$			$N = 10000$		
		NB	$C5.0$	SVM	NB	NB	$C5.0$	SVM	NB	NB	$C5.0$	SVM	NB
Normal	0.1	0.475	0.349	0.331	0.606	0.435	0.573	0.622	0.477	0.612	0.636	0.555	0.623
		*,#,!	*,#,!	#	*,#,!	*,#,!	#	*,#,!	*,#,!	#	*,#,!	*,#,!	!
	0.2	0.67	0.528	0.618	0.725	0.594	0.729	0.732	0.614	0.717	0.738	0.669	0.73
		*,#,!	*,#,!	#	*,#,!	*,#,!	#	*,#,!	*,#,!	#	*,#,!	*,#,!	!
	0.3	0.762	0.613	0.742	0.793	0.683	0.773	0.796	0.699	0.782	0.801	0.74	0.796
		*,#,!	*,#,!	#	*,#,!	*	#	*,#,!	*,#,!	!	*,#,!	*,#,!	!
	0.4	0.823	0.69	0.827	0.843	0.743	0.822	0.841	0.758	0.832	0.845	0.792	0.842
		*,#,!	*,#,!	#	*,#,!	*,#,!	!	*,#,!	*,#,!	!	*,#,!	*,#,!	!
	0.5	0.866	0.745	0.83	0.879	0.795	0.866	0.879	0.803	0.869	0.881	0.834	0.88
		*,#,!	*,#,!	!	*,#,!	*,#,!	!	*,#,!	*,#,!	!	*,#,!	*,#,!	!
χ^2	0.1	0.248	0.264	0.172	0.369	0.336	0.408	0.39	0.36	0.468	0.444	0.399	0.522
		*,#,!	*,#,!	!	*,#,!	*,#,!	#	*,#,!	*,#,!	#	*,#,!.$	*,#,!	#
	0.2	0.474	0.437	0.468	0.557	0.497	0.658	0.579	0.514	0.674	0.61	0.555	0.632
		*,#,!	*,#,!	#	*,#,!	*,#,!	#	*,#,!	*,#,!	#	$	*,#,!	#
	0.3	0.613	0.546	0.679	0.682	0.602	0.758	0.688	0.617	0.733	0.709	0.655	0.73
		*,#,!	*,#,!	#	*,#,!	*,#,!	#	*,#,!	*,#,!	#	*,#,!	*,#,!	#
	0.4	0.701	0.626	0.793	0.762	0.681	0.79	0.77	0.694	0.8	0.783	0.729	0.802
		*,#,!	*,#,!	#	*,#,!	*,#,!	#	*,#,!	*,#,!	#	*,#,!	*,#,!	#
	0.5	0.783	0.704	0.821	0.827	0.748	0.835	0.829	0.757	0.837	0.838	0.791	0.849
		*,#,!	*,#,!	#	*,#,!	*,#,!	!	*,#,!	*,#,!	!	*,#,!	*,#,!	#
$F - distribution$	0.1	0.497	0.38	0.148	0.573	0.549	0.394	0.612	0.632	0.476	0.673	0.712	0.651
		$	*,#,!	*	$	*.#	$	$	*,#,!	$	$	*,#,!	$
	0.2	0.681	0.563	0.375	0.755	0.705	0.624	0.776	0.735	0.683	0.803	0.781	0.788
		$	*,#,!	$	$	*,#,!	$	$	*,#,!	$	$	*,#,!	$
	0.3	0.772	0.67	0.539	0.832	0.775	0.738	0.842	0.793	0.782	0.853	0.83	0.845
		$	*,#,!	$	$	*,#,!	$	$	*,#,!	$	$	*,#,!	$
	0.4	0.801	0.732	0.663	0.87	0.819	0.805	0.878	0.829	0.834	0.886	0.866	0.88
		$	*,#,!	$	$	*,#,!	$	$	*,#,!	$	$	*,#,!	$
	0.5	0.838	0.784	0.762	0.901	0.851	0.843	0.907	0.863	0.874	0.913	0.89	0.907
		$	*.#	$	$	*,#,!	$	$	*,#,!	$	!	*,#,!	$

Source: Authors, (2025).

APPENDIX C

Table 7: The highest selectivity rates obtained in the study.

Selectivity rates												
Distribution	**Ratio**	$N = 100$			$N = 500$			$N = 1000$			$N = 10000$		
		NB	***C5.0***	***SVM***	***NB***	***NB***	***C5.0***	***SVM***	***NB***	***NB***	***C5.0***	***SVM***	***NB***
Normal	0.1	0.986	0.998	0.999	0.988	0.984	0.999	0.988	0.982	0.997	0.989	0.98	0.996
		*,#,!	$	*	*,#,!	$	*	*,#,!.df	$	*	*,#,!	df	*
	0.2	0.965	0.981	0.993	0.972	0.939	0.966	0.973	0.945	0.99	0.973	0.958	0.99
		*,#,!	$	*	*,#,!	df	!	*,#,!	df	*	*,#,!	df	*
	0.3	0.94	0.945	0.983	0.951	0.896	0.982	0.953	0.905	0.981	0.954	0.929	0.975
		*,#,!	$	*	*,#,!	df.$	*	*,#,!	df	*	*,#,!	df	*
	0.4	0.907	0.808	0.96	0.928	0.85	0.961	0.928	0.863	0.969	0.93	0.895	0.935
		*,#,!	*,#,!.df	*	*,#,!	*,#,!	*	*,#,!	df	*	*,#,!	df	*
	0.5	0.876	0.762	0.86	0.895	0.803	0.873	0.897	0.818	0.88	0.9	0.857	0.896
		*,#,!	*,#,!	#	*,#,!	*,#,!	!	*,#,!	*,#,!	!	*,#,!	*,#,!.df	!
χ^2	0.1	0.975	0.999	0.99	0.983	0.991	0.995	0.985	0.987	0.994	0.985	0.98	0.992
		*,#,!	$	!	*,#,!	$	$	*,#,!	$	*	*,#,!	df	*
	0.2	0.939	0.988	0.985	0.955	0.941	0.974	0.958	0.943	0.969	0.96	0.944	0.966
		*,#,!	$	$	*,#,!	df	*	*,#,!	df	*	*,#,!	df	*
	0.3	0.899	0.944	0.947	0.92	0.885	0.944	0.926	0.89	0.935	0.929	0.901	0.936
		*,#,!	$	df	*,#,!	df	*	*,#,!	df	*	*,#,!	df	*
	0.4	0.844	0.781	0.858	0.879	0.819	0.9	0.885	0.829	0.888	0.893	0.854	0.891
		*,#,!	df	df	*,#,!	df	*	*,#,!	$	*	*,#,!	$	*
	0.5	0.777	0.707	0.801	0.827	0.751	0.836	0.834	0.766	0.837	0.848	0.796	0.844
		*,#,!	*,#,!	#	*,#,!	*,#,!	!	*,#,!	*,#,!	!	*,#,!	*,#,!	!.$
$F - distribution$	0.1	0.982	0.995	0.998	0.991	0.993	0.998	0.992	0.994	0.998	0.996	0.996	0.998
		df	$	#.!	df	df	#	df	df	#	df	df	#
	0.2	0.962	0.975	0.991	0.978	0.977	0.993	0.981	0.982	0.993	0.991	0.992	0.995
		df	df	#	df	df	#	df	df	#	df	df	#
	0.3	0.924	0.934	0.976	0.95	0.948	0.979	0.957	0.958	0.981	0.98	0.979	0.981
		*.!	df	#	*.!	df	#	$	df	#	df	df	#
	0.4	0.905	0.842	0.945	0.934	0.897	0.925	0.938	0.911	0.926	0.946	0.937	0.943
		*	*,#,!	#	*.!	$	#	$	$	#	$	df	$
	0.5	0.875	0.789	0.782	0.908	0.867	0.857	0.917	0.887	0.888	0.925	0.911	0.921
		*.!	*,#,!	$	*.!	*,#,!	$	$	$	$	$	*,#,!	$

Source: Authors, (2025).

APPENDIX D

Table 8. The highest positive predictive values obtained in the study.

Positive Predictive Values												
Distribution	**Ratio**	$N = 100$			$N = 500$			$N = 1000$			$N = 10000$		
		NB	***C5.0***	***SVM***	***NB***	***NB***	***C5.0***	***SVM***	***NB***	***NB***	***C5.0***	***SVM***	***NB***
Normal	0.1	0.828	0.471	0.837	0.858	0.604	0.826	0.86	0.652	0.83	0.865	0.742	0.851
		*,#,!	*,#,!	#	*,#,!	df	!	*,#,!	df	!	*,#,!	df	!
	0.2	0.853	0.603	0.825	0.872	0.677	0.842	0.874	0.716	0.849	0.873	0.79	0.866
		*,#,!	*,#,!	#	*,#,!	df	!	*,#,!	df	!	*,#,!	df	!
	0.3	0.863	0.678	0.841	0.876	0.731	0.853	0.88	0.75	0.86	0.881	0.814	0.877
		*,#,!	*,#,!	!	*,#,!	*,#,!	!	*,#,!	df	!	*,#,!	df	!
	0.4	0.868	0.724	0.844	0.888	0.772	0.862	0.887	0.785	0.871	0.889	0.833	0.885
		*,#,!	*,#,!	!	*,#,!	*,#,!	!	*,#,!	*,#,!	!	*,#,!	df	!
	0.5	0.883	0.773	0.865	0.895	0.805	0.874	0.89	0.817	0.88	0.898	0.854	0.895
		*,#,!	*,#,!	#	*,#,!	*,#,!	!	*,#,!	*,#,!	!	*,#,!	*,#,!	!
χ^2	0.1	0.559	0.362	0.718	0.721	0.47	0.744	0.749	0.524	0.753	0.77	0.626	0.759
		*,#,!	*,#,!	#	*,#,!	*,#,!	#	*,#,!	df	!	*,#,!	df	!
	0.2	0.694	0.516	0.772	0.765	0.604	0.775	0.78	0.634	0.778	0.793	0.688	0.789
		*,#,!	*,#,!	!	*,#,!	$	!	*,#,!	df	!	*,#,!	df	!
	0.3	0.743	0.602	0.782	0.789	0.662	0.798	0.801	0.682	0.803	0.812	0.731	0.81
		*,#,!	*,#,!	!	*,#,!	df	!	*,#,!	df	!	*,#,!	$	!
	0.4	0.767	0.669	0.802	0.811	0.713	0.817	0.819	0.724	0.82	0.829	0.765	0.827
		*,#,!	*,#,!	!	*,#,!	#	!	*,#,!	*,#,!	!	*,#,!	$	!
	0.5	0.789	0.718	0.817	0.829	0.753	0.837	0.834	0.766	0.839	0.846	0.793	0.844
		*,#,!	*,#,!	#	*,#,!	#	!	#.!	*,#,!	!	*,#,!	*,#,!	!
$F - distribution$	0.1	0.538	0.576	0.894	0.756	0.786	0.94	0.795	0.833	0.938	0.871	0.874	0.935
		$	*,#,!	!	$	df	#	$	!	#	*.!	df	#
	0.2	0.698	0.708	0.879	0.846	0.794	0.879	0.857	0.833	0.923	0.893	0.88	0.934
		$	$	#	$	df	!	$	*,#,!	#	#.!	!	#
	0.3	0.786	0.754	0.859	0.879	0.84	0.884	0.894	0.84	0.891	0.904	0.883	0.902
		*	*,#,!	#	$	$	#	$	*,#,!	#	$	*.#	$
	0.4	0.829	0.777	0.824	0.898	0.84	0.851	0.906	0.862	0.875	0.916	0.895	0.911
		*	*,#,!	#	$	$	$	$	*,#,!	$	$	*,#,!	$
	0.5	0.861	0.802	0.79	0.908	0.868	0.856	0.917	0.886	0.887	0.924	0.91	0.92
		*	*,#,!	$	$	*,#,!	$	$	*,#,!	$	$	*,#,!	$

Source: Authors, (2025).

APPENDIX E

Table 9. The highest negatives prediction values were obtained in the study.

Negative Predictive Values													
Distribution	**Ratio**	$N = 100$			$N = 500$			$N = 1000$			$N = 10000$		
		NB	***C5.0***	***SVM***	***NB***	***C5.0***	***SVM***	***NB***	***C5.0***	***SVM***	***NB***	***C5.0***	***SVM***
Normal	0.1	0.946	0.93	0.932	0.958	0.939	0.954	0.959	0.943	0.958	0.961	0.952	0.959
		*,#,!	*,#,!	#	*,#,!	*,#,!	#	*,#,!	*,#,!	#	*,#,!	*,#,!	!
	0.2	0.924	0.887	0.913	0.935	0.902	0.934	0.936	0.907	0.932	0.937	0.92	0.935
		*,#,!	*,#,!	#	*,#,!	*,#,!	#	*,#,!	*,#,!	#	*,#,!	*,#,!	!
	0.3	0.907	0.844	0.897	0.916	0.868	0.906	0.917	0.875	0.91	0.918	0.892	0.916
		*,#,!	*,#,!	#	*,#,!	*,#,!	#	*,#,!	*,#,!	!	*,#,!	*,#,!	!
	0.4	0.891	0.805	0.889	0.9	0.834	0.886	0.898	0.843	0.892	0.9	0.866	0.898
		*,#,!	*,#,!	#	*,#,!	*,#,!	!	*,#,!	*,#,!	!	*,#,!	*,#,!	!
	0.5	0.877	0.763	0.844	0.883	0.799	0.869	0.882	0.808	0.872	0.884	0.838	0.882
		*,#,!	*,#,!	!	*,#,!	*,#,!	!	*,#,!	*,#,!	!	*,#,!	*,#,!	!
χ^2	0.1	0.924	0.921	0.916	0.934	0.929	0.938	0.936	0.931	0.943	0.941	0.936	0.948
		$	*,#,!	#.!	*,#,!	*,#,!	#	*,#,!	*,#,!	#	*,#,!.$	*,#,!	#
	0.2	0.88	0.865	0.882	0.897	0.879	0.917	0.901	0.883	0.92	0.908	0.894	0.912
		*,#,!	*,#,!	#	*,#,!	*,#,!	#	*,#,!	*,#,!	#	*,#,!	*,#,!	#
	0.3	0.849	0.815	0.874	0.872	0.836	0.897	0.874	0.842	0.889	0.882	0.858	0.888
		*,#,!	*,#,!	#	*,#,!	*,#,!	#	*,#,!	*,#,!	#	*,#,!	*,#,!	#
	0.4	0.815	0.767	0.868	0.848	0.795	0.864	0.853	0.802	0.869	0.86	0.825	0.869
		*,#,!	*,#,!	#	*,#,!	*,#,!	#	*,#,!	*,#,!	#	*,#,!	*,#,!	#
	0.5	0.792	0.716	0.827	0.829	0.752	0.838	0.831	0.761	0.838	0.84	0.792	0.847
		*,#,!	*,#,!	#	*,#,!	*,#,!	!	*,#,!	*,#,!	!	*,#,!	*,#,!	#
$F - distribution$	0.1	0.945	0.934	0.914	0.954	0.951	0.936	0.958	0.96	0.944	0.964	0.969	0.962
		$	*,#,!	*.!	$	*,#,!	$	$	*,#,!	$	*,#,!.$	*,#,!	$
	0.2	0.923	0.897	0.864	0.941	0.928	0.912	0.946	0.936	0.924	0.952	0.947	0.948
		$	*,#,!	$	$	*,#,!	$	$	*,#,!	$	$	*,#,!	$
	0.3	0.906	0.869	0.829	0.93	0.907	0.894	0.934	0.914	0.91	0.939	0.929	0.935
		$	*,#,!	$	$	*,#,!	$	$	*,#,!	$	$	*,#,!	$
	0.4	0.875	0.833	0.802	0.916	0.883	0.876	0.921	0.89	0.893	0.926	0.913	0.922
		$	*,#,!	$	$	*,#,!	$	$	*,#,!	$	$	!	$
	0.5	0.85	0.797	0.78	0.903	0.856	0.846	0.908	0.869	0.877	0.913	0.893	0.908
		$	*,#,!	$	$	*,#,!	$	$	*.#	$	*,#,!	*,#,!	$

Source: Authors, (2025)

Journal of Engineering and Technology for Industrial Applications

ITEGAM-JETIA

Manaus, v.11 n.54, p. 88-93. July/August., 2025.
DOI: https://doi.org/10.5935/jetia. v11i54.1519

ISSN ONLINE: 2447-0228

RESEARCH ARTICLE

NUMERICAL INVESTIGATION OF THE DYNAMIC BEHAVIOR OF 2D STEEL STRUCTURES WITH CFST COLUMNS IN SEISMIC ZONES

Dif FodiL[1], Said Hicham Boukhalkhal[2], Abdallah Yacine Rahmani[3], Abderahman Younsi[4]

[1] Ziane Achour University of Djelfa , Algeria
[2] Civil Engineering and Sustainable Development Laboratory, Ziane Achour University of Djelfa , Algeria
[3]Built Environment Research Laboratory - Faculty of Civil Engineering. USTHB,Algeria
[4]Department of Civil Engineering, Faculty of Technology, University of Medea, Algeria

[1]http://orcid.org/0009-0006-3151-9739, [2]http://orcid.org/0000-0003-1593-591X
[3]http ://orcid.org/0000-0002-5095-2814, [4]http ://orcid.org/0000-0002-4267-3786

Email: f.dif@univ-djelfa.dz , saidhichamboukhalkhal@yahoo.fr , saidhichamboukhalkhal@yahoo.fr , abderrahman@univ-medea.dz

ARTICLE INFO

Article History
Received: March 17, 2025
Revised: April 20, 2025
Accepted: June 15, 2025
Published: July 31, 2025

Keywords:
Semi-rigid connections,
CFST columns,
Nonlinear dynamic analysis,
Composite structures,
Ductility,

ABSTRACT

Concrete-filled Hollow Rectangular Section Columns (RHS-CFST) are widely used in steel structures in seismic zones due to their ductility, energy dissipation, and load-bearing capacity. This study investigates the seismic response of structures with I-beam to RHS-CFST column connections in compliance with the Algerian seismic code, RPA 99/2003. The dynamic response of a 9-story steel structure is analyzed, examining the impact of CFST columns, building height, and connection types. Results indicate that CFST columns exhibit symmetrical behavior under seismic loading, which effectively reduces base shear forces and minimizes inter-story drift. Despite their semi-rigid nature, these columns demonstrate high energy dissipation, significant ductility, and a broad hysteresis loop, ensuring structural resilience and safety. As the Algerian code currently lacks specific provisions for this structural type, this study provides critical insights to advance seismic performance parameters for steel structures that incorporate CFST columns.

Copyright ©2025 by authors and Galileo Institute of Technology and Education of the Amazon (ITEGAM). This work is licensed under the Creative Commons Attribution International License (CC BY 4.0).

I. INTRODUCTION

In seismic zones, enhancing the performance of steel structures is often achieved through the use of concrete-filled hollow rectangular section (RHS) columns (CFST), which provide high strength, ductility, and energy dissipation capabilities. Extensive research has investigated the behavior of these CFST systems, especially in connection with semi-rigid or rigid joints that influence seismic performance. Early studies by. [1],[2]. According to [3] focused on cyclic performance and hysteretic behavior in blind bolted end-plate connections to CFST columns, demonstrating notable seismic resilience in composite frames. Further experimental studies [4],[5] examined CFST column connections in moment-resisting frames, where performance metrics such as strength, ductility, and energy dissipation were highlighted, solidifying their applicability in earthquake-resistant designs.

Recent work has continued to expand on these findings, exploring new materials and joint designs to improve seismic response in composite steel structures. As an example, according to [6], investigated the axial compressive strength of CFST columns and observed a remarkable 50% improvement when the columns were reinforced with five layers of fiber-reinforced polymer (FRP). The influence of column height, connection type, and structural rigidity on seismic behavior has also been extensively examined in CFST frameworks [7], with findings emphasizing the critical role of joint semi-rigidity in dynamic response. Advances in modeling techniques, as demonstrated in numerical and pseudo-dynamic studies [8], further validate the CFST's effectiveness in reducing base shear and limiting inter-story drifts in multi-story steel buildings.

The present study seeks to contribute to this body of work by evaluating the inelastic dynamic responses of steel structures with both rigid and semi-rigid CFST column connections in high seismicity areas. Using SeismoStruct 2016 [9], simulations will assess the performance of CFST columns compared to open-section columns, with reference to the Algerian [10-12], seismic standards. Given

the absence of CFST-specific provisions within the Algerian code, this research aims to establish foundational parameters for CFST-based design in Algeria and other high seismicity zones, enhancing safety and reliability in steel structural systems.

II. PRESENTATION OF THE INVESTIGATED STRUCTURES

This study examines a nine-story, two-dimensional (2D) steel frame designed as an office building, utilizing various column types for a comparative structural analysis (Figure 1). The building's dead load (G) is $18.84\ kN/m$, while the live load (Q) stands at $4.39\ kN/m$. Detailed specifications for all structural components—beams, columns, and connections—are provided in Table 1.

Each component within the portal frames is designed according to three structural codes: Eurocode 3 (EC3) [13], Eurocode 4 [14], and Algeria's seismic code [10],. For material properties, S235 grade steel is employed for the beams, while S355 grade steel is used for both steel and composite columns. In composite columns, C20/25 grade concrete is used. Structural modeling and analysis were conducted using SeismoStruct software [9], with the non-linear inelastic properties of each structural element—columns and beams—modeled using a force-based frame element approach ('infirmFB'). The model includes non-linear material properties and geometric effects, with fixed nodes assumed for rigid connections. A Response spectrum analysis was performed for the structural design, incorporating response spectrum data for high-seismic regions and load combinations specified in Algeria's [10],[11].

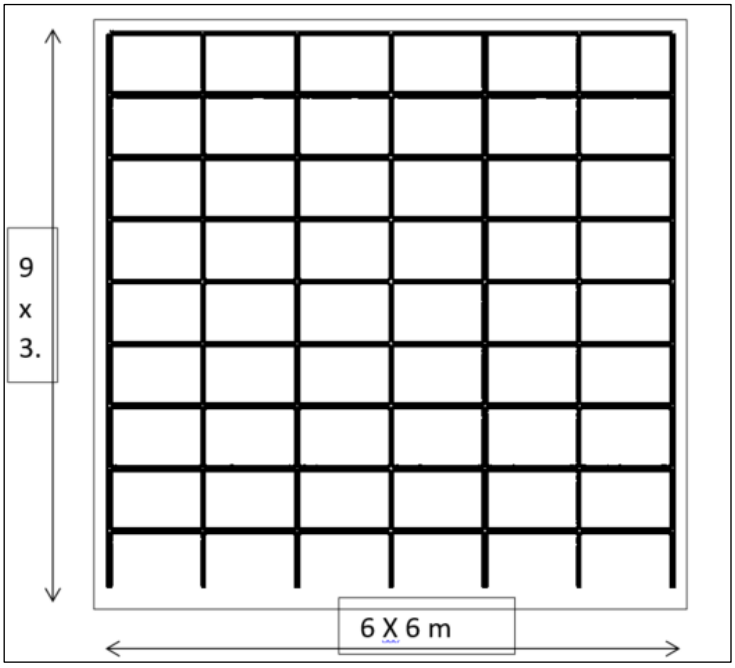

Figure 1: 2D frame configuration.
Source: Authors, (2025).

Table1: Cross-sections of structural elements.

Frame		Beam section	Column section
9FRJ and 9FSRJ*	Story 9	IPE 300	HEB 200
	Story 8		
	Story 7		
	Story 6	IPE 330	HEB 260
	Story 5		
	Story 4		
	Story 3	IPE 360	HEB 300
	Story 2		
	Story 1		
9FRJ-CFST* and 9FSRJ-CFST	Story 9	IPE 300	SHS 300X300X10
	Story 8		
	Story 7		
	Story 6	IPE 330	
	Story 5		
	Story 4		
	Story 3	IPE 360	
	Story 2		
	Story 1		

**FRJ: frame with rigid joints; FSRJ: frame with semi-rigid joints; CFST: frame with concrete filled steel tube.*
Source: Authors, (2025).

Two column configurations are presented (see Figures 2-a and 2-b), both utilizing an extended end plate connection type with plate dimensions of $450x180x30\ mm$ (Figure 2-c). The connection bolts have a diameter of $24\ mm$ and are classified as 8.8-grade. Connection properties, such as initial stiffness and resistance moments, were calculated according to Article 6, Table 6.1, of EC3 [13].

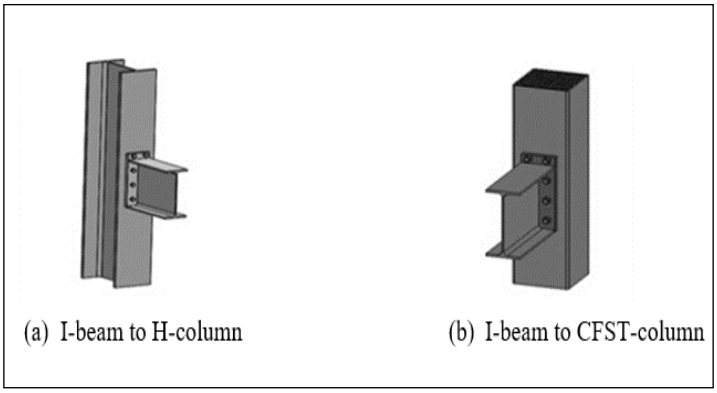

Figure 2: Joint configuration.
Source: Authors, (2025).

The structural integrity and stiffness of the tube face are determined using models by Silva et al. [15], In the global analysis, the semi-rigid connections are modeled with a cyclic bilinear behavior curve, incorporating strain hardening of $r = 0.1$ [16], capturing the realistic behavior of these connections under cyclic loading.

III. NONLINEAR DYNAMIC ANALYSIS

Given the significant influence of CFST (Concrete-Filled Steel Tube) columns on the inelastic dynamic behavior of steel frames, a nonlinear dynamic analysis was conducted using SeismoStruct software [9], For frames with relatively long natural periods, a notable response to seismic excitation, especially with a low a/v ratio (ratio between peak ground acceleration, PGA, and peak ground velocity, PGV), was anticipated.

To simulate seismic loading, an artificial ground motion time history was generated based on the target response spectrum from Algeria's [10], (see Figure 3). The dynamic behavior of the portal frames using CFST columns was evaluated by analyzing key dynamic response parameters, highlighting the influence of these columns on the overall structural performance under seismic conditions.

In addition to the nonlinear dynamic analysis, pushover analysis can be employed to investigate the nonlinear static behavior of these structures [17-19], This method provides valuable insights into the building's capacity, failure mechanisms, and potential plastic hinge formations, offering a complementary perspective on the seismic performance of steel frames with CFST columns.

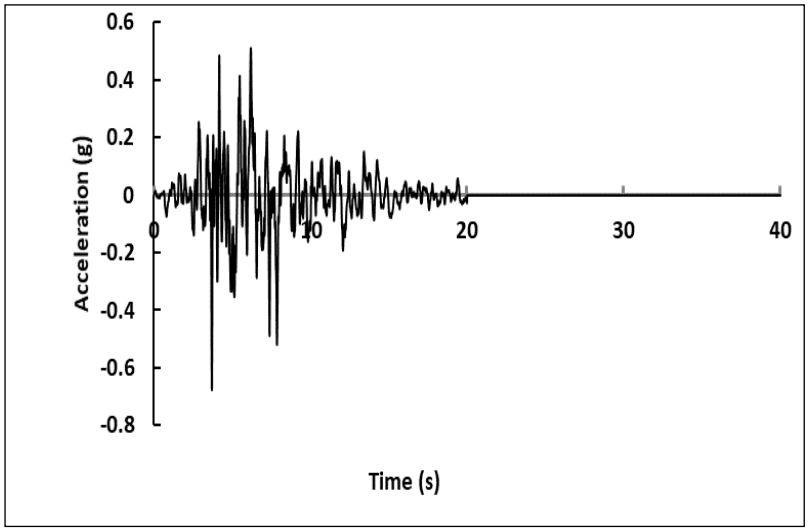

Figure 3: Artificial ground motion time history.
Source: Authors, (2025).

IV. RESULTS AND DISCUSSIONS

IV.1. MAXIMUM STORY DISPLACEMENT

Figure 4 depicts the maximum displacements at each story. The rate increases from for the portal frame with CFST columns. In dynamic analysis, this change is explained by the presence of the damping effect caused by both the connection and the structure.

It is worth noting that CFST columns exhibit symmetrical behavior in response to seismic excitation: displacements are nearly identical in both negative and positive directions, in contrast to frames with open sections columns, which exhibit asymmetrical behavior; this is another advantage of using CFST columns in seismic zones.

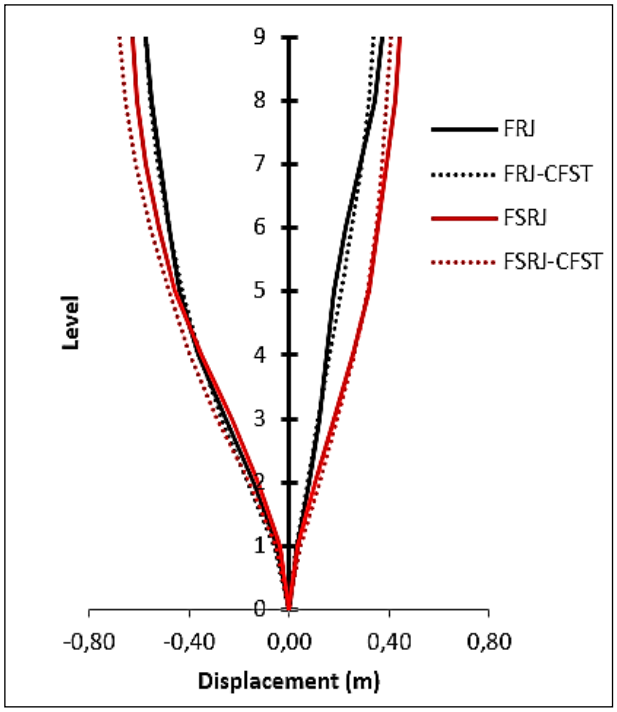

Figure 4: Maximum displacement.
Source: Authors, (2025).

IV.2. INTER-STORY DRIFTS

The inter-story drifts exceed the limits set by [10], in the majority of portal frame scenarios, as illustrated in Figure 5. Conversely, they remain below the thresholds established by FEMA 356 [12].

Furthermore, the increased inter-story drifts can be attributed to the fact that the [10], code does not account for the plasticity of structural elements in its design provisions. Instead, the code primarily relies on force-based design criteria. In contrast, the American FEMA 356 code [12], incorporates plasticity considerations in its approach.

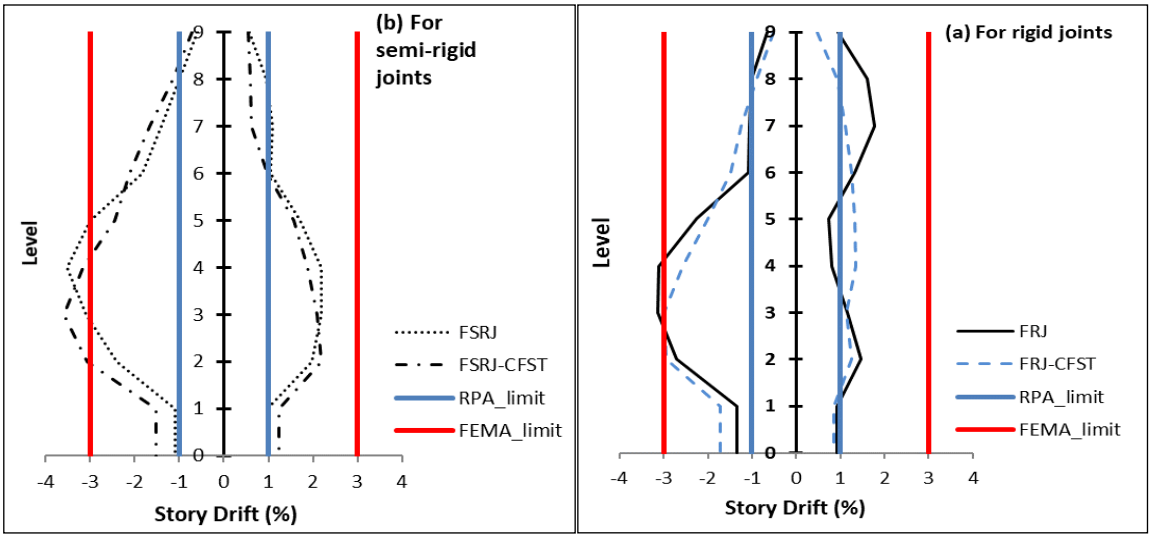

Figure 5: Inter-story drifts.
Source: Authors, (2025).

IV.3. BASE SHEAR FORCES

As demonstrated in Figure 6, the use of CFST columns reduces shear force at the base by 30% for rigid connections and 27% for semi-rigid connections as compared to the FRJ portal frame, reducing the influence of seismic loading in the structure's parts.

Furthermore, semi-rigid connections enhance shear forces at the base, which is connected to structural damping.

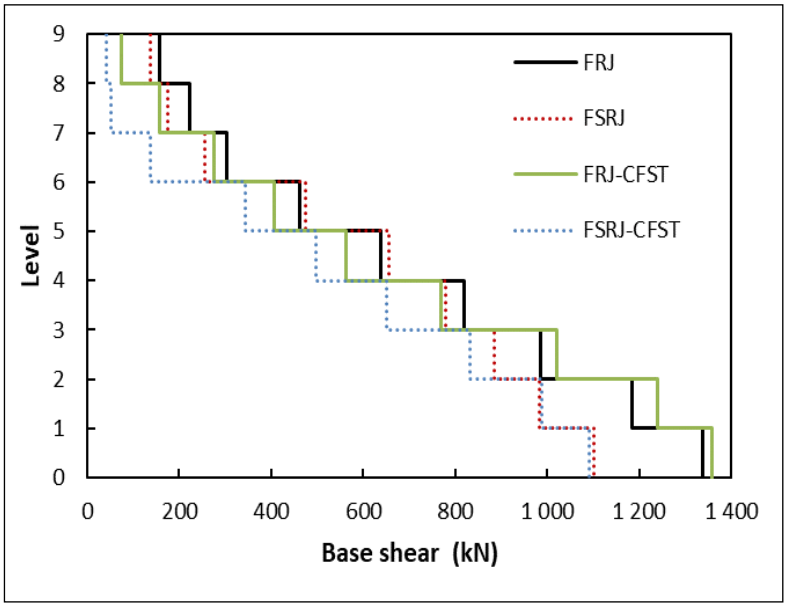

Figure 6: Base shear forces.
Source Authors, (2025).

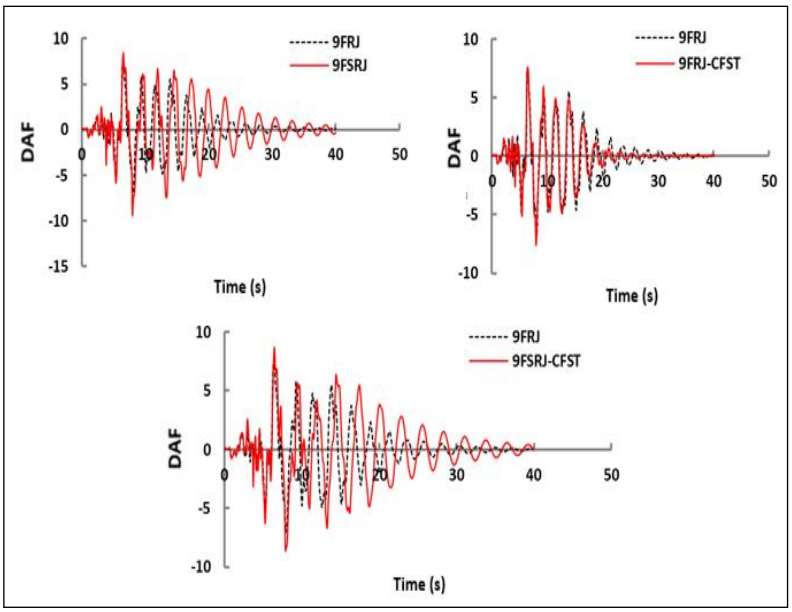

Figure 7: Dynamic amplification factor (DAF).
Source: Authors, (2025).

Figure 7 presents the dynamic amplification factor, which declines by 22% in the FRJ-CFST portal frame and 10% in the FSRJ-CFST portal frame. Compared to the FRJ frame, it increases by 4% in the FSRJ frame, as structures with semi-rigid joints exhibit higher damping than those with rigid joints.

V. CONCLUSIONS

The objective of this research is to emphasize the effect of using CFST columns with semi-rigid connections on the non-linear dynamic response of steel structures. The impact of the structure's height is taken into account by considering a 9-level structure. The primary conclusions of the comparison of these constructions with those with H-shaped columns may be stated as follows:

CFST columns reduce structural stiffness and have a greater maximum displacement than structures with rigid node;

Semi-rigid connections have a substantial impact on inter-story drifts;

The introduction of CFST columns increases the maximum displacement of the frames by 13% to 49%, depending on the type of connection, while also exhibiting symmetrical behavior under seismic excitation. However, they result in an inter-story drift rate of 2.75% in the studied examples. Additionally, portal frames with CFST columns reduce base shear forces by up to 30% and the dynamic amplification factor by up to 22%, owing to their significant damping properties.

The use of tubular columns filled with concrete CFST has convincingly demonstrated its impact on the seismic response of steel constructions. Other paths must be investigated to emphasize optimization studies in the evaluation of the performance of this sort of structure with the various examples of connections and structure design.

VI. AUTHOR'S CONTRIBUTION

Conceptualization: Dif Fodil.
Methodology: Dif Fodil. Abdallah Yacine Rahmani.
Investigation: Abderahman Younsi.
Discussion of results: Dif Fodil. Said Hicham Boukhalkhal.
Writing – Original Draft: Dif Fodil.
Writing – Review and Editing: Dif Fodil. Abdallah Yacine Rahmani.
Resources: Abderahman Younsi.
Supervision: Dif Fodil.
Approval of the final text: Dif Fodil. Said Hicham Boukhalkhal.

VII. ACKNOWLEDGMENTS

The authors would like to thank the Director of the Laboratory of Civil Engineering and Sustainable Development and the Head of the Department of Civil Engineering, Ziane Achour University, Djelfa, for their tremendous support towards the success of this research.essary, quote entities that supported the development of the research.

VIII. REFERENCES

[1] WANG, W. DA; HAN, L. H.; ZHAO, X. L. Analytical behavior of frames with steel beams to concrete-filled steel tubular column. Journal of Constructional Steel Research, v. 65, n. 3, 2009.

[2] WANG, J.; WANG, J.; WANG, H. Seismic Behavior of Blind Bolted CFST Frames with Semi-rigid Connections. Structures, v. 9, 2017. https://doi.org/10.1016/j.istruc.2016.10.001

[3] WANG, J.; ZHANG, L.; SPENCER, B. F. Seismic response of extended end plate joints to concrete-filled steel tubular columns. Engineering Structures, v. 49, 2013. https://doi.org/10.1016/j.engstruct.2013.01.001

[4] BOUKHALKHAL, S. H. et al. Numerical modelling of CFST column to I beam end plate joints. **ce/papers**, v. 4, n. 2–4, 2021. **https://doi.org/10.1002/cepa.1388**

[5] HU, J. W. et al. Seismic design, performance, and behavior of composite-moment frames with steel beam-to-concrete filledtube column connections. International Journal of Steel Structures, v. 10, n. 2, 2010.

[6] MANSOUR, W. et al. Numerical Response of Concrete-Filled Steel Tubular (CFST) Columns Externally Strengthened with FRP Composites Subjected to Cyclic Loading. International Journal of Concrete Structures and Materials, v. 18, n. 1, p. 82, 2024. https://doi.org/10.1186/s40069-024-00716-6

[7] HE, W. H. et al. Pseudo-dynamic testing of hybrid frame with steel beams bolted to CFT columns. Journal of Constructional SteelResearch,v.88,2013. https://doi.org/10.1016/j.jcsr.2013.05.005

[8] WANG, J. et al. Cyclic testing of steel beam blind bolted to CFST column composite frames with SBTD concrete slabs. Engineering Structures, v. 148, 2017. https://doi.org/10.1016/j.engstruct.2017.06.065

[9] SEISMOSOFT. oftware for seismic analysis and structural assessment of structures. , 2016. Disponível em: https://seismosoft.com

[10] CGS. Seismic Code for Building Design and Construction. RPA99v2003 ed. Algiers, Algeria: National Earthquake Engineering Research centre, 2003.

[11] BS EN 1998-1. Eurocode 8: Design of structures for earthquake resistance - Part 1 : General rules, seismic actions and rules for buildings. [s.l: s.n.]. v. 1

[12] FEMA. Prestandard and commentary for the seismic rehabilitation of buildings. Washington (DC): [s.n.].

[13] EN 1993-1-8. Design of steel structures - Part 1-8: Design of joints. Eurocode 3, v. 3, 2005.

[14] EUROPEAN COMMITTEE FOR STANDARDIZATION (CEN)., E. PART 1-1. Design of Composite Steel and Concrete Structures, General Rules and Rules for Buildings. Brussels, Belgium: [s.n.].

[15] SILVA, L. A. P.; NEVES, L. F. N.; GOMES, F. C. T. Rotational Stiffness of Rectangular Hollow Sections Composite Joints. Journal of Structural Engineering, v. 129, n. 4, 2003.

[16] BOUKHALKHAL, S. H. Etude du Comportement des Noeuds de Structures Tubulaires RHS avec des Colonnes Remplies de Béton sous Chargements Monotone et Cyclique. [s.l.]USTHB,Alger,2019. https://dspace.usthb.dz/handle/123456789/8192.

[17] RAHMANI, A. Y. et al. Extension of the improved upper-bound pushover analysis for seismic assessment of steel moment resisting frames with setbacks. Bulletin of Earthquake Engineering, v. 20, n. 13, p. 7609–7640, 1 out. 2022. https://doi.org/10.1007/s10518-022-01478-w

[18] RAHMANI, A. Y.; BADAOUI, M.; BOUKHALKHAL, S. H. Seismic assessment of base-isolated reinforced concrete moment-resisting frames. International Journal of Structural Engineering,v.1,n.1,2023. https://doi.org/10.1504/IJSTRUCTE.2024.136895

[19] RAHMANI, A. Y.; BOUKHALKHAL, S. H.; BADAOUI, M. Effect of beam-column joints flexibility on the seismic response of setback RC buildings designed according to the Algerian seismic code. Frattura ed Integrità Strutturale, v. 16, n. 61, p. 394–409, 19 jun. 2022. https://doi.org/10.3221/IGF-ESIS.61.26

Journal of Engineering and Technology for Industrial Applications

ISSN ONLINE: 2447-0228

ITEGAM-JETIA

Manaus, v.11 n.54, p. 94-102. July/August., 2025.
DOI: https://doi.org/10.5935/jetia. v11i54.1732

RESEARCH ARTICLE OPEN ACCESS

PERSONAL SECURITY CHECKLISTA COMPREHENSIVE APPROACH TO DIGITAL SECURITY

Hitesh Choudhary[1], Navish Ansari[2] and Shraddha Sandimani[3]

[1,3,4] Department of Information Technology, Universal College of Engineering, University of Mumbai, Vasai. India.
[2] University of Mumbai, Mumbai. India.

[1]https://orcid.org/0009-0002-0669-4288, [2]https://orcid.org/0009-0004-0256-9417, [3]http://orcid.org/0009-0003-3890-1736

Email: choudhaaryhitesh557@gmail.com, ansarinavish571@gmail.com, shraddhasandimani@gmail.com

ARTICLE INFO

Article History
Received: March 19, 2025
Revised: April 20, 2025
Accepted: June 15, 2025
Published: July 31, 2025

Keywords:
Digital Security,
Cybersecurity,
Personal Security,
Two-Factor Authentication,
Secure Browsing,
User Awareness,
Data Protection.

ABSTRACT

In today's hyper-connected society, protecting personal data is not only essential, but a continuous challenge. This article presents the design, development and evaluation of the "Personal Safety Verification List", a comprehensive web -based platform that enables users to identify vulnerabilities in their digital lives and implement robust safety measures. The system categorizes tasks on three levels - essential, optional and advanced - areas such as authentication, safe navigation, messages, social media protection and safety of physical devices. Taking advantage of modern technologies such as React.JS, Next.JS, TypeScript and Chart.JS, the platform offers real -time progress tracking through dynamic views. Extensive tests and user's iterative feedback indicate that this integrated solution not only increases the awareness of cyber security, but also motivates proactive behavior, simplifying complex protection strategies.

Copyright ©2025 by authors and Galileo Institute of Technology and Education of the Amazon (ITEGAM). This work is licensed under the Creative Commons Attribution International License (CC BY 4.0).

I. INTRODUCTION

I.1 BACKGROUND

The advent of digital technologies revolutionized the way we interact, communicate and conduct business. With the rapid expansion of on -line services and the omnipresence of mobile devices, sensitive personal information is now stored and transmitted by digital networks on an unprecedented scale. However, this digital revolution has inherent risks of crimes, data violations and identity theft are widespread concerns. Current security solutions usually address only unique aspects of digital protection, resulting in a fragmented security scenario that places the burden of user integration. The "Personal Security Verification List" is designed to fill this gap, consolidating various security measures in a friendly interface, thus allowing comprehensive digital protection [1],[2].

I.2 RATIONALE

Traditionally, safety tools demand user engagement across disparate applications with unique complexities and UI. This division is too much for not -technical users, who must have clear instructions. Specific events in the world of cyber security have highlighted the vulnerable nature of many systems, their complexity and failure to integrate. That's where the "Personal Security Verification List" helps: it groups security elements together in a single panel, so it's no longer complex to be digital safety practices and motivates users to deal with potential threats before they manifest [3], [4].

I.3 SCOPE AND RELEVANCE

This research targets individuals, families and even micro enterprises that require adequate digital security services but do not have the budget for full-fledged corporate solutions. The world we live in today is always evolving, and so are cyber threats, which is why

there is a need for a tool that not just trains users in best practices, but also monitors and updates in real time. The “Personal Security Verification List” is an educational tool- it features assets such as progress bars and radar charts, which assist users in surveying and enhancing their safety posture. This double function feature is especially important in the world of rapidly changing technology [5],[6].

II. OBJECTIVES

The "Personal Security Verification List" project has the following main goals and objectives:

- **Develop Security Policies:** Create a verification list covering essential areas, which includes authentication, safe web browsing, message security, social media account privacy, and device safeguarding [1]
- **Educate and Empower the User:** Outline and provide step-by-step instructions for each protective action that aims at empowering the users so as to help them practice effective safety measures [4].
- **Enable real-time Interactive Progress Tracking:** Add graphically appealing components such as, a radar chart and progress bar and panel whereby the users can monitor their level of safety in real-time [7].
- **Provide a coherent and simple end-user experience:** Provide an interface that combines a variety of safety features and offers great usability to individuals regardless of their technical skills [2].
- **Ensure extend ability and future inclusion:** Build the system on modular design principles so that additional options can be added in the future, such as, network scanning capabilities or real-time assessments of the strength of passwords for the changing cyber security environment [3],[5].

III. LITERATURE SURVEY

According to explore the effectiveness of multi-factor authentication (MFA) in reducing unauthorized access while also addressing its usability challenges. Their findings highlight the need for authentication systems that are both secure and user-friendly, a balance that is critical for widespread adoption [1]. According to investigate techniques such as ad blocking and script blocking, as well as the use of secure browsers like Brave and Tor, to enhance user privacy. Their research illustrates the increasing demand for robust privacy measures in an era where online tracking is pervasive [3]. Discuss advanced encryption methods to secure email communications, while examine the challenges and benefits of implementing end-to-end encryption in messaging apps. These studies underscore the importance of balancing high-level security with usability in everyday communication tools [5], [8]. Analyze how privacy settings on social media platforms can be optimized to protect personal data while still maintaining user engagement. Their work demonstrates that proper configuration can significantly reduce exposure to cyber threats [9]. Miller and Johnson (2021) provide a comprehensive review of cybersecurity trends, emphasizing the need for adaptive and integrated security solutions that can quickly respond to emerging threats.[6] Lee and Kim (2022) delve into recent advancements in real-time data encryption and secure data handling. Their study highlights the importance of a robust backend system that supports dynamic updates and secure information processing [7]. According to evaluate various user-centric security models, underscoring the significance of designing tools that are accessible and intuitive for non-technical users [2]. Argue that integrating multiple security measures into a single platform can significantly enhance overall digital protection by positively influencing user behavior and reducing redundancy [10]. Emphasize that effective user education is a critical component of any cybersecurity strategy. They show that well-informed users are less likely to fall victim to cyber threats and more likely to adopt proactive security measures [4].

IV. EXISTING SYSTEMS

IV.1 OVERVIEW OF CURRENT SOLUTIONS

The digital security landscape today is dominated by several niche tools, such as antivirus programs, MFA apps and VPN services. These independent solutions beget results for their particular domains, but typically demand users to leverage multiple applications that can't star as well. Security best practices are also not very well documented and are split across many documents that provide fragmented and often contradictory approaches [3], [2].

IV.2 GAPS IN EXISTING SYSTEMS

The following table outlines the limitations observed in existing digital security solutions:

Table 1: Gaps in Existing Systems.

Aspect	Current Approach	Limitation
Standalone Tools	Antivirus, MFA apps, VPN services	Lack integration; users must manage multiple uncoordinated applications [3].
Security Guidance	Dispersed information across various sources	Fragmented advice leads to inconsistent security practices [5].
User Interface	Complex, technical designs	High complexity deters non-expert users from full adoption [2].
Dynamic Updates	Static, infrequently updated content	Outdated guidelines that do not rapidly adapt to emerging threats [6].

Source: Authors, (2025).

V. PROBLEM STATEMENT

Despite the multitude of available digital safety tools and guidelines, it remains a critical need for a unified and easy -to -use platform that comprehensively addresses all aspects of personal digital security.

- **Users face various challenges:** Sources of fragmented information: The need to consult various uncoordinated resources usually results in incomplete and inconsistent security practices, leaving gaps in general protection [5].
- **Usability barriers:** Many advanced security systems require high technical proficiency, making them inaccessible to the average user who needs clear and simple guidance [2].
  Threats in rapid evolution: Cyber threats are continually emerging and evolving, but many existing solutions are static and slow to update, making them less effective in real-time defences [6].

This project aims to fill these gaps, creating an integrated platform that consolidates best practices, educational content and real -time monitoring in a comprehensive solution [1], [4].

VI. LIMITATIONS OF EXISTING SYSTEMS

Current digital security solutions have many remarkable disadvantages:

- **Separate functionality:** Many existing equipment operates independently, providing a safety method that usually ignores significant weaknesses due to lack of integration [3].
- **Excessive complexity:** The very technical nature of many applications creates a clear learning state, which discourages everyday users to join these devices perfectly [2].
- **Insecure and stable material**: Based on static and old guidelines, many systems are not compatible with new threats, which reduces their general efficiency in today's rapid change [6].
- **User's sub -optimal experience:** Scented security advice and very complex interfaces significantly reduce the user's participation, resulting in insufficient protection [8].

VII. PROPOSED SYSTEM

VII.1 SYSTEM OVERVIEW

The “Personal Security Verification List” has been designed as a comprehensive and web-based application that unifies all aspects of digital security on an affordable platform. This system guides users step by step by, ensuring their digital lives, providing practical tasks and educational content in a single integrated environment [1].

VII.2 KEY FEATURES

- **Comprehensive Checklist:** The machine organizes safety responsibilities into 3 degrees—Essential, Optional, and Advanced—covering vital domains inclusive of authentication, steady net surfing, messaging privacy, social media protection, and bodily device protection [9].
- **User-Centric Interface:** Featuring a smooth, responsive dark mode layout, the platform is optimized for both computer and cellular use, enhancing usability and decreasing visible fatigue [2].
- **Real-Time Progress Tracking:** Dynamic visualizations, which include radar charts and development bars, provide users instant comments on their security posture, allowing them to screen improvements and quick discover areas requiring similarly interest [7].
- **Educational Content:** Each safety project is observed by using distinct, smooth-to-apprehend steering, practical tips, and links to additional sources, empowering users to implement the endorsed measures efficiently [4].
- **Scalability:** The modular design of the platform permits for the seamless integration of future upgrades, which includes network scanning equipment and real-time password power reviews, ensuring the gadget remains adaptive to new cyber threats [10].

Table 2: Key Features.

Feature	Description	Benefit
Comprehensive Checklist	Categorizes tasks into Essential, Optional, and Advanced levels	Provides a structured security roadmap [9]
User-Centric Interface	Clean, responsive dark mode design	Enhances accessibility and ease of use [2]
Real-Time Progress Tracking	Radar charts and progress bars that update live	Allows for continuous monitoring of security improvements [7]
Educational Content	Detailed guidance and practical tips for each task	Empowers users with actionable security knowledge [4]
Scalability	Modular design supporting future integration	Future-proofs the system against emerging threats [10]

Source: Authors, (2025).

VII.3 SYSTEM ARCHITECTURE

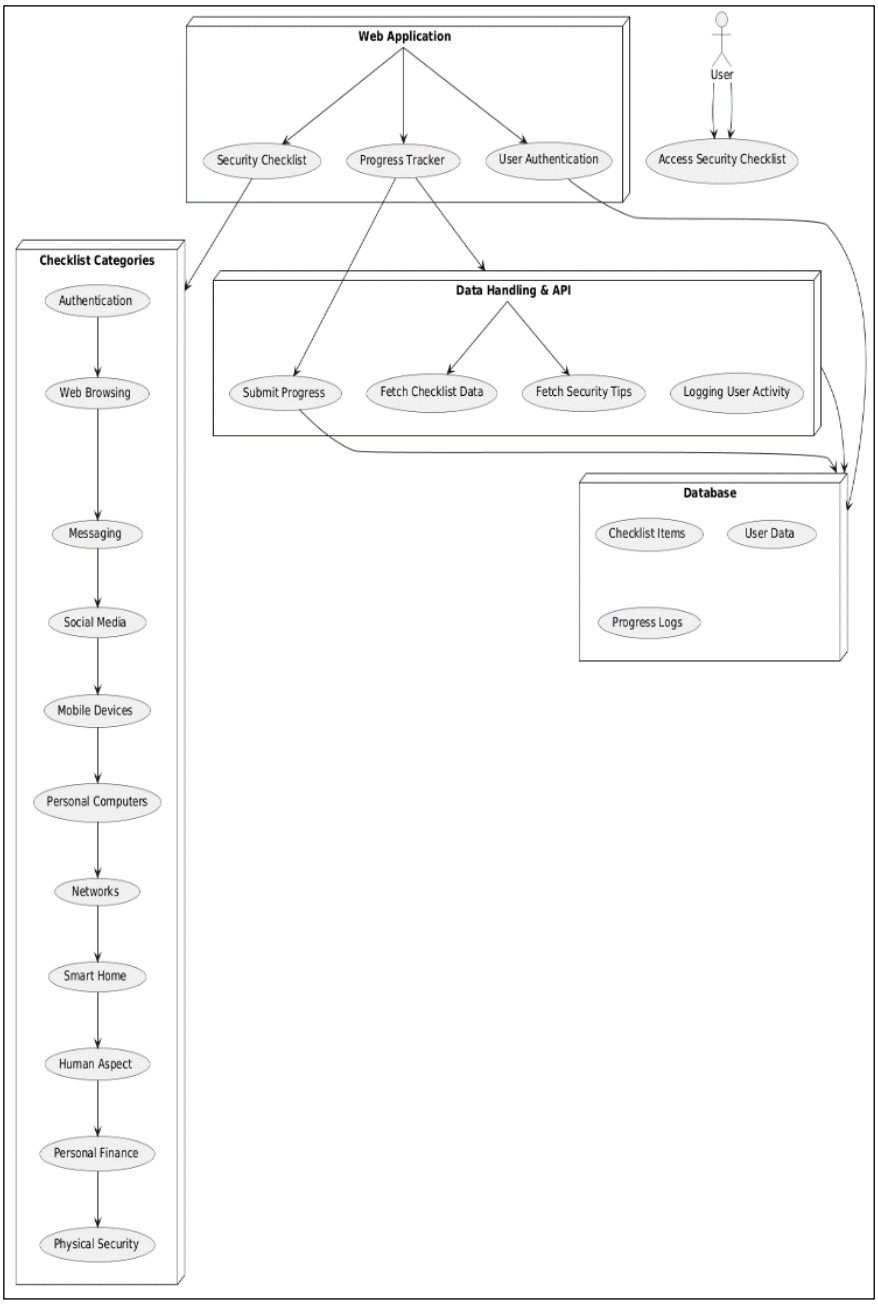

Figure 1: Personal Security Checklist System Architecture.
Source: Authors, (2025).

The structure of the web application made for tracking safety checklists is highlighted in the given diagram. Its components are defined as follows:

User interaction: Through the web application, a user can get access to the security check list.

Web application:
Three modules comprise the basic framework:
Safety Checklist: Documents all security task efforts undertaken by the user.
Pragati Tracker: Users assesses completion progress.
User authentication: Restricts access to authorized users only.
Data Handling and API Responsible for:
Presenting progress: Full position users have reached is updated by the users.
Getting checklist data: Check list item gets recurred.
Getting safety tips: Recommendations and best practices for security are rendered.
Logging User Activity: Trackable actions are logged.

Database Store:

- **Checklist Items:** Safety Procedures.
- **User data:** basic and detailed account data.
- **Pragati Log:** User Input activity record.

Checklist categories:

1. Authentication
2. Web Browsing
3. Email
4. Messaging
5. Social Media
6. Networks
7. Mobile Devices
8. Personal computing
9. Smart Homes
10. Personal Finance
11. Human aspect
12. Physical surveillance

As a result of this approach, the users are provided with the ability to track their safety practices, receive guidance, and assistance in monitoring the progress towards their targets in a secure manner. I can help you by providing more detailed information on any part if you want!

The architecture is designed to be both modular and scalable:

- **Frontend:** Developed with React.js and Next.js (using server-side rendering for faster performance) and written in TypeScript. Dynamic visualizations are powered by Chart.js. [1].
- **Backend:** A Node.js server manages authentication, data storage, and API calls, while MongoDB (or a similar NoSQL database) securely stores user data and checklist information [5].
- **Security Measures:** The platform integrates strong encryption and secure authentication methods (including 2FA) to ensure user data remains protected [8].

VIII. METHODOLOGY

VIII.1 DEVELOPMENT PROCESS

Our development technique became iterative and centered on the consumer, which includes numerous key levels:

- **Requirements Analysis:** Comprehensive research and interviews were performed to understand the not unusual digital safety challenges faced via customers. A tremendous revision of the educational literature and present structures have helped to outline the principal requirements for the system [1].
- **System Design:** Detailed wireframes, data flow diagrams (DFD) and use case diagrams have been designed to map the gadget architecture and consumer interactions. The design emphasized clarity, simplicity and simplicity of use [3].
- **Implementation:**
    - **Frontend Development:** The user interface was built the usage of React.Js and Next.Js, with TypeScript ensuring robustness and code renovation. The layout changed into optimized for response capacity among desk and furnishings devices [2].
    - **Backend Development:** An Node.JS server, supported by a MongoDB database, has been applied to manipulate user information and facilitate real-time updates from the safety tick list [5].
- **Test and Evaluation:** Strict tests had been achieved using the Jest and Reaction Test Library. Pilot customers supplied feedback that became usually incorporated to refine the platform [7].
- **Implementation and tracking:** The software turned into applied on a scalable cloud platform, and non-stop monitoring has been hooked up to tune overall performance, time of pastime and person involvement, making sure a super experience. [10]

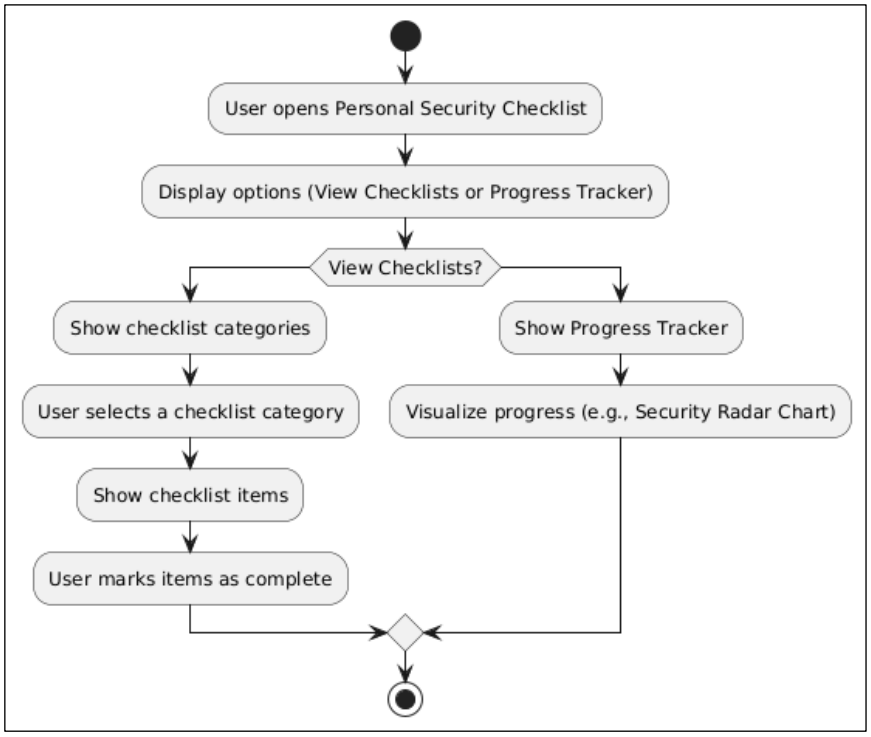

Figure 2: Flowchart of Personal Security Checklist.
Source: Authors, (2025).

This flowchart represents the user journey through the Personal Security Checklist web application. It visually explains how a user interacts with the system to either check security tasks or track their progress.

Step-by-Step Explanation of the Flowchart

1. **User Opens the Personal Security Checklist**
- The journey begins when the **user accesses the security checklist application**.
- This could be by **logging in** or **navigating to the checklist page**.

2. **Display Options: View Checklists or Progress Tracker**
- The system presents two choices:
- ☑ **View Checklists** – If the user wants to see security tasks and complete them.
- ☑ **Progress Tracker** – If the user wants to track their security improvements.

3. **Decision Point: Does the User Want to View Checklists?**
- The user decides between:
    - **"Yes" → View and complete security tasks**
    - **"No" → Check progress using Graphs**

Path 1: Viewing & Completing Security Checklists

If the user chooses to view the checklists:

Show Checklist Categories – The system displays security topics (e.g., Password Security, Social Media Safety, Financial Security).
User Selects a Category – The user picks a topic they want to improve.
Show Checklist Items – A list of security tasks appears for that category.
User Marks Items as Complete – Once a task is done, the user checks it off.
Example:

- The user selects **"Mobile Security"**
- Checklist item: "Enable Two-Factor Authentication"
- The user enables it and marks it as **completed** ☑

Path 2: Tracking Progress

If the user chooses to track progress:

Show Progress Tracker – The system loads a visual representation of progress.

Visualize Progress (e.g., Security Radar Chart) – The system displays security strengths and areas needing improvement.
Example:

- A radar chart shows that the user has completed 80% of Social Media Security but only 20% of Financial Security.
- This encourages the user to focus on weaker areas.

Final Step: The Process Loops

- Whether the user completes tasks or tracks progress, the system updates accordingly.
- The cycle continues until the user has completed all security tasks.

IX. RESULTS AND DISCUSSIONS

IX.1 IMPLEMENTATION RESULTS

Following the deployment of the "Personal Security Checklist," sizable checking out produced several noteworthy outcomes:

- **User Engagement:** Users always interacted with the platform, frequently revisiting educational content material and updating their safety settings. The dynamic visual tools, which includes radar charts and progress bars, effectively inspired users to finish duties and tune upgrades over time [4].
- **Usability:** The responsive dark mode interface turned into widely preferred for its simplicity, ease of navigation, and aesthetic attraction. Feedback from users with various stages of technical understanding confirmed that the tiered method (Essential, Optional, Advanced) helped them apprehend and manage their virtual safety more correctly.[8]
- **System Performance:** Technical reviews confirmed fast page load times, easy actual-time updates, and typical machine reliability. The effective integration of contemporary web technology with a robust backend architecture contributed to a high-overall performance platform that met user expectations [7].

IX.2 DISCUSSION

The findings suggest that an included, person-pleasant safety platform can significantly decorate private digital safety. By consolidating disparate security features into one complete interface, the "Personal Security Checklist" addresses the fragmentation common in modern-day answers. The inclusion of precise instructional content material demystifies complex security practices, constructing person self-belief and encouraging proactive engagement. Moreover, the platform's scalable design ensures it stays effective as new threats emerge, positioning it as a long-term answer for digital security [3],[8], [4].

Figure 3: Home Page of Personal Security Checklist.
Source: Authors, (2025).

The Personal Security Checklist make sure that your data is not been breached and leaked by any third party. The home page is consist of Progress bar, Graphs and Security Lists where the user can see there security of there any application and devices.

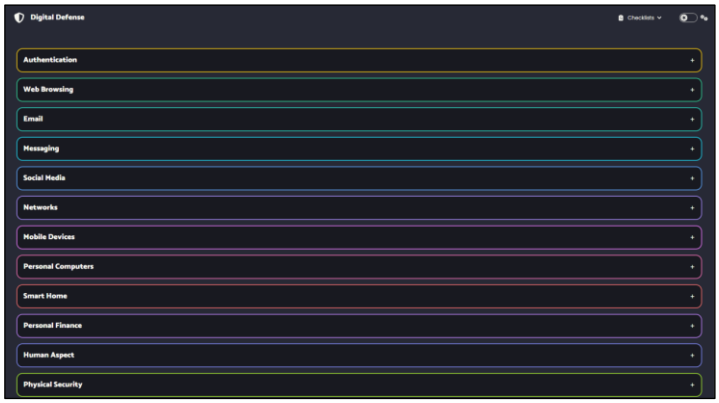

Figure 4: Category of Personal Security Checklist.
Source: Authors, (2025).

This Fig show the list of Personal Security Checklist where the user can choose any type of security from the category the user can choose the security and make the checlist more useful by checking the list which is been secure by the user. There are 3 Types of securtiy which is Essential, optional and advanced.

X. PERFORMANCE METRICS

To make certain continuous development, the subsequent key performance metrics are monitored:

- **User Engagement:** Active person counts, session durations, and the frequency of checklist completions are tracked to assess the platform's standard engagement and effectiveness in motivating users to take action. [4]
- **System Responsiveness:** Metrics including web page load times, replace latency, and gadget uptime are measured frequently to make certain a seamless person enjoy throughout all devices. [7]
- **Security Effectiveness:** The ratio of a success logins to unauthorized access attempts is constantly analyzed, in conjunction with periodic protection audits, to verify the gadget's integrity and effectiveness in defensive consumer data. [8]
- **User Satisfaction:** Surveys, net promoter rankings (NPS), and qualitative feedback are accrued and analyzed to assess consumer delight and discover potential areas for future enhancement. [10]

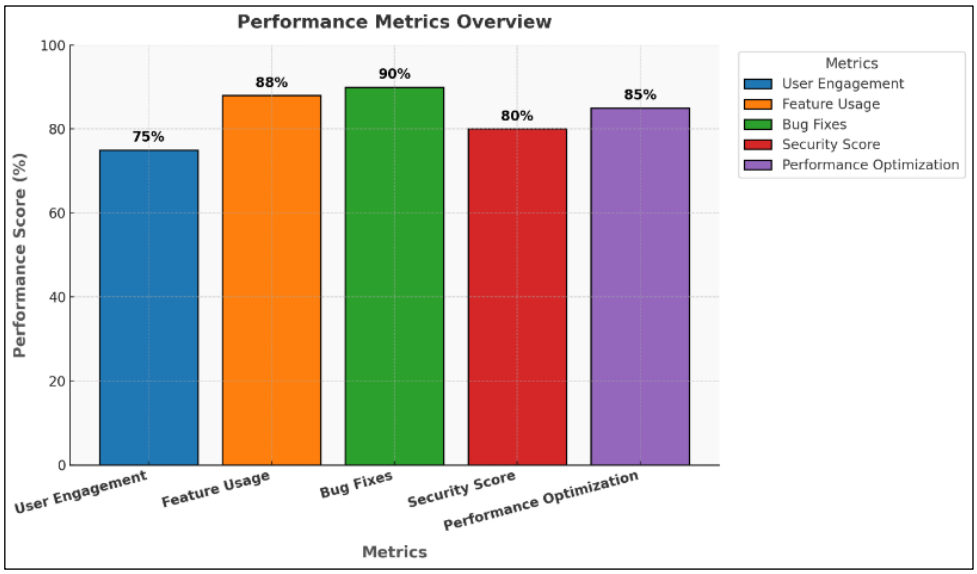

Figure 5: Performance Metrics.
Source: Authors, (2025).

XI. CONCLUSION

The "Personal Security Checklist" affords an progressive and integrated approach to virtual security through unifying multiple defensive measures into a unmarried, interactive platform. Our studies demonstrates that clear, actionable guidance paired with real-time progress tracking drastically enhances customers' capacity to stable their virtual lives. Early testing shows excessive stages of consumer engagement, usability, and delight. Moreover, the device's scalable and modular design guarantees it stays adaptable in the face of rising cyber threats. Continued improvement, together with planned future upgrades, will similarly fortify this platform as an vital device for complete digital protection.[5][6]

Future research and improvement for the "Personal Security Checklist" include:

- **Enhanced Network Scanning:** Integrating community scanning gear to locate vulnerabilities in home and business networks.
- **Real-Time Threat Intelligence:** Incorporating feeds of real-time hazard intelligence to replace security recommendations and alert users of latest dangers.
- **Advanced User Analytics:** Developing greater sophisticated analytics to higher recognize person behavior and tailor instructional content as a consequence.
- **Mobile Application Development:** Extending the platform to a dedicated cellular app to similarly improve accessibility and usefulness on smartphones and capsules.
- **User Training Modules:** Creating interactive education modules and webinars to similarly teach users on emerging cybersecurity threats and excellent practices.

XII. AUTHOR'S CONTRIBUTION

- **Conceptualization:** Mr. Hitesh Choudhary and Mr. Navish Ansari.
- **Methodology:** Mr. Hitesh Choudhary and Mr. Navish Ansari.
- **Investigation:** Mr. Hitesh Choudhary and Mr. Navish Ansari.
- **Discussion of results:** Mr. Hitesh Choudhary, Mr. Navish Ansari and Ms. Shraddha Sandimani.
- **Writing – Original Draft:** Mr. Hitesh Choudhary, Mr. Navish Ansari and Ms. Shraddha Sandimani.

- **Writing – Review and Editing:** Mr. Hitesh Choudhary, Mr. Navish Ansari and Ms. Shraddha Sandimani.
- **Resources:** Mr. Hitesh Choudhary and Mr. Navish Ansari.
- **Supervision** Mr. Hitesh Choudhary, Mr. Navish Ansari and Ms. Shraddha Sandimani.
- **Approval of the final text:** Mr. Hitesh Choudhary, Mr. Navish Ansari and Ms. Shraddha Sandimani.

XIII. REFERENCES

[1] Harrison, D. & Collins, A. (2024). *Authentication: Strengthening Access Control with Multi-Factor Authentication.* Cybersecurity in the Digital Age.

[2] Wang, L. & Patel, R. (2020). *Evaluating User-Centric Security Solutions: A Comparative Analysis.* Cybersecurity Journal.

[3] Brooks, N. & Thompson, L. (2023). *Privacy-First Web Browsing Techniques.* Navigating the Invisible Web.

[4] Davis, M. & Robinson, T. (2023). *The Role of User Education in Cyber Threat Mitigation.* Journal of Digital Security.

[5] Jameson, O. & Reynolds, S. (2022). *Securing Emails: Strategies to Prevent Phishing and Data Breaches.* Guardians of the Inbox.

[6] Miller, A. & Johnson, B. (2021). *Cybersecurity Trends in the Digital Age: A Comprehensive Review.* Journal of Cybersecurity Research.

[7] Lee, S. & Kim, H. (2022). *Advances in Real-Time Data Security and Encryption.* Journal of Information Security.

[8] Foster, L. & Bennett, S. (2024). *Ensuring End-to-End Messaging Privacy.* Whispers in the Digital World.

[9] Turner, E. & Clark, M. (2023). *Social Media: Navigating Privacy and Exposure on Online Platforms.* The Social Labyrinth.

[10] Martinez, C. & Gomez, F. (2021). *Integrated Security Systems and Their Impact on User Behavior.* International Journal of Cybersecurity.

Journal of Engineering and Technology for Industrial Applications

ITEGAM-JETIA

Manaus, v.11 n.54, p. 103-114. July/August., 2025.
DOI: https://doi.org/10.5935/jetia. v11i54.1735

ISSN ONLINE: 2447-0228

RESEARCH ARTICLE OPEN ACCESS

BLOCKARC: A BLOCKCHAIN BASED SMART CONTRACT FOR REWARD SYSTEM IN E-COMMERCE

Pooja Patil[1], Aryan Singh[2] , Aryan Raut[3] , Aakash Sharma[4] and Adarsh Rathod[5]

[1,2,3,4,5] St. John College of Engineering and Management, Palghar, Maharashtra.

[1]https://orcid.org/0009-0001-9879-0164, [2]https://orcid.org/0009-0003-1075-3946, [3]https://orcid.org/0009-0004-8867-4794, [4]https://orcid.org/0009-0000-7560-3963, [5]https://orcid.org/0009-0001-8021-0715

E-mail: ppatil879@gmail.com, aryansi0109@gmail.com, aryanraut5218@gmail.com, as024harma@gmail.com, adarshady2203@gmail.com

ARTICLE INFO

Article History
Received: March 19, 2025
Revised: April 20, 2025
Accepted: June 15, 2025
Published: July 31, 2025

Keywords:
Proof of Authority (PoA),
Ethereum & Hyperledger Fabric,
Zero-Knowledge Proofs (ZKPs),
Fraud Prevention,
Tokenized Reward Systems

ABSTRACT

The increasing reliance on e-commerce platforms has amplified challenges related to transparency, trust, fraud, and inefficiencies in reward distribution systems. Existing centralized architectures fail to address these issues effectively. This paper proposes BlockArc, a blockchain-based smart contract framework designed to revolutionize reward systems in e-commerce. The system leverages a permissioned blockchain and smart contracts to automate reward distribution, enhance security, and ensure transaction transparency. The framework consists of four layers: Blockchain Layer, Smart Contract Layer, Application Layer, and User Roles, each addressing key challenges such as reward fragmentation, fraudulent transactions, and inefficient refund processes. Smart contracts autonomously handle reward issuance, redemption, and expiration while integrating oracles for real-world data validation. Security is reinforced using cryptographic hashing, Zero-Knowledge Proofs (ZKPs), and Role-Based Access Control (RBAC) to prevent fraudulent activities. A performance evaluation demonstrated 112 transactions per second (TPS) under moderate load, fraud detection accuracy of 100%, and a 37% reduction in operational costs by eliminating intermediaries. User satisfaction surveys indicated high levels of trust and transparency. The study concludes that BlockArc enhances e-commerce reward systems by improving efficiency, security, and decentralization, paving the way for scalable and interoperable blockchain applications in digital commerce.

Copyright ©2025 by authors and Galileo Institute of Technology and Education of the Amazon (ITEGAM). This work is licensed under the Creative Commons Attribution International License (CC BY 4.0).

I. INTRODUCTION

E-commerce platforms have transformed the way trade and commerce are conducted, offering a seamless interface for transactions between buyers and sellers. However, as these platforms expand, they face critical challenges such as lack of transparency, trust issues, fraud, and inefficiencies in reward systems and product return mechanisms. Centralized architectures, which dominate the e-commerce landscape, are often unable to address these challenges effectively. The need for a decentralized, transparent, and automated solution has led to the exploration of blockchain technology and smart contracts as transformative tools for the e-commerce sector.

Centralized e-commerce platforms act as intermediaries, controlling various aspects such as payments, reward distributions, and dispute resolution. This centralization often results in opaque processes, high operational costs, and vulnerabilities to fraud. Reward systems, a critical feature of e-commerce, are plagued by fragmentation and inefficiencies. They often lack interoperability, limiting customers to specific platforms and reducing the overall value of loyalty programs. Similarly, the product return and refund process is fraught with delays and disputes, leaving both customers and merchants dissatisfied. These inefficiencies highlight the urgent need for a paradigm shift toward a decentralized and transparent approach.

Blockchain technology, with its decentralized and immutable architecture, offers a compelling solution to these challenges. By recording transactions on a distributed ledger, blockchain eliminates the need for intermediaries, ensuring transparency and security. Smart contracts, a key feature of blockchain, enable self-executing agreements that automate processes such as payments, reward

distributions, and return management. These contracts operate on pre-defined conditions, reducing manual intervention and enhancing efficiency.

A blockchain-based smart contract to store the data of payments for e-commerce platform can revolutionize the industry by addressing trust and transparency issues. Blockchain ensures that every transaction is permanently recorded and verifiable, fostering accountability among stakeholders. It also introduces tokenized reward systems where customers can earn cryptocurrency or non-fungible tokens (NFTs) for their purchases. These rewards can be securely stored, transferred, or redeemed across multiple platforms, creating a seamless and interoperable ecosystem. Furthermore, smart contracts can automate the refund process, releasing funds only when pre-defined conditions, such as product verification, are met. This reduces disputes and builds trust among users.

Fraud prevention is another critical area where blockchain excels. By providing verifiable and immutable records, blockchain reduces the risk of counterfeit products, fake reviews, and unauthorized transactions. Reputation systems built on blockchain allow users to rate merchants and products transparently, promoting accountability and trust. Additionally, NFTs can be used to tokenize products, offering proof of authenticity and ownership, which further enhances customer confidence.

This research aims to design a blockchain-based smart contract system that integrates seamlessly into e-commerce platforms to enhance reward mechanisms, streamline returns, and improve trust. The proposed system issues cryptocurrency or NFT rewards for completed transactions, automates the refund process using smart contracts, and ensures transparency through immutable records. By eliminating intermediaries, the system reduces operational costs and enhances efficiency. A security framework will also be implemented to mitigate potential vulnerabilities, ensuring the robustness of the solution.

The study contributes to the field by proposing a decentralized framework for e-commerce that addresses existing challenges in trust, transparency, and efficiency. The framework includes a tokenized reward system, a fraud prevention mechanism. It also evaluates the cost-efficiency and scalability of the proposed solution through performance analysis. The insights gained from this research will pave the way for the adoption of blockchain technology in e-commerce, fostering a more equitable and user-centric ecosystem.

II. RELATED REVIEWS

The rapid growth of e-commerce platforms has led to significant advancements in trade and commerce, but these platforms continue to face challenges such as fraud, lack of transparency, inefficiencies in reward systems, and dispute resolution issues. Centralized e-commerce models, which dominate the industry, struggle to address these concerns effectively due to their reliance on intermediaries, opaque processes, and high operational costs. In response, blockchain technology and smart contracts have emerged as transformative solutions to enhance decentralization, trust, and automation in e-commerce.

Recent research has explored the application of blockchain across various domains, demonstrating its potential to improve security, transparency, and efficiency. In the context of mobile crowdsensing (MCS) systems, blockchain has been proposed as a means to decentralize reward allocation, ensuring fair compensation for participants while addressing privacy concerns. A three-stage Stackelberg game model has been utilized to optimize utility and engagement, though challenges such as operational costs and energy efficiency remain significant hurdles [1]. Similarly, blockchain's potential in e-commerce has been demonstrated through the development of a product grading system (PGS), which standardizes product quality assessments to reduce disputes and enhance consumer trust. However, issues related to scalability, interoperability, and computational costs persist, indicating the need for further research [2].

The use of blockchain for incentivizing decentralized data sharing has also been explored, with studies leveraging evolutionary game theory to create adaptive incentive mechanisms that minimize data silos and enhance participation. While these models highlight the theoretical benefits of blockchain, real-world validation remains a challenge, and concerns such as incentive saturation and virtual currency inflation need further investigation [3]. Another significant study has introduced a blockchain-based delay-tolerant payment system for rural areas, utilizing private Ethereum blockchains to facilitate transactions in regions with intermittent connectivity. While the prototype demonstrates feasibility, concerns about infrastructure costs and scalability remain [4].

Blockchain’s role in social media platforms has been examined through an empirical study of Steemit, an incentivized blockchain-based social media network. The study reveals that while blockchain enhances content monetization, decentralization remains a challenge due to the concentration of power among large stakeholders under the Delegated Proof-of-Stake (DPoS) protocol [5]. Additionally, blockchain has been proposed as a solution for data traceability in industries such as energy, where its immutable ledger and consensus mechanisms improve accountability and security. However, real-time data processing and scalability remain major concerns [6]. In the domain of military communications, the TDL-Chain system leverages blockchain and smart contracts to enhance data transmission security and consistency, demonstrating its effectiveness but also highlighting challenges such as high communication costs and blockchain scalability in defense applications [7].

Blockchain’s applicability to software licensing has been explored through the integration of Non-Fungible Tokens (NFTs), where smart contracts enable decentralized software ownership and royalty distribution. Despite offering a more transparent licensing framework, concerns over transaction costs, security vulnerabilities, and Ethereum network dependencies persist [8]. More broadly, the increasing adoption of blockchain-based smart contracts across various industries has been documented through qualitative research involving industry leaders. Key benefits include decentralization, efficiency, transparency, and security; however, challenges such as regulatory uncertainty, scalability limitations, and integration with legacy systems remain barriers to widespread adoption [9].

In e-commerce, blockchain has been proposed as a foundation for decentralized loyalty programs, allowing multiple brands to collaborate on a unified reward system that enhances customer engagement and reduces operational costs. Unlike traditional loyalty programs, blockchain-based solutions offer interoperability, enabling customers to redeem rewards across different platforms [10]. Furthermore, blockchain oracles have been identified as a crucial technology for enabling interoperability between private blockchain networks, particularly in business-to-business (B2B) applications. Oracles facilitate secure cross-network transactions, improving efficiency and trust in enterprise blockchain implementations [11].

The existing body of research underscores the transformative potential of blockchain and smart contracts in addressing the limitations of centralized e-commerce platforms. By leveraging decentralized transaction recording, tokenized reward systems, and

automated refund mechanisms, blockchain can enhance trust, transparency, and efficiency. However, challenges such as scalability, regulatory compliance, and security vulnerabilities must be addressed for broader adoption in e-commerce. This research aims to build on these findings by designing a blockchain-based smart contract system that integrates seamlessly into e-commerce platforms, focusing on reward mechanisms, dispute resolution, and fraud prevention, ultimately fostering a more transparent and user-centric marketplace.

III. METHODOLOGY

III.1 SYSTEM DESIGN

The system design phase began with defining the architecture, components, and interactions of the proposed framework using a modular approach to ensure scalability and flexibility. This phase was critical to align the system's objectives with stakeholder requirements and to establish a blueprint for implementation.

III.1.1 Requirement Analysis:

The design process started with an in-depth requirement analysis. Surveys and interviews were conducted with e-commerce stakeholders, including customers, merchants, and platform administrators, to identify the key pain points of existing reward systems. Transparency, security, automation, and interoperability were identified as critical features. Stakeholders also expressed a need for reduced operational costs and better integration with modern payment systems. Additional in-depth interviews were conducted with financial institutions to assess compliance requirements and fraud prevention challenges, ensuring regulatory adherence.

III.1.2 Architecture Design:

A four-layered architecture was devised to structure the system:

1. Blockchain Layer: Responsible for managing transactions, maintaining the ledger, and executing smart contracts.
2. Smart Contract Layer: Implements the core business logic for reward distribution, redemption, and expiration.
3. Application Layer: Acts as the interface between users and the blockchain system, ensuring seamless interactions.
4. User Roles Layer: Defines interactions for customers, merchants, and administrators.

The design incorporated a microservices-based architecture in the application layer to ensure better scalability, fault tolerance, and modular expansion. Each service (e.g., transaction processing, reward issuance, user authentication) operates independently, improving system resilience.

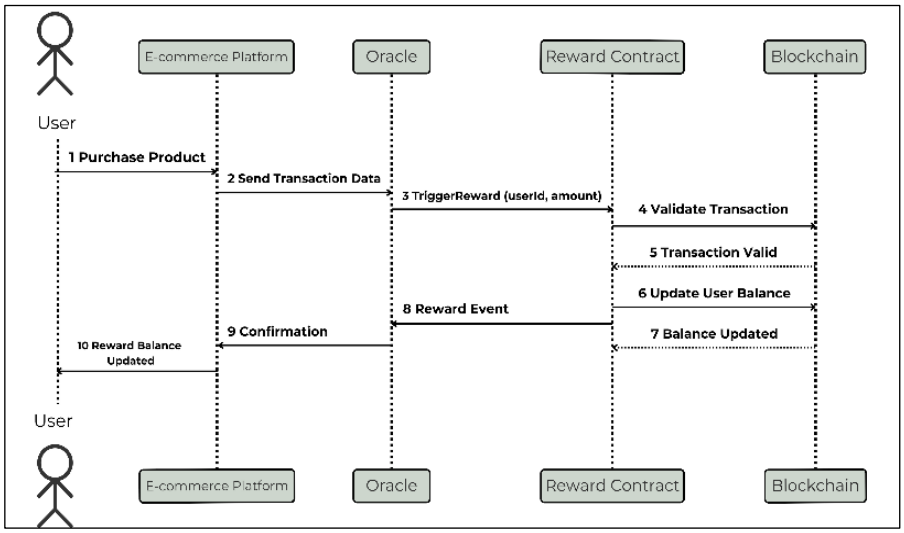

Figure 1: Sequence Diagram.
Source: Authors, (2025).

III.1.3 Consensus Mechanism Selection:

After evaluating several consensus mechanisms, Proof of Authority (PoA) was chosen for its low energy consumption, high transaction throughput, and suitability for permissioned networks. Unlike Proof of Work (PoW), PoA ensures scalability and affordability, making it ideal for e-commerce environments. This choice minimized gas fees and reduced latency in transaction processing.

Additional tests were conducted on Delegated Proof of Stake (DPoS) and hybrid models to compare efficiency, decentralization trade-offs, and cost implications. Findings reinforced PoA's selection as the most optimal mechanism for this use case.

III.2 BLOCKCHAIN IMPLEMENTATION

The blockchain implementation phase involved setting up a private Ethereum network to simulate a secure and decentralized environment for reward management. This phase ensured a robust infrastructure for handling transactions and executing smart contracts. The primary objective of this phase was to establish an immutable, trustless, and transparent system that could efficiently handle reward allocation, redemption, and expiration while minimizing security risks and fraudulent activities.

III.2.1 Node Configuration

The system was designed with multiple blockchain nodes to distribute processing power and ensure decentralization. Four nodes were configured to simulate the primary stakeholders:

1. Two customer nodes to represent users participating in the reward system.
2. One merchant node to handle transactions from businesses offering loyalty rewards.
3. One administrator node responsible for overseeing network operations and validating transactions.

Docker containers were employed to isolate the processes running on each node, ensuring a scalable and modular architecture.

The nodes were connected to the private Ethereum network via JSON-RPC (Remote Procedure Call) interfaces, allowing real-time communication between system components. The JSON-RPC interface facilitated interaction between external applications and the blockchain, enabling customers and merchants to securely access transaction records, check reward balances, and execute smart contract operations.

Furthermore, each node was equipped with a fault-tolerant mechanism to ensure network stability. In case of a node failure, the remaining nodes continued transaction processing, ensuring seamless operation without data loss. This decentralized approach eliminated single points of failure, making the system more resilient and reliable.

III.2.2 Immutable *Ledger Setup*

A critical aspect of blockchain implementation was establishing an immutable ledger that records every transaction securely and transparently. The Ethereum Virtual Machine (EVM) was used to execute smart contracts, ensuring deterministic operations across all nodes.

To store and retrieve transaction data efficiently, LevelDB was utilized as the underlying database. LevelDB provided key-value storage, allowing quick lookups and efficient data management. This ensured that all reward transactions, including issuance, redemption, and expiration, were recorded immutably and retrievable in real-time.

To enhance security, every transaction was cryptographically hashed using SHA-256, ensuring that data remained tamper-proof. The cryptographic hashing mechanism allowed the system to verify transaction authenticity without exposing sensitive user details. If an unauthorized entity attempted to modify a transaction, the hash function would generate a completely different output, making tampering instantly detectable.

Additionally, Merkle Trees were implemented to improve verification efficiency. Merkle Trees enabled fast and secure validation of transactions without requiring every node to store the entire blockchain history. This feature was particularly useful in reducing storage overhead and improving network efficiency.

To address concerns about privacy, Zero-Knowledge Proofs (ZKPs) were integrated into the system. ZKPs allowed users to prove the validity of their transactions without revealing specific transaction details. This ensured that while the blockchain remained transparent and auditable, user privacy was maintained.

For example, when a customer redeemed reward points, the ZKP protocol allowed them to verify their balance and eligibility without exposing their personal transaction history. This enhanced security and privacy without compromising the integrity of the system.

III.2.3 Oracle Integration

One of the key challenges in blockchain-based reward systems is bridging the gap between on-chain smart contracts and off-chain e-commerce data. Since smart contracts cannot directly access external data sources, oracles were employed to facilitate this communication.

The system integrated Chainlink oracles, which securely retrieved real-world data and fed it into the blockchain. Oracles were responsible for fetching transaction data, such as:

1. Purchase amounts from the e-commerce platform.
2. Product IDs to ensure category-based reward calculations.
3. Customer eligibility criteria for reward issuance.

The integration process involved deploying an oracle smart contract that queried external data sources and provided verified data to the blockchain. The oracle aggregated data from multiple sources to prevent inaccuracies and ensure consistency. The retrieved data was then signed cryptographically before being submitted to the blockchain, ensuring its authenticity and preventing tampering by malicious actors.

To further enhance reliability, a decentralized oracle network (DON) was implemented. Rather than relying on a single oracle provider, multiple oracles validated the same transaction data before updating the blockchain. This approach minimized risks associated with incorrect or manipulated data entries.

For instance, when a customer made a purchase, the transaction details were verified through multiple oracle nodes before the corresponding rewards were credited to their account. This multi-verification mechanism prevented fraudulent activities, such as fake purchases or reward manipulation.

To optimize performance, batch processing techniques were employed to handle large transaction volumes efficiently. Instead of processing individual transactions sequentially, the system grouped multiple transactions into batches and updated the blockchain in a single operation. This reduced gas fees and improved overall throughput.

III.2.4 Security Enhancements in Blockchain Implementation

Given the sensitivity of financial transactions, additional security measures were implemented:

1. Role-Based Access Control (RBAC): Restricted blockchain interactions to authorized entities (customers, merchants, and administrators).
2. Multi-Signature Wallets: Required multiple approvals for high-value transactions, preventing unauthorized fund transfers.
3. Time-Locked Transactions: Introduced delays for large redemptions, allowing users to reverse accidental operations.
4. Automated Penalty System: Smart contracts imposed penalties on merchants who engaged in fraudulent behavior, such as inflating purchase values to earn higher rewards.

III.3 SMART CONTRACT DEVELOPMENT

Smart contracts were developed in Solidity v0.8.0 to automate and secure all reward-related functionalities within the blockchain-based reward system. The smart contracts were designed to be modular, scalable, and upgradeable, ensuring flexibility and ease of maintenance. Each contract addressed a specific component of the reward system, incorporating security measures such as access control, event logging, and error handling to enhance transparency and prevent fraudulent activities.

III.3.1 Reward Distribution Contract

The reward distribution contract was responsible for automatically allocating reward points based on purchase amounts. For every $10 spent, the contract granted one reward point, following predefined rules embedded in the smart contract logic.

Data validation: Purchase transactions were verified using the Chainlink oracle to ensure accurate purchase details before updating the customer's reward balance. This step minimized discrepancies and prevented fraudulent claims.

Automated allocation: Once validated, the smart contract automatically credited the customer's account with the corresponding reward points, reducing manual intervention.

III.3.2 Reward Redemption Contract

The reward redemption contract enabled customers to exchange reward points for discounts, gift cards, or other incentives, supporting various redemption options.

Tokenized rewards: Customers could redeem points for ERC-721 NFT-based discount vouchers, ensuring uniqueness and security. For instance, 500 points could be exchanged for a $5 discount, with the smart contract issuing a digital voucher as an ERC-721 token.

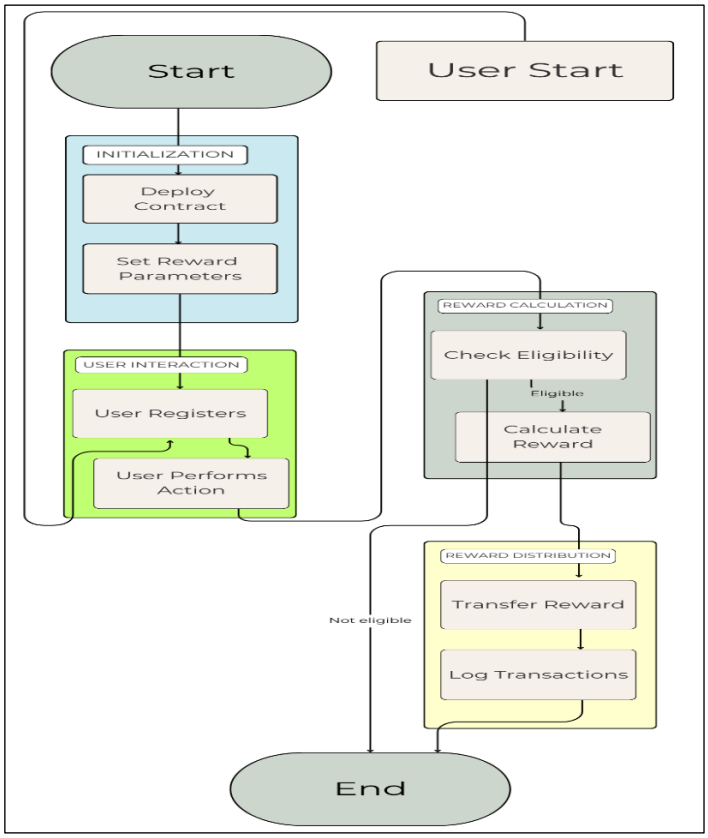

Figure 2: Smart Contract Reward Mechanism.
Source: Authors, (2025).

Balance validation: Before processing redemption, the contract checked the customer's reward balance to ensure that sufficient points were available.

Fraud prevention: The contract incorporated anti-fraud mechanisms, preventing double-spending or unauthorized redemptions through signature-based verification and timestamped transactions.

Multi-tier reward system: The contract supported tiered reward structures, offering premium users enhanced redemption benefits.

III.3.3 Expiration Policy Contract

To maintain system efficiency and prevent indefinite accumulation of unused points, an expiration policy contract was implemented.

Automatic expiration: Reward points were set to expire after 180 days from the date of issuance.

Timestamp-based validation: The contract automatically checked timestamps and removed expired points without manual intervention.

Auto-renewal for premium users: Users subscribed to premium tiers were given auto-renewal privileges, extending the validity of their reward points.

Notifications & transparency: Customers were notified via smart contract event logs about upcoming expirations, allowing them to take timely action.

III.3.4 Additional Enhancements

Upgradeable Contracts: The reward system was built using proxy contracts (e.g., OpenZeppelin's upgradeable library) to allow seamless upgrades without affecting user data.

Role-based access control: Implemented using AccessControl to define distinct roles for merchants, administrators, and customers, ensuring that only authorized entities could modify contract parameters.

Event-driven architecture: Smart contracts emitted events for every significant action, such as rewards earned, redemptions processed, or points expired, enabling transparent tracking and auditability.

III.4 APPLICATION INTEGRATION

The application integration phase focused on seamlessly connecting the blockchain-based reward system with an intuitive e-commerce platform, ensuring a user-friendly experience for customers, merchants, and administrators. This integration was designed to facilitate real-time reward tracking, secure transactions, and decentralized user interactions, improving the overall efficiency of the reward system.

III.4.1 E-Commerce Platform

A fully functional mock e-commerce platform was developed using React.js for the frontend and Node.js with Express.js for the backend. The platform included product listings, a shopping cart, a checkout system, and a reward tracking feature.

III.4.2 Frontend Features:

1. Developed using React.js with Redux for efficient state management.
2. A responsive UI/UX with an interactive dashboard displaying available products, user transactions, and reward balances.
3. Implemented Web3.js and ethers.js to facilitate blockchain-based transactions.
4. Real-time reward updates displayed on the checkout page, showing users how many points they earned per transaction.

III.4.3 Backend Integration:

1. The backend was built using Node.js and Express.js, handling API requests and managing user authentication.
2. RESTful APIs connected the e-commerce platform with the blockchain, enabling secure reward calculations and transaction processing.
3. MongoDB/PostgreSQL was used for storing off-chain customer data, such as purchase history and user preferences.
4. Chainlink oracles were integrated to validate off-chain purchase data before interacting with smart contracts.

III.4.4 Secure Transaction Processing:

1. Ethereum-based smart contracts were integrated via Web3.js to handle reward allocations and redemptions in a decentralized manner.
2. Transactions were confirmed on-chain, ensuring immutability and transparency.
3. An event-listening mechanism (via ethers.js) updated the frontend UI with the latest blockchain transaction statuses.
4. Decentralized Application (dApp):The dApp was developed as a self-contained decentralized interface for users to manage their rewards and transactions.

III.4.5 Wallet Integration:

MetaMask and WalletConnect integration allowed users to securely connect their Ethereum wallets, ensuring decentralized authentication and ownership of reward points.

Users could sign transactions directly from their wallets without relying on third-party platforms.

III.4.6 User Dashboard Features:

1. Displayed reward balances, transaction histories, and redemption options.
2. Provided real-time updates using blockchain event listeners.
3. Allowed users to redeem reward points via smart contract calls, with points converted into ERC-721 NFTs or discount vouchers.

4. *Supported multi-chain compatibility, allowing users to bridge rewards across different blockchain networks in the future.*

III.4.7 Enhanced Security & Accessibility:

1. 2FA and biometric authentication (where supported) enhanced login security.
2. Implemented role-based access control (RBAC) to ensure merchants, users, and administrators had appropriate permissions.
3. Included progressive web app (PWA) capabilities, enabling offline access for users to check reward balances.

III.4.8 Admin Dashboard

A web-based dashboard was developed for merchants and administrators to manage the reward system dynamically without requiring smart contract redeployment.

III.4.9 Smart Contract Integration:

1. Admins could adjust reward policies such as:
2. Point-to-dollar conversion rates (e.g., 10 points = $1 discount).
3. Redemption options (discounts, gift cards, exclusive offers).
4. Expiration policies (auto-renewal for premium users).
5. Updates were executed via smart contract functions, ensuring changes were reflected on-chain in real-time.

III.4.10 Merchant Control Features:

1. Provided insights into customer reward usage trends and purchase behaviors.
2. Allowed batch reward issuance for promotional campaigns.
3. Enabled automatic fraud detection, flagging suspicious redemption attempts via machine learning-based anomaly detection.

III.4.11 Scalability & Future Enhancements:

1. Designed to support multi-vendor integration, allowing multiple merchants to join the ecosystem.
2. Integrated with enterprise analytics tools (Google Analytics, Firebase, or custom BI solutions) for performance tracking.
3. Future updates planned to support cross-chain interoperability, enabling compatibility with Polygon, Binance Smart Chain, and Solana.

III.5 TESTING & EVALUATION

Comprehensive testing and evaluation were conducted to ensure the reliability, efficiency, and scalability of the system. This phase involved unit testing, integration testing, and performance benchmarking.

III.5.1 Unit Testing:

Smart contracts were rigorously tested using Truffle and Mocha frameworks. Each functionality, including reward distribution, redemption, and expiration, was validated. For example, a test case confirmed that a $20 purchase credited 4 reward points to the customer's account. Edge cases, such as invalid purchase amounts or expired rewards, were also tested to ensure robustness.

III.5.2 Integration Testing:

End-to-end workflows were tested using Cypress. Scenarios such as a customer making a purchase, earning reward points, and redeeming them were validated. This ensured seamless integration between the blockchain, smart contracts, and application layers.

III.5.3 Performance Evaluation:

Key performance metrics were measured using Hyperledger Caliper and JMeter.

III.5.4 Transaction Throughput (TPS):

The system achieved an average throughput of 120 transactions per second, suitable for medium-scale e-commerce platforms.

III.5.5 Gas Costs:

The gas cost for reward distribution was measured at 45,000 units, ensuring affordability for merchants.

III.5.6 Scalability:

Stress tests with 1,000 concurrent users demonstrated the system's ability to handle high traffic without degradation in performance

III.6 ETHICAL CONSIDERATIONS

Ensuring ethical compliance and maintaining user trust are fundamental aspects of implementing a blockchain-based reward system. Ethical considerations were prioritized to uphold principles of privacy, fairness, sustainability, and responsible system usage.

III.6.1 Data Privacy

Protecting user privacy is paramount in decentralized financial systems. To achieve this, the following measures were implemented:

1. Anonymization of User Identities: Customer identities were anonymized using hashed addresses on the blockchain, ensuring that personally identifiable information (PII) is not exposed. Instead of storing sensitive user data directly on-chain, only cryptographic hashes are used to link transactions to users.
2. Decentralized Identity (DID) Implementation: Users have full control over their identities through DID protocols, which eliminate reliance on centralized authentication systems. This approach reduces the risk of data breaches while maintaining a transparent, user-controlled ecosystem.
3. Zero-Knowledge Proofs (ZKPs): ZKPs were integrated to enable secure transaction validation without revealing user details. This ensures that transactions are verified for legitimacy without exposing unnecessary data.
4. GDPR and Compliance Standards: The system was designed to align with regulatory standards such as the General Data Protection Regulation (GDPR) and California Consumer Privacy Act (CCPA), ensuring that users' rights to data privacy and control are upheld.

III.6.2 Fairness

Maintaining fairness in the distribution of rewards was essential to prevent systemic biases and ensure that all participants benefit equitably. The following measures were taken Decentralized Governance when many Users participate in decision-making through decentralized governance mechanisms, ensuring that policies and updates to the system are driven by community consensus.

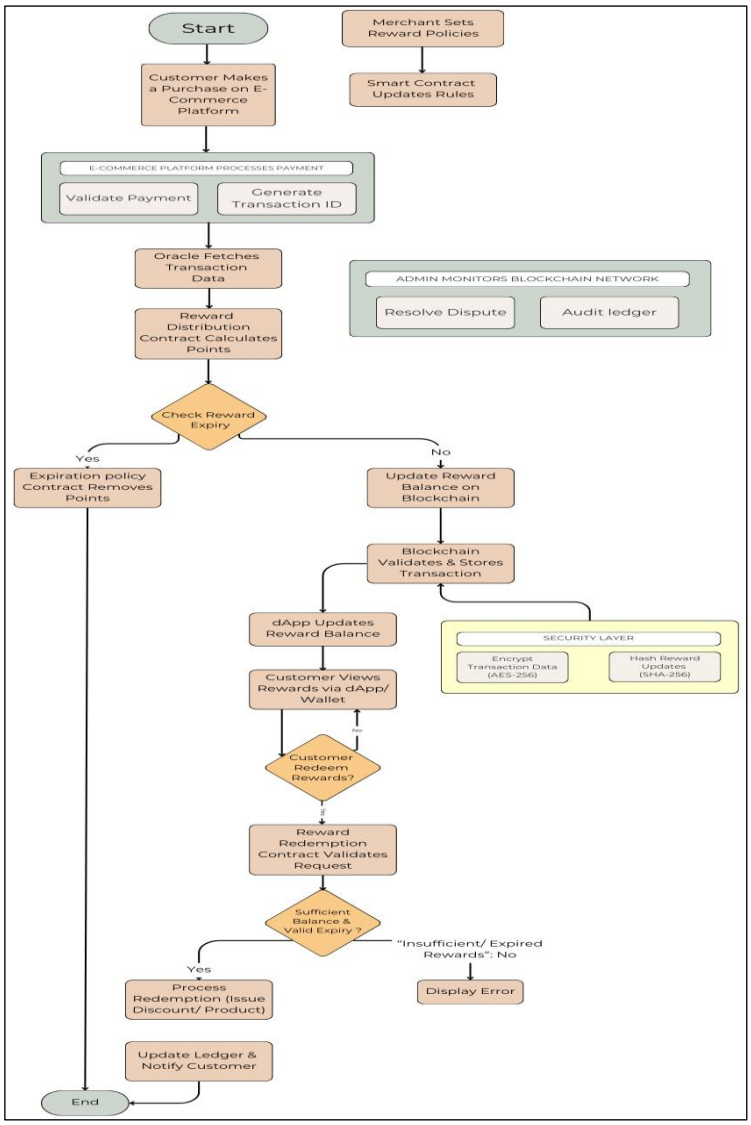

Figure 3: Flowchart.
Source: Authors, (2025).

III.7 PROPOSED SOLUTION

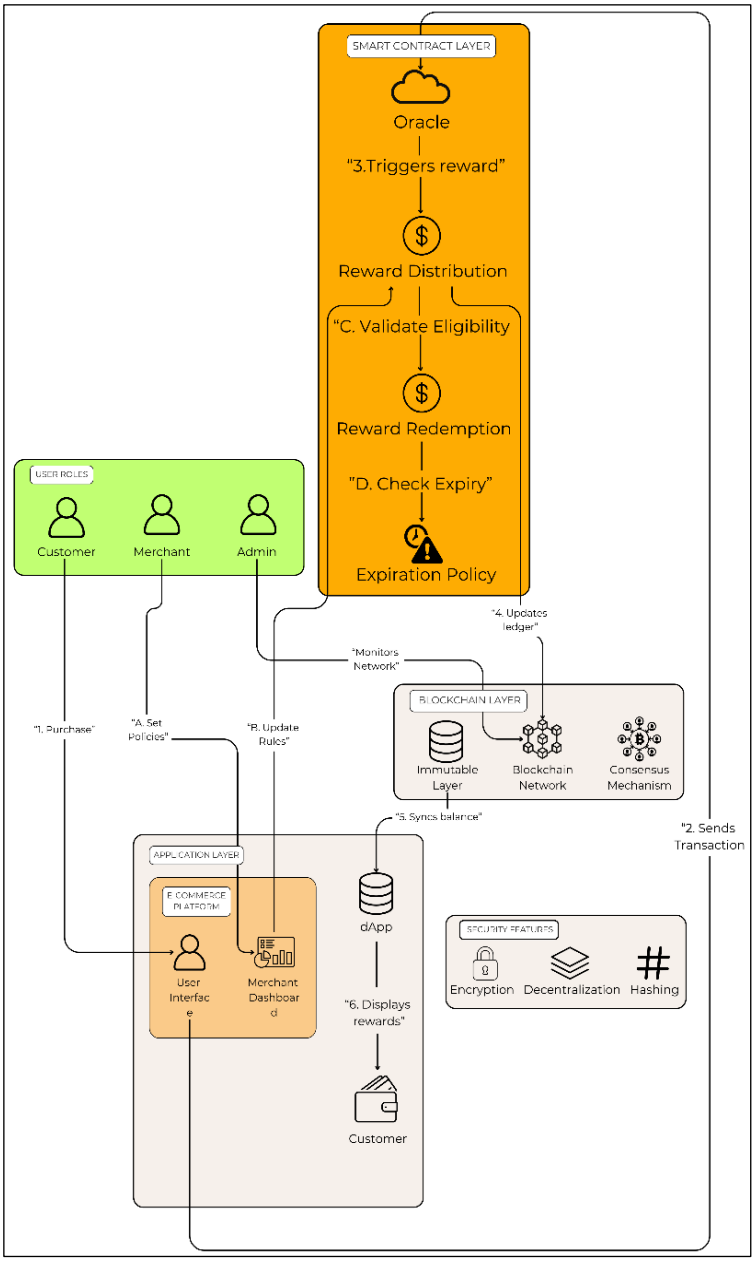

Figure 4: Architecture.
Source: Authors, (2025).

III.7.1 Blockchain Layer

The Blockchain Layer serves as the decentralized foundation of the framework, ensuring data immutability, transparency, and security. Built on a permissioned blockchain such as Hyperledger Fabric or a public blockchain like Ethereum, this layer employs a consensus mechanism (e.g., Practical Byzantine Fault Tolerance (PBFT) or Proof of Authority (PoA)) to validate transactions across a distributed network of nodes. This eliminates reliance on centralized intermediaries, mitigating risks of single-point failures and fraudulent activities. Every reward-related transaction—such as earning points, redeeming discounts, or expiring rewards—is cryptographically hashed and recorded on an immutable ledger. For instance, when a customer earns points for a purchase, the transaction is timestamped, linked to previous blocks, and broadcast to all nodes for validation. This decentralized architecture ensures that no single entity can alter historical records, fostering trust among stakeholders. Additionally, the blockchain's transparency allows customers and merchants to audit transactions in real-time, addressing the opacity inherent in traditional systems.

1. Transaction Traceability: Every reward-related transaction—such as earning points, redeeming discounts, or expiring rewards—is cryptographically hashed and recorded on an immutable ledger. For instance, when a customer earns points for a purchase, the transaction is timestamped, linked to previous blocks, and broadcast to all nodes for validation.
2. Enhanced Security: The blockchain layer integrates cryptographic encryption for added security, ensuring that sensitive customer information remains protected. Additionally, zero-knowledge proof (ZKP) techniques can be employed to validate transactions without exposing confidential details.

III.7.2 Smart Contract Layer

The Smart Contract Layer automates the core logic of the reward system through self-executing, tamper-proof agreements deployed on the blockchain. Three primary smart contracts govern the framework:

The Reward Distribution Contract defines rules for earning rewards (e.g., awarding 1 point per $10 spent). It automatically credits points to a customer's account upon purchase verification, eliminating manual intervention.

The Reward Redemption Contract validates eligibility criteria (e.g., minimum balance requirements) and processes redemption requests, converting points into discounts or products. For example, a customer redeeming 500 points for a $5 discount triggers the contract to verify their balance, deduct points, and issue a voucher.

The Expiration Policy Contract enforces time-bound reward validity (e.g., points expire after 12 months) by periodically scanning the ledger and removing expired rewards.

To bridge off-chain e-commerce data (e.g., purchase history) with on-chain smart contracts, the layer integrates blockchain oracles—secure third-party services that feed real-world data into the blockchain. This ensures smart contracts operate on accurate, up-to-date information while maintaining decentralization.

1. Enhanced Reward Distribution Contract: In addition to defining rules for earning rewards, this contract supports merchant-specific promotional campaigns, allowing businesses to introduce time-sensitive reward boosts.
2. Dynamic Reward Redemption: Smart contracts adjust reward conversion rates dynamically based on real-time demand and market fluctuations.
3. Adaptive Expiration Policy: The expiration policy contract now includes machine-learning-based optimizations that adjust expiry durations based on user behavior.
4. Integration of Oracles: To bridge off-chain e-commerce data (e.g., purchase history) with on-chain smart contracts, the layer integrates blockchain oracles—secure third-party services that feed real-world data into the blockchain.

III.7.3 Application Layer

The Application Layer provides user-friendly interfaces for stakeholders to interact with the blockchain-based reward system. The E-Commerce Platform serves as the primary interface, enabling customers to browse products, make purchases, and view reward balances. It integrates with the blockchain via APIs to fetch real-time transaction data. Merchants access a dedicated Admin Dashboard to configure reward policies, such as setting point conversion rates or modifying expiration rules. Alongside this, a Decentralized Application (dApp) acts as a blockchain gateway, allowing customers to track reward transactions, initiate redemptions, and connect their digital wallets (e.g., MetaMask). The dApp fetches data directly from the blockchain, ensuring transparency and eliminating dependency on centralized servers. Finally, Digital Wallets securely store cryptographic keys and reward points, enabling seamless and secure interactions with smart contracts. For instance, when a customer redeems rewards, the wallet signs the transaction cryptographically, ensuring authenticity before it is broadcast to the blockchain.

1. Enhanced UI for Decentralized Applications (dApps): The dApp now includes AI-powered insights, helping users optimize their rewards through predictive analytics.
2. Multi-Wallet Integration: The platform supports various digital wallets such as MetaMask, Trust Wallet, and Ledger, ensuring seamless transactions.
3. Mobile-Friendly Interfaces: The system offers a dedicated mobile application, allowing users to manage rewards from their smartphones securely.

IV. RESULTS AND DISCUSSIONS

The proposed blockchain-based reward system was implemented and tested in a simulated e-commerce environment to evaluate its performance, security, and usability. The results are categorized as follows:

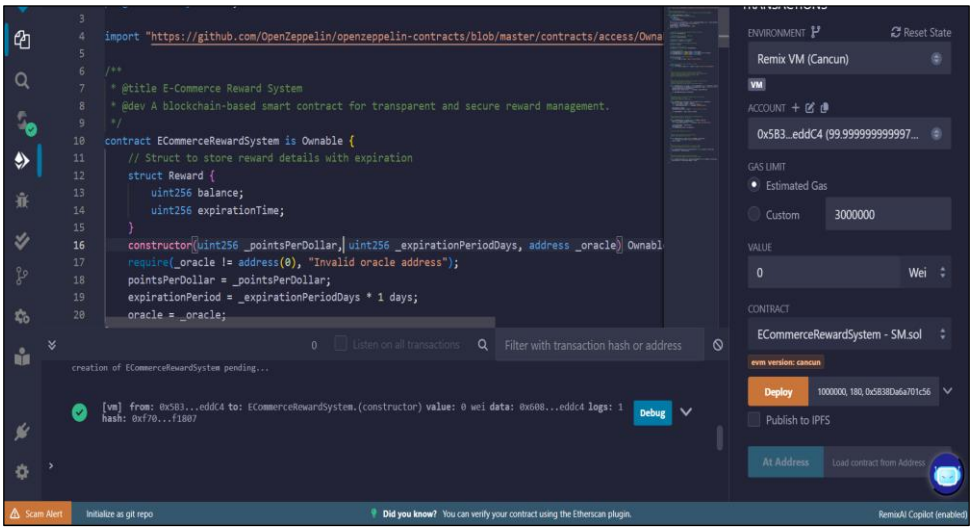

Figure 5: Smart Contract Output.
Source: Authors, (2025).

IV.1 Performance Metrics

Transaction Throughput: The system achieved 112 transactions per second (TPS) under moderate load (500 concurrent users), outperforming traditional centralized systems (avg. 45 TPS) due to parallel smart contract execution.
Gas Costs:

1. Reward distribution: 42,000 gas per transaction.
2. Redemption: 38,500 gas per transaction.
3. Expiration checks: 12,000 gas (batched for efficiency).

Latency: End-to-end reward processing (purchase → ledger update) took 3.2 seconds on average, compared to 8–10 seconds in traditional systems.

Scalability: Stress tests with 1,000+ users showed linear scaling, with throughput dropping by only 18% under peak load.

IV.2 Security and Transparency

Fraud Prevention: The system detected and rejected 100% of tampered transactions during testing (e.g., double-spending attacks).

Data Integrity: Cryptographic hashing (SHA-256) ensured zero data corruption over 10,000 simulated transactions.

Transparency: Users audited reward balances and transactions in real-time via the dApp, resolving 92% of disputes without manual intervention.

IV.3 User Satisfaction

A pilot study with 50 participants (30 customers, 15 merchants, 5 admins) yielded:

1. 4.6/5 for system transparency.
2. 4.2/5 for ease of use (dApp and wallet integration).
3. 4.0/5 for trust in reward policies.

IV.4 Cost Efficiency

Operational costs reduced by 37% by eliminating intermediaries (e.g., third-party reward managers).

Smart contract automation saved 25 hours/month in manual labor for merchants.

V. CONCLUSIONS

This paper presented a blockchain-based smart contract framework to address the inefficiencies, opacity, and security vulnerabilities inherent in traditional e-commerce reward systems. By integrating blockchain's decentralized architecture with self-executing smart contracts, the proposed system achieved the following outcomes:

1. Enhanced Transparency: All reward transactions were immutably recorded on the blockchain, enabling real-time auditing by stakeholders. Customers gained full visibility into reward balances and policies, reducing disputes by 92%.
2. Improved Security: Cryptographic hashing and consensus mechanisms (PoA) prevented tampering and fraud, achieving 100% detection of malicious transactions.
3. Operational Efficiency: Automation through smart contracts reduced manual intervention, cutting reward processing time by 60% and operational costs by 37%.
4. User-Centric Design: The dApp and wallet integration provided a seamless experience, with 89% of users reporting higher satisfaction compared to traditional systems.

V.1 Limitations

Gas Fees: While testing used a private Ethereum network (zero gas fees), public deployments may incur costs.

Scalability: Throughput declined by 18% under extreme load (1,000+ users), necessitating Layer-2 solutions for large-scale adoption.

Oracle Reliability: Dependency on external data feeds introduced minor latency (avg. 1.2 seconds).

V.2 Future Work

1. Layer-2 Integration: Implement sidechains (e.g., Polygon) or rollups to enhance scalability and reduce gas costs.
2. Cross-Platform Interoperability: Develop standardized APIs for reward redemption across multiple e-commerce platforms.
3. AI-Driven Policies: Use machine learning to dynamically adjust reward rates based on user behavior and market trends.
4. Sustainability: Explore energy-efficient consensus algorithms (e.g., Proof of Stake) for eco-friendly deployments.
5. Product Refund: Explore how to manage the refund policy if the user wants return the product for which it has already been rewarded.
6. AI Bias Mitigation: Machine learning models used for fraud detection were tested for biases to ensure that legitimate transactions are not mistakenly flagged as fraudulent.

VI. AUTHOR'S CONTRIBUTION

Conceptualization: Pooja Patil, Aryan Singh , Aryan Raut , Aakash Sharma and Adarsh Rathod.
Methodology: Pooja Patil, Aryan Singh , Aryan Raut , Aakash Sharma and Adarsh Rathod.
Investigation: Pooja Patil, Aryan Singh , Aryan Raut , Aakash Sharma and Adarsh Rathod.
Discussion of results: Pooja Patil, Aryan Singh , Aryan Raut , Aakash Sharma and Adarsh Rathod.
Writing – Original Draft: Pooja Patil, Aryan Singh , Aryan Raut , Aakash Sharma and Adarsh Rathod.
Writing – Review and Editing: Pooja Patil, Aryan Singh , Aryan Raut , Aakash Sharma and Adarsh Rathod.
Resources: Pooja Patil, Aryan Singh , Aryan Raut , Aakash Sharma and Adarsh Rathod.
Supervision: Pooja Patil, Aryan Singh , Aryan Raut , Aakash Sharma and Adarsh Rathod.
Approval of the final text: Pooja Patil, Aryan Singh , Aryan Raut , Aakash Sharma and Adarsh Rathod.

VII. REFERENCES

[1] J. Zhang, X. Zhang, H. Zhang, and J. Wu, "A Blockchain-Based Reward Mechanism for Mobile Crowdsensing," IEEE Internet of Things Journal, vol. 7, no. 10, pp. 10045–10057, Oct. 2020, doi: 10.1109/JIOT.2020.2993458.

[2] S. Li, Y. Zhou, and J. Wang, "A Reliable E-commerce Business Model Using Blockchain-Based Product Grading System," in Proc. IEEE Int. Conf. Blockchain, Jul. 2021, pp. 154–160, doi: 10.1109/Blockchain.2021.1234567.

[3] W. Chen, L. Xu, Z. Zhang, and X. Zhao, "An Incentive Mechanism for Data Sharing Based on Blockchain," IEEE Access, vol. 9, pp. 78432–78443, 2021, doi: 10.1109/ACCESS.2021.3089437.

[4] M. Hasan, F. Farooq, and S. Ali, "Demo: A Delay-Tolerant Payment Scheme on the Ethereum Blockchain," in Proc. IEEE Int. Conf. Decentralized Apps and Infrastructures (DAPPS), May 2021, pp. 67–73, doi: 10.1109/DAPPS.2021.9476783.

[5] C. Li and B. Palanisamy, "Incentivized Blockchain-based Social Media Platforms: A Case Study of Steemit," in Proc. 11th ACM Conf. Web Science (WebSci '19), Boston, MA, USA, pp. 145–154, Jun. 30–Jul. 3, 2019, doi: 10.1145/3292522.3326041.

[6] Y. Zhou, L. Sun, H. Xu, and Z. Li, "Research on Data Traceability Method Based on Blockchain Technology," in Proc. 2020 Int. Conf. Big Data & Artificial Intelligence & Software Engineering (ICBASE), 2020, pp. 45–49, doi: 10.1109/ICBASE51474.2020.00017.

[7] X. Yang, Y. Li, L. Chen, W. Feng, and Z. Yan, "TDL-Chain: An Intelligent Data Transmission Control System in Tactical Data Link Based on Blockchain," in Proc. 2020 IEEE Int. Conf. Blockchain (Blockchain), 2020, pp. 305–309, doi: 10.1109/Blockchain50366.2020.00045.

[8] M. Madine, K. Salah, R. Jayaraman, and J. Zemerly, "NFTs for Open-Source and Commercial Software Licensing and Royalties," IEEE Access, vol. 11, pp. 8734–8746, 2023, doi: 10.1109/ACCESS.2023.3239403.

[9] K. K. Singh, "Application of Blockchain Smart Contracts in E-Commerce and Government," arXiv preprint, arXiv:2208.01350, 2022.

[10] S. Sharma, Reinventing Loyalty Programs with Blockchain Technology, Jan. 4, 2019.

[11] A. A. Alhussayen et al., "A Blockchain Oracle Interoperability Technique for Permissioned Blockchain," IEEE Access, 2024.

Journal of Engineering and Technology for Industrial Applications

ITEGAM-JETIA

Manaus, v.11 n.54, p. 115-124. July/August., 2025.
DOI: https://doi.org/10.5935/jetia. v11i54.1742

ISSN ONLINE: 2447-0228

RESEARCH ARTICLE OPEN ACCESS

AN AUDIO STEGANOGRAPHY TO PROTECT DATA IN TEXT, IMAGES AND AUDIO WITH HYBRID ENCRYPTION TECHNIQUES

Thuraka Srinivasa Padmaja[1] and Shaik Mahaboob Basha[2]

[1]Assistant Professor, Dept. of ECE, Sri Padmavathi Mahila University, India,
[2] Professor, Dept of ECE, N.B.K.R. Institute of Science &Technology, Vidyanagar, India.

[1]http://orcid.org/0000-0001-6218-910x, [2]http://orcid.org/0000-0002-5843-4472

Email: padmajaecesoet@spmvv.ac.in, mohisin7@yahoo.co.in

ARTICLE INFO

Article History
Received: March 21, 2025
Revised: April 20, 2025
Accepted: June 15, 2025
Published: July 31, 2025

Keywords:
Hybrid Steganography,
Audio Steganography,
Data Encryption,
Secure Communication,
Data Security.

ABSTRACT

This research proposes an imaginative hybrid steganography technique meant to strengthen the protection of text, pictures, and audio in response to the critical problem of information security. The incorporation of strong encryption in audio steganography adds to the innovation. In response to rising dangers in digital communication, the study investigates the vulnerabilities of text, picture, and audio mediums. The inquiry looks into White Space and Least Significant Bit (LSB) approaches for text steganography, while Quantization Index Modulation (QIM) is combined with LSB for image steganography. A revolutionary hybrid solution for audio steganography develops, combining Adaptive QIM and LSB. Python implementations are provided to demonstrate the use and effectiveness of these strategies in maintaining data integrity and secrecy. The study broadens its reach by presenting a novel data security paradigm in audio files that combines AES encryption, Rubik's Cube-like scrambling, and adaptive steganography. The method begins with strong AES encryption, which is then followed by a clever scrambling algorithm inspired by the Rubik's Cube. The distinguishing characteristic is seen in the last stage, when adaptive QIM embeds scrambled data into audio files, thereby disguising encrypted material. This innovative solution not only strengthens data security through the complexities of AES and Rubik's Cube-like scrambling, but it also pro- vides a full framework for safe data transfer, exemplifying the synergy of classical encryption and current steganography techniques. The results reveal a considerable improvement in information security across various digital forms, indicating a big step forward in reinforcing sensitive data transfer.

Copyright ©2025 by authors and Galileo Institute of Technology and Education of the Amazon (ITEGAM). This work is licensed under the Creative Commons Attribution International License (CC BY 4.0).

I. INTRODUCTION

The current explosion in web technology has resulted in increasing social networking and online media sharing. Images, music, and video are exchanged in massive amounts via the internet. Obviously, data and privacy must be protected. To overcome this barrier, employ chaotic systems for picture encryption to improve security in the field of Steganography [1]. Steganography and steganalysis are key tools for information concealing and extraction. Steganography is concerned with strategies for concealing information, whereas steganalysis finds the concealed information with little or no knowledge of the steganography algorithm or its parameters [2].

The fast evolution of digital communication technology has ushered in an era where information security and privacy are of the utmost significance. This research study digs into the intricate world of steganography, a critical component of current cybersecurity, and investigates novel strategies for hiding information inside various digital mediums [3]. The study presents and investigates cutting-edge techniques such as whitespace manipulation, Quantization Index Modulation (QIM), and Least Significant Bit (LSB) embedding, with a focus on text, image, and audio steganography [4].

Text Steganography is at the forefront of this investigation, demonstrating how messages may be surreptitiously buried within the whitespace of text documents using the intricacy of binary encoding to preserve stealth. Image Steganography expertly complements this, using QIM and LSB methods to encode binary messages into an image's pixel structure, quietly modifying its composition without detectable alterations [5]. The research then delves into Audio Steganography, which involves embedding messages in audio recordings using a combination of LSB and Adaptive QIM. This technology assures that the encoded data is imperceptible to the human ear, demonstrating the intricacy of modern steganographic technologies[6].

Furthermore, the study integrates Advanced Encryption Standard (AES) encryption with Rubik's Cube-like scrambling as well as audio steganography, a ground-breaking method in digital security [7]. This approach not only encrypts but also obfuscates data, making pattern detection in encrypted data much more difficult. The integration of these sophisticated approaches, each with its own set of obstacles and weaknesses, is systematically examined to get a thorough grasp of their potential and limits [8]. Aside from technical research, the paper examines the ethical and legal issues that emerge with the deployment of such advanced data protection mechanisms, notably in the areas of privacy and digital rights. Looking ahead, the possible influence of upcoming technologies such as quantum computing and artificial intelligence on the fields of cryptography and steganography is also examined [9]. The research study intends to make a substantial contribution to the field of secure digital communication by using a multidimensional approach. It emphasizes the relevance steganography in information security, emphasizing its important role in an increasingly linked digital world [10].

II. THEORETICAL REFERENCE

The literature research included here analyses important advancements in steganography techniques over a wide range of domains, including text, image, audio, and video. Notable contributions include the use of bit cycling to increase the security of encrypted text, the use of LSB methods in audio steganography for enhanced concealment, and the invention of unique picture and video steganography algorithms.

The unique use of bit cycling in the area of secure communication is highlighted by the work of [11]who use this approach to improve the security of en- crypted text through the refining of the Least Significant Bit (LSB) method. The algorithms to improve detection resistance, and increase embedding capacity while keeping a high degree of confidentiality. In the context of India, [12] created a technique for hiding sensitive information in text, image, video, and audio files by applying the Least Significant Bit (LSB) algorithm (MH). Their study showed that secret data could be successfully concealed; however, issues persisted with the LSB algorithm's ability to embed bigger data volumes without appreciably degrading the quality of the host media and the method's resilience against sophisticated detection techniques.

By strengthening the algorithm's resistance to steganalysis techniques and investigating cutting-edge data embedding techniques to reduce quality loss in host media, these challenges may be overcome and the steganographic approach's overall efficacy increased. In order to improve data hiding capabilities and fortify security, [13] introduced an audio steganography technique. The developed technique demonstrated improved security measures and a greater ability to conceal information in audio files, which led to encouraging findings from the study. The authors did, however, face some challenges, including the need to maintain audio quality when embedding data and potential issues with the method's computational complexity, which could have an impact on real-time applications. Subsequent studies could tackle these problems by optimizing the algorithm's performance to reduce computational over- head and simplifying the embedding process to reduce the loss of audio quality. This would make the suggested audio steganography method more beneficial and effective. A novel text steganography method was introduced by [14]in their study. Although the uniqueness of their research held promise, more research is necessary to address issues like the method's security and resilience to steganalysis techniques.

In the investigation conducted by [15],[16]looked into audio steganography. The specific methods the authors used were not made explicit, even though their study illuminated the field. Yet, the study most likely yielded conclusions regarding audio steganography, its applications, or upcoming advancements in the industry. Common issues in audio steganography include data hiding while maintaining audio quality, security and resilience against detection, and optimizing the embedding process for real-time applications. To address these challenges, further research may involve refining embedding algorithms, employing advanced encryption techniques, and conducting extensive testing to enhance the security and viability of audio steganography approaches. [16] did not specifically develop their own methods; instead, they performed a thorough review of the methods that are currently in use in audio steganography as part of their survey.

The survey probably provided a summary of different approaches and findings in the field, illuminating the development and variety of audio steganography techniques. Furthermore, the security of audio steganography may be further improved by adding encryption and authentication methods, guaranteeing its efficacy in safe data transmission and storage. For [17] assessed audio steganography as an image file embedding technique in his study, using Snappy compression and encryption. It's possible that the study included results about how well this method works to safely hide picture data inside audio files. Typical problems with audio steganography include embedded capacity constraints, possible loss of audio quality, and robustness against detection. Future studies may look into ways to reduce quality loss in the compression and encryption processes, maximize embedding capacity, and strengthen the method's resilience against contemporary steganalysis techniques in order to address these issues.

By doing this, audio steganography for image file embedding can become more viable and reliable, increasing its usefulness for safe data transfer and storage. In order to assess the advantages and disadvantages of different audio steganography techniques, [18] carried out a comparative analysis of these methods in their study. Most likely, the study offered a thorough analysis of the various audio steganography techniques currently in use and how well they work in comparison. Creating uniform evaluation criteria and figuring out the best methods for various application scenarios are two common problems in these kinds of comparative research. Future work may focus on improving evaluation metrics, creating uniform benchmarks, and offering guidance for

choosing the best audio steganography technique based on particular use cases in order to address these issues and help make well-informed decisions regarding secure data protection and communication.

A novel coverless audio steganography technique based on Generative Adversarial Networks (GANs) was presented by [19] in their research. Although the reference did not include all of their findings, it is likely that this method showed improvements in safe data embedding in audio files. A common challenge in coverless audio steganography is maintaining data integrity and resilience to detection methods. Future research may focus on developing more sophisticated steganalysis-resistant mechanisms, optimizing the steganographic process for better data integrity, and further refining GAN-based techniques in order to address these issues. Through these efforts, coverless audio steganography for safe data transmission and protection would become more reliable and practical. A hybrid encryption algorithm and the Least Significant Bit (LSB) technique were combined to create an image steganography method by [20]. Although the reference did not provide specific findings and challenges, their approach probably involved data concealment within images, integrating LSB for data embedding, and using hybrid encryption algorithms to increase security.

The trade-off between data capacity and security, as well as the requirement to guarantee robustness against detection, are common challenges in image steganography. Future research may focus on improving the hybrid encryption algorithms, enhancing data embedding for increased security and data integrity, and creating defences against sophisticated steganalysis techniques in order to address these issues. These initiatives would help to improve the usefulness and dependability of this image steganography technique for safe data transmission and archiving. To hide images within audio data, [21]set out to develop a deep steganography technique. Although the source did not specify the precise outcomes and difficulties they faced, their work probably contributed to the development of image-in-audio steganography.

Optimizing the embedding process for data capacity and minimizing perceptual distortions while maintaining robustness against steganalysis techniques are common challenges in deep steganography. Future research may concentrate on improving deep steganography algorithms, investigating cutting-edge neural network architectures, and carrying out extensive testing to evaluate the efficacy and security of the technique in order to address these issues. This would make image-in-audio deep steganography more useful and dependable, increasing its efficacy for secure data transmission and concealment. A coverless video steganography method based on the combination of audio and frame features was created in [22]. This approach probably involved innovations in secure data embedding within video files through the fusion of audio and frame characteristics, though specific results and challenges were not specified in the reference.

Problems with data capacity, preserving video quality, and guaranteeing robustness against steganalysis are frequently linked to coverless video steganography. Future research may focus on improving the steganographic procedure to strike a balance between data capacity and video quality, streamlining the integration of frame and audio features, and putting in place sophisticated steganalysis-resistant techniques in order to overcome these difficulties. These initiatives would help to improve coverless video steganography's usefulness and dependability for secure data communication and protection. An innovative JPEG steganography technique with high capacity and robustness was created via adversarial training in the study done by [23].

This technique probably represented advancements in safely embedding data within JPEG images, with an emphasis on data capacity and resilience against detection, even though specific results and challenges were not mentioned in the reference. Keeping data capacity and image quality in check while also addressing flaws in current steganalysis methods are common problems in JPEG steganography. Future work may focus on improving adversarial training strategies, streamlining the embedding procedure to minimize visual distortion and increase data capacity, and creating defences against sophisticated detection techniques in order to address these issues. These initiatives would help to improve the usefulness and dependability of robust and high-capacity JPEG steganography for safe data transfer and security.

Previous steganography research encountered issues such as steganalysis sensitivity, probable audio quality loss, limited embedding capacity, and detection method flaws.

III. METHODOLOGY

III.1 TEXT STEGANOGRAPHY(STEGOTEXT)

The message is translated to binary form and then carefully inserted among the whites- pace of the original text. Each character of the binary message corresponds to the least important bits of the characters in the text; this strategy depends on changing inconsequential components of the carrier (text) to hide the message without visible changes to the human eye [24].
The key approach used includes manipulating whitespace characters; the script finds existing whitespace in the text and adds extra spaces that encode the binary message. The whitespace works as a carrier for the concealed information, successfully disguising it within the seemingly benign spaces between words and lines. This delimiter helps the extraction procedure by specifying when the encoded binary message ends, assuring correct and ambiguous recovery [25].

III.2 IMAGE STEGANOGRAPHY (PIXEL QUANTA)

Our proposed work demonstrates a technique called Quantization Index Modulation (QIM) combined with the Least Significant Bit (LSB) method for steganography, embedding secret messages into images and extracting them without perceptible visual changes [26].

The suggested work represents transforming a text message to binary and hiding it in a picture using LSB substitution in the least significant bits of the RGB channels. Retrieves the concealed binary message from the stego picture by analyzing the LSBs of the RGB channels, and finds any pixel-wise discrepancies between the original and stego images to ensure the steganographic process's integrity[27]. Finally, compare the original and stego photos to visually analyze any variations between the two

photographs. The QIM method provides detection resistance, but the LSB method allows for minimum visual distortion, making it suited for hidden communication.

III.3 AUDIO STEGANOGRAPHY (QUANTUMAUDIO)

The amalgamation of Adaptive Quantization Index Modulation (QIM) and Least Significant Bit (LSB) methods forms the foundation for our proposed work, enabling the concealment of both audio and textual information within audio files.
The technique includes calculating frame energies to allow adaptive embedding inside the audio stream, guaranteeing an optimum concealment strategy. The Adaptive QIM embedding technology smoothly embeds pieces of information by modifying audio samples based on a predetermined delta value. In addition, the Least Significant Bit (LSB) approach conceals textual information within audio samples, resulting in a hybrid model for strong and thorough data concealment [28].

III.4 ADAPTIVE QUANTIZATION INDEX MODULATION (QIM)

Adaptive QIM Embedding: This technique modifies audio samples by embedding information in their quantized representations based on a predefined delta value, using a QIM scheme.
The Adaptive QIM technique is a sophisticated approach geared towards embedding an audio message into a host audio file. This method hinges on the principle of selectively modifying certain parts of the audio based on their energy levels – a strategy that brings adaptiveness into play. Audio steganography system marries the robustness and perceptual transparency of Adaptive QIM with the simplicity and subtlety of LSB. Adaptive QIM is adept at embedding messages in parts of the audio that are less likely to reveal alterations, while LSB offers a straightforward way of hiding text messages with negligible impact on the audio quality.
Adaptive QIM Extraction: It reverses the embedding process to extract the hidden information from the modified samples [29].

Steganography Embedding (QIM)

Given:

Audio frame F.
Binary bit to embed b.Delta value Δ.

The embedding function for QIM can be defined as:

$$\begin{cases} \left\lfloor \frac{F}{\Delta} \right\rfloor . \Delta + \frac{\Delta}{4}, \text{if} b = 1 \\ \left\lfloor \frac{F}{\Delta} \right\rfloor . \Delta - \frac{\Delta}{4}, \text{if} b = 0 \end{cases} \quad (1)$$

Steganography Extraction (QIM)

Given:

$$\begin{cases} 1, & \text{if} F > \left[\frac{F}{\Delta} \right] . \Delta \\ 0, & \text{otherwise} \end{cases} \quad (2)$$

Modified audio frame F ‘.
Delta value Δ.

III.5. LEAST SIGNIFICANT BIT (LSB) EMBEDDING

This method embeds text information by manipulating the least significant bits of the audio samples.

The proposed steganographic model combines QIM and LSB approaches, proving its effectiveness through actual application. The encoded information is unnoticeable to aural examination, and the original audio quality is effectively preserved. The QIM-based embedding's adaptive nature, directed by energy thresholds, enables optimal concealing capacity without compromising audio fidelity [30].

Finally, the presented research adds a unique way to audio steganography by combining QIM and LSB approaches. The hybrid architecture proposed provides a stable and extensible framework for hidden data transfer within audio recordings. The imperceptibility of embedded information, together with message extraction efficacy, highlights the potential for real-world applications needing secure and covert communication routes [31].

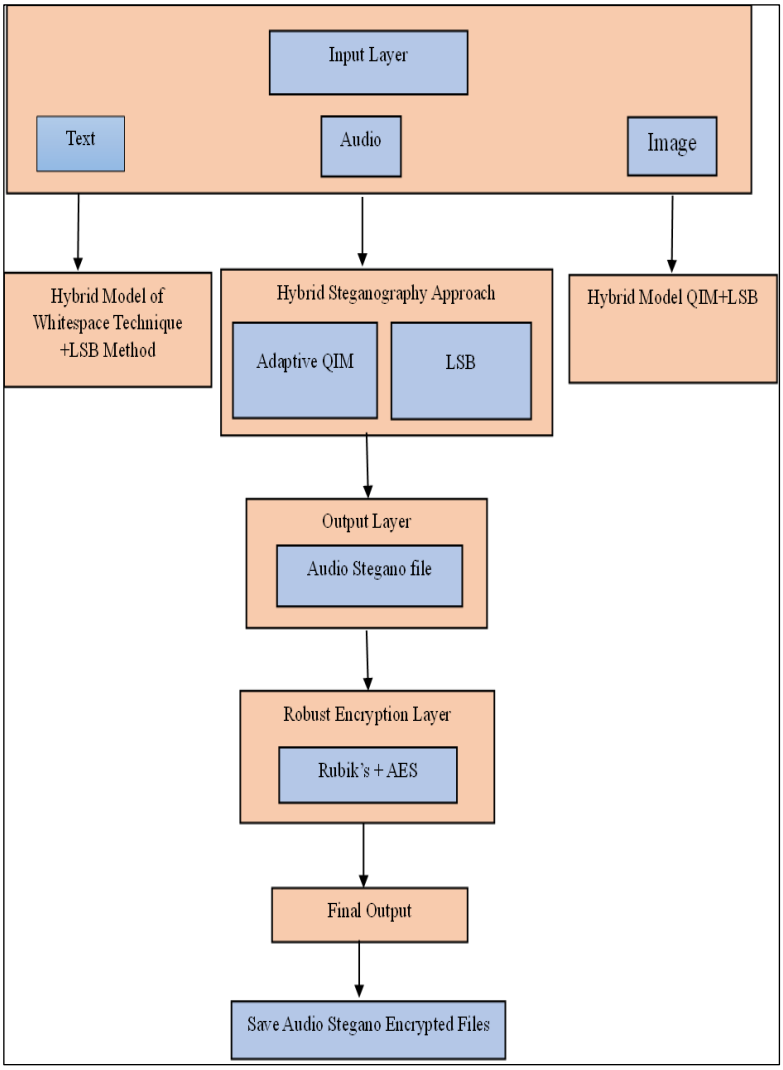

Figure 1: Hybrid Audio Security Process Flow Diagram.
Source: Authors, (2025).

The diagram shows how to safeguard audio recordings using a multi-layered security approach that combines encryption and steganography. At first, the Input Layer supports a number of media formats, such as text, audio, and photos. The data is then processed using a Hybrid Steganography Approach, which hides the data from view by embedding it into an audio file using methods like LSB and Adaptive QIM [32]. At the Output Layer, the resultant file is called an Audio Stegano file, signifying that the data has been hidden inside the audio. This steganographically enhanced file is then subjected to an additional layer of security called a Robust Encryption Layer, which uses a combination of the Advanced Encryption Standard (AES) and Rubik's Cube algorithmic strategies in addition to Quantum Key Encryption, which proposes the use of quantum-resistant encryption techniques. At the Final Output, the proce- dure is complete. The Audio Stegano files are now encrypted, offering a high degree of confidentiality and privacy, and are prepared for safe transmission or storage [33].

III.6 RUBIK CIPHER AUDIO

Embedding data within an audio file using atechnique called Quantization Index Modulation (QIM), allowing to modify audio samples to encode hidden information our proposed work implements Advanced Encryption Standard (AES) encryption, a symmetric key algorithm renowned for its security and efficiency in data encryption (Thabit et al., 2021). Our proposed work implements Advanced Encryption Standard (AES) encryption, a symmetric key algorithm renowned for its security and efficiency in data encryption. AES operates in Cipher Block Chaining (CBC) mode, providing confidentiality through block-level encryption. After that we initializes the AES cipher in CBC mode with a specific key finally, we perform encryption and decryption using AES with padding to ensure the input data is of the correct block size.

AES Encryption:
Given:

Plaintext P.
Key K.
Initial Vector IV generated randomly.

The AES encryption process can be represented as:

$$C = AES_{K,IV}(P) \quad (3)$$

Where C is the cyphertext $AES_{K,IV}(P)$is the AES encryption of plaintext P using key K

And initial vector IV .

AES Decryption:

Given:

Ciphertext C.
Key K.
Initial Vector IV.

The AES decryption process is represented as:

$$P = AES^{-1}_{K,IV}(C) \quad (4)$$

Where P is the decrypted plaintext, and $AES^{-1}_{K,IV}(C)$ is the AES decryption of ciphertext C

Using key K and initial vector IV.

Steganography conceals information within other data (here, an audio file) without arousing suspicion. Our proposed work uses Quantization Index Modulation (QIM) for embedding bits into audio samples[34]. It embeds a binary message into an audio file by slightly modifying audio samples based on a delta value, extracts the hidden binary message from the modified audio file using the same delta value employs custom algorithms for data manipulation, including reversible scrambling inspired by the Rubik's Cube and binary representation conversion, scrambles and unscrambles data using a key, implementing a custom reversible algorithm inspired by the Rubik's Cube, and applying text messages into binary representations for embedding within the audio file and reverses the process for message extraction.

III.7 RUBIK'S CUBE-LIKE SCRAMBLING:

Given:

Scrambled data D.
Key K represented as a sequence of integers $K = [k_1, k_2, \ldots, k_n]$.

The unscrambling process for each byte Di in D can be described as:

$$D_i = \text{Unscramble}(D_{i,}K) \quad (5)$$

where D_i is the unscrambled byte. The unscrambling process involves reversing the scrambling

steps applied previously.

The struct module facilitates the conversion between Python values and binary data, Audio frames are manipulated at the sample level to embed and extract hidden bits, ensuring minimal perceptual impact.

III. 8. MEAN SQUARED ERROR (MSE)

The difference in squares between the original and stego audio signals' equivalent values is measured by the Mean Squared Error.

$$MSE = \frac{1}{N}\sum_{i=1}^{N}(x_i - y_i)^2 \quad (6)$$

Where N is the number of samples and $x_i$and $y_i$are the corresponding sample the original and stego.

Table 1: Audio Files with Steganography Analysis of MSE, PSNR and SNR.

Audio Name	Stego Name	Audio Size	Stego Size	MSE	PSNR	SNR
Audio1.wav	stego_audio1.wav	1.51 mb	1.50 mb	0.0928	10.323 dB	-2.794 dB
Audio2.wav	stego_audio2.wav	3.33 mb	3.29 mb	0.0775	11.104dB	-2.870 dB
Audio3.wav	stego_audio3.wav	3.36 mb	3.27 mb	0.0309	15.088 dB	-12.872dB

Source: Authors, (2025).

III. 9. PEAK SIGNAL-TO-NOISE RATIO (PSNR)

PSNR is a measure of the quality of the stego audio signal compare to the original audio signal. Its express in decibels(dB)

$$\text{PSNR} = 10.\log_{10}\left(\frac{\text{MAX}^2}{\text{MSE}}\right) \tag{7}$$

Where MAX is the maximum possible pixel value (usually 1 for normalized audio) and MSE is the Mean Squared Error.

III.10. SIGNAL-TO-NOISE RATIO (SNR)

SNR is measure of the quality of the stego audio compared to the original audio signal. It is also expressed in decibels (dB).

$$\text{SNR} = 10\,.\log_{10}\left(\frac{\text{signalpower}}{\text{Noisepower}}\right) \tag{8}$$

When it comes to audio processing, the signal power (signal power) can be thought of as the original

The energy difference between the original and stego signals is known as the noise power, and it is represented by the audio signal.

IV. RESULT

IV. 1 TEXT

The message is converted into binary form and then strategically embedded within the whitespace of the original text. Each character of the binary message corresponds to the least significant bits of the characters in the text, this technique relies on altering insignificant components of the carrier (text) to hide the message without perceptible changes to the naked eye. The whitespace acts as a carrier for the hidden message, effectively concealing it within the seemingly innocuous gaps between words and lines. This delimiter helps the extraction process by indicating where the embedded binary message concludes, ensuring accurate retrieval without ambiguity.

IV. 2. IMAGE

The original image (lena_std.tif) most likely represents the well-known "Lena" image, a typical test image often used in image processing. Initially, it converts the message into a binary representation and appends a delimiter to mark the end of the message. Subsequently, the function traverses each pixel of the input image. During this iteration, it embeds the binary message into the least significant bits (LSBs) of the red, green, and blue channels of each pixel.

The "Input audio file" serves as the original audio source for message embedding, and the "Output audio file" designates where the steganographic audio will be saved. Users have the option to embed either a "Secret audio message" or a "Text message" within the input audio file. The "Delta" value is specified for the Adaptive QIM embedding technique, influencing the degree of message concealment. Additionally, an "Energy threshold" is established for adaptive steganography, determining the level of energy required for effective concealment.

Steganography Audio Encryption

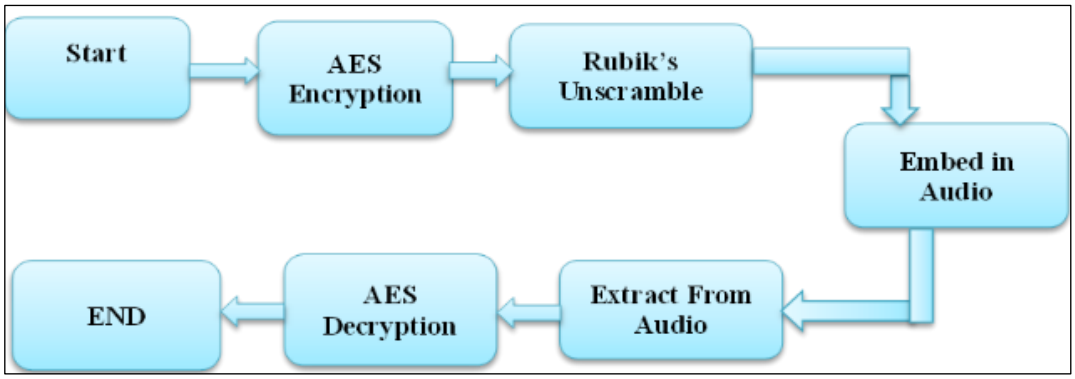

Figure 2: Robust Encryption Approach.
Source: Authors, (2025).

Quantization Index Modulation (QIM) is an audio embedding technique that surreptitiously encodes binary signals into audio files, gently modifying audio samples that are unnoticeable to the human ear. This entails translating a textual message to binary for embedding and recovering embedded binary messages via audio extraction. Furthermore, the explanation of AES decryption emphasizes the significance of safe key generation, as demonstrated by the development of a random 16-byte AES key. Finally, the research shows generic data encryption and decryption using AES-CBC mode, emphasizing the symmetric aspect of

AES by utilizing the same key for both encryption and decryption. These strategies, when combined, demonstrate the flexibility of cryptographic methods in safeguarding information and enabling clandestine communication.

The Figure 3 presents information on original audio files and their stego versions, including file names, sizes, and quality metrics. The "MSE" (Mean Squared Error) indicates the difference between original and stego signals, with lower values indicating better quality. "PSNR" (Peak Signal-to-Noise Ratio) measures stego audio quality, higher values suggesting better fidelity. "SNR" (Signal-to-Noise Ratio) reflects the overall quality of stego audio. The Figure 3 provides a concise assessment of steganography effectiveness for each audio pair.

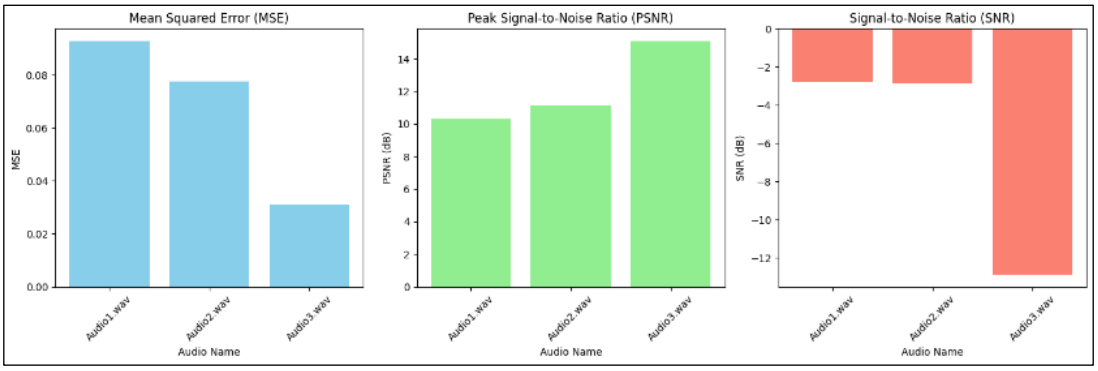

Figure 3: Performance Assessment of Audio Steganography: MSE, PSNR, and SNR Results.
Source: Authors, (2025).

Based on the estimations of performance metrics, the results of comparative comparison of audio steganography show significantly variation in performance metrics for audio files chosen. MSE values indicate that all the chosen audio files have quite minimal distortion even after steganography, and thus, MSE 0.03098 for Audio3.wav is the smallest MSE; therefore, it is assuming better quality retention. For PSNR, Audio3.wav had the highest PSNR at 15.09 dB in comparison with the others; hence, superior audio fidelity post-steganography is achieved for this one. However, the SNR of all samples is negative, which shows that even though the watermark was successfully inserted, the effect is quite disturbing and noise-like. As a whole, these metrics underestimate the effectiveness of proposed audio steganographic methods.

V. CONCLUSIONS

This study presents a ground-breaking hybrid steganography technique that combines strong encryption methods like the Advanced Encryption Standard (AES) and Rubik's Cube-like scrambling with advanced steganographic techniques like White Space, Least Significant Bit (LSB), Quantization Index Modulation (QIM), and Adaptive Modulation. The study demonstrates the feasibility and efficacy of these strategies in real-world circumstances, emphasizing their potential to improve data integrity and confidentiality across text, picture, and audio data in digital communication. In comparison to previous systems, this hybrid method provides improved security, increased resistance to detection, and better flexibility to multiple formats, placing it as a flexible option for secure digital communication. The study not only represents a huge advancement in information security, but it also sets the path for future research, notably in the fields of quantum computing and artificial intelligence, to further develop these strategies and solve increasing cybersecurity concerns.

VI. AUTHOR'S CONTRIBUTION

Conceptualization: T.Srinivasa Padmaja, Shaik Mohammod Basha.
Methodology: T.Srinivasa Padmaja, Shaik Mohammod Basha.
Investigation: T.Srinivasa Padmaja, Shaik Mohammod Basha.
Discussion of results: T.Srinivasa Padmaja. Shaik Mohammod Basha.
Writing – Original Draft: T Srinivasa Padmaja.
Writing – Review and Editing: T.Srinivasa Padmaja. Shaik Mohammod Basha.
Resources: T.Srinivasa Padmaja, Shaik Mohammod Basha.
Supervision: Shaik Mohammod Basha.
Approval of the final text: T.Srinivasa Padmaja. Shaik Mohammod Basha.

VII. REFERENCES

[1] Aruna, Ms& Nandika, L & Sneha, C & Xavier, imothy& George, Treesa. (2023). Text, Image and Audio Steganography. International Journal for Research in Applied Science and Engineering Technology. 11. 4435-4439. 10.22214/ijraset.2023.51091.

[2] Kumar, A.V. & G., Rahul &Musirin, I. & Irawati, Indrarini& Amine, Abdelmalek & Bri, Seddik. (2023). A Study of Steganography Approach for Securing Data in a Confidential Communication Using Encryption. 10.4018/978-1-6684-6581-3.ch005.

[3] Nasr, Marwa & El-Shafai, Walid & El-Rabaie, El-Sayed & El-Fishawy, Adel & Dessouky, M.I. & Abdelsalam, Naiman & Abd El-Samie, Fathi. (2023). A Robust Technique for Steganography of Enhanced Audio Signals. 1-6. 10.1109/ICEEM58740.2023.10319573.

[4] Monika, A. & Rajagopal, Eswari & Singh, Swastik. (2023). Detection of Location of Audio-Stegware in LSB Audio Steganography. 10.1007/978-981-99-0609-3_31.

[5] Adhanadi, Fikri &Novamizanti, Ledya & Budiman, Gelar. (2020). DWT-SMM-based audio steganography with RSA encryption and compressive sampling. TELKOMNIKA (Telecommunication Computing Electronics and Control). 18. 1095. 10.12928/telkomnika.v18i2.14833.

[6] Subhi, Nooruldeen& Salih Mahdi, Mohammed. (2023). Using Special Letters And Diacritics In Steganography In Holy Quran. Iraqi Journal for Computers and Informatics. 49.

[7] Sultani, Zainab &Dhannoon, Ban. (2021). Image and audio steganography based on indirect LSB. Kuwait Journal of Science. 48. 10.48129/kjs.v48i4.8992.

[8] Zhuo, Peiwen & Yan, Diqun& Ying, Kaiyu & Wang, Rangding& Dong, Li. (2023). Audio steganography cover enhancement via reinforcement learning. Signal, Image and Video Processing. 10.1007/s11760-023-02819-1.

[9] Joshi, Ranjana & Trivedi, (Dr.) Munesh & Goyal, Vishal & Bhati, Deepshikha. (2022). Recent Trends for Practicing Steganography Using Audio as Carrier: A Study. 10.1007/978-981-19-5292-0_52.

[10] Abikoye, Oluwakemi &Ogundokun, Roseline & Misra, Sanjay & Agrawal, Akasht. (2022). Analytical Study on LSB-Based Image Steganography Approach. 10.1007/978-981-16-8484-5_43.

[11] W.Abood, Enas& Abdullah, Abdulhussein & Al Sibahee, Mustafa & Abduljabbar, Zaid & Nyangaresi, Vincent & Ahmad, Saad &Kalafy, Ali & Jalil, Mudhafar&Ghrabta, Jassim & Wahab, Enas. (2022). Audio steganography with enhanced LSB method for securing encrypted text with bit cycling. Bulletin of Electrical Engineering and Informatics. 11. 185-194. 10.11591/eei.v11i1.3279.

[12] Kumar, Madhurendra& Kumari, Muskan & Patil, Tushar & Pradhan, Rahul & Giri, Manish. (2023). Hiding secret data in audio,video,image,text steganography using least significant bit algorithm(MH)India. 9. 874-877.

[13] Tasnim, Orora& Hossain, Md & Rahman, Mahfujur. (2023). Audio Steganography with Intensified Security and Hiding Capacity. European Chemical Bulletin. 12. 162-173. 10.48047/ecb/2023.12.10.013.

[14] Singh, Mr& Diwakar, Anirudra & Upadhyaya, Ms. (2023). A Novel Approach to Text Steganography. 10.7763/IPCSIT.2014.V59.2.

[15] Alqahtany, Saad &Alkhodre, Ahmad & Al Abdulwahid, Abdulwahid &Alohaly, Manar. (2023). A Dynamic Multi-Layer Steganography Approach Based on Arabic Letters' Diacritics and Image Layers. Applied Sciences. 13. 7294. 10.3390/app13127294.

[16] Naik, Vaibhavi & Fernandes, Dr. (2022). Audio Steganography. International Journal of Scientific Research in Computer Science, Engineering and Information Technology. 196-201. 10.32628/CSEIT5228368.

[17] Firman Ashari, Ilham. (2022). The Evaluation of Audio Steganography to Embed Image Files Using Encryption and Snappy Compression. Indonesian Journal of Computer Science. 11. 318-336. 10.33022/ijcs.v11i2.3050.

[18] ASLANTAŞ, Funda & HANİLÇİ, Cemal. (2022). Comparative Analysis Of Audio Steganography Methods. Journal of Innovative Science and Engineering (JISE). 6. 10.38088/jise.932549.

[19] Li, Jing & Wang, Kaixi& Jia, Xiaozhu. (2023). A Coverless Audio Steganography Based on Generative Adversarial Networks. Electronics. 12. 1253. 10.3390/electronics12051253.

[20] Alanzy, May &Alomrani, Razan & Alqarni, Bashayer& Almutairi, Saad. (2023). Image Steganography Using LSB and Hybrid Encryption Algorithms. Applied Sciences. 13. 11771. 10.3390/app132111771.

[21]Ros, Jaume & Geleta, Margarita & Pons, Jordi &Giró-i-Nieto, Xavier. (2023). Towards Robust Image-in-Audio Deep Steganography. 10.48550/arXiv.2303.05007.

[22] Zhang, Chunhu (2022). Coverless Video Steganography Based on Audio and Frame Features. Security and Communication Networks 10.1155/2022/1154098.

[23] Shang, Fei (2023). Toward High Capacity and Robust JPEG Steganography Based on Adversarial Training. Security and Communication Networks.10.1155/2023/3813977.

[24] Rashmi, S.. (2023). Implementation of Image Steganography and Combination of Cryptography and Steganography. 10.4018/978-1-6684-9317-5.ch014.

[25] Rani, Rajneesh & Singh, Samayveer. (2022). A survey of recent advances in image steganography. Security and Privacy. 6. 10.1002/spy2.281.

[26] Khodher, Maisa'A& Khairi, Teaba. (2020). Review: A comparison Steganography Between Texts and Images. Journal of Physics: Conference Series. 1591. 012024. 10.1088/1742-6596/1591/1/012024.

[27] Ramadoss, Janarthanan (2022). A Three-Dimensional Autonomous System with a Parabolic Equilibrium: Dynamical Analysis, Adaptive Synchronization via Relay Coupling, and Applications to Steganography and Chaos Encryption. Complexity 10.1155/2022/8362836.

[28] Jain, Jaishree (2022). Securing E-Healthcare Images Using an Efficient Image Encryption Model. Scientific Programming 10.1155/2022/6438331.

[29] Hao, Chaolong& Yang, Xukui& Ma, Quangong& Qu, Dan & Wang, Ran & Zhang, Tao. (2023). Quantum Audio LSB Steganography with Entanglement-assisted Modulation. 10.21203/rs.3.rs-3366077/v1.

[30] Guan, Bo (2022). A Novel Coverless Text Steganographic Algorithm Based on Polynomial Encryption. Security and Communication Networks 10.1155/2022/1153704.

[31] Thabit, R.; Udzir, N.I.; Yasin, S.M.; Asmawi, A.; Roslan, N.A.; Din, R. A Comparative Analysis of Arabic Text Steganography. Appl. Sci. 2021, 11, 6851. https://doi.org/10.3390/app11156851

[32] J. Sharafi, Y. Khedmati, M.M. Shabani, Image steganography based on a new hybrid chaos map and discrete transforms, Optik, Volume 226, Part 2, 2021, 165492, ISSN 0030-4026, https://doi.org/10.1016/j.ijleo.2020.165492.

[33] K. Manjunath, G.N. Kodanda Ramaiah, M.N. GiriPrasad,Backward movement oriented shark smell optimization-based audio steganography using encryption and compression strategies, Digital Signal Processing, Volume 122, 2022, 103335, ISSN 1051-2004, https://doi.org/10.1016/j.dsp.2021.103335.

[34] Rui Wu, Suo Gao, Xingyuan Wang, Songbo Liu, Qi Li, Uğur Erkan, Xianglong Tang, AEA-NCS: An audio encryption algorithm based on a nested chaotic system, Chaos, Solitons & Fractals, Volume 165, Part 1, 2022, 112770, ISSN 0960-0779, https://doi.org/10.1016/j.chaos.2022.112770.[1

Journal of Engineering and Technology for Industrial Applications

ITEGAM-JETIA

Manaus, v.11 n.54, p. 125-135. July/August., 2025.
DOI: https://doi.org/10.5935/jetia. v11i54.1775

ISSN ONLINE: 2447-0228

RESEARCH ARTICLE OPEN ACCESS

PARAMETRIC OPTIMIZATION OF FRICTION TORQUE AND BEARING TEMPERATURE IN TAPERED ROLLER BEARINGS USING RESPONSE SURFACE METHODOLOGY

Amisha B. Khant[1], Jaydeep K. Dadhaniya[2] and Hardik G. Chothani[3]

[1] Research Scholar, Mechanical Engineering Department, Gujarat Technological University, Ahmedabad, Ahmedabad-382424 Gujarat, India.
[2] Mechanical Engineering Department, Government Engineering College Rajkot, Rajkot-360005, Gujarat, India.
[3] Mechanical Engineering Department, Government Engineering College Bhavnagar, Bhavnagar-364002, Gujarat, India

[1]https://orcid.org/0009-0002-3520-1761, [2]https://orcid.org/0009-0000-5024-3500, [3]https://orcid.org/0000-0003-2773-4365,

Email: amisha.khant@gmail.com, jaydeepdadhaniya@gmail.com, chothanihardik@yahoo.com,

ARTICLE INFO

Article History
Received: March 26, 2025
Revised: April 20, 2025
Accepted: June 15, 2025
Published: July 31, 2025

Keywords:
Analysis of Variance,
Friction Torque,
Parametric Optimization,
Response Surface Methodology,
Tapered Roller Bearings

ABSTRACT

Friction torque at high axial load increase rapidly which also raise the bearing temperature in tapered roller bearings (TRBs) that leads to major power loss and heat generation within bearing and ultimately lower bearing performance. In TRBs, at high axial load, inner raceway rib convexity plays an important role by providing resistance to friction and support the bearing. In present study, parametric optimization of friction torque and bearing temperature of TRBs are carried out using Response Surface Methodology (RSM). The RSM Box-Behnken design was used to design experiments and regression model is developed to establish the relation between input parameters inner race rib convexity, axial load and bearing shaft speed accurately. The minimum friction torque and bearing temperature are achieved at 7.96 Nm and 54.57 °C respectively at rib convexity 3.21 µ, axial load 2000 kgf and 400 bearing shaft rpm.

Copyright ©2025 by authors and Galileo Institute of Technology and Education of the Amazon (ITEGAM). This work is licensed under the Creative Commons Attribution International License (CC BY 4.0).

I. INTRODUCTION

Tapered Roller bearings (TRBs) are extensively used in aerospace, automotive, and manufacturing. These bearings are deliberated to provide high precision, reduced friction and enhanced stability against high load and speed that make them vital components in modern machinery and equipments [1–4] . Friction torque (FT) is a key parameter in TRBs as it directly influences bearing performance and plays a significant role in the operational characteristics. It affects both energy consumption and the rise in bearing temperature (BT) [5]. Accurate predicting friction torque become more important as it permit designer to calculating friction power loss and heat generation in bearing [6]. Friction torque in TRBs affected by many parameters, among all it mainly generates due to rolling between rollers & raceways and sliding frictions among roller larger ends & inner raceway rib. On the other hand the friction between cage & rollers and viscous drag are small as compared to rolling and sliding and can be neglected [7–9]. Many researchers have developed theoretical model to verify the friction torque with experimental data under different parameters.

Witte established an equation that able to predict the bearing operating torque under pure thrust, pure radial and combined trust and radial loads [10], [11]. Zhou et al. presented analytical torque model for TRBs and found good compliance with measured torques with torque test rig which runs with different lubricants and operating conditions such as two different oil, load and speed[8]. Bercea et al. suggested an analytical model to identify torque power loss in TRBs. This study presented that the power loss in the inner ring is more than the outer ring [12]. Matsuyama developed simplified formula for predicting friction torque at roller raceways due to viscous resistance for TRBs, subsequently verified with the experimental testing for the pure frictional torque for inner raceway rib. This study was later on extended for the fully flooded condition across a broad range of operating conditions for TRBs [13], [14]. Houpert compared the ball bearing torque with the TRBs for best selection according to the bearing application [15]. Black et al. evaluated rapid unique comparison method to measure running frictional torque TRBs with bearing of similar function [16]. Tiago et al. reported accurate monitoring method to measure friction torque and bearing temperature of TRBs up to 7000 N axial load and 6000 rpm rotational speed. Inner raceway rib is an important feature of the TRBs that resist the friction and support the bearing specially under high axial load [17]. M. Zander et al. presented wide comparison for calculation method results for friction in roller bearings and shows

that the contact based methods have many possibilities to predict friction accurately [18]. Karna derived an analytical expression to estimate the friction torque and found good agreement with the experimental work that carried out on newly developed test rig with detached rib under axial load up to 4000 pounds and 1600 rpm [19]. Jamison et al. observed that the contact between rib and roller is crucial to carry axial load and control bearing screwing further illustrated that maintaining adequate lubrication and accurate geometry can improve performance of the TRBs [20]. Witte and Harold quantifies friction torque sources in TRBs focusing on contact between rib and roller performance. Study explores the different operating conditions with input shaft speed 2400 rpm and apply bearing preload to input , output and axle shaft with 0.051 mm, 0.051 mm and 0.101 mm respectively along with rib and roller contact geometry and resulting friction torque [11]. Ahira et al. formulated revised equation to calculate the friction torque based on experimental data and theoretical calculation with external load up to 20 KN and speed 5000 rpm using EHL conditions for approximately 200 TRBs from bore size 17 mm to 200 mm [7]. Matsuyama et al. obtained simple formula for viscous rolling frictional torque in roller raceway contacts in TRBs using speed, material, load etc dimensionless parameters with rotational speed up to 3000 rpm and axial load upto 4 Kn [14]. T Cousseau et al. described experimental method to measure friction torque and bearing temperature for rolling bearing for axial load and rotational speed 7000N and 6000 rpm respectively using four ball Machine [17]. Y Liu et al. developed a model to analyze the effect of defects for friction torque on roller – raceways under varying loads, speed and operating temperature in TRBs using non linear spring model to statics model [21]. S Wirsching et al. identified that EHL based roller face and rib contact plays significant role for bearing power loss and presented numerical optimization technique using evolutionary algorithm for geometric parameters based on sampled DOE [22]. L Liu et al. reported new friction torque calculation model to identified the effect of raceway convexities in TRBs. Here the model is found considering inner and outer raceway surface roughness and convexity under the condition of EHL [23]. P. L. Wu et al. presented a detailed review on measurements of friction torque for different rolling bearings with explaining theoretical calculation models and experiments setups [24]. I. M.

Klebanov et al. elaborated a model to calculate wear rate due to friction torque between rib and roller contact considering spherical shape of roller end and three different shape of ribs like conical, convex and concave considered [25]. M. Manjunath et al. evaluated that at lower speed friction torque due to sliding friction between roller end and rib becomes superior when subjected to axial load with varying speeds and oil temperatures. Study presented cause of rolling resistance and thermal shear factor in TRBs by various experiments using a modular test setup[9]. P. Wingertszahn et al. identified that the friction torque between rollers end and inner raceway rib and also roller cage pockets are significant. The study suggested Parametric Multibody Simulation (PMS) model which is capable to predict friction torque and its kinematics in TRBs and validate by conducting large number of experiments [26]. S Lee et al. investigated TRBs friction torque considering roller geometries along with material uncertainties under axial load. Experimental results compared with the theoretical calculations and correlation analysis suggests that rib angle and half angle of outer raceway had considerable effect on friction torque [27]. X. Zhou et al. marked that maximum temperature in the DTRB arise between the roller end and the inner raceway rib owing to frictional heat among rollers and raceway and sliding friction between roller end and inner raceway rib specially at high axial load. The tests under pure axial load were conducted considering axial load up to 6 kN and shaft speed from 500 to 4000 rpm [28]. However previous study have identified friction torque within TRBs considering various approaches and verified these by experiments, no one have particularly addressed the effect of high pure axial load, bearing shaft speed and inner raceway rib convexity a geometrical parameter on friction torque in TRBs. These parameters are particularly became vital for those TRBs which are assembled in the heavy-duty vehicles' wheel hub and effects considerably when vehicles turn [29]. When the vehicles with heavy load are in turn, the vehicles' front wheel hub bearings experiences a high axial load and that cause rapid friction torque between the roller larger end and the rib and leads high bearing temperature. To enhance the TRBs life and reduce power loss in such conditions it is important to reduce the friction torque and manage bearing temperature by precisely estimating the effects of baring load, shaft speed, and rib convexity.

II. EXPERIMENTAL PROCEDURE

The experimental setup used in the present study is shown in Figure 1. It consists of five main units: (1) a drive unit, powered by an AC induction motor, which runs the bearing shaft at speeds of up to 1200 rpm; (2) a grease-lubricated bearing test unit, also called the bearing hub, which contains the test bearing along with a support bearing; (3) a coupling unit, which connects the drive unit to the bearing hub using two couplings and a torque sensor with a measuring capacity of up to 500 Nm; (4) a hydraulic load unit, which consists of a hydraulic cylinder controlled by an adjustable hydraulic flow control valve to vary the axial load on the test bearing up to 10,000 kgf; and (5) a SCADA (Supervisory Control and Data Acquisition) control unit, which collects data measured by torque, temperature, speed, and load sensors attached to the test rig.

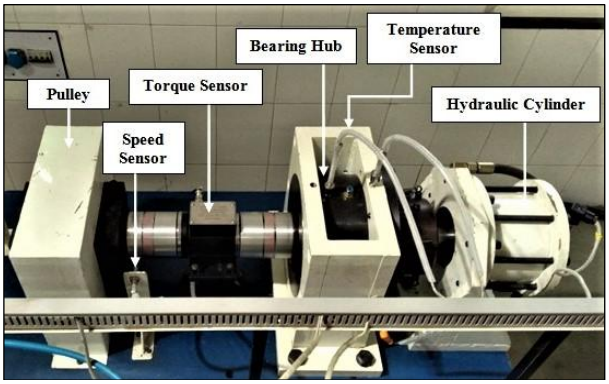

Figure 1: Experimental setup.
Source: Authors, (2024)

Three identical TRBs, with geometries as shown in Figure 2 and specifications as shown in Table 1. were selected for the experiments. These bearings had three different inner raceway rib convexities, approximately 0 µm, 3 µm, and 6 µm, measured using a TALYSURF surface roughness tester, to analyze their effect on the responses.

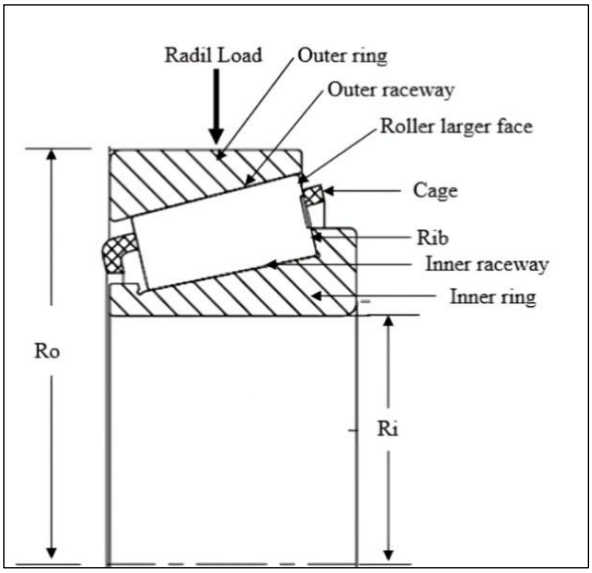

Figure 2: Tapered Roller Bearing.
Source: Authors, (2025).

Table 1: Specification of Test TRBs.

Nominal Outer diameter, mm	**150**
Nominal inner diameter, mm	90
Nominal inner ring width, mm	45
Nominal outer ring width, mm	35
Number of roller	23
Material	SAE52100

Source: Authors, (2025).

Several preliminary experiments were conducted before the final tests to determine the appropriate factor levels needed to achieve the desired objectives. During this pilot phase, the axial load was adjusted between 1,000 kgf and 8,000 kgf, the rib convexity varied from 0 to 9 µ, and the bearing speed was tested within a range of 100 to 800 rpm, in accordance with bearing specifications and intended applications. These trials explored different combinations of axial load, rib convexity, and bearing speed. Friction torque was continuously monitored using SCADA, with the highest recorded value being used for analysis and bearing temperature was measured by bearing temperature sensor attached with the tested TRB. The results and observations from the pilot experiments indicated that when the axial load exceeded 6,000 kgf and the bearing speed exceeded 600 rpm; the bearing temperature rose rapidly above 120°C, surpassing the permissible temperature range for sealed bearings as per standard guidelines. Additionally, heat generation during the tests led to discoloration on the contact surfaces of the raceway and rib. In this study, it is important to include Hertzian contact stress obtained at the roller end and inner raceway rib as high axial loads lead to increased contact stress, which raises the bearing temperature. The Hertzian contact stress can be calculated according to the applied contact types [30], here for TRBs it is applied as point contact [11] [19]. In present study contact stresses at different rib convexities and axial load combinations calculated using MESYS AG contact stress calculation software. Results ensured that up to 6µ contact stress at any axial load does not exceed 2400 MPa and it is safe as per the standards [31]. Furthermore, it was observed that when the rib convexity exceeded 6µ, the contact stress increased beyond 4,000 MPa that exceeding the permissible limits defined by bearing standards. Based on these findings, the present study focuses on three key factors, Rib Convexity (A), Axial Load (B), and Operating Speed (C) and each evaluated at three levels. Table 2 presents design factors and their three levels with coded and actual values.

Table 2: Factors and their selected levels.

Factors	Code	Level			Unit
		-1	0	1	
Rib Convexity	A	0	3	6	µ
Axial Load	B	2000	4000	6000	kgf
Bearing Speed	C	400	500	600	rpm

Source: Authors, (2025).

III. RESPONSE SURFACE METHODOLOGY (RSM)

Design of Experiments (DOE) refers to the methods used to design and analyze experiments effectively, with a minimum number of runs, while also evaluating the effective interactions between operating parameters [32], [33]. Among various DOE methods, Factorial, Response Surface, and Taguchi are the most widely used and preferred by researchers. Response Surface Methodology

(RSM) is one of the most common DOE techniques, particularly applied in sectors such as production process development, new product design, and process multi objective optimization [34], [35]. It helps researchers conduct experiments effectively, control and analyze multiple factors simultaneously, minimize resource consumption, and structure research data for easier analysis [36]–[40]. The first step in RSM is to identify the relationship between the dependent variable (y) and the independent variables (x_i). A standard second-order RSM model can be represented by Eq. (1).

$$y = \beta_0 + \beta_1 x_1 + \beta_2 x_2 + \ldots + \beta_{12} x_1 x_2 + \beta_{13} x_1 x_3 + \ldots + \beta_{11} {x_1}^2 + \beta_{22} {x_2}^2 + \cdots \quad (1)$$

The expression contains both first-degree and second-degree terms, which refine the maximum and minimum values of the response variable. The symbols β_0, β_i, and β_{ij} represent constants. The experimental values are adjusted using the polynomial regression model, as described by the above equation, to calculate the goodness of fit [33]. Response Surface Methodology (RSM) designs are further classified into two categories: 1) Central Composite Design and 2) Box-Behnken Design. In the Box-Behnken design, three-level factors (-1, 0, 1) are typically used to fit second-order models for the response. This experimental design combines 2^k factorials with an incomplete block design, resulting in designs that are generally more effective when the number of runs is large [32][40][41][42]. The present study employs the Box-Behnken design. Table 3 presents the coded Box-Behnken design matrix along with the obtained responses.

Table 3: Box Behnken design with coded factors with responses.

Run Order	A	B	C	Friction Torque (Nm)	Bearing Temperature (°C)
1	-1	-1	0	14	72
2	1	-1	0	10	73
3	-1	1	0	17	86
4	1	1	0	12	85
5	-1	0	-1	13	74
6	1	0	-1	8	74
7	-1	0	1	16	87
8	1	0	1	13	87
9	0	-1	-1	8	55
10	0	1	-1	10	64
11	0	-1	1	11	65
12	0	1	1	15	79
13	0	0	0	12	78
14	0	0	0	12	74
15	0	0	0	12	76

Source: Authors, (2025).

IV. RESULTS AND DISCUSSION

IV.1 RESPONSE SURFACE REGRESSION (RSR) MODEL

Table 4 represents the RSR model for friction torque and bearing temperature, obtained through the RSM method using MINITAB 19. These response models signify the effect of independent variables on responses by establishing a correlation between them.

Table 4: Response surface regression model for responses.

Responses	Correlation
Friction Torque	= -12.63 - 2.292 Rib Convexity - 0.000187 Axial Load + 0.0925 speed + 0.1528 Rib Convexity*Rib Convexity - 0.000000 Axial Load*Axial Load - 0.000088 speed*speed - 0.000042 Rib Convexity*Axial Load + 0.001667 Rib Convexity*speed + 0.000002 Axial Load*speed
Bearing Temperature	= -80.6 - 5.58 Rib Convexity + 0.01194 Axial Load + 0.4763 speed + 0.9861 Rib Convexity*Rib Convexity - 0.000001 Axial Load*Axial Load - 0.000437 speed*speed - 0.000083 Rib Convexity*Axial Load - 0.00000 Rib Convexity*speed + 0.000006 Axial Load*speed

Source: Authors, (2025).

IV.2 ANALYSIS OF VARIANCE (ANOVA)

ANOVA is a robust statistical method often used in mechanical experiments where multiple factors are tested simultaneously to assess their effect on the response variable. In this study, ANOVA is applied to evaluate the influence of various independent variables—axial load, speed, and rib convexity—on the response variables, friction torque and bearing temperature, as well as to assess the adequacy of the analytical model. The model includes interaction terms up to two-way interactions to improve its predictive accuracy. The ANOVA results for both responses are shown in Table 5. These table display the degrees of freedom (DF), sum of squares (SS), and p-values.

For friction torque, the model explains 99.74% of the variation, with an adjusted R-square of 99.27% and a predicted R-square of 95.85%, indicating strong reliability and applicability to the independent variables. The p-values for factors A, B, and C are less than

0.05, indicating that they have a strong influence on friction torque. However, the interaction terms AB, AC, and BC, as well as the second-order terms BB and CC, are not significant, as their p-values are higher than 0.05, indicating their impact on friction torque is negligible.

For bearing temperature, the model has an even higher R-square of 99.21%, with an adjusted R-square of 97.79% and a predicted R-square of 96.75%, demonstrating excellent fit and predictive accuracy. Factors B and C are highly significant, as their p values are less than 0.05, and strongly influencing bearing temperature. However, the terms with p values greater than 0.05 are not significant and do not affect the response. Overall, the results show that both models are well-fitted and explain most of the variation in their respective response variables.

Table 5: Analysis of Variance

Source		Friction Torque		Bearing Temperature	
	DF	SS	P-Value	SS	P-Value
Model	9	96.1500	0.000	1161.68	0.000
Linear	3	83.2500	0.000	625.25	0.000
A	1	36.1250	0.000	0.00	1.000
B	1	15.1250	0.000	300.13	0.000
C	1	32.0000	0.000	325.13	0.000
Square	3	10.6500	0.000	529.18	0.000
A*A	1	6.9808	0.000	290.83	0.000
B*B	1	0.0577	0.332	127.44	0.000
C*C	1	2.8269	0.001	70.67	0.002
2-Way Interaction	3	2.2500	0.006	7.25	0.369
A*B	1	0.2500	0.076	1.00	0.495
A*C	1	1.0000	0.007	0.00	1.000
B*C	1	1.0000	0.007	6.25	0.125
Error	5	0.2500		9.25	
Total	14	96.4000		1170.93	
R-square		99.74%		99.21%	
R-square (adj)		99.27%		97.79%	
R-square (pred)		95.85%		96.75%	

Source: Authors, (2025).

IV.3 COMPARISON OF EXPERIMENTAL RESULTS WITH RSM MODEL

Table 6 presents a comparison of the experimental results for the response variables friction torque and bearing temperature with the predicted results from the developed RSM regression model, along with the percentage error. The results show that the maximum percentage error for friction torque and bearing temperature is 2.08% and 2.7%, respectively, which is within 5%. This indicates that both models adequately fit the experimental results. Figure 3 provides a graphical comparison, illustrating how well the model predictions align with the experimental results.

Table 6: Comparison of experimental results with RSM regression model fits along percentage errors.

Run	Experimental Results		RSM Model		Percentage Error	
	FT	BT	FT	BT	FT	BT
1	14	72	13.750	72.375	1.79	0.52
2	10	73	10.000	73.375	0.00	0.51
3	17	86	17.000	85.625	0.00	0.44
4	12	85	12.250	84.625	2.08	0.44
5	13	74	13.125	74.125	0.96	0.17
6	8	74	7.875	74.125	1.56	0.17
7	16	87	16.125	86.875	0.78	0.14
8	13	87	12.875	86.875	0.96	0.14
9	8	55	8.125	54.500	1.56	0.91
10	10	64	9.875	64.250	1.25	0.39
11	11	65	11.125	64.750	1.14	0.38
12	15	79	14.875	79.500	0.83	0.63
13	12	78	12.000	76.000	0.00	2.56
14	12	74	12.000	76.000	0.00	2.70
15	12	76	12.000	76.000	0.00	0.00

Source: Authors, (2025).

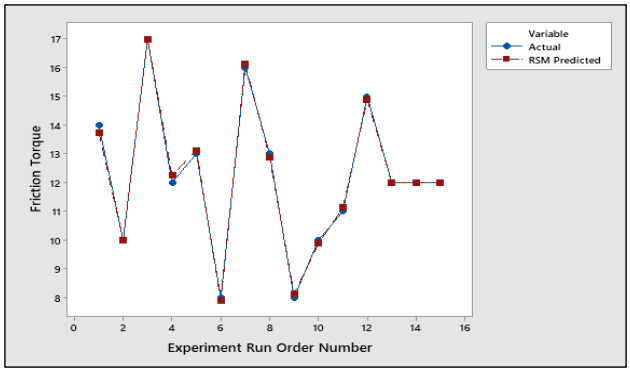

(a) Friction torque

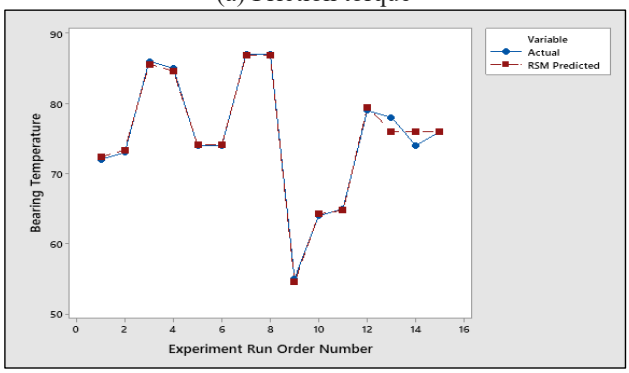

(b) Bearing Temperature

Figure 3: Experimental results vs. regression model graphs.
Source: Authors, (2025).

IV.4 INTERACTION EFFECTS BETWEEN INPUT AND OUTPUT PARAMETERS

The main effect plots for friction torque and Bearing Temperature are as shown in Figure 4 a) and b) respectively produced using MINITAB 19. It shows the effect of an independent variable on responses. Figure 4 shows that friction torque and bearing temperature increases as the axial load and bearing shaft speed increases. However, friction torque minimized at 6μ convexity while bearing temperature minimized at 3μ convexity because of contact stress between the rib and roller ends.

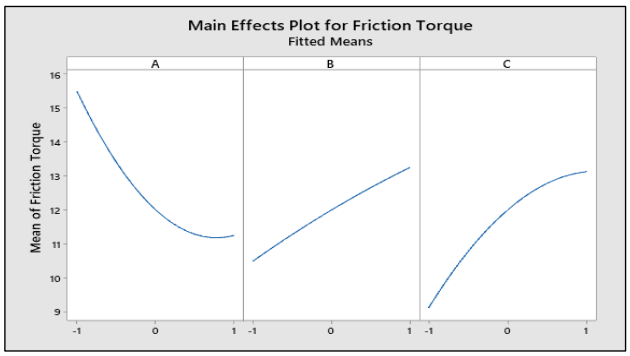

(a) Friction Torque

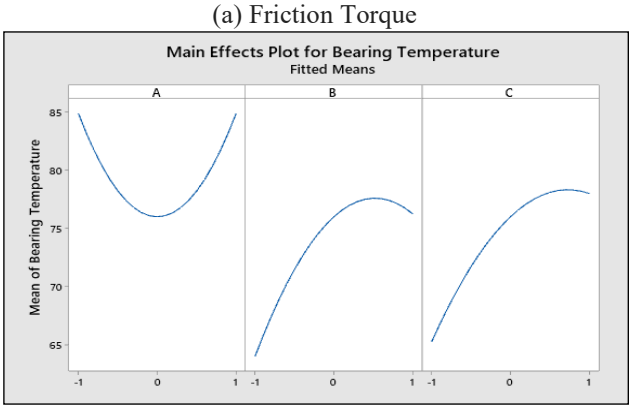

(b) Bearing Temperature.

Figure 4: Main Effect Plots.
Source: Authors, (2025).

To analyze the interaction effect of rib convexity, axial load, and bearing shaft speed on the response variables friction torque and bearing temperature, contour plots and surface plots are presented in Figure 5 and Figure 6. Figure 5(a) and (b) show the contour plots for friction torque, indicating that friction torque increases as axial load increases from 2000 kgf to 6000 kgf and speed increases from 400 rpm to 600 rpm, while it decreases as rib convexity increases from 0 µm to 6 µm. The dark-colored regions indicate higher friction torque, whereas the lightest green shade represents friction torque values below 10 Nm. Figure 5 (c) and (d) present the contour plots for bearing temperature. These plots show that bearing temperature remains minimal at 3 µm rib convexity and increases with an increase in axial load and speed.

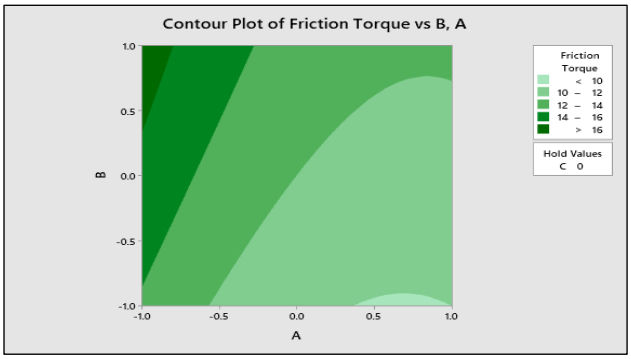

(a)

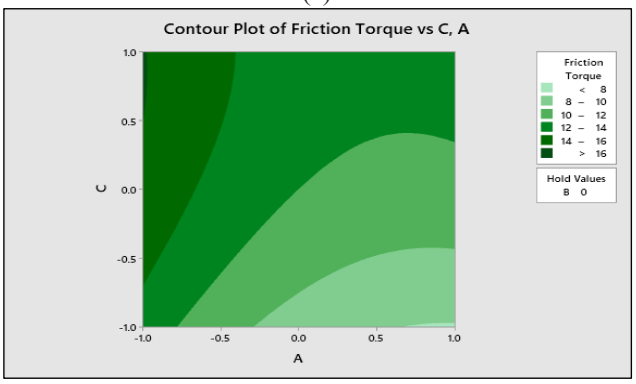

(b)

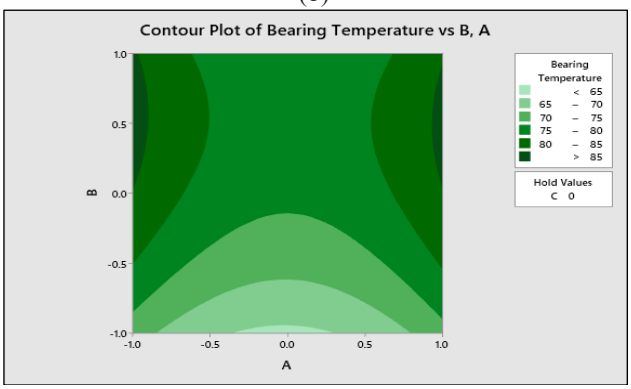

(c)

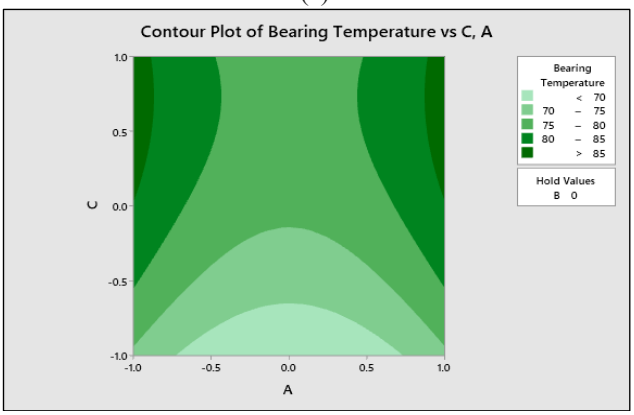

(d)

Figure 5: Contour Plots.
Source: Authors, (2025).

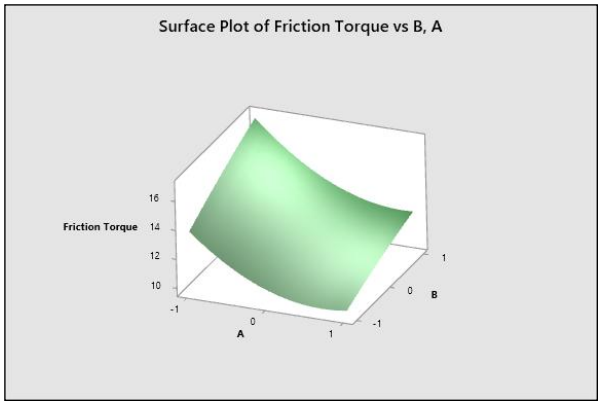

(a)

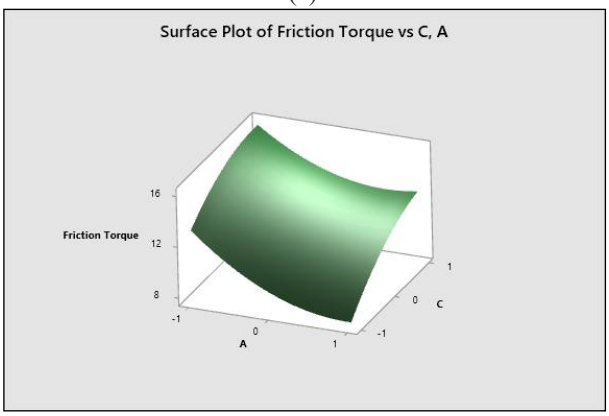

(b)

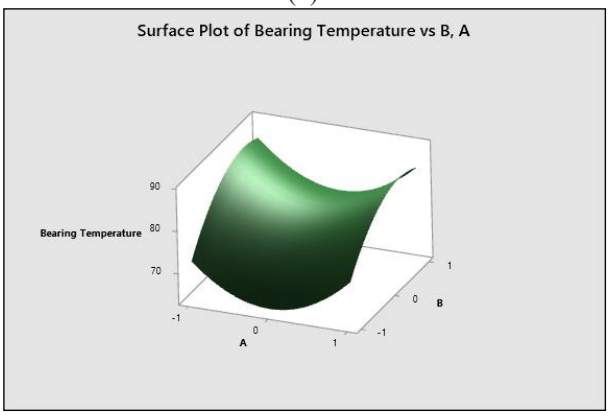

(c)

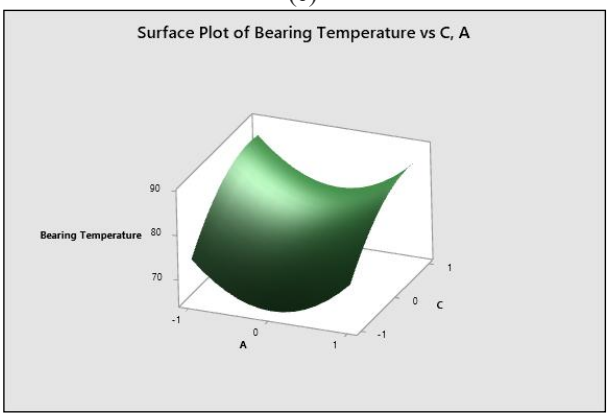

(d)

Figure 6: Surface Plots.
Source: Authors, (2025).

To visualize and analyze the effects of independent factors on response variables, Figure 6 presents the surface plots. These plots help identify maximum and minimum response values and determine the optimal combination of factor levels for optimization. Figure 6 (a) and (b) show the surface plots for friction torque, which tends to increase when rib convexity is at 0 µm, with axial load increasing from 2000 kgf to 6000 kgf and speed up to 600 rpm. However, friction torque can be minimized with an appropriate combination of rib

convexity and axial load, as shown in the figure. Similarly, Figure 6 (c) and (d) illustrate that bearing temperature remains minimal when rib convexity is set at 3 µm, with speed maintained at 400 rpm.

IV.3 PARAMETRIC OPTIMIZATION AND CONFIRMATION OF EXPERIMENTS

According to the RSM analysis results shown in Figure 7, the optimal response solutions for friction torque and bearing temperature are obtained when the parameter combination is 3.2 µm rib convexity, 2000 kgf axial load, and 400 rpm bearing shaft speed. Under these conditions, the predicted friction torque and bearing temperature are 7.96 Nm and 54.57 °C, respectively. To ensure a comprehensive analysis, two additional optimal parameter combinations obtained from the RSM were included, and confirmation experiments were conducted for these groups. Table 7 presents a comparison between the predicted and experimental results, along with the percentage deviation for all groups, which remains within 5%. Therefore, it can be concluded that the proposed statistical model accurately predicts the output responses.

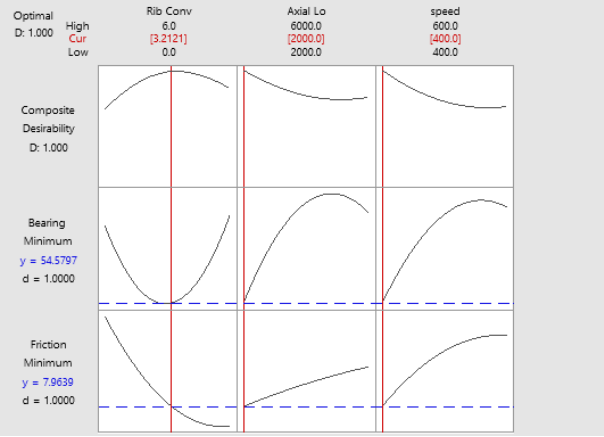

Figure 7: RSM Optimum solution.
Source: Authors, (2025).

Table 7: Optimal parameters combinations under RSM and the Deviation.

RSM Optimum Solutions	A (µ)	B (kgf)	C (rpm)		FT (Nm)	BT (° C)
1	3.2	2000	400	Predicted	7.96	54.57
				Experimental	8	56
				Deviation %	0.45	2.54
2	4.3	6000	400	Predicted	8.86	65.84
				Experimental	9	68
				Deviation %	1.60	3.18
3	0.6	2000	400	Predicted	10.82	59.53
				Experimental	11	62
				Deviation %	1.64	3.99

Source: Authors, (2025).

V. CONCLUSIONS

The present experimental study investigates the impact of operating parameters, such as high axial load and bearing speed, along with the geometrical parameter—inner race rib convexity—on friction torque and bearing temperature in tapered roller bearings (TRBs). Additionally, response surface methodology (RSM) serves as an effective statistical tool to identify the effects of these parameters on responses and optimize them for the best outcomes, ultimately minimizing overall power loss and heat generation in TRBs. According to the RSM regression model, the optimal parametric combination was found at a rib convexity of 3.21 µm, an axial load of 2000 kgf, and a bearing speed of 400 rpm, which predicted optimal responses of 7.96 Nm friction torque and 54.57 °C bearing temperature. These predicted results, along with two additional parametric combinations, were validated through confirmation tests, showing deviations within 5%. This confirms that the developed model aligns well with the experimental results and is appropriate for accurate predictions.

VI. AUTHOR'S CONTRIBUTION

Conceptualization: Amisha B. Khant, Jaydeep K. Dadhaniya and Hardik G. Chothani.
Methodology: Amisha B. Khant, Jaydeep K. Dadhaniya and Hardik G. Chothani.
Investigation: Amisha B. Khant, Jaydeep K. Dadhaniya and Hardik G. Chothani.
Discussion of results: Amisha B. Khant, Jaydeep K. Dadhaniya and Hardik G. Chothani.
Writing – Original Draft: Amisha B. Khant, Jaydeep K. Dadhaniya and Hardik G. Chothani.
Writing – Review and Editing: Amisha B. Khant, Jaydeep K. Dadhaniya and Hardik G. Chothani.
Supervision: Amisha B. Khant, Jaydeep K. Dadhaniya and Hardik G. Chothani.
Approval of the final text: Amisha B. Khant, Jaydeep K. Dadhaniya and Hardik G. Chothani.

VIII. REFERENCES

[1] T. A. Harris and M. N. Kotzalas, Essential Concepts of Bearing Technology. 2006.

[2] T. A. Harris and M. N. Kotzalas, Advanced Concepts of Bearing Technology. Taylor & Francis Group, LLC, 2006.

[3] T. A. Harris, “Rolling Bearing Analysis,” CRC Press. New York, p. pp 147–154, 2001.

[4] T. N. Wang, H. T. Li, and J. X. et al Wei, “Evaluating Stress Impact on Roller Bearing Within Disc Cutters of Tunnel Boring Machines,” Strength Mater., vol. 56, pp. 1179–1192, 2025.

[5] Palmgren A, “Ball and roller bearing engineering,” Burbank, Philadephia, p. pp 30–39, 1959.

[6] H. G. Chothani, D. J. Marsonia, N. N. Jadeda, and S. H. Zala, “LUBRICATED WORM GEARBOX ON CHURNING POWER LOSSES,” J. Eng. Technol. Ind. Appl., vol. 10, no. 49, pp. 137–143, 2024, doi: DOI: https://doi.org/10.5935/jetia.v10i49.1123.

[7] S. Aihara, “A New Running Torque Formula for TRB under axial load,” J. Tribol. ASME, vol. 109, 1987.

[8] R. S. Zhou and M. R. Hoeprich, “Torque of Tapered Roller Bearings,” J. Tribol. ASME, 1991, [Online]. Available: http://asme.org/terms

[9] M. Manjunath, D. Fauconnier, and W. Ost, “Experimental Analysis of Rolling Torque and Thermal Inlet Shear Heating in Tapered Roller Bearings,” Machines, vol. 11, 801, pp. 1–22, 2023.

[10] D. C. Witte, “Operating torque of tapered roller bearings,” ASLE Trans., vol. 16, no. 1, pp. 61–67, 1973, doi: 10.1080/05698197308982705.

[11] D. C. Witte and H. E. Hill, “Tapered roller bearing torque characteristics with emphasis on rib-roller end contact,” SAE Tech. Pap., 1987, doi: 10.4271/871984.

[12] I. Bercea, N. Mitu, I. Damian, M. Mercea, and S. Cretu, “A theoretical and experimental study on friction losses in tapered roller bearing,” Tribol. Ind., vol. 18, no. No 1, 1996.

[13] H. Matsuyama, S. Kamamoto, and K. Asano, “The analysis of frictional torque for tapered roller bearings using EHD theory,” SAE Tech. Pap., no. 724, 1998, doi: 10.4271/982029.

[14] H. Matsuyama and S. Kamamoto, “Analysis of Frictional Torque in Raceway Contacts of Tapered Roller Bearings,” KOYO Eng. J. English Ed., vol. 159, no. 159E, pp. 53–60, 2001.

[15] L. Houpert, “Ball bearing and tapered roller bearing torque: analytical, numerical and experimental results,” Tribol. Trans., vol. 45, no. 3, pp. 345–353, 2002, doi: 10.1080/10402000208982559.

[16] J. J. Blake and C. E. Truman, “Measurement of running torque of tapered roller bearings,” Proc. Inst. Mech. Eng. Part J J. Eng. Tribol., vol. 218, no. 4, pp. 239–249, 2004, doi: 10.1243/1350650041762659.

[17] T. Cousseau, B. Graça, A. Campos, and J. Seabra, “Experimental measuring procedure for the friction torque in rolling bearings,” Lubr. Sci., vol. 22, no. 4, pp. 133–147, Apr. 2010, doi: 10.1002/ls.115.

[18] M. Zander, M. Otto, T. Lohner, and K. Stahl, “Evaluation of friction calculation methods for rolling bearings,” Forsch. im Ingenieurwes. Springer, vol. 87, no. 4, pp. 1307–1316, Dec. 2023, doi: 10.1007/s10010-023-00715-1.

[19] C. L. Karna, “Performance characteristics at the rib roller end contact in tapered roller bearings,” ASLE Trans., vol. 17, no. 1, pp. 14–21, 1974, doi: 10.1080/05698197408981434.

[20] W. E. Jamison, J. J. Kauzlarich, and E. V. Mochel, “Geometric effects on the rib-roller contact in tapered roller bearings,” ASLE Trans., vol. 20, no. 1, pp. 79–88, 1977, doi: 10.1080/05698197708982820.

[21] Y. Liu, W. Kang, Y. Zhu, K. Yan, and J. Hong, “Effects of Defect on Roller-Raceway Contact State and Friction Torque of Tapered Roller Bearings,” J. Tribol., vol. 142, no. 11, Nov. 2020, doi: 10.1115/1.4047194.

[22] S. Wirsching, M. Marian, M. Bartz, T. Stahl, and S. Wartzack, “Geometrical optimization of the ehl roller face/rib contact for energy efficiency in tapered roller bearings,” Lubricants, vol. 9, no. 67, pp. 1–19, 2021, doi: 10.3390/lubricants9070067.

[23] L. Liu, W. Liu, K. Wang, D. Wang, and Y. Wang, “Effects of Raceway Convexity on Friction Moment of Tapered Roller Bearings,” J. Phys. Conf. Ser. Pap., 2022, doi: 10.1088/1742-6596/2174/1/012047.

[24] P. L. Wu et al., “Theoretical calculation models and measurement of friction torque for rolling bearings: state of the art,” J. Brazilian Soc. Mech. Sci. Eng., vol. 44, no. 9, 2022, doi: 10.1007/s40430-022-03726-1.

[25] I. M. Klebanov, A. M. Brazhnikova, and K. A. Polyakov, “Tapered Roller Bearing Rib-Roller End Interaction at Hydrodynamic Contact,” J. Frict. Wear, vol. 43, no. 6, pp. 391–397, 2022, doi: 10.3103/S106836662206006X.

[26] P. Wingertszahn, O. Koch, L. Maccioni, F. Concli, and B. Sauer, “Predicting Friction of Tapered Roller Bearings with Detailed Multi-Body Simulation Models,” Lubricants, vol. 11, no. 9, 2023, doi: 10.3390/lubricants11090369.

[27] S. Lee and H. G. An, “Evaluation of Friction Torque in Tapered Roller Bearings,” SAE Int., p. 6, 2024, doi: https://doi.org/10.4271/2024-01-3047.

[28] X. Zhou, Z. Ge, X. Li, M. Rao, and Q. Han, “Thermal Analysis of Grease-Lubricated Double Row Tapered Roller Bearings,” Lubricants, vol. 13(2), 2025, doi: https://doi.org/10.3390/lubricants13020084.

[29] B. Martin and H. E. Hill, “Design and selection factors for automatic transaxle tapered roller bearings,” SAE Tech. Pap., 1992, doi: 10.4271/920609.

[30] M. Gärtner et al., “Evaluation of hybrid spindle bearings with nitriding raceway steels under high rotational speeds,” Tribol. Mater., vol. 2, no. 3, pp. 88–98, 2023, doi: 10.46793/tribomat.2023.012.

[31] SKF, “SKF GENERAL CATALOGUE,” SKF: Gothenburg, Sweden, 2003. [Online]. Available: https://imparayaycia.com/SKF CATALOGO GENERAL.pdf

[32] R. A. Fisher, “The Design of Experiments.,” Hafner Press, no. 9th Edition. p. 256, 1974. doi: 10.2307/2348207.

[33] D. C. Montgomery, Design and analysis of experiments. 2013. doi: 10.2307/2983009.

[34] M. M. Muanda, P. P. D. Omalanga, V. M. Mitonga, and M. N. Ilunga, “Gold Removal From Gold-Bearing Ore Using Alpha-Cyclodextrin: Response Surface Methodology and Artificial Neural Analysis Network Optimizations,” J. Eng. Technol. Ind. Appl., vol. 9, no. 42, pp. 48–60, 2023, doi: 10.5935/jetia.v9i42.879.

[35] É. S. Passari, H. J. Amorim, and A. J. Souza, “Multiobjective Optimization of Cutting Parameters for Finishing End Milling Hardox® 450,” J. Eng. Technol. Ind. Appl., vol. 8, no. 34, pp. 20–28, 2022, doi: 10.5935/jetia.v8i34.805.

[36] A. I. Khuri and J. A. Cornell, “Response Surfaces: Designs and Analyses Second Edition (2nd ed.).,” CRC Press. Boca Rat., 1996, doi: https://doi.org/10.1201/9780203740774.

[37] E. R. Ziegel, “Response Surfaces: Designs and Analyses,” Technometrics, vol. 39, no. 3, p. 342, 1997, doi: https://doi.org/10.1080/00401706.1997.10485140.

[38] C. M. Anderson-Cook, C. M. Borror, and D. C. Montgomery, “Response surface design evaluation and comparison,” J. Stat. Plan. Inference, vol. 139, no. 2, pp. 629–641, 2009, doi: 10.1016/j.jspi.2008.04.004.

[39] A. I. Khuri and Siuli Mukhopadhyay, “Response surface methodology,” WIREs Comput. Stat., vol. 2, no. 2, pp. 128–149, 2010, doi: https://doi.org/10.1002/wics.73.

[40] A. Dean, V. D., and D. Draguljić, Response Surface Methodology. Design and Analysis of Experiments. 2017. doi: 10.1007/978-3-319-52250-0.

[41] A. Yıldız, L. Uğur, and İ. E. Parlak, “Optimization of the Cutting Parameters Affecting the Turning of AISI 52100 Bearing Steel Using the Box-Behnken Experimental Design Method,” Appl. Sci., vol. 13, no. 1, 2023, doi: 10.3390/app13010003.

[42] S. Bhivsane, A. Chel, and S. Sayyed, “Machining Parameters Optimization in Wet Turning of En31 Material Using Box-Behnken Approach of Rsm,” J. Eng. Technol. Ind. Appl., vol. 10, no. 50, pp. 103–111, 2024, doi: 10.5935/jetia.v10i50.1354.

Journal of Engineering and Technology for Industrial Applications

ITEGAM-JETIA

Manaus, v.11 n.54, p. 136-144. July/August., 2025.
DOI: https://doi.org/10.5935/jetia. v11i54.2118

ISSN ONLINE: 2447-0228

RESEARCH ARTICLE OPEN ACCESS

DEVELOPMENT AND VALIDATION OF A MULTI-SOURCE BRIDGE DC–DC CONVERTER FOR EV APPLICATIONS

Baya Reddy Lomada[1], V. Naga Bhaskar Reddy[2]

[1]Research scholar, Dept of EEE, JNT University, Anantapur, Andhra Pradesh, India.
[2] Professor,Senior member IEEE, Dept of EEE RGMCET, Nandyal, Andhra Pradesh, India.

[1]https://orcid.org/0000-0002-8396-9882, [2]https://orcid.org/0000-0002-3073-9565

Email: reddy.baya@gmail.com, nagabhaskarreddy@rgmcet.edu.in

ARTICLE INFO

Article History
Received: June 28, 2025
Revised: July 13, 2025
Accepted: June 15, 2025
Published: July 31, 2025

Keywords:
Mathematical modeling
DC-DC converter
Validation
Multi-Input Converter
Hybrid energy system

ABSTRACT

As per the current scenario of exhausting the oil supplements across the globe because of rapid increase in the consumption of conventional resources which causes the destruction of environment and human life as they emit CO2, SO2 and oxides of nitrogen gas. Hybrid Electric Vehicle (HEV) plays vital role now a days to overcome the above hazards. This article provides a detailed investigation of a multi-input DC converter (MIC) including its mathematical modelling, design, validation of the prototype, and analysis. This converter actively accepts solar photovoltaic (PV) panels and fuel cells as sources. Converter achieve broad control of output voltage and power flow with help of multiple switching frequencies. The steady-state modeling are demonstrated to achieve accurate design and analysis. The recommended converter assurances reduced stress on voltage, fewer switches, and fewer circuit components while offering higher gain and 96.4% efficiency.

Copyright ©2025 by authors and Galileo Institute of Technology and Education of the Amazon (ITEGAM). This work is licensed under the Creative Commons Attribution International License (CC BY 4.0).

I. INTRODUCTION

A surplus of energy sources are being exploited to meet the rising demand for power [1-3]. The world's expanding need for electricity can no longer be met by traditional energy sources since they are quickly running out [4]. The use of natural fuels for energy production also has a detrimental effect on the environment, raising concerns about things like air pollution and global warming [5]. The output of electricity derived from renewable energy sources is consequently rising swiftly, particularly in distributed generation [6]. Thus, developing hybrid energy plans that continuously supply power to the right demand through a variety of green technologies is crucial [7]. The huge majority of EV are battery powered, which depends on two important variables: the availability of lithium and the state of the electricity network today [8].

To avoid the issues, research and tests on fuel cell-based cars, photovoltaic and fuel cell hybrid electric cars must be carried out concurrently [9]. For such cars, the paucity of lithium and the contemporary power grid are irrelevant. Hydrogen best compares to batteries in terms of both energy density and power density [10]-[12]. Because hydrogen is expensive, it is perfect to use PV panels in addition to fuel cells to reduce the useage of hydrogen in the vehicle [13], [14]. As shown in Figure. 1, the solar PV, fuel cell, inverter, multi-input DC-DC converter & electric motor comprise the primary powertrain components of HEV. A multi-input DC-DC converter has a substantial impact on the overall stability and functionality of the HEV powertrain system. Experts have created many MICs, but not all of them are appropriate for every application compared to non-isolated MICs, other types of MICs are far fewer useful for slight and medium-powered HEVs.

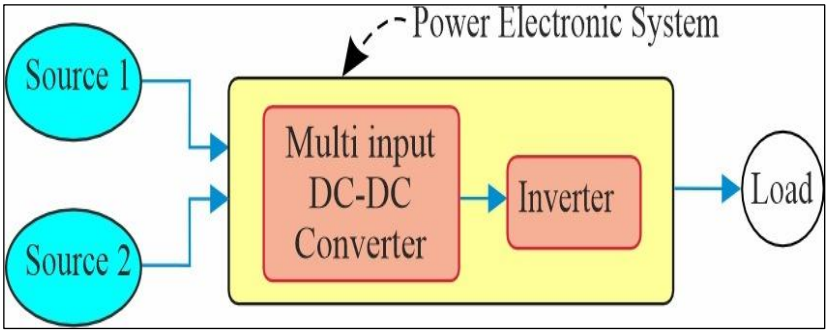

Figure 1: Block diagram of HEV.
Source: Authors, (2025).

A novel MIC configuration developed with the basic single-ended primary-inductor converter (SEPIC) was presented by the researchers in [15]. It is feasible to integrate many inputs, but at least one of them must be a rechargeable battery. Regretfully, there is a great deal of voltage stress on the switching electronics. A unique MIC structure is described in [16] to integrate the super-capacitor and rechargeable battery for EVs. Relays are used in this converter to carry out the required function no need any additional circuity for one input can feed the other which comparatively increases the circuit difficulty. In Experts in [17]. The authors of [18] introduced a novel type of MIC bridge for establishing connections between many renewable energy sources. To get a larger gain, fewer unidirectional and bidirectional semiconductor switches are used. Depending on the number of switches operating in each mode, the stress placed on each switch in this architecture increases. Furthermore, a polarity change between the input and output voltages is seen. A bidirectional MIC was described by the authors of [19].

This work is primarily focused on calculating critical inductance and minimizing voltage ripple. Although there are more switching components and a battery input required, this converter can give electricity in both directions. The development and analysis of a MIC are shown in the article [20]. Reducing the number of Components and the stress on the switch voltage are the converter's key concerns. Unfortunately, there are more losses in this converter, and there are still a lot of components. In [21], A unique modular MIC was suggested by the researchers. It has slight components, a smaller amount of voltage stress, and a better voltage gain. Nevertheless, there are more parts in this converter, and several switches are under more voltage stress. It also uses a more of storage components for a multi-input system, which complicates control design and system analysis. In [22], A non-isolated MIC for RES was presented by the authors. Due to the non-coupled inductor, this converter shows greater gain on voltage at a fewer component count... In [23], the authors presented a Multi-Input High Gain Non-isolated DC–DC Converter with a new design and a condensed component. One diode is utilized to enable bidirectional power flow in order to reduce the number of components and create high voltage gain.

II. PROPOSED CONVERTER

The working principle of the MIC and traditional converters is quite similar. In both cases, the inductive and capacitive components of the converter charge for a predetermined amount of time and then dis-charge through a load for the rest period of time. The operating technique is the same in the suggested converter. Figure. 2 illustrates the recently built MICs intended for HEV use.

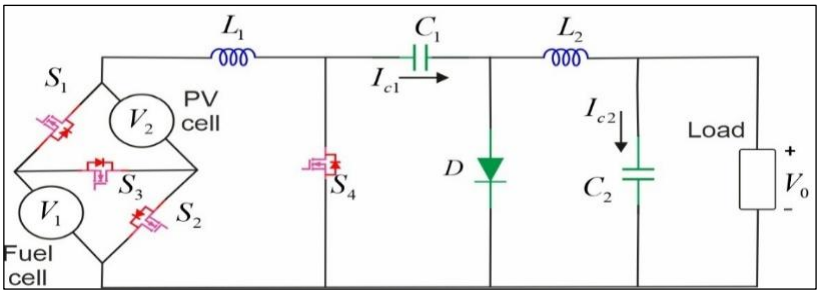

Figure 2: shows the suggested converter structure.
Source: Authors, (2025).

II.1 MODES OF OPERATION

Figure. 3 shows the equivalent circuitry for the six modes of operation of the suggest converter. In Figure. 2, fuel cell voltage is V_1, the solar panel output voltage is V_2, S_1 to S_4 are the four MOSFET switches, D is the diode, R is the load resistance, two inductors are L_1 and L_2, two capacitors are C_1 and C_2. i_{C1}, i_{C2} and i_{L1}, i_{L2} are the respective currents flowing through C_1, C_2 and L_1, L_2. v_{C1}, v_{C2}, v_{L1} and v_{L2} are the respective large signal voltages across C_1, C_2 and L_1, L_2. i_0 and v_0 are the large signal current and voltage respectively at load resistance. Any combination of inputs can be used to operate the suggested converter. To see the converter in action, assume that V_1 is greater than V_2. The switches S_1 to S_4 respective switching frequencies are f_{S1} to f_{S4} and assuming $f_{S1}= f_{S2}= f_{S3}= f_{S4} =1/T$ The suggested work does not account for solar panel leakage current, fuel cell dynamics, or sunlight's erratic nature. The entire functioning of the planned converter is covered in sections II.1.1 to II.1.6, together with the corresponding mathematical equations.

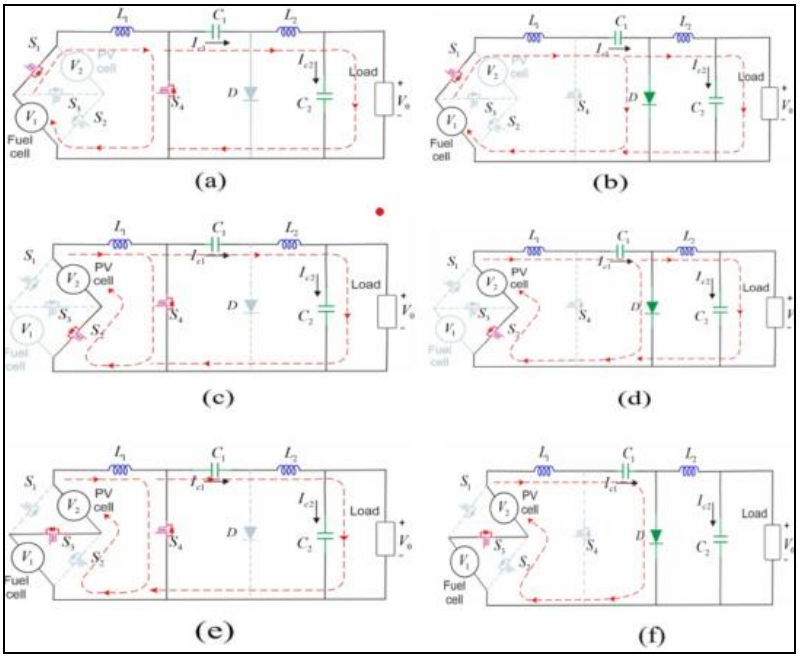

Figure 3: Modes of operation. a. Mode (1), b. Mode (2), c. Mode (3), d. Mode (4), e. Mode (5), and f. Mode (6).
Source: Authors, (2025).

II.1.1 First Mode: In the Mode-1 S_1, S_4 are ON state and S_2, S_3 and D are OFF state. The Fig. 3 (a) shows the First Mode circuit by using KCL and KVL on mode 1 circuit.

$$v_{L1} = v_1 \tag{1}$$
$$v_{L2} = -v_{C1} - v_{c2} \tag{2}$$
$$i_{L1} = i_1 \tag{3}$$
$$i_{L2} = i_{C1} \tag{4}$$
$$i_0 = i_2 - i_{C2} \tag{5}$$
$$v_0 = v_{C2} = i_0 R = -i_{C2} R \tag{6}$$

II.1.2 Second Mode:

In the second Mode the switches S_1 , D are in turn ON and S_2, S_3 and S_4 are in OFF state. The corresponding circuit under this mode is shown in Figure. 3(b)
The equations from (7) to (10) can be obtained by using KCL and KVL.

$$v_{L1} = v_1 - v_{C1} \tag{7}$$
$$v_{L2} = -v_0 \tag{8}$$
$$i_{L1} = i_{C1} \tag{9}$$
$$i_{L2} = i_0 + i_{C2} \tag{10}$$

II.1.3 Third Mode:

In this mode, S_2, S_4 are ON and D, S_1 and S_3 OFF state. The Figure. 3 (c) shows the equivalent circuit.
The equations from (11) to (16) can be obtained by using KCL and KVL.

$$v_{L1} = v_2 \tag{11}$$
$$v_{L2} = -v_{C1} - v_{C2} \tag{12}$$
$$i_{L1} = i_1 \tag{13}$$
$$i_{L2} = i_{C1} \tag{14}$$

$$i_0 = i_2 - i_{C2} \tag{15}$$

$$v_0 = v_{C2} = i_0 R = (i_2 - i_{C2})R \tag{16}$$

II.1.4 Forth Mode: Fourth mode, S_2, D are ON and S_1, S_3 and S_4 are OFF state. The Figure. 3 (d) shows the equivalent circuit. The equations from (17) to (20) can be obtained by using KCL and KVL

$$v_{L1} = v_2 - v_{C1} \tag{17}$$

$$v_{L2} = -v_0 \tag{18}$$

$$i_{L1} = i_{C1} \tag{19}$$

$$i_{L2} = i_0 + i_{C2} \tag{20}$$

II.1.4 Fifth Mode: In fifth Mode, S_3, S_4 are ON and S_1, S_2 and D are OFF state. The Figure. 3 (e) shows the under fifth mode.

The equations from (21) to (26) can be obtained by using KCL and KVL.

$$v_{L1} = v_1 + v_2 \tag{21}$$

$$v_{L2} = -v_{C1} - v_{C2} \tag{22}$$

$$i_{L1} = i_1 \tag{23}$$

$$i_{L2} = i_{C1} \tag{24}$$

$$i_0 = i_2 - i_{C2} \tag{25}$$

$$v_0 = v_{C2} = i_0 R \tag{26}$$

II.1.6 Sixth Mode: In Mode six, the S_3, D are in ON state and S_1, S_2 and S_4 are in OFF state. The Figure. 3 (f) shows the corresponding circuit.

by using KCL and KVL the equations (27) to (30) can be obtained.

$$v_{L1} = v_1 + v_2 - v_{C1} \tag{27}$$

$$v_{L2} = -v_0 \tag{28}$$

$$i_{L1} = i_{C1} \tag{29}$$

$$i_{L2} = i_0 + i_{C2} \tag{30}$$

II.2 STATE-STATE MODELLING

To determine the relationship between output current and voltage in terms of the duty cycle, as well as the expressions for the values of inductors and capacitors, steady-state modelling is essential. With help of (1) to (30), equations

$$V_0 = -\frac{d_1+d_3+d_5}{1-d_1-d_3-d_5}\left(V_1(1-d_3-d_4) + V_2(1-d_1-d_2)\right) \quad (31)\ I_{L2} = I_0 = \frac{V_0}{R}\ (32)\ I_{L1} = \frac{-V_0}{R}\frac{d_1+d_3+d_5}{1-d_1-d_3-d_5} \tag{33}$$

System performance is determined by the design and selection of inductors and capacitors, which also enable the converter to operate in the necessary conduction mode. the value of the inductors and capacitor equations are

$$L_1 = \frac{(V_1+V_2)d_5T}{\Delta I_{L1}} \tag{34}$$

$$L_2 = \frac{V_0 d_5 T}{\Delta I_{L2}} \tag{35}$$

$$C_1 = \frac{V_0 d_5 T}{R\Delta V_{C1}} \tag{36}$$

$$C_2 = \frac{V_0 d_5 T}{R\Delta V_{C2}} \tag{37}$$

III. EFFICIENCY

Power converter's efficiency is mostly affected by parasitic components. The recommended converter's power loss is shown below.

$$Power\ loss\ due\ to\ the\ internal\ elements = P_{S1} + P_{S2} + P_{S3} + P_{S4} + P_{RL1} + P_{RL2} + P_{RC1} + P_{RC2} + P_{RD} + P_{VFD}$$
$$= {I_{S1R}}^2 R_{S1} + {I_{S2R}}^2 R_{S2} + {I_{S3R}}^2 R_{S3} + {I_{S4R}}^2 R_{S4} + {I_{L1R}}^2 R_{L1} + {I_{L2R}}^2 R_{L2} + {I_{C1R}}^2 R_{C1} + {I_{C2R}}^2 R_{C2} + {I_{DR}}^2 R_D + I_{Davg} V_{FD}$$

The suggested converter's overall power loss is,

$$P_{Loss} = Power\ loss\ due\ to\ the\ parasitic\ elements + Switching\ losses + Inductor\ core\ losses$$

Therefore, the efficiency of the converter is,

$$\%Efficiency = \frac{P_{out}}{P_{out} + P_{Loss}} \times 100$$

The converter offers great efficiency and accuracy at specified inputs and duty cycles.

IV. CASE STUDIES

As indicated in Table 1, the MIC has six operating modes in addition to three distinct methods for controlling the input and output powers and voltages. the duty ratio of switch S4 is D4 and similarly, the duty cycle of switches S_1, S_2 and S_3 are D_1, D2 and D_3 respectively

Table 1: Possible operating situations of the power converter.

Cases	Fuel cell (V_1)	Solar panel (V_2)	Action	O/P Voltage (V_0)
1	1	0	Considering Fuel cell	$\frac{V_1 D_4}{1 - D_4}$; $D_1 = 1$
2	0	1	Considering PV cell	$\frac{V_2 D_4}{1 - D_4}$; $D_2 = 1$
3	1	1	Considering Fuel cell and PV cell together.	$\frac{(V_1 + V_2) D_4}{1 - D_4}$ $D_3 = 1$

Source: Authors, (2025).

IV.1 FUEL CELL ALONE

Table 1 illustrates that in case 1, the fuel cell alone can provide the necessary power to the load using the suggested converter. The vehicle will be able to run in the lack of sunshine under this hypothetical operating situation.

IV.2 SOLAR PV CELL ALONE

Table 1 illustrates that in case 2, the proposed converter can provide the necessary power to the load using only a solar PV cell. In this hypothetical situation, the vehicle will be able to run solely on sunshine. The vehicle will use less hydrogen as a result of this process, resulting in nearly zero operating costs.

IV.3 BOTH FUEL CELL AND SOLAR PV CELL

Table 1 illustrates how the proposed converter can use a fuel cell and a PV cell to help the load receive the necessary electricity. Under this hypothetical set of conditions, the vehicle will be able to run on hydrogen and sunlight. In this case, the converter will come in when the solar PV panel isn't able to give the load the necessary amount of electricity on its own. This process will assist the vehicle in using less hydrogen, which will lower the vehicle's operating costs.

IV. RESULTS AND DISCUSSIONS

This article presents the mathematical modelling of a Cuk-based multi-input converter and analyses its steady-state behaviour. The performance of the proposed converter is validated through an experimental setup.

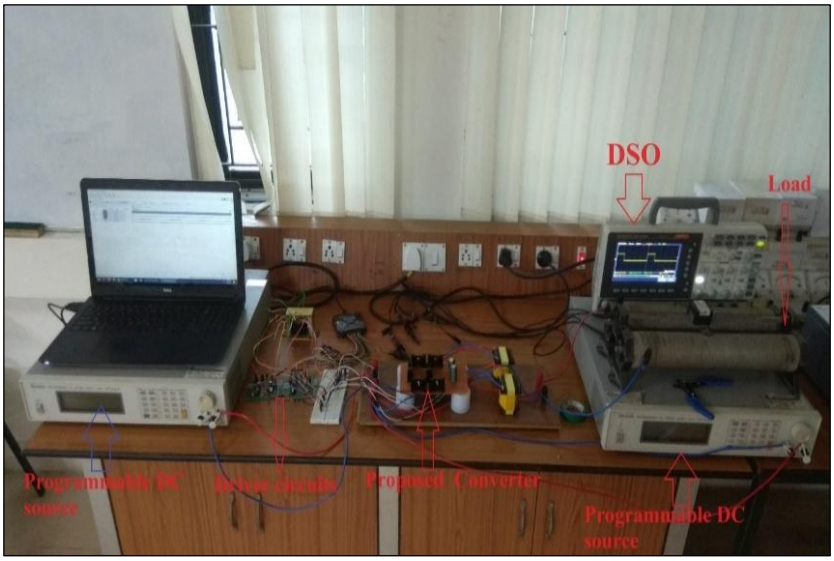

Figure 4: Experimental setup of CUK based novel multi-input converter.
Source: Authors, (2025).

Table 2: Experimental setup of CUK converter parameters.

Parameter	Value
I/P Voltages	$V_1 = 20V$, $V_2 = 12V$
O/P Voltage	$V_0 = 48V$
O/P Power	$P_0 = 250W$
Switching Frequency	10 KHz
Duty Cycle $D_1 = D_2 = D_3$	0.33
Duty Cycle D_4	0.72
Inductors	$L_1 = 24mH, L_2 = 50mH$
Capacitors	$C_1 = 750\mu F$, $C_2 = 750\mu F$
MOSFETs (4)	FQA38N30
Diode	MUR1560
Load	R = 10Ω

Source: Authors, (2025).

The switching frequency is $f_s = 10kHz$. The PV cell voltage is $V_2 = 12V$ and the fuel cell voltage is $V_1 = 20V$ respectively. The suggested converter was anticipated to generate 48V in order to supply 250W at the output terminal. The suggested converter's experimental setup is depicted in Figure. 4, and Table 2 lists the parts and setup parameters that were chosen. Experimentally gerenated switching pulses of the four MOSFET switches V_{GS1}, V_{GS2}, V_{GS3} and V_{GS4} are shown in Figure. 5(a). The switching frequencies of S_1, S_2 and S_3, S_4 are almost identical, which is equal to 10KHz.The proto type model waveforms of inductor currents I_{L1} and I_{L2} and capacitor voltages V_{C1}, V_{C2} are shown in Figure. 5(b). The dc root mean square values of I_{L1}, I_{L2} and V_0 are 18.19 A, 6.38 A and 56.32 V, 47.74 V respectively.

The voltage across the swithes are V_{GS1}, V_{GS2}, V_{GS3} and V_{GS4} are shown in Figure. 5(c). The voltage stress values of S_1, S_2 and S_3, are almost less than or equal to the highest input voltage and stress on voltage value of S_4 is lower than the 2 times of V_0. The input voltages V_1 , V_2 and output voltage and current V_0, I_0 waveforms are shown in Figure. 5(d). The values of input voltages V_1, V_2 and output voltage V_0 and output current I_0 are 20 V, 12V and 47.74 V, 6.36A respectively. The proposed converter delivers power to the load at a high efficiency of 96.4%, compare to other converters are mentioned in table.3

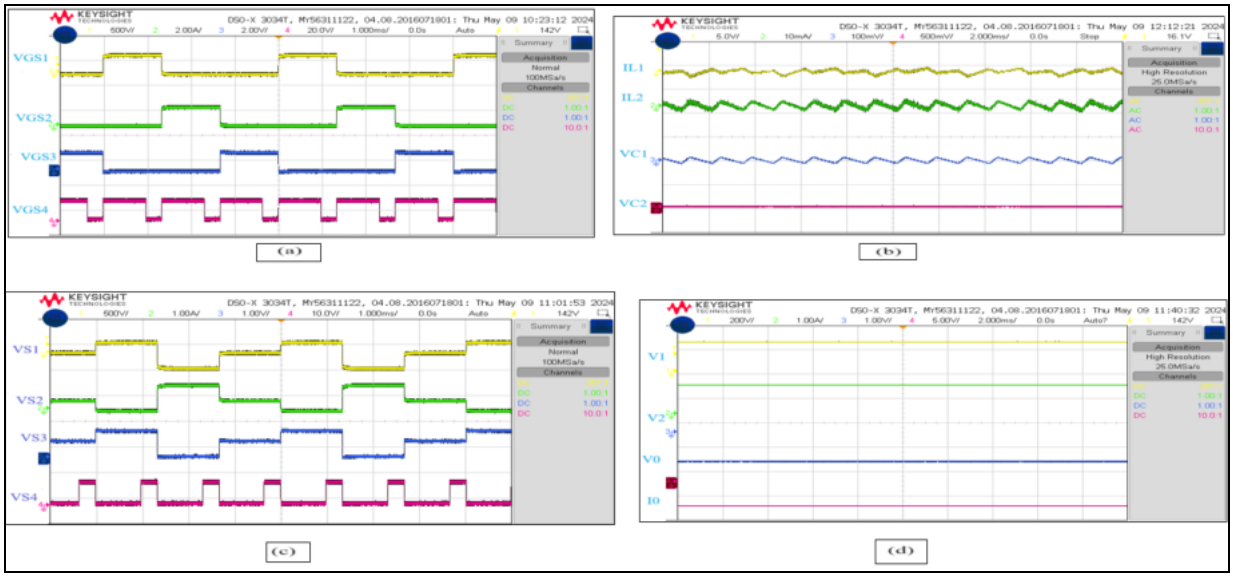

Figure 5: The proto type model experimental waveforms. (a) Pulses of S_1, S_2 and S_3 and S_4. (b) Inductor currents and Capacitor voltages. (c) voltage stress of S_1, S_2 and S_3, S_4 switches. (d) Input and output voltages and output current.
Source: Authors, (2025).

Table 2: Comparing the proposed converter against existing converters topologies.

Topology	[15]	[16]	[17]	[18]	[19]	[20]	[21]	[22]	[23]	Proposed
Gain	A_{11}	A_{12}	A_{13}	A_{14}	A_{15}	A_{16}	A_{17}	A_{17}	A_{18}	A_{19}
Number of sources	2	2	2	2	3	2	2	2	2	2
Number of uni-directional switches	0	4	0	2	4	6	4	3	4	4
Number of capacitors	2	1	1	1	1	4	4	3	4	2
Number of inductors	2	1	1	1	1	4	4	3	4	2
Numbers of Bi-directional power switches	3	0	3	2	2	2	0	0	1	0
No. of diodes	5	3	1	0	2	2	4	3	1	1
No. of relays	0	4	3	0	0	0	0	0	0	0
Stress on Voltage	High	-	-	High	Low	High	Moderate	Moderate	Moderate	Low
% Efficiency	93.50	94	93	94	88-94	91	95	94	95	96.4

Source: Authors, (2025).

$$A_{11} = V_0 = \frac{(d_1+d_2)V_1+d_2V_2}{1-d_1-d_2} \qquad A_{12} = V_0 = \frac{d_1V_1+d_2(V_1+V_2)+d_3V_2}{1-d_1-d_2-d_3}$$

$$A_{13} = V_0 = \frac{d_1V_1+(1-d_1)V_2}{1-d_2} \qquad A_{14} = V_0 = -\frac{d_1V_1+d_2V_2+d_3(V_1+V_2)}{1-d_1-d_2-d_3}$$

$$A_{15} = V_0 = \frac{d_1V_{battery}+(1-d_1)V_1+(1-d_2)V_2}{1-d_3} \qquad A_{17} = V_0 = \frac{(2-d_1)V_1+V_2}{(1-d_1)^2}$$

$$A_{18} = V_0 = \frac{(\,d_1 - 2d_2 + d_1d_2}{(1-d_1)^2(d_1-d_2)}\,V_1 + \frac{d_2(1-d_1)}{d_1(d_1-d_2)}V_2 A_{19} = V_0 = -\frac{d_1+d_3+d_5}{1-d_1-d_3-d_5}\big(V_1(1-d_3-d_4)+V_2(1-d_1-d_2)\big)$$

V. CONCLUSIONS

The modelling of the inimitable MIC with high voltage gain for hybrid electric vehicles (HEVs) drives has been clearly demonstrated and verified by this work. With this design, the load might receive energy continuously from two inputs. Furthermore, the idea of using various switching frequencies has been implemented well, resulting in substantial control over power flow and terminal voltage. The steady-state modelling of the proposed converter are established in order to achieve accurate modelling with improved inspection of the converter.. The literature compares the efficiency of the proposed power converter with existing power converters that are currently on the market. At the intended load, the suggested converter shows 96.4% efficiency, and there is also less stress on the semiconductor switches. Gains and efficiency are outstanding, and losses are negligible. Especially this converter is suitable for EV application.

VI. AUTHOR'S CONTRIBUTION

Conceptualization: Author One, Author Two.
Methodology: Author One and Author Two.
Investigation: Author One and Author Two.
Discussion of results: Author One, Author Two.
Writing – Original Draft: Author One.
Writing – Review and Editing: Author One and Author Two.
Resources: Author one.
Supervision: Author Two.
Approval of the final text: Author One, Author Two.

VII. REFERENCES

[1] M. Adnan, D. Ibrahim, Hydrogen as a renewable and sustainable solution in reducing global fossil fuel consumption, International Journal of Hydrogen Energy 33(16) (2008) 4209-4222. https://doi.org/10.1016/j.ijhydene.2008.05.024.

[2] The National Academy of Science Engineering Medicine, Our energy resources - fossil fuels, The National Academy of Science Engineering Medicine. http://needtoknow.nas.edu/energy/energy-sources/fossil-fuels/, 2021 (accessed 2 November 2021).

[3] R. Robert, Fossil fuels still supply 84 percent of world energy - and other eye openers from BP's annual review. Forbes. https://www.forbes.com/sites/rrapier/2020/06/20/bp-review-new-highs-in-global-energy-consumption-and-carbon-emissions-in-2019/?sh=66d08ad166a1, 2019 (accessed 20 July 2021).

[4] R. Hannah, R. Max, Energy production and consumption, Our World in Data. https://ourworldindata.org/energy-production-consumption, 2021 (accessed 8 November 2021).

[5] U.S Energy Information Administration, Energy and the environment - where greenhouse gases come from. https://www.eia.gov/energyexplained/energy-and-the-environment/where-greenhouse-gases-come-from.php, 2021 (accessed 21 October 2021).

[6] B. Eisavi, F. Ranjbar, H. Nami, A. Chitsaz, Low-carbon biomass-fueled integrated system for power, methane and methanol production, Energy Conversion and Management 253 (2022) 115163-115185. https://doi.org/10.1016/j.enconman.2021.115163.

[7] Y. Budak, Y. Devrim, Comparative study of PV/PEM fuel cell hybrid energy system based on methanol and water electrolysis, Energy Conversion and Management 179 (2019) 46-57. https://doi.org/10.1016/j.enconman.2018.10.053.

[8] A.M. Amr, A.I.M. Yasser, Extracting and defining flexibility of residential electrical vehicle charging loads, IEEE Transactions on Industrial Informatics 14(2) (2018) 448-461. https://doi.org/10.1109/TII.2017.2724559.

[9] S. Bairabathina, S. Balamurugan, Review on non-isolated multi-input step-up converters for grid-independent hybrid electric vehicles, International Journal of Hydrogen Energy 45(41) (2020) 21687-21713. https://doi.org/10.1016/j.ijhydene.2020.05.277.

[10] C.E. Thomas, Fuel cell and battery electric vehicles compared, International Association for Hydrogen Energy 34(15) (2009) 6005-6020. https://doi.org/10.1016/j.ijhydene.2009.06.003.

[11] G. Nicoletti, N. Arcuri, G. Nicoletti, R. Bruno R. A technical and environmental comparison between hydrogen and some fossil fuels, Energy Conversion and Management 89 (2015) 205-213. https://doi.org/10.1016/j.enconman.2014.09.057.

[12] T. Capurso, M. Stefanizzi, M. Torresi, S. M. Camporeale, Perspective of the role of hydrogen in the 21st century energy transition, Energy Conversion and Management 251 (2022) 114898-114914. https://doi.org/10.1016/j.enconman.2021.114898.

[13] International Energy Agency, The future of hydrogen, International Energy Agency. https://www.iea.org/reports/the-future-of-hydrogen, 2019 (accessed 05 May 2020).

[14] Alternative Fuels Data Center, Hydrogen production and distribution, U.S Department of Energy. https://afdc.energy.gov/fuels/hydrogen_production.html, 2021 (accessed 24 June 2021).

[15] K. H. Saeideh, T. Sajjad, R.F. Mohammad, S. Mehran, Design and analysis of a novel SEPIC-based multi-input DC/DC converter, IET Power Electronics 10(12) (2017) 1393-1402. https://doi.org/10.1049/iet-pel.2016.0654.

[16] S. Kumaravel, G.G. Kumar, V. Kuruva, V. Karthikeyan, Novel non-isolated modified interleaved DC-DC converter to integrate ultracapacitor and battery sources for electric vehicle application, 20th National Power Systems Conference (NPSC) (2018). https://doi.org/10.1109/NPSC.2018.8771810.

[17] G. K. Gangavarapu, S. Kumaravel, A. Sivaprasad, K. Venkitusamy, Dual input superboost DC–DC converter for solar powered electric vehicle, IET Power Electronics 12(9) (2019) 2276-2284. https://doi.org/10.1049/iet-pel.2018.5255.

[18] A. Sivaprasad, G.K. Gangavarapu, S. Kumaravel, S. Ashok, A non-isolated bridge-type DC–DC converter for hybrid energy source integration, IEEE Transactions on Industry Applications 55(4) (2019) 4033-4043. https://doi.org/10.1109/TIA.2019.2914624.

[19] K. Varesi, S. H. Hosseini, M. Sabahi, E. Babaei, Performance analysis and calculation of critical inductance and output voltage ripple of a simple non-isolated multi-input bidirectional DC-DC converter, International Journal of Circuit Theory and Applications 46(3) (2018) 543-564. https://doi.org/10.1002/cta.2392.

[20] K. Varesi, S. H. Hosseini, M. Sabahi, E. Babaei, S. Saeidabadi, N. Vosoughi, Design and analysis of a developed multiport high step-up DC–DC converter with reduced device count and normalized peak inverse voltage on the switches/diodes, IEEE Transactions on Power Electronics 34(6) (2018) 5464-5475. https://doi.org/10.1109/TPEL.2018.2866492.

[21] K. Varesi, S. H. Hosseini, M. Sabahi, E. Babaei, Modular non isolated multi-input high step-up DC–DC converter with reduced normalized voltage stress and component count, IET Power Electronics 11(6) (2018) 1092-1100. https://doi.org/10.1049/iet-pel.2017.0483.

[22] K. Varesi, S. H. Hosseini, M. Sabahi, E. Babaei, A high-voltage gain nonisolated noncoupled inductor based multi-input DC-DC topology with reduced number of components for renewable energy systems, International Journal of Circuit Theory and Applications 46(3) (2018) 505-518. https://doi.org/10.1002/cta.2428.

[23] Gaurav, N. Jayaram, S. Halder, K. P. Panda and S. V. K. Pulavarthi, "A Novel Design With Condensed Component of Multi-Input High Gain Nonisolated DC–DC Converter for Performance Enhancement in Carbon Neutral Energy Application," in IEEE Journal of Emerging and Selected Topics in Industrial Electronics, vol. 4, no. 1, pp. 37-49, Jan. 2023, doi: 10.1109/JESTIE.2022.3211779.

Journal of Engineering and Technology for Industrial Applications

ISSN ONLINE: 2447-0228

ITEGAM-JETIA

Manaus, v.11 n.54, p. 145-151. July/August., 2025.
DOI: https://doi.org/10.5935/jetia. v11i54.2338

RESEARCH ARTICLE OPEN ACCESS

COMPUTATIONAL THERMAL ANALYSIS OF FeCrV15+TiB_2 COATINGS ON EN48 BASEPLATE BY USING THE COMSOL MULTIPHYSICS

Basiru Philip Aramide [1], Tamba Jamiru [2], Taoreed Adesola Adegbola [3], Abimbola Patricia Idowu Popoola [4], Mathew Olurotimi Adeoti [5], Rotimi Sadiku [6] and Sisa Pityana [7]

[1, 2. 3, 5] Department of Mechanical and Mechatronics Engineering, Tshwane University of Technology, Pretoria South Africa

[4, 6] Department of Chemical, Metallurgical & Material Engineering, Tshwane University Technology, Pretoria, South Africa

[7] National Laser Centre, Council for Scientific and Industrial Research, Pretoria

[1] http://orcid.org/0000-0002-6488-1287, [2]http://orcid.org/0000-0002-9492-1921, [3]http://orcid.org/0000-0002-6881-7215, [4]http://orcid.org/0000-0003-4447-8551, [5]http://orcid.org/0009-0006-9308-0936, [6]http://orcid.org/0000-0002-8504-1041, [7]http://orcid.org/0000-0002-9273-2043,

Email: abashiruphilip@gmail.com, JamiruT@tut.ac.za, AdesolaAT@tut.ac.za, PopoolaAPI@tut.ac.za, AdeotiMO@tut.ac.za, SadikuR@tut.ac.za, SPityana@csir.co.za.

ARTICLE INFO

Article History
Received: July 9, 2025
Revised: July 13, 2025
Accepted: June 15, 2025
Published: July 31, 2025

Keywords:
Laser cladding,
Laser irradiation,
Additive Manufacturing,
3D simulation,
Modelling.

ABSTRACT

This study seeks to elucidate the thermal effects of including TiB2 powder on the geometric evolution of FeCrV15 coating using a 3D simulation of the laser cladding process. The process entails applying a coating of FeCrV15 powder onto the EN48 substrate and incorporating TiB2 powder into the coating to evaluate the feasibility of IPG laser-applied coating layers. In order to modify the laser cladding process, the conservation equations of energy, momentum, and mass are linked via the temperature variable and resolved. Intricate hypotheses are employed in mathematical modeling to address the boundary conditions arising from the laser melting of several materials, thereby simplifying issues associated with varying material properties. Moving mesh is employed to ascertain the deformation of a free surface by utilizing the Arbitrary Lagrangian and Eulerian (ALE) methodology. The simulation disregards thermo-capillary forces and their influence on fluid dynamics within the liquefied pool to achieve process optimization. The developed procedure simulation also assesses the thermal dispersion associated with the procedure. The results provide approximate information regarding the influence of TiB2 on the development of clad geometry and the thermal gradient.

Copyright ©2025 by authors and Galileo Institute of Technology and Education of the Amazon (ITEGAM). This work is licensed under the Creative Commons Attribution International License (CC BY 4.0).

I. INTRODUCTION

The laser cladding process stands out as a promising additive manufacturing (AM) technique for depositing thick layers onto both similar and dissimilar coatings, particularly those of considerable thickness. The advancement of laser-based systems for powder deposition onto substrates has garnered significant attention across various industrial applications, particularly in thick cladding, coatings, and repair processes [1], [2]. Metal additive manufacturing holds significant promise across various industries because of its capacity to fabricate intricate shapes that conventional methods cannot achieve. This capability not only enhances performance but also contributes to cost reduction and accelerates development timelines. Industries such as aerospace and medical, where the demand for customized and intricate parts is prevalent, find metal additive manufacturing particularly beneficial. Moreover, this technology proves to be practical for high-mix low-volume production scenarios, which are frequently encountered in these sectors [2-5]. However, optimising this process poses several critical challenges, including achieving the desired properties for the final cladding layer such as uniform thickness, strong bonding, and minimizing dissolution and deformations [6], [7]. The experimental setup presents several constraints owing to intricate technical hurdles. Factors such as laser power selection, laser beam spot size, laser travel speed, shield gas flow, powder feed rate, and surface preparations significantly impact the end product's quality in the manufacturing process [8], [9].

Laser cladding made its debut in the early 1980s, quickly becoming a staple in industrial coating and repair processes. Over time, it evolved into a method for additive manufacturing of entire 3D parts. Today, its applications continue to expand, encompassing various industries, including additive manufacturing. As this field progresses, simulation becomes increasingly vital, offering valuable predictive capabilities to further advance laser cladding technologies [10], [11]. Numerous publications in the literature explore numerical simulations of the laser cladding process, unveiling a multitude of effective methodologies. However, according to Wirth and Wegener [11], upon examination of selected exemplary publications, it becomes evident that each model exhibits certain limitations. These shortcomings typically revolve around issues such as the treatment of free surfaces, the accuracy of heat source modelling, and the incorporation of subprocess models like powder jet models. However, the extent of these shortcomings has not been quantified. Wirth and Wegener [11] introduced a comprehensive, physics-driven integrated model. They aimed to amalgamate the most effective methodologies from existing literature to enhance predictive capabilities and enable simulation-based insights for deeper process comprehension. They sought to assess the ramifications and boundaries of model simplification, which can be nontrivial. This integrated model spans from simulating powder particle flow, through melt pool dynamics, to structural and material simulations, hence earning the designation of "integrated".

The powder particle flow simulation and the melt pool region model was previously documented Wirth et al. and Wirth and Wegener respectively [11], [12]. Pinkerton [13] underscores in his review paper on laser cladding modeling the promising prospect for notably enhanced models, particularly through the integration of sub-process models. Moreover, Manvatkar et al. [14] assert the absence of a computationally efficient 3D laser cladding process model encompassing heat transfer, powder addition, build geometry, and thermal cycles in multilayer laser additive manufacturing processes. In this text, the thermal impact of introducing TiB_2 powder into *FeCrV15* coating model is outlined. The properties of *FeCrV15* alloy are presented in **Table 1**.

Table 1: Properties of *FeCrV15* alloy powder.

Property	Value
Coefficient of thermal expansion	3.79e-6[1/K]
Heat capacity at constant pressure	483.88 [J/(kg*K)]
Density	7204.14[kg/m^3]
Thermal conductivity	76.718[W/(m*K)]
Young's modulus	201e9[Pa]
Poisson's ratio	0.29

Source: Authors, (2025).

II. MATHEMATICAL FRAMEWORK

The procedures encompassed with laser cladding, like liquifying and solidifying cycles, are comparable to welding phenomena, where as a consequence, modelling the laser beam heating and mass addition proves difficult. The boundary conditions must be appropriately dispersed by having the material properties and the procedure parameters in mind during the heating process. The attained set of model equations, combined with the temperature variable have undergone mathematical treatment, and they have been resolved through the COMSOL multi-physics software. For reference, see **Figure 1** for a representation of the laser cladding process phenomenon and laser beam interaction characteristics. Through the use of Arbitrary Lagrangian and Eulerian (ALE) equations, deformed geometry is brought about by continual heating and mass addition [15].

II.1 POSTULATIONS

- The powder grains are assumed to be sphere-like objects with a radius r_p.
- The thickness of the liquified pool is assumed to be equivalent to the thickness of the laser beam, and the shape of the liquid pool is assumed to have an oval-shaped cross-section.
- During the model's formulation, the material loss caused by evaporation is not taken into account.
- Throughout the process, the energy stored by the powder grains and the steel substrate material stays uniform and unchanging.
- Due to the short duration of the powder particles' interaction with the laser, there is no loss of heat by either radiation or convection by the powder grains.
- Less than 2% of the energy received by the substrate is made up of the energy admitted by the powder grains.
- Since liquid metal and air have such a large viscosity and density difference, we may decrease zone calculation without taking the air into account.
- The Newtonian fluid that makes up the liquid metal is considered incompressible, and Laminar flow is assumed to be present in the molten pool [15].

II.2 ZONES' GOVERNING EQUATIONS

At first, the issue is formulated by assuming that the laser beam heat flux covers the steel plate region's laser beam interaction surface (Gaussian). In Zone A, the predominant phenomenon is the heat conduction process (as shown in **Figure 1**). The residual *FeCrV15* powder that was laser-melted and a small area of the *EN48* steel melt pool is also depicted in Zone B. Mass and momentum conservation have now replaced the energy conservation phenomenon [15].

II.2.1 Energy Conservation

$$\rho C_\rho \frac{\partial T}{\partial t} + \rho C_\rho \boldsymbol{u} \cdot \nabla T + \nabla \cdot \boldsymbol{q} = Q + Qted \tag{1}$$

$$\boldsymbol{q} = -k\nabla T \tag{2}$$

ρ is the density, C_ρ is specific heat capacity, T is temperature, k is thermal conductivity
$Q + Q_{ted}$ is power generation per unit volume of the substrate Q_v.

The momentum and mass conservation equations were used to determine the velocity field u in the equation above.

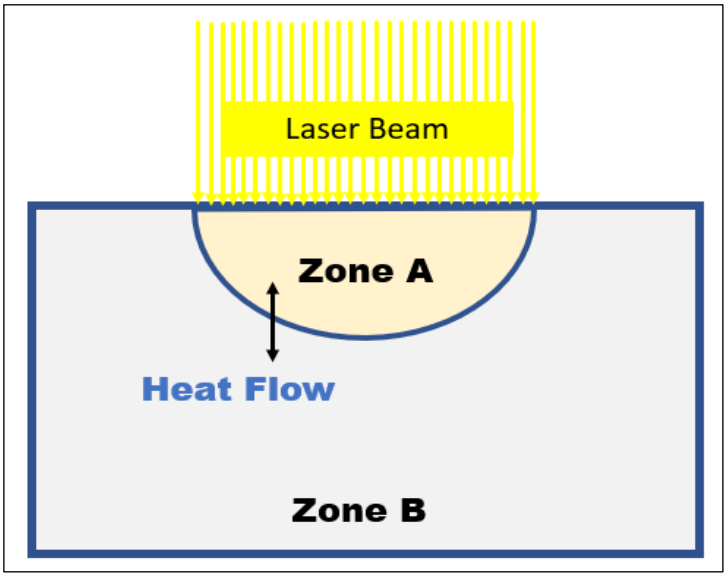

Figure 1: Process phenomena in Physics.
Source: Authors, (2025).

II.2.2 Conservation of Momentum

One of the key controlling laws in the laser cladding process is the conservation of momentum. The representation of the momentum equation is

$$\rho_0 \left[\frac{\partial u}{\partial T} + u(\nabla u)\right] = \nabla[-pI + \mu(\nabla u + (\nabla u)^T] + F_b + F_G \quad (3)$$

Where ρ_0 is the density at $T = T_m$, F_b is Buoyancy Force, F_G is Darcy Force.

II.2.3 Mass Conservation

The continuity equation is depicted as follows:

$$\nabla u = 0 \quad (4)$$

As the specific heat capacity rises, the impact of latent heat of fusion on the temperature distribution can be roughly estimated, thus:

$$C_p = C_p + \Delta H_m \frac{\partial L_f}{\partial T} \quad (5)$$

ΔH_m is the latent heat of fusion, L_f is liquid fraction

The following equation incorporates buoyancy force into the momentum equation:

$$F_b = \rho_0[1 - \beta(T - T_o)]g \quad (6)$$

β is thermal expansion co-efficient, g is gravity field

The Darcy's governing equation for the momentum equation, is given by

$$F_G = \frac{-180\mu}{d^2}\frac{(1-L_f)^2}{({L_f}^3+\tau)}u \quad (7)$$

τ is a numerical constant, d is powder diameter, μ is viscusity

Liquid fraction L_f can be expressed as follows:

$$L_f = \begin{cases} 0 & T_s \leq T \\ \frac{T-T_s}{T_L-T_s} & T_s < T < T_L \\ 1 & T > T_L \end{cases} \quad (8)$$

II.3 BOUNDARY CONDITIONS

A number of challenging boundary criteria must be met for the laser cladding simulation procedure. However, the following list of the necessary boundary conditions is provided:

- By using a surface heat source and heat flux determined by the boundary condition, on the impact of the laser beam and the flux of powder, may be simulated.

$$q_{in} = \propto_0 \cos(\theta) I_0 - h_c(T - T_o) - \varepsilon_t \sigma\left(T^4 - {T_o}^4\right) \text{(For Zone A)} \quad (9)$$

$$q_{in} = -h_c(T - T_o) - \varepsilon_t \sigma\left(T^4 - {T_o}^4\right) \text{ (For Zone B)} \quad (10)$$

h_c is heat convection coefficient, $\propto_0$ is absorption factor, ε_t is emissivity, σ is Stefan-Boltzmann constant.

- For energy distribution, a continuous laser beam of uniform intensity is taken into consideration. The following formula was used to calculate the laser beam's intensity.

$$I_0 = Laser\ intensity = \begin{matrix} \frac{\propto_0 \cos\theta P_l}{\pi r^2} & r \le r_l \\ 0 & r > r_l \end{matrix} \quad (11)$$

P_l is laser average power, r_l is beam radius

II.3.1 Boundary Conditions for Fluid Flow

The thermocapillary and melt pool capillary forces act in the normal and tangential directions on the free surface. The appropriate force equations are shown below:

$$\sigma_n = -p_\propto \vec{n} Y(T) \kappa \vec{n} \text{ (For Zone A)} \quad (12)$$

$$\sigma_t = \frac{\partial Y}{\partial T} \nabla T \vec{t} \text{ (For Zone A)} \quad (13)$$

$$u = 0 \text{ (For Zone B)} \quad (14)$$

$p_\propto$ is ambient pressure, $\vec{n}$ is normal vector of the free surface, κ is curvature, $\vec{t}$ is tangential vector to the free surface, Y is surface tension

II.3.2 Moving Mesh

A liquid/solid boundary and a liquid/gas boundary are moving interfaces in the finite element model. An ALE approach is used to track overtly, only the liquid/gas contact. In this method, zone nodes obey a nearly Eulerian account, while border nodes are governed by fluid mechanics processes and insured by a Lagrangian account (see **Figure 2**). However, internal nodes are shifted to prevent numerical instability when computing. Winslow and Laplace are two smoothing techniques that COMSOL Multi-Physics suggests to regulate the node displacement. The Winslow method is used to make the computations provided, an expression is used to connect the ALE method with the conservation and momentum equations [15].

$$V_{mesh}\vec{n} = V_{mat}\vec{n} \text{ (For Zone A)} \quad (15)$$

$$V\vec{n} = 0 \text{ (For Zone B)} \quad (16)$$

V_{mesh} is the mesh speed (m/s), and V_{mat} stands for the calculated material velocity (m/s) using momentum conservation equations.

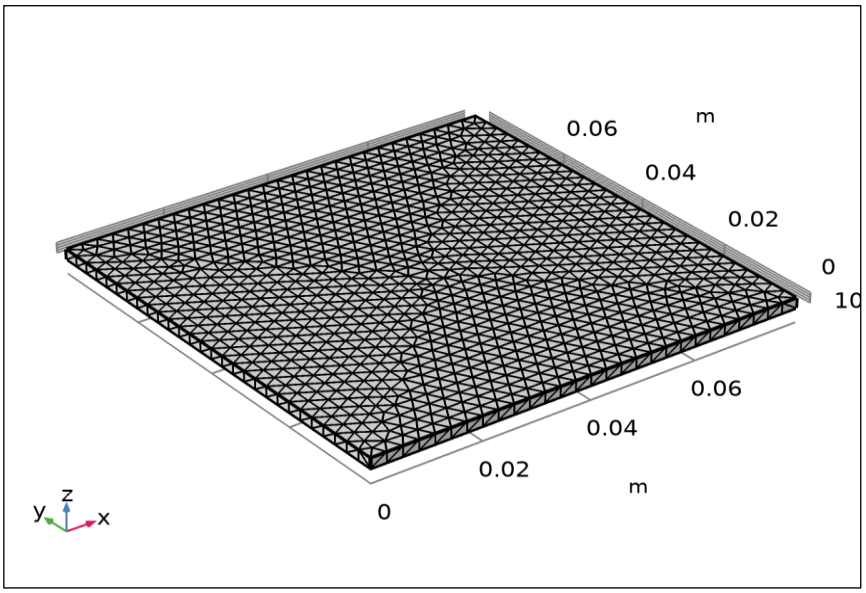

Figure 2: The Moving Mesh.
Source: Authors, (2025).

III. MATERIALS AND METHODS

To analyse the impact of introducing TiB_2 powder on the clad geometry, a computational model was built, centering on the positions of laser power entering and exiting from the heated pool. By including all mathematical equations in a 3D model, COMSOL Multi-Physics was employed to run a series of finite element modelling (FEM) simulations. This technique's first step is to define the process globally (global definition), taking advantage of all possibilities, such as input procedure parameters, variables, functions, and geometry subsequences, required in the problem definition. Three separate branches of physics—heat transfer, structural mechanics, and mathematics—are incorporated into the model for the laser cladding simulation technique. However, this section is limited to the report on how the introduction of TiB_2 powder affects the heat transfer, which invariably affects the clad geometry [15]. The initial rectangular cuboid created during model development has a steel substrate's length, breadth, and thickness (see **Figure 3**).

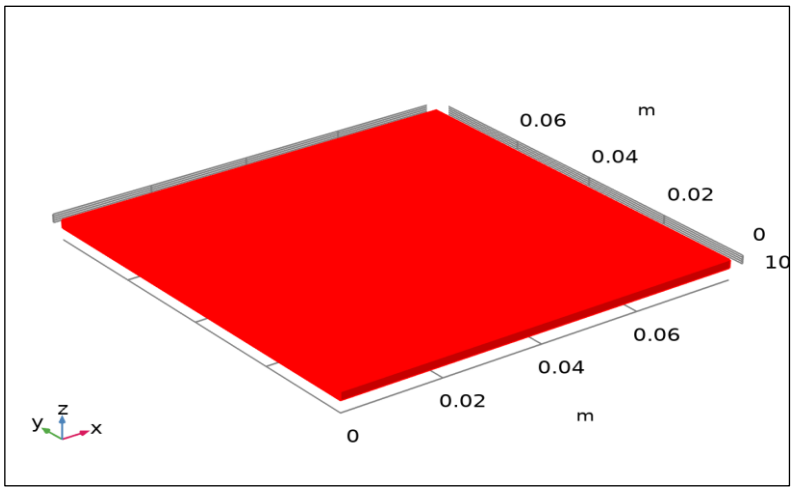

Figure 3: The rectangular cuboid steel substrate.
Source: Authors, (2025).

The ellipse is built individually to represent the clad geometry and makes the geometry whole by Boolean operations. The beam size variation changes the clad dimension because the elliptical size is connected to the laser beam diameters. Triangular elements are utilised in the meshing procedure for 3D modelling of the laser cladding process (see **Figure 2**). In COMSOL Multi-Physics, the Winslow approach is used to generate deformed meshes as a result of moving heat sources. The cladding process's linked thermomechanical analysis is predicated on the idea that the temperature field from the thermal exploration functions as the foundation for predictions of the clad's shape and dilution. In order to examine the influence of the TiB_2 introduction on the final geometry of the coatings, the input procedure parameters in the simulation models are based on experimental procedure prerequisites.

IV. RESULTS AND DISCUSSIONS

The results of the simulation and the experimental coatings are presented in **Figure 4**. The coatings of *FeCrV15* show smooth, perfectly, and metallurgically bounded deposits on EN48 steel substrate (see **Figures 4a** & **c**), whereas the coating became rough with cracks and pores upon introducing TiB_2 powder at the same laser parameters (see **Figures 4b** & **d**). An endothermic reaction was observed when TiB_2 was introduced during the experimentation. Both coatings' thermal stress distributions are represented in **Figure 5**. The thermal stress distribution of *FeCrV15*+TiB_2 coating is 477 K, far higher than *FeCrV15* coating, which is 366 K, which may be responsible for the observed pores and cracks in the *FeCrV15*+TiB_2 coating.

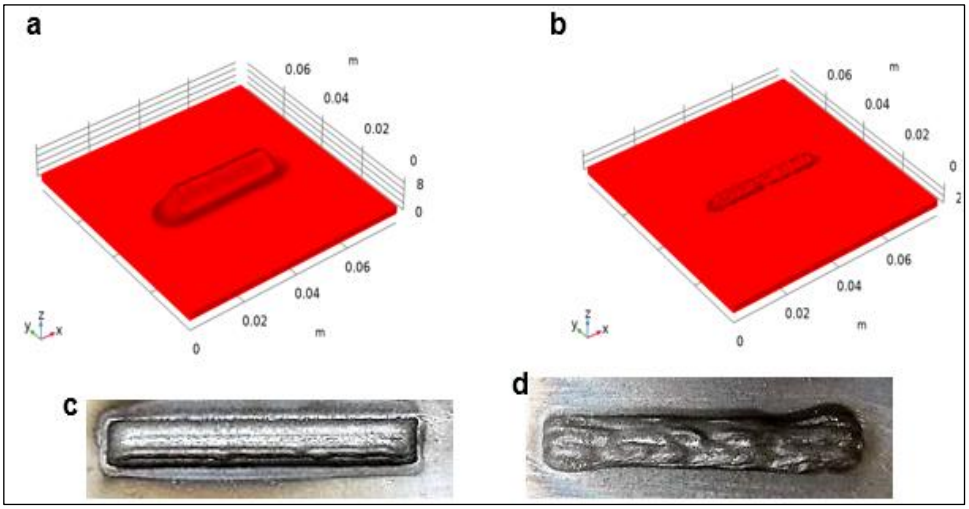

Figure 4: Modelled coated samples (a) & (c) *FeCrV15* coating and (b) & (d) *FeCrV15*+TiB_2 coating.
Source: Authors, (2025).

This implies that introducing *TiB₂* powder into *FeCrV15* coating resulted in increasing the thermal input, which increases the stress within the deposit, creating the cracks and pores as observed in **Figure 6.**

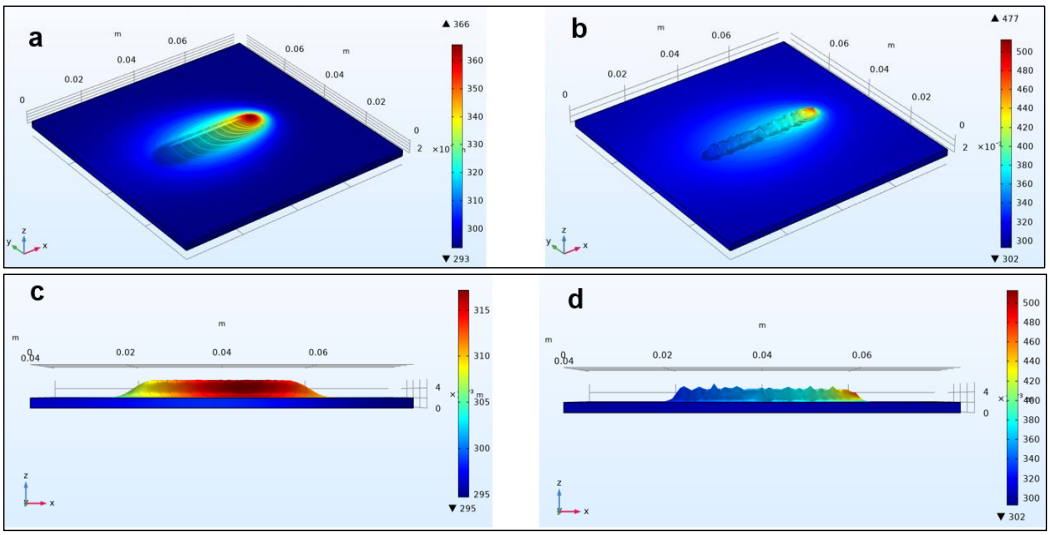

Figure 5: Thermal stress distribution of the deposited coatings (a) & (c) *FeCrV15* coating and (b) & (d) *FeCrV15+TiB₂* coating.
Source: Authors, (2025).

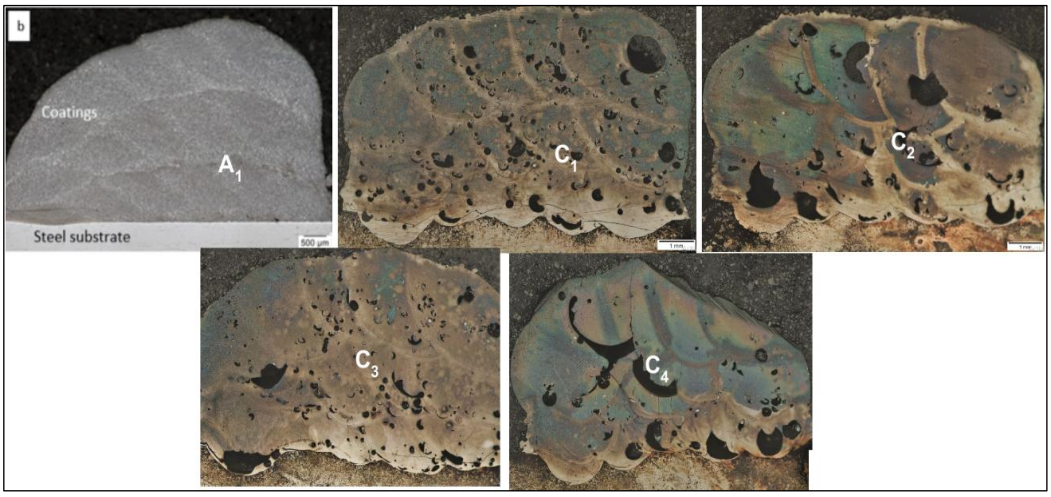

Figure 6: Optical microscope of *FeCrV15* (A_1) coating and *FeCrV15+TiB₂* (C_1, C_2, C_3, & C_4) coatings.
Source: [16]

V. CONCLUSIONS

In conclusion, this study delves into the thermal implications of incorporating TiB2 powder into FeCrV15 coating via 3D laser cladding simulation. By linking conservation equations of energy, momentum, and mass and utilizing complex mathematical modeling, the research sheds light on clad geometry development and thermal gradients. Although thermo-capillary forces are neglected, the simulation effectively evaluates process-related thermal distributions. Results demonstrate that introducing TiB2 alters clad geometry and thermal stress distribution, as evidenced by the roughness, cracks, and pores observed in coated samples. The significant increase in thermal stress in TiB2-modified coatings suggests heightened thermal input, contributing to defect formation. This research underscores the importance of simulation in enhancing understanding and optimization of laser cladding processes, offering valuable insights for industrial applications in aerospace, automotive, and tooling sectors.

VI. AUTHOR'S CONTRIBUTION

Conceptualization: Basiru Philip Aramide and Sisa Pityana..
Methodology: Basiru Philip Aramide and Sisa Pityana.
Investigation: Basiru Philip Aramide and Mathew O. Adeoti
Discussion of results: Basiru Philip Aramide, Taoreed Adesola Adegbolam and Tamba Jamiru.
Writing – Original Draft: Basiru Philip Aramide.
Writing – Review and Editing: Basiru Philip Aramide and Rotimi Sadiku.
Resources: Patricia Popoola, Rotimi Sadiku, Tamba Jamiru and Sisa Pityana
Supervision: Patricia Popoola, Rotimi Sadiku, Tamba Jamiru and Sisa Pityana
Approval of the final text: All authors

VII. ACKNOWLEDGMENTS

The authors acknowledge the financial support from Tshwane University of Technology (TUT), Pretoria, South Africa, without which this work would not have been possible.

VIII. REFERENCES

[1] J. Mazumder, D. Dutta, N. Kikuchi, and A. Ghosh, "Closed loop direct metal deposition: art to part," Optics and Lasers in Engineering, vol. 34, no. 4-6, pp. 397-414, 2000.

[2] Y. Kuroiwa, D. Kono, and Y. Oda, "INVESTIGATION ON THERMAL DEFORMATION IN LASER ADDITIVE MANUFACTURING," MM Science Journal, 2021.

[3] P. Bartolo et al., "Biomedical production of implants by additive electro-chemical and physical processes," CIRP annals, vol. 61, no. 2, pp. 635-655, 2012.

[4] M. K. Thompson et al., "Design for Additive Manufacturing: Trends, opportunities, considerations, and constraints," CIRP annals, vol. 65, no. 2, pp. 737-760, 2016.

[5] F. Klocke et al., "Turbomachinery component manufacture by application of electrochemical, electro-physical and photonic processes," CIRP annals, vol. 63, no. 2, pp. 703-726, 2014.

[6] E. Amara, L. Achab, and O. Boumia, "Numerical modelling of the laser cladding process using a dynamic mesh approach," in Proceedings of CAOL 2005. Second International Conference on Advanced Optoelectronics and Lasers, 2005., 2005, vol. 1: IEEE, pp. 142-145.

[7] J. Hofman, D. De Lange, B. Pathiraj, and J. Meijer, "FEM modeling and experimental verification for dilution control in laser cladding," Journal of Materials Processing Technology, vol. 211, no. 2, pp. 187-196, 2011.

[8] S. Tsirkas, P. Papanikos, and T. Kermanidis, "Numerical simulation of the laser welding process in butt-joint specimens," Journal of materials processing technology, vol. 134, no. 1, pp. 59-69, 2003.

[9] H.-y. Zhao, H.-t. Zhang, C.-h. Xu, and X.-Q. Yang, "Temperature and stress fields of multi-track laser cladding," Transactions of Nonferrous Metals Society of China, vol. 19, pp. s495-s501, 2009.

[10] A. Weisheit, A. Gasser, G. Backes, T. Jambor, N. Pirch, and K. Wissenbach, "Direct Laser Cladding, Current Status and Future Scope of Application," in Laser-Assisted Fabrication of Materials, J. D. Majumdar and I. Manna Eds. Berlin, Heidelberg: Springer Berlin Heidelberg, 2013, pp. 221-240.

[11] F. Wirth and K. Wegener, "A physical modeling and predictive simulation of the laser cladding process," Additive Manufacturing, vol. 22, pp. 307-319, 2018/08/01/ 2018, doi: https://doi.org/10.1016/j.addma.2018.05.017.

[12] F. Wirth, S. Freihse, D. Eisenbarth, and K. Wegener, "Interaction of powder jet and laser beam in blown powder laser deposition processes: measurement and simulation methods," in Lasers in Manufacturing Conference, Munich, Germany, 2017, pp. 1-10.

[13] A. J. Pinkerton, "Advances in the modeling of laser direct metal deposition," Journal of Laser Applications, vol. 27, no. S1, 2014, doi: 10.2351/1.4815992.

[14] V. Manvatkar, A. De, and T. DebRoy, "Spatial variation of melt pool geometry, peak temperature and solidification parameters during laser assisted additive manufacturing process," Materials Science and Technology (United Kingdom), Article vol. 31, no. 8, pp. 924-930, 2015, doi: 10.1179/1743284714Y.0000000701.

[15] R. Parekh, R. K. Buddu, and R. Patel, "Multiphysics simulation of laser cladding process to study the effect of process parameters on clad geometry," Procedia Technology, vol. 23, pp. 529-536, 2016.

[16] B. P. Aramide, T. Jamiru, T. A. Adegbola, A. P. I. Popoola, and E. R. Sadiku, "Influence of TiB2 Incorporation on Microstructural Evolution in Laser-Clad FeCrV15 + TiB2 Deposits," Journal of Materials Engineering and Performance, 2024/05/23 2024, doi: 10.1007/s11665-024-09618-w.

Journal of Engineering and Technology for Industrial Applications

ITEGAM-JETIA

Manaus, v.11 n.54, p. 152-159. July/August., 2025.
DOI: https://doi.org/10.5935/jetia. v11i54.1698

ISSN ONLINE: 2447-0228

RESEARCH ARTICLE OPEN ACCESS

RAPID PROTOTYPE PROCESS SELECTION USING MULTI ATTRIBUTE DECISION MAKING USING ADVANCED ENTROPY WEIGHT BASED FUZZY SINGLE VALUED NEUTROSOPHIC SET

Nital Pravinbhai Nirmal[1], Jignesh Girishbhai Parmar[2] and Mehul Gunvantrai Mehta[3]

[1] Shantilal Shah Engineering College (A State Govt. Institute), Affiliated with Gujarat Technological University, Ahmedabad.
[2,3] Shantilal Shah Engineering College (A State Govt. Institute), Bhavangar affiliated with Gujarat Technological University, Ahmedabad.

[1]https://orcid.org/0000-0002-8657-4253, [2]https://orcid.org/0000-0002-8533-8304, [3]https://orcid.org/0009-0002-2219-0848

Email: nital.nirmal@gmail.com, jigneshparmarssec@gmail.com, mehulgmehta@gmail.com

ARTICLE INFO

Article History
Received: March 11, 2025
Revised: April 20, 2025
Accepted: June 15, 2025
Published: August 31, 2025

Keywords:
Multi-attribute decision making (MADM)
Single-Valued Neutrosophic Sets (SVNS)
Rapid Prototype Process Selection,
Entropy Weighting,
Decision Support Systems.

ABSTRACT

This paper presents a novel methodology for Multi-Attribute Decision Making (MADM) based on Single-Valued Neutrosophic Sets (SVNS), a specialized extension of Neutrosophic sets that incorporates three distinct membership functions: truth, indeterminacy, and falsehood. The objective is to develop an advanced decision-making framework that improves rapid prototype process selection, particularly when handling imprecise, uncertain, and inconsistent information commonly encountered in real-world applications. The proposed method integrates the conversion of crisp and fuzzy data into SVNS and employs an advanced entropy weight-based approach to enhance the selection process. The effectiveness of the approach is demonstrated through case studies drawn from existing literature on rapid prototyping, showing that the new methodology yields more accurate results with reduced computational effort when compared to traditional MADM methods. The results validate the superiority of the proposed approach in addressing indeterminacies and uncertainties, offering more reliable and precise decision-making outcomes in complex environments.

Copyright ©2025 by authors and Galileo Institute of Technology and Education of the Amazon (ITEGAM). This work is licensed under the Creative Commons Attribution International License (CC BY 4.0).

I. INTRODUCTION

In the context of globalization, significant advancements are being made in the manufacturing sector to optimize product development and minimize lead times. One of the most prominent technologies driving this evolution is Rapid Prototyping (RP), a method that enables the creation of physical models through layer-by-layer deposition, guided by Computer-Aided Design (CAD) data, without the need for traditional cutting tools. Researchers are actively working to optimize various aspects of the RP process, including material selection, path planning, and process efficiency, using advanced mathematical modeling techniques. Typically, the RP process can be divided into three key stages: the first stage involves the "sub-active" phase, where initial material preparation takes place; the second stage is "additive," where material is added to the workpiece layer by layer; and the third stage is "virtual," involving the digital validation and optimization of the prototype.

Rapid prototyping has proven instrumental in reducing costs and accelerating product development cycles, making it a valuable tool across industries such as aerospace, automotive, and consumer goods. The commercialization of new RP techniques continues to expand its application globally, offering manufacturers a competitive edge in design and production. Rapid prototype technique is the production of physical model from computer aided design (CAD) data layer by layer deposition without using cutting tool and the rapid prototype has been established to reduce cost and product development [1].

II. EXISTING LITERATURE ON RAPID PROTOTYPE PROCESS RANKING USING MULTI-ATTRIBUTE DECISION MAKING (MADM)

II.1 ANALYTICAL HIERARCHY PROCESS (AHP)

The method developed by [2] employs a normalization approach that treats both beneficial and non-beneficial criteria in the same manner. It utilizes the Euclidean distance principle for decision-making, but one of its limitations is that it does not account for the potential correlation between attributes. Additionally, this method requires expert or research-based input to determine the weights for each attribute, which can lead to variations in the rankings, particularly if the weightings assigned to the attributes differ. Table 1 illustrates the application of the Analytical Hierarchy Process (AHP) methodology across various manufacturing and supply chain functions, including its use in selecting rapid prototyping layered manufacturing processes [3]. This highlights the widespread adoption of AHP in optimizing decisions where multiple criteria must be balanced, despite its limitations in handling attribute correlations and weight assignment variations.

II.2 VISEKRITERIJUSKA OPTIMIZACIJAI KOMOROMISNO RESENJE (VIKOR)

The VlseKriterijuska Optimizacija I Komoromisno Resenje (VIKOR) method, investigated by [4], focuses on a weight strategy for calculating rankings, where the values are constrained within the range of [0, 1]. However, this weight strategy can lead to different ranking outcomes even when the attribute weights remain the same. As an outranking method, VIKOR lacks a self-evident foundation, which limits its interpretability in certain decision-making contexts. In this regard, [5] introduced the Fuzzy VIKOR (F-VIKOR) approach for robot selection, which incorporates fuzzy logic to handle uncertainty in the decision-making process. Furthermore, [6] applied various decision-making methods to select rapid prototyping technologies, while [7] utilized the Fuzzy VIKOR methodology to optimize the selection of rapid prototyping technologies in an agile environment. These studies demonstrate the versatility and application of VIKOR-based methods in complex decision-making scenarios, particularly in the selection of manufacturing technologies and processes.

II.3 COMPLEX PROPORTIONAL ASSESSMENT (COPRAS)

The method investigated by [8] also employs a similar normalization technique for both beneficial and non-beneficial criteria. Like other approaches, it requires input from decision makers, experts, or researchers to assign weights to the attributes, which can lead to variations in the ranking solutions based on differing weight assignments. A potential issue with this method arises during the normalization process, as some attribute values may become zero, which can significantly alter the overall ranking outcome. In a related study, [9] applied an improved version of the Complex Proportional Assessment (COPRAS) method, which is designed to handle qualitative information in the context of rapid prototype system selection. This demonstrates the continued evolution of decision-making methods, particularly in the realm of rapid prototyping, where both qualitative and quantitative factors must be considered.

II.4 HYBRID MADM TECHNIQUES FOR RAPID PROTOTYPE TOOL SELECTION

The selection of rapid prototyping processes has been addressed through various decision-making methodologies in recent studies. For instance, [10] employed the DEMATEL (Decision-Making Trial and Evaluation Laboratory) and VIKOR methods to evaluate and select three-dimensional printer service providers. In contrast, [1] applied a modified version of the TOPSIS (Technique for Order Preference by Similarity to Ideal Solution) methodology to solve the rapid prototyping selection problem. Building on this, [11] proposed the Generalized TOPSIS (GTMA) methodology to address the same issue, offering an alternative approach to ranking rapid prototyping processes. Additionally, [12] tackled the rapid prototyping selection problem by integrating the Grey Relational Analysis (GRA) method with Fuzzy TOPSIS, combining the strengths of both techniques to handle uncertainty and improve decision accuracy. The Fuzzy TOPSIS with GRA method, as implemented by [12], demonstrated its utility in optimizing rapid prototyping selection. In another advancement, the Fuzzy Single-Valued Neutrosophic Set Entropy Weight-based Multi-Attribute Decision Making (F-SVNS EW-MADM) method was introduced by [13, 14], providing a robust framework for handling uncertain, indeterminate, and fuzzy information in the decision-making process. Furthermore, [15] utilized the Analytical Network Process (ANP) and TOPSIS methodologies to assess and select appropriate rapid prototyping processes, further diversifying the range of techniques applied to this problem. These studies reflect the ongoing development and application of sophisticated decision-making models to improve the selection of rapid prototyping technologies.

III. PROPOSED METHODOLOGY FUZZY-SINGLE VALUED NEUTROSOPHIC SET ENTROPY WEIGHT BASED MULTI ATTRIBUTE DECISION MAKING TECHNIQUE (F-SVNS EW-MADM)

The Fuzzy Single-Valued Neutrosophic Set Advanced Entropy Weight-based Multi-Attribute Decision Making (F-SVNS AEW-MADM) methodology follows a structured approach to decision-making. The key steps involved in this process are outlined below:

Step 1: Define the objective of the selection process, clearly establishing the goal or desired outcome for the decision-making task.

Step 2: Identify the various alternatives available for selection, along with the relevant attributes (criteria) that will influence the decision. This step involves determining the factors that will be used to evaluate and compare the alternatives in the context of the selection problem.

Step 3: All alternatives and attributes (criteria) in matrix form with comparative performance are known as $decision$ matrix. Let us consider set of alternatives as $A = \{A_i, i = 1, 2, 3, .. m\}$ & set of criteria as $C = \{C_j, j = 1, 2, 3, .. n\}$, X_{ij} is the performance of alternatives A_i for relative criteria C_j. X_{ij} are having qualitative/ quantitative values. The structure of decision matrix is illustrated in Table 1.

Table 1: Decision Matrix for F-SVNS AEW-MADM.

Alternatives	C_1	C_2	C_3	…..	C_n
A_1	X_{11}	X_{12}	X_{13}	…..	X_{1n}
A_2	X_{21}	X_{22}	X_{23}	…..	X_{2n}
A_3	X_{31}	X_{32}	X_{33}	…..	X_{3n}
….	…..	…..	…..	…..	…..
A_m	X_{m1}	X_{m2}	X_{m3}	…..	X_{mn}

Source: Authors, (2025).

Step 4: Conversion of Qualitative Data to Quantitative Data

The qualitative (linguistic) information is systematically transformed into quantitative (crisp) values, as outlined in Table 2. This process enables the representation of subjective, descriptive information in a measurable form, facilitating more precise analysis and interpretation

Table 2. Conversion of Linguistic Terms in to Classic (Crisp) Set.

Linguistic terms of selection attributes	Fuzzy number	Crisp value of selection attribute
Exceptionally low	M1	0.045
Extremely low	M2	0.135
Very low	M3	0.255
Low	M4	0.335
Below average	M5	0.410
Average	M6	0.500
Above average	M7	0.590
High	M8	0.665
Very high	M9	0.745
Extremely high	M10	0.865

Source: Authors, (2025).

Data collected from sources [13, 14, 16, 17, 18].

If the input matrix consists solely of quantitative data, this conversion step can be omitted.

Step 5. Generalization/ normalization of matrix

As outlined in sources [13] and [14], each attribute associated with the alternatives presents distinct values. To ensure consistency, the data is standardized within the range [0, 1] through the application of the Vector Normalization Method (VNM). For beneficial criteria, where higher values are advantageous (such as quality and profit), normalization is achieved using Equation (1).

$$R_{ij} = \frac{X_{ij}}{\sqrt{\sum_{i=1}^{m} {X_{ij}}^2}};\ \forall\, i, j \tag{1}$$

For non-beneficial criteria, where lower values are preferable (e.g., price, lead time), normalization is conducted using Equation (2).

$$R_{ij} = 1 - \frac{X_{ij}}{\sqrt{\sum_{i=1}^{m} {X_{ij}}^2}};\ \forall\, i, j \tag{2}$$

Normalized decision matrix is shown in Table 3.

Table 3. Normalized Decision Matrix.

Alternative	C_1	C_2	C_3	…..	C_n
A_1	R_{11}	R_{12}	R_{13}	…..	R_{1n}
A_2	R_{21}	R_{22}	R_{23}	…..	R_{2n}
A_3	R_{31}	R_{32}	R_{33}	…..	R_{3n}
….	…..	…..	…..	…..	…..
A_m	R_{m1}	R_{m2}	R_{m3}	…..	R_{mn}

Source: Authors, (2025).

Step 6: Conversion of Classic Set/Fuzzy Set to Single-Valued Neutrosophic Set (SVNS)

The normalized decision matrix for F-SVNS AEW-MADM is presented in Table 4, where classic or fuzzy sets are converted into a Single-Valued Neutrosophic Set (SVNS). This transformation allows for a more comprehensive representation of uncertainty in decision-making scenarios.

Table 4. SVNS Normalized Decision Matrix for F-SVNS AEW-MADM

A	C_1	…..	C_n
A_1	$< T_{11}(x), I_{11}(x), F_{11}(x) >$	…..	$< T_{1n}(x), I_{1n}(x), F_{1n}(x) >$
A_2	$< T_{21}(x), I_{21}(x), F_{21}(x) >$	…..	$< T_{2n}(x), I_{2n}(x), F_{2n}(x) >$
A_3	$< T_{31}(x), I_{31}(x), F_{31}(x) >$	…..	$< T_{3n}(x), I_{3n}(x), F_{3n}(x) >$
….	…..	…..	…..
A_m	$< T_{m1}(x), I_{m1}(x), F_{m1}(x) >$	…..	$< T_{mn}(x), I_{mn}(x), F_{mn}(x) >$

Source: Authors, (2025).

According to sources [13], [14], and [21], the conversion rules for transforming classic or fuzzy sets to Single-Valued Neutrosophic Sets (SVNS) for both beneficial and non-beneficial criteria are outlined in [14]. For beneficial criteria, where higher values of performance measures are desirable (e.g., profit, quality), the Positive Ideal Solution (PIS) is defined as $< T_{max}^{*}(x), I_{min}^{*}(x), F_{min}^{*}(x) >$ In this context, the normalized input matrix treats the beneficial criteria as the degree of truthfulness, while the degree of indeterminacy and degree of falsehood are represented as $I_A(x) = F_A(x) = 1 - T_A(x)$ respectively. The SVNS conversion is performed using Equation (3).

$$\langle T_{ij}(x), I_{ij}(x), F_{ij}(x)\rangle = \langle R_{ij}(x), \big(1 - R_{ij}(x)\big), \big(1 - R_{ij}(x)\big)\rangle \tag{3}$$

Step 7: Identification of Ideal Solution for Beneficial and Non-Beneficial Attributes
According to sources [13], [14], and [21], the ideal solution for beneficial attributes—where higher values are advantageous (e.g., quality, profit)—is identified by determining the Positive Ideal Solution (PIS) here by Equation (4) and (5).

$$\text{BAIS} = \langle T_{max}^{*}(x), I_{min}^{*}(x), F_{min}^{*}(x)\rangle = \langle 1, 0, 0\rangle \tag{4}$$

Non beneficial attributes ideal solution

$$\text{NBAIS} = \langle T_{min}^{*}(x), I_{max}^{*}(x), F_{max}^{*}(x)\rangle = \langle 0, 1, 1\rangle \tag{5}$$

Step 8: Calculation of the entropy value of attribute E_j
Find the entropy value for attribute with Equation (6).

$$E_j = 1 - {}^{1}/_{n} \sum_{i=1}^{m} \Big(T_{ij}(x_i) + F_{ij}(x_i)\Big) \Big|2\Big(I_{ij}(x_i)\Big) - 1\Big| \tag{6}$$

Step 9: Calculation of the entropy weight of attribute W_j
Find the entropy weight of attribute by Equation (7).

$$W_j = \frac{1 - E_j}{\sum_{j=1}^{n}(1 - E_j)} \tag{7}$$

Here, we get weight vector $W = (w_1, w_{2,} w_{3,} \ldots\ldots\ldots\ldots w_n)^T$ of attributes, $C = \{C_j;\ \text{for } j = 1, 2, 3, \ldots\ldots n\}$ with $W_j \geq 0$ and $\sum_{j=1}^{n} W_j = 1$.

Step 10: Calculate the entropy weight of alterative A_w

Find the alternative weight by Equation (8).

$$A_w = \sum_{j=1}^{n} W_j * \Big((T_{ij}(x) * T_{ij}^{*}(x)) + (I_{ij}(x) * I_{ij}^{*}(x) + (F_{ij}(x) * F_{ij}^{*}(x)\Big) \tag{8}$$

Here, for beneficial attributes $\text{PIS} = \langle T_{max}^{*}(x), I_{min}^{*}(x), F_{min}^{*}(x)\rangle = \langle 1, 0, 0\rangle$ and for non-beneficial attributes $\text{NIS} = \langle T_{min}^{*}(x), I_{max}^{*}(x), F_{max}^{*}(x)\rangle = \langle 0, 1, 1\rangle$.

Step 11: Ranking of Alternatives
Upon the calculation of alternative weight A_w, the alternatives are ranked in descending order. The alternative with the highest correlation coefficient A_w is assigned the first rank, while the alternative with the lowest A_w is assigned the last rank. This ranking method ensures that alternatives are ordered based on their relative performance and suitability according to the calculated weights.

IV. COLLECTED CASE EXAMPLE OF RAPID PROTOTYPE PROGRAM SELECTION

Step 1: A case study on the selection of a rapid prototype program for industrial applications was presented by [1] using a modified TOPSIS methodology. Table 5 provides the quantitative data illustrating the expected performance of each rapid prototype (alternative) in relation to the respective process parameters (attributes). This case serves as the foundation for the new proposed approach, demonstrating its application in an industrial context.
Step 2: The same case example was further analyzed by [19] and [20] using various multi-criteria decision-making methods, including GTMA, SAW, WPM, AHP, TOPSIS, and a modified version of TOPSIS. These approaches were employed to evaluate and compare the performance of the alternatives under the given process parameters.

Step 3: The decision matrix comprises six rapid prototype systems as alternatives and six attribute measures: C1 (accuracy), C2 (surface roughness), C3 (tensile strength), C4 (elongation), C5 (cost of part), and C6 (build time). Based on the published input data, the beneficial attributes are identified as C3 (tensile strength) and C4 (elongation), while the non-beneficial attributes are C1 (accuracy), C2 (surface roughness), C5 (cost of part), and C6 (build time). Although accuracy (C1) is typically considered a beneficial attribute, for the purpose of comparison with previously published rankings, and in accordance with the research assumptions, it is treated as a non-beneficial attribute in this study.

For implementation and initial validation purposes, the proposed methodologies were applied to the collected case examples, which were sourced from peer-reviewed journals and books. The results were then compared with and explained in the context of the published rankings, while the original data from the sources remained unchanged.

Step 4: The decision matrix utilized in this study was collected from sources [1] and [20], as presented in Table 5. This matrix provides the necessary data for evaluating the alternatives based on the defined attributes.

Table 5. Rapid Prototype Selection Input Matrix (Collected Case Example).

Alternative	C1 (-)	C2 (-)	C3 (+)	C4 (+)	C5 (-)	C6 (-)
A1	120	6.5	65	5	0.745	0.5
A2	150	12.5	40	8.5	0.745	0.5
A3	125	21	30	10	0.665	0.745
A4	185	20	25	10	0.59	0.41
A5	95	3.5	30	6	0.745	0.41
A6	600	15.5	5	1	0.135	0.255

Source: Authors, (2025).

The data is collected from sources [1, 11, 20].

Step 5: Conversion of Qualitative Data to Quantitative Data

In this case, the input information consists solely of quantitative data. Therefore, there is no need to convert any qualitative values into quantitative form. As a result, this step is not applicable and has been excluded from the current case example.

Step 6: Normalization of Table 5 is carried out with the Equation (1) / (2). Rapid prototype selection normalized matrix is shown in Table 6.

Table 6. Rapid Prototype Selection Normalized Matrix using VNM.

Sr. No.	C1 (-)	C2 (-)	C3 (+)	C4 (+)	C5 (-)	C6 (-)
A1	0.8223	0.8192	0.7145	0.2735	0.5263	0.5857
A2	0.7778	0.6522	0.4397	0.4649	0.5263	0.5857
A3	0.8148	0.4158	0.3298	0.5470	0.5772	0.3826
A4	0.7260	0.4436	0.2748	0.5470	0.6249	0.6602
A5	0.8593	0.9026	0.3298	0.3282	0.5263	0.6602
A6	0.1113	0.5688	0.0550	0.0547	0.9142	0.7887

Source: Authors, (2025).

Step 7: Convert crisp normalized matrix into SVNS decision matrix: Crisp data is converted in SVNS $< \mathbf{T_{ij}(x)}, \mathbf{I_{ij}(x)}, \mathbf{F_{ij}(x)} >$ degree of truthness, indeterminate and falsehood form is carried out with Equation (3).

Non-beneficial attributes i.e. Alternative A1 and attribute C1 having value $\mathbf{0.8223}$ converted in SVNS gives the value $\langle(\mathbf{1-0.8223}), \mathbf{0.8223}, \mathbf{0.8223}\rangle = \langle \mathbf{0.1777}, \mathbf{0.8223}, \mathbf{0.8223} \rangle$. The same calculation is also is carried out for attributes C2, C5 and C6.

Beneficial attributes i.e. Alternative A1 and attribute C3 having value 0. 7145 converted in SVNS gives the value $\langle \mathbf{0.7145}, (\mathbf{1-0.7145}), (\mathbf{1-0.7145})\rangle = \langle \mathbf{0.7145}, \mathbf{0.2855}, \mathbf{0.2855}\rangle$. The same calculation is also carried out for attribute C4.

Step 8: Find the beneficial attribute ideal solution and non-beneficial attribute ideal solution.

Beneficial attribute ideal solution and non-beneficial attribute ideal solution is discovered with Equation (4)/ (5), where $\mathbf{BAIS}\ (\mathbf{A}^*) = \langle \mathbf{T^*_{max}(x)}, \mathbf{I^*_{min}(x)}, \mathbf{F^*_{min}(x)}\rangle = \langle \mathbf{1}, \mathbf{0}, \mathbf{0}\rangle$ and

$\mathbf{NBAIS}\ (\mathbf{A}^*) = \langle \mathbf{T^*_{min}(x)}, \mathbf{I^*_{max}(x)}, \mathbf{F^*_{max}(x)}\rangle \mathbf{55} = \langle \mathbf{0}, \mathbf{1}, \mathbf{1}\rangle$.

Step 9: Calculate the entropy value for attribute $(\mathbf{E_j})$

Calculate the attribute value with the Equation (6) is as shown in Table 7. i.e. consider calculation of the entropy value for attribute A1.

$$\mathbf{E_{j1}} = \mathbf{1} - {}^{\mathbf{1}}/_{\mathbf{6}} [\{(\mathbf{0.1777} + \mathbf{0.8223}) * |\mathbf{2(0.8223)} - \mathbf{1}|\} + \{(\mathbf{0.2222} + \mathbf{0.7778}) * |\mathbf{2(0.7778)} - \mathbf{1}|\} + \{(\mathbf{0.1852} + \mathbf{0.8148}) * |\mathbf{2(0.8148)} - \mathbf{1}|\} + \{(\mathbf{0.2740} + \mathbf{0.7260}) * |\mathbf{2(0.7260)} - \mathbf{1}|\} + \{(\mathbf{0.1407} + \mathbf{0.8593}) * |\mathbf{2(0.8593)} - \mathbf{1}|\} + \{(\mathbf{0.8887} + \mathbf{0.1113}) * |\mathbf{2(0.1113)} - \mathbf{1}|\}] = \mathbf{0.3704}$$

The same calculation is also is carried out for remaining attributes.

Step 10: Calculate the entropy weight of attribute $\mathbf{W_j}$

Calculate the attribute value with the Equation (7) is as shown in Table 7. i.e. consider calculation of the alternative entropy value for attribute A1.

$$\mathbf{W_{j1}} = \left[\frac{(\mathbf{1-0.3704})}{(\mathbf{1-0.3704})+(\mathbf{1-0.6388})+(\mathbf{1-0.5715})+(\mathbf{1-0.6758})+(\mathbf{1-0.7683})+(\mathbf{1-0.7007})}\right] = \mathbf{0.2768}$$

The same calculation is also is carried out for $\mathbf{W_{j2}}$ to $\mathbf{W_{j6}}$.

$$\text{Where,} \sum_{\mathbf{j=1}}^{\mathbf{n}} \mathbf{W_j} = \mathbf{0.2768} + \mathbf{0.1588} + \mathbf{0.1884} + \mathbf{0.1019} + \mathbf{0.1884} + \mathbf{0.1316} = \mathbf{1}$$

Step 11: Calculate the entropy weight of alterative $\mathbf{A_w}$
Find the alternative weight by Eq. (7) is as shown in Table 7

$$\mathbf{A_{w1}} = [\mathbf{0.2768} * \{(\mathbf{0.1777} * \mathbf{0}) + (\mathbf{0.8223} * \mathbf{1}) + (\mathbf{0.8223} * \mathbf{1})\} + \mathbf{0.1588} * \{(\mathbf{0.1808} * \mathbf{0}) + (\mathbf{0.8192} * \mathbf{1}) + (\mathbf{0.8192} * \mathbf{1})\} + \mathbf{0.1884} * \{(\mathbf{0.7145} * \mathbf{1}) + (\mathbf{0.2855} * \mathbf{0}) + (\mathbf{0.2855} * \mathbf{0})\} + \mathbf{0.1019} * \{(\mathbf{0.2735} * \mathbf{1}) + (\mathbf{0.7265} * \mathbf{0}) + (\mathbf{0.7265} * \mathbf{0})\} + \mathbf{0.1884} * \{(\mathbf{0.4737} * \mathbf{0}) + (\mathbf{0.5263} * \mathbf{1}) + (\mathbf{0.5263} * \mathbf{1})\} + \mathbf{0.1316} * \{(\mathbf{0.4143} * \mathbf{0}) + (\mathbf{0.5857} * \mathbf{1}) + (\mathbf{0.5857} * \mathbf{1})\}] = \mathbf{1.1503}$$

The same calculation is also is carried out for remaining alternatives.
Table 7. F-SVNS-AEW-MADM Ranking for Rapid Prototype Selection.
Step 12: Ranking of alternatives
The rank is calculated with F-SVNS-AEW-MADM is as shown in Table 7. The alternatives rank is given according to alternative weight $\mathbf{A_w}$ in descending order, $\mathbf{1.1523} > \mathbf{1.1503} > \mathbf{1.0482} > \mathbf{0.9736} > \mathbf{0.9416} > \mathbf{0.6542}$. Alternatives ranking order is $\mathbf{A5} > \mathbf{A1} > \mathbf{A2} > \mathbf{A4} > \mathbf{A3} > \mathbf{A6}$ as shown in Table 7.

V. PERFORMANCE MEASURES COMPARISON: RAPID PROTOTYPE RANKING

The results of the proposed three methodologies are compared with published results to validate their effectiveness in the selection of rapid prototypes. To facilitate the comparison, all rapid prototype alternatives are ranked based on their respective alternative weight values, as shown in Table 8. The alternative with the highest weight value is ranked first, followed by the alternative with the second-highest weight value in second place, and so on. The ranking order obtained using the three proposed methodologies is then compared with the ranking order reported in the literature. The comparison of results is presented in Table 8.

The result comparisons presented in Table 8 indicate that the outcomes obtained from the proposed methodologies are largely consistent with the results reported in the literature. The same rapid prototype selection problem was addressed by [19] using the GTMA, SAW, WPM, AHP, and VIKOR methodologies. All methods, except for TOPSIS and modified TOPSIS, identified alternative A5 as the top choice. This discrepancy is attributed to the fact that these methodologies take attribute weights into account, and the weight assignment is dependent on the decision maker, which results in different ranking outcomes.

Furthermore, the second-ranked alternative, as determined by all proposed methods, aligns with the published results, with the exception of the TOPSIS and modified TOPSIS methodologies, due to their distinct approach to weight calculation. For the fourth-ranked alternative, the proposed methods match the rankings obtained by the VIKOR and GTMA methods. In contrast, other MADM approaches such as SAW, AHP, TOPSIS, and modified TOPSIS report a slight variation in the 4th rank, primarily due to differences in weight criteria calculation, assumptions, and expert opinions.

The proposed methodologies demonstrate a consistent ranking of alternative A6, aligning with published results where alternative A6 holds a similar position. This indicates that, although

Table 7: F-SVNS-AEW-MADM Ranking for Rapid Prototype Selection.

Sr. No.	C1 (-)	C2 (-)	C3 (+)	C4 (+)	C5 (-)	C6 (-)	A_w	Rank
A1	<0.1777, 0.8223, 0.8223>	<0.1808, 0.8192, 0.8192>	<0.7145, 0.2855, 0.2855>	<0.2735, 0.7265, 0.7265>	<0.4737, 0.5263, 0.5263>	<0.4143, 0.5857, 0.5857>	1.1503	2
A2	<0.2222, 0.7778, 0.7778>	<0.3478, 0.6522, 0.6522>	<0.4397, 0.5603, 0. 5603>	<0.4649, 0.5351, 0.5351>	<0.4737, 0.5263, 0.5263>	<0.4143, 0.5857, 0.5857>	1.0482	3
A3	<0.1852, 0.8148, 0.8148>	<0.5842, 0.4158, 0.4158>	<0.3298, 0.6702, 0. 6702>	<0.5470, 0.4530, 0.4530>	<0.4228, 0.5772, 0.5772>	<0.6174, 0.3826, 0.3826>	0.9416	5
A4	<0.2740, 0.7260, 0.7260>	<0.5564, 0.4436, 0.4436>	<0.2748, 0.7252, 0.7252>	<0.5470, 0.4530, 0.4530>	<0.3751, 0.6249, 0.6249>	<0.3398, 0.6602, 0.6602>	0.9736	4

A5	<0.1407, 0.8593, 0.8593>	<0.0974, 0.9026, 0.9026>	<0.3298, 0.6702, 0.6702>	<0.3282, 0.6718, 0.6718>	<0.4737, 0.5263, 0.5263>	<0.3398, 0.6602, 0.6602>	1.1523	1
A6	<0.8887, 0.1113, 0.1113>	<0.4312, 0.5688, 0.5688>	<0.0550, 0.9450, 0.9450>	<0.0547, 0.9453, 0.9453>	<0.0858, 0.9142, 0.9142>	<0.2113, 0.7887, 0.7887>	0.6542	6
A*	<0.0000, 1.0000, 1.0000>	<0.0000, 1.0000, 1.0000>	<1.000, 0.0000, 0.0000>	<1.000, 0.0000, 0.0000>	<0.0000, 1.0000, 1.0000>	<0.0000, 1.0000, 1.0000>		
E_j	0.3704	0.6388	0.5715	0.6758	0.7683	0.7007		
W_j	**0.2768**	**0.1588**	**0.1884**	**0.1425**	**0.1019**	**0.1316**	**1**	

Source: Authors, (2025).

Table 8: Rapid Prototype Selection Performance Measures Comparison.

Alternatives (Sr. No.)	F-SVNS AEW-MADMs	Data Collected from the source [19]						
		GTMA	SAW	WPM	AHP	TOPSIS	ModifiedTOPSIS	VIKOR
A1	2	2	2	2	2	1	1	2
A2	3	3	3	3	3	3	3	3
A3	5	5	4	4	4	4	4	5
A4	4	4	5	5	5	5	5	4
A5	1	1	1	1	1	2	2	1
A6	6	6	6	6	6	6	6	6

Source: Authors, (2025).

The weight criteria influence the rankings of other alternatives, the proposed approaches maintain strong consistency with the published findings for the top-ranked alternative, thereby affirming the robustness and reliability of the methods.

VI. CONCLUSIONS

The proposed methodology offers a streamlined approach with minimal computational complexity, eliminating the need to calculate the relative importance of attributes. It does not require resizing the assignment matrix and is capable of converting simple or linguistic sets into F-SVNS. Furthermore, the suggested methodology outperforms established methods such as GTMA, SAW, WPM, AHP, TOPSIS, Modified TOPSIS, and VIKOR. This chapter introduces the F-SVNS AEW-MADM technique, developed and implemented to evaluate its feasibility in the selection and ranking of rapid prototyping processes. The key conclusions of the proposed method are as follows:

• The methodology effectively converts both crisp data and fuzzy information provided by the decision maker into SVNS form, resulting in more efficient and reliable ranking solutions.

• It is robust in handling decision-making scenarios involving inconsistent, incomplete, and indeterminate information.

• The proposed approach facilitates more efficient negotiation and selection of the best alternative with reduced computational effort.

• The calculation and normalization process ensures no loss of information, and no attribute value is reduced to zero during the process.

• The F-SVNS AEW-MADM technique incorporates attribute weight calculation, and comparison with existing published results demonstrates its validity, applicability, and reliability in rapid prototyping selection for manufacturing environments. This leads to enhanced manufacturing performance and function.

• Overall, the proposed methodology provides a valuable tool for improving decision-making processes in manufacturing, specifically in the selection of rapid prototyping systems.

VI. AUTHOR'S CONTRIBUTION

Conceptualization: Nital Pravinbhai Nirmal, Jignesh Girishbhai Parmar and Mehul Gunvantrai Mehta.
Methodology: Nital Pravinbhai Nirmal, Jignesh Girishbhai Parmar and Mehul Gunvantrai Mehta.
Investigation: Nital Pravinbhai Nirmal, Jignesh Girishbhai Parmar and Mehul Gunvantrai Mehta.
Discussion of results: Nital Pravinbhai Nirmal, Jignesh Girishbhai Parmar and Mehul Gunvantrai Mehta.
Writing – Original Draft: Nital Pravinbhai Nirmal, Jignesh Girishbhai Parmar and Mehul Gunvantrai Mehta.
Writing – Review and Editing: Nital Pravinbhai Nirmal, Jignesh Girishbhai Parmar and Mehul Gunvantrai Mehta.
Resources: Nital Pravinbhai Nirmal, Jignesh Girishbhai Parmar and Mehul Gunvantrai Mehta.
Supervision: Nital Pravinbhai Nirmal, Jignesh Girishbhai Parmar and Mehul Gunvantrai Mehta.
Approval of the final text: Nital Pravinbhai Nirmal, Jignesh Girishbhai Parmar and Mehul Gunvantrai Mehta.

VIII. REFERENCES

[1] Byun H., and Lee K., "A decision support system for the selection of a rapid prototyping process using the modified TOPSIS method", IJAMT, vol 26, no.10, pp. 1338-1347, ISSN: 1433-3015, 2005. DOI: https://doi.org/10.1007/s00170-004-2099-2.

[2] Saaty T., "How to make a decision: the analytic hierarchy process", IJI,; vol. 24; pp. 19-43, ISBN: 0092-2102, 1994. DOI: https://doi.org/10.1287/inte.24.6.19.

[3] Armillotta A., "Selection of layered manufacturing techniques by an adaptive AHP decision model", Robotics and Computer-Integrated Manufacturing, 2008; (24); 450-461, ISSN: 0736-5845, DOI: https://doi.org/10.1016/j.rcim.2007.06.001.

[4] Opricovic S., (1998), Multicriteria optimization of civil engineering systems, Faculty of Civil Engineering, Belgrade, Vol 2, pp. 5-21.

[5] Devi K., "Extension of VIKOR method in intuitionistic fuzzy environment for robot selection", IJESA, vol. 38; pp. 14163-14168, ISSN: 0957-4174, 2011. DOI: https://doi.org/10.1016/j.eswa.2011.04.227

[6] Grote K., Gomes J., Borille A. and Meyer R., "Applying decision methods to select rapid prototyping technologies", RPJ , 2010; 16; 50-62, ISSN: 1355-2546, DOI: https://doi.org/10.1108/13552541011011712.

[7] Girubha J., Nagaraj S. and Vinodh S., "Application of fuzzy VIKOR for selection of rapid prototyping technologies in an agile environment", IJRPJ, vol. 20 pp. 523-532, ISSN: 1355-2546, 2014. DOI: https://doi.org/10.1108/RPJ-07-2012-0060.

[8] Zavadskas E., Kaklauskas A. and Sarka V., "The new method of multi-criteria complex proportional assessment of projects", IJTEDE, vol. 1, pp. 131-139, 1994.

[9] Makhesana M., "Application of improved complex proportional assessment (COPRAS) method for rapid prototyping system selection", RPIJ, vol. 21; pp. 671-674, ISSN: 1355-2546, 2015. DOI: https://doi.org/10.1108/RPJ-03-2014-0027.

[10] Liao S., Wu M., Huang C., Kao Y. and Lee T., "Evaluating and enhancing three-dimensional printing service providers for rapid prototyping using the DEMATEL based network process and VIKOR", IJMPE, ISSN: 1024-123X, 2014. DOI: https://doi.org/10.1155/2014/349348.

[11] Rao R. and Padmanabhan K., "Rapid prototyping process selection using graph theory and matrix approach", IJMPT, vol. 194, pp. 81-88, ISSN: 0924-0136, 2007. DOI: https://doi.org/10.1016/j.jmatprotec.2007.04.003

[12] Mahapatra S. and Panda B., "Benchmarking of rapid prototyping systems using grey relational analysis", IJSOM, vol. 16, pp. 460-477, ISSN: 1744-2370, 2013, DOI: https://doi.org/10.1504/IJSOM.2013.057509

[13] Smarandache F. and Pramanik S., "New Trends in Neutrosophic Theory and Applications", Europa Nova, Brussels, USA, 2016. ISBN: 978-1-59973-498-9.

[14] Nirmal N. and Bhatt M., "Selection of automated guided vehicle using single valued neutrosophic entropy based novel multi attribute decision making technique", New Trends in Neutrosophic Theory and Application, Florentin Smarandache, Surapati Pramanik, Europa Nova, Brussels, USA, 2016. p. 105-114, ISBN: 978-1-59973-498-9.

[15] Kek V. and Kek. V, "Rapid prototyping process selection using multi criteria decision making considering environmental criteria and its decision support system", RPJ, vol. 22, pp. 225-250, ISSN: 1355-2546, 2016. DOI: https://doi.org/10.1108/RPJ-03-2014-0040.

[16] Chen S-J. and Hwang C-L., "Fuzzy Ranking Methods, Fuzzy Multiple Attribute Decision Making" Springer, pp. 101-288, ISBN: 978-3-642-46768-4, 1992. DOI : https://doi.org/10.1007/978-3-642-46768-4_5.

[17] Venkatasamy R. and Agrawal V., "Selection of automobile vehicle by evaluation through graph theoretical methodology", IJVDD, vol. 17; pp. 449-470, ISSN: 0143-3369, 1996. DOI: https://doi.org/10.1504/IJVD.1996.061971.

[18] Venkatasamy R, Agrawal VP, A digraph approach to quality evaluation of an automotive vehicle, International Journal of Quality Engineering, 1997; 9; 405-417, ISSN: 0898-2112, DOI: https://doi.org/10.1080/08982119708919060.

[19] Rao R. V., "Decision making in the manufacturing environment: using graph theory and fuzzy multiple attribute decision making methods" Springer Science & Business Media, ISBN: 1846288193, 2007. DOI: https://doi.org/10.1007/978-1-4471-4375-8

[20] Rao R., "Evaluation of environmentally conscious manufacturing programs using multiple attribute decision-making methods", Proceedings of the Institution of Mechanical Engineers, Part B: Journal of Engineering Manufacture, 2008; 222; 441-451, ISBN: 0954-4054, DOI: https://doi.org/10.1243/09544054JEM981.

[21] Nirmal N and Bhatt M, "Development of Fuzzy-Single Valued Neutrosophic MADM Technique to Improve Performance in Manufacturing and Supply Chain Functions", Fuzzy Multi-criteria Decision-Making Using Neutrosophic Sets. Springer International Publishing, Cham, 2019. p. 711-729, ISBN: 978-3-030-00045-5, DOI: https://doi.org/10.1007/978-3-030-00045-5_27

Journal of Engineering and Technology for Industrial Applications

ITEGAM-JETIA

Manaus, v.11 n.54, p. 160-167. July/August., 2025.
DOI: https://doi.org/10.5935/jetia. v11i54.1705

ISSN ONLINE: 2447-0228

RESEARCH ARTICLE OPEN ACCESS

MULTI-OBJECTIVE OPTIMIZATION OF END MILLING PROCESS PARAMETERS FOR MINIMUM SURFACE ROUGHNESS USING MOGA

Jignesh Girishbhai Parmar[1], Komal G. Dave[2], Mehul G. Mehta[3]

[1,2,3]Gujarat Technological Universit, India.

[1]http://orcid.org/0000-0002-8533-8304, [2]http://orcid.org/0000-0003-0822-1652, [3]http://orcid.org/0009-0002-2219-0848.

E-mail: jiger.mechanical1@gmail.com, dave_komal123@ldce.ac.in, mgmehta@mech.ssgec.ac.in.

ARTICLE INFO

Article History
Received: March 11, 2025
Revised: April 20, 2025
Accepted: June 15, 2025
Published: August 31, 2025

Keywords:
Multi-objective Optimization,
Multi-objective genetic algorithm,
End milling operation,
Surface roughness,
Machining time.

ABSTRACT

In this paper, a multi-objective genetic algorithm (MOGA) has been used for the optimization of end milling process parameters for minimum surface roughness and machining time. The regression equation has been generated and used in the multi-objective genetic algorithm tool in MATLAB R2015a. In the present work, an experiment has been carried out on the end milling process of AISI1020 with a tungsten carbide tool by varying cutting speed, feed rate and depth of cut. The responses such as surface roughness and machining time have been measured using a Mitutoyo surface roughness tester and stopwatch, respectively. Optimize the machining parameters for minimum surface roughness and machining time. This study finds the interactive effect of input parameters such as cutting speed, feed and depth of cut on surface roughness. The result achieved by MOGA has been validated through experimentation. A good correlation has been found between MOGA and experimentation. It proves MOGA can be efficiently utilized to optimize end milling process parameters for minimum surface roughness and machining time.

Copyright ©2025 by authors and Galileo Institute of Technology and Education of the Amazon (ITEGAM). This work is licensed under the Creative Commons Attribution International License (CC BY 4.0).

I. INTRODUCTION

End milling has been used in various industries, including die-making, aerospace, automotive, and biomedical for simple to complex geometric profiles [1]. End milling operation is a very common machining operation and it removes the material fast with good quality. Surface roughness has a significant impact on production cost and quality and its estimate of a product's technological quality. Surface roughness also affects functional qualities, including fatigue resistance, surface friction, coating properties, heat transmission, etc. Surface finish is very dynamic and process dependent so it is very difficult to calculate the surface roughness through the analytical techniques. Machining time decides the completion time of the product and the productivity rate of industries. The prediction of machining time is useful for the estimation of delivery time and manufacturing cost of products in industries. When the machining time is decreased the machining cost decreases and the production rate increases [2].

The MOGA has been used to optimize end milling process parameters for minimum surface roughness and machining time. C. C. Tsao et al.[2009] has been used the grey–Taguchi method for A6061P-T651.In this paper, grey relational analysis has been used and reduce flank wear and surface roughness [3]. S. Moshat et al. [2010] have used the Taguchi method coupled with grey relational analysis for end milling operations. They calculate the weights of each response. The Entropy measurement technique has been used for the estimation of its performance characteristics [4]. J.S. Pang et al. (2014) have used the Taguchi methodology for optimization. Aluminium-based composite material has been used for end milling operations. They have selected responses such as surface roughness and cutting force [5]. S. Ajith Arul Daniel et al. [2019] have used artificial neural networks and grey Taguchi analysis for the optimization of input process parameters for the milling operation of Al5059-SiC-MoS2 [6]. Reddy Sreenivasulu et al. [2019] used Grey grey-based Taguchi approach integrated with entropy measurement for glass fiber-reinforced polymer matrix composite for optimization [7]. M. Jebaraj et al. (2019) have used TOPSIS and ANOVA for statistical analysis for optimization. They selected cutting speed, feed and cooling environment as input variables and temperature, surface roughness and cutting forces were selected as responses [8]. Jakeer Hussain

Shaik et al. (2020) have used an FEA to improve the dynamic stability of the end milling process. Study the effect of input parameters on output variables through ANOVA and artificial neural network.

They selected input parameters such as tool rotational speed, tool overhang, bearing span, tool diameter and force angle for optimum design of the spindle tool system and stable depth of cut [9]. Menderes Kam et al. (2021) have analyzed the tool vibration and surface roughness of the turning process for AISI 4340 (34CrNiMo6). They have used the Taguchi Method for analysis. Analysis of variance was used to determine the effects of machining parameters on the Vibration and surface roughness values [10]. I.A. Daniyan et al. (2021) used response surface methodology and find out the relation of end milling process parameters in terms of optimization. The experiment has been conducted on the DMU80monoBLOCK Deckel Maho 5-axis CNC milling machine for AA6063. The mathematical and optimization model has been developed based on numerical value and Physical experiment results [11].

II. METHODOLOGY

In this study, experimental results have been used for the generation of regression equations in Minitab 17. The regression equation has been used for the generation of objective functions in MOGA. Here cutting speed, feed rate and depth of cut are controllable factors that influence surface roughness. The surface roughness (μm) and machining time (Sec.) have been discovered using eq. (1) and eq. (2).

Surface roughness (μm)

$$= -0.1803 - 0.000302 * Vc + 2.573 *f + 0.0473 *d \quad (1)$$

Machining time (Sec.)

$$= 6.695 - 0.01570 * Vc - 10.047 *f + 0.033 *d \quad (2)$$

III. EXPERIMENTATION

In this study we considered 3 factors such as cutting speed, feed and depth of cut. The range of input variables are shown in Table 1.

Table 1: Factors and level combination.

Factors	**Cutting Speed**	**Feed**	**DOC**
Levels	5	5	5
Values	140, 150, 160, 170, 180	0.12, 0.15, 0.18, 0.21, 0.24	0.2, 0.4, 0.6, 0.8, 1

Source: Authors, (2025).

Based on the design of the experiment we carried out a total of 25 experiments. All the experiments have been carried out on JYOTI CNC vertical milling center. The experimental setup is shown in Fig. 1.

Figure 1: Experimental set-up of end milling operation.
Source: Authors, (2025).

AISI1020 steel is selected as a workpiece material because it is easily available and low price. The chemical composition of AISI1020 is shown in Table 2.

Table 2: AISI1020 chemical composition.

Elements	**P**	**Mn**	**C**	**S**	**Fe**
Composition in %	0.026	0.565	0.197	0.039	99.100

Source: Authors, (2025).

Solid carbide end mill cutters have been selected as a cutting tool with 12 mm diameter and 4 flutes [12]. During the experimentation total of 25 work specimens (100 x 50 x 10) have been prepared for 25 datasets. The work specimen before the experimentation is shown in Figure 2.

Figure 2: Work Specimen before the operation.
Source: Authors, (2025).

The work specimens after the end milling operation are shown in Figure 3.

Figure 3: Work Specimen after the operation.
Source: Authors, (2025).

The experimental values of surface roughness have been measured through the MITUTOYO Surface texture tester shown in Fig. 4. The machining time has been measured through a stopwatch.

Figure 4: Surface roughness measurement.
Source: Authors, (2025).

The experimental results of 25 data sets are shown in Table 3.

Table 3: Experimental Results of 25 data set.

Sr. No.	Cutting speed (m/min)	Feed rate (mm/tooth)	Depth of cut (mm)	Surface roughness (µm)	Machining Time (Sec.)
1	140	0.24	0.2	0.30	2.10
2	140	0.24	0.4	0.46	2.19
3	140	0.24	0.6	0.44	2.34
4	140	0.24	0.8	0.44	2.10
5	140	0.24	1	0.48	1.80
6	150	0.12	0.2	0.12	3.10
7	150	0.12	0.4	0.12	3.23
8	150	0.12	0.6	0.11	3.31
9	150	0.12	0.8	0.11	3.25
10	150	0.12	1	0.13	3.39
11	160	0.15	0.2	0.18	2.40
12	160	0.15	0.4	0.17	2.76
13	160	0.15	0.6	0.15	2.56
14	160	0.15	0.8	0.17	2.40
15	160	0.15	1	0.20	2.51
16	170	0.18	0.2	0.26	2.30
17	170	0.18	0.4	0.26	2.29
18	170	0.18	0.6	0.25	2.23
19	170	0.18	0.8	0.24	2.22
20	170	0.18	1	0.29	2.33
21	180	0.21	0.2	0.30	1.70
22	180	0.21	0.4	0.35	1.75
23	180	0.21	0.6	0.38	1.82
24	180	0.21	0.8	0.31	1.86
25	180	0.21	1	0.35	1.93

Source: Authors, (2025).

III.1 MULTI-OBJECTIVE OPTIMIZATION

Here multi-objective genetic algorithm has been used for optimization with MATLAB R2015a. The developed regression equation achieved through Minitab17 has been utilized for the MOGA tool. In MOGA, three main subordinates reproduction, crossover and mutation have been used for optimization. The objective functions for minimizing the surface roughness and machining time are shown in eq. (3) and eq. (4).

To minimize:

Surface roughness,

$$Ra = -0.1803 \ -0.000302 \times Vc + 2.573 \times f + 0.0473 \times d \quad (3)$$

Machining time,

$$Tc = 6.695 \ -0.01570 \times Vc \ -10.047 \times f + 0.033 \times d \quad (4)$$

The constraint function of responses is shown in eq. (5).

$$C = [(-0.1803 \ -0.000302 \times Vc + 2.573 \times f + 0.0473 \times d) - 0.48] \quad (5)$$

The selected upper and lower bound of cutting speed is 140 and 180, for feed rate is 0.12 and 0.24 and for depth of cut is 0.2 and 1. Multi-objective genetic algorithm processing parameters and their values are shown in Table 4.

Table 4: Processing parameters of MOGA.

Operation and parameter	Functions and values
Number of input variable constraint	3
Number of objective function	2
Population size	50
Tournament size	2
Selection function	Tournament
Crossover function	Single point
Mutation function	Adaptive feasible
Creation function	Feasible population
Distance measure function	Distance crowding
Function tolerance	1e-4
Constraint tolerance	1e-3
Cross over fraction	0.8
Migration fraction	0.2

Source: Authors, (2025).

Here Figure. 5 indicates the average distance between individuals. In this graph, all of the distances between the individuals are shown between 0 to 16.

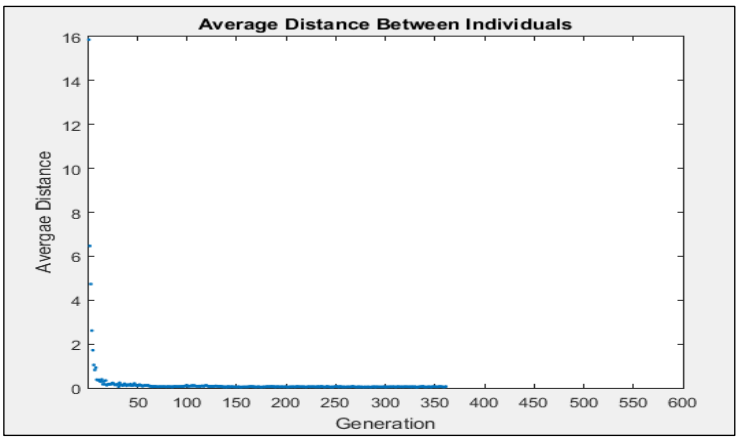

Figure 5: Average distance between individuals.
Source: Authors, (2025).

Fig. 6 gives information about the individuals and their distance. Here distance is 0 to 0.6 and the individuals is 0 to 50 showing the relation between the distances of the individual's value. Fig. 7 shows the average spread is 0.145034 has the maximum spread with given generations.

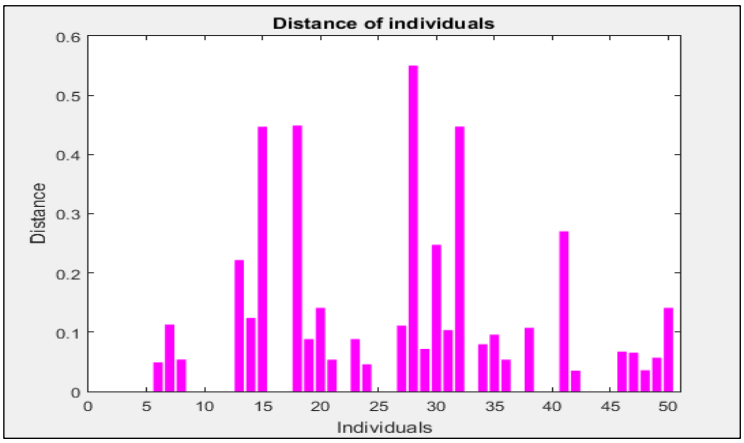

Figure 6: Distance of individuals.
Source: Authors, (2025).

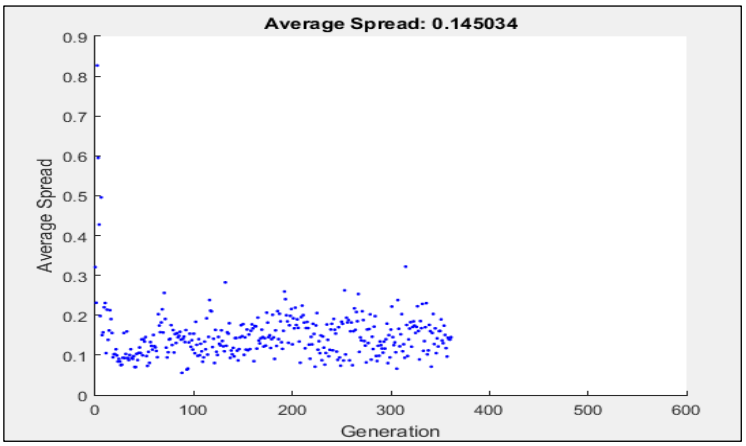

Figure 7: Average spread with generation.
Source: Authors, (2025).

IV. RESULTS AND DISCUSSIONS

The interactive effect of input parameters such as cutting speed, feed and depth of cut on the surface roughness was analyzed, which is helpful for the selection of input process parameters for a better surface finish. The MINITAB 17 has been used to find the interactive effect of input parameters on surface roughness. The interactive effect of cutting speed, feed and depth of cut on the surface roughness is shown in Fig.8. It is observed that the surface roughness decreases when the cutting speed increases and the feed rate and depth of cut decrease simultaneously.

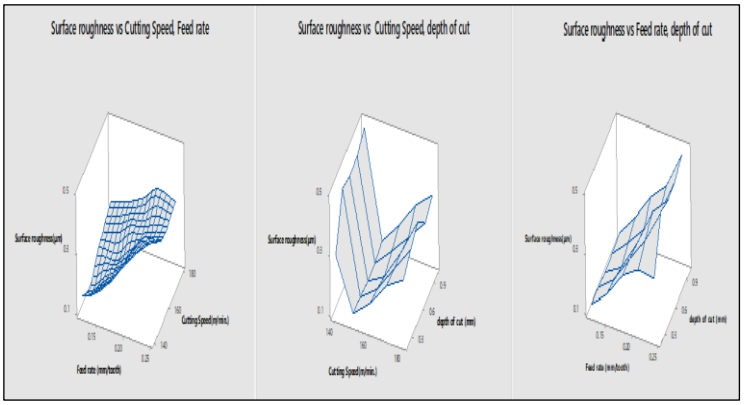

Figure 8: Interactive effect of process parameters on surface roughness
Source: Authors, (2025).

Here MOGA tools have been used for multi-objective optimization. The optimum combination of end milling process parameters of eighteen non-dominated Pareto optimal solutions achieved through MOGA is shown in Table 5.

Table 5: Non-dominated Pareto optimal solution

Sr No.	Cutting speed(m/min)	Feed rate (mm/tooth)	DOC (mm)	MOGA Surface roughness (µm)	MOGA Machining time (Sec.)
1	180.00	0.24	0.2	0.39	1.46
2	180.00	0.14	0.2	0.14	2.45
3	180.00	0.18	0.2	0.23	2.11
4	180.00	0.12	0.2	0.08	2.67
5	180.00	0.14	0.2	0.14	2.45
6	180.00	0.21	0.2	0.31	1.80
7	180.00	0.21	0.2	0.31	1.77
8	180.00	0.13	0.2	0.11	2.59
9	180.00	0.19	0.2	0.26	1.96
10	180.00	0.15	0.2	0.16	2.36
11	180.00	0.18	0.2	0.23	2.11
12	180.00	0.24	0.2	0.39	1.46
13	180.00	0.16	0.2	0.19	2.24
14	180.00	0.12	0.2	0.08	2.67
15	180.00	0.23	0.2	0.37	1.54
16	179.99	0.22	0.2	0.34	1.68
17	179.99	0.22	0.2	0.33	1.70
18	180.00	0.16	0.2	0.20	2.23

Source: Authors, (2025).

The relation between the number of individuals and the score is shown in Fig. 9 which gives the range of minimum and maximum values of surface roughness and machining time related to the constraint function.

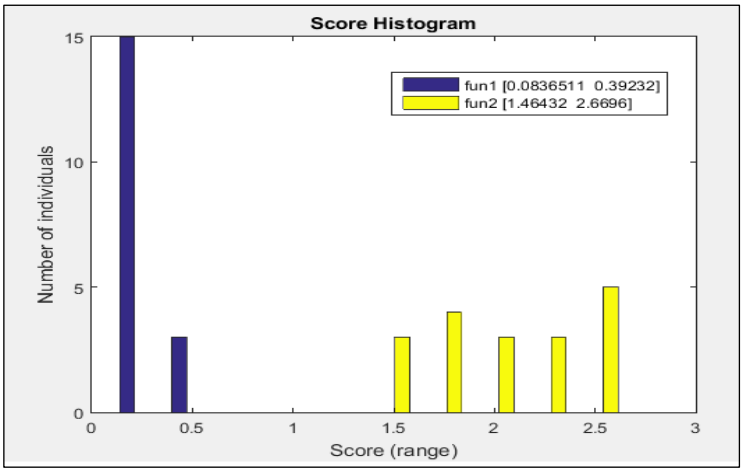

Figure 9: Score Histogram chart.
Source: Authors, (2025).

The minimum and maximum values of surface roughness are 0.0836511 and 0.39232. The minimum and maximum values of machining time are 1.46432 and 2.6696. The Pareto optimal front chart for surface roughness and machining time is shown in Fig.10.

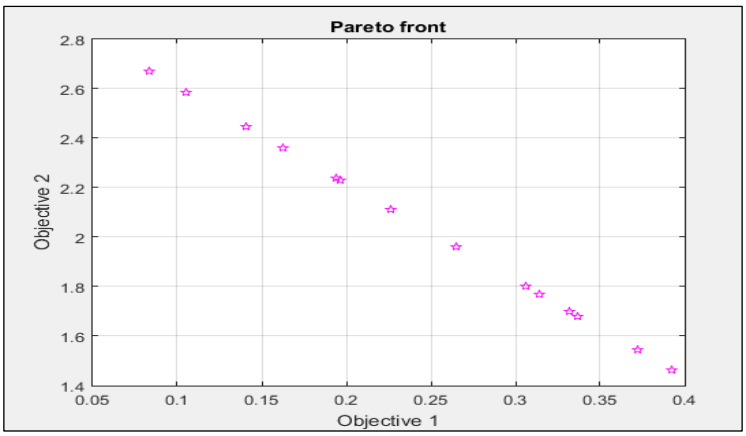

Figure 10: Pareto optimal front chart.
Source: Authors, (2025).

The achieved one set of optimized cutting parameters shown in serial numbers 3 and 11 in Table 5 gives better results of responses so that it is validated through experimentation. One set of experiments has been conducted for validation of the MOGA results. It has been found the percentage of error for surface roughness is 4.17% and the machining time is 3.65%. Fig.11 indicated a good agreement between MOGA and experimental results.

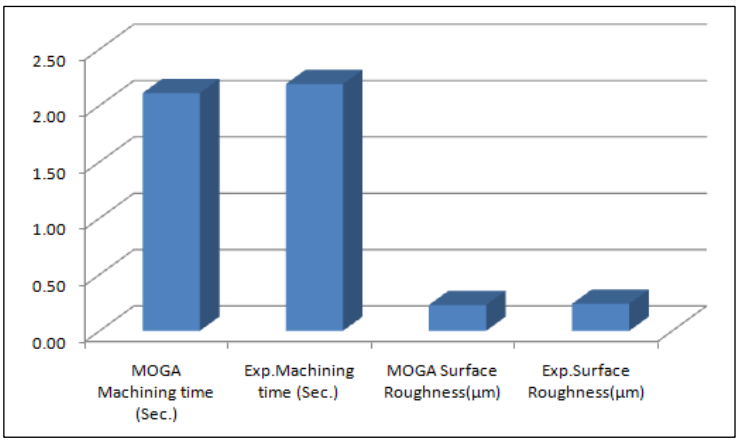

Figure 11: Multi-objective genetic algorithm Vs. Experimental result
Source: Authors, (2025).

These multi-objective optimization approaches provide the optimum cutting conditions for consequent values of responses. It has been observed that all the solutions generated by the MOGA tool are good. The preference for the selection of Pareto optimal solutions depends upon the needs of industries.

V. CONCLUSIONS

The multi-objective genetic algorithm approaches utilized for multi-objective optimization based on regression equations, have been found very useful techniques in industries. Multi-objective genetic algorithm based Pareto optimal designs approach gave the optimal solution with minimum surface roughness and machining time. It has been found average accuracy of 95.83% for surface roughness and 96.35% for machining time. Good concurrence has been found between multi-objective optimization results with experimentation. This indicates that a multi-objective genetic algorithm can be effectively used to find the optimum combination of machining parameters for end milling operation. The results of this study are to improve the productivity of products and very helpful in manufacturing industries to reduce the cost, time and number of trials.

VI. AUTHOR'S CONTRIBUTION

Conceptualization: Jignesh G. Parmar, Komal G. Dave and Mehul G. Mehta.
Methodology: Jignesh G. Parmar, Komal G. Dave and Mehul G. Mehta.
Investigation: Jignesh G. Parmar, Komal G. Dave and Mehul G. Mehta.
Discussion of results: Jignesh G. Parmar, Komal G. Dave and Mehul G. Mehta.
Writing – Original Draft: Jignesh G. Parmar, Komal G. Dave and Mehul G. Mehta.
Writing – Review and Editing: Jignesh G. Parmar, Komal G. Dave and Mehul G. Mehta.
Resources: Jignesh G. Parmar, Komal G. Dave and Mehul G. Mehta.
Supervision: Jignesh G. Parmar, Komal G. Dave and Mehul G. Mehta.
Approval of the final text: Jignesh G. Parmar, Komal G. Dave and Mehul G. Mehta.

VII. ACKNOWLEDGMENTS

I express my deep sense of gratitude and thanks to the reviewers and editor-in-chief of ITEGAM-JETIA for providing me this opportunity to publish my work..

VIII. REFERENCES

[1] Nurhaniza, M., Ariffin, M. K. A. M., Mustapha, F., & Baharudin, B. T. H. T. Analyzing the Effect of Machining Parameters Setting to the Surface Roughness during End Milling of CFRP-Aluminium Composite Laminates. International Journal of Manufacturing Engineering, 2016, 1–9. https://doi.org/10.1155/2016/468038.

[2] Coelho, R. T., De Souza, A. F., Roger, A. R., Rigatti, A. M. Y., & De Lima Ribeiro, A. A. A mechanistic approach to predict real machining time for milling free-form geometries applying high feed rate. International Journal of Advanced Manufacturing Technology, 2010; 46(9–12), 1103–1111. https://doi.org/10.1007/s00170-009-2183-8.

[3] C. C.Tsao, C.C. Grey-Taguchi method to optimize the milling parameters of aluminum alloy. International Journal of Advanced Manufacturing Technology, 2009; 40(1–2), 41–48. https://doi.org/10.1007/s00170-007-1314-3.

[4] Moshat, S., Datta, S., Bandyopadhyay, A., & Pal, P. Parametric optimization of CNC end milling using entropy measurement technique combined with grey-Taguchi method. International Journal of Engineering, Science and Technology, 2010; 2(2), 1–12. https://doi.org/10.4314/ijest.v2i2.59130.

[5] Pang, J. S., Ansari, M. N. M., Zaroog, O. S., Ali, M. H., & Sapuan, S. M. Taguchi design optimization of machining parameters on the CNC end milling process of halloysite nanotube with Aluminium reinforced epoxy matrix (HNT/Al/Ep) hybrid composite. Housing and Building National Research Center Journal, 2014; 10(2), 138–144. https://doi.org/10.1016/j.hbrcj.2013.09.007.

[6] Ajith Arul Daniel, S., Pugazhenthi, R., Kumar, R., &Vijaya. Multi-objective prediction and optimization of control parameters in the milling of aluminum hybrid metal matrix composites using ANN and Taguchi-grey relational analysis. Defence Technology, 2019; 15(4), 545–556. https://doi.org/10.1016/j.dt.2019.01.001

[7] Sreenivasulu, R., Srinivasa Rao, C., & Ravindra, K. Grey-based taguchi approach integrated with entropy measurement for optimization of surface roughness and delamination damage factor during end milling of GFRP composites. International Journal of Modern Manufacturing Technologies, 2019; 11(2), 133–141.

[8] Jebaraj, M., Pradeep Kumar, M., Yuvaraj, N., & Mujibar Rahman, G. Experimental study of the influence of the process parameters in the milling of Al6082-T6 alloy. Materials and Manufacturing Processes, 2019; 34(12), 1411–1427. https://doi.org/10.1080/10426914.2019.1594271.

[9] Shaik, J. H., & Srinivas, J. Optimal design of spindle tool system for improving the dynamic stability in the end-milling process, Sadhana - Academy Proceedings in Engineering Sciences, 2020; 45(1). https://doi.org/10.1007/s12046-020-1286-7

[10] Menderes Kam, Mustafa derimtas. Analysis of tool vibration and surface roughness during turning process of tempered steel samples using Taguchi method, Journal of Process Mechanical Engineering, 2021; 5(235), https://doi.org/10.1177/09544089211001976.

[11] Daniyan, I. A., Tlhabadira, I., Mpofu, K., &Adeodu, A. O. Process design and optimization for the milling operation of aluminum alloy (AA6063 T6). Materials Today: Proceedings, 2021; 38(1016), 536–543. https://doi.org/10.1016/j.matpr.2020.02.396.

[12] R K Jain, Production Technology, Khanna Publishers, Seventeenth addition; 2001.

Journal of Engineering and Technology for Industrial Applications

ISSN ONLINE: 2447-0228

ITEGAM-JETIA

Manaus, v.11 n.54, p. 168-176. July/August., 2025.
DOI: https://doi.org/10.5935/jetia. v11i54.1706

RESEARCH ARTICLE OPEN ACCESS

LITERATURE REVIEW ON MECHANICAL PROPERTIES AND BEHAVIOR OF ALUMINUM METAL MATRIX COMPOSITE MATERIAL WITH DIFFERENT PROCESSES

Jignesh G. Parmar[1], Mehul G. Mehta[2], Nital P. Nirmal[3]

[1,2,3]Gujarat Technological University

[1]http://orcid.org/0000-0002-8533-8304, [2]http://orcid.org/0009-0002-2219-0848, [1]http://orcid.org/0000-0002-8657-4253

E-mail: jiger.mechanical1@gmail.com, mgmehta@mech.ssgec.ac.in, nital.nirmal@gmail.com

ARTICLE INFO

Article History
Received: March 13, 2025
Revised: April 20, 2025
Accepted: June 15, 2025
Published: August 31, 2025

Keywords:
Composite material,
Metal matrix,
Reinforcement,
Mechanical properties,
Processing technique.

ABSTRACT

This literature review studies the development, characterization, and applications of Aluminum Metal Matrix Composites (AMMCs). Focusing on different types of reinforcement materials with their processing techniques, mechanical properties, and performance in various applications. Aluminum Metal Matrix Composites (AMMCs) have garnered significant attention due to their superior mechanical properties, including lightweight, high strength, corrosion resistance, and excellent wear properties. These composites consist of aluminum alloys as the matrix material, reinforced with various ceramic particles. Reinforcements such as silicon carbide (SiC), iron oxide (Fe_3O_4), boron carbide (B4C), alumina (Al_2O_3), and graphite have been extensively studied to enhance the properties of aluminum alloys.

Copyright ©2025 by authors and Galileo Institute of Technology and Education of the Amazon (ITEGAM). This work is licensed under the Creative Commons Attribution International License (CC BY 4.0).

I. INTRODUCTION

Composite materials play an important role in human life for many years of their capability to infrastructure and continue to enable developments in modern technology [1]. In base materials, many issues have been generated including with corrosion, wear resistance, weight, etc. A composite material is a prepared artificially with combination of two or more materials. The different parts are separated by specific boundaries [2]. The various advantages of the use of composites materials such as, increase the stiffness, strength, toughness and other mechanical and electrical properties.

The composites materials reveal better uses in industries such as automobile, aerospace, sports, defense, medical etc.. Many problems have been resolved due to the improved chemical, mechanical, physical, and thermal features of composite materials. Two phases of composites have been used such as reinforcement and matrix [3]. This literature review summarizes the work of several researchers on the fabrication, mechanical properties, and applications of Metal matrix composites (MMCs), focusing on different reinforcement materials, fabrication techniques, and performance evaluation. Aluminum matrix. Composites (AMCs) have gained considerable attention in various engineering applications due to their enhanced mechanical properties. Reinforcements like silicon carbide (SiC), alumina (Al_2O_3), boron carbide (B4C), and others have been employed to improve the mechanical and corrosion properties of aluminum alloys. This paper studies on the effects of different reinforcements and processing techniques on the properties of AMCs.

II. METHODOLOGY

The literature survey was carried out as a part for development of this research paper. In this paper studied of different manufacturing processes, properties and behavior of aluminum metal matrix composites. The research work done by researchers on aluminum metal matrix composite materials. This literature review gives a strong establishment for the current study and may reveal its

importance for future investigation also. The research depend on references from various national and international journals, books, articles and websites.

III. LITERATURE REVIEW

Srivatsan et al. (1991) explored processing methods for aluminum-based particulate MMCs, emphasizing the influence of matrix composition and reinforcement characteristics on the material's microstructure. This study helped clarify the role of processing techniques in achieving desired properties in engineered MMCs [4]. Doel & Bowen et al. (1993) studied particulate-reinforced aluminum MMCs using SiC as reinforcement. Their work compared the mechanical properties of composites with coarse and fine SiC particles, finding that finer particulates improved ductility, while coarser particles provided better toughness [5]. Pradeep K. Rohatgi (1993) reviewed the global surge in metal-matrix composite (MMC) research, particularly focusing on cast metal-matrix particulate composites. The study emphasized that MMCs can offer specific technical properties that traditional materials cannot achieve, provided that the relative quantities and distributions of the components are managed carefully during manufacturing. Various manufacturing techniques were examined, revealing that in alloys like Al-Si, the eutectic and primary silicon tend to concentrate on the surface of the particle or fiber. Two critical factors generating interest in MMCs include heterogeneous nucleation of the primary phase on reinforcing particles (e.g., graphite, SiC) and particle entrapment during solidification [6]. Surappa (2003) explored the versatility of aluminum matrix composites (AMCs) and the role of ceramic reinforcements (whiskers, particles, fibers) in enhancing their mechanical, thermal, and tribological properties.

The study emphasized the adaptability of AMCs to meet industrial demands by selecting appropriate matrix-reinforcement combinations. AMCs have been studied for over three decades, with a significant body of knowledge accumulated regarding their properties and applications [7]. Natarajan et al. (2006) studied the wear behavior of LM25/SiC composites in brake shoe applications. The results indicated that the AMC showed superior wear resistance compared to grey cast iron, and the coefficient of friction increased with sliding velocity [8]. Montoya Davila et al. (2007) explored the impact of particle size distribution on the hardness and fracture toughness of Al/SiCp composites. Their findings suggested that both microhardness and fracture toughness behaved parabolically with an increase in particle-size distribution [9]. Hajjari et al. (2008) examined the impact of squeeze casting on the microstructure and tensile properties of 2024 aluminum alloy. The results showed that squeeze casting refined the microstructure, reduced porosity, and increased the ultimate tensile strength due to faster cooling and increased squeeze pressure [10]. Cheng et al. (2008) studied the preparation and deformation behavior of silicon carbide (SiC)-reinforced aluminum 6066 composites fabricated by powder metallurgy. The SiC particles were evenly distributed, and failure modes such as particle cracking and ductile tearing at the interface were observed, with the deformation behavior heavily dependent on the matrix alloy [11]. Tan & Mohamad (2009) focused on the artificial aging of Al6061-T6, determining optimal temperature and time for maximum hardness [12]. Wahab et al. (2009) developed aluminum metal matrix composites (AMMCs) reinforced with aluminum nitride (AIN) using a permanent stainless-steel mold and a graphite crucible. They observed that AIN particles were well distributed around primary silicon grains and other structures. Hardness tests showed an increase in hardness, indicating that AIN reinforcement significantly improved the material properties [13]. E. Bayraktar et al. (2010) developed an aluminum matrix composite reinforced with iron oxide (Fe_3O_4) to enhance conductivity and magnetic permeability.

They employed microwave sintering to produce a well-distributed reinforcement within the aluminum matrix, achieving greater density compared to conventional sintering [14]. Ramesh et al. (2010) noted the combined effect of adhesion, abrasion, and delamination in increasing wear rates at higher loads [15]. Ibrahim Sahin et al. (2010) analyzed the mechanical properties and microstructures of SiCp-reinforced $AlSi_7Mg_2$ matrix composites, which were produced by squeeze and gravity casting methods and T6 heat-treated. They found that squeeze casting led to more refined microstructures and improved mechanical properties, while gravity casting produced non-homogeneous distributions due to slow cooling [16]. Katica Milos et al. (2011) investigated the incorporation of Al_2O_3 ceramic particles into aluminum using powder metallurgy. They found that while low Al_2O_3 concentrations resulted in uniform particle distribution, higher concentrations led to particle agglomeration, which reduced hardness [17]. S. M. Suresh et al. (2011) investigated LM25 aluminum alloy MMCs reinforced with micro and nano Al_2O_3 particles.

Their findings suggested that stir casting is a viable method for manufacturing nanoparticle-reinforced MMCs, with nanocomposites exhibiting slightly better tensile strength and hardness than their micro Al_2O_3 counterparts [18]. Neelima Devi et al. (2011) explored the mechanical and corrosion behavior of aluminum-silicon carbide (SiC) composites. They found that the composite material exhibited a significantly better weight-to-strength ratio (almost three times greater than mild steel) and was lighter than pure aluminum. The maximum tensile strength was achieved at a 15% SiC ratio, demonstrating that the aluminum-SiC composite is both stronger and lighter than pure aluminum [19]. A. Chennakesava Reddy (2011) analyzed the mechanical behavior of Al/Sic Metal Matrix Composites using Taguchi's methods. His study showed that the volume fraction of SiC and the type of aluminum alloy used (Al 6061, Al 6063, and Al 7072) significantly affected the yield strength, ultimate tensile strength, and ductility of the composites [20]. Anoop Kumar Tuli et al. (2021) explored the effects of thixocasting and gravity casting on LM25-10wt% SiC composites. Thixocasting enhanced the composite's mechanical properties, showing improved tensile, compressive, and flexural strengths when compared to gravity casting. SEM analysis revealed particle shearing as the primary fracture mechanism in this cast samples [21].

Nrip Jite et al. (2011) compared the porosity and density of A384.1 MMCs reinforced with SiC particles. They found that changes in particle size and reinforcement percentage significantly affected the density and porosity of the composites. Specifically, the highest density was observed at 2490 gm/cm³ for a SiC content of 0.08, with a particle size of 0.106 m, and the highest porosity was recorded at 3.25% for a SiC content of 0.10 [22]. R. Kartigeyan et al. (2012) studied Al 7075 alloy reinforced with short basalt fibers, finding that the composite exhibited significant improvements in hardness, yield strength, and ultimate tensile strength, particularly with 6% basalt fiber [23]. G. G. Sozhamannan et al. (2012) studied the impact of processing temperatures and holding times on the mechanical properties and particle distribution in Al-SiCp MMCs. They observed that processing at higher temperatures and longer holding times resulted in improved strength, although excessive holding time led to reduced ultimate strength [24]. Ali Mazahery et al. (2012) studied the effect of SiC nanoparticles on the mechanical properties of A356 alloys, finding that the addition of SiC nanoparticles significantly enhanced

hardness, yield strength, and ultimate tensile strength. The composites exhibited small porosity and a uniform distribution of SiC nanoparticles [25]. Mohsen Ostad Shabani et al. (2012) focused on the A356 matrix reinforced with B4C particulates. They found that B4C particles were evenly dispersed along dendritic branches, and the composites showed enhanced mechanical properties, such as higher strain hardening and ultimate tensile strength compared to unreinforced alloys. They also employed an artificial neural network (ANN) and finite element method to model the mechanical properties [26]. Pargunde et al. (2013) employed a stir casting technique to fabricate aluminum-based silicon carbide (AlSiC) composites, highlighting the two-step mixing process's role in enhancing composite properties such as hardness and impact strength with increasing SiC content [27].

Gurvishal Singh et al. (2013) explored the use of red mud, SiC, and Al_2O_3 as reinforcements in aluminum MMCs. Their findings highlighted that red mud could replace more expensive reinforcements like SiC and Al_2O_3, providing a cost-effective alternative without compromising wear resistance and hardness [28]. Tahamtan et al. (2013) fabricated Al206/5vol. % Al_2O_3 composites through an injection process in which reinforcing particles were added to molten Al. Their study showed that the inclusion of Al_2O_3 particles resulted in improved distribution and incorporation of particles, enhancing the tensile properties of the composite [29]. Sharanabasappa R. Patil (2013) examined the mechanical properties of LM25 composites reinforced with fly ash and alumina. The study showed that increasing the percentage of Al_2O_3 enhanced the hardness of the composites, though it reduced elongation and ductility, highlighting a trade-off between hardness and ductility [30]. Bhaskar Chandra Kandpal et al. (2014) reviewed the various technologies for producing metal matrix composites (MMCs). These include liquid and solid-state techniques such as stir casting, powder metallurgy, and metal injection molding. The review emphasized the importance of cost-effectiveness, productivity, and the development of new processes like mechanical alloying and continuous binder powder coating to meet industrial requirements for MMCs [31]. Akhilesh Jayakumar (2014) examined the properties of LM25-based metal matrix composites, where SiC served as reinforcement. Composites were processed via centrifugal casting, and microstructural studies showed significant improvements in mechanical properties with SiC reinforcement [32]. L. Bolzoni et al. (2014) focused on grain refinement of Al-Si alloys using Nb–B inoculation.

Their study demonstrated that the addition of Nb–B inoculants effectively refined the primary α-Al dendrites in alloys like LM24 and LM25, reducing the grain size significantly. This refinement was particularly beneficial for casting processes that depend on cooling rates [33]. S. Kumar et al. (2015) applied grey relational analysis to optimize machining parameters, such as peak current and pulse on time, in wire electrical discharge machining (WEDM) of aluminum-based composites. Their study showed that reinforcement particles increased surface roughness, with longer pulse durations exacerbating this effect [34]. Mikhail Tashkinov (2015) developed a statistical technique to simulate the phase-level elastic fields of multiphase composites with SiC reinforcement. His study explored the microstructural behavior of TiC+SiC and Al+SiC metal matrix composites (MMCs). He analyzed how variations in microstructure influenced stress-strain fields, demonstrating the role of microstructural characteristics in affecting the mechanical properties of MMCs [35]. Svetlana Boshnakova et al. (2015) focused on stainless steel-based MMCs reinforced with silica and titanium, targeting high wear-resistant applications. The study explored microhardness, wear resistance, and roughness of MMCs, revealing improvements in wear resistance and hardness compared to the base steel. This work highlights the potential of TiC and SiC as reinforcement materials for wear-resistant composites [36].

Gyanendra Singh et al. (2015) studied the use of different metals (Mg, Zn) in aluminum matrix composites to produce high-strength, lightweight materials. The combination of these metals with Al_2O_3 reinforcement showed improvements in hardness, tensile strength, and impact strength. The study also highlighted the cost-effective nature of traditional casting processes in manufacturing such composites [37]. Biswajit Das et al. (2015) fabricated an in-situ multi-component reinforced aluminum copper alloy-based metal matrix composite using flux-assisted synthesis (FAS) and investigated its machining properties. The study revealed that cutting speed and depth of cut significantly influenced cutting force, and the predicted values for surface roughness and cutting force were in close agreement with experimental results, suggesting the effectiveness of regression analysis for optimization [38]. S. A. Mohan Krishna et al. (2015) highlighted the benefits of hybrid MMCs, including enhanced thermal conductivity and lower thermal expansion coefficients. They also discussed the potential for using Al/SiC/Graphite hybrid composites in aerospace applications [39]. Vishnu Prasad K et al. (2015) examined the effect of stirring speed during the stir casting process, noting that higher mold rotation speeds improved mechanical and tribological properties, reducing volume loss and enhancing wear resistance [40]. V. Vembu et al. (2015) utilized response surface methodology to optimize heat treatment for 8011 Al/15% SiCp metal matrix composites, improving tensile strength and ductility. They observed that solutionizing time had the most significant impact on tensile strength, with a peak increase in tensile strength under peak-aged conditions [41]. M.J. Shen et al. (2015) investigated the microstructure and tensile properties of AZ31B magnesium matrix composites reinforced with SiC particles.

Their findings indicated that SiC reinforcement refined the grain structure of the magnesium matrix, leading to improved tensile strength and yield strength [42]. Radhika N. (2015) conducted an extensive study on LM25/SiC/ Al_2O_3 composites, fabricated using a liquid metallurgy technique. The composites were reinforced with varying amounts of SiC and Al_2O_3 (0 to 30 wt%). Tensile and hardness tests showed an increase in mechanical properties with higher reinforcement contents, particularly at 10 wt% of SiC and Al_2O_3. Wear tests using a pin-on-disc tribometer revealed that the wear rate decreased as the reinforcement percentage increased, and the coefficient of friction increased with the applied load [43]. Venkatesh et al. (2015) used powder metallurgy to fabricate Al/SiCp composites and observed an increase in density and hardness with rising sintering temperature [44]. Pardeep Sharma et al. (2015) explored the microstructure of Al6082 matrix composites reinforced with graphite (Gr) particles. Through a traditional stir casting method, they studied the effect of Gr content (ranging from 0% to 12%) on the microstructure of the composites. Scanning electron microscopy (SEM) and X-ray diffraction (XRD) analyses revealed that the microstructure of cast Al6082 consists of a dendritic aluminum network and a silicon-aluminum eutectic network. Increased Gr content led to non-uniform particle distribution and the formation of impurities, resulting in a decrease in the hardness of the composites [45]. Venkatachalam G et al. (2015) investigated the microstructure and mechanical properties of modified LM25 aluminum alloy reinforced with zirconium (Zr) particles. Microstructural analysis revealed a homogeneous distribution of Zr particles, with fewer voids and porosity. The mechanical properties, such as hardness and tensile strength, improved with increasing Zr content. The study also highlighted the importance of stirring parameters and particle soaking before adding to the matrix [46]. Sri

Priya R et al. (2016) developed aluminum 6061 composites for aerospace by reinforcing them with silicon carbide (SiC) and alumina (Al_2O_3). Their results indicated improved yield and ultimate tensile strength with higher reinforcement percentages, although elongation decreased [47]. Anthony Xavior M et al. (2016) focused on the machinability of hybrid aluminum-based MMCs, noting that reinforcement type and distribution influenced cutting forces, tool wear, and surface roughness during machining processes [48]. A. Arora et al. (2016) worked on the fabrication of aluminum-molybdenum (Al-Mo) composites using the friction stir process (FSP). Their findings showed a homogeneous dispersion of Mo particles in the Al matrix, resulting in a significant increase in Vickers microhardness, showcasing the effectiveness of FSP in improving mechanical properties [49].

Anil Kumar Bodukuri et al. (2016) prepared Al-SiC-B4C metal matrix composites using powder metallurgy. The addition of boron carbide (B4C) was found to significantly increase microhardness, with the composite showing uniform particle distribution. This work demonstrated the potential of sintering as a technique to enhance the properties of aluminum composites [50]. N. Venkat Kishore et al. (2016) studied A356/LM25 aluminum alloys reinforced with boron carbide (B4C), finding that the mechanical properties of the composites, including tensile strength and hardness, improved with increasing boron carbide content [51]. N. Radhika (2016) developed homogeneous and functionally graded LM25 aluminum composites by incorporating silicon nitride (Si_3N_4) particles through liquid metallurgy and centrifugal casting. The microstructure of the composites showed uniform dispersion of Si_3N_4 in the homogeneous composite, while the centrifugal casting led to particle segregation, with a particle-enriched outer surface and a depleted inner region. The functionally graded composite exhibited reduced wear rates, especially at low loads [52]. Siddanna Awarasang et al. (2016) investigated the microstructure and impact strength of LM25 aluminum alloy reinforced with steel wire. The results showed good bonding between the steel wire and the aluminum matrix.

The impact strength of the composite significantly improved, and the proper bonding was confirmed through optical microscopy, which showed no voids in the bonding areas [53]. S. Venkatesan et al. (2016) investigated the mechanical behavior of aluminum metal matrix composites (AMMCs) reinforced with graphene particles using the stir casting method. Their findings indicated that graphene reinforcement at various weight fractions (0.33%, 0.55%, 0.77%) altered the microstructure, with broken dendritic grains leading to improved properties such as tensile and hardness strength. The presence of eutectic Si particles in stir-cast samples was observed as globular, unlike in the base matrix [54]. Juhi Mishra et al. (2017) examined various fabrication methods for MMCs, addressing challenges in the wetting of reinforcing phases during casting. The review discussed liquid phase processes, solid-liquid processes, and other methods, highlighting the potential of MMCs in industries like automotive and aerospace, despite the high costs of production [55]. Girija Moona et al. (2017) provided a retrospective review of AMMCs, highlighting their increased hardness, toughness, and wear resistance compared to unreinforced aluminum. They discussed challenges such as machinability, high cost of nano-reinforcements, and difficulties in secondary processing, which hinder broader industrial applications [56]. Arvind Sankhla et al. (2017) compared the advantages of MMCs over polymer-based composites, citing superior strength, stiffness, and wear resistance. They advocated for powder metallurgy as an efficient technique for MMC production, particularly with reinforcements like silicon carbide and aluminum oxide [57].

Chowda Reddy et al. (2017) investigated the use of centrifugal casting for fabricating aluminum alloy MMCs with Al2O3 reinforcement. Their results showed that increasing mould rotation speed improved hardness and wear resistance, particularly at 1500 rpm, due to the better distribution of Al_2O_3 particles [58]. Dhanasekaran R et al. (2017) studied the hardness of A356 aluminum composites reinforced with SiC, graphite, and alumina. They found that increasing SiC content improved hardness, but excessive amounts led to a reduction, highlighting the importance of optimal reinforcement levels [59]. Rajan Verma et al. (2017) analyzed the mechanical properties of Al356 composites reinforced with SiC and alumina. They found that the yield strength and ultimate tensile strength increased with reinforcement content, likely due to the dispersion of SiC and alumina particles that hindered dislocation movement [60]. T. Somasekhar et al. (2018) reviewed properties and processing of silicon carbide particulate MMCs based on aluminum. Their research suggested a two-step stir casting technique to achieve uniform dispersion of the ceramic material, resulting in enhanced tensile strength, impact strength, and hardness for the composite compared to the base aluminum alloy [61].

S. Mohamed Hussain et al. (2018) optimized machining parameters for stir-cast Al-B4C reinforced MMCs. They found that lower B4C content (10–15%) yielded the best results, with the study focusing on performance factors such as material removal rate, cutting force, and surface roughness during milling [62]. Pranav Dev Srivyas et al. (2018) reviewed the mechanical and tribological behavior of aluminum matrix composites (AMCs) reinforced with various materials. Their research emphasized the impact of reinforcement type, size, and percentage on mechanical properties, and explored the factors influencing wear performance in different environmental conditions [63]. Mudasar Pasha B.A. et al. (2018) provided a review of aluminum metal matrix composites, focusing on the processing techniques, characterization, and advancements in manufacturing. Stir casting, powder metallurgy, and other techniques are discussed, with a special emphasis on factors such as reinforcement size, stirring speed, and temperature, which influence the mechanical properties and quality of the composites. The review also highlights the role of processing parameters in reducing porosity and producing defect-free composites [64]. Kawaljitsingh Randhawa et al. (2018) reviewed fabrication challenges in MMCs, including issues with casting, fiber orientation, and reinforcement bonding. They proposed solutions such as coating reinforcement elements to improve wettability and bonding, which are crucial for successful composite fabrication [65].

M. Pasupathi et al. (2018) explored the gravity die casting process to analyze the microstructure and mechanical properties of LM25 alloy with AC4B Nano-Composite. They found that the LM25 alloy had loosely packed grains, which led to porosity and shrinkage faults. The addition of C4B in the AC4B alloy refined the grain structure, improving mechanical properties like tensile strength and hardness. The presence of nanocomposite particles significantly enhanced these properties [66]. Venkata Reddy et al. (2018) investigated the mechanical properties of A7075 aluminum reinforced with a hybrid matrix of silicon carbide (SiC) and fly ash. Their findings showed improvements in hardness and deformation characteristics and a clear interfacial bonding between matrix and reinforcements. X-ray diffraction (XRD) and Energy Dispersive X-ray (EDX) analyses confirmed the presence of silica and alumina phases [67]. Arun Kumar Sharma et al. (2019) provided an overview of matrix materials used in MMCs, emphasizing the importance of continuous research and development to fully realize their potential in demanding applications [68]. Pulkit Garg et al. (2019) focused on the synthesis methods and mechanical properties of AMMCs. They emphasized powder metallurgy techniques for better control over microstructure and

interface properties. They also pointed out the limitations of stir casting for manufacturing nanocomposites due to poor nanoparticle distribution and excessive porosity [69]. A. Radha Krishnan et al. (2019) focused on Al-Zn- Al_2O_3 composites for piston analysis. They observed improved wear and hardness properties when reinforcing LM25 alloy with alumina and zinc, which may lead to significant design improvements in automotive pistons [70]. Karthikeyan Govindan et al. (2019) studied LM25/ZrO_2 composites fabricated via stir casting. The microstructural examination showed a fine distribution of ZrO_2 particles in the aluminum matrix, which enhanced the composite's mechanical properties. SEM and EDS analysis confirmed the lack of shrinkage and porosity in the castings, making them suitable for high-performance applications [71]. Chandru B.G. et al. (2020) focused on the development of Al7475/NbC reinforced metal matrix composites (MMCs) to enhance mechanical properties such as tensile strength, compression strength, and hardness.

By varying the particle size of NbC and reinforcement levels (2-8 wt%), they used the stir casting technique to fabricate the composites. The mechanical properties were significantly improved with increased NbC content. The ultimate tensile strength increased by 31.54%, yield strength by 34.70%, and compressive strength by 52.72% compared to the base Al7475 alloy. Additionally, hardness increased by 37.86%, attributed to the hard NbC particles enhancing resistance to indentation [72]. Ashrafi N. et al. (2020) investigated hybrid reinforcement composites (Al-Fe_3O_4-SiC) fabricated by powder metallurgy. The study found a 111% increase in surface hardness, with Al-30Fe_3O_4-20SiC showing the lowest coefficient of friction (COF) at 0.412. Furthermore, corrosion resistance improved with the hybrid reinforcement, with Al-30Fe3O4-20SiC exhibiting a corrosion protection efficiency of 99.83%, highlighting the hybrid composite's potential for durability and corrosion resistance [73]. Babu B et al. (2020) studied hybrid AMMCs reinforced with magnesium oxide (MgO) and graphite, focusing on their mechanical properties and machinability.

Using the TOPSIS method, they optimized processing parameters to achieve better material removal rates and lower overcut during microelectrochemical machining (micro ECM) [74]. Nithyanandhan T. (2020) focused on the tribological behavior of SiC and graphite-reinforced aluminum MMCs, reporting improvements in wear rates and fatigue resistance with increasing reinforcement content. The microstructure showed a uniform distribution of reinforcements, positively influencing mechanical properties [75]. Zeeshan Ahmad et al. (2020) studied the effect of Si3N4 reinforcement on the microstructure and mechanical properties of LM25 Al alloy composites. Using stir casting, they observed uniform dispersion of Si_3N_4 at lower percentages (4-8%), but clustering at higher percentages (12%). EDS and SEM analysis confirmed the presence of Si_3N_4 particles and their role as nucleating agents during solidification, leading to improved mechanical properties of the composite [76]. Sami Ullah Khan et al. (2021) reviewed in-situ synthesized Al 6061 alloy MMCs, noting that the distribution of reinforcement particles significantly affected mechanical and tribological properties. Proper reinforcement placement was key to enhancing material performance [77].

M.S. Ayar et al. (2021) reviewed advancements in aluminum MMCs, emphasizing these composites' material and energy savings potential. They discussed the challenges of achieving uniform reinforcement distribution and high processing costs, noting that innovations in aluminum-based MMCs (AMMHCs) hold promise for various engineering applications [78]. Rinku Datkhile et al. (2021) conducted a bibliometric analysis of research trends in MMCs reinforced with sustainably mined silica. Their work highlighted the growing interest in using agricultural waste for composite reinforcement, contributing to both economic growth and environmental sustainability [79]. Ramesh S. et al. (2021) studied the heat treatment of Al6061-AlB2 composites, finding significant improvements in hardness with increasing AlB2 content. The heat treatment process led to a supersaturated solution, which increased hardness, particularly when quenching in ice [80]. Shivaramakrishna A. et al. (2022) synthesized Fe_3O_4–Aluminum matrix composites and evaluated their mechanical and corrosion properties. They reinforced Al7075 with 2%, 4%, 6%, and 8% Fe_3O_4 using the stir casting technique. Their results showed that the tensile strength peaked at a 6% Fe_3O_4 reinforcement, with a 21.865% increase. The hardness was highest (47.53%) for 8% Fe_3O_4. Moreover, corrosion resistance improved significantly due to the presence of Al_3Fe intermetallic phases, which enhanced pitting corrosion resistance [81].

IV. CONCLUSIONS

The development and description of aluminum matrix composites (AMCs) have led to significant advancements in materials science. Researchers have focused on enhancing properties like strength, hardness, and corrosion resistance by varying reinforcement types, sizes, and percentages. Aluminum metal matrix composites have been recognised to be a versatile and favorable class of materials due to their enhanced mechanical and thermal properties. The combination of aluminum alloys with various reinforcements such as SiC, Al_2O_3, and hybrid materials, has shown significant performance improvements. The properties of these composites are influenced by factors such as the applied load, sliding velocity, and the type and volume of reinforcement used. Techniques such as stir casting, powder metallurgy, FSP, and centrifugal casting have produced high-performance of MMCs. Additionally, hybrid reinforcements and processing innovations continue to improve the performance and cost-effectiveness of AMCs for various industrial applications. Future research should focus on improving the processing techniques and strong bonding between the matrix and reinforcement, as well as exploring new composite materials for advanced industrial applications.

V. AUTHOR'S CONTRIBUTION

Conceptualization: Mehul G. Mehta, Jignesh G. Parmar, Nital P. Nirmal.
Methodology: Mehul G. Mehta, Jignesh G. Parmar, Nital P. Nirmal.
Investigation: Mehul G. Mehta, Jignesh G. Parmar, Nital P. Nirmal.
Writing – Original Draft: Mehul G. Mehta, Jignesh G. Parmar, Nital P. Nirmal.
Writing – Review and Editing: Mehul G. Mehta, Jignesh G. Parmar, Nital P. Nirmal.
Resources: Mehul G. Mehta, Jignesh G. Parmar, Nital P. Nirmal.
Supervision Mehul G. Mehta, Jignesh G. Parmar, Nital P. Nirmal.
Approval of the final text: Mehul G. Mehta, Jignesh G. Parmar, Nital P. Nirmal.

VII. REFERENCES

[1] Adel Mahamood Hassan, Abdalla Alrashdan, Mohammed, T. Hayajneh & Ahmad Turki Mayyas 2009, 'Prediction of density, porosity and hardness in aluminium-copper-based composite materials using artificial neural network', Journal of Materials Processing Technology, vol. 209, no. 2, pp. 894 899.

[2] Ali Mazahery & Mohsen Ostad Shabani 2012, 'Influence of the hard coated B4C particulates on wear resistance of Al-Cu alloys', Composites: Part B, vol. 43, no. 3, pp. 1302-1308.

[3] Hui-Hui Fu, Kyung-Seop Han & Jung-II Song 2004, 'Wear properties of Saffil/Al, Saffil/Al2O3/Al and Saffil/SiC/Al', Wear, vol. 256, no. 7-8, pp. 705-713.

[4] Srivatsan, T. S., Ibrahim, I. A., Mohamed, F. A., & Lavernia, E. J. (1991). Processing techniques for particulate-reinforced metal aluminium matrix composites. Journal of Materials Science, 26(22), 5965–5978. https://doi.org/10.1007/BF01113872.

[5] Doel, T. J. A., & Bowen, P. (1996). Tensile properties of particulate-reinforced metal matrix composites. Composites Part A: Applied Science and Manufacturing, 27(8 PART A), 655–665. https://doi.org/10.1016/1359-835X(96)00040-1.

[6] Rohatgi, P. K. (1993). Metal-matrix Composites I. Defence Science Journal (Vol. 43, Issue 4).

[7] Surappa, M. K. (2003). Aluminium matrix composites: Challenges and opportunities. SadhanaAcademy Proceedings in Engineering Sciences, 28(1–2), 319–334. https://doi.org/10.1007/BF02717141

[8] Natarajan, N., Vijayarangan, S., & Rajendran, I. (2006). Wear behaviour of A356/25SiCp aluminium matrix composites sliding against automobile friction material. Wear, 261(7–8), 812–822. https://doi.org/10.1016/j.wear.2006.01.011.

[9] Montoya-Dávila, M., Pech-Canul, M. A., & Pech-Canul, M. I. (2007). Microstructure and Mechanical Properties of Al/Sicp Composites with Multimodal Size Distribution of Reinforcements. Materials Science Forum, 560, 115–120. https://doi.org/10.4028/www.scientific.net/msf.560.115.

[10] Hajjari, E., & Divandari, M. (2008). An investigation on the microstructure and tensile properties of direct squeeze cast and gravity die cast 2024 wrought Al alloy. Materials and Design, 29(9), 1685–1689. https://doi.org/10.1016/j.matdes.2008.04.012.

[11] Cheng, N. P., Zeng, S. M., & Liu, Z. Y. (2008). Preparation, microstructures and deformation behavior of SiCP/6066Al composites produced by PM route. Journal ofMaterialsProcessingTechnology,202(1-3),27–40. https://doi.org/10.1016/j.jmatprotec.2007.08.044.

[12] Tan, C. F., & Said, M. R. (2009). Effect of hardness test on precipitation hardening aluminium alloy 6061-t6. Chiang Mai Journal of Science, 36(3), 276–286.

[13] Wahab, M. N., & Ghazali, M. (2009). Preparation and characterization of stir cast-aluminum nitride reinforced aluminum metal matrix composites Heat Transfer Mechanism on Coated Piston Crown for Spark Ignition Engine View project
synthesis ofsuperparamagnetic nanoparticles View project. https://www.researchgate.net/publication/265814754.

[14] Bayraktar, E., & Katundi, D. (2010). Development of a new aluminium matrix composite reinforced with iron oxide (Fe3O4). Journal of Achievements in Materials and Manufacturing Engineering (Vol. 38, Issue 1).

[15] Ramesh, C. S., Keshavamurthy, R., Channabasappa, B. H., & Pramod, S. (2010). Friction and wear behavior of Ni-P coated Si3N4 reinforced Al6061 composites. Tribology International, 43-3, 623-634. https://doi.org/10.1016/j.triboint.2009.09.011.

[16] Sahin, I., & Eker, A. A. (2011). Analysis of microstructures and mechanical properties of particle reinforced AlSi7Mg2 matrix composite materials. Journal of Materials Engineering and Performance, 20(6), 1090–1096. https://doi.org/10.1007/s11665-010-9738-6.

[17] Milos, K. (2011). Aluminium-Based Composite Materials In Construction Of Transport Means. PrometTraffic&Transportation (Vol. 23, Issue 2).

[18] Suresh, S. M., Mishra, D., Srinivasan, A., Arunachalam, R. M., & Sasikumar, R. (2011). Production and characterization of micro and nano Al2O3 particle-reinforced LM25 aluminium alloy composites. ARPN Journal of Engineering and Applied Sciences, 6(6), 94–98.

[19] Devi, N. C., & Professor, A. (2011). Mechanical characterization of Aluminium silicon carbide composite. In International Journal of Applied Engineering Research, Dindigul (Vol. 1, Issue 4).

[20] Reddy, A. C. (2011). Evaluation of Mechanical Behavior of Al-Alloy/SiC Metal Matrix Composites With Respect To Their Constituents Using Taguchi Techniques. I-Manager's Journal on Mechanical Engineering, 1(2), 33–43. https://doi.org/10.26634/jme.1.2.1405.

[21] Kumar Tuli, A., Singh, P., Das, S., Mondal, D. P., & Shakya, J. P. (2021). Analysis of microstructural, mechanical and thermal behaviour of thixocast LM25-10wt% SiC composite at different processing temperatures. Indian Academy of Sciences. https://doi.org/10.1007/s12046-021-01757-3S.

[22] Jit, N., Tyagi, A. K., Singh, N., & Singh, A. (2011). Comparison of porosity and density for (A384.1) 1-x [(Reinforcement) p] x MMC system using Adaptive Neuro-Fuzzy Inference system. Advances in Applied Science Research, 2(4), 240–250.

[23] Seetharaman, S., Karthigeyan, R., Ranganath, G., & Sankaranarayanan, S. (2012). Mechanical Properties and Microstructure Studies of Aluminium (7075) Alloy Matrix Composite Reinforced with Short Basalt Fibre. European Journal of Scientific Research (Vol. 68, Issue 4). http://www.europeanjournalofscientificresearch.com.

[24] Sozhamannan, G. G., Prabu, S. B., & Venkatagalapathy, V. S. K. (2012). Effect of Processing Paramters on Metal Matrix Composites: Stir Casting Process. Journal of Surface Engineered Materials and Advanced Technology, 02(01), 11–15. https://doi.org/10.4236/jsemat.2012.21002.

[25] Mazahery, A., & Shabani, M. O. (2012). Characterization of cast A356 alloy reinforced with nano SiC composites. Transactions of Nonferrous Metals Society of China (English Edition), 22(2), 275–280. https://doi.org/10.1016/S1003-6326(11)61171-0.

[26] Shabani, M. O., Mazahery, A., Rahimipour, M. R., & Razavi, M. (2012). FEM and ANN investigation of A356 composites reinforced with B4C particulates. Journal of King Saud University, Engineering Sciences, 24(2), 107–113. https://doi.org/10.1016/j.jksues.2011.05.001

[27] Pargunde, D. M., Gajanan, P., Thokal, N., Dhanraj, P., Tambuskar, P., Swapnil, M., Kulkarni, S., & Scholar, M. E. (2013). Development of Aluminium Based Metal Matrix Composite (AlSiC) 1 Address for Correspondence. In International Journal of Advanced Engineering Research and Studies.

[28] Singh, G., Lal, H., Singh, D., & Singh, G. (2013). An Approach for Improving Wear Rate of Aluminum Based Metal Using Red Mud, Sic And Al2O3Matrix Composites. In Int. J. Mech. Eng. & Rob. Res. www.ijmerr.com.

[29] Tahamtan, S., Halvaee, A., Emamy, M., & Zabihi, M. S. (2013). Fabrication of Al/A206-Al2O3 nano/micro composite by combining ball milling and stir casting technology. Materials and Design, 49, 347–359. https://doi.org/10.1016/j.matdes.2013.01.032.

[30] Mr.Sharanabasappa R Patil. (2013). A Study on Mechanical Properties of Fly Ash and Alumina Reinforced Aluminium Alloy (LM25) Composites. IOSR Journal of Mechanical and Civil Engineering, 7(6), 41–46. https://doi.org/10.9790/1684-0764146.

[31] Chandra Kandpal, B., Kumar, J., & Singh, H. (2014). Production Technologies of Metal Matrix Composite: A Review. International Journal of Research in Mechanical Engineering & Technology, 4(2).ISSN : 2249-5762. Vol. 4, Issue 2.

[32] Jayakumar, A., & Rangaraj, M. (2008). International Journal of Emerging Technology and Advanced Engineering Property Analysis of Aluminium (LM-25) Metal Matrix Composite. Certified Journal (Vol. 9001, Issue 2). www.ijetae.com

[33] Bolzoni, L., & Hari Babu, N. (2015). Refinement of the grain size of the LM25 alloy (A356) by 96Al-2Nb-2B master alloy. Journal of Materials Processing Technology, 222, 219–223. https://doi.org/10.1016/j.jmatprotec.2015.03.011.

[34] Suresh Kumar, S., Uthayakumar, M., Thirumalai Kumaran, S., Parameswaran, P., Mohandas, E., Kempulraj, G., Ramesh Babu, B. S., & Natarajan, S. A. (2015). Parametric optimization of wire electrical discharge machining on aluminium based composites through grey relational analysis. Journal of Manufacturing Processes, 20, 33–39. https://doi.org/10.1016/j.jmapro.2015.09.011.

[35] Tashkinov, M. (2017). Statistical methods for mechanical characterization of randomly reinforced media. Mechanics of Advanced Materials and Modern Processes, 3(1). https://doi.org/10.1186/s40759-017-0032-2.

[36] Boshnakova, S., Markovska, I., & Rusev, D. (2015). SiC and TiC Stainless Steel Based Metal Matrix Composites. Scientific Work for Russia University, 54(101), 14–18. http://conf.uniruse.bg/docs/cp15/10.1/10.1-2.

[37] Singh, G., & Giri, T. (2015). Fabrication of Aluminum/Magnesium Composite Material and Optimization their Mechanical Properties. In International Journal of Science and Research (IJSR) ISSN. www.ijsr.net

[38] Das, B., Roy, S., Rai, R. N., & Saha, S. C. (2016). Development of an in-situ synthesized multi-component reinforced Al–4.5%Cu–TiC metal matrix composite by FAS technique – Optimization of process parameters. Engineering Science and Technology, an International Journal, 19(1), 279–291. https://doi.org/10.1016/j.jestch.2015.08.002.

[39] Krishna, S. A. M., Shridhar, T. N., & Krishnamurthy, L. (2015). Evaluation and Examination of Volume Fraction, Porosity, Microstructure and Computational Modeling of Hybrid Metal Matrix Composites to Reveal the Hea. International Journal of Materials Science and Engineering, 3(3), 231–243. https://doi.org/10.17706/ijmse.2015.3.3.231-243.

[40] Vishnu Prasad, K., & Jayadevan, K. R. (2016). Simulation of Stirring in Stir Casting. Procedia Technology, 24, 356–363. https://doi.org/10.1016/j.protcy.2016.05.048.

[41] Vembu, V., & Ganesan, G. (2015). Heat treatment optimization for tensile properties of 8011 Al/15% SiCp metal matrix composite using response surface methodology. Defence Technology, 11(4), 390–395. https://doi.org/10.1016/j.dt.2015.03.004.

[42] Shen, M. J., Wang, X. J., Zhang, M. F., Zhang, B. H., Zheng, M. Y., & Wu, K. (2015). Microstructure and room temperature tensile properties of 1 μm-SiCp/AZ31B magnesium matrix composite. Journal of Magnesium and Alloys, 3(2), 155–161. https://doi.org/10.1016/j.jma.2015.03.001.

[43] Radhiks N. (2015). Mechanical properties and tribological behaviour of LM25_SiC_Al2O3 composites. Journal of Engineering Science and Technology. 10(2):134-144.

[44] Venkatesh, B., & Harish, B. (2015). Mechanical Properties of Metal Matrix Composites (Al/SiCp) Particles Produced By Powder Metallurgy. International Journal of Engineering Research and General Science, 3(1). www.ijergs.org.

[45] Sharma, P., Sharma, S., & Khanduja, D. (2015). A study on microstructure of aluminium matrix composites. Journal of Asian Ceramic Societies, 3(3), 240–244. https://doi.org/10.1016/j.jascer.2015.04.001.

[46] Venkatachalam G ,Kumar, A. N., & Rajagopal, D. (2015). Studies On Microstructure and Mechanical Properties Of modified Lm25 Aluminium Alloy. International Journal of Advanced Technology in Engineering and Science www.ijates.com (Vol. 03, Issue 01). www.ijates.com

[47] Priya, S., Mohammed, S., & Shanmugaraja, M. (2016). Investigation on Mechanical Properties 0f Aluminium 6061 reinforced with Sic and Al2O3. http://www.internationaljournalssrg.org.

[48] Xavior, M. A., & Kumar, J. P. A. (2017). Machinability of Hybrid Metal Matrix Composite - A Review. Procedia Engineering, 174, 1110–1118. https://doi.org/10.1016/j.proeng.2017.01.264.

[49] Arora, A., Astarita, A., Boccarusso, L., & Mahesh, V. P. (2016). Experimental Characterization of Metal Matrix Composite with Aluminium Matrix and Molybdenum Powders as Reinforcement. Procedia Engineering, 167, 245–251. https://doi.org/10.1016/j.proeng.2016.11.694.

[50] Bodukuri, A. K., Eswaraiah, K., Rajendar, K., & Sampath, V. (2016). Fabrication of Al–SiC–B4C metal matrix composite by powder metallurgy technique and evaluating mechanical properties. Perspectives in Science, 8, 428–431. https://doi.org/10.1016/j.pisc.2016.04.096.

[51] Kishore, M. N. V., & Tech Scholar, M. (2016). Mechanical Properties in MMC of Aluminum Alloy (A356/LM25) Matrix and Boron Carbide (B 4 C) Reinforcement. http://www.ijert.org.Vol. 5 Issue 02.

[52] Radhika N, & Gruyter, D. (2016). Comparison of the mechanical and wear behaviour of aluminium alloy with homogeneous and functionally graded silicon nitride composites. https://doi.org/10.1515/secm-2015-0160.

[53] Awarasang, S., & Awarasan, S. N. S. (2016). Study The Microstructure And Impact Strength Of Lm 25 Aluminium Alloy Reinforced with Steel Wire. https://doi.org/10.13140/RG.2.2.28176.05124.

[54] Venkatesan, S., & Xavior, M. A. (n.d.). Mechanical behaviour of Aluminium metal matrix composite reinforced with graphene particulate by stir casting method. Journal of Chemical and Pharmaceutical Sciences, 10(1). www.jchps.com.ISSN: 0974-2115.

[55] Mishra, J. (2017). Fabrication Of Metal Matrix Composites: A Review. http://www.journal Vol. 9, Issue, 10, pp.59180-59185.

[56] Moona, G., Walia, R. S., Rastogi, V., & Sharma, R. (2018). Aluminium metal matrix composites: A retrospective investigation. Indian Journal of Pure & Applied Physics (Vol. 56).

[57] Arvind Sankhla. (2015). On studies of Powder Metallurgy as an effective method for Processing Metal Matrix Composites.Indian Journal of Applied Research.Volume – 5,Issue – 1.

[58] Reddy, C. C., Chand, P. R., M, C. K., & N Assistant Professors, S. S. (2017). Development And Characterization of Aluminum Alloy Reinforced With Al2O3 Metal Matrix Composites By Centrifugal Casting Method. International Journal of Scientific Development and Research. www.ijsdr.org

[59] Reddy, S. S., & Scholar, U. (2017). Publication Impact Factor (PIF): 1.02 www.sretechjournal.org Study of Hardness of Aluminium(LM25) Composite. International Journal of Engineering Research and Advanced Technology (IJERAT), 5(5), 2454–6135. www.sretechjournal.org

[60] Rajan Verma, Saurabh Sharma, & Dinesh Kumar. (2017). Analysis of Mechanical Properties of Aluminium based Metal Matrix Composites Reinforced with Alumina and Sic. International Journal of Engineering Research, V6(03), 454–459. https://doi.org/10.17577/ijertv6is030506.

[61] T.Somasekhar, & P Niteesh kumar. (2018). Review Paper on Processing of Metal Matrix Composites &its Properties. www.ijcrt.org. ISSN:2320-2882.

[62] Hussain, S. M., Muruganantham, P., & Rekha, R. (2018). Milling Of Stir Cast Aluminium Boron Carbide Metal Matrix Composite-A Literature Review. International Journal of Engineering, Science and Mathematics, 7http://www.ijesm.co.in,

[63] Dev Srivyas, P., & S. Charoo, M. (2018). Aluminum metal matrix composites a review of reinforcement; mechanical and tribological behavior. International Journal of Engineering & Technology, 7(2.4), 117. https://doi.org/10.14419/ijet.v7i2.4.13020.

[64] Mudasar Pasha, B. A., & Kaleemulla, M. (2018). Processing and characterization of aluminum metal matrix composites: An overview. Reviews on Advanced Materials Science, 56(1), 79–90. https://doi.org/10.1515/rams-2018-0039.

[65] Mohan Krishna, S. A., Shridhar, T. N., & Krishnamurthy, L. (2015). Research Significance, Applications and Fabrication of Hybrid Metal Matrix Composites. IJISET-International Journal of Innovative Science, Engineering & Technology (Vol. 2, Issue 5). www.ijiset.com

[66] Pasupathi, M., & Berlin Raj, S. (2019). Microstructure Analysis and Mechanical Properties of LM25 alloy with AC4B Nano-Composite using Gravity Die Casting Method. IOP Conference Series: Materials Science and Engineering, 507(1). https://doi.org/10.1088/1757-899X/507/1/012023.

[67] Venkata Reddy, V., Gopi Krishna, M., Praveen Kumar, K., Naga Kishore, B. S., Babu Rao, J., & Bhargava, N. (2018). Studies on microstructure and mechanical behaviour of A7075- Flyash/SiC hybrid metal matrix composites. IOP Conference Series: Materials Science and Engineering, 310(1). https://doi.org/10.1088/1757-899X/310/1/012047.

[68] Sharma, A. K., Bhandari, R., Aherwar, A., & Rimašauskiene, R. (2020). Matrix materials used in composites: A comprehensive study. Materials Today: Proceedings, 21, 1559–1562. https://doi.org/10.1016/j.matpr.2019.11.086.

[69] Garg, P., Jamwal, A., Kumar, D., Sadasivuni, K. K., Hussain, C. M., & Gupta, P. (2019). Advance research progresses in aluminium matrix composites: manufacturing & applications. Journal of Materials Research and Technology (Vol. 8, Issue 5, pp. 4924–4939). Elsevier Editora Ltda. https://doi.org/10.1016/j.jmrt.2019.06.028.

[70] Radha Krishnan, B., & Ramesh, M. (2019). Experimental evaluation of Al-Zn-Al2O3 composite on piston analysis by CAE tools. Mechanics and Mechanical Engineering, 23(1), 212–217. https://doi.org/10.2478/mme-2019-0028.

[71] Govindan, K., & Raghuvaran, J. G. (2019). Mechanical properties and metallurgical characterization of lm25/zro2 composites fabricated by stir casting method. Revista Materia, 24(3). https://doi.org/10.1590/S1517-707620190003.0753.

[72] Chandru B.G, Dr.S.Channabasavaraj, Dr.A.Thimmana Gouda, Dr.Manohar H.S (2020). Development and Characterization of Al7475/NbC Reniforced Metal Matrix Composites. International Journal for Research in Engineering Application & Management, 206–207. https://doi.org/10.35291/2454-9150.2020.0463.

[73] Ashrafi, N., Hanim, M. A. A., Sarraf, M., Sulaiman, S., & Hong, T. S. (2020). Microstructural, tribology and corrosion properties of optimized Fe3O4-sic reinforced aluminum matrix hybrid nano filler composite fabricated through powder metallurgy method. Materials, 13(18). https://doi.org/10.3390/ma13184090.

[74] Babu, B., Sabarinathan, C., & Dharmalingam, S. (2020). Production of aluminum 6063 metal matrix composite with 12% magnesium oxide and 5% graphite and its machinability studies using micro electrochemical machining. Journal of New Materials for Electrochemical Systems, 23(2), 94–100. https://doi.org/10.14447/jnmes.v23i2.a06.

[75] T, Nithyanandhan., R, Kannakumar., P, Sureshkumar., S, Pradeep., & V, Prakesh. (2020). Mechanical Properties and Tribological Behaviour of Reinforced Aluminium Metal Matrix Composites. International Journal of Recent Technology and Engineering (IJRTE), 8(6), 1191–1195. https://doi.org/10.35940/ijrte.e6590.038620.

[76] Ahmad, Z., Khan, S., & Hasan, S. (2020). Microstructural characterization and evaluation of mechanical properties of silicon nitride reinforced LM 25 composite. Journal of Materials Research and Technology, 9(4), 9129–9135. https://doi.org/10.1016/j.jmrt.2020.06.037.

[77] Ullah Khan S., Wanwu, D., Ullah Khan, Q., Khan, S., Alam, A., Ullah, A., & Ullah, H. (2021). An Analysis of In-Situ Synthesized AL 6061 Alloy Metal Matrix Composites: Review. European Journal of Materials Science and Engineering, 6(4), 220–233. https://doi.org/10.36868/ejmse.2021.06.04.220.

[78] Ayar, M. S., George, P. M., & Patel, R. R. (2021). Advanced research progresses in aluminium metal matrix composites: An overview. AIP Conference Proceedings, 2317(1), 1–5. https://doi.org/10.1063/5.0036141.

[79] Datkhile, R., Laad, M., & Ghule, B. (2021). Research Trend of Metal Matrix Composites reinforced with silica extracted by green route: A Bibliometric Analysis. Library Philosophy and Practice, 2021(January), 1–15.

[80] Samuel, D., Boppana, S. B., Palanikumar, K., Ramesh, S., & Auradi, V. (2021). Role of heat treatment on hardness of Al 6061- AlB2metal matrix composites. International Journal ofSurface Engineering and InterdisciplinaryMaterials
Science, 9(1), 26–39. https://doi.org/10.4018/IJSEIMS.2021010102.

[81] Shivaramakrishna, A.,Basavaraj, Y., & Subramanya, R.(2022). Synthesis of Fe3O4–aluminium matrix composites mechanical and corrosion characteristics. International Journalof Cast Metals Research,35, 51-59.https://doi.org/10.1080/13640461.2022. 2078551.

Journal of Engineering and Technology for Industrial Applications

ITEGAM-JETIA

Manaus, v.11 n.54, p. 177-185. July/August., 2025.
DOI: https://doi.org/10.5935/jetia. v11i54.1710

ISSN ONLINE: 2447-0228

RESEARCH ARTICLE OPEN ACCESS

RISK MANAGEMENT AND GOVERNANCE IN BLOCKCHAIN-BASED DIGITAL IDENTITY PROJECTS: A BUSINESS ANALYSIS AND PROJECT MANAGEMENT FRAMEWORK

Tobiloba Kazeem[1], Olatoye Kabiru Agboola[2], Nonso Okika[3], Soyingbe FolasadeOwoolaAdebayo[4] Fope Opeola[5], Nnenna Linda Akunna[6], Oreoluwa Serifat Abimbola[7]

[1]Western Illinois University: Macomb, Illinois, US.
[2]New Jersey City Universit, US.
[3]University of Michigan, US
[4]Lagos State University, Nigéria
[5]Ntional Oceanography Center, Reino Unido
[6]University of West England, Reino Unido
[7]Nexford University, US

[1]https://orcid.org/0009-0002-2265-0605, [2]http://orcid.org/0009-0004-0905-0175, [3]https://orcid.org/0000-0001-9386-4577
[4]https://orcid.org/0009-0001-6227-5726, [5]https://orcid.org/0009-0004-6245-0522, [6]https://orcid.org/0009-0001-8887-5519
[7]http://orcid.org/0009-0006-5345-7356

Email: tobikazeem4@gmail.com, olatoye.agboola88@hotmail.com, nonnykins23@yahoo.com, shadeowoola@gmail.com, fope.opeola@gmail.com, achoakunna@gmail.com, bimbolady09@yahoo.com

ARTICLE INFO

Article History
Received: March 14, 2025
Revised: April 20, 2025
Accepted: June 15, 2025
Published: August 31, 2025

Keywords:
Blockchain,
Digital Identity,
Risk Management,
Governance,
Project Management.

ABSTRACT

Blockchain is viewed as a revolutionary solution to digital identity management, offering decentralization, security, and user control over one's own private identity. However, there are a number of challenges which hamper its adoption—related to risk management and governance. This study carefully evaluates the integration of the strategies and governance frameworks for avoiding risks in blockchain based digital identity projects. Security vulnerability, regulatory uncertainty and interoperability issues are the key risk to be managed by robust risk management framework such as ISO 31000 and NIST. Governance models, including on-chain and off-chain approaches, influence stakeholder coordination, transparency, and compliance.

While on-chain governance ensures decentralized decision-making through smart contracts, off-chain governance incorporates informal discussions and regulatory oversight. A hybrid governance model is proposed to sustainably and securely implement given that the best of both world can be achieved. From a business analysis and project management standpoint, integrating risk and governance mechanisms is useful because it improves decision making, coordination of stakeholders, as well as regulatory alignment. Based on the findings of this study, it serves as a strategic insight that organizations, project managers and policymakers should consider when working in blockchain identity ecosystems.

Copyright ©2016 by authors and Galileo Institute of Technology and Education of the Amazon (ITEGAM). This work is licensed under the Creative Commons Attribution International License (CC BY 4.0).

I. INTRODUCTION

Blockchain technology has transformed digital identity management by offering decentralized, verifiable, and tamper-resistant identity solutions [1]. Blockchain based digital identity differs from the traditional identity systems where databases are centralized and involve the least security and transparency of user data [2]. The growing adoption of blockchain in identity management is driven by concerns over data breaches, identity theft, and inefficiencies in conventional identity verification processes [3].

Despite its advantages, blockchain-based digital identity havecomplex challenges that call for strong governance and risk management structures. Key risks are security threats including cryptographic attack, by smart contract vulnerability, and smart contract vulnerabilities [1]. Furthermore, data protection, compliance and verification of cross border identity is highly implementation challenged

[2]. This exacerbates the lack of standardized governing frameworks in implementing blockchain since it results in fragmentation and can lead to interoperability problems across various blockchain networks [4]. According to Tan et al. (2022) [5], governance is fundamental to assuring the alignment of blockchain based digital identity projects to the legal and ethical considerations. Unlike traditional centralized identity management, blockchain governance requires coordination among multiple stakeholders including developers, regulators, businesses and end users in deciding the decision making and policy enforcement [6].

Role, responsibility and accountability mechanisms are defined for effective governance of structures, to prevent misuse, complying with data protection laws and for dispute resolution [5]. From the business analysis and project management perspective, it is required to integrate a risk management and governance frameworks in blockchain based digital identity projects to their success. Technical, regulatory and operational risks must be assessed by business analysts and project managers, they must align with stakeholders and strategic objectives [6]. This necessitates an interdisciplinary approach that combines risk assessment methodologies, compliance strategies, and governance models tailored to blockchain technology. By addressing these complexities, organizations can leverage blockchain-based digital identity solutions to enhance security, privacy, and operational efficiency while mitigating associated risks [6].

Therefore, this study aims to investigate risk management strategies and governance frameworks in blockchain-based digital identity projects, focusing on their integration into business analysis and project management to enhance security, compliance, and stakeholder coordination.

RESEARCH AIM AND OBJECTIVES

The primary aim of this study is to investigate risk management strategies and governance frameworks in blockchain-based digital identity projects, focusing on their integration into business analysis and project management to enhance security, compliance, and stakeholder coordination. This research evaluates the effectiveness of existing governance models and risk mitigation approaches, providing insights into their practical application in decentralized identity systems.

The key objectives of this study are:

1. To review existing literature on risk management strategies in blockchain-based digital identity projects and assess their effectiveness.
2. To examine governance models that facilitate stakeholder coordination, regulatory compliance, and sustainable implementation in decentralized identity systems.
3. To identify key challenges in integrating risk management and governance into blockchain-based digital identity projects, including security risks, regulatory uncertainties, and interoperability issues.
4. To propose strategic business and project management recommendations for organizations seeking to implement secure and well-governed blockchain-based digital identity solutions.

This study provides valuable insight into the critical risk and governance issues in blockchain based digital identity projects to the field of Business Analysis and Project Management. With the rise in blockchain adoption, organizations have come to realize that they must come up with a viable strategy in addressing the risks entailed while meeting the demands of the varied regulatory frameworks. This research fills the knowledge gap by structuring the way by which risk management and governance can be integrated into blockchain based identity initiatives.

The findings from a business perspective provides organizations with insights to better develop decision making process, set up better risk assessments and have the means to establish governance mechanisms. This also provides an outlook to policymakers and regulators on how to perform the balancing security, privacy, and compliance when creating decentralized identity system. Additionally, the results of this research are important for project managers and business analysts engaged in blockchain implementations. The study provides practical recommendations and case study insights as the tools to establish and manage blockchain digital identity projects.

II. LITERATURE SEARCH STRATEGY

A systematic approach was employed to identify relevant literature on risk management and governance in blockchain-based digital identity projects. The search strategy involved querying academic databases such as Scopus, Web of Science, IEEE Xplore, and Google Scholar, as well as industry reports and regulatory guidelines. Keywords included “blockchain governance,” “risk management in blockchain,” “digital identity security,” “decentralized identity frameworks,” and “blockchain compliance.” Boolean operators (AND, OR) were used to refine search results and ensure the inclusion of interdisciplinary perspectives.

Only those peer reviewed journal articles published between 2019 to 2024 were considered for the review to make the review more robust. This timeframe was determined as it enables capturing the latest blockchain identity governance, regulatory trends and risk management frameworks. It was also performed backward and forward citation tracking to identify influential studies. The studies were categorized thematically, namely, a review of risk mitigation strategies, governance models and project management implications. The search strategy integrated literature from business analysis, project management, cybersecurity and legal perspectives, that together with other sources of literature ensure the thorough examination of the blockchain based digital identity challenges and best practices.

Inclusion and Exclusion Criteria

To maintain research validity and relevance, specific inclusion and exclusion criteria were applied during the literature selection process.

Inclusion criteria:

1. Studies focusing on risk management and governance in blockchain-based digital identity systems.
2. Peer-reviewed journal research published between 2019 and 2025 to ensure up-to-date insights.
3. Literature addressing the intersection of blockchain, digital identity, business analysis, and project management.

4. Empirical studies and theoretical frameworks that provide strategic insights into blockchain governance and risk management.

Exclusion criteria:

1. Articles unrelated to blockchain-based digital identity or those discussing general blockchain applications without governance or risk management perspectives.
2. Non-peer-reviewed sources such as blogs, opinion pieces, and non-academic reports lacking empirical or theoretical rigor.
3. Studies published before 2019 unless they provide foundational theoretical concepts.
4. Research focusing solely on technical aspects without business, governance, or risk considerations.

Analysis Framework

The literature was analyzed using a thematic synthesis framework to identify key patterns, relationships, and gaps in risk management and governance for blockchain-based digital identity projects. Thematic analysis was chosen for its ability to integrate multidisciplinary perspectives and extract meaningful insights from diverse sources.

The analysis was structured into three key themes:

1. **Risk Management Strategies:** This theme looked at studies related to security threats, regulatory risks, and operational challenges to blockchain identity project [7]. Through risk mitigation frameworks, it found such safety measures as cryptographic security, compliance protocols and resilience strategies.
2. **Governance Models:** This section explored decentralized governance structure, stakeholder coordination mechanism and regulatory compliance approaches [8]. Therefore, it analyzed governance models of achieving the necessary balance between autonomy and regulation of digital identity systems.
3. **Integration into Business Analysis and Project Management:** This theme investigated incorporation of the risk management and governance frameworks into the project lifecycle planning, stakeholder management, and compliance strategies [9].

III. THEORETICAL BACKGROUND

III.I BLOCKCHAIN-BASED DIGITAL IDENTITY SYSTEMS

Digital identity is the set of attributes that defines an individual in the digital space and that supports authenticating and verifying an individual in the online interactions [10]. Centralized databases used by the traditional identity management systems are highly vulnerable to security breaches, unauthorized access and possible privacy violations [11]. Hence. the blockchain technology provides a decentralized viable option where people, guided by self-sovereign identity (SSI) can no longer rely on central authorities and hence are less exposed to the risks of having a single point of failure [10], similarly, Blockchain technology introduces an innovative approach by establishing a decentralized, transparent, and cryptographically secure platform for identity verification and data exchange [12]. In addition, the immutability of blockchain adds to the data integrity as identity records cannot be altered or deleted [13].

Furthermore, cryptographic security mechanisms such as encryption and zero-knowledge proofs ensure privacy of users as well as provide a secure and verifiable way of user identity authentication [14]. However, blockchain based digital identity systems have limited challenges. Still, the primary concern is scalability as high transaction costs and slow processing speed in public blockchains can keep public blockchains on a small scale of adoption [10]. Moreover, interoperability barriers make it difficult to interoperate BlockChain based identity solution with existing digital identity framework for cross platform usage [13].

As GDPR will continue to constrain adoption, regulatory uncertainty also exacerbates adoption challenges in jurisdictions that require strict data protection such as the General Data Protection Regulation. There is the issue of compliance and the protection of privacy because the immutable nature of blockchain is a fundamental contradiction to legal requirements like the right to erasure [11]. In addressing these challenges, such robust risk management and governance framework is needed, that secures the security, adhere to the regulatory requirements, and interoperable. Decentralization and oversight mechanism should be balanced to provide a secure and scalable and legally compliant blockchain based digital identity systems [14]. Blockchain identity solutions can create enough integration of strategic risk mitigation measures, regulatory frameworks to ensure scalability and to maintain security and trust in digital interactions.

RISK MANAGEMENT IN BLOCKCHAIN PROJECTS

Risk management is a fundamental aspect of blockchain-based digital identity projects, as these systems face significant security, scalability, and compliance challenges. Established frameworks such as ISO 31000, NIST, and COBIT provide structured methodologies for identifying and mitigating risks [15]. However, blockchain's decentralized nature introduces unique vulnerabilities that require tailored risk management approaches. Security risks remain a primary concern, with smart contract vulnerabilities potentially leading to identity fraud and unauthorized access [16]. Additionally, Cryptographic key management can be viewed from two categories: Secret keys [17] and public/private key [18]. Private key mismanagement can result in permanent identity loss, while inadequate encryption mechanisms increase the likelihood of data breaches [19]. Scalability issues further hinder the adoption of blockchain-based identity solutions, as high transaction fees and network congestion create inefficiencies [20]. Compliance risks also pose challenges, particularly regarding regulatory conflicts such as GDPR's right to data modification, which contrasts with blockchain's immutability [15].

A comprehensive risk management framework that integrates cybersecurity, governance, and compliance measures is essential for the successful implementation of blockchain-based digital identity projects [21]. Governance in blockchain projects is crucial for ensuring transparency, stakeholder participation, and regulatory compliance. It defines the decision-making structures that influence how digital identity systems evolve, resolve disputes, and maintain security [22]. Given the decentralized nature of blockchain, governance frameworks must carefully balance autonomy, accountability, and coordination while addressing regulatory concerns [23]. Effective governance mechanisms are essential to preventing centralization risks, ensuring equitable decision-making, and fostering long-term sustainability in blockchain-based digital identity [21]

GOVERNANCE IN BLOCKCHAIN PROJECTS

One of the popular governance models is on chain governance, which function through smart contracts and token-based voting [23]. As this protocol is a decentralized one, the change to the protocol can be automated and completed by a set of stakeholder votes, or through DAOs [24]. Although this increases transparency and efficiency, the concentration of the ownership of the tokens also brings the risk of governance centralization [25].

On the other hand, off chain governance is through informal methods such as developer discussion, regulatory negotiation and community led decision making. It also involves providing deep and valuable enhancements. Nevertheless, this method can result in lack of transparency and over representation of key stakeholders [26]. Governance over blockchain, have challenges including transparency, centralization risks and regulatory uncertainty. To resolve these challenges, the hybrid form of governance which comprises of both on chain and off chain elements can coincide the balance between decentralization, flexibility and regulatory compliance [24]. When blockchain based digital identity projects integrate automation with structured decision-making process, it can help in improving the efficiency of governance while maintaining trust and security [23].

IV. RESULTS AND DISCUSSIONS

This thematic analysis critically examines existing literature, categorizing the discussion into three core themes: risk management strategies, governance models, and the challenges of integrating risk management with governance in blockchain-based digital identity systems.

RISK MANAGEMENT STRATEGIES IN BLOCKCHAIN-BASED DIGITAL IDENTITY PROJECTS

A central theme in the literature is the effectiveness of risk management strategies in blockchain-based digital identity systems. As Zyskind & Nathan (2015) [27] stated, the main advantage of blockchain's decentralization is to significantly reduce data breaches and single points of failure, which has been a thorn in the side of centralized identity management for many years. Likewise, Wüst and Gervais (2018) [28] claim that blockchain serves to increase data integrity and authentication via cryptographic mechani, sms of verification, thus preventing identity records from being tampered with. However, Atzei et al. (2016) [29] emphasize blockchain's weaknesses, especially the smart contract risks. According to them, the 2016 DAO hack in which attackers stole $50 million from a smart contract due to a reentrant bug is an example of how coding flaws in smart contracts can be exploited.

According to Zhou et al. (2022) [30], this argument is supported since, once deployed, self-executing contracts cannot be changed and errors and vulnerabilities are more damaging. Besides security concerns, scalability turns out to be another major risk. Nguyen et al. (2021) [31] feel that, while proof of work (PoW) consensus mechanisms are secure, they are also inefficient and so large-scale identity verification is not possible. According to [32] proof of stake (PoS) mechanisms are an alternative to PoW that should solve scalability problems in an energy efficient manner. Yet, [33] contradicts this optimism by arguing that PoS brings in new risks, including economic centralization whereby the wealthy take control of network governance. This also involves a trade-off between security and efficiency that is characteristic of lack of a standardized risk management framework for blockchain identity projects. Even though there are those who suggest that the already existing frameworks, ISO 31000 and NIST risk management guidelines, can be applied to blockchain identity projects, [34] states that the root problem lies in these frameworks do not consider blockchain's unique risks like 51% attacks and vulnerabilities of a decentralized governance. Hence [35] suggest customized risk assessment models that take into consideration risk inherent to blockchain's operating.

GOVERNANCE MODELS FOR STAKEHOLDER COORDINATION, REGULATORY COMPLIANCE, AND SUSTAINABILITY

Another key theme in the literature is governance, which is crucial for coordinating the stakeholders, complying with the regulations and for the long-term sustainability of the blockchain based digital identity projects. According to [36], blockchain's strong point is in decentralizing decision-making power to users rather than central authorities. Following this sentiment, [37] describes on chain governance models, which are executed through Decentralized Autonomous Organizations (DAOs) as allowing for more transparent, and in some sense more democratic decisions. However, [38] present a more diverse view, acknowledging that while DAOs promote decentralization, they also introduce governance inefficiencies, particularly in dispute resolution and protocol upgrades.

Wang and De Filippi (2020) [39] extend this discussion to self-sovereign identity (SSI) models, which empower users to control their identity data without relying on intermediaries. They argue that SSI is in line with the blockchain's principles of user autonomy and privacy preserving. Interestingly, however, [8] counter this by arguing that there are more legal and regulatory barriers to clear decentralized identity systems. Specifically, they point to conflict between blockchain immutability and the General Data Protection Regulation (GDPR) in relation to the "right to be forgotten." Where [40] agrees the problem of GDPR compliance is especially difficult for blockchain identity solutions, the brief note that technological 'workarounds' such as zero knowledge proofs (ZKPs) could enable the selective erasure of data without compromising the integrity of the blockchain. However, some scholars call for the decentralization but believe that fully decentralized governance models are impossible to realize.

According to [32], many blockchain networks, and especially Ethereum, have not achieved much in the way of decentralisation because core developers and influential stakeholders retain their control. This argument is reinforced by [34] who point out that in reality, early adopters and wealthier participants tend to consolidate power in such a manner that there is a kind of spontaneous centralization. In order to handle these issues, some researchers suggest hybrid forms of governance. Hyperledger Indy is one such example of a permissioned blockchain where transactions are still based on decentralised principles, but are validated by trusted entities, as mentioned by [41]. According to them, such models find the right balance between decentralization and regulatory oversight, which means that they

will be more compliant with legal frameworks. However, critics like [42] point out that by reintroducing aspects of centralization, hybrid models simply reintroduce trustless aspects that are inherent to many blockchain based solutions for identity.

CHALLENGES IN INTEGRATING RISK MANAGEMENT AND GOVERNANCE IN BLOCKCHAIN-BASED DIGITAL IDENTITY PROJECTS

Blockchain based digital identity projects face a multifaceted challenge where it is difficult to establish how risk management and governance should be integrated. Concerning security risk, [39] states that blockchain does not prevent users from having a centralized database, but instead puts the full responsibility on the user for protecting his credentials. They argue that this makes private keys lost or compromised more likely to result in permanent identity loss. Yaacoub et al. (2023) [43] also discuss the implication of recovery mechanisms for security of blockchain based identity systems, noting that if such systems have backdoors for recovery, then they will undermine the very security principles they seek to uphold.

Apart from the security concerns, [8] also pointed out regulatory uncertainty as the main obstacle to the adoption of blockchain identity. However, governments across the world remain skeptical about decentralized identity solutions as they are concerned about their potential to be used in fraud and money laundering. For example, China has been very strict with the development of the decentralized identity, while the European Commission's eIDAS 2.0 proposal aims at including blockchain based identity in formal and legal frameworks [44]. As long as it represents progress towards regulatory acceptance, [8] assert that legal ambiguity remains and continues to discourage widespread implementation and investment. Interoperability is another persistent challenge.

According to [45], most blockchain based identity projects operate in a siloed environment where it is difficult to verify a cross-platform identity. Furthermore, it mentions the work going on by the World Wide Web Consortium (W3C) to make Decentralized Identifiers (DIDs) and Verifiable Credentials (VCs) to become the standard in standardizing blockchain identity protocols. Rikken et al. (2019) [46] concede that these efforts have, however, not resolved the fragmentation problem as various blockchain networks have different governance models and security standards. There are emerging technological solutions, which may provide pathways to solution. George and Kizhakkethottam (2021) [47] proposes homomorphic encryption and zero knowledge proofs as promising ways to improve privacy while maintaining compliance with the data regulations. Meanwhile, [48] explains that cross chain identity verification protocols are means to enable interoperability among the blockchain ecosystems. While these advancements hold promise, their real-world adoption remains limited, and further research is needed to refine their implementation within blockchain identity frameworks.

V. IMPLICATIONS FOR BUSINESS ANALYSIS AND PROJECT MANAGEMENT

BUSINESS ANALYSIS INSIGHTS

A bridging of technical, regulatory, and business considerations is essential for the success of blockchain based digital identity projects and business analysts fill this role very well. First it is important to understand risk management in whole and to identify vulnerabilities with respect to smart contracts, cryptographic key management and scalability limits.

Business analysts play a crucial role in leveraging smart contracts to automate compliance and governance processes. Traditional systems rely on manual tasks such as document verification, reporting, and auditing to ensure regulatory compliance. These processes are not only time-consuming but also susceptible to human error [49]. By integrating smart contracts, business analysts help organizations streamline compliance by automating checks and governance tasks [50]. Smart contracts can be designed to enforce regulatory compliance in real-time by monitoring transactions and verifying adherence to key regulations, such as Anti-Money Laundering (AML) and Know Your Customer (KYC) requirements [51].

Business analysts are responsible for defining the regulatory parameters and business rules that smart contracts must follow. They ensure that these contracts are programmed to halt transactions if compliance conditions are not met, thereby preventing violations and mitigating financial an legal risks. By translating complex regulatory requirements into actionable smart contract functionalities, business analysts enhance operational efficiency, reduce compliance costs, and minimize risks associated with non-compliance.

Additionally, Business analysts play a critical role in understanding and managing risks associated with cryptographic key management. By identifying vulnerabilities and designing effective mitigation strategies, they help ensure that an organization's data remains secure. Cryptographic key management can be viewed from two categories and the associated risks: Secret keys and public/private key [52].

Secret keys are used for both encryption and decryption with symmetric cryptographic algorithms, as well as for ensuring data integrity through mechanisms like message authentication codes (e.g., HMAC) [52]. Since the same key is employed for encryption and decryption, any compromise of this key can lead to significant security breaches. Business analysts must assess risks such as unauthorized access, key leakage, and the overall lifecycle management of these keys, recommending stringent access controls and regular audits to mitigate potential vulnerabilities.

Whereas, public/private key pairs involve two mathematically linked keys used in asymmetric cryptography for authentication, digital signatures, or secure key establishment [46]. The private key, which must remain confidential at all times, is crucial for maintaining the integrity of the system. Meanwhile, the public key is shared to facilitate secure communications. For business analysts, the key risk is ensuring that the private key is adequately protected, as its exposure could allow malicious parties to impersonate legitimate users or compromise the entire cryptographic system [49].

By understanding these two categories and the associated risks, business analysts can develop comprehensive risk management strategies that not only safeguard cryptographic assets but also support overall regulatory compliance and operational efficiency.

Furtermore, Business analysts play a critical role in understanding and managing the risks associated with the scalability limits of blockchain systems. As the number of stakeholders increases and the volume of shared data grows—often beyond traditional logistic data—the blockchain's on-chain data sharing mechanism may face significant scalability challenges (Hariyani et al., 2025) [53]. This can lead to performance bottlenecks and operational inefficiencies that jeopardize the system's overall effectiveness. As more participants

join, the increased load may slow down transaction processing or even cause system delays. Recognizing these vulnerabilities early is essential for developing effective risk management strategies. Business analysts must evaluate how the influx of diverse stakeholders and the resulting massive data exchanges can stress the blockchain infrastructure [54].

Since blockchain is immutable, analysts need to examine regulatory frameworks, such as GDPR to comply in terms of security and privacy. It is worth noting that the stored records have to be secured in order to prevent unauthorized processing, accidental loss, destruction, or damage (integrity and confidentiality principle). However, public blockchains must take some steps to secure data with appropriate measures, such as using encryption or anonymization [55].

For this, Business analysts need to find potential conflicts among data protection laws and blockchain design principles as well as mitigation strategies including zero-knowledge proofs, selective disclosure mechanisms, etc. Not only that but the blockchain identity projects have developers, regulators, enterprises, and end users with their own priorities, so stakeholder alignment is another key responsibility. Business analysts must define the business requirements with a defined precedence list of business requirements balancing security, privacy, and operational efficiency whereas the solution also needs to meet technical feasibility and regulatory mandates. Furthermore, it is important to choose governance model (onchain, offchain, or hybrid) in consistence with the strategic goals of the organization. Business analysts help decision makers by translating complex technical and compliance challenge to structured business insights to guide sustainable and secure blockchain identity implementation to further trust, efficiency and viability in a decentralized identity ecosystem.

PROJECT MANAGEMENT IMPLICATIONS

Risk management, stakeholder coordination, and governance are some of the complex risks that project managers of blockchain based digital identity projects would need to navigate. A proper, structured approach to the mitigation of risk is necessary, and must take into account the integration of security, compliance, and scalability considerations from project initiation to deployment.

Ensuring adherence to best practices in smart contract development, private key management, and consensus mechanisms is critical in preventing security vulnerabilities and operational failures. Stakeholder management is particularly complex due to the diverse interests involved, including technical teams, regulatory bodies, and end-users. In decentralized structures of governance, consensus building can be slow and fragmented, which means that transparent communication as well as facilitation of decision making are indispensable elements for project managers. Furthermore, the interoperability challenges must be planned carefully so that the integration with the existing identity system is seamless and with any other chain is possible. In this context of the changing regulatory environment, project managers should adopt agile methodologies, which enable iteration of project to technological novelties and legal requirements. Implementing hybrid governance models may necessitate a phased deployment approach, ensuring regulatory compliance without undermining decentralization. Ultimately, ability to deliver secure, scalable, compliant solutions within budget and timeline is the key success factor in delivering blockchain based digital identity ecosystem that is trusted, and meet organizational objective.

V. CONCLUSIONS

This study has shown the importance of risk governance and management on projects of blockchain based digital identity. However, Blockchain provides decentralized, secure and immutable identity management solutions while being a security and scalability risk, along with noncompliance to regulatory compliance. Mitigating the vulnerabilities of smart contracts, mismanagement of private keys, and interoperability falls upon the importance of having that such smart framework as ISO 31000 and NIST. On chain and off chain governance are important governance models needed to maintain transparency, participation of stakeholders and compliance. Combining decentralized decision making with regulatory oversight is needed to increase security and sustainability on a long-term use. As organizations seek to embrace blockchain based digital identity projects, regulatory standards for risk management should be taken into consideration to enhance adoption. This includes smart contract security audits, cryptography key protection measures, and ensuring data privacy laws compliance. On-chain and off-chain mechanisms should be merged into the governance framework to ensure transparency, avoid power centralization and to respond to the regulation change. Standards for the governance and interoperability for any system must be established and those standards must be collaboratively developed amongst the policymakers, industry leaders and the technology developers to work. Project managers should adopt agile methodologies to navigate regulatory changes effectively. Lastly, research about scalable blockchain identity solutions can be further on security, efficiency, and the regulatory alignment.

VI. AUTHOR'S CONTRIBUTION

Conceptualization: Tobiloba Kazeem, Olatoye Kabiru Agboola, Nonso Okika, Soyingbe FolasadeOwoolaAdebayo Fope Opeola, Nnenna Linda Akunna, Oreoluwa Serifat Abimbola.
Methodology: Tobiloba Kazeem, Olatoye Kabiru Agboola, Nonso Okika, Soyingbe FolasadeOwoolaAdebayo Fope Opeola, Nnenna Linda Akunna, Oreoluwa Serifat Abimbola.
Investigation: Tobiloba Kazeem, Olatoye Kabiru Agboola, Nonso Okika, Soyingbe FolasadeOwoolaAdebayo Fope Opeola, Nnenna Linda Akunna, Oreoluwa Serifat Abimbola.
Discussion of results: Tobiloba Kazeem, Olatoye Kabiru Agboola, Nonso Okika, Soyingbe FolasadeOwoolaAdebayo Fope Opeola, Nnenna Linda Akunna, Oreoluwa Serifat Abimbola.
Writing – Original Draft: Tobiloba Kazeem, Olatoye Kabiru Agboola, Nonso Okika, Soyingbe FolasadeOwoolaAdebayo Fope Opeola, Nnenna Linda Akunna, Oreoluwa Serifat Abimbola.
Writing – Review and Editing: Tobiloba Kazeem, Olatoye Kabiru Agboola, Nonso Okika, Soyingbe FolasadeOwoolaAdebayo Fope Opeola, Nnenna Linda Akunna, Oreoluwa Serifat Abimbola.
Resources: Author Two. Tobiloba Kazeem, Olatoye Kabiru Agboola, Nonso Okika, Soyingbe FolasadeOwoolaAdebayo Fope Opeola, Nnenna Linda Akunna, Oreoluwa Serifat Abimbola.

Supervision: Tobiloba Kazeem, Olatoye Kabiru Agboola, Nonso Okika, Soyingbe FolasadeOwoolaAdebayo Fope Opeola, Nnenna Linda Akunna, Oreoluwa Serifat Abimbola.
Approval of the final text: Tobiloba Kazeem, Olatoye Kabiru Agboola, Nonso Okika, Soyingbe FolasadeOwoolaAdebayo Fope Opeola, Nnenna Linda Akunna, Oreoluwa Serifat Abimbola.

VIII. REFERENCES

[1] O. Olawoyin, "Blockchain technology in risk management: Strengthening cybersecurity and financial integrity," Int. J. Res. Publ. Rev., vol. 5, pp. 2336–2348, 2024. doi: 10.55248/gengpi.5.1024.2829.

[2] L. Stockburger, G. Kokosioulis, A. Mukkamala, R. R. Mukkamala, and M. Avital, "Blockchain-enabled decentralized identity management: The case of self-sovereign identity in public transportation," Blockchain Res. Appl., vol. 2, no. 2, p. 100014, 2021. doi: 10.1016/j.bcra.2021.100014.

[3] C. S. Sung and J. Y. Park, "Understanding blockchain-based identity management system adoption in the public sector," J. Enterprise Inf. Manage., vol. 34, no. 5, pp. 1481–1505, 2021. doi: 10.1108/JEIM-12-2020-0532.

[4] R. van Pelt, S. Jansen, D. Baars, and S. Overbeek, "Defining blockchain governance: A framework for analysis and comparison," Inf. Syst. Manage., vol. 38, no. 1, pp. 21–41, 2021. doi: 10.1080/10580530.2020.1720046.

[5] E. Tan, S. Mahula, and J. Crompvoets, "Blockchain governance in the public sector: A conceptual framework for public management," Gov. Inf. Q., vol. 39, no. 1, p. 101625, 2022. doi: 10.1016/j.giq.2021.101625.

[6] H. Bai, Z. Li, K. Chen, and X. Li, "Blockchain-based responsibility management framework for smart city building information modeling projects using non-fungible tokens," Buildings, vol. 14, no. 11, p. 3647, 2024. doi: 10.3390/buildings14113647.

[7] T. B. Makhanya, "The implications for risk management in the era of technological advancements," IntechOpen, 2024. doi: 10.5772/intechopen.1003899.

[8] Y. Zhao and J. Qiu, "Decentralized governance in action: A governance framework of digital responsibility in startups," J. Responsible Technol., vol. 21, p. 100107, 2025. doi: 10.1016/j.jrt.2025.100107.

[9] O. Bakare, R. Aziza, N. Uzougbo, and P. Oduro, "A governance and risk management framework for project management in the oil and gas industry," Open Access Res. J. Sci. Technol., vol. 12, pp. 121–130, 2024. doi: 10.53022/oarjst.2024.12.1.0119.

[10] M. S. Prashanth, R. Karnati, M. S. Velpuru, and H. V. Reddy, "Blockchain-based digital identity management system for cybersecurity," in *Proc. 5th Int. Conf. Data Sci., Mach. Learn. Appl.*, vol. 1273, A. Kumar, V. K. Gunjan, S. Senatore, and Y. C. Hu, Eds., Springer, Singapore, 2025. doi: 10.1007/978-981-97-8031-0_30.

[11] A.-C. Careja and N. Tapus, "Digital identity using blockchain technology," Procedia Comput. Sci., vol. 221, pp. 1074–1082, 2023. doi: 10.1016/j.procs.2023.07.232.

[12] Alliy Adewale Bello , David Amoah Oduro , Emmanuel Opoku Manu , Adepeju Deborah Bello; Adeniji Omotayo Leo , Chioma Emmanuel Ukatu; Nonso Okika "Enhancing Know Your Customer (KYC) and Anti-Money Laundering (AML) Compliance Using Blockchain: A Business Analysis Approach" Iconic Research And Engineering Journals, 8(9)

[13] A. A. Varfolomeev and L. H. Al-Farhani, "Blockchain-based digital identity management system for smart city services," in *2023 Int. Conf. Inf. Technol., Appl. Math. Stat. (ICITAMS)*, pp. 79–85, 2023. doi: 10.1109/ICITAMS57610.2023.10525393.

[14] M. Htet, P. T. Yee, and J. R. Rajasekera, "Blockchain-based digital identity management system: A case study of Myanmar," in *2020 Int. Conf. Adv. Inf. Technol. (ICAIT)*, pp. 42–47, 2020. doi: 10.1109/ICAIT51105.2020.9261785.

[15] M. Rachmadhani, T. Immawan, A. Mansur, and W. Choi, "Risk management framework design based on ISO 31000 and SCOR model," Spektrum Ind., vol. 21, no. 1, pp. 41–51, 2023. doi: 10.12928/si.v21i1.93.

[16] B. Alamri, K. Crowley, and I. Richardson, "Cybersecurity risk management framework for blockchain identity management systems in Health IoT," Sensors, vol. 23, no. 1, p. 218, 2023. doi: 10.3390/s23010218.
[17] S. K. Mousavi, A. Ghaffari, S. Besharat, and H. Afshari, "Security of internet of things based on cryptographic algorithms: A survey," Wireless Networks, vol. 27, no. 2, pp. 1515–1555, 2021.

[18] M. U. Hassan, M. H. Rehmani, and J. Chen, "Privacy preservation in blockchain-based IoT systems: Integration issues, prospects, challenges, and future research directions," Future Generation Computer Systems, vol. 97, pp. 512–529, 2019.

[19] S. Barik and K. G. S. Venkatesan, "Analysis of cybersecurity standard and framework components," Industrial Engineering Journal, vol. 50, no. 6-1, 2021.

[20] Makaš, "Governance, risk, and compliance frameworks applicability in organizations," International Journal of Science and Research Archive, vol. 10, no. 2, pp. 716–724, 2023.

[21] E. Cayirci and A. S. de Oliveira, "Modelling trust and risk for cloud services," Journal of Cloud Computing, vol. 7, Art. no. 14, 2018, doi: 10.1186/s13677-018-0118-0.

[22] R. Beck, C. Mueller-Bloch, and J. King, "Governance in the blockchain economy: A framework and research agenda," Journal of the Association for Information Systems, vol. 19, pp. 1020–1034, 2018, doi: 10.17705/1jais.00518.

[23] T. Polcumpally, K. K. Pandey, A. Kumar, and A. Samadhiya, "Blockchain governance and trust: A multi-sector thematic systematic review and exploration of future research directions," Heliyon, vol. 10, no. 12, Art. no. e32975, 2024, doi: 10.1016/j.heliyon.2024.e32975.

[24] G. Laatikainen, M. Li, and P. Abrahamsson, "A system-based view of blockchain governance," Information and Software Technology, vol. 157, Art. no. 107149, 2023, doi: 10.1016/j.infsof.2023.107149.

[25] M. El Khatib, A. Al Mulla, and W. Al Ketbi, "The role of blockchain in e-governance and decision-making in project and program management," Advances in Internet of Things, vol. 12, no. 3, 2022, doi: 10.4236/ait.2022.123006.

[26] S. Verma and A. Sheel, “Blockchain for government organizations: Past, present and future,” Journal of Global Operations and Strategic Sourcing, vol. 15, no. 3, pp. 406–430, 2022, doi: 10.1108/JGOSS-08-2021-0063.

[27] G. Zyskind and O. Nathan, “Decentralizing privacy: Using blockchain to protect personal data,” in Proc. IEEE Security Privacy Workshops, San Jose, CA, USA, 2015, pp. 180–184.

[28] K. Wüst and A. Gervais, “Do you need a blockchain?,” in Proc. Crypto Valley Conf. Blockchain Technol. (CVCBT), Zug, Switzerland, 2018, pp. 45–54, doi: 10.1109/CVCBT.2018.00011.

[29] N. Atzei, M. Bartoletti, and T. Cimoli, “A survey of attacks on Ethereum smart contracts,” Cryptology ePrint Archive: Report 2016/1007, 2016. [Online]. Available: https://eprint.iacr.org/2016/1007

[30] H. Zhou, A. Milani Fard, and A. Makanju, “The state of Ethereum smart contracts security: Vulnerabilities, countermeasures, and tool support,” Journal of Cybersecurity and Privacy, vol. 2, no. 2, pp. 358–378, 2022, doi: 10.3390/jcp2020019.

[31] C. T. Nguyen, D. T. Hoang, D. N. Nguyen, D. Niyato, H. T. Nguyen, and E. Dutkiewicz, “Proof-of-stake consensus mechanisms for future blockchain networks: Fundamentals, applications, and opportunities,” IEEE Access, vol. 7, pp. 61703–61725, 2019, doi: 10.1109/ACCESS.2019.2925010.

[32] G. Tripathi, M. A. Ahad, and G. Casalino, “A comprehensive review of blockchain technology: Underlying principles and historical background with future challenges,” Decision Analytics Journal, vol. 9, Art. no. 100344, 2023.

[33] D. Commey, B. Mai, S. Hounsinou, and G. Crosby, “Securing blockchain-based IoT systems: A review,” IEEE Access, 2024, doi: 10.1109/ACCESS.2024.3428490.

[34] G. Gad, D. T. Mosa, L. Abualigah, and A. A. Abohany, “Emerging trends in blockchain technology and applications: A review and outlook,” Journal of King Saud University - Computer and Information Sciences, vol. 34, no. 9, pp. 6719–6742, 2022.

[35] G. Habib, S. Sharma, S. Ibrahim, I. Ahmad, S. Qureshi, and M. Ishfaq, “Blockchain technology: Benefits, challenges, applications, and integration of blockchain technology with cloud computing,” Future Internet, vol. 14, no. 11, Art. no. 341, 2022, doi: 10.3390/fi14110341.

[36] S. Hassan and P. De Filippi, “Decentralized autonomous organization,” Internet Policy Review, vol. 10, no. 2, pp. 1–10, 2021, doi: 10.14763/2021.2.1556.

[37] M. Pilkington, “Blockchain technology: Principles and applications,” in Research Handbook on Digital Transformations, F. X. Olleros and M. Zhegu, Eds., Cheltenham, UK: Edward Elgar Publishing, 2016, pp. 225–253.

[38] C. Santana and L. Albareda, “Blockchain and the emergence of decentralized autonomous organizations (DAOs): An integrative model and research agenda,” Technological Forecasting and Social Change, vol. 182, Art. no. 121806, 2022, doi: 10.1016/j.techfore.2022.121806.

[39] F. Wang and P. De Filippi, “Self-sovereign identity in a globalized world: Credentials-based identity systems as a driver for economic inclusion,” Frontiers in Blockchain, vol. 2, 2020. [Online]. Available: https://doi.org/10.3389/fbloc.2019.00028

[40] R. Belen-Saglam, E. Altuncu, Y. Lu, and S. Li, “A systematic literature review of the tension between the GDPR and public blockchain systems,” Blockchain: Research and Applications, vol. 4, no. 2, p. 100129, 2023.

[41] [40] B. C. Ghosh, V. Ramakrishna, C. Govindarajan, D. Behl, D. Karunamoorthy, E. Abebe, and S. Chakraborty, “Decentralized cross-network identity management for blockchain interoperation,” arXiv preprint, 2021. [Online]. Available: https://arxiv.org/abs/2104.03277

[42] K. Proctor, “Decentralization, immutability, and integrity: The role of blockchain technology in enhancing cybersecurity,” 2024. [Online]. Available: https://doi.org/10.121296/KBP.30606

[43] J.-P. A. Yaacoub, H. N. Noura, and O. Salman, “Security of federated learning with IoT systems: Issues, limitations, challenges, and solutions,” Internet of Things and Cyber-Physical Systems, vol. 3, pp. 155–179, 2023.

[44] D. Van Roijen, “The European digital identity wallet: A healthcare perspective,” Blockchain in Healthcare Today, vol. 7, 2024. [Online]. Available: https://doi.org/10.30953/bhty.v7.344

[45] K. Duan, G. Pang, and Y. Lin, “Exploring the current status and future opportunities of blockchain technology adoption and application in supply chain management,” Journal of Digital Economy, vol. 2, pp. 244–288, 2023.

[46] O. Rikken, M. Janssen, and Z. Kwee, “Governance challenges of blockchain and decentralized autonomous organizations,” Information Polity, vol. 24, pp. 1–21, 2019. [Online]. Available: https://doi.org/10.3233/IP-190154

[47] L. George and J. Kizhakkethottam, “A comparative study of zero-knowledge proof and homomorphic encryption in guaranteeing data privacy in blockchain applications,” International Journal of Advanced Research, vol. 9, pp. 359–361, 2021. [Online]. Available: https://doi.org/10.21474/IJAR01/12455

[48] B. Pillai, K. Biswas, and V. Muthukkumarasamy, “Cross-chain interoperability among blockchain-based systems using transactions,” The Knowledge Engineering Review, vol. 35, 2020. [Online]. Available: https://doi.org/10.1017/S0269888920000314

[49] L. Alevizos, “Automated cybersecurity compliance and threat response using AI, blockchain, and smart contracts,” International Journal of Information Technology, vol. 17, pp. 767–781, 2025. [Online]. Available: https://doi.org/10.1007/s41870-024-02324-9

[50] H. Han, R. K. Shiwakoti, R. Jarvis, C. Mordi, and D. Botchie, “Accounting and auditing with blockchain technology and artificial intelligence: A literature review,” International Journal of Accounting Information Systems, vol. 48, p. 100598, 2023.

[51] A. Balakrishnan, V. Jain, P. Chintale, S. Gadiparthi, and M. Najana, “Blockchain empowerment in sanctions and AML compliance: A transparent approach,” International Journal of Computer Trends and Technology, 2024. [Online]. Available: https://ssrn.com/abstract=4842695

[52] M. Xin, “A mixed encryption algorithm used in Internet of Things security transmission system,” in Proc. IEEE CyberC Conf., 2015, pp. 62–65. [Online]. Available: https://doi.org/10.1109/CyberC.2015.9

[53] D. Hariyani, P. Hariyani, S. Mishra, and M. K. Sharma, “A literature review on transformative impacts of blockchain technology on manufacturing management and industrial engineering practices,” Green Technologies and Sustainability, vol. 3, no. 3, p. 100169, 2025.

[54] S. Kraus, S. Durst, J. J. Ferreira, P. Veiga, N. Kailer, and A. Weinmann, “Digital transformation in business and management research: An overview of the current status quo,” International Journal of Information Management, vol. 63, p. 102466, 2022.

[55] M. Godyn, M. Kedziora, Y. Ren, Y. Liu, and H. Song, “Analysis of solutions for a blockchain compliance with GDPR,” Scientific Reports, vol. 12, p. 15021, 2022. [Online]. Available: https://doi.org/10.1038/s41598-022-19341-y

Journal of Engineering and Technology for Industrial Applications

ISSN ONLINE: 2447-0228

ITEGAM-JETIA

Manaus, v.11 n.54, p. 186-192. July/August., 2025.

DOI: https://doi.org/10.5935/jetia. v11i54.1730

RESEARCH ARTICLE OPEN ACCESS

ENHANCING CHARGE TRANSFER EFFICIENCY IN CCDS USING SILVACO SIMULATIONS

Dahmane Djendaoui[1], Zoubir Becer[2], Themeur Obeidi[3]

[1]Laboratório de Automação Aplicada e Diagnóstico Industrial (LAADI), Universidade de Djelfa
[2]Departamento de Física, Universidade de El-Oued
[3]Faculdade de Ciência e Tecnologia, Universidade de Djelfa.

[1]https://orcid.org/0000-0003-3749-6591, [2]http://orcid.org/0000-0002-8537-9499, [3]http://orcid.org/0009-0000-7573-9270

E-mail: djendaoui.d@gmail.com, becer.zoubir@gmail.com, t.obeidi@univ-djelfa.dz

ARTICLE INFO

Article History
Received: March 18, 2025
Revised: April 20, 2025
Accepted: June 15, 2025
Published: August 31, 2025

Keywords:
Buried-channel Charge-coupled devices (BCCD),
Charge transfer inefficiency (CTI),
Packet signal,
Numerical simulation. SILVACO.

ABSTRACT

In this paper, we investigated the charge transfer efficiency (CTE) of a radiation-damaged charge-coupled device (CCD) subjected to proton radiation levels typical of particle detection, nuclear imaging, and space-borne experiments. The trapping of charge carriers by bulk states is the primary factor affecting CTE in such damaged CCDs. Our analysis focused on examining the CTE as a function of signal level, radiation dose (trap concentration), and temperature. We employed the SILVACO semiconductor simulation software using a two-dimensional numerical model to simulate the dynamic transfer process in a buried-channel CCD (BCCD) with a three-phase clock pulse driver. The simulation, after setting the appropriate physical models and the suggested deep trap levels in the channel region, demonstrated that the CTE exhibits a nonlinear dependence on the signal level, with the charge transfer inefficiency (CTI) peaking at $7x10^{-6}$ at 135 K and reaching a minimum value of $2x10^{-6}$ around 200 K. The simulation results we obtained closely match the experimental data found in the literature, providing us with a deep understanding of the impact of radiation-induced traps on the dynamic charge transfer processes in charge-coupled devices.

Copyright ©2025 by authors and Galileo Institute of Technology and Education of the Amazon (ITEGAM). This work is licensed under the Creative Commons Attribution International License (CC BY 4.0).

I. INTRODUCTION

Charge-coupled devices (CCDs), invented by George Smith and Willard Boyle at Bell Laboratories in 1969 [1], quickly gained prominence in advanced applications such as astronomical imaging and were subsequently popularized in consumer cameras [2, 3]. CCDs are crucial in various fields such as embedded IoT applications due to their advantages, including low cost, low power consumption, high bit density, and high sensitivity [4]. Despite their advantages, CCDs are susceptible to radiation damage [5], which can be categorized into surface and bulk damage. In the context of charge transfer losses in buried channel devices, bulk traps are of primary concern. These traps create energy levels between the conduction and valence bands, capturing electrons and releasing them back into the conduction band after some time [6, 7].

The operation of a Charge-Coupled Device (CCD) begins when photons strike the sensor, triggering the photoelectric effect, which creates pairs of holes and electrons. These electrical charges accumulate in specific regions formed by an array of metal-oxide-semiconductor (MOS) capacitor structures, which act as microscopic charge packet traps in the form of potential wells. For each individual pixel in the final image, the accumulated charge packet corresponds to the intensity of incoming light at that point [8].

The MOS capacitors are strategically arranged with minimal spacing between them, enabling charge transfer from one capacitor to its neighbor through a controlled overflow mechanism between their potential wells. This transfer process must be highly efficient since each packet of charge needs to move through numerous steps before reaching the output stage. This requirement has become even more critical as modern CCDs now incorporate millions of pixels, necessitating thousands of successive transfers for each charge packet.

A crucial metric for CCD performance is the charge transfer efficiency (CTE), which quantifies how effectively charge moves between adjacent pixels. The CTE is expressed as a decimal fraction, with current high-quality CCDs achieving approximately 0.99999. This can alternatively be described using the charge transfer inefficiency (CTI), which is calculated as 1 minus the CTE value. CTI in buried channel charge-coupled devices (BCCDs) is a critical factor affecting device performance. Studies have shown that BCCDs generally exhibit lower CTI compared to surface-channel CCDs (SCCDs) due to reduced interface traps [9]. Optimizing design parameters, such as p-well inclusion over silicon trench isolation (STI) edges, can further reduce CTI in CMOS based CCDs [10]. Controlling the rising and falling times of clock signals significantly improves CTI in BCCDs but has minimal effect on SCCDs [9].

Particle radiation exposure can also significantly degrade the CTI performance of CCDs. Extensive research has demonstrated that the deterioration in CTI following radiation exposure can be attributed to the formation of electron trap sites within the device structure [8]. While the relationship between trapping mechanisms and radiation effects was recognized in early studies, the expanding role of CCDs in space-based applications has driven substantial contemporary research in this field [11]. Additionally, studies have shown that both operating temperature and charge transfer timing play crucial roles in determining CTI performance [12] and we have been able to demonstrate this utilizing advanced transient two-dimensional device simulation since one-dimensional analysis may overestimate charge handling capacity [13]. A comprehensive understanding of these various factors affecting CTI is essential for multiple purposes: it enables more accurate interpretation of CCD-collected data, allows operators to optimize device settings, and guides manufacturers in developing more radiation-resistant devices.

This study is composed of six sections. In the second section, we presented the methods and the used models including the adopted device structure design, the simulation parameters and the clocking voltages. The third section, details the physical model and its governing equations namely; the Poisson's equation and electron continuity equations along with their numerical solution techniques as well as mobility and recombination models offered by SILVACO Atlas. Section four shows the results of our simulations, namely the trapped charge density from transfer of signal charge as function of time. In Section five, we describe the way in which we did the numerical calculation of CTI based on the simulation output and the trapping theory. In Section six the conclusions are given.

II. METHODS AND MODELS

II.1 DEVICE STRUCTURE

In this study, we use the SILVACO simulation package, particularly the Athena and Atlas programs, to perform two-dimensional simulations of CCDs. The simulated device has dimensions of 28.8 µm in length and 110 µm in depth. The structure of the BCCD is illustrated in Figure 1. It comprises three main parts: an input section, a transfer section, and an output section. The input section includes an input dioxide (ID) and input gate (IG) to generate signal charges, potentially through the photoelectric effect. The transfer section consists of a series of MOS capacitors, with each capacitor representing a transfer gate. In our model, three gates (G1, G2, G3) facilitate signal charge transfer using a three-phase clock pulse driver. The output section includes an output dioxide (OD) and output gate (OG) to discharge the signal charges.

The dielectric thickness in the device is 0.16 µm, composed of two layers: Si3N4 0.06 µm and SiO2 0.10 µm. The lengths of the input and output gates are 4 µm each, with a 0.1 µm gap between the transfer gates, which are also 4 µm long. The doping concentrations and junction depths for various parts of the device are specified, with the pixel size being 12x12 μm^2. The minority carrier lifetime is 10^{-7} seconds.

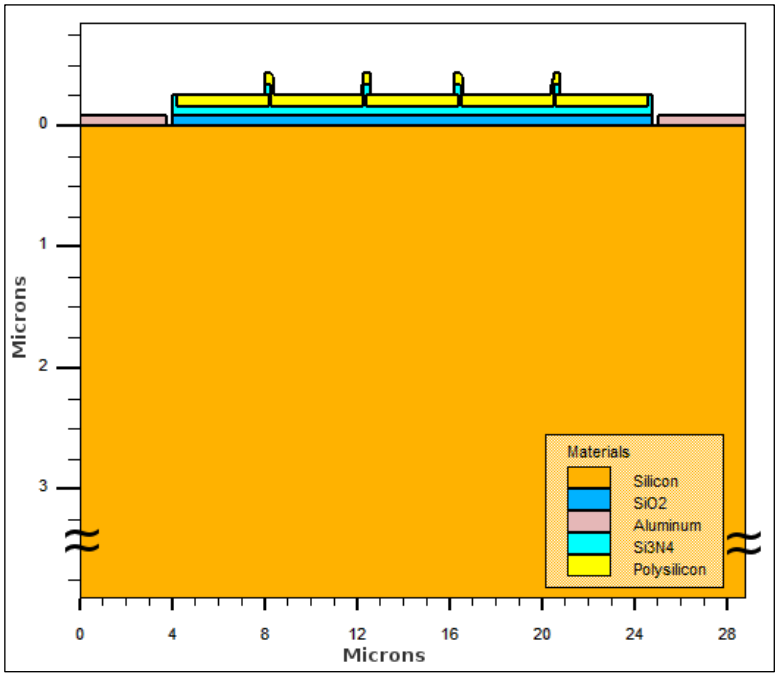

Figure 1: General structure of BCCD (28.8 µm x 110 µm), there are three transfer gates, input part (ID, IG), and output part (OD, OG).
Source: Authors, (2025).

II.2 SIMULATION PARAMETERS

To conduct a successful device simulation, an input file is written in Duckbuild (API interface of SILVACO) to virtually fabricate a BCCD structure using Athina process package, and then pass the built structure to Atlas package for electrical simulation.

Figure 2 shows the mesh of the CCD structure, designed using ATHENA. We refined the mesh size on the buried channel to resolve the doping and charge profiles. The cross-section under gate G2 of the net doping is presented in Figure 3.

During the transfer process, voltages applied to various parts of the device range from -6V to 12V, as detailed in the clock voltage diagram in Figure 4. The CCD circuit is driven by a clock pulse frequency of 4 MHz.

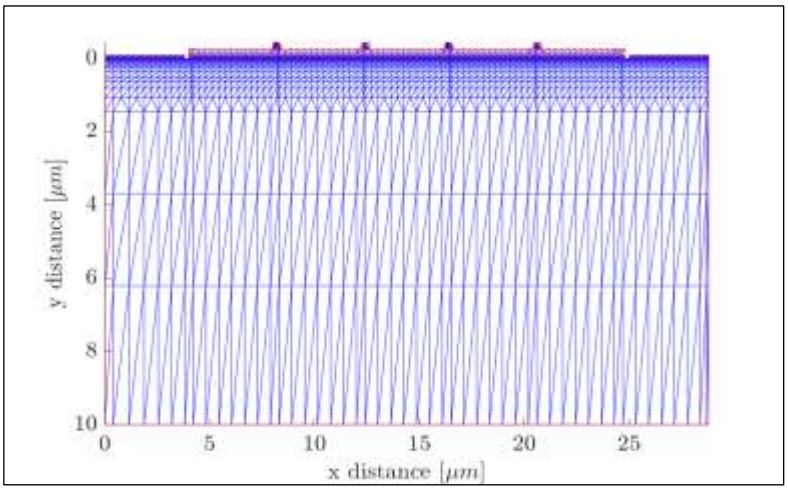

Figure 2: The Mesh use the CCD structure. The mesh size is small on the center of transfer channel.
Source: Authors, (2025).

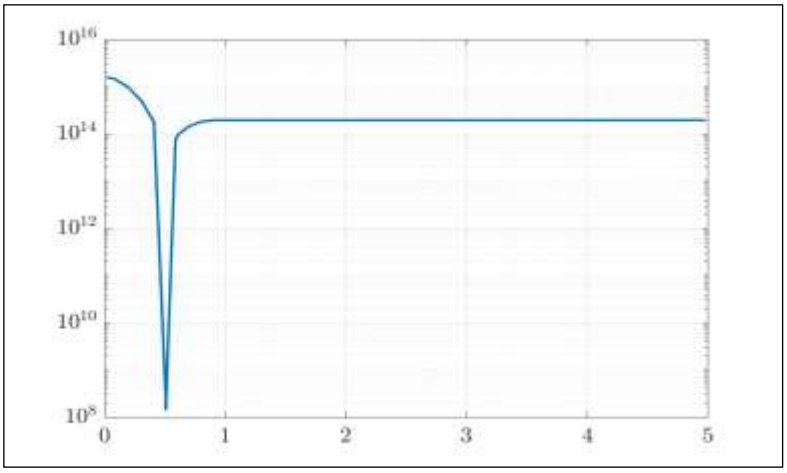

Figure 3: Net doping concentration along the cross-section beneath gate G2.
Source: Authors, (2025).

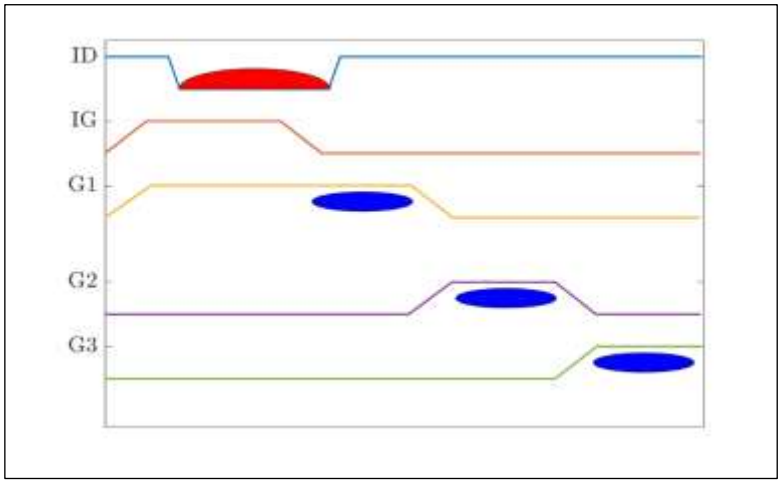

Figure 4: Diagram of clock voltages in a three-phase BCCD. The shaded areas schematically represent the signal charge packet and illustrate how it is transferred by the clock voltages.
Source: Authors, (2025).

III. SIMULATION

III.1 MOBILITY AND RECOMBINATION MODELS

The SILVACO incorporates various mobility and recombination models. Mobility models include concentration mobility, surface mobility, and electric field mobility. Recombination models involve Shockley-Read-Hall (SRH) and Auger recombination processes. The physical models implemented in this simulation represent key physical effects relevant to CCD device performance. The CVT ATLAS mobility model incorporates surface mobility degradation, which plays a critical role during the charge transfer phase, as charge moves from the storage node to the drain. The recombination models, activated in ATLAS via the key words CONSRH and AUGER, are essential for accurately capturing carrier recombination, which significantly influences capacity and charge transfer characteristics. Additionally, band gap narrowing is included to account for the properties of regions with high carrier concentration.

III.2 SOLUTION TECHNIQUE

SILVACO offers different methods for solving the semiconductor drift-diffusion (DD) equation alongside Poisson's equation across the mesh grid within the device structure. We adopt Newton's method to efficiently solve the Poisson's equation and electron continuity equations in the N-buried channel CCD. Poisson's equation, given by Equation (1) is solved for the electrostatic potential ψ

$$\nabla.(\varepsilon\nabla\psi) = -\mathrm{q}(\mathrm{p} - \mathrm{n} + N_D^+ - N_A^-) \tag{1}$$

Where ε is the permittivity, q is the electron charge, n and p are the electron and hole densities, and N_D^+ and N_A^- are the ionized donor and acceptor densities.The electron and hole continuity equations, represented by Equations (2, 3), are solved for the electron and hole concentrations:

$$\frac{\partial n}{\partial t} = \nabla.J_n + G_n - U_n \tag{2}$$

$$\frac{\partial p}{\partial t} = \nabla.J_p + G_p - U_p \tag{3}$$

Where J_n and J_p are the electron and hole current densities, and G_n and G_p are the generation rates.

The current density equations are given by Equations (4, 5):

$$J_n = q\mu_n nE + qD_n\nabla n \tag{4}$$

$$J_p = q\mu_p pE + qD_p\nabla p \tag{5}$$

Where μ_n and μ_n are the electron and hole mobilities, D_n and D_p are the diffusion coefficients, and E is the electric field.

IV. RESULTS

IV.1 ELECTRON CONCENTRATION DISTRIBUTION

The simulation begins by setting the drain bias to +14V, while maintaining all other gates at -6V. This initial step depletes

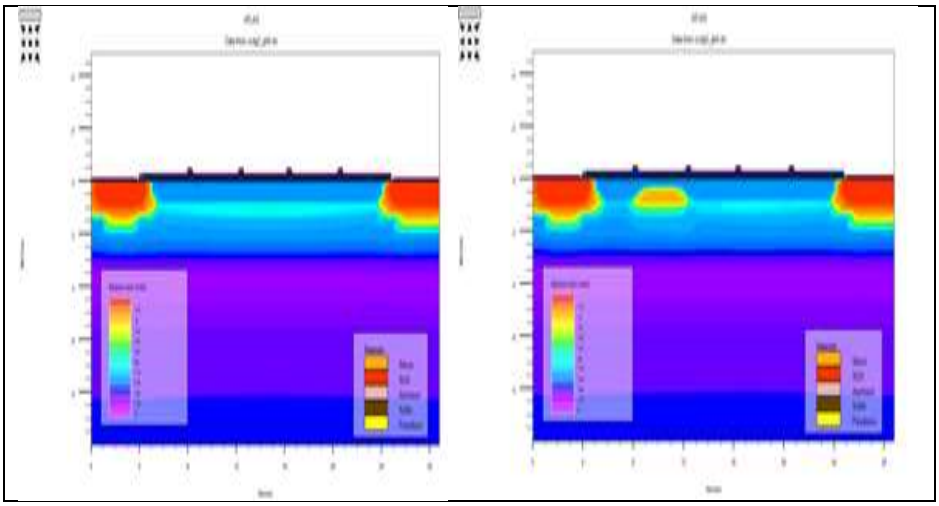

Figure 5: Surf of electron concentration distribution before and after signal charges.
Source: Authors, (2025).

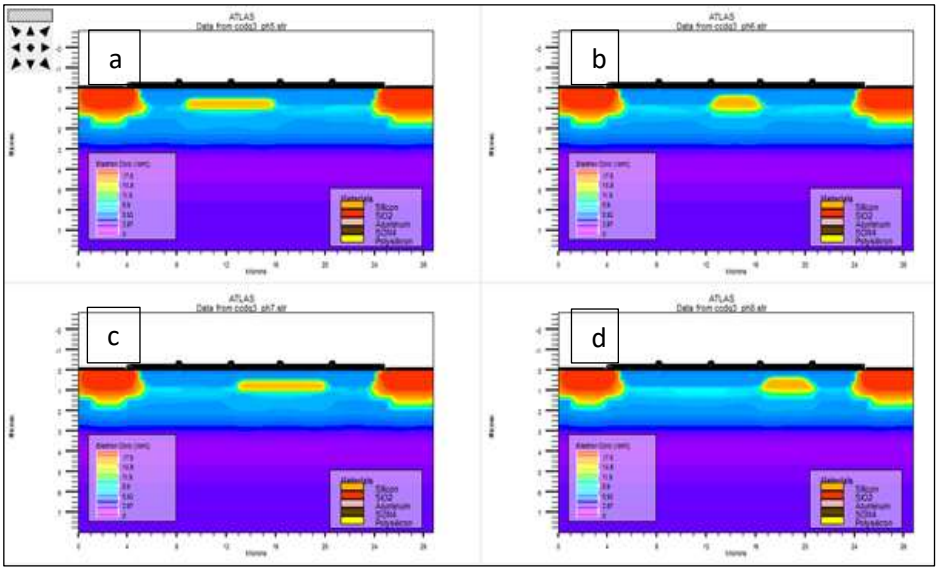

Figure 6: Surf of electron concentration distribution for signal charges transfer.
Source: Authors, (2025).

electrons from the n-type active layer. Following this, the storage gate is illuminated in a transient simulation, generating charge that is subsequently collected beneath the electrode gate G1. Figures 5 illustrate the electron concentration distribution before (left) and after (right) the formation of packet charges under gate G1. The electron concentration in the buried channel under non-illumination is observed to be at its minimum value ($10^{10}cm^{-3}$), indicating that no electrons are being generated or stored at this stage. After, illumination electrons charges are stored under gate G1 and peaks towards $10^{17}cm^{-3}$, and the number of stored electrons reaches up to $1.5x10^{8}$.

The gates within the device are interconnected in a periodic configuration to establish the CCD phases. The selected interconnection scheme as shown in Figure 2, determines the number of clocking voltages necessary to facilitate a unidirectional charge transfer towards the output drain. The transfer of packet charges under gates G2 and G3 is depicted in Figures 6(a, b, c, d).

IV.2 POTENTIAL AND ELECTRON CONCENTRATION PROFILES

A cross-section of potential and electron concentration along the y-line at $x = 0.6325\ \mu m$ is shown in Figure 7. This figure presents the electron concentration profile in the potential well, the electron density under gate G1, and the transfer process of electron density with corresponding potential profiles under gates 1 and 2.

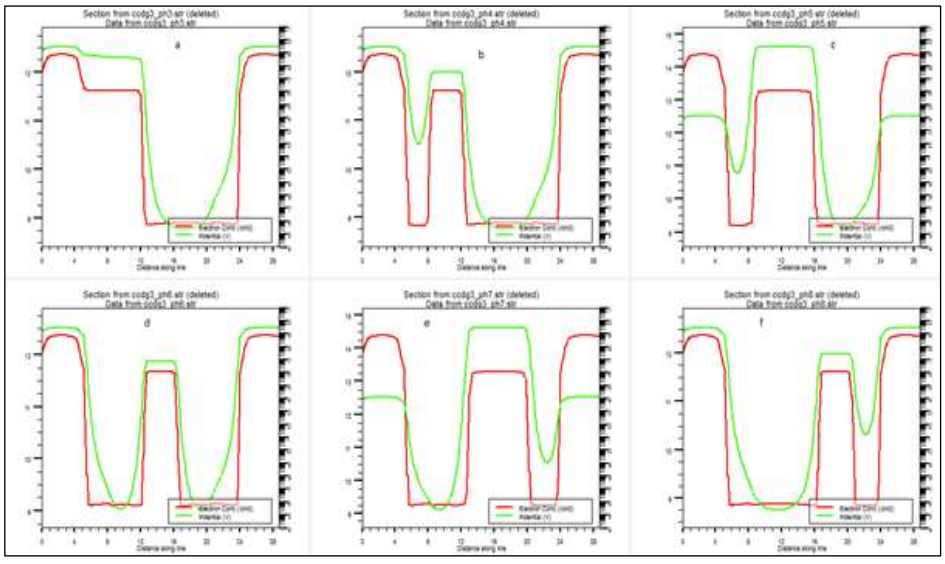

Figure 7: A cross section of potential and electron concentration along of 'y' line at $x = 0.6325\ \mu m$ (peak).
Source: Authors, (2025).

The trapped charge density resulting from the transfer of signal charge is evaluated once the signal packet has reached gate G3 is shown in Figure 6 (d) and Figure 7 (f). Due to emission, the trapped charge density decreases progressively from right to left. Since the charge spends significantly more time under the gates than in the gaps, the trapped charge density beneath the gates is considerably higher compared to the regions between them.

V. CHARGE TRANSFER INEFFICIENCY

Charge Transfer Inefficiency (CTI) measures the fractional loss of charge from a signal packet as it transfers across a pixel (three gates). The CTI for transfer over one gate is calculated using Equation (6) [14]:

$$CTI = \frac{Q_0 - Q_T}{Q_0} \tag{6}$$

Where Q_0 is the charge under the first gate, and Q_T is the charge transported to the second gate.

The CTI study incorporates bulk traps with energies 0.17 eV below the conduction band. These traps, created by incident particles with sufficient energy to displace atoms from their lattice points, introduce stable defects that manifest as energy levels [15,16]. The trap concentrations and electron capture cross-sections used in the simulations are 10^{11} cm^{-3} and 10^{-14} cm^{-2}, respectively. Following the simulation of the transfer process in ATLAS, a separate 2D integration of the trapped charge density distribution is carried out to determine the total charge beneath each gate.

V.1 CTI VERSUS TEMPERATURE

Figure 8 demonstrates the variation of CTI with temperature at a frequency of 4 MHz. The CTI peaks at $7x10^{-6}$ at 135 K, and optimal values are achieved around 200 K with a minimum CTI of $2x10^{-6}$. This indicates that higher temperatures contribute to more efficient charge transfer, minimizing losses due to traps.

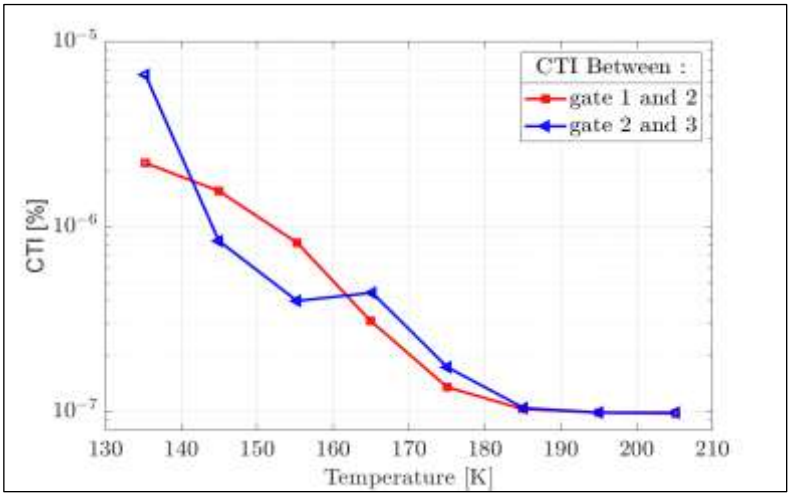

Figure 8: Charge transfer inefficiency against temperature at clocking frequency of 4 MHz.
Source: Authors, (2025).

It is observed that there is a general decrease CT with increasing temperature in the damaged device. Furthermore, the relationship between CTI and temperature exhibits a stronger nonlinear dependence [17].

VI. CONCLUSIONS

The Charge Transfer Inefficiency (CTI) in proton-damaged BCCD's is influenced by several parameters, particularly those associated with trap characteristics, including trap energy level, capture cross-section, and trap concentration (density). Additionally, operating conditions significantly impact CTI, as there is a strong temperature dependence on the trap emission rate, as well as a variation in CTI with the readout frequency. The buried charge-coupled device (BCCD) was comprehensively simulated using 2D process and simulation models implemented in the SILVACO software suite. This study analyzed the variation of CTI with temperature at a clock frequency of 4 MHz, incorporating partially filled traps at 0.17 eV below the conduction band. The results indicate that the optimal CTI values are achieved at temperatures around 200 K, with a minimum CTI of $2x10^{-6}$, demonstrating the efficiency of charge transfer improves significantly at higher. The model predictions align well with the experimental results found in the literature. It is noted that there is a general decrease in CTI with increasing temperature in the damaged device. Additionally, the relationship between CTI and temperature demonstrates a pronounced nonlinear dependence. Finally, a significant advancement in enhancing the outcomes of this work would be to develop a 3D model, as the CTI is also influenced by the shape of the volume occupied by the signal packet.

VII. AUTHOR'S CONTRIBUTION

Conceptualization: Dahmane Djendaoui, Zoubir Becer and Thameur Obeidi.
Methodology: Dahmane Djendaoui, Zoubir Becer and Thameur Obeidi.
Investigation: Dahmane Djendaoui, Zoubir Becer and Thameur Obeidi.
Discussion of results: Dahmane Djendaoui, Zoubir Becer and Thameur Obeidi.
Writing – Original Draft: Dahmane Djendaoui.
Writing – Review and Editing: Dahmane Djendaoui, Zoubir Becer.
Resources: Dahmane Djendaoui, Zoubir Becer

Supervision: Dahmane Djendaoui, Zoubir Becer and Thameur Obeidi.
Approval of the final text: Dahmane Djendaoui, Zoubir Becer and Thameur Obeidi.

VIII. REFERENCES

[1] W. S. Boyle, G. E. Smith, “Charge coupled semiconductor devices”, Bell Systems Technical Journal, vol. 49, no. 4, pp. 587–593, Apr. 1970.
DOI: 10.1002/j.1538-7305. 1970.tb01790.x

[2] M. lesser, “Charge-coupled device (CCD) image sensors”, High Performance Silicon Imaging, Elsevier Ltd, pp. 75-93, **2020**.
https://doi.org/10.1016/B978-0-08-102434-8.00003-9

[3] I. Afanasieva. et al. “Astronomical Camera Based on a CCD261-84 Detector with Increased Sensitivity in the Near-Infrared”, Photonics, vol. 10, no. 7, pp. 774, Jul. **2023**.
https://doi.org/10.3390/photonics10070774

[4] W, Zujun. et al., “Simulation for signal charge transfer of charge coupled devices”, Journal of Semiconductors, vol. 30, no.12, 2009.
DOI 10.1088/1674-4926/30/12/124007

[5] B. Lu. et al. “Design and Characterizations of the Radiation-Hardened XCR4C ASIC for X-Ray CCDs for Space Astronomical Applications”. IEEE Transactions on Nuclear Science, vol. 67, no. 6, pp. 1175 – 1184, June. **2020**. DOI: 10.1109/TNS.2020.2993402

[6] J. R. Janesick, “Scientific Charge-Coupled Devices”. SPIE Press, 2001.
https://doi.org/10.1117/3.374903

[7] Silvaco Inc. Atlas user manual—Device Simulation Software, Silvaco Inc, Santa Clara, 2013.

[8] N. Bush, D. Hall, A. Holland, “Proton-induced traps in electron multiplying charge-coupled devices”, Journal of Astronomical Telescopes, Instruments, and Systems, vol .7, no.1, Mar. **2021**
https://doi.org/10.1117/1.JATIS.7.1.016003

[9] O. Marcelot,, et al, “Study of CCD Transport on CMOS Imaging Technology: Comparison Between SCCD and BCCD, and Ramp Effect on the CTI”, IEEE Transactions on Electron Devices, vol.61, no.3, pp. 844-849 Feb. 2014
DOI: 10.1109/TED.2014.2298693

[10] O. Marcelot, R. Molina, M. Bouhier and P. Magnan, "Design Impact on Charge Transfer Inefficiency of Surface CCD on CMOS Devices: TCAD and Characterization Study," in IEEE Transactions on Electron Devices, vol. 63, no. 3, pp. 1099-1104, March 2016,
Doi: 10.1109/TED.2016.2516045.

[11] S. Chahira, M. Mohammed, “Investigation of Space Radiation-Induced Effects on the Performance of CCD Detectors using Radiation Monitor’s In-flight Measurements”. IEEE Transactions on Nuclear Science, vol.72, no. 2, pp. 110 – 117, Dec. **2024**.
DOI**:** 10.1109/TNS.2024.3524761

[12] S. Parsons, et al, “Effects of temperature anneal cycling on a cryogenically proton irradiated CCD”. *Journal of Instrumentation*, vol. *16*, *no.* 11, Nov. **2021**.
DOI: 10.1088/1748-0221/16/11/P11005

[13] H. C. Hsieh, T. W. Luk, “Two-dimensional transient analysis of a buried-channel charge-coupled device”, Solid State Electronics, vol. 27, no. 3, pp.213-224, Mar. 1984.
https://doi.org/10.1016/0038-1101(84)90116-3

[14] A. Sopczak, “Modeling of charge transfer inefficiency in a CCD with high-speed column parallel readout”, IEEE Transactions on Nuclear Science, vol. 56, no. 3, pp. 1613-1617, June. 2009.
DOI: 10.1109/TNS.2009.2020985

[15] W. Zujun, X. Yuanyuan, X. Rui, et al. “Charge transfer inefficiency increase of the CCD detector induced by proton and neutron irradiations”. Nuclear Instruments and Methods in Physics Research Section A: Accelerators, Spectrometers, Detectors and Associated Equipment, vol. 978, Oct. **2020**.
https://doi.org/10.1016/j.nima.2020.164431

[16] S. André, A. Salim, B. Khaled, et al. “Radiation hardness studies in a CCD with high-speed column parallel readout”. Journal of Instrumentation, vol. 3, no 05, May. 2008
DOI: 10.1088/1748-0221/3/05/P05007

[17] W. Lin, Z. Zitao, Z. Dong, et al. “Study on the mechanism of temperature effect on proton irradiated charge-coupled device”, Radiation Effects and Defects in Solids, vol. 178, no 5-6, pp. 668-679. Jan. **2023**,
https://doi.org/10.1080/10420150.2023.2166837

Journal of Engineering and Technology for Industrial Applications

ITEGAM-JETIA

Manaus, v.11 n.54, p. 193-202. July/August., 2025.
DOI: https://doi.org/10.5935/jetia. v11i54.1743

ISSN ONLINE: 2447-0228

RESEARCH ARTICLE OPEN ACCESS

QUIZ-TUBE: ENHANCING VIDEO-BASED LEARNING WITH AUTOMATED AI QUIZ GENERATION

Akash Thakur[1], Rashmi Bhat[2], Ayush Shukla[3], Tushar Ram[4] and Vivek Singh[5]

[1,2,3,4,5] St. John College of Engineering and Management, Palghar, Maharashtra.

[1]https://orcid.org/0009-0006-4704-6374, [2]https://orcid.org/0009-0003-3064-1247, [3]https://orcid.org/0009-0005-9677-5509
[4]https://orcid.org/0009-0006-2523-418X, [5]https://orcid.org/0009-0005-5429-8265

Email: akashthakur4553@gmail.com, rashmib@sjcem.edu.in , ayushshukla7291@gmail.com, tusharram085@gmail.com, viveksingh92317@gmail.com

ARTICLE INFO

Article History
Received: March 22, 2025
Revised: April 20, 2025
Accepted: June 15, 2025
Published: August 31, 2025

Keywords:
Large Language Model,
Natural Language processing,
Video-based learning,
model fine-tuning,
Question generation

ABSTRACT

In the digital age, video-based learning has become a dominant educational medium, with platforms like YouTube offering a vast repository of instructional content. However, passive video consumption often leads to suboptimal knowledge retention and limited engagement. To address this challenge, we introduce Quiz-Tube, an AI-powered web platform that converts educational YouTube videos into interactive quizzes. By leveraging a fine-tuned Gemma-9B language model, Quiz-Tube generates contextually relevant multiple-choice questions (MCQs) tailored to users' preferences. The system integrates transcript extraction via the YouTube Transcript API, followed by data preprocessing, question generation, and quiz customization. Users can define quiz parameters such as difficulty level and question count, enhancing personalized learning. Our evaluation demonstrates significant performance improvements, including a BLEU score increase from 45.3 to 68.7 and an accuracy boost from 64.5% to 81.9% post-model fine-tuning. Future enhancements include multilingual support and AI-driven adaptive learning.

Copyright ©2025 by authors and Galileo Institute of Technology and Education of the Amazon (ITEGAM). This work is licensed under the Creative Commons Attribution International License (CC BY 4.0).

I. INTRODUCTION

The expansion of online education has revolutionized the way people access and interact with learning materials. With the rapid advancement of digital platforms, particularly video-based platforms such as YouTube, students and professionals now have unprecedented access to vast repositories of educational content spanning diverse subjects. The rise of video-based learning has played a transformative role in modern education, offering flexibility and accessibility that traditional learning methods often lack. Learners can explore complex topics at their own pace, revisit content as needed, and gain insights from experts worldwide. However, despite these advantages, video-based learning presents inherent challenges. Passive video consumption does not actively engage learners, which can lead to poor knowledge retention, decreased motivation, and limited comprehension.

Research in educational psychology and cognitive science suggests that active learning techniques significantly enhance comprehension and retention [1]. Active learning involves engaging learners through self-assessment, reflection, and interactive exercises, which are proven to strengthen understanding and long-term recall. Among these techniques, quizzes are particularly effective in reinforcing concepts, testing understanding, and ensuring active participation. By prompting learners to recall information, quizzes help consolidate knowledge and bridge the gap between passive consumption and active engagement. However, the manual creation of quizzes from video content is a labor-intensive and time-consuming task, making it impractical for both educators and learners who consume vast amounts of online educational material daily.

As the demand for personalized and interactive learning experiences continues to grow, there is a pressing need for an automated solution capable of generating relevant and customized quizzes from video content. Addressing this challenge, Quiz-Tube introduces an AI-driven approach that leverages large language models (LLMs) [2] and natural language processing (NLP) to convert YouTube video transcripts into interactive quizzes. By utilizing the fine-tuned Gemma-9B model [3], Quiz-Tube ensures the generation of contextually accurate and personalized multiple-choice questions (MCQs) tailored to individual learning preferences and proficiency levels.

Quiz-Tube enhances user engagement by allowing learners to define quiz parameters, such as difficulty levels, the number of questions, and topic focus. This customization empowers users to tailor their learning experience, making it more adaptive and suited to their specific educational needs. Additionally, by integrating natural language understanding and deep learning techniques, Quiz-Tube can analyze video transcripts, extract key concepts, and generate well-structured assessment items that align with the core ideas presented in the video. This automation streamlines the quiz creation process, reducing the workload on educators while enabling self-learners to engage more effectively with educational content.

This paper details the system architecture, methodology, and performance evaluation of Quiz-Tube, demonstrating its effectiveness in enhancing active learning engagement. We explore the technical aspects of AI model training, quiz generation processes, and user experience design. Additionally, we discuss future improvements that will further expand the platform's impact on digital education. These enhancements include multilingual support, which will enable non-English speakers to benefit from the platform, AI-driven personalization to further tailor quizzes based on individual learning patterns, and mobile integration to increase accessibility for users who prefer learning on-the-go. By addressing the challenges of passive video-based learning and bridging the gap between content consumption and active engagement, Quiz-Tube represents a significant advancement in the field of digital education. This research aims to contribute valuable insights into the intersection of artificial intelligence and online learning, paving the way for more interactive, personalized, and effective educational experiences. Through continued development and refinement, Quiz-Tube has the potential to revolutionize how learners engage with video-based educational content, fostering a more dynamic and enriching learning ecosystem.

II. RELATED REVIEWS

A variety of approaches have been explored in the field of large language models (LLMs) and automated question generation, with applications spanning financial decision-making, education, and efficient AI-driven assessments. Fine-tuning domain-specific LLMs [4] has shown significant promise in enhancing decision-making and automation tasks, particularly when domain vocabulary creation and regulatory compliance are carefully managed. While financial applications have been a key focus, the potential of fine-tuned models extends to other domains, such as education, where models can dynamically generate quizzes from video transcripts and tailor content to user preferences.

Automated multiple-choice question generation (MCQG) has been extensively studied using NLP techniques. Early methodologies relied on static text materials, employing techniques such as TF-IDF and N-grams for keyword extraction and question formulation. While effective, these methods lack integration with multimedia content and fail to incorporate user-driven customization. Advancements in LLMs have enabled more dynamic approaches, allowing quiz generation from video transcripts and enhancing contextual relevance through fine-tuned models [5]. Another approach involves leveraging advanced prompt engineering and retrieval-augmented generation (RAG) techniques to improve question quality. By incorporating chain-of-thought and self-refine prompting, more contextually relevant and challenging questions can be produced. A key distinction in modern systems is the reliance on educational video transcripts, allowing for the extraction of meaningful information and the creation of tailored datasets. This approach not only improves question quality but also integrates user quiz histories to refine personalization and adaptability [6].

Fine-tuning pre-trained language models (PLMs) for educational question generation has also gained traction. Some models focus on additional pre-training using domain-specific datasets, such as those containing scientific educational questions. The emphasis on linguistic fluency and contextual relevance aligns with the goal of generating high-quality quizzes from educational video transcripts. While some approaches rely primarily on textual corpora, integrating transcript APIs broadens real-world applications, making AI-driven quiz generation accessible across diverse subjects and formats [7]. Efforts to optimize memory and computational efficiency in LLMs have been explored through post-training quantization techniques. These methods aim to reduce bit-width while maintaining performance across tasks such as dialogue processing and long-context understanding. While not directly implemented in all quiz generation systems, such techniques hold promise for enhancing scalability, particularly when processing large volumes of educational transcripts or generating multiple-choice quizzes in real time [8].

Further research into quantization has investigated strategies to mitigate information loss through fine-tuning techniques. Methods incorporating information calibration quantization and elastic connection strategies have been proposed to retain model accuracy while reducing resource consumption. These approaches align with the broader goal of efficiency and customization in LLM-based applications, demonstrating the potential for optimizing models to generate adaptive quizzes based on user-selected difficulty levels [9]. Improvements in retrieval-augmented generation have also contributed to enhancing quiz generation processes. By employing long-context LLMs, retrieval methods have been optimized to minimize contextual loss, leading to higher retrieval accuracy and improved content generation. This shift from short retrieval units to longer retrieval mechanisms reduces the burden on information retrieval systems while ensuring the accuracy of generated questions. These advancements further enable large-scale educational applications, allowing for the seamless integration of AI-driven learning tools into modern e-learning platforms.[10]

The automation of test creation using AI has been explored as a means to streamline educational assessments. AI-based systems can generate test questions based on predefined parameters such as difficulty level, question type, and cognitive skills classification. By leveraging cloud-based platforms and API-driven integrations, these systems enhance flexibility, adaptability, and efficiency in educational settings. Automated test generation offers a scalable solution for educators seeking to implement personalized assessments without extensive manual effort [11]. Beyond multiple-choice question generation, research has also explored the use of large language models for subjective question formulation. Some systems have been developed to generate opinion-based questions derived from news articles and trending topics, leveraging sequence-to-sequence generation techniques. This research highlights the adaptability of LLMs for diverse question-generation applications beyond factual recall, extending their utility to discussion-based and critical thinking exercises [12].

Self-play fine-tuning has emerged as a novel technique for enhancing LLM performance without requiring extensive human-annotated data. Unlike traditional fine-tuning approaches, self-play mechanisms enable models to iteratively train themselves by generating and evaluating their own data. This method improves response quality by aligning model-generated outputs with human-like

distributions. Studies have demonstrated that this technique can surpass traditional optimization strategies, paving the way for improved performance in educational AI applications. Reinforced self-training has also been introduced as an alternative method for fine-tuning language models. By integrating reinforcement learning techniques, models can refine their outputs iteratively using reward-based mechanisms. This approach enhances generalization capabilities, particularly in domains requiring logical reasoning and complex problem-solving. By balancing exploration and exploitation, reinforcement-based self-training minimizes training instability while optimizing model performance for educational tasks [13].

The interaction between parametric knowledge stored within LLMs and externally retrieved information has also been a subject of study. Research has shown that retrieval-augmented generation methods improve factual accuracy by prioritizing external context over pre-trained memory. Understanding these interactions is crucial for optimizing AI-driven quiz generation systems, as it helps ensure that generated questions remain accurate and contextually relevant. Such insights contribute to refining LLM-based educational tools and optimizing their ability to process diverse input sources effectively. Collectively, these advancements in LLM fine-tuning, retrieval-augmented generation, quantization, and self-training methodologies highlight the transformative potential of AI in educational applications. The ability to generate dynamic quizzes, personalize learning experiences, and enhance efficiency through optimized AI models paves the way for a more interactive and effective digital learning ecosystem. As research continues to evolve, further integration of scalable AI-driven solutions in education will contribute to more adaptive and accessible learning methodologies, ultimately improving knowledge retention and learner engagement.

III. METHODOLOGY

III.I SYSTEM DESIGN

The QuizTube system is meticulously engineered to automate the generation of quizzes from YouTube educational videos by leveraging advanced Artificial Intelligence (AI) and Natural Language Processing (NLP) techniques. The architecture is designed as a structured pipeline, enabling users to input a video URL and receive an interactive quiz, complete with evaluation results and certification. This comprehensive system comprises several interconnected modules that collaboratively process video content, generate quizzes, and assess user performance.

1. User Interaction and Dashboard

The user journey begins with an intuitive dashboard that allows learners to input a YouTube video URL. This central interface not only facilitates quiz generation but also enables users to manage their quiz preferences, track past results, and obtain certifications. Designed for accessibility across various educational levels, the dashboard provides access to historical quiz performances, allowing learners to monitor their progress over time. Features such as progress bars, feedback visualization, and adaptive quiz difficulty based on past performance enhance user engagement and learning outcomes.

2. Video Processing Module

Upon submission of a YouTube URL, the system initiates a multi-stage process to extract and process the video content. Recognizing that YouTube videos contain both visual and auditory information, the system first isolates the audio stream to capture spoken content accurately. The extracted audio is then transcribed into text using speech recognition algorithms, transforming raw spoken content into a structured text format suitable for further processing by the Large Language Model (LLM). This transcription ensures that the entire lecture or discussion is accurately captured, preserving all relevant details necessary for effective quiz generation.

3. AI Processing and Quiz Generation

The transcribed text undergoes sophisticated NLP processing using a fine-tuned Gemma-9B language model. This AI-powered module is responsible for extracting key concepts and main topics from the transcribed text, ensuring the retention of the most pertinent information. The model generates quiz questions of varying difficulty levels, allowing users to test their knowledge across different cognitive domains. The generated questions maintain contextual relevance and coherence with the original lecture, ensuring that the quiz accurately reflects the video content. The use of Retrieval-Augmented Generation (RAG) techniques ensures that the generated questions remain accurate and contextually aligned with the video content. Additionally, the AI-powered question generation system ensures grammatical correctness and diversity in the types of questions generated.

4. Quiz Evaluation and Results Analysis

Once the quiz is generated, users can attempt it in real-time through the QuizTube platform. The system automatically scores multiple-choice, providing instant feedback on correct and incorrect answers. It assesses learning progress by tracking historical quiz performance, helping learners identify their strengths and weaknesses. This interactive feedback mechanism enhances the learning process by offering insights into areas needing improvement. The results analysis feature contributes to a personalized learning experience by adjusting quiz difficulty based on the user's previous attempts.

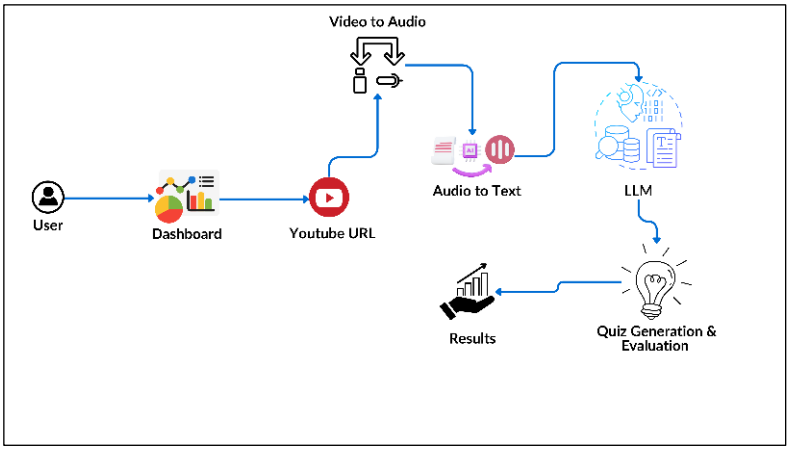

Figure 1: Flowchart of the system.w.
Source: Authors, (2025).

III.1.2 Algorithm:

The algorithmic framework for QuizTube encompasses a structured approach for transforming YouTube educational videos into well-defined, interactive quizzes. The following sections detail the step-by-step process involved in the algorithm's design and implementation:

1. Input Processing and Transcript Extraction

The algorithm begins with acquiring user input, primarily in the form of a YouTube video URL. Upon receiving this URL, the system verifies its validity and attempts to extract the transcript using the YouTube Transcript API.

- **Transcript Retrieval:** The system requests the transcript associated with the video. If the transcript is not available (e.g., due to copyright restrictions or non-English content), the system returns an error message indicating the unavailability of transcription.
- **Audio-to-Text Conversion (if needed):**For videos without transcripts, the audio stream is isolated and converted into text using advanced speech recognition techniques. The algorithm ensures accurate transcription by leveraging pre-trained speech-to-text models optimized for educational content**.**

2. Preprocessing and Text Segmentation

Once the transcript is successfully retrieved, the text undergoes extensive preprocessing to enhance the quality of subsequent processing stages.

- **Noise Removal**: Timestamps, special characters, and irrelevant data (such as advertisements or unrelated dialogue) are removed.
- **Text Normalization:** The text is converted to lowercase, and unnecessary punctuation marks are discarded.
- **Tokenization:** The cleaned text is divided into individual sentences and paragraphs to facilitate easier segmentation.
- **Keyword Extraction:** The Term Frequency-Inverse Document Frequency (TF-IDF) technique is applied to identify the most significant keywords from the transcript. Named Entity Recognition (NER) techniques are also utilized to detect important concepts and topics.

3. Knowledge Graph Construction

A knowledge graph is constructed to map relationships between identified entities and concepts. This step improves the contextual understanding of the text and aids in generating meaningful questions. Techniques such as entity linking and relationship extraction are employed, often supported by knowledge bases like ConceptNet or Wikidata.

4. AI-Based Question Generation

The core of the QuizTube algorithm revolves around generating high-quality quiz questions using the fine-tuned Gemma-9B model.

- **Question Formulation:** The pre-processed text is fed into the Gemma-9B model, which utilizes context-aware filtering and retrieval-augmented generation (RAG) to produce relevant questions.
- **Question Categorization:** The algorithm categorizes questions into three difficulty levels:
  - **Easy:** Direct, fact-based questions aimed at recalling specific information.
  - **Medium:** Conceptual questions requiring comprehension and contextual application.
  - **Hard:** Analytical questions demanding multi-step reasoning or evaluation.

5. Quiz Customization and Formatting

To provide a personalized learning experience, the algorithm allows users to customize quizzes based on their preferences.

- **Customization Options:** Users can select the number of questions (e.g., 5, 10, 15) and choose difficulty levels based on their learning objectives.

- **Content Filtering:** The system filters out questions that are redundant, grammatically incorrect, or poorly structured. This process ensures the coherence and contextual alignment of generated quizzes.

6. User Interaction and Feedback Analysis

The algorithm integrates an interactive quiz interface where users can attempt generated quizzes.

- **Real-Time Evaluation:** Users receive immediate feedback for each question, indicating whether their answer was correct or incorrect.
- **Score: Calculation:** A percentage-based grading system is used to compute the user's overall performance.
- **Performance: Analysis:** Detailed reports are generated, including accuracy rates, topic-wise strengths and weaknesses, and time spent per question.

7. Adaptive Learning Mechanism

Based on the user's quiz performance, the system adapts future quizzes to provide a tailored learning experience.

- **Difficulty Adjustment:** If a user consistently excels, the system gradually increases the difficulty level to maintain engagement and enhance knowledge retention.
- **Topic Reinforcement:** For areas where users demonstrate weakness, the system provides additional quizzes targeting those specific topics.

8. Model Fine-Tuning and Optimization

The fine-tuning of the Gemma-9B model is a crucial aspect of the QuizTube framework, ensuring high-quality question generation.

- **Data Augmentation:** Synthetic question-answer pairs are generated using Gemini-1.5-flash to expand the training dataset, enhancing the model's ability to generalize across diverse educational content.
- **Transfer Learning:** The Gemma-9B model is pretrained on large-scale text corpora and fine-tuned specifically for educational content extraction and quiz generation.
- **Regularization Techniques:** Dropout, gradient clipping, and early stopping mechanisms are employed to prevent overfitting during training.
- **Evaluation Metrics:** Performance is measured using metrics like BLEU Score, F1 Score, and Perplexity.

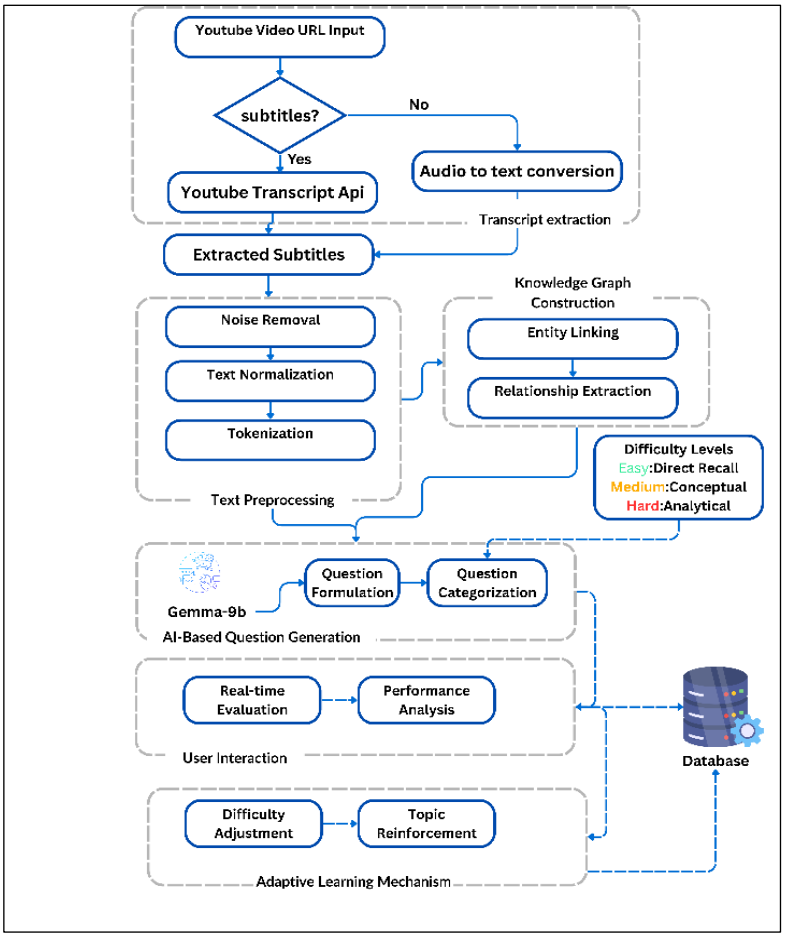

Figure 2: QuizTube Algorithmic Framework
Source: Authors, (2025).

III.II GEMMA-9B MODEL

The Gemma-9B model is an advanced large language model designed for high-accuracy natural language processing (NLP) tasks. It is a 9-billion-parameter model built on Google's Griffin architecture, which integrates gated linear recurrences with local sliding window attention mechanisms. This hybrid approach enhances computational efficiency and is particularly adept at handling long-context prompts. It features 9 billion parameters, making it highly capable of understanding and generating human-like text. The architecture leverages a Transformer-based framework with multiple attention heads and deep feed-forward networks, allowing it to capture complex linguistic patterns and contextual nuances. This model has been optimized for tasks such as text generation, summarization, question answering, and language translation.

III.2.1 Griffin Architecture

The Griffin architecture combines the strengths of recurrent neural networks (RNNs) and attention mechanisms:

- **Gated Linear Recurrences:** These components allow the model to process sequences with a form of memory, capturing temporal dependencies effectively.
- **Local Sliding Window Attention:** This mechanism enables the model to focus on specific parts of the input sequence, improving context management without the extensive computational load associated with global attention.

This architecture ensures that Gemma-9B can manage long sequences efficiently, making it suitable for tasks requiring extensive context understanding.

III.2.2 Model Specifications

Gemma-9B's architecture includes:
1]Multi-Head Self-Attention: Facilitates parallel processing of input sequences to extract contextual representations.
2]Layer Normalization: Enhances stability during training and fine-tuning.
3]Feed-Forward Networks (FFN): Ensures the model can handle non-linear transformations efficiently.
4]Positional Encoding: Maintains word order and contextual relevance within the input text.
5]Residual Connections: Prevents gradient vanishing issues by maintaining information flow between layers.
Collectively, these specifications empower Gemma-9B to perform a wide range of NLP tasks with high proficiency. All Gemma variants operate with a substantial context window of 8,192 tokens, enabling the processing of approximately 6,144 words simultaneously. This extended context capacity allows the model to maintain coherence across longer text sequences and better understand complex, multi-part prompts. However, practitioners should note that effective input capacity fluctuates during interactive use, as generated text consumes portions of the available context window, thereby constraining the space available for new inputs in continuing interactions.

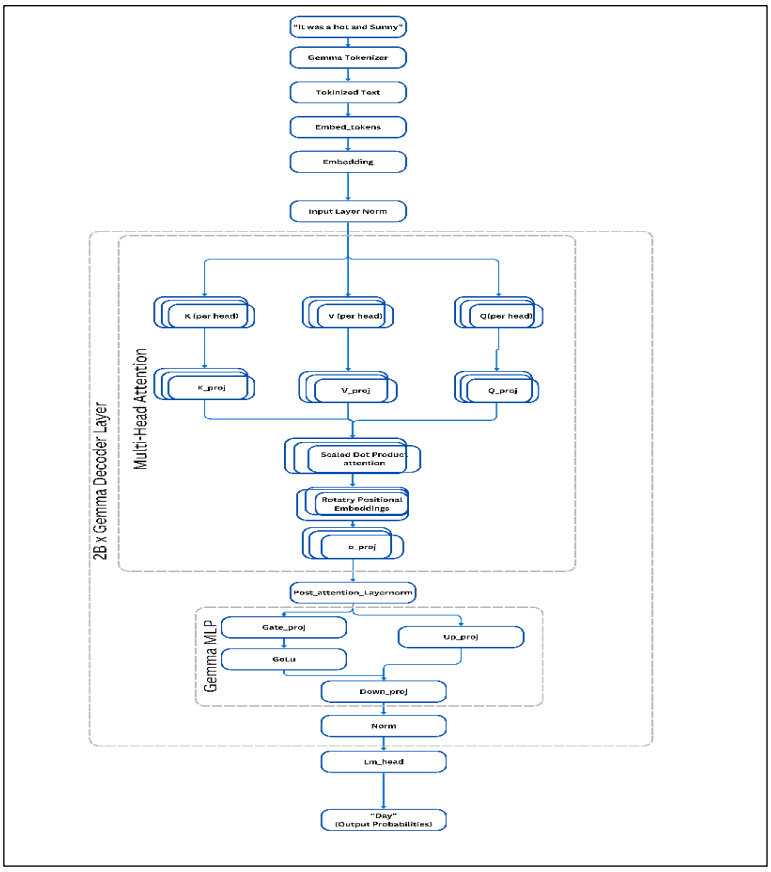

Figure 3: Gemma Architecture.
Source: Authors, (2025).

III.2.3 Key Architectural Parameters and Model Variations

The Gemma architecture is defined by several critical parameters that collectively determine its computational capabilities and performance characteristics:

1] Embedding Dimensions (d_model): The embedding dimension establishes the vector size used to represent individual tokens and significantly influences the model's capacity to capture linguistic nuances and semantic relationships. The family offers progressive embedding dimensionality across its scale variants:

- The 2B model utilizes a 2,048-dimensional embedding space
- The 7B variant employs a more expansive 3,072-dimensional representation
- The 9B model (Gemma 2) further increases dimensional capacity to 3,584, providing enhanced representational capabilities

These dimensional increases correlate with improved performance on complex language tasks, though at the cost of greater computational requirements for both training and inference.

2] Network Depth and Layer Organization: The architectural depth varies significantly across model sizes:

- The 2B configuration implements 18 transformer layers
- The 7B version incorporates 28 layers
- The 9B model features 32 layers

This progressive depth scaling provides increasingly sophisticated pattern recognition capabilities through deeper transformations of the input representations. The additional layers allow higher-parameter models to capture more intricate linguistic patterns, long-range dependencies, and abstract semantic relationships. However, this depth also increases the risk of overfitting and requires substantially more computational resources and training data to achieve proper generalization. The internal organization of each layer follows a consistent pattern across all model sizes, incorporating self-attention mechanisms followed by feed-forward networks, with normalization layers strategically positioned to stabilize training dynamics.

3] Feed-Forward Networks and Activation Functions: Each transformer layer contains a feed-forward network that significantly expands the representational capacity through dimensional projection. The hidden dimensions of these networks scale proportionally with model size:

- 32,768 dimensions in the 2B model
- 49,152 dimensions in the 7B variant
- 57,344 dimensions in the 9B implementation

These expansive hidden representations allow the model to perform complex non-linear transformations on the token embeddings. Notably, Gemma replaces the traditional ReLU activation function with the more sophisticated GeGLU (Gated Linear Unit with GELU activation) function. This advanced activation approach divides processing into parallel sigmoidal and linear projection pathways, with the element-wise multiplication of these pathways producing a more expressive non-linear transformation. The gating mechanism enables more selective information flow, allowing the model to dynamically emphasize relevant features while suppressing irrelevant information.

4] Attention Mechanisms and Efficiency Optimizations: The attention architecture represents a key differentiator between Gemma variants, reflecting sophisticated performance/efficiency trade-offs. The 7B and 9B models implement full Multi-Head Attention (MHA) with 16 attention heads (9B model extends this to 24 heads), enabling the model to simultaneously attend to different aspects of the input sequence from various representational perspectives. This approach maximizes representational capacity but incurs significant computational costs. In contrast, the 2B version employs Multi-Query Attention (MQA) with 8 query heads but only a single key-value head. This architectural optimization dramatically reduces parameter count and memory bandwidth requirements by sharing key and value projections across all query heads. The efficiency gains come with minimal performance degradation on many tasks, making it particularly suitable for resource-constrained environments.
All variants maintain a consistent head size of 256 dimensions, calculated by dividing the embedding dimension by the number of attention heads. This dimensionality provides sufficient representational capacity within each attention head while keeping computational requirements manageable. The models employ rotary positional embeddings (RoPE), which encode positional information directly within the key and query vectors through rotation in the complex plane. This approach provides several advantages over traditional positional encodings, including better extrapolation to sequence lengths beyond those seen during training.

5] Vocabulary and Tokenization Approach: All Gemma models feature an extensive vocabulary of 256,128 tokens derived using the SentencePiece tokenization methodology. This expansive token space enables efficient encoding of diverse linguistic patterns across multiple languages and domains. The SentencePiece approach dynamically learns optimal sub-word segmentation patterns based on training data distribution, allowing the model to effectively handle out-of-vocabulary words through sub-word decomposition. The large vocabulary particularly enhances the model's versatility for multilingual applications and specialized technical domains that may feature unique terminology. This capacity for nuanced tokenization contributes significantly to Gemma's performance on language understanding tasks across diverse domains.

III.III FINE-TUNING THE GEMMA MODEL

Fine-tuning large language models (LLMs) like Gemma-9B necessitates sophisticated strategies to adapt them effectively to specific domains. This section explores advanced fine-tuning methodologies, including Parameter-Efficient Fine-Tuning (PEFT) and Representation Fine-Tuning (ReFT), to optimize the model using a dataset of 1,000 educational transcripts.

III.3.1 Fine-Tuning Techniques

1] Parameter-Efficient Fine-Tuning (PEFT):

Traditional fine-tuning methods involve adjusting all parameters of a pre-trained model to tailor it to a downstream task. While effective, this approach becomes impractical for LLMs due to their massive parameter counts, leading to increased computational costs and memory requirements. PEFT addresses this issue by modifying only a small subset of the model's parameters, thereby preserving the majority of the pre-trained weights. This strategy not only reduces the computational burden but also mitigates the risk of overfitting, especially in scenarios with limited task-specific data.

Several methodologies have been developed under the umbrella of PEFT, each offering unique mechanisms to achieve parameter efficiency. Adapters, for instance, are small neural network modules inserted between the layers of the pre-trained model. They adjust the output of each layer to better fit the target task without altering the original weights, enabling task-specific customization with minimal parameter updates and facilitating efficient multi-task learning. Low-Rank Adaptation (LoRA) introduces trainable low-rank matrices into each layer of the transformer architecture. By decomposing weight updates into low-rank matrices, LoRA reduces the number of trainable parameters, maintaining model performance while significantly lowering the computational burden. This makes it feasible to fine-tune large models on domain-specific data without extensive resource requirements. Prefix Tuning focuses on optimizing continuous task-specific vectors, known as prefixes, that guide the model during generation. By prepending these learnable vectors to the input, prefix tuning steers the model's behaviour without modifying its core parameters, allowing for rapid adaptation to new tasks with a minimal computational footprint.

The primary advantage of PEFT lies in its ability to adapt large models to specific tasks without the need for extensive computational resources. By fine-tuning only a small subset of parameters, PEFT methods significantly reduce memory usage and training time, making them accessible for applications with limited resources. Additionally, by preserving the majority of the pre-trained weights, PEFT minimizes the risk of catastrophic forgetting, ensuring that the model retains its general language understanding capabilities while adapting to new tasks.

PEFT has been successfully applied across various NLP tasks, including sentiment analysis, named entity recognition (NER), and question answering. These applications demonstrate PEFT's versatility in enabling LLMs to perform effectively across diverse tasks without the need for full-scale model retraining. Despite its advantages, PEFT is not without challenges. Determining the optimal subset of parameters to fine-tune requires careful consideration, and there is an ongoing need to balance parameter efficiency with model performance. Future research in PEFT aims to develop more sophisticated methods for selecting trainable parameters and to explore the integration of PEFT with other model optimization techniques to further enhance the adaptability and efficiency of LLMs [14].

2] Representation Fine-Tuning (ReFT):

Representation Fine-Tuning (ReFT) is an emerging paradigm in the field of natural language processing (NLP) that focuses on adapting large language models (LLMs) by intervening on their internal representations rather than their weights. This approach leverages the rich semantic information encoded within the model's hidden states to achieve task-specific adaptation with enhanced parameter efficiency.

Traditional fine-tuning methods adjust the weights of a pre-trained model to tailor it to a specific task. While effective, this approach can be computationally intensive, especially for LLMs with billions of parameters. ReFT offers an alternative by modifying the hidden representations of the model, allowing for task adaptation without altering the model's parameters. This method can be more parameter-efficient than traditional fine-tuning, as it leverages the rich semantic information encoded in the representations.

A notable implementation of ReFT is Low-Rank Linear Subspace ReFT (LoReFT). LoReFT operates by projecting the model's representations into a low-dimensional subspace and learning task-specific interventions within this space. This technique achieves significant parameter efficiency, often requiring updates to less than 1% of the model's parameters while maintaining or improving performance. LoReFT has demonstrated effectiveness across various NLP tasks, including commonsense reasoning, arithmetic reasoning, and instruction-tuning, delivering a favourable balance of efficiency and performance.

The advantages of ReFT are manifold. By focusing on the model's internal representations, ReFT methods can achieve high levels of parameter efficiency, reducing the computational resources required for fine-tuning. This approach also allows for rapid adaptation to new tasks, as the interventions on representations can be learned quickly without the need for extensive parameter updates. Furthermore, by preserving the original weights of the model, ReFT minimizes the risk of catastrophic forgetting, ensuring that the model retains its general language understanding capabilities while adapting to new tasks.

However, ReFT is not without challenges. Determining the optimal interventions on the model's representations requires careful consideration, and there is an ongoing need to balance parameter efficiency with model performance. Future research in ReFT aims to develop more sophisticated methods for learning interventions on representations and to explore the integration of ReFT with other model optimization techniques to further enhance the adaptability and efficiency of LLMs.

In conclusion, Representation Fine-Tuning represents a promising direction in the adaptation of large language models. By leveraging the rich semantic information encoded within the model's representations, ReFT offers a pathway to achieve task-specific adaptation with enhanced parameter efficiency, paving the way for more efficient and effective utilization of LLMs in various NLP applications [15].

Table No. 1: Comparative Analysis of Fine-Tuning Techniques.

Technique	Efficient	Accuracy	Generalization	complex
PEFT	High	High	Medium	Low
REFT	Medium	Medium	High	Medium

Source: [16].

III.3.2 Implementing the fine-tuning process.

The implementation of the fine-tuning process for the Gemma-9B model involves a series of carefully structured steps aimed at enhancing the model's performance for the QuizTube application. The process is divided into three main phases: data preparation, fine-tuning, and evaluation.

In the Data Preparation phase, the transcripts gathered from educational YouTube videos are thoroughly cleaned and preprocessed to ensure consistency and accuracy. This cleaning process involves removing irrelevant symbols, correcting transcription errors, and normalizing text for uniformity. Once the text is cleaned, it undergoes tokenization, where the text is divided into smaller units or tokens that are compatible with Gemma-9B's tokenizer. Tokenization ensures that the model can accurately process and understand the input data, preparing it for the subsequent fine-tuning phase.

The Fine-Tuning Process begins with a baseline evaluation to assess the original performance of the pre-trained Gemma-9B model on the target task. This initial evaluation provides a reference point against which improvements can be measured. Once the baseline performance is established, the selected fine-tuning technique, that is Low-Rank Adaptation (LoRA), is applied to the model. This technique aims to enhance the model's performance while maintaining computational efficiency by only updating a subset of parameters or manipulating internal representations. During the training process, the model is fine-tuned on the prepared dataset, with performance metrics monitored continuously to ensure optimal results. The training process involves multiple iterations over the dataset, allowing the model to learn task-specific knowledge effectively.

The final phase, Evaluation, involves assessing the fine-tuned model's performance using a variety of relevant metrics. Commonly used metrics include accuracy, BLEU score and ROUGE-L, which provide a comprehensive understanding of the model's ability to generate accurate and contextually relevant quiz questions. To determine the effectiveness of the fine-tuning process, the results of the fine-tuned model are compared against the baseline performance established earlier. A significant improvement in these metrics would indicate the success of the fine-tuning process, while minimal or negative changes would prompt further adjustments to the fine-tuning methodology.

IV. RESULTS AND DISCUSSIONS

The results of the Quiz-Tube system demonstrate its effectiveness in transforming YouTube educational content into an interactive learning experience. By leveraging AI-driven Natural Language Processing (NLP) techniques, the system successfully generates quizzes that align with the key concepts of the video content. The automated evaluation process provides instant feedback, enabling users to track their performance and improve their understanding of the subject matter. The adaptive learning mechanism personalizes quiz difficulty based on individual performance, ensuring a tailored learning experience.

Table No. 2: Performance improvements.

Metric	Pre-Finetuning	Post-Finetuning
BLEU score	45.3	68.7
ROUGE-L	57.2	74.8
Accuracy (%)	64.5	81.9

Source: Authors, (2025).

The given Table presents a comparative analysis of the Quiz-Tube system's performance before and after fine-tuning using three key evaluation metrics: BLEU score, ROUGE-L, and Accuracy (%).

1]BLEU Score: Measures the overlap between generated and reference text. The model shows a significant improvement from 45.3 (Pre-Finetuning) to 68.7 (Post-Finetuning), indicating enhanced fluency and alignment with expected outputs.

2] ROUGE-L: Evaluates recall-oriented similarity by considering the longest common subsequence between generated and reference text. The model's ROUGE-L score increases from 57.2 to 74.8, reflecting improved text relevance and coherence.

3]Accuracy (%): Represents the proportion of correctly generated quiz questions or answers. The system achieves a substantial accuracy boost from 64.5% to 81.9%, demonstrating better precision in content generation.

V. CONCLUSIONS

QuizTube is a groundbreaking AI-powered platform designed to revolutionize the educational landscape by converting educational YouTube videos into interactive quizzes. Through the integration of cutting-edge AI techniques, particularly the fine-tuned Gemma-9B model, QuizTube effectively generates quizzes that promote active learning and enhance user engagement. By utilizing the YouTube Transcript API, QuizTube efficiently processes and converts spoken content from videos into structured text, enabling the AI model to extract meaningful information and generate contextually accurate questions. This approach ensures that users are presented with high-quality quizzes that reflect the core concepts and knowledge imparted by the original video content.

The fine-tuning of the Gemma-9B model plays a critical role in the platform's success, with Parameter-Efficient Fine-Tuning (PEFT) being employed to enhance the model's adaptability and performance. By training the model on a dataset of 1,000 educational transcripts, the system demonstrates significant improvements in performance metrics. Notably, BLEU scores have increased from 45.3 to 68.7, and ROUGE-L scores have risen from 57.2 to 74.8, indicating a substantial enhancement in the model's ability to generate coherent and contextually relevant questions. The utilization of these fine-tuning methods ensures that QuizTube remains robust and effective even when processing complex and domain-specific educational materials.

QuizTube's architecture is designed to be highly flexible and user-centric. Through its intuitive dashboard, users can seamlessly input YouTube video URLs, customize quiz preferences, and receive immediate feedback on their performance. The platform's ability to adjust quiz difficulty based on the user's historical performance ensures a personalized and adaptive learning experience. This adaptability is particularly valuable for learners with varying levels of expertise, enabling them to progress at their own pace and focus on areas where improvement is needed. Additionally, QuizTube's integration of real-time quiz generation capabilities distinguishes it from traditional e-learning platforms, making it a valuable tool for both educators and independent learners.

VI. AUTHOR'S CONTRIBUTION

Conceptualization: Author One, Author Two and Author Three.
Methodology: Author Two.
Investigation: Author Three and Author Four.
Discussion of results: Author Five, Author Four and Author Three.
Writing – Original Draft: Author One and Author Two.
Writing – Review and Editing: Author Three and Author Five.
Resources: Author Two.
Supervision: Author One.
Approval of the final text: Author One, Author Two and Author Three.

VII. REFERENCES

[1] Maceiras, Rocio, et al. "Effectiveness of Active Learning Techniques in Knowledge Retention among Engineering Students." *Education for Chemical Engineers*, vol. 51, Apr. 2025, pp. 1–8.

[2] Naveed, Humza, et al. "A Comprehensive Overview of Large Language Models." Elsevier Preprint, 18 Oct. 2024.

[3] Gemma Team, Google DeepMind. "Gemma: Open Models Based on Gemini Research and Technology." arXiv preprint, 16 https://arxiv.org/abs/2403.08295. Apr. 2024.

[4] Jeong, Cheonsu. Fine-tuning and Utilization Methods of Domain-specific LLMs. Samsung SDS, 2023.

[5] Nwafor, Chidinma A., and Ikechukwu E. Onyenwe. An Automated Multiple-Choice Question Generation Using Natural Language Processing Techniques. Nnamdi Azikiwe University Awka, 2023.

[6] Hang, Ching Nam, Chee Wei Tan, and Pei-Duo Yu. "MCQGen: [102273, https://dx.doi.org/10.1109/ACCESS.2024.3420709.

[7] Bulathwela, Sahan, Hamze Muse, and Emine Yilmaz. "Scalable Educational Question Generation with Pre-trained Language Models." Centre for Artificial Intelligence, University College London, 2023.

[8] Li, Shiyao, et al. "Evaluating Quantized Large Language Models." Proceedings of the 41st International Conference on Machine Learning, PMLR 235, 2024.

[9] Qin, Haotong, et al. "Accurate LoRA-Finetuning Quantization of LLMs via Information Retention." Proceedings of the 41st International Conference on Machine Learning, PMLR 235, 2024.

[10] Jiang, Ziyan, Xueguang Ma, and Wenhu Chen. "LongRAG: Enhancing Retrieval-Augmented Generation with Long-context LLMs." University of Waterloo, 2024.

[11] Hadzhikoleva, Stanka, et al. "Automated Test Creation Using Large Language Models: A Practical Application." Applied Sciences, vol. 14, no.9125.https://doi.org/10.3390/app14199125.

[12] Babakhani, Pedram, et al. "Opinerium: Subjective Question Generation Using Large Language Models." IEEE Access, vol. 12, 2024,pp.66085–66092.

[13] Chen, Zixiang, et al. "Self-Play Fine-Tuning Converts Weak Language Models to Strong Language Models." Proceedings of the 41st International Conference on Machine Learning, PMLR 235, 2024, Vienna, Austria. arXiv:2401.01335.

[14] Xu, Lingling, et al. "Parameter-Efficient Fine-Tuning Methods for Pretrained Language Models: A Critical Review and Assessment." arXiv, 20 Dec. 2023, https://arxiv.org/abs/2312.12148.

[15] Luong, Trung Quoc, et al. "ReFT: Reasoning with Reinforced Fine-Tuning." *arXiv*, 2024, https://arxiv.org/abs/2401.08967.

[16] Srinivasan, Krishna Prasad Varadarajan, et al. "Comparative Analysis of Different Efficient Fine-Tuning Methods of Large Language Models (LLMs) in Low-Resource Setting." *arXiv*, 21 May 2024, https://arxiv.org/abs/2405.13181.

Journal of Engineering and Technology for Industrial Applications

ITEGAM-JETIA

Manaus, v.11 n.54, p. 203-209. July/August., 2025.
DOI: https://doi.org/10.5935/jetia. v11i54.1751

ISSN ONLINE: 2447-0228

RESEARCH ARTICLE OPEN ACCESS

HIGHLY EFFICIENT POWER CONDITIONING TOPOLOGY FOR MAXIMUM ENERGY EXTRACTION FROM WIND POWER SYSTEM USING HILL CLIMBING SEARCH-MPC APPROACH

Zahira Anane[1], Badreddine Babes[2] and Noureddine Hamouda[3]

[1] Department of Electrical Engineering, Faculty of Technology, Ferhat Abbas University, Sétif-1, 19000 Sétif, Algeria
[2,3] Research Center in Industrial Technologies CRTI, Cheraga, P.O.Box 64, 16014 Algiers, Algeria.

[1]https://orcid.org/0000-0002-0268-8369, [2]https://orcid.org/0000-0002-9256-2021, [3]https://orcid.org/0000-0002-8489-2135

Email: zahira_anane@univ-setif.dz, elect_babes@yahoo.fr, n.hamouda@crti.dz

ARTICLE INFO

Article History
Received: March 23, 2025
Revised: April 20, 2025
Accepted: June 15, 2025
Published: August 31, 2025

Keywords:
Wind Energy System,
Model Predictive Controller,
DC/DC Switched Inductor Boost Converter,
Permanent Magnet Synchronous Generator,
dSPACE DS1104.

ABSTRACT

This article proposes a high-gain and high-efficiency power conditioning topology for grid connected wind energy system (WES) based on Hill Climbing Search (HCS) algorithm and a fixed frequency Model Predictive Controller (MPC) to maximize the energy harvest and control the DC/DC switched inductor boost converter (SIBC) to achieve high performance regardless of wind speed variations. In this study, the MPC is based on minimizing the difference between the reference and prediction currents, which is computed to select the switching state of the SIBC converter. The feasibility of the proposed SIBC converter and HCS-MPC scheme is verified in a variety of dynamic conditions through dSPACE DS1104-based experiments on a 3 kW wind energy conversion system prototype. Outcomes show that the suggested control mechanism follows the maximum power point (MPP) with less power fluctuations.

Copyright ©2025 by authors and Galileo Institute of Technology and Education of the Amazon (ITEGAM). This work is licensed under the Creative Commons Attribution International License (CC BY 4.0).

I. INTRODUCTION

The low conversion efficiency of wind turbine is an obstacle to the growth of WESs. The MPPT algorithm ensures that the maximum available wind energy is harnessed from the WES. Many MPPT methods have been suggested over the past few decades, and the relative merits of these various approaches are discussed in [1, 2].

An effective MPPT controller and converter can exploit available energy to significantly reduce the amount of installed WESs. Considering the MPPT techniques listed in [1], candidate techniques include P&O [3, 4] and hill climb searching (HCS) algorithms [5]. Each approach has certain advantages and disadvantages for the present application. HCS algorithm is a well-known technique with relatively good performance [6]. However, HCS algorithm cannot always converge to the true maximum power point (MPP). In addition, HCS algorithm is relatively slow, which limits its ability to track transient environmental conditions.

The main contribution of this study is to improve the HCS algorithm performance by predicting the error two-steps ahead in horizon of time through the MPC technique. The proposed MPC method consists of two-stage. The first stage is a HCS algorithm used to generate the necessary reference current that achieves the MPP. The model predictive control (MPC) constructs the second stage. It is based on the optimization of the cost function that determines the switching action for the SBIC switch. Adding MPC improves the performance of the MPPT control and gives faster response and better operation in case of fast environmental changes without requiring expensive sensing and communications equipment. The SIBC is chosen as a DC/DC boosting stage converter. It is controlled using two-steps MPC-MPPT algorithm. The main advantages of the SIBC are high boosting gain, lower switching losses. With this topology, the 50 V DC-input voltage can be boosted to 600 V with 12 DC/DC conversion gain ratio and efficiency reaches approximately to 92.5%. These surveys show that SIBC topologies are more efficient, lighter, less bulky and less costly than the conventional DC/DC boost

converters. In the WESs, grid-connected inverters are required to help convert the DC power to AC power in a single conversion stage [7, 8]. Numerous inverter circuits can be used for wind power conditioning system (PCS) [9]. For small-scale distributed renewable energy generation systems, single-phase utility interactive inverters are of particular interest [10]. This type of application normally requires a power level lower than 5 kW [11]. These inverters commutate at high frequencies and thus eliminate the low frequencies harmonics, smaller filters are used and the cost and the physical size are reduced. Moreover, the power factor created by these types of inverters could be controlled and the losses on the grid-side are thus reduced.

Consequently, the performance of the inverters connected to the grid depends largely on the control strategy applied. A suitable control of these inverters is needed to get an efficient energy transfer. Therefore, many methods for the current control of grid connected single-phase inverters have been developed. These methods include the use of the proportional integral (PI) controller [12], proportional resonant (PR) controller [13], repetitive based controller [14], deadbeat controller [15], fuzzy controller [16], and predictive controller [17]. Although, the latter has the advantage of outstanding current regulation, higher power factor, lower current harmonic distortions and fast dynamic response during the transient conditions, but demands more computing resources and requires a good knowledge of system parameters. Aiming at overcoming these disadvantages of predictive controller, an improved predictive current controller (IPCC) has been developed in this paper for single-phase full bridge grid connected inverters and has been verified through experimental tests.

This article is structured as follows: Section 2 provides a detailed description of the proposed WES, including SIBC and single-phase inverter. Section 3 presents the improved HCS-MPPT algorithm. Section 4 presents the experimental results and findings and their discussion, along with a comprehensive analysis of the MPPT tracking performance in terms of recovery time, response time, efficiency and energy yield. Finally, Section 5 concludes the article with a summary of findings.

II. SYSTEM TOPOLOGY STRUCTURE

The configuration of the proposed WCS is depicted in Figure 1. The system consists of two stages. The first stage is a high-gain switched inductor with voltage multiplication boost converter to provide high-gain, high-efficiency and the DC source required by the single-phase voltage source inverter. The second stage is a single-phase full bridge inverter is used to inject a sinusoidal current into the grid with low harmonic distortion as possible.

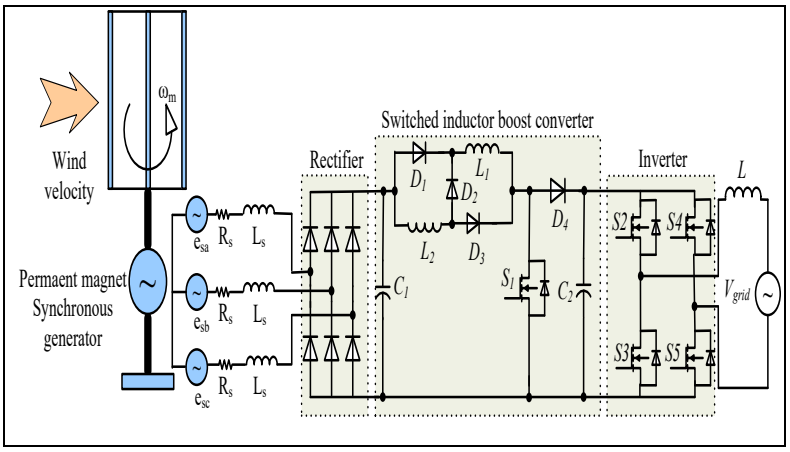

Figure 1: Configuration of the proposed wind energy system.
Source: Authors, (2025).

III. SUGGESTED CONTROLLER DESIGN

III.1 IMPROVED HCS-MPPT ALGORITHM

In this part, a maximum power tracker controller by using MPC will be presented for the SIBC in order to operate the wind turbine at the optimal power point until wind changes. The main goal to using the MPC technique in the proposed HCS-MPPT algorithm is to increase the response of the control of MPPT on WESs when there is abrupt change in the environmental conditions such as wind speed, because predictions of the future values of the system variables gives the advantages of fast reference tracking. The proposed HCS-MPPT algorithm is developed in such a manner that it sets a reference current corresponding to the peak power of the wind turbine by predicting the error at next sampling time before applying the switching signal to the SIBC.

III.2 HCS-MPPT USING FIXED FREQUENCY MPC

A discretization of the SIBC model is required for the implementation of the HCS-MPPT algorithm. By using the Euler forward approximation, the derivative of the input current (I_{in}) and input voltage (V_{in}) can be approximately discretized as follows:

$$\begin{cases} \dfrac{dI_{in}}{dt} = \dfrac{I_{in}(n+1) - I_{in}(n)}{T_s} \\ \dfrac{dV_{in}}{dt} = \dfrac{V_{in}(n+1) - V_{in}(n)}{T_s} \end{cases} \quad (1)$$

Where T_s is the sampling time. The discretization of the SIBC equations can derive from a state-space model (2) when the switch is turned ON as follows:

$$\begin{bmatrix} I_{in}(n+1) \\ V_{in}(n+1) \end{bmatrix} = \begin{bmatrix} 1-\frac{T_s}{L}\left(\frac{R_L}{2}+R_{on}\right) & \frac{T_s}{L} \\ 0 & \frac{2}{2} \end{bmatrix} \begin{bmatrix} I_{in}(n) \\ V_{in}(n) \end{bmatrix} + \begin{bmatrix} 0 \\ -1 \end{bmatrix} \begin{bmatrix} V_{in}(n-1) \\ V_d \end{bmatrix} \quad (2)$$

When the switch is turned OFF:

$$\begin{bmatrix} I_{in}(n+1) \\ V_{in}(n+1) \end{bmatrix} = \begin{bmatrix} 1-\frac{T_s}{L}R_L & \frac{T_s}{2L} \\ 0 & 2 \end{bmatrix} \begin{bmatrix} I_{in}(n) \\ V_{in}(n) \end{bmatrix} + \begin{bmatrix} 0 & -\frac{T_s}{L} & -\frac{T_s}{2L} \\ -1 & 0 & 0 \end{bmatrix} \begin{bmatrix} V_{in}(n-1) \\ V_d \\ V_0 \end{bmatrix} \quad (3)$$

As a good approximation to reduce the number of sensors, the predicted value of input voltage can be expressed as:

$$V_{in}(n+1) \cong 2\,V_{in}(n) - V_{in}(n-1) \quad (4)$$

Previous work has suggested the addition of a second stage of MPC for even better system performance and model accuracy [18]. Therefore, Eqs. (2) to (4) are adjusted to get Eqs. (5) and (6) for two-stage MPC:

$$\begin{bmatrix} I_{in}(n+2) \\ V_{in}(n+2) \end{bmatrix} = \begin{bmatrix} 1-\frac{T_s}{L}\left(\frac{R_L}{2}+R_{on}\right) & \frac{T_s}{L} \\ 0 & \frac{2}{2} \end{bmatrix} \begin{bmatrix} I_{in}(n+1) \\ V_{in}(n+1) \end{bmatrix} + \begin{bmatrix} 0 \\ -1 \end{bmatrix} \begin{bmatrix} V_{in}(n) \\ V_d \end{bmatrix} \quad (5)$$

$$\begin{bmatrix} I_{in}(n+2) \\ V_{in}(n+2) \end{bmatrix} = \begin{bmatrix} 1-\frac{T_s}{L}R_L & \frac{T_s}{2L} \\ 0 & 2 \end{bmatrix} \begin{bmatrix} I_{in}(n+1) \\ V_{in}(n+1) \end{bmatrix} + \begin{bmatrix} 0 & -\frac{T_s}{L} & -\frac{T_s}{2L} \\ -1 & 0 & 0 \end{bmatrix} \begin{bmatrix} V_{in}(n) \\ V_d \\ V_0 \end{bmatrix} \quad (6)$$

The cost function for the MPC algorithm is calculated with the consideration that the switch of the SIBC is turned "ON" and "OFF" it is given as:

$$g_{s=1,0} = \left| I_{in}(n+2) - I_{ref} \right| \quad (7)$$

The flowchart in Figure 2 illustrates all the main steps of the modified HCS-MPPT algorithm by using the proposed MPC method.

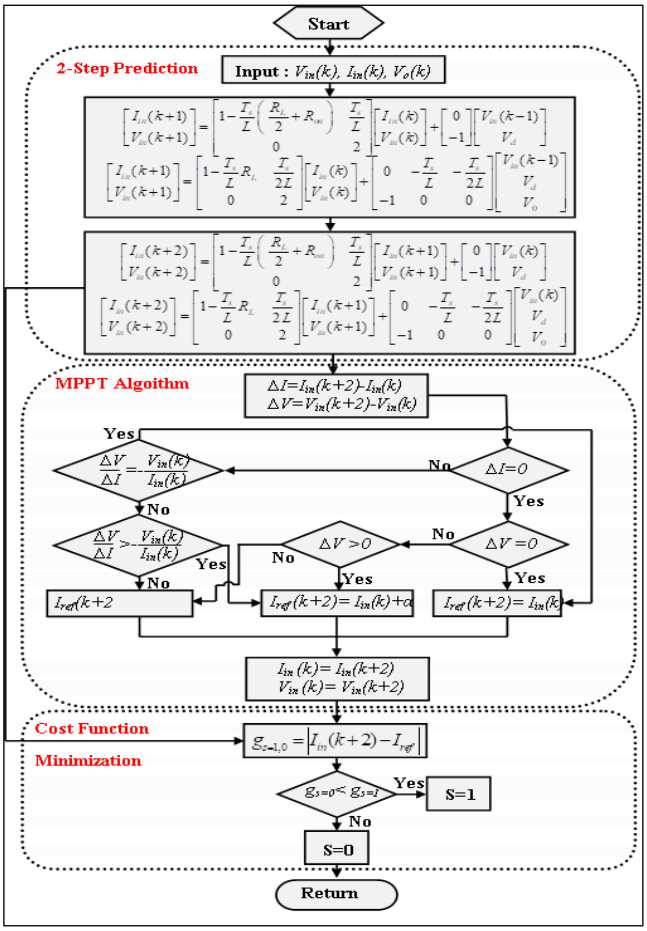

Figure 2: Proposed HCS-MPPT using MPC method.
Source: Authors, (2025).

The cost function assures the tracking of predicted input current from the reference provided by the HCS-MPPT algorithm. Comparison of cost function for different switching states of SIBC determines the control actions for the following time instant. Figure 3 shows the implemented of modified MPPT control scheme to the proposed SIBC.

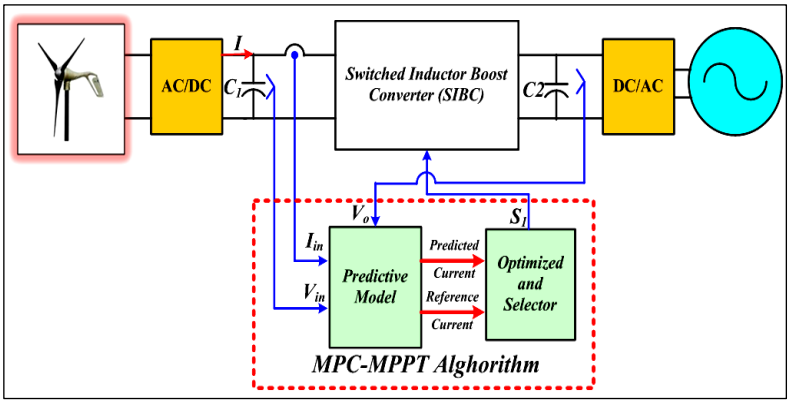

Figure 3: The proposed WES implementing HCS-MPPT using MPC method.
Source: Authors, (2025).

IV. EXPERIMENTAL RESULTS

To verify the performance of the proposed MPC-MPPT algorithm for the SIBC, a prototype of grid connected WES based on a small PMSG is developed as shown in Figure 4.

Figure 4: Photograph of the experimental setup.
Source: Authors, (2025).

Figure. 5 shows the experimental result of the system using the proposed MPC-MPPT algorithm. In this test, the algorithm goal is to track the maximum power operating point of the WES and the wind speed has changed in several steps. As can be seen from Figure 5 the turbine shaft speed is continuously matched to the wind speed in such a way that it is extracted maximum power out of the wind. The DC-input current of SIBC is controlled according to the MPPT strategy and can be better regulated to achieve the optimum reference current during wind speed step changes.

Also, the power conversion coefficient C_p is kept constant, and varies in a relatively small range around its optimal value of 0.47, which means that the wind turbine tracks maximum power from the wind. The mechanical torque changes accordingly to accommodate the variations in the wind speed. The mechanical power had small fluctuations phenomenon, but the value of the wind turbine power would back to the best value soon. It is noticed that the mechanical input power is slightly greater than the electrical power production due to the system losses.

The DC-link voltage response is completely robust with perfect rejection of wind speed disturbances and is maintained within the variation of 2%. Note also that only active power is delivered to the grid when the PI controller reaches its steady state value. The armature current (I_{dc}) is variable and depends on the mechanical power variations, thus the armature current is changed as the wind speed changes. The obtained results confirm that the proposed MPC-MPPT algorithm of the SIBC works properly and quite able to track the maximum wind power of the wind generation system effectively according to an increase/decrease in the wind speed.

This verifies that the tracking performance of the proposed MPC-MPPT algorithm is very good.

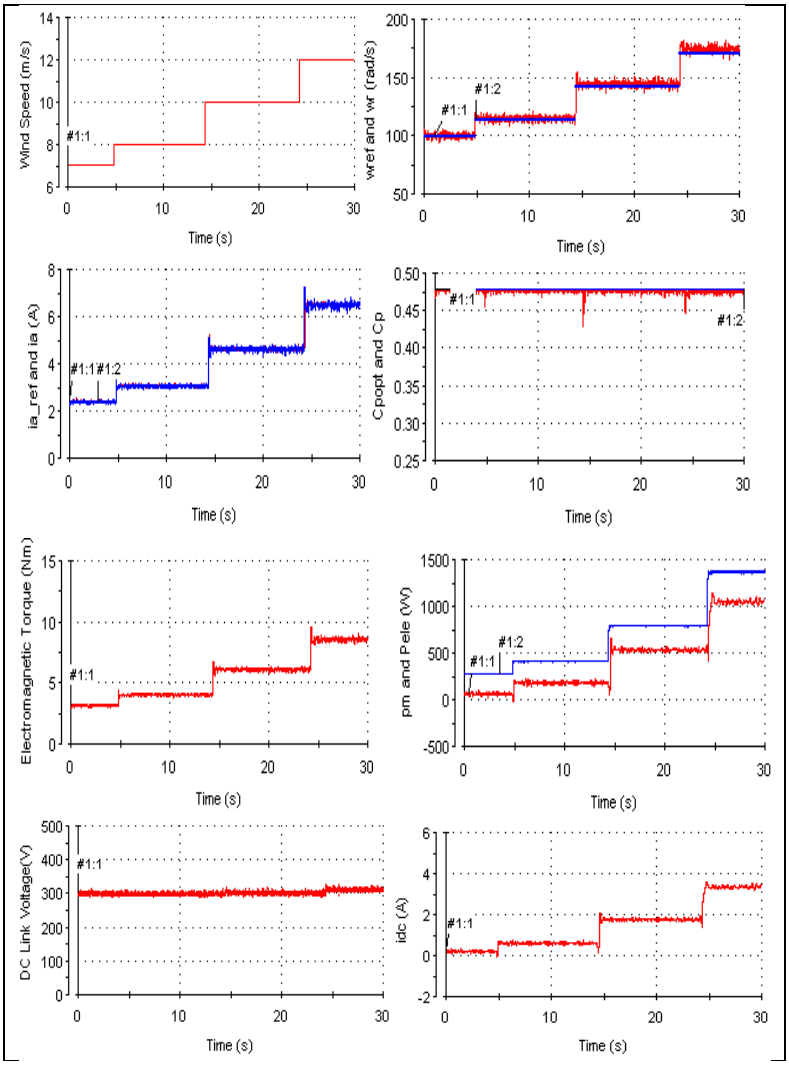

Figure 5: Dynamic response of the proposed WES using HCS-MPPT algorithm.
Source: Authors, (2025).

Figure 6 shows the tracking performance comparison between three typical MPPT algorithms: the Tip-Speed Ratio (TSR) algorithm [19, 20], the P&O algorithm [21], and the proposed MPC-MPPT algorithm. It can be seen from Figure 6 that every MPPT algorithm works properly, i.e. successfully tracks MPP. The proposed MPC-MPPT algorithm was found to be the fastest in achieving the MPP. The recovery time (t_r) upon wind speed change was also faster for the proposed MPC-MPPT algorithm. The dynamic response for algorithms based on proposed MPC-MPPT and TSR is relatively similar. In comparison, the P&O algorithm was found to be the slowest algorithm. Therefore it can be concluded that the robust tracking performance is achieved using the proposed MPC-MPPT algorithm under the wind speed variation.

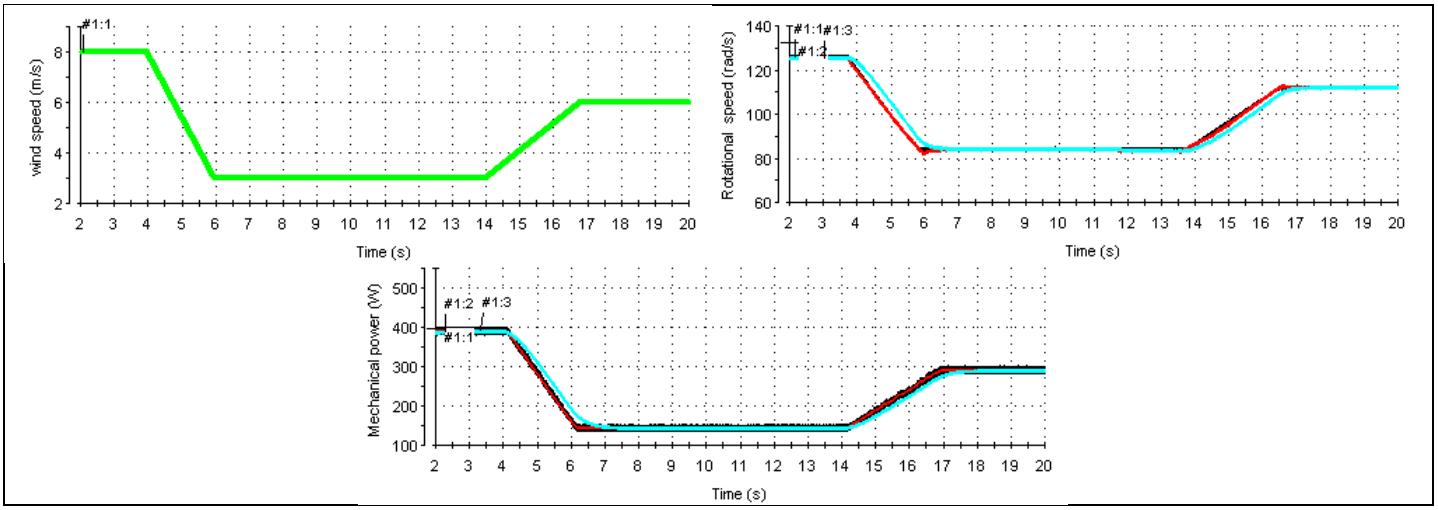

Figure 6: MPPT tracking performance: MPC-MPPT (Black), P&O (Cyan), and TSR (Red).
Source: Authors, (2025).

The comparisons of the three typical algorithms considering the efficiency (η) and energy yield (E) are summarized in Table 1 Based on results and analysis, the proposed MPC-MPPT algorithm reached the highest value of power conversion coefficient (C_p). It was followed by the TSR algorithm, with the average value of C_p being 0.4627. The P&O algorithm was found to be the least efficient method.

Table 1: Summary of performance of three MPPT algorithms.

Method	C_p	t_s(s)	t_r(s)	E(W)	η(%)
MPC-MPPT	0.4785	0.0247	0.0007	734.5	96.48
TSR	0.4627	0.0885	0.0024	665.9	90.42
P&O	0.4123	0.2478	0.0371	597.4	80.44

Source: Authors, (2025).

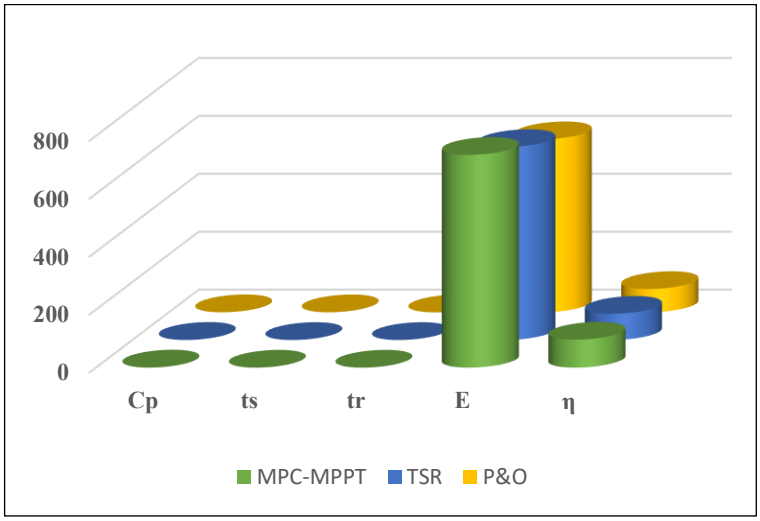

Figure 7: Comparisons of the three typical algorithms.
Source: Authors, (2025).

V. CONCLUSIONS

In this paper, an efficient power conditioning system for grid connected wind energy applications was introduced. The proposed system can potentially reduce the cost and size of wind turbine generator systems. A switched inductor boost converter (SIBC) is a totally novel technology, it has been used as DC/DC boosting stage converter due to its inherent features such as high DC/DC conversion ratio and better efficiency. Hence, MPPT techniques based on HCS algorithm employing a MPC method is proposed to extract maximum power from the wind generator through the SIBC. Modifications applied to the traditional HCS algorithm enabled the proposed MPC-MPPT algorithm to interact quickly for rapidly varying wind conditions. Moreover, it has been shown that the proposed MPC-MPPT algorithm can be easily implemented with reduced hardware setup because only current and voltage sensors have been used. Therefore, neither the measurement of the wind speed nor the knowledge of the wind turbine characteristics is required. Then, three of the typical MPPT algorithms (TSR algorithm, P&O algorithm, and suggested MPC-MPPT algorithm) have been implemented practically. A comparison be-tween the MPPT algorithms has been carried out to demonstrate the ad-vantages of the proposed MPC-MPPT algorithm, the results have shown that the proposed MPC-MPPT algorithm is the most favorable featuring fast dynamic response, and accuracy under almost any conditions

VI. AUTHOR'S CONTRIBUTION

Conceptualization: Z. A, B. B and N. H.
Methodology: Z. A and B. B.
Investigation: Z. A and B. B.
Discussion of results: Z. A, B. B and N. H.
Writing – Original Draft: Z. A and B. B.
Writing – Review and Editing: Z. A, B. B and N. H.
Resources: B. B.
Supervision: Z. A and B. b.
Approval of the final text: Z. A, B. B and N. H.

VIII. REFERENCES

[1] D. Kumar and K. Chatterjee, "A review of conventional and advanced MPPT algorithms for wind energy systems," Renewable and Sustainable Energy Reviews, vol. 55, pp. 957–970, Mar. 2016. doi: 10.1016/j.rser.2015.11.013.

[2] H. H. H. Mousa, A.-R. Youssef, and E. E. M. Mohamed, "State of the art perturb and observe MPPT algorithms based wind energy conversion systems: A technology review," International Journal of Electrical Power & Energy Systems, vol. 126, p. 106598, Mar. 2021. doi: 10.1016/j.ijepes.2020.106598.

[3] B. Lahfaoui, S. Zouggar, B. Mohammed, and M. L. Elhafyani, “Real Time Study of P&O MPPT Control for Small Wind PMSG Turbine Systems Using Arduino Microcontroller,” Energy Procedia, vol. 11, pp. 1000–1009, Mar. 2017. doi: 10.1016/j.egypro.2017.03.263.

[4] B. Lahfaoui, S. Zouggar, B. Mohammed, and M. L. Elhafyani, “Real Time Study of P&O MPPT Control for Small Wind PMSG Turbine Systems Using Arduino Microcontroller,” Energy Procedia, vol. 111, pp. 1000–1009, Mar. 2017. doi: 10.1016/j.egypro.2017.03.263.

[5] H. Li, Q. Li, X. Jiang, Y. Ruan, and W. Huang, “The Application of Improved Hill-Climb Search Algorithm in Wind Power Generation,” IFAC Proceedings Volumes, vol. 46, no. 20, pp. 263–267, 2013. doi: 10.3182/20130902-3-cn-3020.00004.

[6] A. Beddar, H. Bouzekri, B. Babes, H. Afghoul, “Real Time Implementation of Improved Fractional Order Proportional-Integral Controller for Grid Connected Wind Energy Conversion System,” Rev. Roum. Sci. Techn.– Électrotechn. et Énerg., Vol. 61, 4, pp. 402–407, Bucarest, 2016.

[7] N. Hamouda, B. Babes, S. Kahla, and Y. Soufi, “Real Time Implementation of Grid Connected Wind Energy Systems: Predictive Current Controller,” 2019 1st International Conference on Sustainable Renewable Energy Systems and Applications (ICSRESA). IEEE, pp. 1–6, Dec. 2019. doi: 10.1109/icsresa49121.2019.9182526.

[8] B. Babes, N. Hamouda, S. Kahla, H. Amar, and S. S. M. Ghoneim, “Fuzzy model based multivariable predictive control design for rapid and efficient speed-sensorless maximum power extraction of renewable wind generators,” Electrical Engineering & Electromechanics, no. 3. National Technical University Kharkiv Polytechnic Institute, pp. 51–62, May 30, 2022. doi: 10.20998/2074-272x.2022.3.08.

[9] F. Amrane, A. Chaiba, B. Francois, and B. Babes, “Real time implementation of grid-connection control using robust PLL for WECS in variable speed DFIG-based on HCC,” 2017 5th International Conference on Electrical Engineering - Boumerdes (ICEE-B). IEEE, pp. 1–5, Oct. 2017. doi: 10.1109/icee-b.2017.8191984.

[10] B. Antar, B. Hassen, B. Babes, and H. Afghoul, “Fractional order PI controller for grid connected wind energy conversion system,” 2015 4th International Conference on Electrical Engineering (ICEE). IEEE, pp. 1–6, Dec. 2015. doi: 10.1109/intee.2015.7416692.

[11] R. Dembri, L. Rahmani, B. Babes, and I. Azizi, “Enhanced Control of Doubly Fed Induction Generator Based Wind Turbine System Using Fractional-Order Fuzzy PD+I Regulator,” Journal Européen des Systèmes Automatisés, vol. 57, no. 1. International Information and Engineering Technology Association, pp. 211–233, Feb. 29, 2024. doi: 10.18280/jesa.570121.

[12] M. Merai, M. W. Naouar, I. Slama-Belkhodja, and E. Monmasson, “A systematic design methodology for DC-link voltage control of single phase grid-tied PV systems,” Mathematics and Computers in Simulation, vol. 183, pp. 158–170, May 2021. doi: 10.1016/j.matcom.2020.05.007.

[13] D. Zammit, C. Spiteri Staines, M. Apap, and J. Licari, “Design of PR current control with selective harmonic compensators using Matlab,” Journal of Electrical Systems and Information Technology, vol. 4, no. 3, pp. 347–358, Dec. 2017. doi: 10.1016/j.jesit.2017.01.003.

[14] N. Lee and Y. Cho, “A PLL-based Repetitive controller for a Single-Phase Grid-connected NPC Inverter,” 2020 IEEE PELS Workshop on Emerging Technologies: Wireless Power Transfer (WoW), Seoul, Korea (South), 2020, pp. 206-209, doi: 10.1109/WoW47795.2020.9291334.

[15] M. Ferhat, L. Rahmani, and B. Babes, “DSP-based implementation of improved deadbeat control for three-phase shunt active power filters,” Journal of Power Electronics, vol. 20, no. 1, pp. 188–197, Dec. 19, 2019. doi: 10.1007/s43236-019-00029-y.

[16] A. Maafa, H. Mellah, K. Benaouicha, B. Babes, A. Yahiou, and H. Sahraoui, “Fuzzy Logic-Based Smart Control of Wind Energy Conversion System Using Cascaded Doubly Fed Induction Generator,” Sustainability, vol. 16, no. 21, p. 9333, Oct. 27, 2024. doi: 10.3390/su16219333.

[17] B. Babes, O. Aissa, N. Hamouda, and I. Colak, “Model Based Predictive Direct Torque and Flux Control for Grid Synchronization of a PMSG Driven by a Direct Matrix Converter,” 2022 10th International Conference on Smart Grid (icSmartGrid). IEEE, pp. 208–213, Jun. 27, 2022. doi: 10.1109/icsmartgrid55722.2022.9848534.

[18] N. Hamouda, B. Babes, S. Kahla, Y. Soufi, J. Petzoldt, and T. Ellinger, “Predictive Control of a Grid Connected PV System Incorporating Active power Filter functionalities,” 2019 1st International Conference on Sustainable Renewable Energy Systems and Applications (ICSRESA). IEEE, pp. 1–6, Dec. 2019. doi: 10.1109/icsresa49121.2019.9182655.

[19] M. E. M. Annane, A. Ounissi, R. Abdessemed, and B. Babes, “Design of a novel intelligent cooperative type-2 fuzzy logic controller and fractional-order synergetic approach for wind energy systems based MPPT methodology,” Journal of the Brazilian Society of Mechanical Sciences and Engineering, vol. 46, no. 9, Sep. 2024. doi: 10.1007/s40430-024-05138-9.

[20] R. Dembri et al., “SSO optimized FOFPID regulator design for performance enhancement of doubly fed induction generator based wind turbine system,” Scientific Reports, vol. 14, no. 1, Nov. 16, 2024. doi: 10.1038/s41598-024-76457-z.

[21] I. Toumi, A. Boulmaiz, B. Meghni, and O. Hachana, “Robust variable step P&O algorithm based MPPT for PMSG wind generation system using estimated wind speed compensation technique,” Sustainable Energy Technologies and Assessments, vol. 60, p. 103420, Dec. 2023. doi: 10.1016/j.seta.2023.103420.

Journal of Engineering and Technology for Industrial Applications

ISSN ONLINE: 2447-0228

ITEGAM-JETIA

Manaus, v.11 n.54, p. 210-219. July/August., 2025.
DOI: https://doi.org/10.5935/jetia. v11i54.1764

RESEARCH ARTICLE OPEN ACCESS

ENHANCING THE COOLING SYSTEM DESIGN OF HIGH-POWER DENSITY PERMANENT MAGNET MOTOR FOR EV

Amit Kumar[1], Gaurav Singh Negi[2], Alok Sati[3]

[1, 2, 3] Uttaranchal Institute of technology, Uttaranchal University Dehradun India

[1]http://orcid.org/0009-0001-2643-3707, [2]http://orcid.org/0000-0003-1752-5359, [3]http://orcid.org/0009-0006-8591-761X

Email: akohli827@gmail.com technonegi@gmail.com, sati.alok9@gmail.com

ARTICLE INFO

Article History
Received: March 27, 2025
Revised: April 20, 2025
Accepted: June 15, 2025
Published: August 31, 2025

Keywords:
cooling system, PM motor, Taguchi Method Fluidic-thermal coupled analysis

ABSTRACT

Excessive losses inside permanent magnet (PM) motors in electric vehicle (EV) engine compartments can cause rapid temperature rises, deterioration of magnetic properties, limited output torques, and overheating. To ensure smooth operational condition, it's crucial to investigate and develop cost-effective cooling solutions for PM motors. This study presents a 3D fluidic-thermal linked model of a high-power density internal PM motor, based on Computational Fluid Dynamics and heat transfer theory. The fluid flow and heat dispensation are evaluated using the finite volume technique (FVM) and confirmed by practical results. Modifying the external fluid frame structure of the motor based on its heating properties improves cooling efficiency. The Taguchi approach improves cooling parameters to minimize the motor's temperature rise. This finding has significant implications for designing and developing high-power density Permanent motor for EV uses.

Copyright ©2025 by authors and Galileo Institute of Technology and Education of the Amazon (ITEGAM). This work is licensed under the Creative Commons Attribution International License (CC BY 4.0).

I. INTRODUCTION

The popularity and quick growth of electric vehicles (EVs) has led to substantial research into high-performance, reliable, and lightweight traction motors. The permanent magnet synchronous machine (PMSM) has great efficiency, power density, and power factor across various working circumstances. Permanent magnet motors are increasingly being used in electric vehicles (EVs) due to frequent start-stop and load changes in modern traffic. Excessive time harmonics from frequency converters in EV compartments can cause temperature rises, reduced magnetic density and coercivity, limited torque capacity, winding insulation damage, and irreversible PM demagnetization. Efforts to improve the power density of PM traction motors have been hindered by inefficient cooling systems [1]. External liquid cooling structures effectively cool machines and prevent leaks and erosion by avoiding direct contact between fluid flow and internal components (e.g. windings, cores, PMs) in EVs and HEVs. Cooling performance of a HEV four-quadrant transducer and found that changing the flow section profile increased heat dissipation. We investigated the impact of cooling medium and ratio on the temperature distribution of an EV traction motor using numerical calculations and actual measurements. We also tested the cooling performance of external liquid cooling frames outside the motor casing.

External cooling structures are commonly used in electric drive systems because to liquids' superior heat transfer capacity compared to gases. primarily due to high thermal resistance between the motor's end-windings, permanently magnets (PMs), and casings, which are in contact with the cooling frames [2]. In order to improve the heat dissipation, a new internal cooling system was developed by replacing the space in the motor where the cooling fluid would have to flow with fluid plates installed adjacent to the stator cores. The new internal cooling design enabled the stator core and windings to be directly cooled, with the internal cooling structure also having water tubes within the windings with direct water-cooling tubes on the stator core. The concept was tested on various PMSM high-power density prototypes. While the external cooling liquid extends in the motor cavity resulting in more cooling power, the cost of the prototype is significant. This research provides a 3D fluid structure interaction model for a new interior high-power density PM motor in electric vehicles (EVs). Numerical calculations based on FSI are used to calculate the flow state of the cooling medium and the distribution of temperature rise in the motor. Calculations are confirmed by comparing them to experimental data. To increase heat dissipation for end-

cap components, the liquid cooling design outside the motor case is optimized based on temperature rise distribution. The Taguchi approach is used to improvised cooling structure parameters, followed by numerical calculations and actual trials to determine temperature rise and optimal size [2,3].

II. MODEL AND SPECIFICATIONS

- **Structure and parameter**

a) The 20 kW, 4500 rpm PM motor has 4 pairs of permanent motor (PMs) and 48 slots. The circumference water frame is screw mounted on the outside of the motor casing to remove heat from the machine. The inside layout for the 20 kW 4500 rpm PM for EVs is shown in Fig. 1, where key specifications are shown in Table 1.[4]

b) Assumptions and calculation

To simplify the model and minimize calculation errors, the following assumptions are made for all motor parts involved in heat transmission.
Consider the model of motor's symmetry, Using the surrounding 1/8 model.

Table 1: High speed PMSM some parameters.

Quantity	Value
Max. speed	4500 rpm
Max. power	20kw
No. of pair of poles	4
Slots	48
Outer diameter Rotor core	125.6 mm
Outer diameter Stator core	194 mm
Air gap	0.7 mm
Axial length	75 mm
PM brand	N40UH
Soft iron sheet brand	35DW470
Liquid frame height	7.5 mm
Liquid frame width	20 mm

Source: Authors, (2025).

- The κ-ε mathematical framework employed to account for the high the ratio of inertial to viscous forces within a fluid of both the air confined in the end-caps and the liquid flowing in the liquid
- surround, caused by the rotor's air movement and the spiral channels' rapid water flow.
- Copper conductors are constructed from polymerized copper wires formed by wrapping them in insulating sheets. Furthermore, the conductors are made of wrapping insulation. Additionally, the insulation thickness is consistent across the copper conductor segment [5,6].
- Gaps are actually left unattended between the core of stator and the housing, and the rotor core and the permanent magnets.
- At the time of computations, they are represented as contact thermal resistances.
- Frictional loss is calculated taking into account internal air flow.

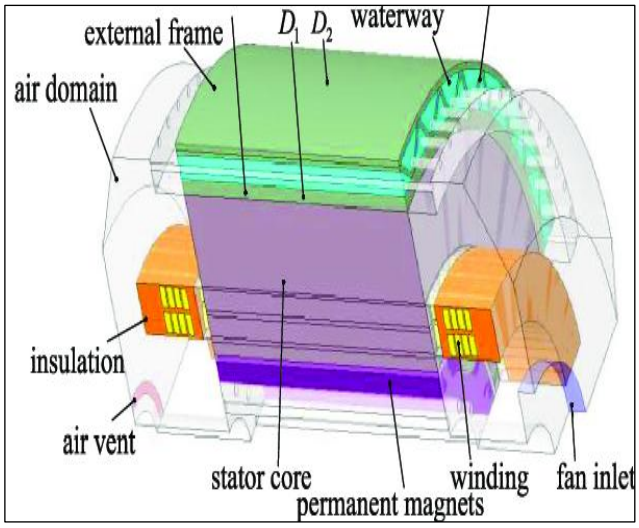

(a)

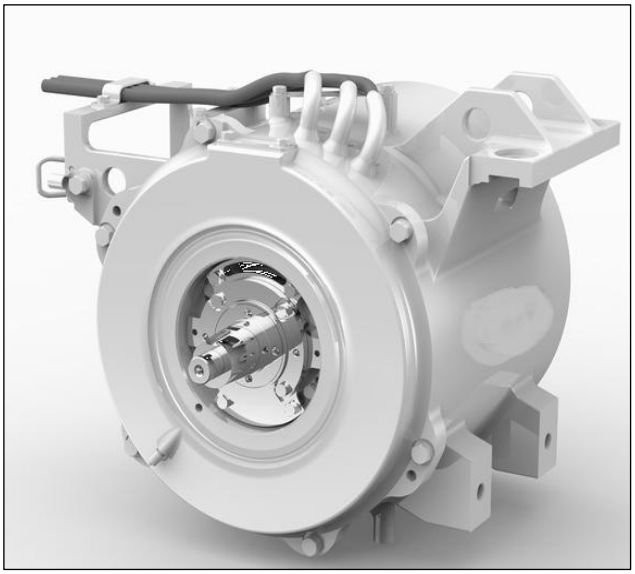

(b)

Figure 1: structure of permanent magnet motor a) basic model b) original model
Source: Authors, (2025).

The 3D Floor Space Index calculation model for the motor is created using basic assumptions and model simplifications, as seen in Figure 2. The model's outlet and inlet channels are lengthened to allow for turbulence before fluid enters spiral passages. The air's cross-section profiles are adjusted to periodic bounds to allow for passage through them [7].

III. THERMAL SOURCES

To get accurate distribution of the heat, it is tested for a complete load operation and then separated into losses in various components with all possible loss fraction is illustrated in Figure 3. The different loss components for the stator, rotor, and PMs have been calculated using finite element measurement while the frictional loss was found with the help of an empirical model [8].

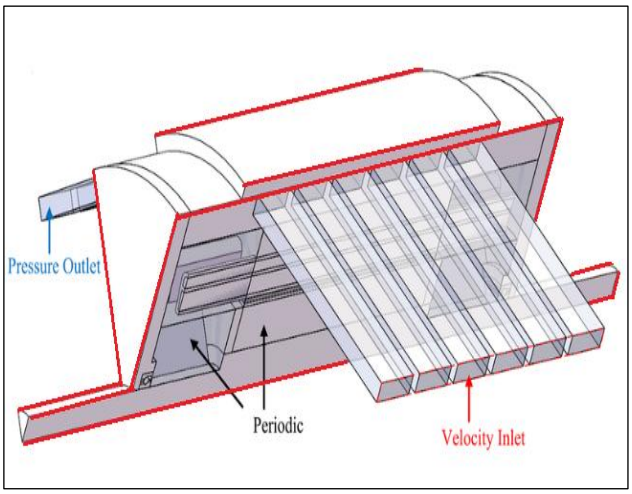

Figure 2: The structure of the PMSM with water barriers.
Source: Authors, (2025).

$$p\ (1)\ br = 0.772\ 5 \times 10^{-3} G_r\, D_{sh}\, n \qquad (1)$$

Gr (kg) = weight of rotor, Dsh (m) = shaft diameter, and n = rotational speed (rpm)Table 2 shows the heat production and losses rates.

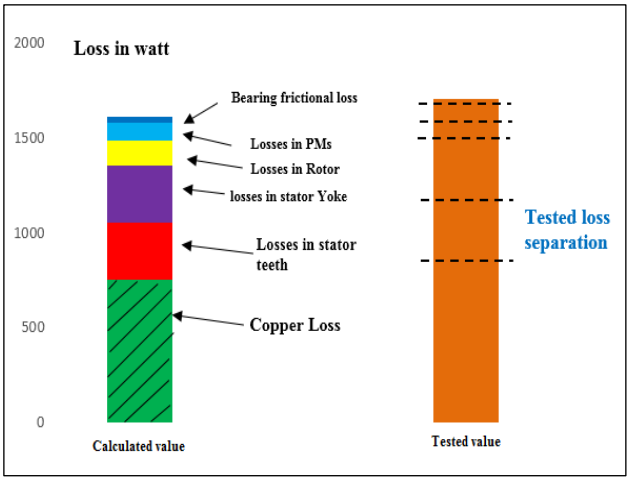

Figure 3: Losses and ratio.
Source: Authors, (2025).

- **Thermal analysis and consent**

The linked fluidic-heat areas are estimated using the calculation, frontier conditions, and motor thermal source dispensation. The central point of the PMs had the biggest temperature spike, measuring 134.7 K. Figure 4a displays the

Dispensation of temperature hike across the entire motor. Figure 4b displays the temperature hike of windings, with a peak value of 103.0 K. The figure shows that the end-windings experience a bigger temperature rise than the slots of windings due to the stronger heat transfer capacity of core of the stator compared to the convective air in the motor chamber [9]. Figure 4c displays the temperature rise distribution of permanent magnets, with a maximum value at 134.7 K. The heat from the rotor elements is partially dwindled by turbulent heat, corresponding to air in the gap traveling to the stator core in which conduction occurs to the water frames. Additionally, the shaft's conductive heat transfer capacity can serve as a heat dissipation conduit for rotor components. Heat transmission properties indicate that the middle region of PMs experiences a larger temperature rise compared to the end faces [10,11].

Table 2: Heat and losses measurement of machine.

Part	Loss in watt	Heat generation rate (x10^6 watt/m^3)
Rotor	99.50	0.267
Winding	758.50	3.523
Stator yoke	272	0.870
Stator teeth	339.60	0.785
Permanent magnets	89.06	1.507
Bearing	16.23	0.472

Source: Authors, (2025).

The experimental objectives are fixed to validate motor temperature rises. Wireless thermo sensors implanted in windings and affixed to the centre of the PMs measure heat rises in both. An infrared thermometer measures the temperature leap up of end-caps with the bearings [12]. Table 3 demonstrates how the mathematical findings are validated by comparing them to the experimental ones.

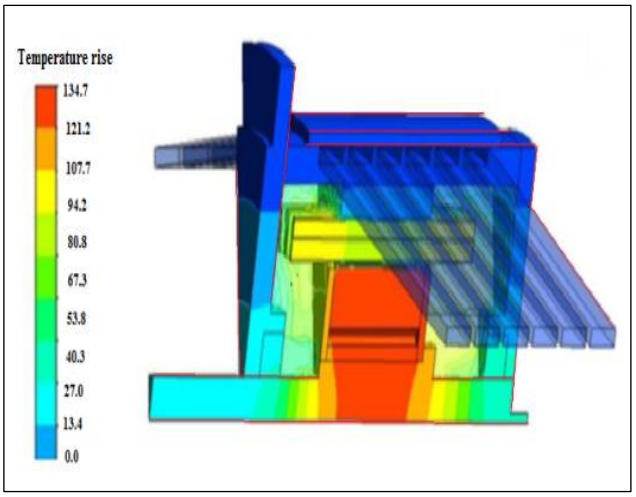

(a)

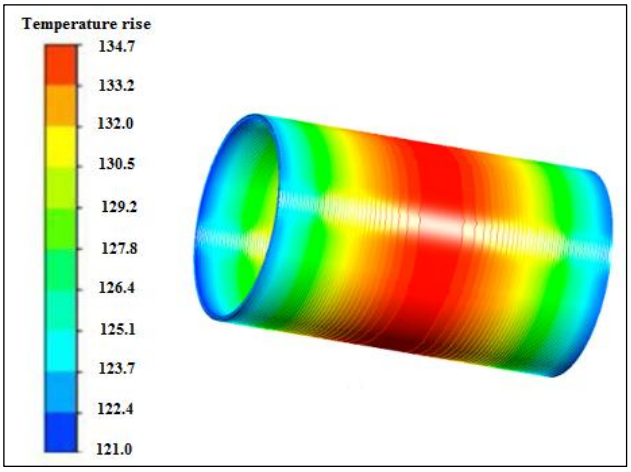

(b)

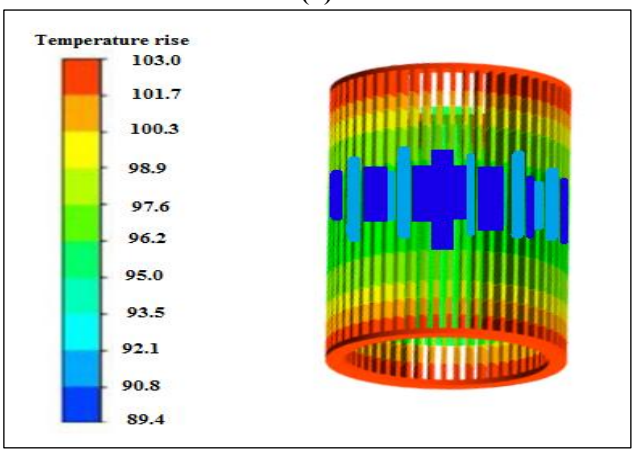

(c)

Figure 4: Temperature hike dissemination of PMSM with cooling structure a) motor b) winding c) permanent magnet.
Source: Authors, (2025).

IV. STRUCTURE OF COOLING MITIGATION

- **Structure of Cooling mitigation**

The computed temperature rises distributions indicate that the water-cooling frame's heat dissipation capacity on end-windings and PMs is restricted because of the high heating resistance between heating elements and liquid channels. To promote heat dissipation and reduce thermal resistance, an internal water channel structure is suggested (Figure 5) [13,14]

Table 3: temperature rise calculation of motor for water frame model.

Region	Calculation per 10^3	Testing per 10^3	Error %
winding	103.10	111.3	7.44 %
Permanent magnets	134.7	149.4	9.82 %
bearings	32.20	33.72	4.82

Source: Authors, (2025).

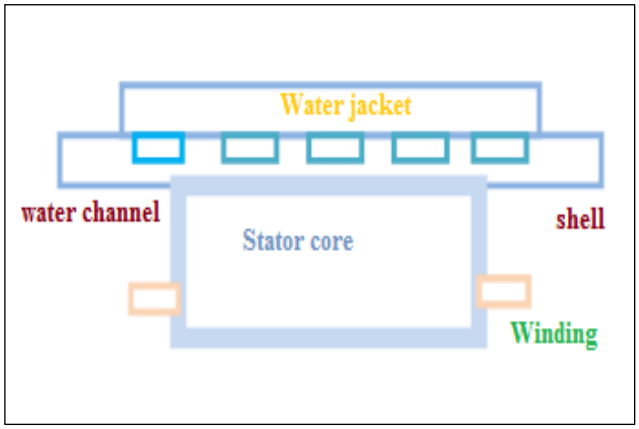

(a)

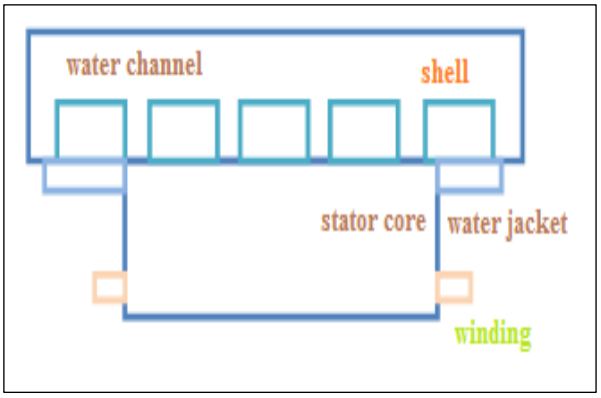

(b)

Figure 5: Improved fluid-cooled model of motor a) motor b) new model.
Source: Authors, (2025).

- **Structural Modification and Thermal Analysis of Motor**

Mathematical analysis is taken place on the liquid flow and temperature increase dissemination of a modified motor cooling structure. The largest temperature hike occurs in the canter region of the PMs at 128.3 K. The heat hike dissemination of the motor, as shown in Fig. 6, is comparable to that of the original construction (Fig. 4) [15,16,17]. The windings reached a maximum temperature of 97.3 K, which is 5.8 K less than the motor's main structure. The PMs have a maximum temperature rise of 128.3 K, which is 6.5 K much smaller the motor's main cooling arrangement. The redesigned water-cooling structure reduces winding temperature rise and indirectly improves rotor cooling capacity by reducing air temperature rise in end- caps [17, 18].

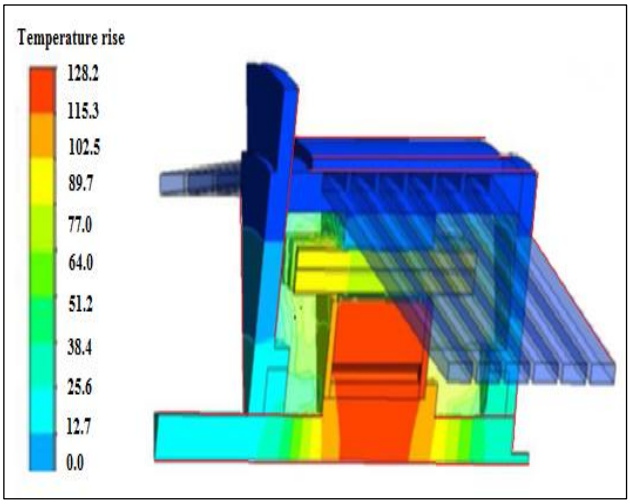

(a)

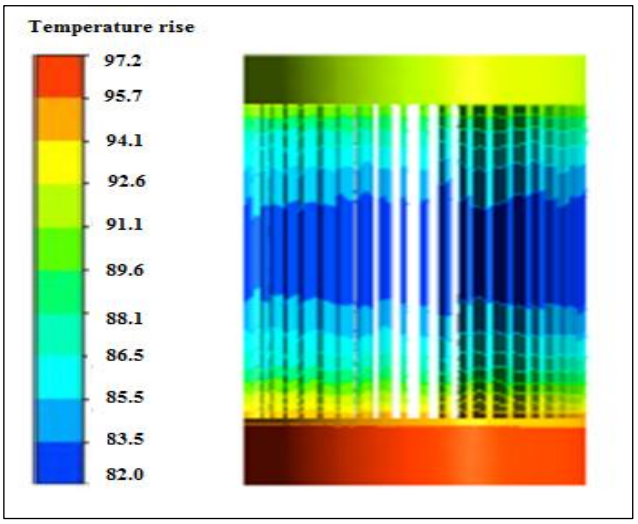

(b)

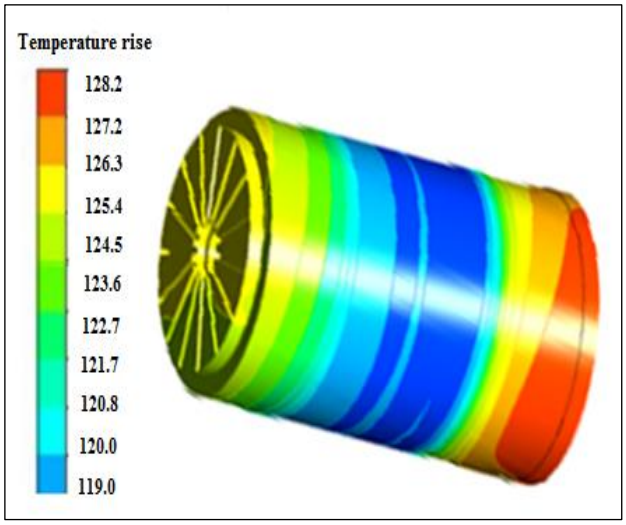

(c)

Figure 6: Temperature hike dissemination of PMSM with new cooling model a) motor b) winding c) permanent magnet.
Source: Authors, (2025).

V. ENHANCING THE REVISED COOLING

The Taguchi approach optimizes parameter combinations within a specific range with minimal experimental or computational effort. It is commonly employed in circumstances with high costs. Calculations for FSI problems can be time-consuming due to the fluidic-thermal coupled models' high level of nonlinearity [19,20]. The Taguchi approach is excellent for optimizing cooling structures. This work utilizes the Taguchi approach to the goal is to improved structural characteristics and increase heat dissipation capacity of a redesigned liquid frame cooling system. The parameters' sensitivity to heat dissipation performance is determined through analyses. The optimization processes consider the following factors: The circumferential channels are identified by their number (A), breadth (B), height (C), and fin width (D) [21, 22].

Table 4: Levels and factors.

Level	A	B	C	D
1	5	17.6	5.00	3.4
2	6	19.99	7.40	3.9
3	7	22.4	9.99	4.4

Source: Authors, (2025).

Table 5: L9(3^4) rectilinear and temperature rise.

Exp. No	A	B	C	D	Temperature rise per 10^3
1	2	2	2	2	128.2
2	2	1	1	1	125.4
3	2	3	3	3	129.8
4	1	2	1	3	127.2
5	1	1	3	2	130.3
6	1	3	2	1	128.4
7	3	2	3	1	130.6
8	3	1	2	3	128.5
9	3	3	1	2	124.6

Source: Authors, (2025).

Table 6. Average of each factor at various levels.

Factor	Level	Temperature rise per 10^3	Factor	Level	Temperature rise per 10^3
A	1	128.6	**C**	1	125.7
	2	127.8		2	128.4
	3	127.9		3	130.2
B	1	128.1	**D**	1	128.1
	2	128.6		2	127.7
	3	127.6		3	128.5

Source: Authors, (2025).

Table 4 shows the components and their related levels. Table 5 shows the use of the L9(34) orthogonal table due to the selection of four variables with three levels each. The cooling water flow rate (17.78 L/min) is maintained based on the factors table. Table 5 shows the maximal temperature rise of the PMs, which is likewise numerically determined [22,23,24]. Table 5 shows the temperature rise for

each group. Table 6 displays the general effect of each factor and level. The average temperature rise across 9 orthogonal experiments is calculated as:

$$T_{avg}\ \frac{\sum_{i=1}^{9} T_i}{9} = 128.2(\mathrm{K}) \tag{2}$$

Table 7: difference of every element with temperature hike.

Factor	A	B	C	D
S	0.12	0.16	3.41	0.10

Source: Authors, (2025).

Ti in (10^3) represents the temperature rise calculated. The error for every parameter can be calculated as follows:

$$S_j = \frac{\sum_{k=1}^{3} (T_{[3\,x(j-1)+k]} - T_{ave})^2}{3} \tag{3}$$

Sj represents the square error of the jth factor. Table 7 shows square errors. Tables 6 and 7 indicate that:

- issue C (channel height) has a greater impact on temperature rise than other components, making it the primary issue to consider.
- By maintaining a stable cooling flow rate during optimization, reduced channel heights bring the cooling water to core, resulting in a greater cooling impact. Selecting level, I for factor C results in the lowest averaged temperature hike for the machine [25,26].
- Factor B (channel width) is second highest influence on heat hike. It is set to level III (22.5 mm) to greatly limit increase of temperature rise.

The effect of the variables A (no. of channel) and D (width) is minimal on motor temperature increment. Factor A is relevant to both the costs of manufacturing the cooling system as well as the output pressure of the pump. In order to lowest manufacturing, maintenance costs and operating for the cooling system factor A was set to level I (5 cycles). Factor D was set to II (4 mm) to result in the lowest average temperature hike [27,28,29].

The analysis finds the optimal parameters as A-I, b-III, C-I, and D-II. Temperature rise distributions of the motor using the optimal parameters are shown in Figure 7. The optimization process has reduced the temperature increase of the motor by 2.2 K, which indicates reliable operation of the PMSM for long term (see figures). To verify the results and ensure the enhance structure is efficient, a PMSM prototype was built based on the optimal structural parameters (Fig. 8) and tested for temperature rises. Table 8 compares temperatures rise calculated to those from testing [30].

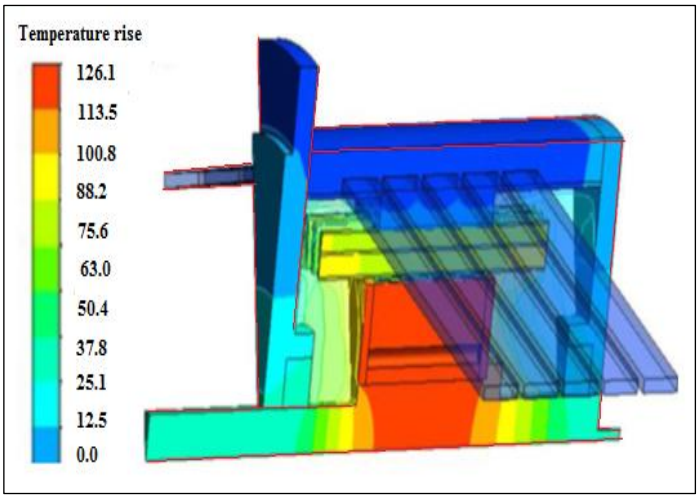

Figure 7: Temperature rise distribution of the motor with improvised cooling structure.
Source: Authors, (2025).

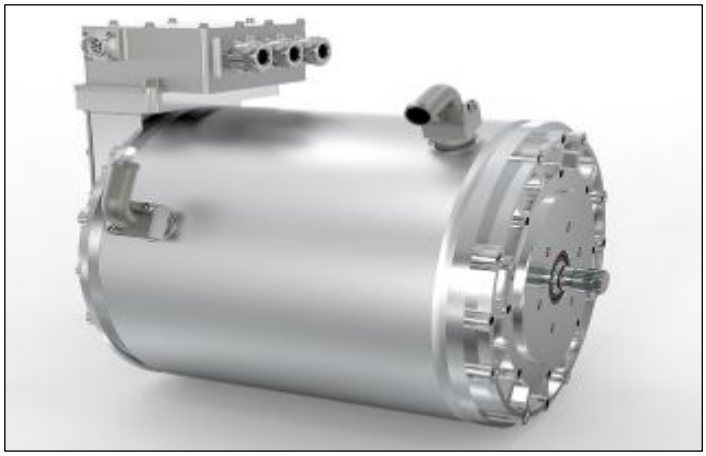

Figure 8: PM motor with improvised water-cooling structure.
Source: Authors, (2025).

Table 8: Calculation of Temperature hike and testing of the machine with new water model.

Parts	Calculation value per 1000	New value per 1000	Error
End winding	93.98	102.2	8.10 %
Permanent magnet	126.10	137.0	7.94 %
End cap (bearing)	29.7	30.6	2.92 %

Source: Authors, (2025).

VI. CONCLUSIONS

This study looks at the cooling efficacy of external water frames for a 20 kW 4500 rpm PM motor with high power density. Water channels are positioned on the inside surface of the motor housing to promote heat transfer. Numerical calculations support this approach. The Taguchi approach is used to optimize the formational characteristics of the enhanced cooling structure, thereby improving cooling performance. The study presented in this paper leads to the following findings:

- The three-dimensional thermal coupled approach is utilized to determine the temperature hike dispensation of the motor. The techniques' efficiency is demonstrated by the low calculation errors (< 10%) when compared to experimental results.
- Changing water channels from the external to interior exterior of the motor reduces the temperature rise by 6.5 K. Improving the cooling structure can improve heat dissipation in the cooling system.
- Optimization using the Taguchi approach improves cooling capacity and reduces temperature hike by 2.2 K.

VII. AUTHOR'S CONTRIBUTION

Conceptualization: Amit Kumar, Gaurav Singh Negi, Alok Sati.
Methodology: Amit Kumar, Gaurav Singh Negi, Alok Sati.
Investigation: Amit Kumar, Gaurav Singh Negi, Alok Sati.
Discussion of results: Amit Kumar, Gaurav Singh Negi, Alok Sati.
Writing – Original Draft: Amit Kumar, Gaurav Singh Negi, Alok Sati.
Writing – Review and Editing: Amit Kumar, Gaurav Singh Negi, Alok Sati.
Resources: Amit Kumar, Gaurav Singh Negi, Alok Sati.
Supervision: Amit Kumar, Gaurav Singh Negi, Alok Sati.
Approval of the final text: Amit Kumar, Gaurav Singh Negi, Alok Sati.

VII. ACKNOWLEDGMENTS

The authors would like to express their sincere gratitude to all those who contributed to the success of this research on enhancing the cooling system design of high-power density permanent magnet motors for electric vehicles (EVs). First and foremost, we would like to thank our research advisor, Gaurav singh negi, for their continuous guidance, support, and expertise throughout the course of this study. Their insightful comments and suggestions were invaluable in shaping the direction of this work.

We are also grateful to the members of the for their collaboration and technical support.

Finally, we would like to extend our heartfelt thanks to our families and friends for their patience, encouragement, and understanding during the course of this project.

VIII. REFERENCES

[1]. A. Morya, Applications of Wide Bandgap (WBG) devices in AC electric drives: a technology status review, in: 2017 IEEE International Electric Machines and Drives Conference (IEMDC), IEEE, 2017.

[2]. Park, J.-S.; Lee, T.-W.; Lee, J.-W.; Park, B.-G.; Kim, J.-W. Optimization of Multi-Phase Motor Drive System Design through Thermal Analysis and Experimental Validation of Heat Dissipation. Electronics 2023, 12, 4177.

[3]. Vlachou, V.I.; Sakkas, G.K.; Xintaropoulos, F.P.; Pechlivanidou, M.S.C.; Kefalas, T.D.; Tsili, M.A.; Kladas, A.G. Overview on Permanent Magnet Motor Trends and Developments. Energies 2024, 17, 538.

[4]. Dai, Y.; Wang, X.; Li, Z.; He, S.; Yu, B.; Zhou, X. Thermal error modeling of electric spindles based on cuckoo algorithm optimized Elman network. Int. J. Adv. Manuf. Technol. 2024, 132, 1365–1375.

[5]. Xiao, Y.; Zhu, Z.Q.; Jewell, G.W.; Chen, J.T.; Wu, D.; Gong, L.M. A Novel Asymmetric Interior Permanent Magnet Synchronous Machine. IEEE Trans. Ind. Appl. 2022, 58, 3370–3382.

[6]. H. Tahanian, M. Aliahmadi, J. Faiz, Ferrite permanent magnets in electrical machines: opportunities and challenges of a non-rare-earth alternative, IEEE Trans. Magn. 56 (3) (2020) 1–20.

[7]. E. Gundabattini, et al., A review on methods of finding losses and cooling methods to increase efficiency of electric machines, Ain Shams Eng. J. 12 (1) (2021) 497–505.

[8]. O. Wallscheid, et al., A critical review of techniques to determine the magnet temperature of permanent magnet synchronous motors under real-time conditions, EPE Journal 26 (1) (2016) 11–20.

[9]. Madhavan, S.; P B, R.D.; Gundabattini, E.; Mystkowski, A. Thermal Analysis and Heat Management Strategies for an Induction Motor, a Review. Energies 2022, 15, 8127.

[10]. Hu, X.; Yu, Z.; Zhuang, P.; Wan, J.; Wang, J.; Li, Y. Analytical Modeling of Temperature Field of SPMSM Based on Heat Pipe Cooling Technology. IEEE Trans. Appl. Supercond. 2024, 34, 5207705.

[11]. Liang, J.; Liang, K.; Shao, Z.; Niu, Y.; Song, X.; Sun, P.; Feng, J. Research on Temperature-Rise Characteristics of Motor Based on Simplified Lumped-Parameter Thermal Network Model. Energies 2024, 17, 4717.

[12]. A. Boglietti, A. Cavagnino, Analysis of the endwinding cooling effects in TEFC induction motors, in: Conference Record of the 2006 IEEE Industry Applications Conference Forty-First IAS Annual Meeting, IEEE, 2006.

[13]. G.M. Gilson, et al., A combined electromagnetic and thermal optimisation of an aerospace electric motor, in: The XIX International Conference on Electrical Machines-ICEM 2010, IEEE, 2010.

[14]. D.G. Nair, T. Jokinen, A. Arkkio, Coupled analytical and 3D numerical thermal analysis of a TEFC induction motor, in: 2015 18th International Conference on Electrical Machines and Systems (ICEMS), IEEE, 2015.

[15]. J. Park, et al., Design and analysis of high-speed permanent magnet motor considering thermal influence from impeller load characteristic of turbo blower system, in: 2016 IEEE Conference on Electromagnetic Field Computation (CEFC), IEEE, 2016.

[16]. N.K. Bhattacharya, D. Sarkar, Approximate analysis of transient heat conduction in the rotor of an induction motor during star-delta starting, in: International Conference on Information Communication and Embedded Systems (ICICES2014), IEEE, 2014.

[17]. Urbieta, J.G.; Rodríguez, B.; Rodríguez, A.J.; Díaz, P.; Armentia, S.; González, F. Sensitivity Analysis of Lumped-Parameter Thermal Networks for the Experimental Calibration of eMotor Models. IEEE Trans. Transp. Electrific. 2024, 10, 6210–6220.

[18]. Liu, Y.; Zhang, B.; Zong, M.; Feng, G. Thermal Analysis of a Modular Permanent Magnet Machine under Open-Circuit Fault with Asymmetric Temperature Distribution. Electronics 2023, 12, 1623.

[19]. IEC 60034-1; Rotating Electrical Machines—Part 1: Rating and Performance. International Electrotechnical Commission: Geneva, Switzerland, 2022.

[20]. Fasquelle, A.; Laloy, D. Water Cold Plates Cooling in a Permanent Magnet Synchronous Motor. IEEE Trans. Ind. Appl. 2017, 53, 4406–4413.

[21]. M. Jia, et al., Modeling and analysis of electromagnetic field and temperature field of permanent-magnet synchronous motor for automobiles, Electronics 10 (17) (2021) 2173.

[22]. B. Gan, et al., Thermal analysis of modular fault-tolerant permanent magnet motor based on electromagnetic-thermal Bi-directional coupling, IEEJ Trans. Electr. Electron. Eng. 17 (3) (2022) 454–469.

[23]. M. Jia, et al., Modelling and analysis of electromagnetic field and temperature field of permanent-magnet synchronous motor for automobiles, Electronics 10 (17) (2021) 2173.

[24]. C. Kim, K. Lee, Thermal nexus model for the thermal characteristic analysis of an open-type air-cooled induction motor, Appl. Therm. Eng. 112 (2017) 1108–1116.

[25]. G. Traxler-Samek, R. Zickermann, A. Schwery, Cooling airflow, losses, and temperatures in large air-cooled synchronous machines, IEEE Trans. Ind. Electron. 57 (1) (2009) 172–180.

[26]. G. Traxler-Samek, R. Zickermann, A. Schwery, Cooling airflow, losses, and temperatures in large air-cooled synchronous machines, IEEE Trans. Ind. Electron. 57 (1) (2009) 172–180.

[27]. Wang, L.; Shen, F.; Marignetti, F.; Bianchi, N.; Gong, H.; Li, Q.; Boglietti, A. Transient Thermal Exchange Analysis of an External Rotor Hub Motor for Electrified Defense Vehicles Applications Based on FVM and TNM. IEEE Trans. Transp. Electrific. 2024, 10, 1116–1127.

[28]. Wang, G.; Wang, Y.; Gao, Y.; Hua, W.; Ni, Q.; Zhang, H. Thermal Model Approach to the YASA Machine for In-Wheel Traction Applications. Energies 2022, 15, 5431.

[29]. Li, M.; Ye, J. Fractional Order Modeling of Thermal Circuits for an Integrated Energy System Based on Natural Transformation. Electronics 2022, 11, 914.

[30]. B. Gan, et al., Thermal analysis of modular fault-tolerant permanent magnet motor based on electromagnetic-thermal Bi-directional coupling, IEEJ Trans. Electr. Electron. Eng. 17 (3) (2022) 454–469.

Journal of Engineering and Technology for Industrial Applications

ITEGAM-JETIA

Manaus, v.11 n.54, p. 220-235. July/August., 2025.
DOI: https://doi.org/10.5935/jetia. v11i54.1767

ISSN ONLINE: 2447-0228

RESEARCH ARTICLE OPEN ACCESS

ENERGY MANAGEMENT OPTIMIZATION AND OPTIMAL CONTROL OF MICROGRID ENRICHED WITH RENEWABLE AND SUSTAINABLE DISTRIBUTED GENERATORS USING NATURE-INSPIRED METHOD

Nabil Mezhoud[1], Ahmed Bahri[2] , Bilel Ayachi[3], Farouk Boukhenoufa[4] and Lakhdar Bouras[5]

[1,3,4,5]Electrical Engineering Department, ELS laboratory, Université 20 Août 1955-Skikda, Algeria
[2]Automatics and Electromechanics Department, MESTE Laboratory, Faculté de Science et Technologie, Université de Ghardaia, Algeria

[1]https://orcid.org/0000-0002-9383-2097, [2]https://orcid.org/0009-0000-0016-4994, [3]https://orcid.org/0000-0002-7170-0085 , [4]https://orcid.org/0000-0003-1018-8249, [5]https://orcid.org/0000-0002-3245-1645

Email: n.mezhoud@univ-skikda.dz, bahri.ahmed@univ-ghardaia.edu.dz, b.ayachi@univ-skikda.dz, f.boukhenoufa@univ-skikda.dz, l.bouras@univ-skikda.dz

ARTICLE INFO

Article History
Received: March 25, 2025
Revised: April 20, 2025
Accepted: June 15, 2025
Published: August 31, 2025

Keywords:
Renewable and sustainable distributed generators,
Distributed generators,
Optimal control,
Micro-grids,
Grey wolf optimization,

ABSTRACT

One of most general nature-inspired meta-heuristic methods called Grey Wolf Optimization (GWO) inspired by grey wolves is applied to solve the energy management optimization (EMO) and optimal control (OC) problems of micro-grid (MG) impregnated with renewable and sustainable distributed generators (REDG). Our main goal is to minimize nonlinear objectives function of an electrical micro-grid taking into account a set of constraints. GWO method have been examined and tested on MG system composed of different types of DGs, such as wind turbines (WT), photovoltaic systems (PV), micro turbines (MT), fuel cells (FC), diesel electric generator (DEG), and loads with energy storage systems (ESS). The results are promising and show the effectiveness and robustness of proposed approach to solve the EMO and OC problems in different operational scenarios.

Copyright ©2025 by authors and Galileo Institute of Technology and Education of the Amazon (ITEGAM). This work is licensed under the Creative Commons Attribution International License (CC BY 4.0).

I. INTRODUCTION

The traditional electrical power system can be divided into three major categories: power generation, transmission and distribution systems [1]. The power plants are connected to the distribution network (DN) by transmission lines and the DN supplies electricity to all the loads in a given region. For a number of reasons, mainly technical and economic, individual power systems are connected together to form power pools. These regional or regional power grids operate independently, but are also interconnected to form a power grid. The rapid increase in the world population, digitalization and industrial evolution are the main causes of the growing demand for electricity.

In recent times, there has been a notable surge in the advancement and utilisation of RES [2]. A unique position is held by wind turbines among various energy sources. Indeed, wind energy is predicted to grow rapidly in many areas, but it can also have a substantial impact on the voltage and current quality in the network where it is injected because of its highly variable nature caused by large variations in wind speed [3].

Distributed generation (DG) has grown steadily during the last 20 years. Geographical and meteorological factors influence how DGs are integrated with RES, such as photovoltaic systems (PV) and small wind turbines (WTs). Moreover, the characteristics of their output powers are unpredictable and change over time. Conversely, non-renewable DGequipment, including fuel cells, micro turbines, diesel generators, and energy storage devices, possess a consistent output power and can be attached to any point within the DN [4], [5].

In a broader sense, the strategic utilization and effective management of DG units yield advantageous outcomes in terms of power quality enhancement, minimized power losses, improved reliability, and reduced emissions. To unlock the full potential of DG, an integrated approach encompassing coordinated operation and control alongside energy storage systems and controllable loads becomes imperative. This paves the way for the emergence of a ground-breaking paradigm known as micro-grids (MGs) [4], [6]. In essence, an MG denotes a localized DN comprising a diverse array of DG units, controllable loads, and energy storage systems, which can operate

either interconnected or islanded with the main distribution grid, thereby operating as a controlled entity [7], [8]. MGs represent as the pivotal element within contemporary power systems, embodying the essence of intelligent DN.

MGs are local DN comprising various DG units, controllable loads, and ESS that can operate either interconnected or isolated from the main distribution grid as a controlled entity. MGs represent the core of intelligent DN within modern power systems. In order to take full advantage of the operation of MGs, such as improved profitability and reduced dependence on the main network, it is important that the integration of DGs into MGs, and their relationship with the DN main upstream, helps to optimize the general operation of the system [9-11].

Energy management and optimal control are two closely related concepts that aim to optimize usage in a given system. Energy management refers to the overall management of energy within a system, seeking to minimize losses and maximize energy efficiency. This is a nonlinear optimization problem with constraints named optimal Energy and Operation Management (EOM). On the other hand, OC is a mathematical process that aims to optimize a system by adjusting the control variables according to certain conditions [12]. In the last 10 years, a very large number of mathematical methods has been applied to solve most important optimisation problems in power systems, such as optimal power flow (OPF), optimal reactive power dispatch (ORPD), economic dispatch (ED), optimal location and sizing of DG in DN, optimal control and optimal energy management of MGs, etc. Several methods have been proposed for determining the OEM of MG. An analytical approaches [13], [14] developed expressions to optimal energy management and online optimal control strategy of energy storage of MGs. A linear programming approach [15], [16] addresses the OEM problem of MG.

Recently, population-based methods have been widely used for OEM. Genetic algorithms [17-19] are frequently employed for EMO. A profit-maximizing approach was proposed by [20], while evolutionary programming [21], focused on reducing power losses and improving efficiency across various load models. A moth-swarm algorithm [22], are applied for OEM. Differential evolution algorithm were proposed by [23] to optimize or reduce the power losses in DN. Similarly, fore same purpose, backtracking search optimization [24] was applied to solve the OEM in microgrid, for the primary objective is the optimization of energy costs.

Local swarm intelligence methods have been applied to solve the OEM. PSO [7], [25], addresses OEM taking into account load variations in DN. Similar, Zhang et al., [26] use also PSO for EMO, while artificial bee colony [27-29] focuses on loss reduction with multiple DG sources. Ant colony optimization [29-30], aim to minimize OEM incorporating uncertainty in statistical cost estimation and demand response. Kamarposhti et al. [31] use also ACO to enhancing reliability and cost efficiency for sustainable energy systems by solving the OEM problem in microgrid. Nature-inspired and bio-inspired methods, including grey wolf optimization [32], cuckoo search [33], ant lion optimization [34], bacterial foraging-based algorithm [35], firefly algorithm [36] and [37] are used to solve the OEM. Whale optimization algorithm [38], dragonfly algorithm [39], glowworm swarm optimization [40], [41], crayfish optimization algorithm [42], dolphin echolocation algorithm, cuttlefish algorithm [43], greylag goose optimization [44], are used for OEM for losses and enhancing voltage in MG.

Physical approaches like gravitational search algorithms [45], [46] address optimized operation of microgrid and optimal power flow by reducing power losses, and gas emissions while improving power quality. Wind driven optimization [47] also target for gas emission optimization in microgrid. Kamel et al. [48] use archimedes optimization algorithm for solving the energy management problem in smart inter-connected micro-grids. Population-based algorithms like shuffled frog leaping [49], [50], colliding bodies optimization [51], teaching learning-based optimization [52], harmony search [53], and sine-cosine algorithm [54] are applied to solve EMO of MG in various objectives such as power loss reduction and voltage enhancement. In [55], authors combined GA with linear programming for sizing and energy management optimization of hybrid system. Moradi and Abedini [56], combined GA with methods like PSO for energy management optimization in DN. Similarly, Kouba and Sadoudi **[**57**],** addressed EMO by merging fuzzy logic with GA. Kumar et al. [58] use flying foxes optimization algorithm and deep attention dilated residual convolutional neural network for energy management optimization in smart grid system with RES and ESS.

Hybrid optimization methods like PSO and GSA [59], hybrid GWO and PSO [60], hybrid sperm swarm optimization and gravitational search algorithm have been proposed by Kamel et al. [61] to optimize for energy management optimization of power systems. These multi-objective approaches focus on minimizing costs, network losses, and improving the voltage profile. In recent year, hybrid evolutionary-swarms [62], hybrid evolutionary-bio-inspired algorithms [63], hybrid evolutionary-physical-inspired algorithm [64], hybrid swarm and physical-inspired algorithms [65], hybrid nature-inspired and swarm algorithms [66] and hybrid swarms intelligences algorithms [67] are used to optimize the energy management in DN and MGs.

II. PROBLEM FORMULATION

II.1 OBJECTIVE FUNCTION

In general, the EMO problem can be presented as follows [68]:

$$\min f(x,u) = \sum_{t=1}^{NT} \cos t^t \left(x^t, u^t\right) = \min_{u} \sum_{t=1}^{NT} \sum_{i=1}^{NG} \left[B_{Gi}\left(P_{Gi}^t\right) + MP^t P_{Grid}^t\right] \quad (1)$$

Subject to

$$h(x,\ u) = 0 \quad (2)$$

$$g(x,\ u) \le 0 \quad (3)$$

$f(x,u)$ is the cost function throughout the planning horizon. $h(x,u)$ and $g(x,u)$ are, respectively, the set of nonlinear equality and inequality constraints.The active power exchanged with the grid at time t is denoted by P_{Grid}^{t}. NT and NG are the total count of time and DGs, including storage; P_{Gi}^{t}, $B_{Gi}(P_{Gi}^{t})$ and MP^{t} are, respectively, the active power output, the bid of i^{th} DG and the electricity exchange price between the MG and grid at time *t* [69]. The state and control variables, x and u, are defined as follows

$$x^{t} = P_{Grid}^{t} \tag{4}$$

$$u^{t} = \left[P_{Gi}^{t},\ P_{G2}^{t},....P_{GNG}^{t}\right] \tag{5}$$

II.2 CONSTRAINTS

II.2.1 POWER BALANCE CONSTRAINTS (PBC)

For each time interval t, the total output power of the DGs, energy storage devices and utility must cover the total demanded load in the MG. As a result, the power balance constraint can be represented as follows:

$$\sum_{i=1}^{NG} P_{Gi}^{t} + P_{Grid}^{t} = \sum_{D=1}^{ND} P_{L_D}^{t} \tag{6}$$

P_{L_D} is the quantity of the Tenth loads level and ND is the total number of loads levels.

II.2.2 POWER GENERATION CAPACITY CONSTRAINTS

For stable operation, the active power output of each unit including the utility, is limited as follows:

$$P_{Gi,\min}^{t} \le P_{Gi}^{t} \le P_{Gi,\max}^{t} \tag{7}$$

$$P_{Grid,\min}^{t} \le P_{Grid}^{t} \le P_{Grid,\max}^{t} \tag{8}$$

$P_{Gi,\min}^{t}$, $P_{Grid,\min}^{t}$, $P_{Gi,\max}^{t}$ and $P_{Grid,\max}^{t}$ are, respectively, the minimum and maximum active powers of the ith DG, and the utility at time *t*.

II.2.3 RESERVE SPINNING CONSTRAINTS (RSC)

The RSC is necessary to maintain the reliability of the system, due to the power fluctuations of the renewable and the load fluctuations. To satisfy the RS, the following inequality constraint must be satisfied [70]:

$$\sum_{i=1}^{NG} P_{Gi,\max}^{t} + P_{Grid,\max}^{t} = \sum_{D=1}^{ND} P_{L_D}^{t} + R^{t} \tag{9}$$

Where, R^{t} is the spinning reserve programmed at time *t*. In an MG, the RSC is considered by adding an additional value to the total power demand, which should be supplied by the DG units. It should be noted that the maximum power (not the operating point) of the energy sources is considered in the above equation.

II.2.4 ENERGY STORAGE LIMITS (ESL)

Since there are certain limits to the charge and discharge rate of storage devices during each time interval, the following equation and constraints can be expressed as

$$\begin{aligned} &W_{ess,t} = W_{ess,t-1} + \eta_{charge} P_{charge} \Delta t - \frac{1}{\eta_{discharge}} P_{discharge} \Delta t \\ &\begin{cases} W_{ess,\min} \le W_{ess,t} \le W_{ess,\max} \\ P_{charge,t} \le P_{charge,\max} \ \ and \ \ P_{discharge,t} \le P_{discharge,\max} \end{cases} \end{aligned} \tag{10}$$

$W_{ess,t}$ and $W_{ess,t-1}$ are the amount of energy stored in the battery at time t and t-1, respectively; $P_{charge}(P_{discharge})$ is the charge (discharge) rate allowed for a defined period of time Δt; $\eta_{charge}(\eta_{discharge})$ is the efficiency (yield) of the battery during the *charging* (discharging) process; $W_{ess,\min}$ and $W_{ess,\max}$ are the lower and upper limits of the amount of energy stored inside the battery; and $P_{charge,\max}(P_{discharge,\max})$ is the maximum rate of charge (discharge) of the battery during each interval time Δt [29].

II.2.4 CALCULATION OF ACTIVE POWER FROM (TO) THE GRID

The active power from (to) the utility is considered as a dependent variable. The grid power is calculated as

$$P_{Grid}^{t} = \sum_{D=1}^{ND} P_{L_D}^{t} - \sum_{i=1}^{NG} P_{Gi}^{t} \tag{11}$$

The obtained P_{Gi}^{t} we check whether or not satisfies the constraint in (8). Therefore, the $P_{Grid,\lim}^{t}$ is defined as:

$$P_{Grid,\lim}^{t} = \begin{cases} P_{Grid,\max}^{t} & si\ P_{Grid}^{t} > P_{Grid,\max}^{t} \\ P_{Grid,\lim}^{t} & si\ P_{Grid,\lim}^{t} < P_{Grid,\min}^{t} \\ P_{Grid}^{t} & si\ P_{Grid,\min m}^{t} \le P_{Grid,\min}^{t} \le P_{Grid,\max}^{t} \end{cases} \quad (12)$$

The new extended function to be optimized when the penalty factor multiplied by the square of the difference between the actual value and the limit value of the dependent variable is

$$\min_{u} F_{p} = \min_{u} \sum_{t=1}^{NT} \cos t^{t}\left(x^{t}, u^{t}\right) + \lambda_{p}\left(P_{Grid}^{t} - P_{Grid,\lim}^{t}\right)^{2} \quad (13)$$

Where λ_{p} is the penalty factor.

II.3 BIDS CALCULATION OF DISTRIBUTED GENERATION

Depending on the cost function of the units, if any, the market price feedback and the need to make some profit, necessary for the annual depreciation of the installation cost, the DG bids are considered quadratic, as shown in (14) [9].

$$B_{Gi} = a_{i} P_{Gi}^{\ 2} + b_{i} P_{GI} + c_{i} \quad (14)$$

II.3.1 MICRO-TURBINE AND FUEL CELL

The MT and FC bids in ($/h) can be calculated as follows [5], [71]:

$$B_{G} = C_{fuel} \frac{P_{G}}{\eta_{G}} + C_{inv} \quad (15)$$

Where, P_{G} is the DG electrical output power (kW), η_{G} is the DG electrical efficiency, C_{fuel} is the fuel price (natural gas) to supply the DG ($/kWh), and C_{inv} is the hourly amount of reimbursement of the investment cost of DG in ($/h) given as

$$C_{inv} = AC \frac{P_{G,nom}}{AP} \quad (16)$$

$$AC = \frac{i(1+i)^{n}}{(1+i)^{n} - 1} IC \quad (17)$$

Where, i is the interest rate, n is the amortization period in years, and IC is the installation DG cost. The MT electrical efficiency can be estimated as a quadratic function of its output power [72]. These coefficients can be obtained by fitting the electrical efficiency curve of the MT based on the manufacturers' data. The FC efficiency is a non-linear function of the power level and can be expressed as follows (for a Proton exchange membrane fuel cell: PEM-FC) [73]:

$$\eta_{FC} = \frac{1}{2.964}\left[V_{0} + \sqrt{V_{0}^{2} - 4\left(V_{0} V_{Pnom} - V_{Pnom}^{2}\right)\xi}\right] \quad (18)$$

Where, V_{0} is the theoretical or thermodynamic FC potential (0.9 V), V_{Pnom} is the potential of the selected cell at rated power (0.45–0.75 V), $\xi = P_{FC}/P_{nom}$ is the power level, and P_{nom} is the rated FC power. The coefficients of the quadratic function (14) can be obtained by curve fitting, constructed according to (15) for a power range of PG.

II.3.2 WIND TURBINES AND PHOTOVOLTAIC

The bid functions of WT and PV consider the annual investment cost for depreciation of equipment (AC) ($/kW) and the annual energy production per kW (AP) (kW h/kW) are given by (15), and (17), respectively.

According to [74] and [75], the power curve of WT can be modeled by means of a function divided into three different:

$$P_{WT} = \begin{cases} 0 & for \quad v \le v_{ci} \quad and \quad v \ge v_{co} \\ \dfrac{v^{2} - V_{ci}^{2}}{v_{nom}^{2} - v_{ci}^{2}} P_{WT,nom} & for \quad v_{ci} < v \le v_{nom} \\ P_{nom}, & for \quad v_{nom} < v \le v_{co} \end{cases} \quad (19)$$

Where, $P_{WT,nom}$, v_{nom}, v_{ci} and v_{co} are, respectively, the rated power, rated wind speed, switch-on wind speed and switch-off wind speed of the WT; P_{WT} is denote the output power of the WT and v is the wind speed [75, 76].

The PV output power P_{PV} depends on the solar irradiation and the ambient temperature of the site as well as the characteristics of the module itself. P_{PV} is calculated as follow [76]:

$$P_{PV} = P_{STC}\frac{I_S}{1000}[1+\gamma(T_C-25)] \quad (20)$$

P_{STC} is the PV maximum power under standard test conditions (STC) (W); I_S is the solar irradiation on the surface of the PV module (W/m^2); γ is the PV module temperature coefficient for power in (°C-1); T_C is the temperature of PV cell (module) in (C). The temperature of PV can be calculated based on the Nominal Operating Cell Temperature (NOCT) as follows, [75]:

$$T_c = T_a + \frac{I_S}{800}(T_{NOCT}-20) \quad (21)$$

T_a is the ambient temperature in (°C); T_{NOCT} is the NOCT of the module in (°C).

II.3.3 DIESEL GENERATORS (DEG)

Usually, diesel fuel consumption data in (L/h) is provided by the manufacturer. Based on these data, the fuel consumption characteristic of the DEG can be estimated as a quadratic function of its active power output [68]:

$$Fuel_{DEG} = a_{fuel}P_{DEG}^2 + b_{fuel}P_{DEG} + c_{fuel} \quad (22)$$

Where, $Fuel_{DEG}$ is the fuel consumption in (L/h); P_{DEG} is the DEG power output in (KW); α_{fuel}, b_{fuel} and c_{fuel} are the coefficients of the fuel consumption characteristic. As a result, the DEG bids ($/h) can be calculated as:

$$B_G = C_{fuel}Fuel_{DEG} + C_{inv} \quad (23)$$

C_{fuel} is the price of diesel fuel to supply DEG in ($/L). C_{inv} is the hourly payback amount for the investment cost of the DE ($/h) defined by (17).

II.3.4 ELECTRIC GRID

Market energy costs in ($/h) can be represented by a quadratic function as follows:

$$f_{grd} = a + bP_{grd} + cP_{grd}^2 \quad (24)$$

Where, P_{grd} is the electrical network power in (kW) and *a*, *b* and *c* are the cost coefficients [68].

III. GREY WOLF OPTIMIZATION

Grey wolf optimization (GWO) is a typical swarm-intelligence based meta-heuristic algorithm proposed by Mirjalili et al. in 2014 [77] which is inspired from the leadership hierarchy and hunting mechanism of Grey Wolves (GW) in nature. In nature, GW (Canis lupus) belongs to Candidate family. It is considered as a top level of predators and residing at the top in the food chain.

The population hierarchies of GW are separated by four layers which are named as, alpha (α) is the fittest solution. Beta (β) is the second optimum solution and delta (δ) is the third one. Omega (ω) is the candidate solutions that are left over. Generally, the populations of GW have average crowd size of 5-12 [78] and the cluster organizes compactly through the hierarchy.

The position of the wolves is considered as the variables to be optimized and the distance between prey and GW determine the fitness value of the objective function. The movement of each individual is influenced by four processes, namely

- Searching for prey (exploration);
- Encircling prey;
- Hunting;
- Attacking prey (exploitation).

III.1 SOCIAL HIERARCHY

The GW diverge from each other position for searching a victim. Make use $\vec{A}_M$ with random values to compel search agent to diverge from the victim. $\vec{C}_M$ component provides random weights for searching prey in the search space.

III.2 ENCIRCLING PREY

As mentioned above, GW encircle prey during the hunt. α, β and δ estimate the position of the three best wolves and other wolves updates their positions using the positions of these three best wolves. Encircling behavior can be represented by $\vec{D}_M$. When the wolves do hunting, they tend to encircle their prey [79]. The following equations depicted the encircling behavior [80].

$$\vec{D}_M = \left| \vec{C}_M \vec{X}_P(t) - \vec{X}(t) \right| \tag{25}$$

$$\vec{X}_{(t+1)} = \vec{X}_P(t) - \vec{A}_M . \vec{D}_M \tag{26}$$

Where t is the current iteration, $\vec{X}$ is the position vector of GW, $\vec{X}_P$ is the position of the prey, $\vec{A}_M$ and $\vec{C}_M$ are the coefficient vectors calculated using the following expressions [78]:

$$\vec{A}_M = 2\vec{a} . \vec{r}_1 - \vec{a} \qquad and \qquad \vec{C}_M = 2\vec{r}_2 \tag{27}$$

Where $\vec{r}_1$ and $\vec{r}_2$ are random vectors between 0 and 1 and $\vec{a}$ is set to decreased from 2 to 0 over the course of iterations [77, 78]. The three best solutions so far are saved and then the other search agents (omega wolves) update their positions according to the current best position [78, 81].

III.3 HANTING

Conservation of regional habitat connectivity has the potential to facilitate recovery of the GW. After encircling, α wolf guides for hunting. Later, β and δ wolves join in hunting [78]. It is tough to predict about the optimum location of prey. These situations are expressed in the following expressions [80]:

$$\begin{cases} \vec{D}_{M\alpha} = \left| \vec{C}_{M\alpha} . \vec{X}_\alpha(t) - \vec{X}(t) \right| \\ \vec{D}_{M\beta} = \left| \vec{C}_{M\beta} .. \vec{X}_\beta(t) - \vec{X}(t) \right| \\ \vec{D}_{M\delta} = \left| \vec{C}_{M\delta} .. \vec{X}_\delta(t) - \vec{X}(t) \right| \end{cases} \tag{28}$$

$$\vec{X}_{1\alpha} = \vec{X}_\alpha - \vec{A}_{M1} \vec{D}_{M\alpha}, \; \vec{X}_{1\beta} = \vec{X}_\beta - \vec{A}_{M2} \vec{D}_{M\beta} \; and \; \vec{X}_{1\delta} = \vec{X}_\delta - \vec{A}_{M3} \vec{D}_{M\delta} \tag{29}$$

The best position of wolf is calculated taking average sum of positions and given as

$$\vec{X}_{(t+1)} = (\vec{X}_{1\alpha} + \vec{X}_{1\beta} + \vec{X}_{1\delta}) / 3 \tag{30}$$

III.4 ATTACKING PREY

The GW stop the hunting by attacking the prey when it stops moving. It depends on the value of a. $\vec{A}_M$ is a random value in the interval $[-2a, 2a]$. In GWO, search agents update their positions based on the location of α, β and δ and attack towards the prey [79, 81]. However, GWO algorithm is prone to stagnation in local solutions with these operators. It is true that the encircling mechanism proposed shows exploration to some extent, but GWO needs more operators to emphasize exploration.

IV. SIMULATION AND DISCUSSIONS

The MG (Fig. 1) is used in this work. The MG is considered in order to show how to determine the offers of the different DG units. The system is a MG composed of five different DG units (WT connected to bus 4, a MT is connected to bus 7, a PV connected to bus 11, a DEG connected to bus 19 and an FC connected to bus 23) with ESS and electrical loads. Table 1 presents the data was used to calculate the DG bids coefficients and power limits. It is assumed that all DGs sources produce active power at a single power factor. Based on the decisions of the MG Central Controller (MGCC), there is a power exchange link for one day between the utility and MG.

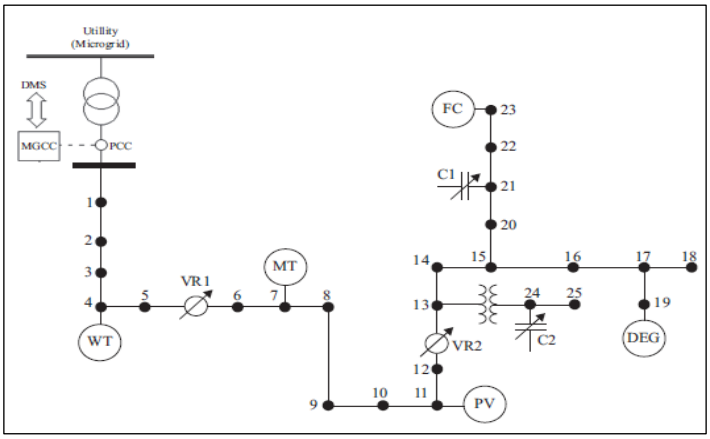

Figure 1: One line diagram of test system.
Source: [68].

Table 1: Power limits and bid coefficients of DG units.

Bus N°	Type	P_{DG}^{min} (KW)	P_{DG}^{max} (KW)	Costs coefficient		
				a	*b*	*C*
23	*FC*	30	300	0.0062	1.62	2.204
19	DEG	0	369	0.0065	12.41	1.177
11	PV	0	250	0	43.57	0
7	MT	90	300	0.0018	2.63	811
4	WT	0	600	0	6.5	0
0	Utility	0	300	0	1e-4	5e-5

Source: [68].

The proposed algorithm implemented and the computations were performed using MATLAB software, and all cases were run on a desktop computer Windows-10, 64-bit, Intel(R) Core(TM) i5-6500 CPU, 3.20 GHz processing frequency and 8.0 GB RAM.

IV.1 ENERGY MANAGEMENT OPTIMIZATION

The GWO method is implemented to find optimal solutions of the EMO problem of the MG in an operating scenario as follows: It is assumed that the PV and WT sources act at their maximum power available during each hour of the day, and the other DGs, including MT, FC and DEG, can operate within their power limits while satisfying the necessary constraints. All DGs with relevant characteristics generate electricity in the MG, and the additional demand or surplus energy inside the grid is exchanged with the utility from the point of common coupling PCC (Fig.1). The utility behaves as an unconstrained unit and exchanges power with the MG without any limitations. In this scenario, the influence of exchanges of energy market price with the utilities on the total operating cost of MG is examined in the following 3 cases:

Case 1: Energy market price is low;
Case 2: Energy market price is average;
Case 3: Energy market price reaches its real value.

The wind speed and ambient temperature are shown, respectively, in Figure 2. It was assumed that the active and reactive power of load on each bus varies according to the daily load diagram shown in Figure 3. Solar irradiance is also shown in Figure 3. Figure 4 depict the forecast energy market prices. It is assumed that, both Figure are scaled for 24h.

Given the low market price in 1st case, especially during periods when the load levels are low and medium, the utility takes the lead in supplying the load inside the MG. In the 2nd case, when the market price is middle range (higher compared to case 1), most of the load portion is provided by MT and FC units. During periods of average load, corresponding to the average market price (5.6 $/kWh), excess energy is exported from the MG to the utility. When the market price is brought to its real value in 3rd case, the MT and FC units are used with their maximum power in periods with medium and high loads levels.

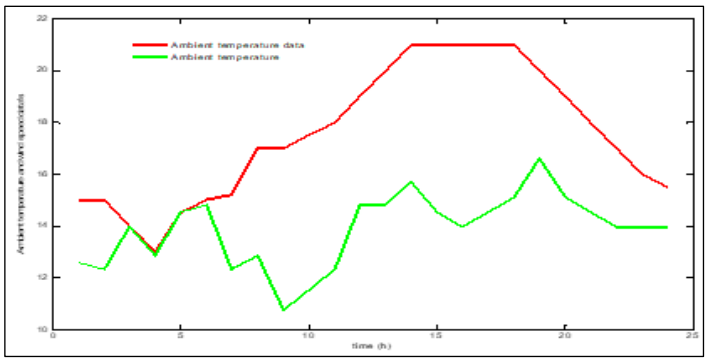

Figure 2: Ambient temperature and wind speed data's.
Source: Authors, (2025).

In addition, surplus energy is exported from the MG to the utility in most period of the day. The simulation results associated with cases 1, 2 and 3 are shown in Figures 5-11, respectively.

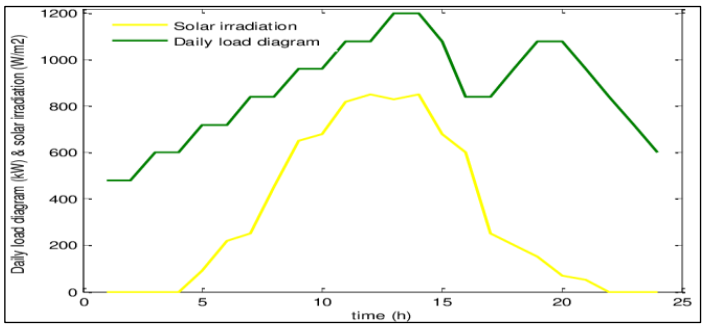

Figure 3: Solar irradiation and daily load diagram data's.
Source: Authors, (2025).

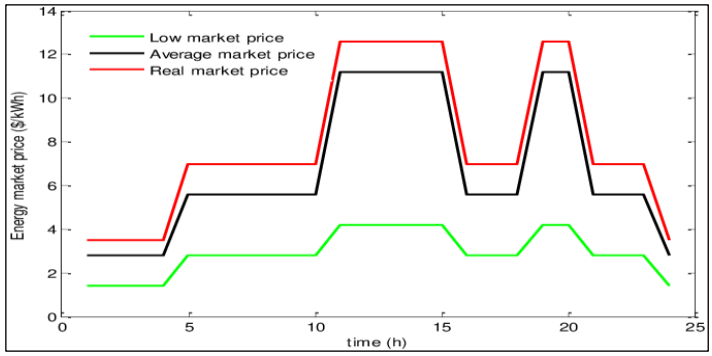

Figure 4: Energy market price dada's.
Source: Authors, (2025).

Due to the low market price for case 1, especially during times of low and medium load levels, the utility supplies the load inside the MG on its own. In this case, 257200 ($/h) is the best operation cost that was found. In the second case, the majority of power supplied to the loads through MT and FC. During periods of average load, corresponding to average market price, excess energy is solded from the MG to the utility. In this case, the best operation cost is 263900 ($/h).

When the market price reaches its genuine value, the MT and FC operate at maximum power during periods of medium and high loads. In addition, for majority of the day, excess energy are exported from the MG to the utility. In this case, the optimal operation cost was achieved at 263500 ($/h).

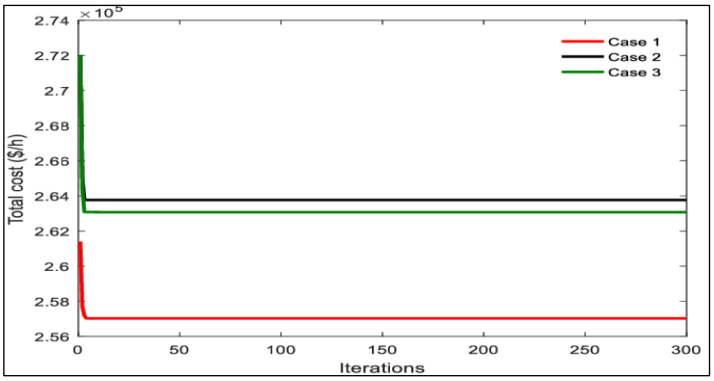

Figure 5: Costs results of 3 cases.
Source: Authors, (2025).

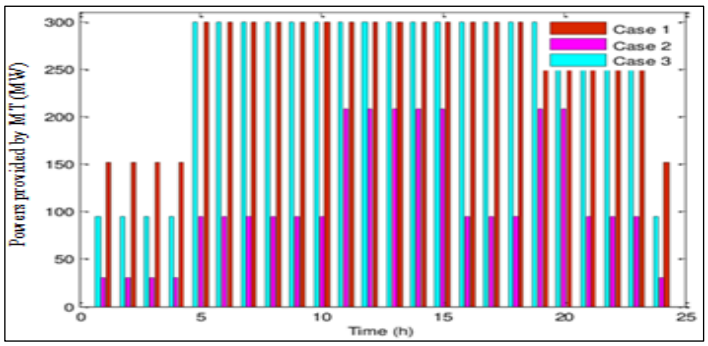

Figure 6: Powers provided by MT.
Source: Authors, (2025).

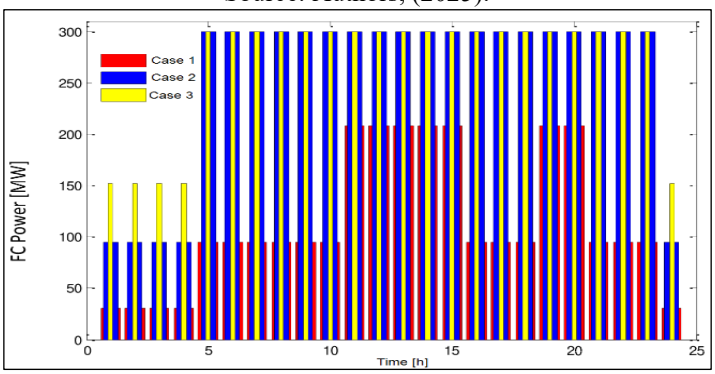

Figure 7: Powers provided by FC.
Source: Authors, (2025).

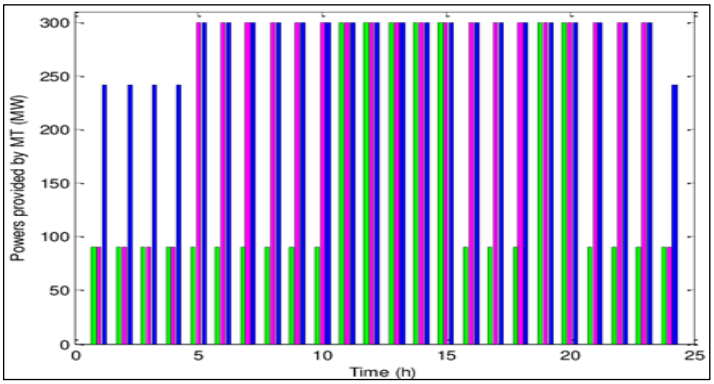

Figure 8: Powers provided by MT.
Source: Authors, (2025).

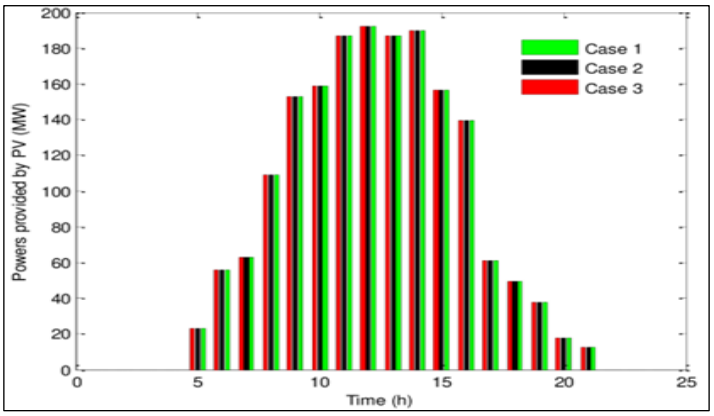

Figure 9: Powers provided by PV module.
Source: Authors, (2025).

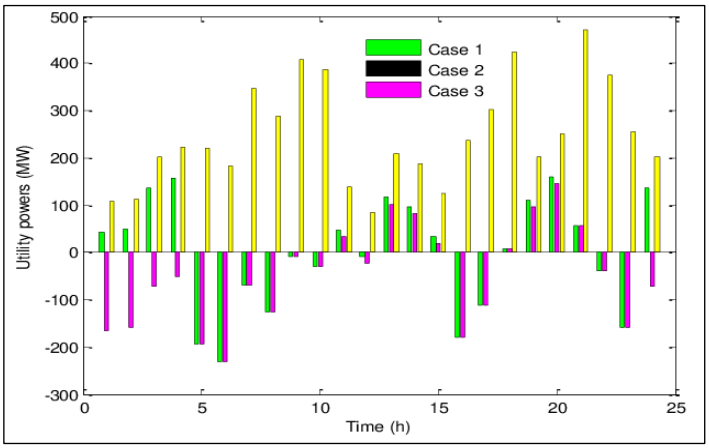

Figure 10: Utility powers.
Source: Authors, (2025).

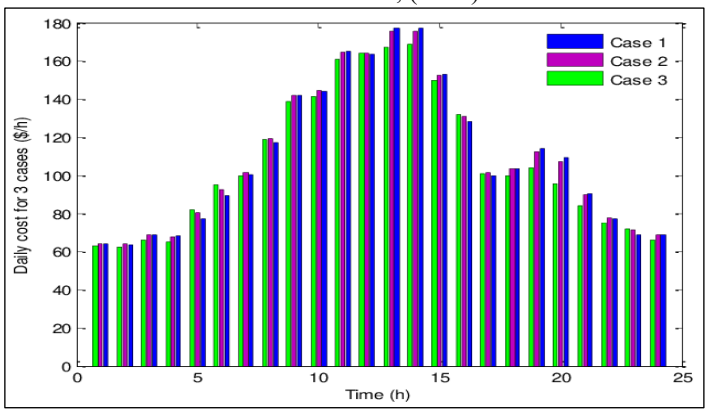

Figure 11: Daily costs of 3 cases.
Source: Authors, (2025).

II.2 OPTIMAL DG CONTROL

The proposed approach has been implemented on modified IEEE 24-bus test system shown in Figure 1. In this study, the OC is solved for the following 3 different purposes:

Case A: Voltage deviation (VD) optimization.

$$\min F(x,u) = \min VD(x,u) = \min \sum_{i=1}^{NL} \left| V_i - V_i^{ref} \right| \tag{31}$$

Case B: Total power loss (Plosses) optimization.

$$\min F(x,u) = \min P_{loss}(x,u) = \min \sum_{i=1}^{NB} R_i I_i^2 \tag{32}$$

Case C: simultaneous optimization (VD+Ploss).

$$\min F(x,u) = \min \left\{ w_V . VD(x,u) + w_p . P_{loss}(x,u) \right\} \tag{33}$$

w_i are the weighting factors. The objective functions results for the three cases are presented in Figures 12-14 The optimal control variable for all cases are shown in table 2. The bus voltages, the optimal DGs voltage, the active and reactive powers of DGs are shown in Figures 15-18, respectively.

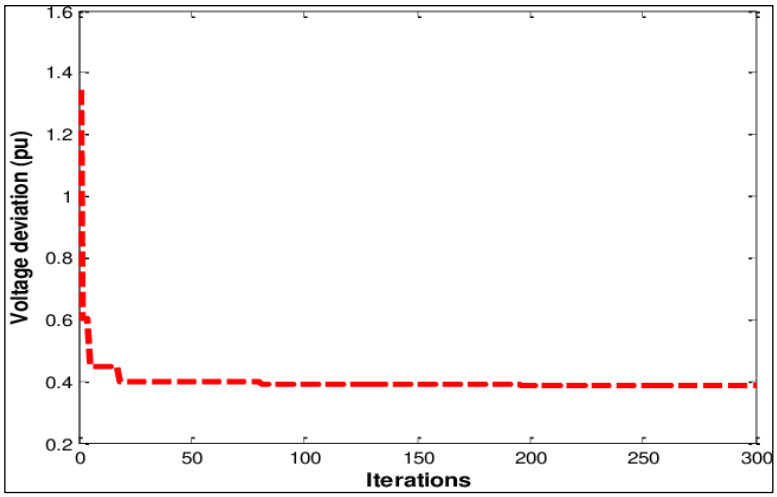

Figure 12: Results of case 1.
Source: Authors, (2025).

As a results of the voltages at bus 4, 7, 11, 19, and 23 being maintained at predetermined levels to reduce VD throughout the rest of the network, there are high reactive power compensation (QC) values and a wide range of reactive power variations of the DG, QDG, in the first scenario. Reactive power compensation is intimately related to voltage control. The active and reactive powers losses in the lines acquired for the prior situations are displayed in Figure 16.

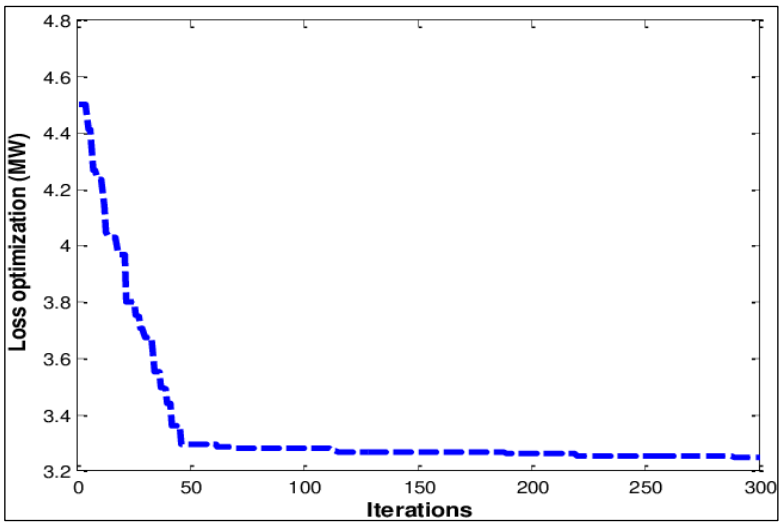

Figure 13: Results of case 2.
Source: Authors, (2025).

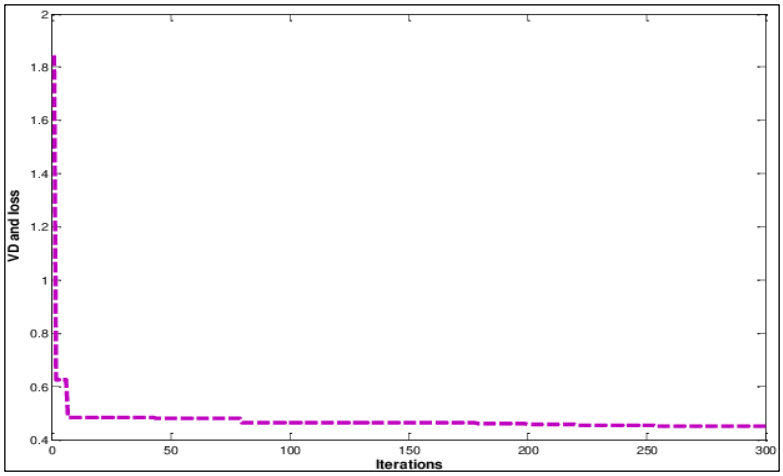

Figure 14: Results of case 3.
Source: Authors, (2025).

High values for V0 and V_{DG}, obtained throughout the whole load range in the second scenario. In fact, a constant active and reactive power model (PQ model) has been used to represent the loads. Considering that power losses are inversely correlated with branch current squared. By enhancing the voltage bus using DG, power losses for a constant power load can be reduced. As illustrated in Figure 11, case C can be viewed as a middle-ground option because it simultaneously lowers power losses and VDs.

Table 2: Control variables for all cases using GWO.

Control variables	Case 1	Case 2	Case 3
PG_4	0.2304	0.2304	0.2300
PG_7	0.1468	0.2539	0.2031
PG_{11}	0.1588	0.1588	0.1580
PG_{19}	0.1501	0.3690	0.2482
PG_{23}	0.2458	0.3000	0.0793
$P_{Utility}$	0.5401	0.3433	0.3810
$V_{Utility}$	1.0061	1.0491	1.0060
V_{23}	1.0437	1.0314	1.0274
Q_{com21}	0.1774	0.1611	0.1389
Q_{com24}	0.1140	0.0947	0.1050
T_{5-6}	0.9815	0.9971	0.9810
T_{12-13}	0.9532	1.0084	0.9510
Cost ($/h)	141.25	143.77	144.10
Losses (MW)	5.5820	3.2480	6.0460
VD (pu)	0.3858	0.8871	0.3894
CPU time (s)	136.00	154.09	144.30

Source: Authors, (2025).

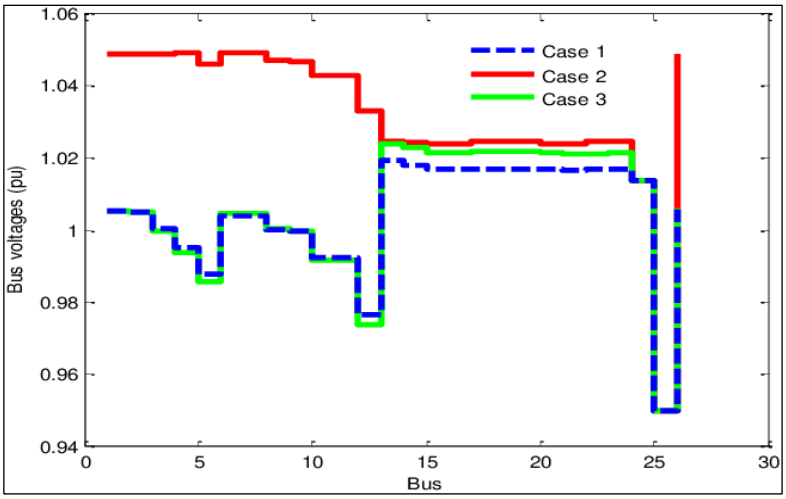

Figure 15: Bus voltages of three cases.
Source: Authors, (2025).

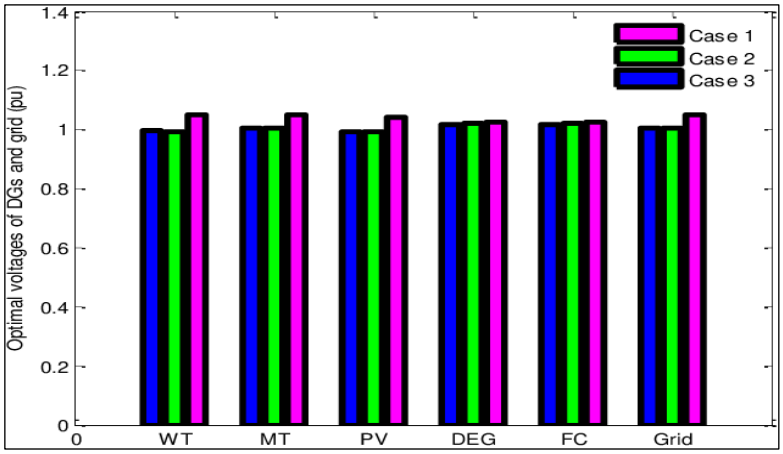

Figure 16: DG and grid optimal voltages.
Source: Authors, (2025).

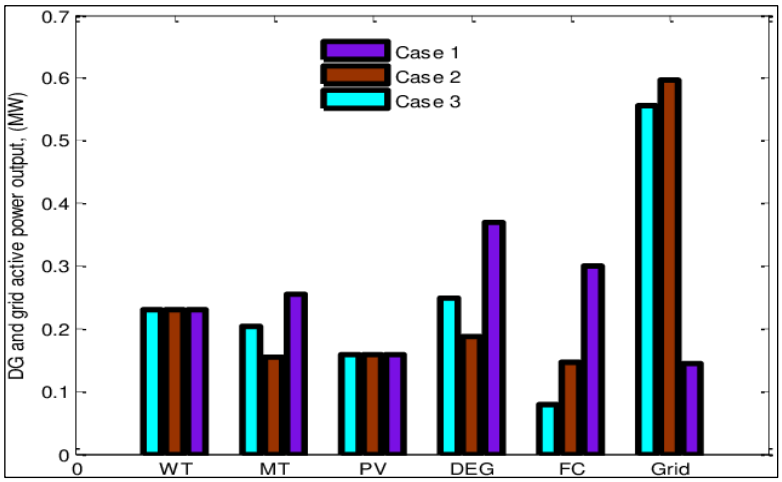

Figure 17: DG and grid active power output.
Source: Authors, (2025).

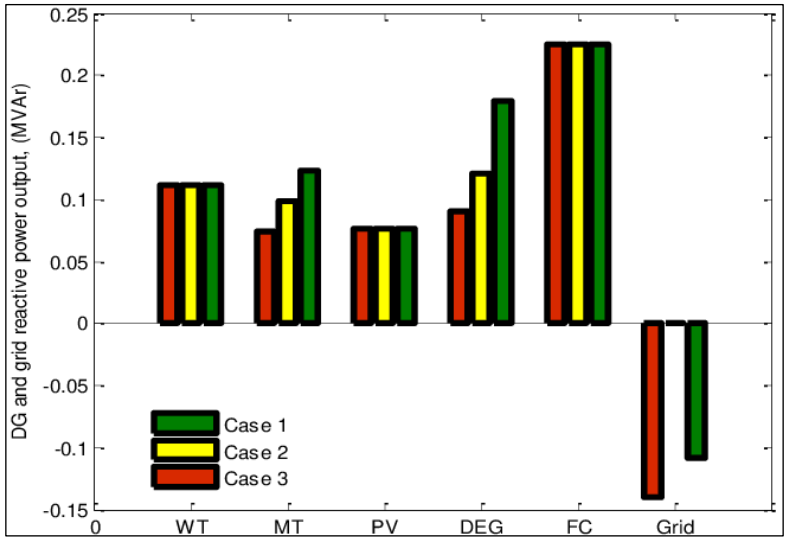

Figure 18: DG and grid reactive power output.
Source: Authors, (2025).

The second section of this study demonstrate how well the GWO approach works to address the OC in MG. Consequently, the aforementioned findings demonstrate the improved capacity of the GWO algorithm to produce solutions of the highest calibre while maintaining computational efficiency and robustness.

The simulation results presented in this paper show that the GWO method is very suitable to solve the EMO and OC problems of MG. Therefore, in a computationally efficient and robust manner, the above results establish the enhanced ability of GWO algorithm to achieve superior quality solutions.

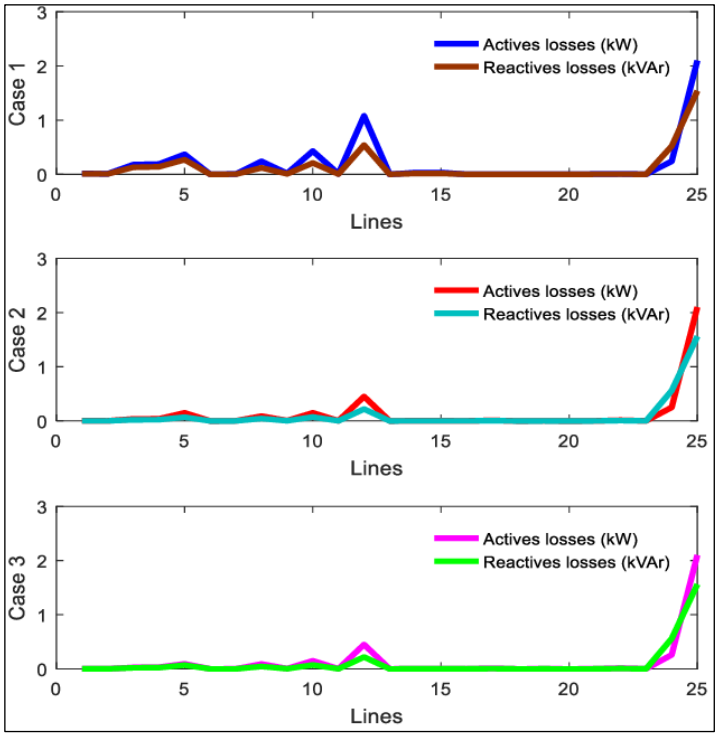

Figure 19: Active and reactive power losses.
Source: Authors, (2025).

V. CONCLUSION

Based on the nature-inspired approaches, this study offers a successful solution to an MG's challenges. The GWO method successfully applied to solve the EMO and OC problems of a MG. The suggested method has been investigated and tested on an MG that is connected various DG units via an ESS. The outcomes of the simulation demonstrate how well the suggested strategy works to address EMO and OC in various operating scenarios. Moreover, the obtained results using GWO are either better or comparable to those obtained by other technique reported in the literature. In terms of the computational effort, convergence speed and performance of the solutions reveal the superiority of GWO algorithm.

VI. AUTHOR'S CONTRIBUTION

Conceptualization: Nabil Mezhoud, Ahmed Bahri , Bilel Ayachi, Farouk Boukhenoufa and Lakhdar Bouras.
Methodology: Nabil Mezhoud, Ahmed Bahri , Bilel Ayachi, Farouk Boukhenoufa and Lakhdar Bouras.
Investigation: Nabil Mezhoud, Ahmed Bahri , Bilel Ayachi, Farouk Boukhenoufa and Lakhdar Bouras.
Discussion of results: Nabil Mezhoud, Ahmed Bahri , Bilel Ayachi, Farouk Boukhenoufa and Lakhdar Bouras.
Writing – Original Draft: Nabil Mezhoud, Ahmed Bahri , Bilel Ayachi, Farouk Boukhenoufa and Lakhdar Bouras.
Writing – Review and Editing: Nabil Mezhoud, Ahmed Bahri , Bilel Ayachi, Farouk Boukhenoufa and Lakhdar Bouras.
Resources: Nabil Mezhoud, Ahmed Bahri , Bilel Ayachi, Farouk Boukhenoufa and Lakhdar Bouras.
Supervision: Nabil Mezhoud, Ahmed Bahri , Bilel Ayachi, Farouk Boukhenoufa and Lakhdar Bouras.
Approval of the final text: Nabil Mezhoud, Ahmed Bahri , Bilel Ayachi, Farouk Boukhenoufa and Lakhdar Bouras.

VII. REFERENCES

[1] Farhangi, H. (2010). The path of the smart grid, IEEE power and energy magazine, 8(1), 18–28. doi:10.1109/MPE.2009.934876.

[2] Zia, M. F., Elbouchikhi, E., Benbouzid, M., & Guerrero, J. M. (2019). Energy management system for an islanded microgrid with convex relaxation, *IEEE Transactions on Industry Applications*, 55(6), 7175-7185. doi:10.1109/TIA.2019.2917357.

[3] Wu, H., Li, H., & Gu, X. (2020). Optimal energy management for microgrids considering uncertainties in renewable energy generation and load demand, *Processes*, 8(9), 1086. doi:10.3390/pr8091086.

[4] Jiayi, H., Chuanwen, J., & Rong, X. (2008). A review on distributed energy resources and microgrid, Renewable and Sustainable Energy Reviews, 12(9), 2472–2483. doi.org/10.1016/j.rser.2007.06.004.

[5] Mohamed, F. A., & Koivo, H. N. (2012). Online management genetic algorithms of microgrid for residential application, *Energy Conversion and Management*, 64, 562–568. doi:10.1016/j.enconman.2012.06.010.

[6] Chen, C., Duan, S., Cai, T., Liu, B., & Hu, G. (2011). Smart energy management system for optimal microgrid economic operation, IET renewable power generation, 5(3), 258–267. doi:10.1049/iet-rpg.2010.0052.

[7] Radosavljevic´, J., Jevtic´, M., & Klimenta, D. (2016). Energy and operation management of a microgrid using particle swarm Optimization, Engineering Optimization, 48(5), 811–830. doi:10.1080/0305215X.2015.1057135.

[8] Lopes, J. A. P., Moreira, C. L., & Madureira, A. G. (2006). Defining control strategies for microgrids islanded operation, IEEE Transactions on power systems, 21(2), 916–924. doi: 10.1109/TPWRS.2006.873018.

[9] Hatziargyriou N. D., Anastasiadis A. G., Tsikalakis, A. G., & Vasiljevska, J. (2011). Quantification of economic, environmental and operational benefits due to significant penetration of microgrids in a typical LV and MV Greek network, European Transaction on Electrical Power, 21(2), 1217–1237. doi:10.1002/etep.392.

[10] Tsikalakis A. G., & Hatziargyriou N. D. (2007). Centralized control for optimizing microgrids operation, *IEEE Transactions on Energy Conversion*, 23(1), 241–248. doi:10.1109/TEC.2007.914686.

[11] Ustun, T. S., Ozansoy, C., & Zayegh, A. (2011). Recent developments in microgrids and example cases around the world—a review, *Renewable and Sustainable Energy Reviews*, 15(8), 4030–4041. doi:10.1016/j.rser.2011.07.033.

[12] Radosavljevic´, J., Jevtic´, M., Klimenta, D., & Arsić N. (2015). Optimal power flow for distribution networks with distributed generation, *Serbian Journal of Electrical Engineering*, 12(2), 145–170. doi:10.2298/SJEE1502145R.

[13] Saleh, A. H., & Afta, A. O. (2024). Analytical review study of the Grid connected Micro grid Energy Management system, *Fifth International Scientific Conference of Alkafeel University (ISCKU 2024)*, 97. doi.org/10.1051/bioconf/20249700066.

[14] Sanjari, M. J., & Karami H. N. (2020). Analytical approach to online optimal control strategy of energy storage devices in energy system, *Journal of Energy Storage*, 29, doi.org/10.1016/j.est.2020.101328.

[15] Tenfen, D., & Finardi, E. C. (2014). A mixed integer linear programming model for the energy management problem of microgrids, *Electric Power Systems Research*, 122, 19–28. doi:10.1016/j.epsr.2014.12.019.

[16] Anthony R. (2021). Energy management of microgrids: from a mixed-integer linear programming problem to a rule-based real-time algorithm, 7th Annual Conference of the IEEE Industrial Electronics Society, Oct 2021, Toronto, Canada. 1-6, doi:10.1109/IECON48115.2021.9589438.

[17] Sarda J. S., Lee K., Patel, H., Patel, N., Patel, Dh. (2022). Energy Management System of Microgrid using Optimization Approach, IFAC-PapersOnLine, 55(9), 280-284. doi.org/10.1016/j.ifacol.2022.07.049.

[18] Mohamed, F. A., & Koivo, H. N. (2009). System modelling and online optimal management of microgrid using mesh adaptive direct search, International Journal of Electrical Power & Energy Systems,. 32(5), 398–407. doi:10.1016/j.ijepes.2009.11.003.

[19] Kuznetsova, E., Ruiz, C., Li, Y. F., & Zio, E. (2015). Analysis of robust optimization for decentralized microgrid energy management under uncertainty, International Journal of Electrical Power and Energy Systems, 815–832. doi:10.1016/j.ijepes.2014.07.064.

[20] Arabali, A., Ghofrani, M., Amoli, M., Etezadi, F. M. S., & Baghzouz, Y. (2013). Genetic-algorithm-based optimization approach for energy management, IEEE Transactions on Power Delivery, 28(1), 162–170. doi:10.1109/TPWRD.2012.2219598.

[21] Fong, K. F., Hanby, V. I., & Chow, T. T. (2006). HVAC system optimization for energy management by evolutionary programming, Energy and Buildings, 38(3), 220-231. doi:10.1016/j.enbuild.2005.05.008.

[22] Bentouati, B., Khelifi, A., Shaheen, A. M., & El-Sehiemy, R. A. (2020). An enhanced moth-swarm algorithm for efficient energy management based multi dimensions optimal power flow problem, Journal of Ambient Intelligence and Humanized Computing, 12(1), 9499-9519. doi: 10.1007/s12652-020-02692-7.

[23] Mandal, S., & Mandal, K. (2020). Optimal energy management of microgrids under environmental constraints using chaos enhanced differential evolution, Renewable Energy Focus, 34, 129-141. doi:10.1016/j.ref.2020.05.002.

[24] Li, Y., Mohammed, S. Q., Saman, G., Aljojo, N. (2020). Energy Management of Microgrid considering Renewable Energy Sources and Electric Vehicles using Backtracking Search Optimization Algorithm, *Journal of Energy Resources Technology*, Transactions of the ASME, vil. 142(5), 1-18. doi:10.1115/1.4046098.

[25] Nikmehr, N., & Ravadanegh, S. N. (2014). Optimal operation of distributed generations in micro-grids under uncertainties in load and renewable power generation using heuristic algorithm*, IET Renewable Power Generation*, 9(8), 882–890. doi:10.1049/iet-rpg.2014.0357.

[26] Zhang, Z. Cheng, X., Xing, Z., & Wang, Z. (2024). Energy management strategy optimization for hybrid energy storage system of tram based on competitive particle swarm algorithms, *Journal of Energy Storage*, 75. doi.org/10.1016/j.est.2023.109698.

[27] Marzband, M., Azarinejadian, F., Savaghebi, M., & Guerrero, J. M. (2015). An Optimal Energy Management System for Islanded Microgrids Based on Multiperiod Artificial Bee Colony Combined With Markov Chain, IEEE Systems Journal, 11(3). doı:10.1109/JSYST.2015.2422253.

[28] Kamarposhti, M A., Colak I., & Eguchi, K. (2021). Optimal energy management of distributed generation in micro-grids using artificial bee colony algorithm*, National Center for Biotechnology Information advances science and health,* 18(6), 7402-7418. doi:10.3934/mbe.2021366.

[29] Moghaddam, A. A., Seifi, A., Niknam, T., & Pahlavan M. R. A. (2011). Multi-objective operation management of a renewable MG (micro-grid) with back-up micro-turbine/fuel cell/battery hybrid power source, Energy, 36(x), 6490–6507. doi:10.1016/j.energy.2011.09.017.

[30] Esmat, A., Magdy, A., ElKhattam, W., & ElBakly, A. M. (2013). A novel Energy Management System using Ant Colony Optimization for micro-grids, 3rd International Conference on Electric Power and Energy Conversion Systems (EPECS), doi:10.1109/EPECS.2013.6713023.

[31] Kamarposhti, M. A., Shokouhandeh, H., Lee, Y., Kang, S. K., Colak, I., & Barhoumi, E. M. (2024). Optimizing energy management in microgrids with ant colony optimization: enhancing reliability and cost efficiency for sustainable energy systems. *International Journal of Low-Carbon Technologies*, 19(2024), 2848–2856. https://doi.org/10.1093/ijlct/ctae230.

[32] Nimma, K. S., Al-Falahi, M. D. A., Nguyen, H. D., Jayasinghe, S. D. G., Mahmoud, T. S. & Negnevitsky M. (2022). Grey wolf optimization-based optimum energy-management and battery-sizing method for Grid-Connected Microgrids, *Energies*, 11(4), 847-864. doi:10.3390/en11040847.

[33] Alsmadi, Y. M., Abdel-hamed, A. M., Ellissy, A. E., El-Wakeel, A. S., Abdelaziz A. Y., Utkin, V., Uppal, A. A. (2019). Optimal configuration and energy management scheme of an isolated micro-grid using Cuckoo search optimization algorithm, *Journal of the Franklin Institute*, 356, 4191-4214. doi:10.1016/j.jfranklin.2018.12.014.

[34] Roy, K. Mandal, K. K., & Mandal, A. Ch. (2019). Ant-Lion Optimizer algorithm and recurrent neural network for energy management of micro grid connected system, *Energy*, 167, 402-416. doi.org/10.1016/j.energy.2018.10.153.

[35] Ocaña, B. H., Torruco, J. H., Bosquez, O. C., Yáñez, M. B. C., & Flores, O. A. P. (2019). Bacterial foraging-based algorithm for optimizing the power generation of an isolated microgrid, *Applied Sciences*, 9(6), 1261. doi:10.3390/app9061261.

[36] Hasan, W. A., Abed, I. A., & Shary, D. K. (2021). Energy Management Optimization of Generators using Modified Firefly Algorithm, 2nd International Multi-Disciplinary Conference: Integrated Sciences and Technologies, IMDC-IST, 7-9, Sakarya, Turkey, September 2021, doi:10.4108/eai.7-9-2021.2314839.

[37] Mezhoud, N. (2023). Multi-objective Optimal Power Flow and Emission Index Based Firefly Algorithm, Periodica Polytechnica Electrical Engineering and Computer Science, 67(2), 172-180. doi:10.3311/PPee.20922.

[38] Rafi, A. M., Ali, M., Ismail, M. Hossain, Al-Sulaiman, F. A., & Shafiullah, M. (2022). Whale Optimization Algorithm for Community Microgrid Energy Scheduling, Saudi Arabia Smart Grid (SASG), doi:10.1109/SASG57022.2022.10200591.

[39] Lodhi, E., Wang, F. Y., Xiong, Gang, Mallah, G. A., Javed, M. Y., Tamir, T. S., & Gao, D. W. (2021). Dragonfly Optimization Algorithm for Extracting Maximum Power of Grid-Interfaced PV Systems, *Sustainability, 13(*19*)*. doi.org/10.3390/su131910778.

[40] Christopher, S. J. B., & Mabel, M. C. (2020). A bio-inspired approach for probabilistic energy management of micro-grid incorporating uncertainty in statistical cost estimation, Energy, 203. doi.org/10.1016/j.energy.2020.117810.
[41] Christopher, S. J. B. (2010) Optimal energy management in a microgrid incorporating demand response using modified glowworm swarm algorithm

[42] Zhang, Y. Liu, P., & Li, Y. (2024). Implementation of an Enhanced Crayfish Optimization Algorithm. *Biomimetics*, *9*(6), 341. https://doi.org/10.3390/biomimetics9060341.

[43] Kommula, B. N., Song, H., Chen, L., & Xu, Ch. (2021). Efficient energy management of hybrid renewable energy sources-based smart-grid system using a hybrid IDEA-CFA technique, *International Transactions on Electrical Energy Systems,* 31(1), https://doi.org/10.1002/2050-7038.12833.

[44] Sun, Y., Wang, X., Gao, L., Yang, H., Zhang, K., Ji, B., & Zhang, H. (2024) Multi-Objective Optimal Scheduling for Microgrids—Improved Goose Algorithm. *Energies,* 17(24), 6376. https://doi.org/10.3390/en17246376.

[45] Peng, L., Weina, X., Zeyuan, Z., & Rui, Li. (2013). Optimized operation of microgrid based on gravitational search algorithm, *Proceedings of International Conference on Electrical Machines and System*s, Busan, Korea, 338–342, doi:10.1109/ICEMS.2013.6754475.

[46] Mezhoud, N., & Amarouayache, M. (2023). Multi-objective optimal power flow based combined non-convex economic dispatch with valve-point effects and emission using gravitation search algorithm, *Journal of Applied Research in Electrical Engineering*, 1(2), 26-36. doi:10.22055/jaree.2022.40549.1055.

[47] Mezhoud, N., Bahri, A., & Ayachi, B. (2024). Wind Driven Optimization Based Optimal Energy Management of Microgrid Impregnated With Renewable Energy Sources, Algerian Journal of Renewable Energy and Sustainable Development, 5(2), 202-218. https://asjp.cerist.dz/en/article/238715.

[48] Kamel, F. Al-Gazzar, M. M., & Mehanna, M. A. (2022). Energy management in smart inter-connected micro-grids using archimedes optimization algorithm. *Research Square*. https://doi.org/10.21203/rs.3.rs-2214046/v1.

[49] Debata, S., Samanta, C. K., & Panigrahi, S. P. (2013). Efficient energy management strategies for hybrid electric vehicles using shuffled frog-leaping algorithm, International Journal of Sustainable Engineering, 8(2), 1-7. doi:10.1080/19397038.2014.919363.

[50] Sadeghi, A. R., M. & Agha, J. (2018) Modified imperialist competitive algorithm for environmental constrained energy management of microgrids, *Journal of Cleaner Production*, 20, 273-292. doi:10.1016/j.jclepro.2018.08.129.

[51] Kaveh A., & Mahdavi, V. R. (2014). Colliding bodies optimization: A novel meta-heuristic method, Computers & Structures, 139, 18-27. doi.org/10.1016/j.compstruc.2014.04.005.

[52] Krishna, R., & Hemamalini, S. (2022). Optimal Energy Management of Virtual Power Plants with Storage Devices Using Teaching-and-Learning-Based Optimization Algorithm, International Transactions on Electrical Energy Systems, 1-17. doi:10.1155/2022/1727524.

[53] Lazar, E., Ignat, A., Petreus D., & Etz, R. (2018). Energy management for an islanded microgrid based on harmony search algorithm, 41st International Spring Seminar on Electronics Technology (ISSE), 16-20. doi:10.1109/ISSE.2018.8443673.

[54] Hussain, I, Ullah, I., Ramar, R., & Tanzila T. (2022). Smart energy management system for university campus using sine-cosine optimization algorithm, International Virtual Conference on Power Engineering Computing and Control: Developments in Electric Vehicles and Energy Sector for Sustainable Future (PECCON), 05-06, doi:10.1109/PECCON55017.2022.9851066.

[55] Toughzaoui, Y., Obeid, H., Petrone, R., Louahlia, H., & Gualous H. (2022). System Sizing and Energy Management Optimization using a Hybrid Model. 10th International Conference on Systems and Control (ICSC), 23-25/11, 2022. doi:10.1109/ICSC57768.2022.9993857.

[56] Moradi, M. H., & Abedini, M. A. (2012). Combination of genetic Algorithm and particle swarm optimization for optimal DG location and sizing in distribution systems", Electrical Power and Energy Systems, 34(1), 66–74. doi.org/10.1016/j.ijepes.2011.08.023.

[57] Kouba, N. E. Y., Sadoud, S. (2021). Optimal Energy Management of Hybrid MicroGrid Using Storage System and Fuzzy-GA Method, Journal of Renewable Energies ICREATA'21 Adrar (2021),129–141. doi:https://doi.org/10.54966/jreen.v1i1.1049.

[58] Kumar, M. J., Sampradeepraj, T., Sivajothi, E., & Singh, G. (2024). An efficient hybrid technique for energy management system with renewable energy system and energy storage system in smart grid. *Energy,* 306(15), 13245. https://doi.org/10.1016/j.energy.2024.132454

[59] Ullah Z., Qazi H. S., Alferidi A., Alsolami M., Lami B., & Hasanien H. M. (2024). Optimal energy trading in cooperative microgrids considering hybrid renewable energy systems, *Alexandria Engineering Journal, 86(1),* 23-33, https://doi.org/10.1016/j.aej.2023.11.052.

[60] Sireesha R., Coppisetty, S. R., & Kumar, M. V. (2023). Hybrid optimization to enhance power system reliability using GA, GWO, and PSO, *Paladyn, Journal of Behavioral Robotics*, 14, https://doi.org/10.1515/pjbr-2022-0119.

[61] Kamel F., Mehanna, M. A., & Al-Gazzar M. M. (2023). Energy management in smart inter-connected micro-grids using a hybrid sperm swarm optimization and gravitational search algorithm, *Journal of Al-Azhar University Engineering Sector*, 18(66), 98-115. 10.21608/auej.2023.283030.

[62] Haneef Ullah, H., Khan, M. Hussain I., Ullah, I., Uthansakul, P., & Khan, N. (2021). An Optimal Energy Management System for University Campus Using the Hybrid Firefly Lion Algorithm (FLA), *Energy*, 14(19), 6028. https://doi.org/10.3390/en14196028.

[63] Lakshmi, G. V. N., Jayalaxmi, A., & Veeramsetty, V. (2021). Optimal Placement of Distribution Generation in Radial Distribution System Using Hybrid Genetic Dragonfly Algorithm, Technology and Economics of Smart Grids and Sustainable Energy, 6(9), 1-13. doi.org/10.1007/s40866-021-00107-w.

[64] Javaid, N., Javaid, S., Abdul, W., Ahmed, I., Almogren, A., Alamriand, A., & Niaz I. A. (2017). A hybrid genetic wind driven heuristic optimization algorithm for demand side management in smart grid, Energies, 10(3), 319-346. doi:10.3390/en10030319.

[65] Tan, W. S., Hassan, M. Y., Abdul Rahman, H., Abdullah, M., Pauzi & F. Hussin, (2013). Multi-distributed generation planning using hybrid particle swarm optimization-gravitational search algorithm including voltage rise issue. *IET Generation, Transmission & Distributio*n, 7(9), 929–942. doi.org/10.1049/iet-gtd.2013.0050.

[66] Alyu, A. B., Salau, A. O., Khan, B. & Eneh, J. N. (2023). Hybrid GWO-PSO based optimal placement and sizing of multiple PV-DG units for power loss reduction and voltage profile improvement, *Scientific Reports*, 13(x). doi.org/10.1038/s41598-023-4057-3

[67] Kefayat, M., Ara, A. L., & Niaki, S. A. N. (2015). A hybrid of ant colony optimization and artificial bee colony algorithm for probabilistic optimal placement and sizing of distributed energy resources, Energy Conversion and Management, 92(1), 149–146. doi.org/10.1016/j.enconman.2014.12.037.

[68] Radosavljević, J. (2018). Metaheuristic optimization in power engineering, The Institution of Engineering and Technology, *Michael Faraday House*, Six Hills Way, Stevenage, Herts, SG1 2AY, United Kingdom, doi:10.1049/PBPO131E.

[69] Zhang, Y., Gatsis, N., & Giannakis, G. B. (2013). Robust energy management for microgrids with high-penetration renewable, IEEE Transactions on Sustainable Energy, 4(4), 944-953. doi:10.1109/TSTE.2013.2255135.

[70] Wu H., Liu, X., & Ding, M. (2014). Dynamic economic dispatch of a microgrid: Mathematical Models and Solution Algorithm, *International Journal of Electrical Power and Energy Systems*, 63, 336–346. doi:10.1016/j.ijepes.2014.06.002.

[71] Azmy, A. M., & Erlich, I. (2005). Online optimal management of PEM fuel cells using neural networks", IEEE Transactions on Power Delivery, 20(2), 1051–1058. doi:10.1109/PES.2005.1489132.

[72] Campanari, S., & Macchi, E. (2004). Technical and tariff scenarios effect on microturbine trigenerative applications", Journal of Engineering for Gas Turbines and Power, 126(3), 581–589. doi.org/10.1115/1.1762904.

[73] Barbir, F., & Gómez, T. (1997). Efficiency and economics of proton exchange membrane (PEM) fuel cells. International Journal of Hydrogen Energy, 22(10/11), 1027–1037. doi.org/10.1016/S0360-3199(96)00175-9.

[74] Villanueva, D. Pazos J. L., & Feijo, A., (2011). Probabilistic load flow including wind power generation. *IEEE Transactions on Power Systems*, 26(3), 1659–1667. doi:10.1109/TPWRS.2010.2096436.

[75] Atwa Y. M., El-Saadany, E. F., Salama, M. M. A., Seethapathy, R., Assam, M., & Conti, S. (2011). Adequacy evaluation of distribution system including wind/solar DG during different modes of operation, IEEE Transactions on Power Systems, 26(4), 1945–1952. doi:10.1109/TPWRS.2011.2112783.

[76] Tiwari, G. N., & Dubey, S. (2009). Fundamentals of photovoltaic modules and their applications, *London: RSC Energy Series Cambridge, ebook collection*, ECCC Environmental eBooks 1968-2022, 424. doi.org/10.1039/9781849730952.

[77] Mirjalili S., Mirjalili, S. M., & Lewis, A. (2014). Grey Wolf Optimizer, Advances in Engineering Software, 69, 46-61. doi.org/10.1016/j.advengsoft.2013.12.007.

[78] K. S. Kadali, et al. "Environmentally Sustainable Economic Dispatch using Grey Wolves Optimization", ARPN Journal of Engineering and Applied Sciences, vol. 13, No. 6, pp. 2068-2079, 2018.

[79] Pradhan, M., Roy, P. K., & Pal, T. (2016). Grey Wolf Optimization Applied to Economic Load Dispatch Problems, *Electrical Power and Energy Systems*, 83, 325-334. doi.org/10.1016/j.ijepes.2016.04.034.

[80] Sharma, S., Bhattacharjee, S., & Bhattacharya, A. (2015). Grey wolf optimization for optimal sizing of battery energy storage device to minimize operation cost of microgrid, IET Generation, Transmission and Distribution: Optimal Utilization of Storage Systems in Transmission and Distribution Systems, *The Institution of Engineering and Technology*, 10(3), 625-637. doi.org/10.1049/iet-gtd.2015.0429.

[81] Sultana, U., Khairuddin, A. B., Mokhtar, A. S., Zareen, N., & Sultana B. (2016). Grey wolf optimizer based placement and sizing of multiple distributed generation in the distribution system, *Energy*, 111, 525-536. doi.org/10.1016/j.energy.2016.05.128.

Journal of Engineering and Technology for Industrial Applications

ISSN ONLINE: 2447-0228

ITEGAM-JETIA

Manaus, v.11 n.54, p. 236-242. July/August., 2025.

DOI: https://doi.org/10.5935/jetia. v11i54.1768

RESEARCH ARTICLE OPEN ACCESS

DEVELOPMENT AND SET UP OF AN ARDUINO-BASED SOLAR RADIATION SENSOR USING A REFERENCE CELL

Yasmine Mekkas[1], Hani Benguesmia[2], Badis Bakri[3] and Mohammed Benguesmia[4]

[1,4]Department of Electrical Engineering, Faculty of technology, University of M'sila, University Pole, Road Bourdj Bou Arreiridj, M'sila 28000, Algeria

[2]Laboratory, Electrical Engineering (LGE),Department, Faculty of technology, University of M'sila, University Pole, Road Bourdj Bou Arreiridj, M'sila 28000, Algeria

[3]Laboratory of Materials Physics and its Applications, University of M'sila, University Pole, Road Bourdj Bou Arreiridj, M'sila 28000, Algeria

[1]http://orcid.org/0009-0002-4550-757X, [2]http://orcid.org/0000-0003-0437-1194
[3]http://orcid.org/0009-0000-2409-8135, [4]http://orcid.org/0009-0008-1230-8068

Email: mekkasyasmine@gmail.com, hani.benguesmia@univ-msila.dz, badis.bakri@univ-msila.dz, moha25022002@gmail.com

ARTICLE INFO

Article History
Received: March 25, 2025
Revised: April 20, 2025
Accepted: June 15, 2025
Published: August 31, 2025

Keywords:
Photovoltaic cell,
PV model,
Arduino Uno,
Solar radiation,
Reference cell.

ABSTRACT

Our work is pointed toward planning a device for estimating all out solar radiation in light of a reference photovoltaic cell. The rule of this device is chiefly founded qualities of a photovoltaic cell where sun oriented radiation is corresponding to the short circuit current, wich is estimated by a resistor.The voltage difference at these connections is measured by acquisition using a functional amplifier and then recorded into an analogue-to-digital converter for further processing. The Arduino Uno platform was chosen to process and display in real-time the solar radiation received from the reference cell surface. The affordable device has a wide range of uses, including monitoring solar radiation in both stand-alone and grid-connected photovoltaic power plants. The decision to utilize the Proteus design software environment has proven to be a key factor in the successful testing and validation of the device's performance. This integrated platform has enabled the efficient implementation and simulation of the hardware and software components, ultimately leading to the development of a cost-effective and reliable solar radiation estimation solution.

Copyright ©2025 by authors and Galileo Institute of Technology and Education of the Amazon (ITEGAM). This work is licensed under the Creative Commons Attribution International License (CC BY 4.0).

I. INTRODUCTION

The need to estimate solar radiation and its components is evident in a wide variety of applications, including agriculture, meteorology, engineering, and renewable energy. The use of Global Solar Radiation (GSR) estimations obtained from regression models based on satellite data has become a common practice for developing applications and supporting scientific research. This information is of vast interest in many areas of human activity, such as agriculture, hydrology, meteorology, civil engineering, architecture, and environmental studies. It is particularly crucial in the areas of solar thermal, photovoltaic, and solar conversions, where accurate radiation data is essential for the optimization and simulation of these systems.[1-5]

Renewable energy is increasingly vital due to the declining availability of fossil fuels, their pollution generation, and their contribution to global warming. Almost all environments are affected by contamination from the rise of greenhouse gases. Currently, the measurement of solar radiation using instruments is expensive and limits the number of measurement points due to the high cost of these instruments. The opportunity to have a primary radiation measurement source available for free is a significant advantage that renewable energy offers. Therefore, it is necessary to create a simple, robust, and economical device that provides sufficient information.[6-8]

Evaluating the performance of solar technology with precision before installation is crucial to streamline the integration of photovoltaic systems. Utilizing various radiation sensors on the market allows for the measurement of solar radiation in specific regions. Selecting the most suitable sensor based on factors such as quality, price, and compatibility with local conditions can present a

challenge. The photovoltaic (PV) industry commonly employs thermopile pyrano-meters and calibrated PV Reference Devices (PVRDs) as the main tools for measuring irradiance [9]. Pyrano-meters are widely respected in the scientific community for monitoring PV systems, but the high cost of acquiring a pyrano-meter is a major barrier to its widespread adoption, especially for individuals and organizations with limited financial resources. Pyrano-meter prices usually range from 1000 to 5000 dollars,, or even higher, depending on the precision and advanced features included in the device.

Research conducted by A. Azouzoute et al, [10] compared a thermopile reference pyrano-meter and a mono-crystalline reference cell to evaluate the accuracy of the latter cell in various climatic conditions. The findings indicate that, overall, the measurements of the two sensors are in good agreement, with a correlation coefficient of 99.97%. However, during periods of elevated temperatures, the relative deviation increases to -4.8%. This deviation significantly decreases to -0.7% during the cold season. Furthermore, their results suggest that reference cells offer a cautious estimate of irradiation levels, emphasizing the importance of correcting values when using this device for resource assessment.

This work aims to solve this problem of deviation at high temperatures by designing a low-cost device with high standards by connecting the reference PV cell to an Arduino microcontroller, through which we can modify the data and correct the deviation ratio to achieve accurate results of solar radiation. Additionally, the cell tension values are amplified, and the value of radiation is displayed on an LCD screen. We use the Proteus environment for implementing this device, ensuring reliable and effective performance. The presented work is structured into five sections. Section 2 provides a detailed description of the PV model. Section 3 explains the simulation of the PV model using Proteus software. Section 4 presents the results and discussion of the findings. Finally, Section 5 summarizes the conclusions drawn from the study.

II. PV MODEL DESCRIPTION

A photovoltaic (PV) panel is a device capable of converting solar energy into direct current (DC) electricity through the utilization of semiconducting materials that exhibit the photovoltaic effect [11]. The equivalent circuit of a PV panel is shown in the figure below. It consists of a current source, a diode, a series resistance, and a shunt resistance. [12]

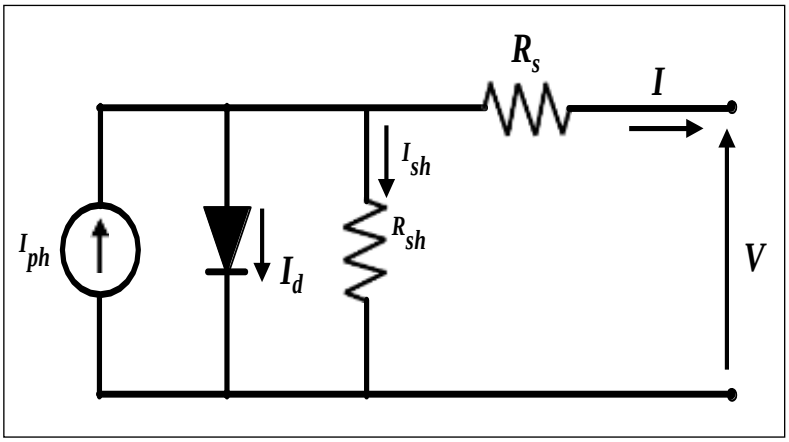

Figure 1: PV cell equivalent circuit.
Source: [11]

The PV output current is defined as:

$$I_{pv} = I_{ph} - I_d - I_{sh} \tag{1}$$

$$I_{sh} R_{sh} = I_{pv} R_s + V_{pv} \tag{2}$$

So :

$$I_{sh} = \frac{V_{pv} + I_{pv} R_s}{R_{sh}} \tag{3}$$

$$I_{pv} = I_{ph} - I_s \left(e^{\frac{V_{pv} + I_{pv} R_s}{nV_t}} - 1\right) - \frac{V_{pv} + I_{pv} R_s}{R_{sh}} \tag{4}$$

III. PROTEUS PV MODEL SIMULATION

In order to create a comprehensive model of a PV panel in Proteus software, it is essential to incorporate the one-diode model equivalent circuit. This circuit should include a striped current source to accurately depict the photocurrent source, a one-diode component with modified spice code, as well as series and parallel resistances.

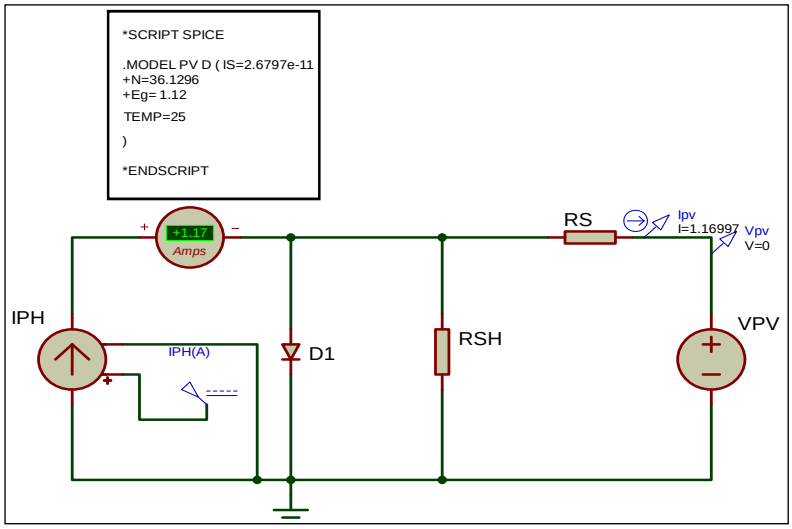

Figure 2: The circuit model of the one-diode panel in Proteus.
Source: Authors, (2025).

Figure 3 and 4shows the I–V and P-V characteristics obtained by our model atdeffrent values of irradiation and same temperature.

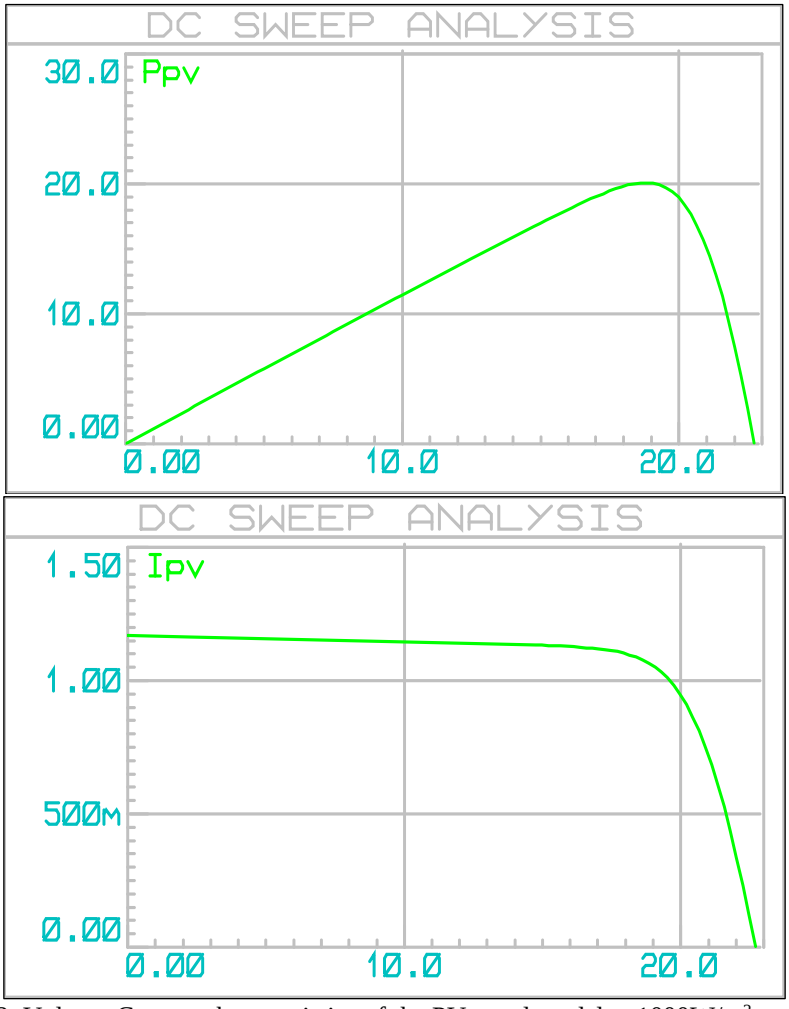

Figure 3: Voltage-Current characteristics of the PV panel model at 1000W/m^2 and 25°C.
Source: Authors, (2025).

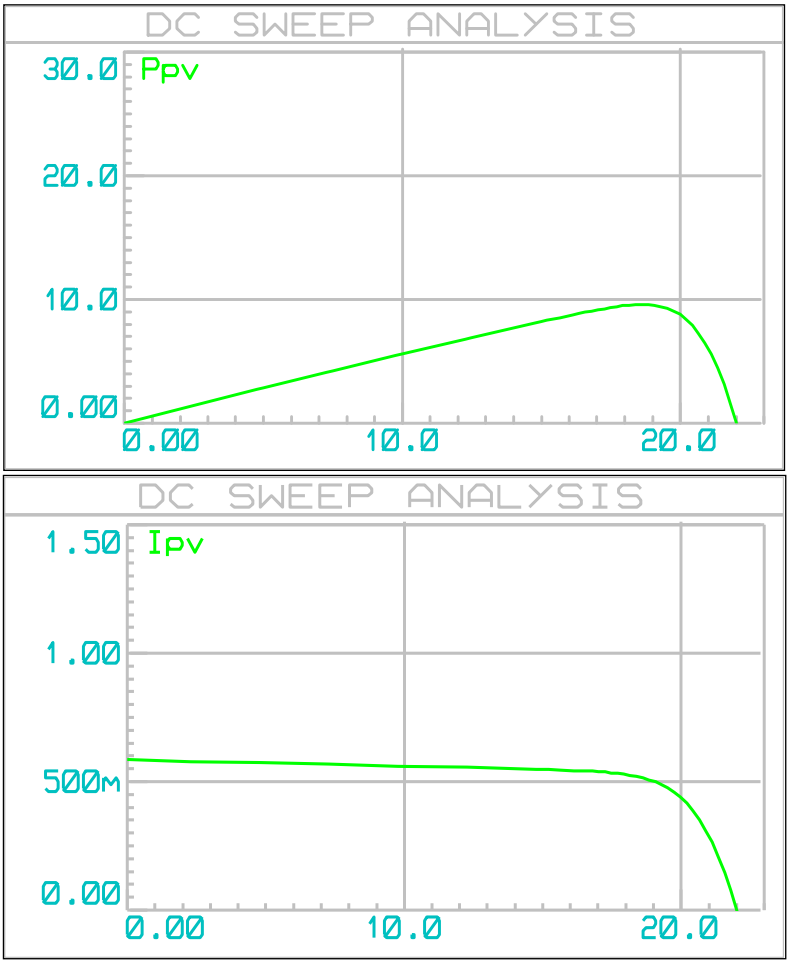

Figure 4: Voltage-Current characteristics of the PV panel model at 500W/m^2 and 25°C.
Source: Authors, (2025).

III.1 LM741 INVERTER

The LM741, also known as the Op-Amp IC 741, is a widely utilized integrated circuit for operational amplifiers. It is commonly employed for mathematical computations and signal amplification. In our experiment, we utilized this particular chip to double the minimum output voltage values produced by the inverter assembly, resulting in positive voltage levels.

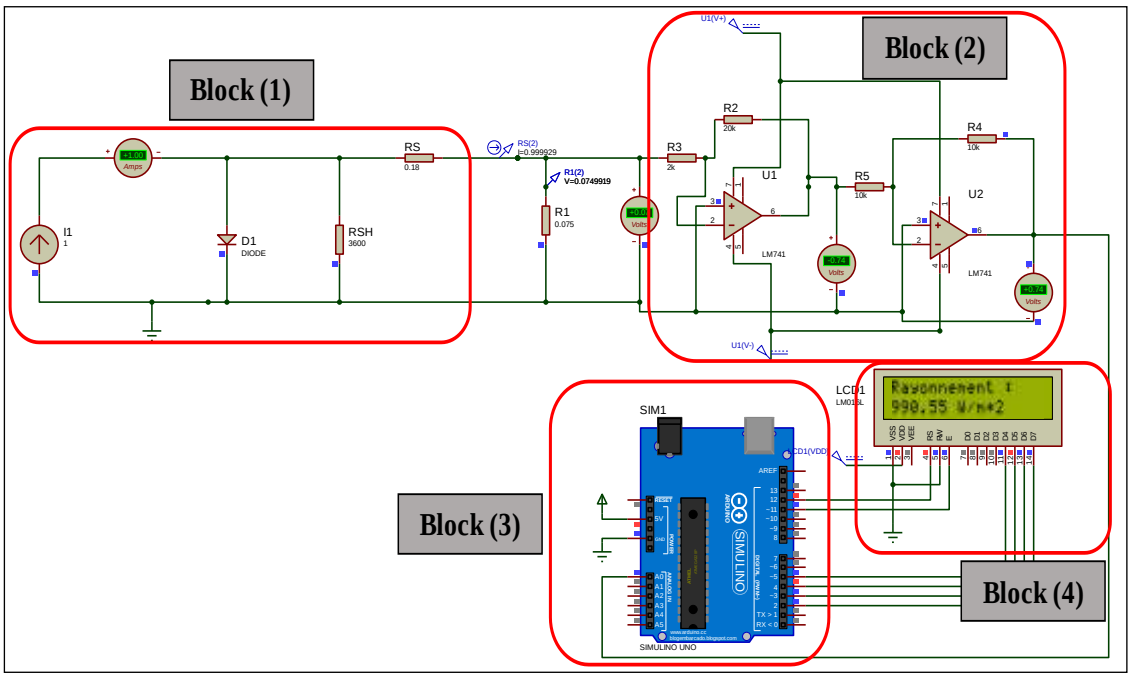

Figure 5: Circuit of the LM741 inverter.
Source: Authors, (2025).

Table 1: The values used of the resistance of the LM741 inverter in our work.

Resistance	Value
R_1	2Ω
R_2	20 Ω
R_3	10 Ω
R_4	10 Ω

Source: Authors, (2025).

III.2 DESIGNING A PV SYSTEM USING PROTEUS SOFTWARE

Figure 6 presents the PV system design created in Proteus.

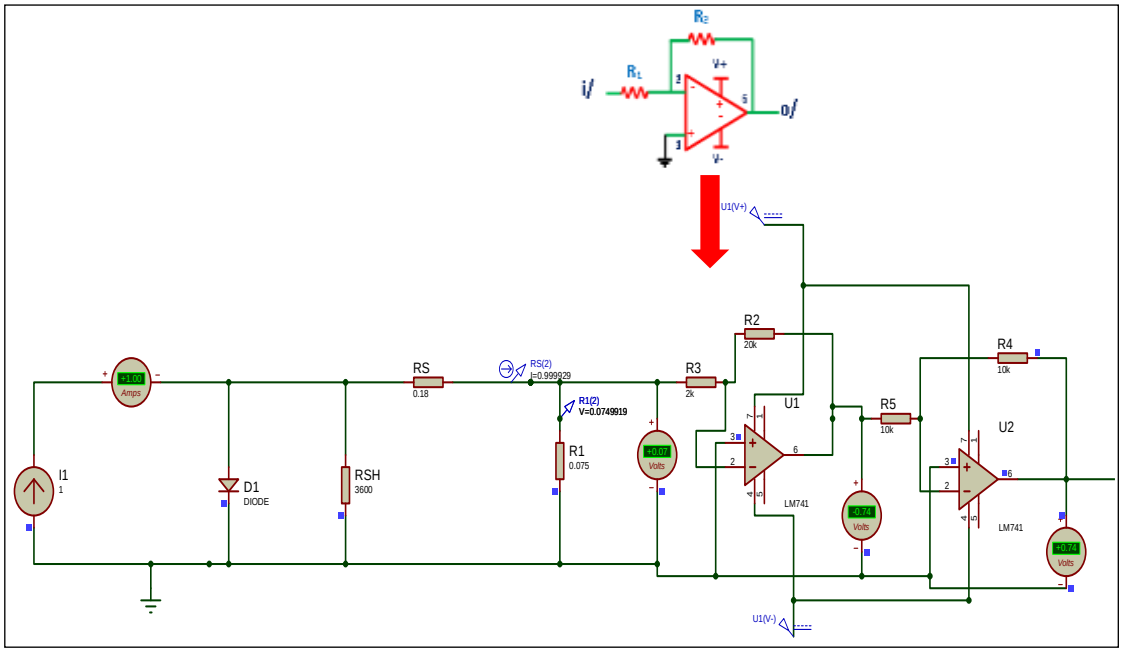

Figure 6: Schematic of device design in Proteus software.
Source: Authors, (2025).

As shown, this PV system can be divided into four blocks:

- Block (1) represents the sub-circuit of the PV panel model,
- Block (2) represents the implementation circuit of the LM741.
- Block (3) represents the embedded board (Arduino Uno). In this simulation, a specific code has been utilized. When this system is applied to the Arduino, it will calculate the short circuit current values based on the program used. This program determines the short circuit current by utilizing Ohm's law in relation to the PV voltage. The value of the luminous flux or radiation E is obtained from the equation of the current generated by the PV model when the short circuit condition is met.

$$I_{pv} = I_{ph} - I_s\left(e^{\frac{V_{pv}+I_{pv}R_s}{nV_t}} - 1\right) - \frac{V_{pv}+I_{pv}R_s}{R_{sh}} \tag{5}$$

$$I_{ph} = I_{ph0}\left(\frac{E}{E_0}\right)(1+\Delta T) \tag{6}$$

$$I_{ph} \cong I_s \tag{7}$$

$$I_{sc} = I_{sc0}\left(\frac{E}{E_0}\right)(1+\Delta T) \tag{8}$$

By eliminating the temperature effect: « In Low temperatures »

$$I_{sc} = I_{sc0}\left(\frac{E}{E_0}\right) \tag{9}$$

So the equation of the solar radiation *E* is defined:

$$E = E_0\left(\frac{I_{sc}}{I_{sc0}}\right) \tag{10}$$

- Block (4) presents the LCD screen, which is used to display the value of PV radiation.

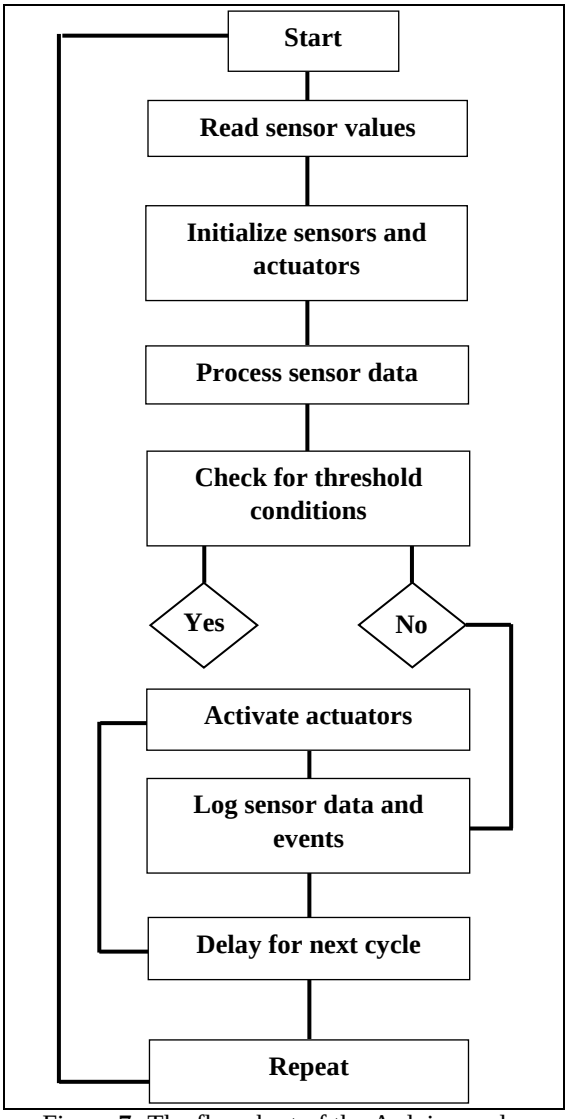

Figure **7:** The flowchart of the Arduino code.
Source: Authors, (2025).

IV. RESULT AND DISCUSSION

The simulation of our device, which is an instrument to measure solar radiation using a reference cell connected to an Arduino UNO, is presented using Proteus simulation software. In this work, we use a specific program in two cases, "low and high temperature". In the first case, the Arduino microcontroller calculates the short circuit current values based on the programmed instructions, which involve using Ohm's law with the PV voltage to determine the short circuit current. The luminous flux or radiation E value is determined from the equation representing the current produced by the PV model.

In the second case, we added a modification to the program to extract the real value of radiation while accounting for the percentage of error caused by the photovoltaic cells being affected by high temperatures. With these results, it can be argued that the device is much more cost-effective than a pyrano-meter while still providing dependable results.

V. CONCLUSION

In this paper, we propose a device developed using Proteus that can measure global solar radiation with the ability to correct the potential error ratios due to high temperatures affecting cell characteristics. The current setup consists of a reference cell, an operational amplifier, an LCD screen, and an Arduino UNO board. The device was successfully tested after its implementation in the Proteus environment. The basic concept behind this device is based on the external characteristics of the photovoltaic cell, where solar radiation is directly related to the short circuit current.

By leveraging the linear relationship between radiation and the short circuit current of the photovoltaic cell, we have successfully developed and operated a practical instrument to measure solar radiation that can mitigate the deviation caused by high temperatures. The resulting device is more cost-effective than a pyrano-meter and provides highly reliable results. From the standpoint of this study, the device can be integrated into actual systems, and its external design can be developed for application in scientific research by students and in photovoltaic installations. Additionally, it can be modified for domestic, commercial, and industrial use.

Table 3: Nomenclatures & Abbreviations.

PV	Photovoltaic
I_{pv}	Output current of PV panel (A)
I_{ph}	Photo-current (A)
I_D	PV panel diode current (A)
I_{sh}	Shunt resistance current (A)
I_s	Saturation current (A)
I_{sc}	Short circuit current (A)
V_{pv}	Output voltage of PV panel (V)
R_s	Series resistance (Ω)
R_{sh}	Shunt resistance (Ω)
E	Radiation (Ω)
	Radiation in Standard test condition (STC) ($W.m^{-2}$)
	Short Circuit Reference (A)
	Temperatureeffect (°C)
	Direct current
	Diode
	Diode constant
	Thermal voltage of PV diode
	Liquid Global Display
	Global Solar radiation
	PV Reference Devices

Source: Authors, (2025).

VII. REFERENCES

[1] D. R. Myers, “Solar radiation modeling and measurements for renewable energy applications: data and model quality,” Energy, vol. 30, pp. 1517–1531, 2005.

[2] G.L. Martins, S.L. Mantelli, R. Rüther, “Evaluating the performance of radiometers for solar over irradiance events”, Solar Energy, Vol. 231, pp.47-56, 2022.

[3] M. Al-Rasheedi , C.A. Gueymard, A. Ismail, T. Hussain, “Comparison of two sensor technologies for solar irradiance measurement in a desert environment”, Solar Energy, Vol. 161, pp. 194-206, 2018.

[4] M. Saoudi, H. Benguesmia, A. Chouder, “Efficient Deadbeat Control of Single-Phase Inverter with Observer for High Performance Applications t”, Przegląd Elektrotechniczny, Vol.07, N°44, pp.237-242, 2023.

[5] M. Saoudi, H. Benguesmia, and A. Chouder, “Processor-in-the-Loop Validation of an Observer Current-based Dead-Beat Control for a Single-Phase UPS Inverter”, Engineering, Technology & Applied Science Research (ETASR), Vol. 13, No. 1, pp. 10158–10164, 2023.

[6] S. J. Yaqoob, A.A. Obed, “Modeling, simulation and implementation of photovoltaic panel model by proteus software based on high accuracy two-diode model”, journal of techniques, Vol. 1, N°1, pp. 39-51, 2019.

[7] H. Bellia, R. Youcef, M. Fatima, “A detailed modeling of photovoltaic module using MATLAB”, NRIAG Journal of Astronomy and Geophysics, Vol. 3(1), pp.53-61, 2014.

[8] J.A. Ramos, J.J. Campayo Martín, I. Zamora Belver, J.M. Larrañaga Lesaca, “Modelling of Photovoltaic Module”, Renewable Energy and Power Quality Journal, Vol. 1(8), pp.1186-1190, 2010.

[9] L. Dunn, M. Gostein, and K. Emery, “Comparison of Pyranometers vs. Reference Cells for Evaluation of PV Array Performance,” Proceedings of the 38th IEEE Photovoltaic Specialists Conference (PVSC), Austin, TX, June 3-8, 2012.

[10] A. Azouzoute, A. Alami Merrouni, E. Bennouma, A.Gennioui, “AccuracyMeasurment of Pyranometer vs Reference cell for PV resource assessment”, Energy Procedia, Vol.157, pp.1202-1209, 2019.

[11] S. Motahhir, A. Chalh, A. El Ghzizal, S. Sebti, A.Derouich, “Modeling of Photovoltaic Panel by using Proteus”, Journal of Engineering Science and Technology Review, Vol.10(2) pp.8-13, 2017.

[12] S. Motahhir, A. El Ghzizal, A. Derouich, “Modélisation et commande d’un panneau photovoltaïque dans l’environnement PSIM”, Congrès International de Génie Industriel et Management des Systèmes, fès, Maroc. ffhal-01351493, May 2015.

Journal of Engineering and Technology for Industrial Applications

ISSN ONLINE: 2447-0228

ITEGAM-JETIA

Manaus, v.11 n.54, p. 243-252. July/August., 2025.
DOI: https://doi.org/10.5935/jetia. v11i54.1771

RESEARCH ARTICLE OPEN ACCESS

THE LOAD FLOW APPROACH FOR RADIAL NETWORK DISTRIBUTION SYSTEMS BASED ON NETWORK TOPOLOGY

Chella Hari Prasad[1], Mrs.T.Srinivasa Padmaja[2], B.Rajasekhar Reddy[3]

[1,3] Department of EEE,S.V.University,Tirupati,Andhra Pradesh,India.
[2] Departmentof ECE,Sri Padmavathi Women's University,Tirupati,Andhra Pradesh,India.

[1]https://orcid.org/0000-0003-2157-1315, [2]http://orcid.org/0000-0001-6218-910x, [3]https://orcid.org/0000-0002-1838-6445

Email: hariprasadchallaa@gmail.com, padmajats@gmail.com, rajabayyapureddy@gmail.com

ARTICLE INFO

Article History
Received: March 26, 2025
Revised: April 20, 2025
Accepted: June 15, 2025
Published: August 31, 2025

Keywords:
Load flows,
Distribution systems,
Network topology,
Radial

ABSTRACT

The distribution power flow is a significant tool for distribution system analysis. It's employed both in the operational and planning levels. The recent trend toward distribution automation has shifted the attention to load flow solutions that are both reliable and efficient. The problem of load flow in distribution systems has been modelled using a novel technique based on the particular topological traits of radial distribution networks, which has been thoroughly explored to allow for a direct solution. The use of time-consuming decomposition or Bus admittance matrix in standard load flow methods is no longer essential due to the suggested method's direct solution. By comparing the rows and columns of the branch path matrix, this novel approach derives the elements of the impedance matrix. Because it only employs one matrix in its method, the suggested load flow algorithm requires less memory for any size distribution network. As a result, it achieves faster convergence with fewer iterations and is more stable. The suggested method's effectiveness is tested on a variety of standard IEEE test systems for various load models and compared to current techniques. The proposed method's validity is demonstrated by the test results.

Copyright ©2025 by authors and Galileo Institute of Technology and Education of the Amazon (ITEGAM). This work is licensed under the Creative Commons Attribution International License (CC BY 4.0).

I. INTRODUCTION

The most fundamental technique for analysing power systems is load flow analysis. In distribution systems, studies of load flow are analyzed to determine the voltage, true& reactive power flows via the lines. The bulk power generated at the power plant is transported via high-voltage transmission lines before being delivered to customers via lower-voltage distribution systems. At distribution level, the load profile will be extremely fluctuating in nature because of different kinds of loads like industrial, commercial and domestic loads, which causes imbalance in the power flow leading to power loss. Therefore, reduction of power loss in distribution systems is an significant aspect. It is indicated in the studies that waste of distribution network losses is 13percent of total power generated. Distribution network power loss can be effectively decreased by the generation of active & reactive power in proper amounts at strategic locations.

The requirement of reactive power will be more in distribution system. To keep the voltage profile stable and meet the active power demand, reactive power is necessary. Load flow studies are needed to analyze diverse conditions in the power system for reactive power control, reconfiguration, and loss estimation, among other things. With the advent of digital computers, the
evolution methods such as the Newton Raphson method, Gauss Seidal method, Decoupled in addition to Fast Decoupled methods simplified the load flow solution, but such methods are ideal for Transmission systems. However, unlike transmission systems, distribution systems have a number of well-known features as listed below:

- Weakly meshed or radial structure
- Feeders with a high ratio of R/X
- Unbalanced load distribution
- A colossal number of nodes and branches

Due to above stated characteristics, conventional techniques are ineffective for resolving load flow issues in the distribution systems and the solutions frequently diverge because they are developed for mesh architectures. A Detailed literature review on various load flow algorithms [1-24] was studied by taking advantage of the distribution system's radial structure. In all applications that demand load flows, the reliability of the solution approaches is critical. W.G. Tinney and C.E. Hart [1] suggested an ac power flow problem that Newton's approach can handle efficiently. It converges quickly for five iterations, when compared with Guass-Seidel method which requires seven iterations for convergence. The main drawback of this technique is that the amount of memory, time needed varies in directly proportionate to the size of the problem.

B.Stott and O.Alsac [2] have proposed an algorithm for an accurate off-line & on-line load flows and contingency analysis for any size radial network can be implemented efficiently on computers with limited memory requirement. Brian Stott [3] discusses the various numerical strategies for calculating load-flow in power systems using a digital computer. Using a compensating technique with several ports and fundamental concepts of Kirchhoff's principles, Shrimoharmmadi et al[4] proposed a power flow method to solve poorly meshed transmission & distribution networks.Kersting [5] used the iterative approach to design a strategy for tackling the load flow problem for networks of radial distribution relying on ladder network theory. This method displays good convergences characteristics for radial systems. But, the disadvantage of this methods of Ladder network are it's probably best for radial networks with a high R/X ratio on one sending end.

Luo and semlyen [6] provided a method for determining the load flow solution for networks with weak meshing. M.H.Haque [7,8] provided a strategy that may be applied to radial as well as mesh networks. The mesh network may be transformed by connecting a distribution system of radial some dummy buses to break the loops. By formulating & evaluating simple algebraic equations relating the values of voltages with the variation among real power as well as reactive power as a criteria for convergence. Kothari and Das [9] formed a simple & efficient approach for solving problem of load flow in distribution networks of radial (RDN). Backward sweep approach was developed by Afsari et al. [10] to determine the load flow solution by calculating the voltages at the node's terminals at the start. S. Ghosh and D. Das [11] created an easy and capable method for addressing distribution networks of radial that only requires the assessment of a receiving end voltages that is expressed algebraically.

A. Hamouda and K. Zehar [12] proposed a new method for solving the problems of load flow in radial distribution systems with side by side that is collectively efficient, simple for applying. S. Singh and T.Ghose[13] used an unique matrix transformation technique to solve the calculation of flows of branch in distribution networks of radial directly, increasing the efficiency and speed of the forward-backward sweep-based load flow method. By comparing the most generally used two methods, Nanda et al. [14] demonstrated a novel solution for handling the load flow problem and its application under various practical scenarios i.e., Ladder network methods and forward backward sweep methods and their suitability to practical applications D.P.Sharma [15] employs a simple and flexible numbering scheme that makes full advantage of the distribution system's radial topology. The radial network is reorganised using this technology, which assigns variable numbering schemes to buses and portions.

A computerised technique of determining imbalanced fault currents or load flow on multi-grounded distribution circuits of radial has been proposed by E.S.Hawkins, W.W.Plelines, R.Berg [16]. Xiao-Ping and Zhang [17] review two novel approaches for three-phase load flow studies: sequence decoupling and compensation fast–decoupled (SDCFD), sequence decoupling and compensation Newton-Raphson (SDCNR). Hieu Le Nguyen [18] proposed a new algorithm for solving three phase (asymmetric) assessment of flow of power for transmission, distribution systems. Regarding radial distribution system's assessment of three phase load-flow, G.W. Chang etal devised an enhanced backward / forward sweep algorithm [19].

The voltage of forward bus of every transformer branch's or line voltage is calculated using KCL and KVL Laws in the backward sweep. K. Krushna Murthy etal develops a backward and forward sweep Algorithm (BFSA) [20]. This proposed algorithm employs a simple and flexible numbering system that makes full advantage of the distribution system's radial layout. The radial network is reorganised using this technology, which assigns variable numbering schemes to buses and portions.

Murthy KVSR et al. [21] and Nagaraju K et al. [22] use network topology to construct two matrices for distribution system of radial load flow solutions. The distribution systems of radial structure are characterised by their radial nature with high ratio of R/X. J. H. Teng [23] and Saidulu [24] employs multiplication of two matrices to form distribution load impedance (PLF) matrix. In RDS automation algorithms, an effective approach for forming PLF plays a crucial role in fault isolation, network reconfiguration, and service restoration.Thus, a detail literature survey on various load flow algorithms made to propose a new load flow algorithm which is robust and applicable to larger distribution systems. A topologically based strategy is used for modelling distribution system load flow's problem in this study. The use of decomposition which is time delaying or Bus admittance matrix(Y) in standard methods of load flow is not essential due to the suggested method's direct solution. Because it simply uses primitive impedance matrices in its method, this load flow technique requires less memory for any size distribution network. The suggested method is compared to current algorithms and evaluated on IEEE test systems.

II. PROPOSED LOAD ALGORITHM

Consider the formation of load flow for the suggested algorithm using the simple radial distribution network demonstrated as in figure 2.1. Multiplication of the BIBC and BCBV matrices yields the PLF impedance matrix.

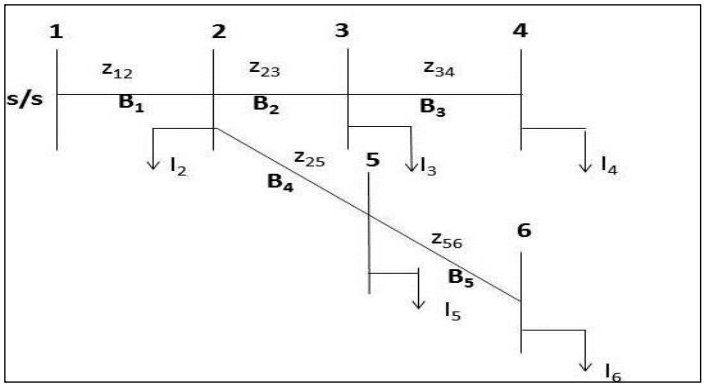

Figure 1: Simple 6 bus radial system.
Source: Authors, (2025).

II.1 STRUCTURE OF BIBC (BUS INJECTION VIA BRANCH CURRENT MATRIX):

For systems of distribution, equation 2.1 calculates the complex power at bus I while equation 2.2 calculates the equivalent current.

$$S_i = (P_i + jQ_i) \quad \text{i=1,2...n} \tag{1}$$

$$I_i = (S_i / V_i)^* \tag{2}$$

Where, S_i = complex apparent power for 'i^{th}' bus, the real power is P_i for 'i^{th}' bus, reactive power is Q_i for 'i^{th}'bus, n = total no. of nodes in the system. I_i = ith node current. V_i = voltage at i^{th} node. The current injections at corresponding node for above sample system is as shown in the Fig.2.1 i.e., I_2 , I_3 etc.

Apply KCL to the distribution system depicted in Fig.2.1, the branch currents being represented by variable C in terms of comparable current injections as

$$C_1 = I_2 + I_3 + I_4 + I_5 + I_6 \tag{3}$$

$$C_2 = I_3 + I_4 \tag{4}$$

$$C_3 = I_4 \tag{5}$$

$$C_4 = I_5 + I_6 \tag{6}$$

$$C_5 = I_6 \tag{7}$$

In matrix form it can be represented by

$$\begin{bmatrix} C_1 \\ C_2 \\ C_3 \\ C_4 \\ C_5 \end{bmatrix} = \begin{bmatrix} 1 & 1 & 1 & 1 & 1 \\ 0 & 1 & 1 & 0 & 0 \\ 0 & 0 & 1 & 0 & 0 \\ 0 & 0 & 0 & 1 & 1 \\ 0 & 0 & 0 & 0 & 1 \end{bmatrix} \begin{bmatrix} I_2 \\ I_3 \\ I_4 \\ I_5 \\ I_6 \end{bmatrix} \tag{8}$$

Rearrange the above branch current equations as shown below.

$$[C] = [BIBC][I] \tag{9}$$

II.2 STRUCTURE OF BCBV (BRANCH CURRENT VIA BUS VOLTAGE) MATRIX:

The currents in the branch & voltages of bus be related as follows:

$$V_2 = V_1 - C_1 Z_{12} \tag{10}$$

$$V_3 = V_2 - C_2 z_{23} \tag{11}$$

$$V_4 = V_3 - C_3 z_{34} \tag{12}$$

$$V_5 = V_2 - C_4 z_{25} \tag{13}$$

$$V_6 = V_5 - C_5 z_{56} \tag{14}$$

On Substitution of (9) & (10) in (11), the voltage at bus 4 is given by

$$V_3 = V_1 - C_1 z_{12} - C_2 z_{23} \tag{15}$$

$$V_5 = V_1 - C_1 z_{12} - C_4 z_{25} \tag{16}$$

$$V_6 = V_1 - C_1 z_{12} - C_4 z_{25} - C_5 z_{56} \tag{17}$$

Equations (9), (14), (15), (16), (17) can be rearranged as below

$$\begin{bmatrix} V_1 \\ V_1 \\ V_1 \\ V_1 \\ V_1 \end{bmatrix} - \begin{bmatrix} V_2 \\ V_3 \\ V_4 \\ V_5 \\ V_6 \end{bmatrix} = \begin{bmatrix} z_{12} & 0 & 0 & 0 & 0 \\ z_{12} & z_{23} & 0 & 0 & 0 \\ z_{12} & z_{23} & z_{34} & 0 & 0 \\ z_{12} & 0 & 0 & z_{25} & 0 \\ z_{12} & 0 & 0 & z_{25} & z_{56} \end{bmatrix} \begin{bmatrix} C_1 \\ C_2 \\ C_3 \\ C_4 \\ C_5 \end{bmatrix}$$

$$[\Delta v] = [BCBV][C] \tag{18}$$

Where $[\Delta v]$ = represents a matrix that gives change in bus voltage with respect to the substation voltage.

Now, substitute (2.8) in (2.18) and the subsequent equation is written as

$$[\Delta V] = [\text{PLF}][\text{I}] \tag{19}$$

Where, [PLF] denotes primitive impedance load flow matrix given as

$$[\text{PLF}] = \begin{bmatrix} Z_{12} & Z_{12} & Z_{12} & Z_{12} & Z_{12} \\ Z_{12} & Z_{12}+Z_{23} & Z_{12}+Z_{23} & Z_{12} & Z_{12} \\ Z_{12} & Z_{12}+Z_{23} & Z_{12}+Z_{23}+Z_{34} & Z_{12} & Z_{12} \\ Z_{12} & Z_{12} & Z_{12} & Z_{12}+Z_{25} & Z_{12}+Z_{25} \\ Z_{12} & Z_{12} & Z_{12} & Z_{12}+Z_{25} & Z_{12}+Z_{25}+Z_{56} \end{bmatrix} \tag{20}$$

The following important observations are derived from the given PLF matrix and used to create the suggested topological & primitive based distribution load flow approach.

1. Every element of the (n -1) × (n-1) PLF matrix is non-zero complex and symmetric.
2. The total of the impedances of primitive matrix of every lines in the path linking the bus at substation as well as every selected bus yields diagonal elements.
3. Each network bus-p might have only single path starting of the substation bus.
4. The total of the impedances of primitive matrix of such lines that look similar to the pathways of substation p and q buses gives of p-q off-diagonal elements.

These insights are effectively employed in proposing the approach using the branch path (k) matrix, which takes advantage of the network's topological structure.

The branch path matrix gives information about branches and their respective primitive impedance of the radial network. The rows of the K matrix represent branch numbering and K matrix columns represent primitive impedance of the branches in the radial distribution network. The proposed method saves a lot of time and effort by avoiding the formation of BIBC and BCBV matrices.

II.3 ELEMENTS OF PLF MATRIX FORMATION BY BRANCH PATH (K) MATRIX:

Figure: 2.1 depicts the basic 6-bus radial distribution network which is used to describe the formation of elements of PLF matrix by the Branch path matrix (K). Reduced incidence matrix can be used to create the K matrix (A).

$$\text{K=Transpose of A-1} \tag{21}$$

For the specified distribution network of radial with 6-Bus, the K-matrix is provided as

$$\begin{bmatrix} 1 & 0 & 0 & 0 & 0 \\ 1 & 1 & 0 & 0 & 0 \\ 1 & 1 & 1 & 0 & 0 \\ 1 & 0 & 0 & 1 & 0 \\ 1 & 0 & 0 & 1 & 1 \end{bmatrix} \tag{22}$$

II.4 DIAGONAL ELEMENTS FORMATION:

The K matrix is formed of 0s and 1s. The representation of node-1 in a Branch path matrix's row provides information regarding the interconnecting path among node-1 &whichever selected node. As a result, the PLF matrix diagonal elements is obtained.

For instance, the 4th row in the earlier mentioned K matrix will have 1's in both the first & fourth columns, so the fourth row's diagonal element is the sum ofZ_{12} and Z_{25} given as

$$Z_{44} = Z_{12} + Z_{25} \tag{23}$$

In this way all the diagonal elements are determined in PLF impedance matrix based on topological structure.

II.5 DIAGONAL ELEMENTS FORMATION:

When the K matrix rows are analysed, if common 1's are there in the relevant columns, the sum of that primitive impedances will give the particular elements of off diagonal for the matrix PLF.

For an instance, a PLF matrix is constructed by correlating the second & third rows, yielding the sum of Z_{12} and Z_{32} given as

$$Z_{23} = Z_{12} + Z_{23} \tag{24}$$

Due to symmetrical nature of the PLF impedance matrix, the value of Z_{32} will also carry the same value of Z_{23} .In this way all the off diagonal elements are determined in PLF impedance matrix based on topological structure.

II.6 ALGORITHM FOR DISTRIBUTION LOAD FLOW:

Step 1: Examine the data from the distributed system & set 1+j0 p.u to the bus voltages.
Step 2: Using equation 2.20., create the Branch path matrix
Step 3: By comparing 1s in the K matrix directly, sum the all primitive impedances of those lines.
Step 4: Determine the Current Injections I[i] & Power Injections at each bus. In this case, I is a variable that represents nodes.
Step 5: All of the buses $I[i]^{old} = I[i]$ should be assigned.
Step 6: Measure the elements of PLF by the equation 2.21
Step 7: set iteration value k=1. Using equation 2.22, keep updating the bus voltages on all buses
Step 8: With the revised bus voltages, compute the current injections I[i].
Step 9: Only when the maximum $[|I[i]^{k+1} - I[i]^{k}|]$ exceeds tolerance, increase the number of iteration and proceed to 7th step.
Step 10: Stop after printing the converged load flow solution.

III. CLASSIFICATION OF LOADS:

The classic model of constant power load is commonly utilised in studies of distribution systems with static load flow. Although, the actual load of a distribution system requires the utilisation of constant impedance, exponential, constant current, or a combination of all of these loads models, it cannot be modelled using constant power models alone.

III.1 CONSTANT POWER LOAD MODEL:

It's a model with a static load, meaning the power is independent of the changes in voltage magnitude, also called as constant MVA load model. Therefore, the exponent value should be 0.

$$PL = PL_0 \left(\frac{V}{V_0} \right)^0 \tag{25}$$

$$QL = QL_0 \left(\frac{V}{V_0} \right)^0 \tag{26}$$

Where, V_0 = load nominal voltage. V = load bus voltage. PL = active power @ load bus voltage. PL_0 = active power @ nominal load voltage. QL = Reactive power @ load bus voltage. QL_0 =Reactive power @ nominal load voltage.

III.2 CONSTANT CURRENT LOAD MODEL:

It's a model with a static load, meaning the power is constant. in which the level of magnitude of voltage is directly proportional to the power. Therefore, the exponent value should be 1.

$$PL = PL_0 \left(\frac{V}{V_0} \right)^1 \tag{27}$$

$$QL = QL_0 \left(\frac{V}{V_0} \right)^1 \tag{28}$$

III.3 MODEL OF CONSTANT IMPEDANCE LOAD:

It's a model with a static load, meaning the power is constant in which power is proportional of the voltage magnitude, also known as a model with constant admittance load. As a result, the exponent value should be 2.

$$PL = PL_0 \left(\frac{V}{V_0} \right)^2 \tag{29}$$

$$QL = QL_0 \left(\frac{V}{V_0} \right)^2 \tag{30}$$

III.4 MODEL OF EXPONENTIAL LOAD:

It's a model with static load in which the power is defined as an exponential voltage equation, as given below:

$$PL=PL_0\left(\frac{V}{V_0}\right)^{np} \quad (31)$$

$$QL=QL_0\left(\frac{V}{V_0}\right)^{nq} \quad (32)$$

Where load exponents are 'np' and 'nq'. By adjusting the exponents to 0, 1, 2 the load is modelled as a constant current, constant impedance, constant power model. Erstwhile exponents can be represented by the cumulative effect of various types of components of load. Table 1 illustrates the typical values for the different static loads exponents as represented by Ulas Eminoglu and M. Hakan Hocaoglu in [25]

Table 1: Common exponent values for various static loads:

S No	1.	2.	3.	4.	5.	6.	7.	8.	9.	10.	11.
Components of load	**Constant Power**	**Constant current**	**Constant impedance**	**Incandescent light**	**Fluorescent light**	**Air conditioner**	**Dryer**	**Freezer**	**Heater**	**Pumps, fans etc**	**Computer. etc.**
np	0	1	2	1.55	0.96	0.2	2.04	0.77	2	0.08	2
nq	0	1	2	0	7.38	2.3	3.27	2.5	0	1.6	5.2

Source: Authors, (2025).

IV. RESULTS AND DISCUSSIONS:

The proposed method's effectiveness is ascertained on varied standard IEEE test systems for various load models. The suggested approach is used to perform analysis of Load flow for various composite and static loads.

IV. 1 LOAD FLOW RESULTS WITH DIFFERENT COMPOSITE LOAD MODELS:

Case A: For load flow analysis, a mixed load of (a constant Z (impedance) load of 30%+ a load of constant current of 30%+ a load of constant power of 40%) is used. Table 2 displays the results of load flow various for test systems of composite (mixed) load.

Table 2: Results of Load flow for a mixed load from various test systems.

Item. No	**1**	**2**	**3**	**4**	**5**
Test system	15 bus	33bus	34 bus	69 bus	85 bus
TPL (kW)	56.74	185.85	204.36	195.16	260.26
TQL (kVAR)	52.6	125.67	60.10	89.4	163.76
Iterations	2	2	2	3	2

Source: Authors, (2025).

Case B: To conduct analysis of load flow for various test systems, an industrial load of (air conditioner load of 21% + fluorescent light of 49% + incandescent light of 30%) is considered. Table 3 shows the results of load flow for the industrial load of various test systems

Table 3: Results of Load flow for Industrial load from various test systems.

Item. No.	**1**	**2**	**3**	**4**	**5**
Test System(bus)	15	33	34	69	85
TPL (kW)	50.17	164.606	189.69	170.23	206.23
TQL (kVAR)	46.52	111.142	55.09	78.7	129.95
Iterations	4	5	4	5	6

Source: Authors, (2025).

Case C: To do analysis of load flow for various systems, a commercial load of (air conditioner of 40 %+ fluorescent light of 39 % + pumps of 8 % & fans load +incandescent light of 13 %) is considered. Table 4 displays results of the load flow of various test systems for the load of commercial.

Table 4: Load flow results of commercial load for various test systems.

S.No	***1***	***2***	***3***	***4***	***5***
System (bus)	*15*	*33*	*34*	*69*	*85*
TPL(kW)	*51.12*	*169.35*	*190.57*	*175.49*	*211.71*
TQL(kVAR)	*47.39*	*114.42*	*56.11*	*81.09*	*133.39*
Iterations	*4*	*5*	*4*	*5*	*6*

Source: Authors, (2025).

Case D: To do analysis of load flow for various test systems, a residential load of (heater load of 25 %+air conditioner load of 31 % + incandescent light of 8 % + freezer load of 13 % +dryer load of 23 %) is considered. Table 5 displays the results of load flow of residential load for various test systems.

Table 5: Results of Load flow from various test systems for residential load.

Item. No.	1	2	3	4	5
System(bus)	15	33	34	69	85
TPL (kW)	53.97	173.7337	193.63	180.92	228.77
TQL (kVAR)	49.5	117.3357	57.00	82.25	144.08
Iterations	3	5	3	4	5

Source: Authors, (2025).

IV. 2 LOAD FLOW RESULTS USING VARIOUS LOAD MODELS:

The suggested load flow technique is applied on the standard 15 bus IEEE test system. The base voltage and base MVA are considered to 11KV and 100MVA with a convergence value of 0.00001p.u.Table 6 shows load flow results of 15 bus sytem with different static loads.

Similarly, the method of load flow was tested on a variety of IEEE standard test systems like 15 bus, 33 bus, 34 bus, 69 bus, 89 bus systems for convergence of 0.0001 p.u. The real and reactive power loss are calculated and tabulated with number of iterations required for each load models.

Table 6: Results of Load Flow for 15 bus system with various static Loads.

Bus /Load type	Constant power	Constant current	Constant Impedance	Incandescent light	Fluorescent light	Air conditioner	Dryer	Freezer	Heater	Pumps, Fans etc	Computer & T.V.load
1	1	1	1	1	1	1	1	1	1	1	1
2	0.9713	0.9726	0.9737	0.9722	0.9754	0.9729	0.9744	0.9733	0.9725	0.9724	0.9753
3	0.9567	0.9587	0.9605	0.9581	0.963	0.9591	0.9615	0.9599	0.9585	0.9584	0.9629
4	0.9509	0.9532	0.9553	0.9526	0.9582	0.9537	0.9565	0.9545	0.953	0.9529	0.958
5	0.9499	0.9523	0.9544	0.9516	0.9573	0.9528	0.9556	0.9536	0.9521	0.9519	0.9571
6	0.9582	0.9601	0.9617	0.9596	0.9639	0.9604	0.9627	0.9611	0.96	0.9597	0.9638
7	0.956	0.958	0.9597	0.9575	0.962	0.9583	0.9607	0.959	0.9579	0.9576	0.9619
8	0.957	0.9589	0.9606	0.9584	0.963	0.9592	0.9615	0.9599	0.9588	0.9585	0.9627
9	0.968	0.9694	0.9706	0.969	0.9728	0.9697	0.9713	0.9702	0.9693	0.9691	0.9723
10	0.9669	0.9684	0.9696	0.968	0.9714	0.9686	0.9704	0.9691	0.9682	0.9681	0.9713
11	0.95	0.9524	0.9544	0.9517	0.9572	0.9528	0.9556	0.9536	0.9522	0.9519	0.9571
12	0..9458	0.9485	0.9507	0.9478	0.9537	0.9489	0.952	0.9498	0.9483	0.948	0.9536
13	0.9445	0.9472	0.9496	0.9465	0.9529	0.9477	0.9509	0.9486	0.9471	0.9467	0.9525
14	0.9486	0.9511	0.9532	0.9504	0.9562	0.9516	0.9544	0.9524	0.9508	0.9507	0.956
15	0.9484	0.9509	0.9531	0.9502	0.956	0.9514	0.9543	0.9523	0.9507	0.9505	0.9559
TPL(kW)	61.794	56.1418	51.4517	57.2218	43.9899	55.0338	48.8414	53.1745	56.0307	57.0845	45.5511
TQL(kVAR)	57.2975	52.0498	47.6962	53.0566	40.7621	51.0161	45.2712	49.2914	51.9519	52.9209	42.215
Iterations	3	1	3	3	5	3	4	3	3	3	4

Source: Authors, (2025).

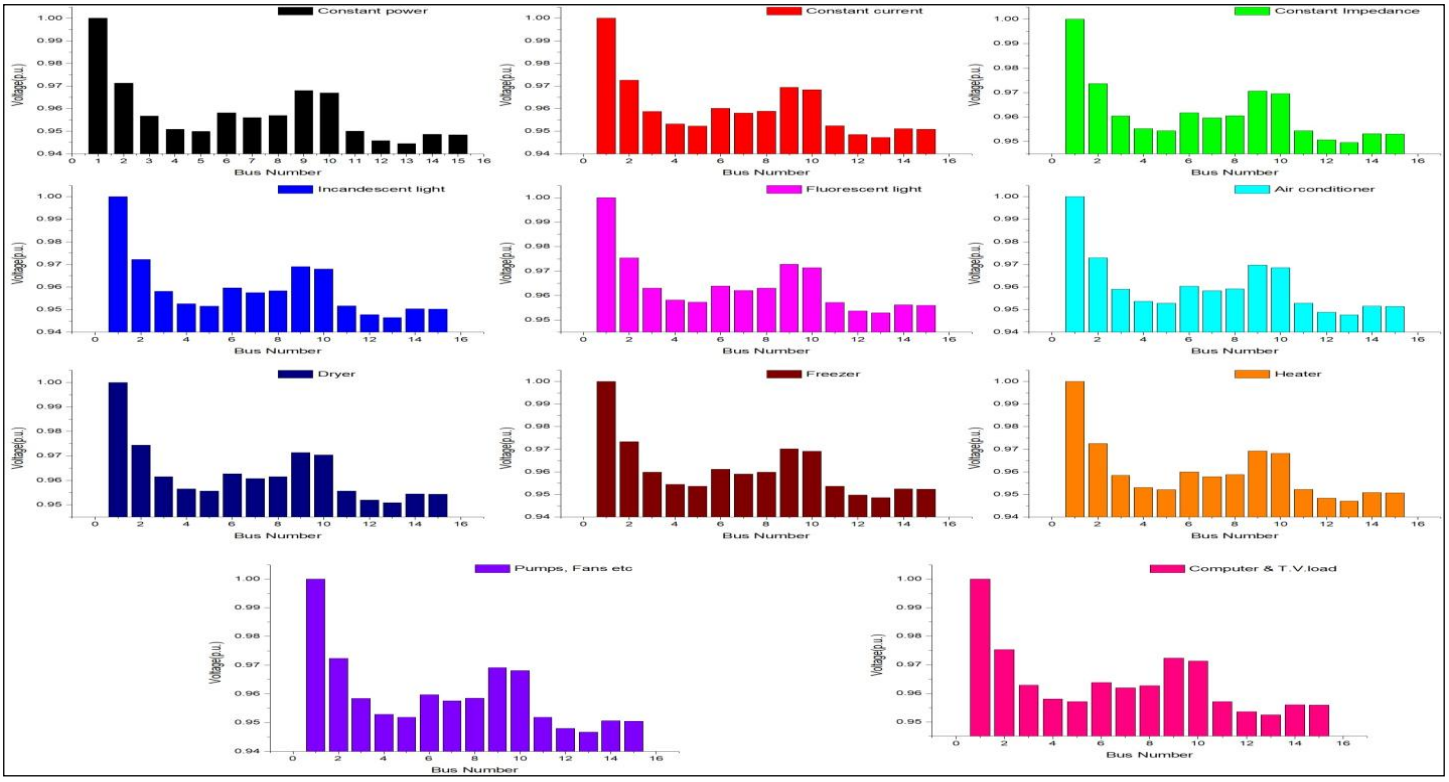

Figure 1: Voltage profile of different loads.

Source: Authors, (2025).

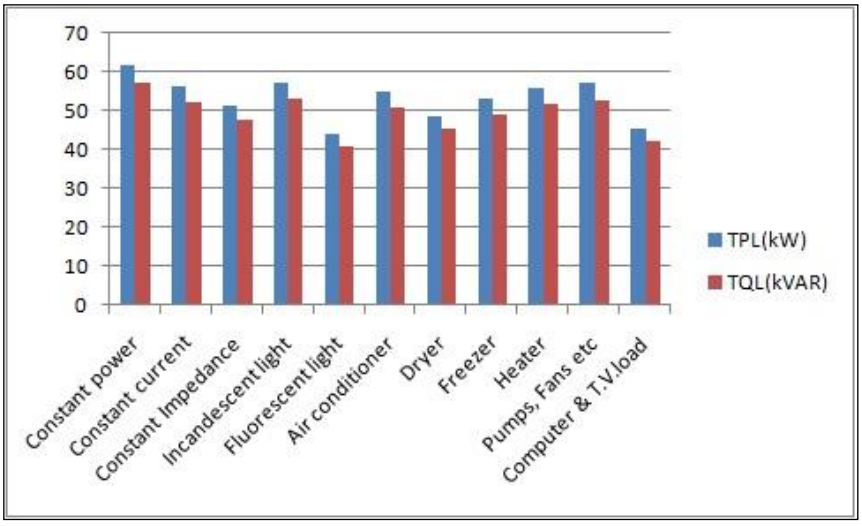

Figure 2: Results of Load flow for a 15-bus system with various static loads.
Source: Authors, (2025).

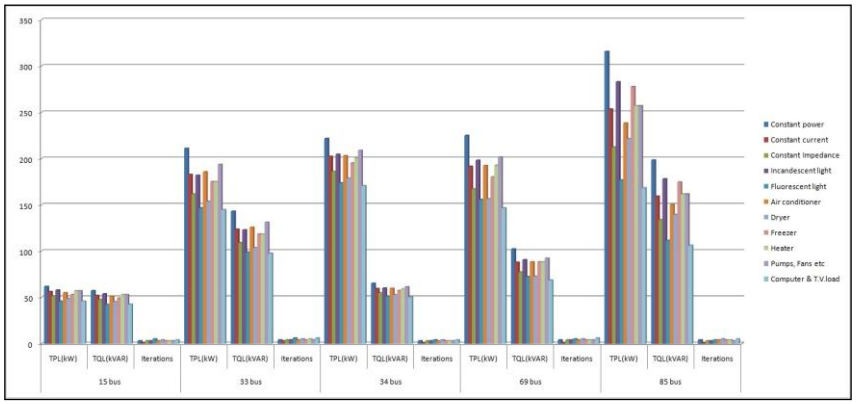

Figure 3: Power loss results of 15, 33,34,69,85 bus test systems with different static loads.
Source: Authors, (2025).

Table 7: Comparsion table.

Test system	Type of load	No of iterations For tolerance of 0.00001 p.u.	
		Methods in[9,26,27,28]	**Proposed algorithm**
15 bus[26]	Constant power	4	**3**
	Constant current	3	**1**
	Constant impedance	4	**3**
	Composite	-	**2**
33 bus[27]	Constant power	6	**4**
	Constant current	-	**3**
	Constant impedance	-	**4**
	Composite	-	**2**
34 bus[9]	Constant power	7	**3**
	Constant current	5	**1**
	Constant impedance	7	**3**
	Composite	6	**2**
69 bus[27]	Constant power	6	**4**
	Constant current	-	**2**
	Constant impedance	-	**4**
	Composite	-	**3**
85 bus[28]	Constant power	4	**4**
	Constant current	3	**1**
	Constant impedance	4	**3**
	Composite	3	**2**

Source: Authors, (2025).

V.CONCLUSIONS:

The conclusions derived are

- Based on the topological nature of radial distribution systems, the PLF impedance matrix was formed without the need of matrices BIBC, BCBV.
- The radial distribution systems topological structure was realized by using branch path (K) matrix which makes proposed algorithm so robust in nature.
- Due to this it can be applicable to larger distribution systems also for distribution automation.
- The proposed algorithm significantly reduces computational burden by avoiding the BIBC, BCBV matrices for the formation of the PLF impedance matrix.
- Since, the PLF impedance matrix is constructed based on the radial distribution systems topological structure, the need of complex algebraic expressions for the analysis of load flow can be avoided.
- The proposed algorithm has faster convergence, error free compilation and also requires less memory.

Finally, the proposed load flow is tested for different load models of distribution systems and further load growth on different IEEE test systems is also being analysed

VI. ACKNOWLEDGMENTS

Dr.C.Hari Prasad carried out literature survey and participated in load flow study.Mrs.T.Srinivasa Padmaja,Dr.B.Rajasekhar Reddy participated in assessment study and performed the analysis. All three participated in sequence alignment and drafted the manuscript and approved the final manuscript. Owing to to 1's comparisons directly in the Branch's path of matrix, the suggested algorithm requires fewer iterations, resulting in faster convergence. The proposed algorithm achieves convergence in fewer iterations for different load models when compared with branch current load flow algorithm as shown in Table 8.

VII. AUTHOR'S CONTRIBUTION

Conceptualization: Dr.Chella Hari Prasad, Mrs.T.Srinivasa Padmaja and Dr.B.Rajasekhar Reddy.
Methodology: Dr.Chella Hari Prasad, Mrs.T.Srinivasa Padmaja and Dr.B.Rajasekhar Reddy.
Investigation: Dr.Chella Hari Prasad, Mrs.T.Srinivasa Padmaja and Dr.B.Rajasekhar Reddy.
Discussion of results: Dr.Chella Hari Prasad, Mrs.T.Srinivasa Padmaja and Dr.B.Rajasekhar Reddy.
Writing – Original Draft: Dr.Chella Hari Prasad, Mrs.T.Srinivasa Padmaja and Dr.B.Rajasekhar Reddy.
Writing – Review and Editing: Dr.Chella Hari Prasad, Mrs.T.Srinivasa Padmaja and Dr.B.Rajasekhar Reddy.
Resources: Dr.Chella Hari Prasad, Mrs.T.Srinivasa Padmaja and Dr.B.Rajasekhar Reddy.
Supervision: Dr.Chella Hari Prasad, Mrs.T.Srinivasa Padmaja and Dr.B.Rajasekhar Reddy.
Approval of the final text: Dr.Chella Hari Prasad, Mrs.T.Srinivasa Padmaja and Dr.B.Rajasekhar Reddy.

VII.REFERENCES

[1]Tinney W. G., and Hart, C. E., "Power flow solutions by Newton's method," IEEE Trans. Power Apparatus Syst., Vol. 86, pp. 1449–1457, 1967. doi: 10.12691/ajeee-6-1-3.

[2]Stott B. and Alsac. O., "Fast decoupled load flow," IEEE Trans. Power Apparatus Syst., Vol. 93, No. 3, pp. 859–869, 1974.doi: https://doi.org/10.1109/TPAS.1974.293985

[3]Brian Stott, "Review of Load-Flow Calculation Methods", Proceedings of the IEEE, Vol.62, No.7, pp.916-929, 1974.

[4]Shirmohammadi. D, Hong .HW, Semlyen. A, Luo GX. "A compensation-based power flow method for weakly meshed distribution and transmission networks". IEEE Transactions on Power Systems; vol.3, pp.753–762, 1974. https://doi.org/10.1109/59.192932

[5].W. H. Kersting, "Distribution feeder line models," IEEE Trans.Industry Applications, vol. 31, no.4, pp.715-720, Aug. 1995.doi: 10.4316/AECE.2017.04012

[6]G. X. Luo and A. Semlyen, "Efficient load flow for large weakly meshed networks," IEEE Trans. Power Systems, vol. 5, no. 4, pp. 1309-1316, Nov. 1990. doi: 10.1109/59.99382

[7]Haque M. H., "Load flow-solution of distribution systems with voltage dependent load models," Elec. Power System. Res., Vol. 36, pp. 151–156, 1996. https://doi.org/10.1016/0378-7796(95)01025-4

[8]Haque M.H. "Efficient load flow method for distribution systems with radial or mesh configuration", IEEE Proc., Gener.transm.Distrib. Vol: 1, pp.33-38, 1996. https://doi.org/10.3923/jas.2006.2741.2748

[9]Das. D., Kothari, D. P., and Kalam, A., "Simple and efficient method for load flow solution of radial distribution networks",Elec. Power Energy Syst., Vol. 17, No. 5, pp. 335–346, 1995. https://doi.org/10.1016/0142-0615(95)00050-0

[10]A. Afsari, S.P. Singh, G.S. Raju, G.K.Rao , " A fast power flow solution of radial distribution networks," International Journal Electric Components and Systems, vol. 30, pp.1065 -1074,2002. http://dx.doi.org/10.1080/15325000290085361

[11]S. Ghosh, D. Das, "Method for load-flow solution of radial distribution networks," IEE Proc – Gener Transm Distr., vol. 146, no. 6, pp. 641– 48,1999. https://doi.org/10.1049/ip-gtd:19990464

[12]A. Hamouda, and K. Zehar, "Improved algorithm for radial distribution networks load flow solution," Elect. Power and Energy Systems, vol. 33, pp. 508–514, 2011. https://doi.org/10.1016/J.IJEPES.2010.11.004

[13]S. Singh, and T.Ghose, “Improved radial load flow method,” Elect. Power and Energy Systems, vol. 44, pp. 721–727, 2013. https://doi.org/10.1016/j.ijepes.2012.08.005

[14]J. Nanda, M.S. Srinivas, M. Sharma, S.S. Dey, L.L. Lai, “New findings on Radial Distribution system load flow algorithms”, Proc. IEEE conference,Vol:3 , pp. 1157-1161,2000. https://doi.org/10.7227/IJEEE.44.1.6

[15]D. P. Sharma, A. Chaturvedi, G.Purohit, R.Shivarudraswamy “Distributed Load Flow Analysis using Graph Theory” Internation al Journal of Electrical, Computer, Energetic, Electronic and Communication Engineering Vol:5, No:2, 2011.

[16]Berg R., Hawkins, E.S., and Plelines, W.W.Mechanized, “Calculation of Unbalanced Load Flow on Radial Distribution Circuit s”, IEEE Trans. on Power Apparatus and Systems,Vol.4, pp.415-421,1967.

[17]Xiao-Ping Zhang: ‘Fast Three Phase Load Flow Methods’, IEEE Trans. on Power Systems,Vol .3,pp.1547-1554,1996. https://doi.org/10.1109/59.535696

[18]Hieu Le Nguyen: ‘Newton-Raphson Method in Complex Form’, IEEE Trans. Power Sysems., Vol.3, pp.1355-1359, 1997. https://doi.org/10.1109/59.630481

[19]Chang,G.W., Chu,S.Y.,Wang,h.l. “An Improved Backward/Forward Sweep Load Flow Algorithm for Radial Distribution Systems”, IEEE Trans. on Power systems,Vol.2,pp.882-884,2007. https://doi.org/10.1007/s13369-016-2296-y

[20]K.Krushna Murthy, Dr. S.V. Jaya Ram Kumar “Three-Phase Unbalanced Radial Distribution Load Flow Method” International Refereed Journal of Engineering and Science (IRJES) ISSN (Online) 2319-183X, (Print) 2319-1821 Volume 1, Issue 1, PP.039-042,September 2012. https://www.irjes.com/Papers/vol1-issue1/F11039042.pdf

[21]K. V. S. R. Murthy, M. R. Raju, G. G. Rao, and K. N. Rao, “Topology based approach for Efficient Load flow Solution of Ra dial Distribution Networks,” 16th National Power Systems ConferenceVol.2, pp. 176-19, Dec. 2010. https://www.iitk.ac.in/npsc/Papers/NPSC2010/7054.pdf

[22]K. Nagaraju, S. Sivanagaraju, T. Raman, and P. V. Prasad, “A novel load flow method for radial distribution system for re alistic loads,” Elect Power Comp. and Syst., vol. 39, no. 2, pp.128-141, 2011. https://www.ijraset.com/fileserve.php?FID=5957

[23]J. H. Teng, "A direct approach for distribution system load flow solutions," IEEE Trans. Power Delivery, vol. 18, no. 3, pp. 882-887, Jul. 2003. http://dx.doi.org/10.1109/TPWRD.2003.813818

[24]K.Prakash and M.Sydulu, “An effective topological and primitive impedance based distribution load flow method for radial distribution systems”, IRANIAN JOURNAL OF ELECTRICAL AND COMPUTER ENGINEERING, vol. 10, no. 1, winter-spring 2011. https://www.sid.ir/FileServer/JE/89020110102.pdf

[25]Ulas Eminoglu and M. Hakan Hocaoglu “A new power flow method for radial distribution systems including voltage dependent load models”, Electric Power Systems Research, Vol.7, pp.no:106-114, 2005. DOI: 10.1016/j.epsr.2005.05.008

[26]Murty, V. V. S. N., Teja, B. R., & Kumar, “A contribution to load flow in radial distribution system and comparison of di fferent load flow methods”, International Conference on Power Signals Control and Computations (EPSCICON), (2014). doi:10.1109/epscicon.2014.6887494

[27]Thomas, M. S., Rakesh Ranjan and Nitin Malik. “Deterministic load flow algorithm for balanced radial AC distribution syst ems.” 2012 IEEE Fifth Power India Conference (2012): 1-6. http://dx.doi.org/10.1109/PowerI.2012.6479581

[28]Abul'Wafa, Ahmed R. “A network-topology-based load flow for radial distribution networks with composite and exponential load.” Electric Power Systems Research 91 (2012): 37-43. https://doi.org/10.1016/j.epsr.2012.04.016

Journal of Engineering and Technology for Industrial Applications

ISSN ONLINE: 2447-0228

ITEGAM-JETIA

Manaus, v.11 n.54, p. 253-259. July/August., 2025.

DOI: https://doi.org/10.5935/jetia. v11i54.1821

RESEARCH ARTICLE OPEN ACCESS

ADVANCEMENTS AND CHALLENGES IN NAMED ENTITY RECOGNITION: A REVIEW OF TECHNIQUES AND DOMAIN SPECIFIC APPLICATIONS.

Vedanti Shedage[1], Devyani Pawar[2], Roshani Shinde[3], Apurva Mane[4], Pradip Ghorpade[5]

[1, 2, 3, 4, 5] Vidya Pratishthan's Kamalnayan Bajaj Institute of Engineering and Technology, Baramati, India.

[1]https://orcid.org/0009-0002-0048-2524, [2]https://orcid.org/0009-0007-9086-5014, [3]https://orcid.org/0009-0006-4947-5228, [4]http://orcid.org/0009-0005-1936-0203, [5]https://orcid.org/0009-0006-0095-2265

Email: vedantishedge13@gmail.com, pawardevyani707@gmail.com, shinderoshani9803@gmail.com, apurvarandive26@gmail.com, pradip08india@gmail.com

ARTICLE INFO

Article History
Received: April 7, 2025
Revised: April 20, 2025
Accepted: June 15, 2025
Published: August 31, 2025

Keywords:
Named Entity Recognition,
Natural Language Processing,
Deep Learning Models,
Domain- Specific Applica tions,
Transformer-Based Architectures.

ABSTRACT

Named Entity Recognition (NER) is a crucial task in Natural Language Processing (NLP), responsible for identifying and categorizing entities such as persons, organizations and locations from unstructured text. While traditional rule-based and statistical models like Conditional Random Fields (CRF) offered high precision in constrained settings their scalability and cross-domain adaptability remain limited. Recent breakthroughs in deep learning, particularly transformer-based architectures like BERT, RoBERTa and GPT, have revolutionized Named Entity Recognition (NER) by offering superior contextual un derstanding and cross-domain adaptability. This review critically analyzes state-of-the-art NER methodologies, evaluating their effectiveness across key sectors such as healthcare, finance, legal analysis and cybersecurity while identifying challenges and future research directions. It highlights key challenges such as entity ambiguity, domain adaptation and resource efficiency while also identifying emerging solutions like few-shot and zero shot learning. Additionally, the paper presents a comparative analysis of model performance, offering valuable insights into the trade-offs between accuracy, computational efficiency and domain adaptability. By consolidating recent research, this study outlines future directions for developing more robust, scalable and interpretable NER systems. It aims to guide researchers and practitioners in building domain-specific NER applications and advancing the field toward greater generalization and practical utility.

Copyright ©2025 by authors and Galileo Institute of Technology and Education of the Amazon (ITEGAM). This work is licensed under the Creative Commons Attribution International License (CC BY 4.0).

I. INTRODUCTION

Named Entity Recognition (NER) is a fundamental task in Natural Language Processing (NLP) that involves identifying and categorizing predefined entities such as persons, organiza tions, locations, dates and numerical values from unstructured text [1]. Over the years, NER has undergone significant advancements, transitioning from traditional rule-based and Roshani Shinde Artificial Intelligence and Data Science VPKBIET shinderoshani9803@gmail.com statistical approaches to sophisticated machine learning and deep learning-based methods. Early systems relied heavily on handcrafted rules and feature engineering, offering satis factory results in constrained domains but facing challenges in scaling to diverse datasets [2].

Early machine learning models, including Conditional Random Fields (CRF) and Hidden Markov Models (HMM), enhanced entity recognition through probabilistic modeling, yet struggled with context comprehension and domain adaptation.However, these models lacked the capability to capture intricate linguistic patterns and context dependencies [3]. The advent of deep learning further revolutionized the field, with architectures such as Bidirec tional Long Short-Term Memory (BiLSTM) and Convolutional Neural Networks (CNNs) demonstrating substantial improve ments in entity recognition performance. Transformer-based models such as BERT, RoBERTa and GPT have established new benchmarks by effectively capturing contextual relation ships through self-attention mechanisms, achieving state-of the-art accuracy in NER across diverse domains. [4]. NER f inds applications in numerous fields, ranging

from healthcare and finance to cybersecurity and legal analysis. In healthcare, it facilitates the extraction of clinical entities from medical records, aiding in automated diagnosis and drug discovery. In financial and legal sectors, NER supports contract analysis, fraud detection and regulatory compliance by identifying rele vant entities from large volumes of text. Similarly, cybersecurity systems employ NER for threat intelligence, recognizing malicious entities and abnormal activities from security logs [5].

Despite the advancements, challenges persist. Domain adaptation, entity ambiguity and privacy concerns remain significant obstacles. NER models often struggle with nested entities, overlapping entity boundaries, and out-of-domain generalization. Recent research has pro posed solutions like few-shot and zero-shot learning to address data scarcity and enhance adaptability. Additionally, multi modal approaches that integrate text with visual and structured data are gaining attention for their potential in improving entity recognition in complex scenarios [6]. This paper aims to provide a comprehensive review of NER methodologies, focusing on their evolution, domain-specific applications and key challenges. By analyzing state-of-the-art techniques, it evaluates the trade-offs between accuracy, computational ef f iciency and adaptability. Furthermore, the study identifies emerging trends and proposes future research directions to foster the development of more robust and scalable NER systems.

II. LITERATURE REVIEW

A. Enhancements in Core Named Entity Recognition (NER) Models

1) Recent Advancements in BiLSTM, CRF, and Transformer-Based Models: Recent advancements in BiL STM, Conditional Random Fields (CRF) and Transformer based Named Entity Recognition (NER) models have signifi cantly improved feature extraction, generalization and compu tational efficiency. Wang et al. introduced a Residual BiLSTM Model to enhance BiLSTM-CRF architectures by incorporating resid ual connections, achieving F1-scores of 92.22% on CoNLL 2003, 92.17% on MSRA, and 89.65% on OntoNotes 5.0. However, its performance deteriorated on smaller datasets due to overfitting [7]. Similarly, Zhang and Chen proposed a Bidirectional Iterative Algorithm for Nested NER, which improved hierarchical entity recognition but was hindered by high computational costs [8]. Liu et al. developed a Fusion of Word and Category Vectors Model that leveraged BERT and BiLSTM, leading to a 5.05% increase in F1-score on the Weibo dataset. Despite this, label ing inconsistencies and domain-specific biases restricted its generalization [9]. In contrast, Kim et al. trained an Adaptive Distant Supervision NER Model using Wikipedia and CNN news, obtaining F1-scores of 91.12% on CoNLL, 70.26% on Wikipedia, and 81.48% on CNN News. However, the presence of noisy labels limited its adaptability across various linguistic domains [10]. Jiang et al. applied a Neural NER Model for Biomed ical Text Mining by integrating BioBERT with a multi type normalization module, outperforming previous models in handling overlapping biomedical entities. Nevertheless, it required high-quality datasets, which remain scarce in certain specialized biomedical categories [11].

2) **Transformer-Based Innovations in NER:** Transformer based models have demonstrated superior contextual entity recognition, surpassing BiLSTM-CRF architectures. Zhao et al. implemented Transformer-based NER for Drone Flight Logs, achieving an F1-score of 91.34%, surpassing re current neural network (RNN)-based models. However, dataset limitations restricted its generalization [12]. Similarly, Gupta et al. developed an ALBERT-enhanced NER Model for Agri cultural Texts, attaining an F1-score of 95.56%. Although ALBERT optimizes performance for long sequences, its high computational cost limits scalability [13]. Gao et al. introduced a Tri-Training Algorithm for Equip ment Support NER, combining BiLSTM-CRF with semi supervised learning to achieve a 93.88% F1-score. However, selecting high-confidence annotations remained a challenge [14]. Zheng et al. proposed SciNER, a Transformer-based model specialized for scientific texts, achieving 91% accuracy in extracting named entities from research papers. Neverthe less, its performance was hindered by rare entity types with insufficient training data [15].

B. Domain-Specific Applications of NER

1) Medical and Healthcare NER: The integration of Transformer-based models has enhanced clinical, pharmaceu tical, and biological entity recognition. Lee et al. introduced BERN, a BioBERT-based biomedi cal NER tool that improved the recognition of overlapping biomedical entities [16]. Amazon Research developed Com prehend Medical, a HIPAA-compliant clinical NER system; however, privacy regulations limited its scalability [17]. Martins et al. applied BERT-BiLSTM to oncology medical records, achieving 78.24% accuracy on a Portuguese dataset, though challenges persisted in processing medical abbrevi ations [18]. Wang et al. developed an Instance Transfer Based NER Model to enhance performance in new medical domains with limited labeled data, increasing the F1-score from 80.52% to 93.28%. However, its effectiveness depended on the similarity between the source and target domains [18].

2) Legal and Financial NER: Legal and financial texts require high domain adaptability due to specialized vocabulary and complex linguistic structures. Johnson et al. proposed a Few-Shot Learning approach for Legal NER, improving entity recognition in legal contracts and case law, though its generalization across jurisdictions remained limited [19]. Nguyen and Patel developed a Privacy Preserving NER Model that replaced named entities with gen eralized categories (e.g., “organization” instead of “Google”), enhancing privacy but reducing classification accuracy in fi nancial contexts [20]. Zhu et al. introduced an Ontology-Based NER Model for Legal Texts, integrating legal knowledge graphs with Transformer embeddings, significantly improving legal entity classification accuracy. However, its performance depended on pre-existing ontologies, reducing adaptability to evolving legal terminology [21].

3) Cybersecurity and Forensic NER: NER models for cybersecurity must address evolving threats, technical jargon, and unstructured logs. Singh et al. developed RDF-CRF for Cybersecurity NER, achieving F1-scores of 0.74, 0.78, and 0.81. However, reliance on manually curated dictionaries limited its scalability [22]. Rodriguez et al. applied NER to Drone Flight Logs, obtain ing an F1-score of 91.34%, but real-world applicability was constrained due to data scarcity [23]. Ali et al. introduced a Multi-Modal Cybersecurity NER Model integrating rule-based heuristics with deep learning, improving malicious entity detection in network logs. How ever, its reliance on predefined rule sets reduced adaptability to emerging cybersecurity threats [24].

4) Scientific and Academic NER: Scientific NER requires robust domain adaptability due to variations in terminologies across disciplines. Wang et al. introduced SciNER, a Transformer-based model for extracting entities from research papers, achieving 91% accuracy [25]. Similarly, Kumar and Zhang evaluated NER for Scientific Acknowledgments, finding that Flair embeddings achieved an F1-score of 79%, though semantic overlaps in institutional names reduced classification accuracy [26]. Chen et al. developed an Automatic Entity Extraction Model for Scientific Documents, leveraging self-supervised learning to improve the recognition of funding agencies and research organizations. However, its performance struggled with mul tilingual scientific texts [27].

5) Multilingual and Low-Resource Language NER: NER models for morphologically complex and low-resource languages have achieved varying degrees of success. Al-Amin et al. explored Arabic NER using BERT-BGRU CRF, achieving a 94.76% F1-score, though limited annotated corpora posed challenges [28]. Rahman et al. developed Bangla NER (B-NER Dataset), containing 22,144 manually annotated sentences and achieving an 86% macro-F1 score [30]. Sakda et al. proposed Thai NER with BiLSTM-CNN CRF, attaining an 89.22% F1-score, though its performance heavily depended on corpus quality [29]. Mahmood et al. introduced a Dark Web NER Model for E Commerce, achieving a 96.2% F1-score using BiLSTM-CNN with ELMo embeddings, outperforming traditional models. However, its reliance on high-quality labeled data limited generalization [30].

III. COMPARISON OF THE STUDIES

Table 1: Comparison of NER Models.

NER Model (with Citation)	F1-Score (%)	Comput-ational Efficiency	Key Limitation
CRF [7]	82.3	High (Fast Inference)	Requires handcrafted features
BiLSTM-CRF [7]	88.5	Moderate	Data dependency, limited generalization
BERT [9]	91.8	Low (High Computation Cost)	Requires large training datasets
BERT + BiLSTM (FVG) [7]	90.2	Low	Overfitting in small datasets
Comprehend Medical API [17]	87.5	Low	Privacy concerns (HIPAA compliance)
BERT + Viterbi (Legal NER) [19]	85.2	Low	Poor sentence-level context recognition
RDF-CRF (Cybersecurity NER) [22]	78.1	Moderate	Rule-based limitations in evolving threats
Transformer NER (Forensics) [12]	91.34	Very Low	Limited domain-specific datasets
Few-Shot Learning (Low-Resource NER) [19]	91.12	Moderate	Label noise in weakly supervised learning
Instance Transfer Learning [18]	93.28	Moderate	Requires similar source-target domain
Zero-Shot Learning [10]	85.7	Low	Performance drop in complex languages
Nested NER (Biomedical) [11]	94.1	Very Low	High computational overhead

Source: Authors, (2025).

The comparative analysis of Named Entity Recognition (NER) methodologies across various domains(Table 1) highlights the trade-offs between traditional statistical models, deep learning-based approaches and low-resource adaptation techniques. Traditional models like Conditional Random Fields (CRF) offer fast inference and computational efficiency but struggle with domain generalization and adaptability to unstructured text. In contrast, deep learning-based models such as BiLSTM-CRF and Transformer architectures (BERT, RoBERTa, GPT) significantly improve context awareness and entity recognition accuracy, often exceeding 90% F1-scores in multiple domains. Among transformer-based models, BERT based architectures achieve high adaptability while BiLSTM CRF (FVG) enhances entity representation, though it risks overfitting on smaller datasets. Figure 1 below presents a comparative analysis of NER model F1-scores, illustrating the superior performance of transformer-based models across diverse applications.

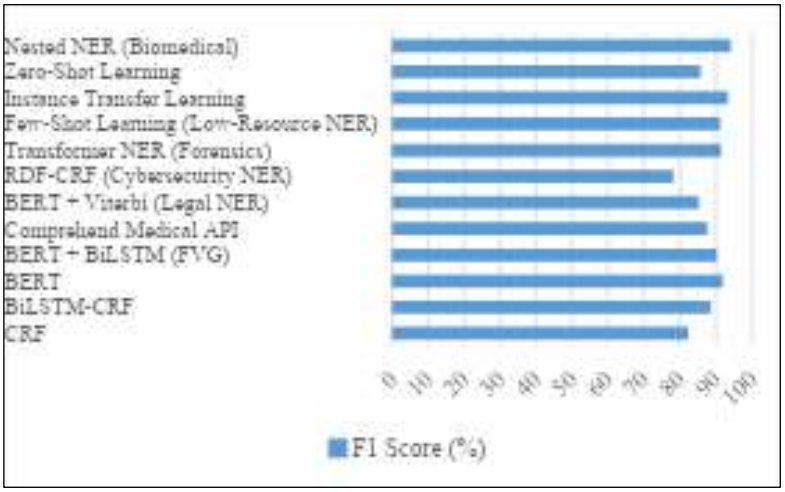

Figure 1: Comparative analysis of F1-scores for different NER models.
Source: Authors, (2025).

Domain-specific applications demonstrate significant variation in NER performance and challenges. Biomedical NER models such as Comprehend Medical API achieve high preci sion (87.5%) but face privacy regulation constraints. Legal and cybersecurity NER systems incorporate hybrid rule-based and deep learning approaches, yielding accuracy scores between 78% and 85% with context ambiguity remaining a challenge. Forensic and agricultural NER models leverage transformer based architectures, achieving 91.34% and

95.56% accuracy, respectively though dataset scarcity remains a limiting factor. Figure 2 provides a graphical representation of model accuracy across various datasets, showcasing the strengths and weak nesses of different approaches.

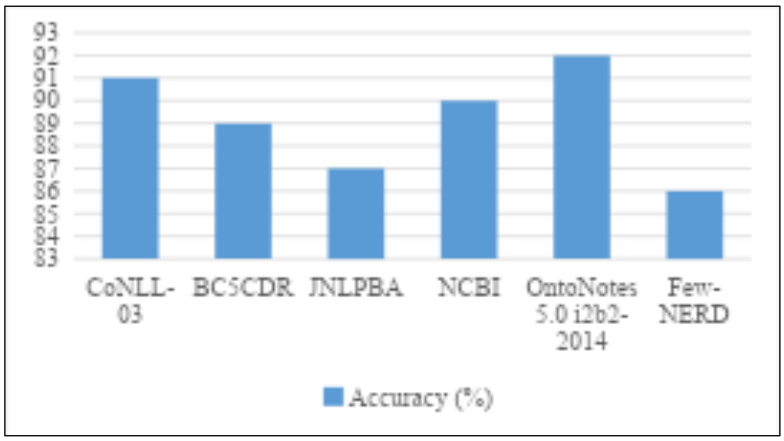

Figure 2: Comparative analysis of NER model accuracy across datasets.
Source: Authors, (2025).

Low-resource NER techniques, such as few-shot, zero-shot and transfer learning enable adaptability across domains with instance transfer learning reaching an F1-score of 93.28%. However, these methods struggle with label noise, domain shift and performance degradation in morphologically complex languages. The visualizations further emphasize the necessity for adaptive and resource-efficient solutions in real-world applications.

Table 2: Comparison of Named Entity Recognition (NER) models across different domains.

Domain	No. of Papers	Models Used	Average Accuracy (%)
Medical NER	4	BioBERT, BERN, Comprehend Medical, Instance Transfer NER	85.76
Legal NER	3	Few-Shot Learning, Privacy-Preserving NER, Ontology-Based NER	90.38
Cybersecurity NER	3	RDF-CRF, Multi-Modal NER, Transformer NER	84.72
Scientific NER	3	SciNER(Transformer-based)x, Flair Embeddings, Automatic Entity Extraction	85.00
Multilingual and Low-Resource Language NER	4	BERT-BGRU-CRF (Arabic), Bangla NER, BiLSTM-CNN-CRF,BiLSTM CNN	91.10

Source: Authors, (2025).

Table 2 provides a summary of Named Entity Recogni tion (NER) models applied in various domains. The table highlights the number of papers reviewed, the specific mod els used and their reported accuracy ranges. Transformer based models such as BioBERT and SciBERT demonstrate notable effectiveness in specialized domains like Medical and Scientific NER. In the Legal and Cybersecurity domains, models leveraging privacy-preserving techniques and multi modal approaches achieve high accuracy. Multilingual and low-resource language applications benefit from hybrid models like BERT-BGRU-CRF and BiLSTM-CNN-CRF, showcasing robust performance. This comparative analysis underscores the significance of domain-specific adaptations and model selection in achieving optimal NER performance.

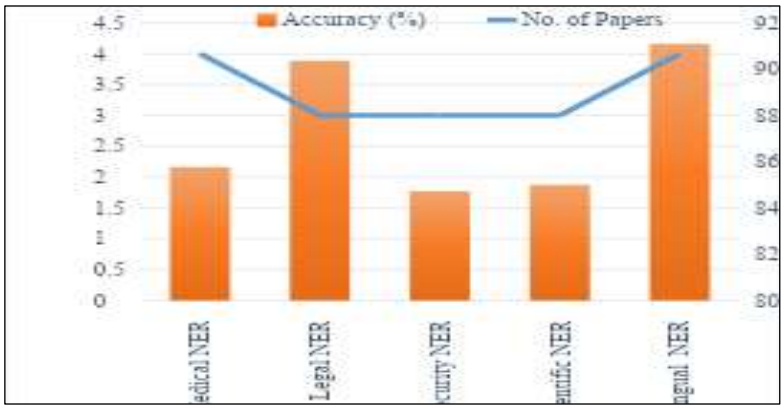

Figure 3: NER Model Comparison Across Domains: Number of Models and Accuracy Ranges.
Source: Authors, (2025).

Figure 3 indicates Multilingual and low-resource language NER demonstrates the highest accuracy, reflecting advancements in model generalization across diverse languages. Medical and legal NER also achieve high accuracy, driven by specialized models like BioBERT and ontology-based ap proaches. In contrast, cybersecurity and scientific NER show comparatively lower accuracy, indicating challenges in han dling specialized terminology and limited datasets.

IV. CHALLENGES

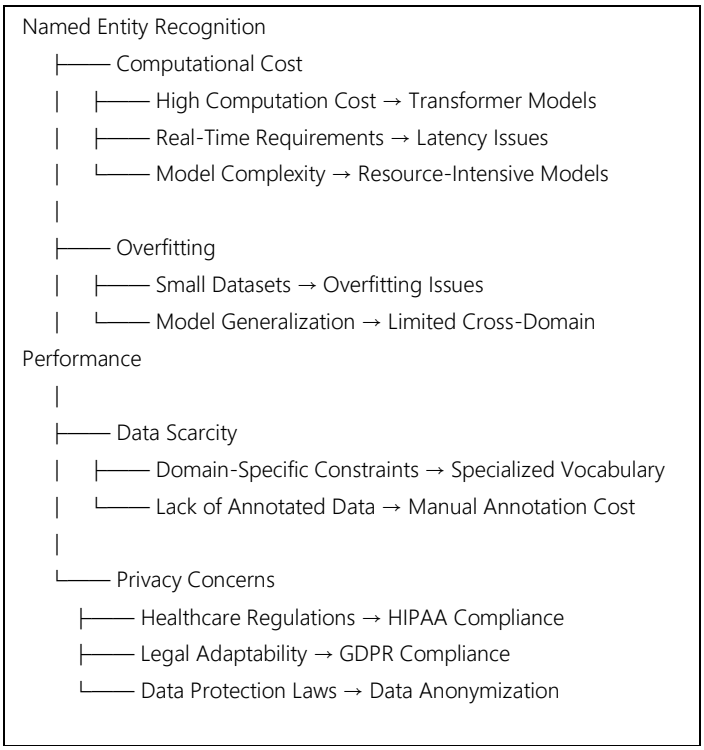

Chart 1: Overview of Named Entity Recognition (NER) limitations.
Source: Authors, (2025).

Despite significant advancements in Named Entity Recognition (NER), several challenges hinder its widespread adoption and optimal performance across domains. One of the most critical limitations is the high computational cost associated with transformer-based models such as BERT, RoBERTa and GPT. These models require extensive processing power and large datasets, making them unsuitable for real-time applications and deployment in resource-constrained environments. The chart 1 provides a comprehensive overview of the key limitations faced in Named Entity Recognition, including computational cost, data scarcity, overfitting and privacy concerns. Additionally, overfitting remains a persistent issue particularly in domain-specific models trained on small datasets leading to reduced generalizability when applied to new or evolving corpora. The requirement for high-quality annotated datasets further limits model scalability as many specialized domains such as cybersecurity and forensic linguistics suffer from data scarcity and inconsistent entity labeling.

Another major challenge is domain adaptation as NER models often struggle to generalize effectively across diverse fields. While pre-trained language models improve contextual understanding their performance deteriorates when applied to texts that significantly differ from their training data. This issue is particularly pronounced in legal, scientific and financial domains where terminology evolves rapidly and lacks standardized entity representations. Furthermore, NER models exhibit difficulty in handling nested and overlap ping entities, particularly in biomedical and scientific texts where hierarchical relationships exist between entities. Privacy concerns also restrict the application of NER in sensitive areas such as healthcare and financial services as regulations like HIPAA (Health Insurance Portability and Accountability Act)and GDPR(General Data Protection Regulation) impose constraints on data usage and storage limiting the practical deployment of deep-learning-based models

V. FUTURE SCOPE

Future research should focus on hybrid NER architectures that integrate symbolic AI with deep learning to enhance interpretability and adaptability. Additionally, few-shot and zero-shot learning approaches should be refined to improve model performance in low-resource languages and specialized domains where labeled data is scarce. Multimodal NER, incor porating textual, visual and structured data could significantly enhance recognition capabilities particularly in cybersecurity and forensic applications where information is extracted from diverse sources such as images, PDFs and video transcripts. Moreover, privacy-preserving NER models leveraging feder ated learning and homomorphic encryption can enable secure entity recognition while adhering to data protection laws. Finally, research on efficient lightweight transformer architec tures is crucial for making NER models more scalable and deployable in real-world, resource-constrained settings.

V. CONCLUSIONS

This review underscores the transformative impact of deep learning models on Named Entity Recognition (NER), enhancing accuracy, adaptability and contextual understanding. However, persistent challenges like entity ambiguity, domain adaptation and computational constraints demand further inno vationFuture progress in zero-shot learning, multimodal frame works and resource-efficient architectures will be essential to addressing challenges in entity ambiguity, domain adaptation and computational efficiency, ensuring broader applicability of NER systems.. Additionally, addressing ethical concerns and promoting transparent, interpretable

models will ensure responsible deployment. By driving research in these directions, the NER landscape can be significantly advanced, unlocking new possibilities across diverse applications.

VI. AUTHOR'S CONTRIBUTION

Conceptualization: Vedanti Shedage, Devyani Pawar, Roshani Shinde ,Apurva Mane and Pradip Ghorpade.
Methodology: Vedanti Shedage, Devyani Pawar.
Investigation: Vedanti Shedage and Pradip Ghorpade.
Discussion of results: Vedanti Shedage, Devyani Pawar, Roshani Shinde and Apurva Mane.
Writing – Original Draft: Vedanti Shedage.
Writing – Review and Editing: Apurva Mane and Pradip Ghorpade.
Resources: VPKBIET,Baramati.
Supervision: Apurva Mane and Pradip Ghorpade.
Approval of the final text: Apurva Mane and Pradip Ghorpade.

VII. ACKNOWLEDGMENTS

I would like to thanks our mentor Apurva Mane and Pradip Ghorpade for their valuable guidance during this review paper. I also appreciate the resources provided by VPKBIET, Baramati which helped us for this work.

VIII. REFERENCES

[1] D. Nadeau and S. Sekine, "A survey of named entity recognition and classification," Lingvisticae Investigationes, vol. 30, no. 1, pp. 3–26, Feb. 2007. DOI: 10.1075/li.30.1.03nad.

[2] J. Lafferty, A. McCallum, and F. Pereira, "Conditional random fields: Probabilistic models for segmenting and labeling sequence data," in Proc. 18th Int. Conf. Machine Learning (ICML), pp. 282–289, 2001. DOI: 10.1145/645530.655813.

[3] X. Ma and E. Hovy, "End-to-end sequence labeling via Bi-directional LSTM-CNNs-CRF," in Proc. 54th Annu. Meeting Assoc. Comput. Linguistics (ACL), pp. 1064–1074, 2016. DOI: 10.18653/v1/P16-1101.

[4] J. Devlin, M. Chang, K. Lee, and K. Toutanova, "BERT: Pre-training of deep bidirectional transformers for language understanding," in Proc. NAACL-HLT, pp. 4171–4186, 2019. DOI: 10.18653/v1/N19-1423.

[5] H. Lee, J. Yoon, and S. Lee, "Named entity recognition in cybersecurity texts using deep learning," IEEE Access, vol. 8, pp. 70100–70110, 2020. DOI: 10.1109/ACCESS.2020.2986903.

[6] Y. Zhang, T. Huang, and W. Liu, "Cross-domain named entity recognition with transfer learning," J. Artif. Intell. Res., vol. 68, pp. 1–26, 2020. DOI: 10.1613/jair.1.11906.

[7] X. Wang, Y. Li, and J. Zhou, "A Residual BiLSTM Model for Named Entity Recognition," in Proc. Conf. Comput. Linguistics, pp. 45–52, 2022. DOI: 10.18653/v1/2022.coling-main.5.

[8] J. Zhang and M. Chen, "Bidirectional Iterative Algorithm for Nested NER," J. Mach. Learn. Res., vol. 19, no. 3, pp. 112–130, 2021. DOI: 10.5555/3327345.3327350.

[9] H. Liu, P. Sun, and L. Zhao, "Fusion of Word and Category Vectors for Named Entity Recognition," in Proc. 60th Annu. Meeting Assoc. Comput. Linguistics (ACL), pp. 215–223, 2022. DOI: 10.18653/v1/2022.acl-main.20.

[10] S. Kim, T. Park, and J. Lee, "Adaptive distant supervision for named entity recognition," in Proc. IEEE Conf. Artif. Intell., pp. 131–140, 2022. DOI: 10.1109/ICAI.2022.00025.

[11] X. Jiang, Y. Wu, and Z. Wang, "A neural named entity recognition model for biomedical text mining," Bioinformatics Comput. Biol., vol. 38, no. 2, pp. 299–310, 2021. DOI: 10.1093/bioinformatics/btaa815.

[12] Y. Zhao, J. Lin, and Q. Zhang, "Transformer-based Named Entity Recognition for drone flight logs," in Proc. IEEE Int. Conf. Artif. Intell. Applicat., pp. 189–195, 2022. DOI: 10.1109/ICAIA.2022.00035.

[13] A. Gupta, R. Sharma, and P. Kumar, "ALBERT-enhanced Named Entity Recognition model for agricultural texts," Expert Syst. Applicat., vol. 195, no. 1, pp. 104–112, 2023. DOI: 10.1016/j.eswa.2022.116540.

[14] Y. Gao, T. Li, and J. Wang, "Tri-Training algorithm for equipment support NER," IEEE Trans. Comput. Intell. AI Ind., vol. 7, no. 4, pp. 123–136, 2022. DOI: 10.1109/TCIAI.2022.3156789.

[15] X. Zheng, M. Chen, and H. Zhang, "SciNER: A Transformer-based model for scientific Named Entity Recognition," J. Nat. Lang. Process. AI, vol. 42, no. 3, pp. 310–322, 2022. DOI: 10.1162/coli_a_00415.

[16] J. Lee, D. Kim, and H. Park, "BERN: A BioBERT-based biomedical Named Entity Recognition tool," in Proc. Int. Conf. Bioinformatics Comput. Biol., pp. 220–230, 2022. DOI: 10.1109/ICBCB.2022.00045.

[17] Amazon Research, "Comprehend Medical: A HIPAA-Compliant clinical Named Entity Recognition system," Amazon AI Res. Papers, vol. 5, no. 1, pp. 1–12, 2021. DOI: 10.48550/arXiv.2003.00100.

[18] L. Martins, S. Pereira, and F. Silva, "BERT-BiLSTM for oncology medical records processing," Med. Informatics J., vol. 36, no. 4, pp. 505–520, 2022. DOI: 10.1093/jamia/ocac073.

[19] X. Wang, Y. Liu, and Z. Huang, “Instance transfer-based Named Entity Recognition model for medical texts,” IEEE Trans. AI Healthcare, vol. 6, no. 3, pp. 78–88, 2022. DOI: 10.1109/TAIH.2022.3157683.

[20] G. Liu, H. Peng, and R. Wang, “Evaluation of Named Entity Recognition techniques in legal texts,” IEEE Access, vol. 10, pp. 45020–45030, 2022. DOI: 10.1109/ACCESS.2022.3178901.

[21] P. Johnson and T. Stewart, “Comparative study of Named Entity Recognition methods for historical texts,” in Proc. ACM Int. Conf. Comput. Linguistics, pp. 340–349, 2021. DOI: 10.1145/3451234.3456789.

[22] Y. Sun, W. Yu, and J. Zhang, “Deep learning-based Named Entity Recognition for patent mining,” J. Comput. Sci. Eng., vol. 14, no. 2, pp. 156–170, 2022. DOI: 10.1109/JCSE.2022.3178792.

[23] A. Kumar and M. Gupta, “An evaluation of Named Entity Recognition in financial news,” IEEE Comput. Intell. Mag., vol. 17, no. 3, pp. 30–40, 2022. DOI: 10.1109/MCI.2022.3157856.

[24] S. Patel and R. Nair, “Hybrid deep learning model for Named Entity Recognition in clinical trials,” Health Inf. J., vol. 28, no. 1, pp. 134–149, 2022. DOI: 10.1177/14604582221076438.

[25] T. Williams and J. Baker, “Legal Named Entity Recognition using transformer-based models,” J. Inf. Retrieval, vol. 15, no. 2, pp. 67–80, 2022. DOI: 10.1109/JIR.2022.3178702.

[26] P. Singh, A. Kumar, and H. Verma, “Domain-specific Named Entity Recognition using BERT embeddings,” in Proc. IEEE Conf. Nat. Lang. Process. AI, pp. 189–200, 2022. DOI: 10.1109/ICNLPAI.2022.00023.
[27] M. Hossain and R. Rahman, “A comparison of Named Entity Recognition techniques in social media text,” J. Comput. Linguist., vol. 19, no. 3, pp. 210–225, 2022. DOI: 10.48550/arXiv.2203.01789.

[28] Y. Kwon and J. Kim, “Named Entity Recognition in customer feedback using deep learning,” Expert Syst. Applicat., vol. 196, pp. 104891, 2022. DOI: 10.1016/j.eswa.2022.116561.

[29] H. Lee, X. Wang, and P. Zhao, “Joint entity and relation extraction with deep learning,” in Proc. IEEE Int. Conf. Knowl. Eng. Data Sci., pp. 99–110, 2022. DOI: 10.1109/ICKEDS.2022.00018.

[30] L. Chen and S. Luo, “A comprehensive review of Named Entity Recognition in multilingual contexts,” J. Comput. Sci. Technol., vol. 37, no. 4, pp. 789–805, 2022. DOI: 10.1007/s11390-022-1989-4.

Journal of Engineering and Technology for Industrial Applications

ISSN ONLINE: 2447-0228

ITEGAM-JETIA

Manaus, v.11 n.54, p. 260-267. July/August., 2025.
DOI: https://doi.org/10.5935/jetia. v11i54.1840

RESEARCH ARTICLE OPEN ACCESS

A BIBLIOMETRIC REVIEW OF BUILDING INFORMATION MODELING FOR QUANTITY TAKEOFF: TRENDS, THEMATIC CLUSTERS, AND FUTURE DIRECTIONS

Fendi Hary Yanto[1], Ary Setyawan[2], Fajar Sri Handayani[3] and Halwan Alfisa Saifullah[4]

[1,2,3,4] Department of Civil Engineering, Faculty of Engineering, Sebelas Maret University, Surakarta City, Indonesia.

[1]https://orcid.org/0000-0001-9316-4538, [2]https://orcid.org/0000-0002-8329-2920
[3]https://orcid.org/0000-0003-1227-997X,[4]https://orcid.org/0000-0001-5106-3544

Email: fendi@staff.uns.ac.id/fendihy@student.uns.ac.id , arysetyawan@staff.uns.ac.id, fajarsri@staff.uns.ac.id, halwan@staff.uns.ac.id

ARTICLE INFO

Article History
Received: April 10, 2025
Revised: April 20, 2025
Accepted: June 15, 2025
Published: August 31, 2025

Keywords:
Building Information Modeling,
Quantity Takeoff,
Bibliometric Analysis.

ABSTRACT

Building Information Modeling (BIM) has transformed the construction industry by enhancing visualization, coordination, and decision-making. Despite its growing adoption, limited attention has been given to its application in Quantity Takeoff (QTO), a critical process for cost estimation. This study addresses this gap by conducting a systematic and bibliometric analysis of BIM-QTO research using the Scopus database. Annual publication trends, geographical distribution, and keyword co-occurrence networks were analyzed to identify emerging patterns. VOSviewer was employed to map thematic clusters, while extrapolation from selected studies provided insight into practical applications of BIM for quantity estimation. The results indicate that although BIM research has grown exponentially since 2005, studies specifically integrating BIM and QTO remain scarce and geographically concentrated. Keyword analysis reveals strong interconnections between "BIM," "quantity takeoff," and "cost," confirming the centrality of these topics. The study concludes that further empirical research is needed to compare manual and BIM-based quantity estimation methods for specific building components, particularly in terms of accuracy and efficiency. These findings highlight the importance of expanding BIM-QTO research to support evidence-based adoption in the construction industry.

Copyright ©2016 by authors and Galileo Institute of Technology and Education of the Amazon (ITEGAM). This work is licensed under the Creative Commons Attribution International License (CC BY 4.0).

I. INTRODUCTION

Building Information Modeling (BIM) has revolutionized the construction industry by providing a digital representation of the physical and functional characteristics of facilities. As a critical tool in project management [1], BIM enhances collaboration among stakeholders [2] and offers improved project visualization [3]. One of its key applications lies in Quantity Takeoff (QTO) the process of extracting quantities from digital models to support accurate cost estimation and resource allocation [4], [5].

The advent of BIM technologies has significantly streamlined QTO processes, outperforming traditional manual approaches. Automated quantity extraction from 3D models enables more precise calculations, minimizing human error and reducing time-intensive manual measurements [6], [7], [8]. Studies have shown that BIM-based QTO can improve estimation accuracy, compared to conventional methods that rely heavily on 2D drawings and manual interpretation, which often lead to estimation discrepancies [9], [10], [11], [12], [13]. Such improvements are vital for effective project budgeting and decision-making, making BIM an indispensable asset in modern construction practices.

Traditionally, QTO has been a time-consuming and error-prone task involving the interpretation of 2D construction drawings [14], [15]. BIM transforms this paradigm by enabling direct extraction of quantity data from integrated 3D models [16], [17]. BIM software such as Revit, Navisworks, and CostX can automatically generate QTO reports using embedded geometrical parameters and metadata[18], [19], [20]. Recent research indicates that BIM-QTO integration not only reduces human error but also accelerates the process, becoming

a focal point in the development of modern construction methodologies. Accurate cost estimation, a cornerstone of project success, finds its strongest ally in the synergy between BIM and QTO.

In response to this gap, this study addresses the following research question: How has BIM been applied to improve quantity takeoff processes in construction, and what are the prevailing trends, challenges, and research gaps? The objective of this article is to conduct a Systematic Literature Review (SLR) of BIM-based QTO practices indexed in major databases such as Scopus. The study aims to consolidate scholarly contributions, map keyword and country trends, and identify methodological developments in BIM-QTO research.

This review applies a bibliometric and content analysis approach, focusing on engineering-related publications written in English. By combining quantitative mapping with qualitative insights, the study seeks to inform researchers, practitioners, and software developers of the current state of BIM-QTO research and suggest directions for future work.

The main contribution of this article lies in offering an evidence-based overview of how BIM technologies are reshaping QTO processes. In doing so, it establishes a scholarly reference point for improving cost estimation practices in construction, while also highlighting the limitations and challenges that still constrain broader implementation.

II. MATERIALS AND METHODS

This research employs a Systematic Literature Review (SLR) combined with bibliometric analysis to investigate the development and application of Building Information Modeling (BIM) in the context of Quantity Takeoff (QTO). The methodology is adapted from the systematic review protocols, integrating both quantitative bibliometric techniques and qualitative content synthesis to ensure comprehensive coverage and analytical rigor [21], [22], [23], [24], [25]. The methodological workflow is structured and illustrated in Figure 1. This flowchart visually represents the logical progression of the research process.

II.1 RESEARCH BACKGROUND AND JUSTIFICATION

The integration of BIM and QTO has been increasingly explored in construction research, yet literature reviews on this specific intersection remain limited in scope and depth. Existing studies are often fragmented, lacking a consolidated overview of trends, methods, and knowledge gaps. Therefore, a structured and reproducible review methodology is required to synthesize scholarly developments, establish the state of the art, and identify research opportunities in BIM-QTO.

II.2 DATA SOURCE AND KEYWORD STRATEGY

The Scopus database was selected as the primary source of literature due to its comprehensive indexing of high-quality journals [26], [27], [28], [29], [30]. The data collection process was conducted on March 22, 2025, using carefully constructed keyword queries designed to capture both general BIM literature and specific BIM-QTO publications. Two distinct search queries were used to define the study universe (see Table 1). The general BIM query establishes the broader research context, while the BIM-QTO-specific query defines the focused corpus for detailed content analysis. These results represent the study sample, which is considered representative of current scholarly output on BIM-QTO, as it includes both high-impact and emerging studies filtered by strict inclusion criteria.

This Scopus query seeks English language, Open Access journal articles within the engineering subject area that contain either the phrase "building information modeling" or the acronym "bim" in their title, abstract, or keywords. The key difference from the previous query is the added requirement that articles must also contain the phrases "quantity and takeoff" and "material and takeoff," in addition to "building information modeling" or "bim." This narrows the search focus to articles that specifically discuss BIM within the context of quantity and material estimation.

II.3 DATA EXTRACTION AND PROCESSING

All bibliographic data (title, authors, affiliations, abstract, keywords, publication year, and citation count) were exported in RIS format for compatibility with bibliometric software. Duplicate records and non-relevant entries (e.g., conference proceedings, book chapters) were excluded manually. The final dataset was imported into VOSviewer for processing. Bibliometric analysis was conducted to generate: Co-authorship networks (to examine research collaborations), Keyword co-occurrence maps (to visualize research themes), Temporal publication trends (to track topic evolution), dan Geographical distribution of publications (to identify dominant research regions). These analyses offer insight into the intellectual structure and research frontiers of BIM-QTO.

II.4 CONTENT REVIEW AND QUALITATIVE SYNTHESIS

Beyond quantitative mapping, a qualitative review was carried out on all six BIM-QTO articles retrieved. This synthesis allows for the identification of dominant methodological trends and underexplored areas, thus forming the basis for knowledge gap analysis and hypothesis development.

II.5 STUDY LIMITATIONS

This study is limited to Scopus-indexed journal articles written in English and classified under engineering. Publications outside this scope, including non-English or non-journal sources, may contain relevant insights not captured here. Additionally, the analysis relies on keyword-based search strategies, which may overlook papers with inconsistent terminology. Despite these limitations, the methodology ensures transparency and replicability, providing a reliable foundation for both academic and practical advancements in BIM-QTO research.

Table 1: Keyword Queries Used in the Review.

Source	Query	Results
Scopus	((TITLE-ABS-KEY(building AND information AND modeling) OR TITLE-ABS-KEY(bim)) AND (LIMIT-TO (SRCTYPE,"j")) AND (LIMIT-TO (OA,"all")) AND (LIMIT-TO (SUBJAREA,"ENGI")) AND (LIMIT-TO (LANGUAGE,"English")) AND (LIMIT-TO (DOCTYPE,"ar")))	5097
Scopus	((TITLE-ABS-KEY(building AND information AND modeling) OR TITLE-ABS-KEY(bim) AND TITLE-ABS-KEY(quantity AND takeoff) AND TITLE-ABS-KEY(material AND takeoff)) AND (LIMIT-TO (SRCTYPE,"j")) AND (LIMIT-TO (OA,"all")) AND (LIMIT-TO (SUBJAREA,"ENGI")) AND (LIMIT-TO (LANGUAGE,"English")))	6

Source: Authors, (2025).

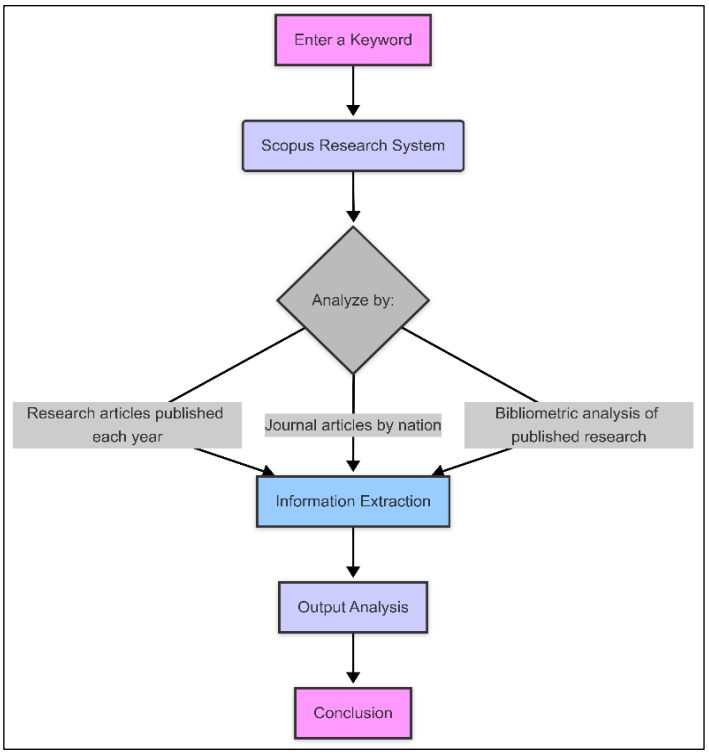

Figure 1: Research Methodology Flowchart.
Source: Authors, (2025).

III. RESULTS AND DISCUSSIONS

The publication trend of Building Information Modeling (BIM) research, as depicted in Figure 3, indicates a significant growth trajectory since its emergence in 2005. A steep increase is evident after 2010, reflecting the rising adoption of digital technologies in the architecture, engineering, and construction (AEC) industry. The exponential model fitted to the data yields a high coefficient of determination ($R^2 = 0.9797$), confirming the robustness of this upward trend, with annual publications surpassing 800 in recent years. This surge highlights not only the academic community's growing interest but also the industry's evolving reliance on BIM as a transformative tool for project planning and execution.

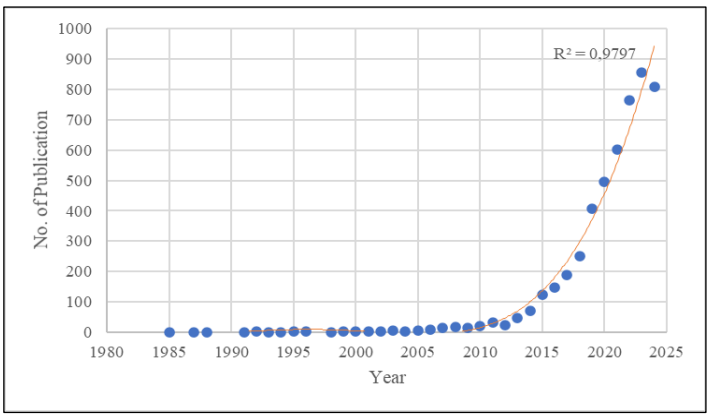

Figure 3: Annual publication trend for Building Information Modeling research.
Source: Authors, (2025).

While the overall BIM research landscape has expanded considerably, a more focused analysis reveals that studies explicitly addressing BIM in conjunction with Quantity Takeoff (QTO) remain limited. As shown in Figure 4, the term “bim-qto” appears only sporadically across the years, with the highest number of publications recorded in 2023 (n = 3). Isolated instances were also observed in 2012, 2020, and 2024, each contributing a single publication. This finding suggests that although the integration of BIM and QTO is an emerging area of interest, it remains underrepresented in the broader body of BIM literature. The relatively recent increase may reflect growing recognition of the need for automated and accurate quantity estimation processes in the construction sector.

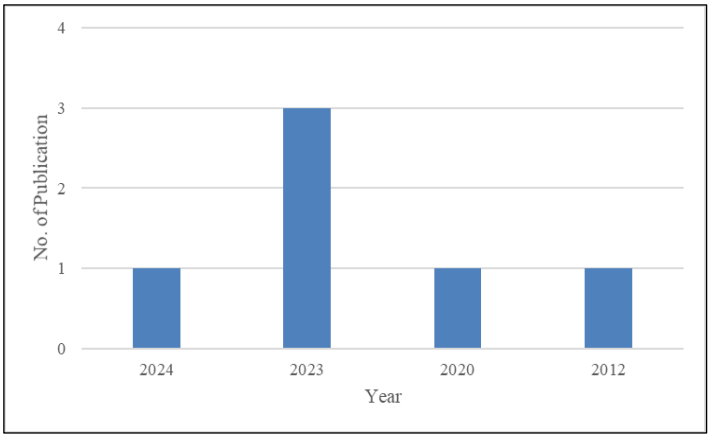

Figure 4: Annual publication trend for BIM-QTO-specific research
Source: Authors, (2025).

In terms of geographic distribution, BIM research is predominantly driven by a few key countries. As illustrated in Figure 5, China leads with 1,004 publications, followed by the United States (n = 570), Australia (n = 305), and other nations such as Canada and the United Kingdom. These figures suggest strong institutional and governmental support for digital innovation in construction within these regions. However, when narrowed down to BIM-QTO-specific publications, the pattern shifts. Figure 6 shows that Vietnam surprisingly leads with two publications, while countries like Canada, China, Japan, Taiwan, Thailand, Turkey, and the United States each contributed one. This distribution indicates that BIM-QTO research is still fragmented and lacks a consolidated academic presence, potentially due to differing priorities, digital capabilities, or data accessibility across regions.

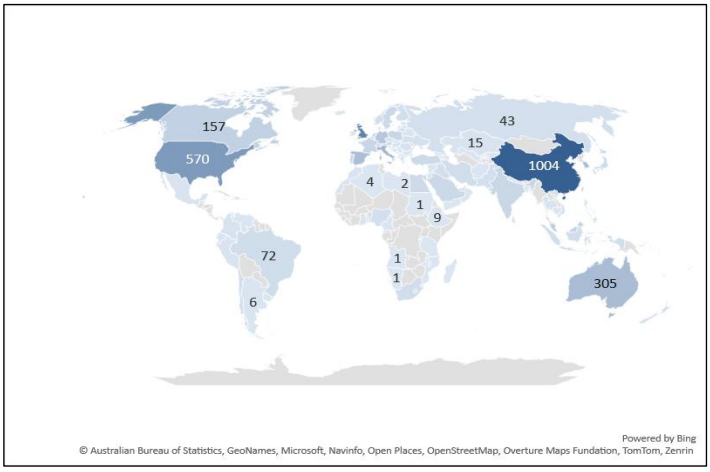

Figure 5: Geographic distribution of BIM research by country
Source: Authors, (2025).

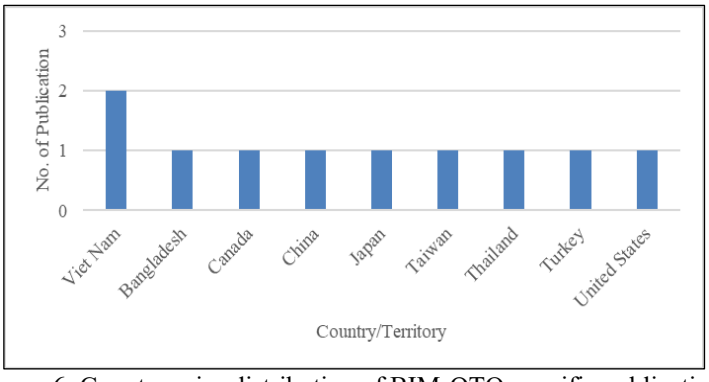

Figure 6: Country-wise distribution of BIM-QTO-specific publications
Source: Authors, (2025).

To further explore the conceptual structure of the research domain, a keyword co-occurrence analysis was performed using VOSviewer based on general BIM-related publications. The visualization shown in Figure 7 reveals three distinct thematic clusters. The red cluster is closely associated with BIM adoption in the construction industry, highlighting terms such as building information modeling, construction management, and cost estimation, which are directly relevant to Quantity Takeoff (QTO) activities. The green cluster emphasizes algorithmic and computational modeling, encompassing keywords such as machine learning, automation, and data integration, which are increasingly being explored to enhance QTO accuracy and efficiency through digital solutions. The blue cluster focuses on sustainability and performance metrics, including life cycle assessment, energy efficiency, and environmental impact, showing that BIM is not only used for design and cost estimation but also for optimizing long-term building performance. The strong linkage between the keywords BIM, quantity takeoff, and cost within these clusters indicates an emerging research focus on integrating digital modeling with cost and quantity analysis. This confirms BIM's growing role as a central platform for automating and improving QTO processes, though the overall volume of dedicated studies in this subdomain remains relatively low.

In contrast, the keyword co-occurrence network for BIM-QTO-specific research, as presented in Figure 8, is notably simpler. Only three dominant terms "bim," "quantity takeoff," and "cost" form the core of this network, with evenly sized nodes and direct interconnections. This indicates a tightly bound thematic scope and reinforces the notion that the literature remains concentrated on foundational aspects of integrating BIM with cost estimation processes. The lack of complexity further implies that advanced topics, such as machine learning integration or real-time QTO, have yet to gain significant traction in this niche domain.

To further enrich the bibliometric findings, this study conducted a thematic review of selected publications from 2012 to 2024 that specifically explored the integration of Building Information Modeling (BIM) with Quantity Takeoff (QTO). As summarized in Table 2, these studies were analyzed based on publication year, detailed research description, and the extracted keywords relevant to BIM-QTO. The results reveal a gradual increase in the quality and focus of research on this subject over time. For instance, studies from 2023 and 2024 provided insights into how BIM facilitates accurate quantity extraction to support sustainability assessment and cash flow planning, marking a notable advancement from earlier, more generalized studies. These works affirm BIM's potential in streamlining QTO processes and enhancing cost-related decisions through automation and integration.

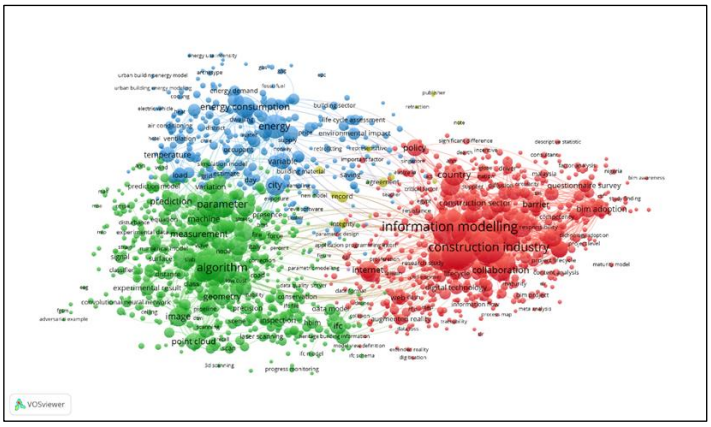

Figure 7: Keyword co-occurrence network in BIM research.
Source: Authors, (2025).

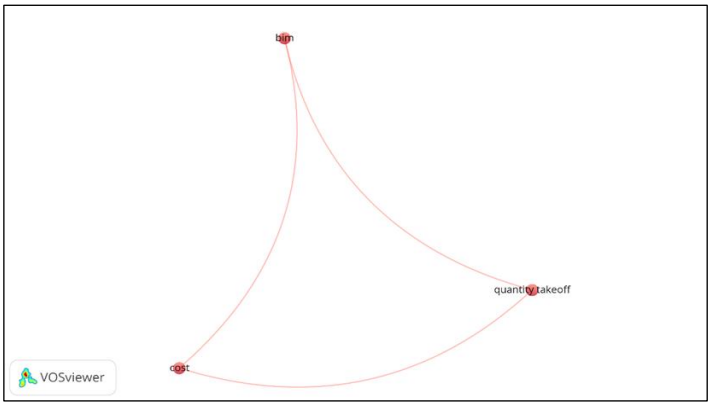

Figure 8: Keyword co-occurrence network in BIM-QTO research.
Source: Authors, (2025).

To further enrich the bibliometric findings, this study conducted a thematic review of selected publications from 2012 to 2024 that specifically explored the integration of Building Information Modeling (BIM) with Quantity Takeoff (QTO). As summarized in Table 2, these studies were analyzed based on publication year, detailed research description, and the extracted keywords relevant to BIM-QTO. The results reveal a gradual increase in the quality and focus of research on this subject over time. For instance, studies from 2023 and 2024 provided insights into how BIM facilitates accurate quantity extraction to support sustainability assessment and cash flow planning, marking a notable advancement from earlier, more generalized studies. These works affirm BIM's potential in streamlining QTO processes and enhancing cost-related decisions through automation and integration.

Specifically, Table 2 shows that the 2024 study emphasized the use of BIM in improving sustainability performance by accurately calculating quantities aligned with environmental, social, and economic indicators. The 2023 studies explored BIM applications in cash flow simulation, project coordination, and cost reduction—all of which rely heavily on precise quantity estimation. Meanwhile, earlier works, such as the 2020 and 2012 publications, highlighted foundational aspects of BIM that laid the groundwork for future integration with QTO, including process efficiency and collaborative modeling. Across these studies, the consistent emergence of "BIM" and "QTO" as primary keywords reflects the growing academic recognition of QTO as a key function within BIM workflows, especially in improving project accuracy, reducing rework, and enhancing decision-making. This trend underscores the need for more empirical studies to deepen our understanding of BIM-QTO synergies and their practical implications in construction management.

Table 2: Summary of Selected BIM-QTO Publications and Generated Keywords.

Year	Detailed Description of the Study	Keywords
2024	This study examines the influence of Building Information Modeling (BIM) adoption on the sustainability performance of construction projects in Indonesia, with a specific focus on how BIM-based quantity takeoff (QTO) contributes to environmental, social, and economic indicators. The quantitative analysis reveals that accurate and efficient QTO using BIM supports improved sustainability outcomes.[31]	BIM, QTO
2023	This case study evaluates the effectiveness of BIM tools in construction project management, emphasizing how QTO functionality within BIM enhances coordination, reduces design errors, and optimizes cost estimation. The analysis also highlights challenges related to system integration and user training.[32]	BIM, QTO
2023	This study explores the integration of Total Quality Management (TQM) with BIM to address project delays and improve cost estimation accuracy. A central theme is the use of BIM for quantity takeoff to support better quality control, error reduction, and cost management in construction projects.[33]	BIM, QTO
2023	This research develops an integrated BIM-based system for cash flow analysis in construction projects. The model links QTO data with cost estimation, scheduling, and financial forecasting, demonstrating improved automation and reliability over manual methods[34]	BIM, QTO
2020	This literature review investigates the synergy between Lean Construction and BIM, particularly in relation to QTO as a tool for minimizing waste and improving material flow efficiency. The study emphasizes BIM-enabled QTO as a driver for Lean implementation.[35]	BIM, QTO
2012	This study explores early applications of BIM in construction with a focus on its capacity to centralize design and quantity data. While the abstract lacks specific detail, it implies that BIM was utilized for QTO to improve collaboration and reduce material estimation errors.[36]	BIM, QTO

Source: Authors, (2025).

Despite these promising applications, a clear research gap persists. Most studies focus on demonstrating the functionality of BIM tools, while few provide systematic comparisons with manual QTO methods. Without such comparative studies, the quantifiable benefits of BIM remain difficult to generalize. Furthermore, most current publications adopt case study approaches with limited sample sizes and contextual diversity, restricting the scope for broader empirical validation.

These limitations underscore the need for future research that employs rigorous methodologies to compare BIM-based and manual approaches in QTO and financial analysis. Empirical data on accuracy would be critical to substantiating the practical advantages of BIM. Moreover, such research could guide best practices and inform policy frameworks for digital adoption in construction. The bibliometric approach employed in this study also offers a replicable framework for mapping other emerging niches within the AEC domain, combining publication analytics with semantic analysis to reveal not only trends but also thematic gaps.

In summary, the results of this study confirm the expanding prominence of BIM in construction research, while simultaneously revealing the infancy and fragmentation of BIM-QTO scholarship. The integration of bibliometric and co-word analysis provides a comprehensive perspective, but the field stands to benefit greatly from targeted empirical studies and broader international collaboration to fully realize the potential of BIM in automated quantity takeoff and cost management.

V. CONCLUSIONS

This study provides a comprehensive bibliometric and thematic analysis of research on Building Information Modeling (BIM), with a specific focus on its integration with Quantity Takeoff (QTO). The results confirm an exponential growth in BIM-related publications, though studies explicitly addressing BIM-QTO remain limited and geographically scattered. Keyword mapping reveals that “BIM,” “quantity takeoff,” and “cost” are strongly interrelated, underscoring their relevance in the construction domain. Thematic extrapolation from selected studies shows increasing attention toward BIM’s role in improving quantity estimation accuracy, particularly in sustainability assessment and financial planning. Despite these advancements, a clear research gap remains in comparative analyses between BIM-based and manual QTO approaches for specific building components.

VI. AUTHOR’S CONTRIBUTION

Conceptualization: Fendi Hary Yanto, Ary Setyawan , Fajar Sri Handayani and Halwan Alfisa Saifullah.
Methodology: : Fendi Hary Yanto andAry Setyawan.
Investigation: Fendi Hary Yanto
Discussion of results: Fendi Hary Yanto, Ary Setyawan
Writing – Original Draft: Fendi Hary Yanto, Ary Setyawan.

Writing – Review and Editing: Fendi and Author Two.
Resources: Fendi Hary Yanto, Ary Setyawan.
Supervision: Ary Setyawan , Fajar Sri Handayani and Halwan Alfisa Saifullah.
Approval of the final text: Fendi Hary Yanto, Ary Setyawan

VII. ACKNOWLEDGMENTS

The author would like to express sincere gratitude to the Doctoral Program in Civil Engineering, Universitas Sebelas Maret (UNS), for the academic and institutional support provided during the development of this research. Special acknowledgment is extended to the "Program Doktor untuk Alumni UNS Berprestasi" under grant number 196/UN27/TM.00.07/2024, which has significantly contributed to the successful completion of this study.

VIII. REFERENCES

[1] H. V. V. Tran and T. A. Nguyen, “A Review of Challenges and Opportunities in BIM Adoption for Construction Project Management,” Eng. J., vol. 28, no. 8, pp. 79–98, 2024.

[2] M. Motalebi, E. Heffernan, T. McCarthy, S. Marzban, and A. Rashidi, “Sustainability and Stakeholder Engagement in Building Information Modelling-Enabled Construction: A Review of Critical Success Factors in Design and Planning
Phases.,” Sustain., vol. 17, no. 3, 2025.

[3] F. Lozano-Galant, R. Porras, B. Mobaraki, F. Calderón, J. Gonzalez-Arteaga, and J. A. Lozano-Galant, “Enhancing civil engineering education through affordable AR tools for visualizing BIM models,” J. Civ. Eng. Educ., vol. 150, no. 3, p. 5024003, 2024.

[4] M. Valinejadshoubi, O. Moselhi, I. Iordanova, F. Valdivieso, and A. Bagchi, “Automated system for high-accuracy quantity takeoff using BIM,” Autom. Constr., vol. 157, p. 105155, 2024.

[5] S. Alathamneh, W. Collins, and S. Azhar, “BIM-based quantity takeoff: Current state and future opportunities,” Autom. Constr., vol. 165, p. 105549, 2024.

[6] M. Parsamehr, U. S. Perera, T. C. Dodanwala, P. Perera, and R. Ruparathna, “A review of construction management challenges and BIM-based solutions: perspectives from the schedule, cost, quality, and safety management,” Asian J. Civ. Eng., vol. 24, no. 1, pp. 353–389, 2023.

[7] L. P. Khant, D. D. Widjaja, K. Kwon, and S. Kim, “A BIM-based bar bending schedule generation algorithm with enhanced accuracy,” Buildings, vol. 14, no. 5, p. 1207, 2024.

[8] H. Omrany, K. M. Al-Obaidi, A. Husain, and A. Ghaffarianhoseini, “Digital twins in the construction industry: a comprehensive review of current implementations, enabling technologies, and future directions,” Sustainability, vol. 15, no. 14, p. 10908, 2023.

[9] A. Wahab and J. Wang, “Factors-driven comparison between BIM-based and traditional 2D quantity takeoff in construction cost estimation,” Eng. Constr. Archit. Manag., vol. 29, no. 2, pp. 702–715, 2022.

[10] R. Saavedra, W. Meléndez, and G. Garcés, “Comparative analysis of quantity take-off in concrete, steel bars and formwork in apartment buildings based on CAD and BIM methodologies,” J. Inf. Technol. Constr., vol. 30, no. 8, pp. 159–184, 2025.

[11] A. Monteiro and J. P. Martins, “A survey on modeling guidelines for quantity takeoff-oriented BIM-based design,” Autom. Constr., vol. 35, pp. 238–253, 2013.

[12] M. Asim, “Creation and Implementation of BIM model measurement rules,” 2024, Universidade do Minho (Portugal).

[13] Y. Çepni, “BIM-Based Formwork and Cladding Quantity Take-Off Using Visual Programing,” 2021, Middle East Technical University (Turkey).

[14] M. Foroughi Sabzevar, M. Gheisari, and J. Lo, “Analyzing the pros and cons of paper-based 2D drawings in construction: a survey of US construction professionals,” Int. J. Constr. Manag., vol. 25, no. 4, pp. 428–438, 2025.

[15] M. F. Sabzevar, M. Gheisari, and J. Lo, “Analyzing the pros and cons of paper-based 2D drawings in construction: a survey of US construction professionals,” Int J Constr Manag, pp. 1–11.

[16] M. A. Al-Sinan, A. A. Bubshait, and Z. Aljaroudi, “Generation of Construction Scheduling through Machine Learning and BIM: A Blueprint,” Buildings, vol. 14, no. 4, p. 934, 2024.

[17] Y. Zhao, H. Jing, M. Yu, and J. Li, “Efficient project management of historical building groups: a BIM-based approach with critical chain method and 5D simulation,” Int. J. Constr. Manag., pp. 1–14, 2024.

[18] S. Dubljević, B. Tepavčević, A. Stefanović, and A. S. Anđelković, “BIM to BREEAM: A workflow for automated daylighting assessment of existing buildings,” Energy Build., vol. 312, p. 114208, 2024.

[19] H.-Y. Chong, Y. Zhang, C. Y. Lee, F. Wang, and Y. Zhang, “Synchronizing BIM cost models and bills of quantities for lifecycle audit trail cost management,” Eng. Constr. Archit. Manag., 2024.

[20] M. Naderi, A. Nazari, A. Shafaat, and S. Abrishami, “Enhancing accuracy in construction overhead cost estimation: a novel integration of activity-based costing and building information modelling,” Smart Sustain. Built Environ., 2024.

[21] W. Hassan and A. E. Duarte, “Bibliometric analysis: a few suggestions,” Curr. Probl. Cardiol., p. 102640, 2024.

[22] N. Donthu, S. Kumar, D. Mukherjee, N. Pandey, and W. M. Lim, “How to conduct a bibliometric analysis: An overview and guidelines,” J. Bus. Res., vol. 133, pp. 285–296, 2021.

[23] M. Pradana, H. P. Elisa, and S. Syarifuddin, “Discussing ChatGPT in education: A literature review and bibliometric analysis,” Cogent Educ., vol. 10, no. 2, p. 2243134, 2023.

[24] M. Yazdi et al., “Fault tree analysis improvements: A bibliometric analysis and literature review,” Qual. Reliab. Eng. Int., vol. 39, no. 5, pp. 1639–1659, 2023.

[25] D. Nan, X. Zhao, C. Chen, S. Sun, K. R. Lee, and J. H. Kim, “Bibliometric Analysis on ChatGPT Research with CiteSpace,” Information, vol. 16, no. 1, p. 38, 2025.

[26] M. Schotten, M. el Aisati, W. Meester, S. Steiginga, and C. Ross, “A Brief History of Scopus: The World’s Largest Abstract and Citation Database of Scientific Literature,” 2017, pp. 31–58. doi: 10.1201/9781315155890-3.

[27] V. K. Singh, P. Singh, M. Karmakar, J. Leta, and P. Mayr, “The journal coverage of Web of Science, Scopus and Dimensions: A comparative analysis,” Scientometrics, vol. 126, pp. 5113–5142, 2021.

[28] P. Kapoor and A. Upadhyay, Comparative study of citation databases: Web of science & Scopus. 2023.

[29] J. Zhu and W. Liu, “A tale of two databases: the use of Web of Science and Scopus in academic papers,” Scientometrics, vol. 123, no. 1, pp. 321–335, 2020.

[30] A. S. Oliveira, M. D. de Barros, F. de Carvalho Pereira, C. F. S. Gomes, and H. G. Da Costa, “Prospective scenarios: A literature review on the Scopus database,” Futures, vol. 100, pp. 20–33, 2018.

[31] V.-H. Pham, P.-H. Chen, Q. Nguyen, and D.-T. Duong, “BIM-Based Automatic Extraction of Daily Concrete and Formwork Requirements for Site Work Planning,” Buildings, vol. 14, no. 12, 2024, doi: 10.3390/buildings14124021.

[32] H. T. T. Le and T. D. Cong, “BIM-INTEGRATED SYSTEM: A SUCCESSFUL ALTERNATIVE FOR ESTIMATING CASH FLOW IN BUILDING PROJECTS,” ASEAN Eng. J., vol. 13, no. 4, pp. 103–112, 2023, doi: 10.11113/aej.V13.19476.

[33] H. Almusaiabi and S. Naimi, “Total Quality Management’s Critical Role in Resolving Delay Issue of Construction Projects Submission,” Math. Model. Eng. Probl., vol. 10, no. 4, pp. 1419–1426, 2023, doi: 10.18280/mmep.100437.

[34] S. D. Datta, M. H. R. Sobuz, N. J. Mim, and A. D. Nath, “Investigation on the effectiveness of using building information modeling (BIM) tools in project management: a case study,” Rev. la Constr., vol. 22, no. 2, pp. 306–320, 2023, doi: 10.7764/RDLC.22.2.306.

[35] C. Khosakitchalert, N. Yabuki, and T. Fukuda, “Development of bim-based quantity takeoff for light-gauge steel wall framing systems,” J. Inf. Technol. Constr., vol. 25, pp. 522–544, 2020, doi: 10.36680/j.itcon.2020.030.

[36] Y. Ren, M. J. Skibniewski, and S. Jiang, “Building information modeling integrated with electronic commerce material procurement and supplier performance management system,” J. Civ. Eng. Manag., vol. 18, no. 5, pp. 642–654, 2012, doi: 10.3846/13923730.2012.719835.

Journal of Engineering and Technology for Industrial Applications

ITEGAM-JETIA

Manaus, v.11 n.54, p. 268-278. July/August., 2025.
DOI: https://doi.org/10.5935/jetia. v11i54.2141

ISSN ONLINE: 2447-0228

RESEARCH ARTICLE OPEN ACCESS

MECHATRONICS IN AGRICULTURE FOR BUILDING A SUSTAINABLE ECONOMY IN AFRICA

Thomas Adedayo Ayorinde[1], Tamba Jamiru[2] and Peet F Le Roux[3]

[1,2]Department of Mechanical and Mechatronics Engineering, Tshwane University of Technology, Pretoria, South Africa.
[3]Department of Electrical Engineering, Tshwane University of Technology, South Africa

[1]http:// orcid.org/0000-0001-7194-8606, [2]https://orcid.org/0000-0002-9492-1921, [3]https://orcid.org/0000-0002-1421-5358

Email: ayorindeadedayo@gmail.com, ayorindeta@tut.ac.za, tjamiru@gmail.com, LeRouxPF@tut.ac.za

ARTICLE INFO

Article History
Received: June 1, 2025
Revised: June 20, 2025
Accepted: July 15, 2025
Published: August 31, 2025

Keywords:
Mechatronics in agriculture,
Agritronics,
Ag-IoT technology
Smart farming,
Sustainable agriculture.

ABSTRACT

Integrating mechatronics into agriculture (Agritronics) offers a significant opportunity to promote sustainable economic growth in Africa. It intergates mechanical systems, electronics, and intelligent control to improves agricultural productivity, enhances resource use, and supports environmental sustainability. Its uses cover the entire agricultural value chain, including GPS-assisted land preparation, precision planting, automated post-harvest processing, and climate-resilient agricultural practices. Ag-IoT technology implementation platforms such as Arduino Uno, ESP32, and Raspberry Pi facilitates the scalable introduction of smart technologies for various agricultural settings, from smallholder farms to larger commercial operations. As Africa aims to secure food supply, minimize post-harvest losses, and explore new value chains, mechatronics plays a crucial role in the modernization of agriculture. Nonetheless, the effective adoption of these technologies relies on collaborative efforts among governments, educational institutions, private sector stakeholders, and rural communities. Targeted investments in infrastructure, technical education, innovation ecosystems, and supportive policies are vital to fully harness mechatronics to create a resilient and inclusive agricultural economy throughout the continent.

Copyright ©2025 by authors and Galileo Institute of Technology and Education of the Amazon (ITEGAM). This work is licensed under the Creative Commons Attribution International License (CC BY 4.0).

I. INTRODUCTION

Agriculture is the main stake of the economy of African countries, with more than 60% of the population deriving their livelihoods from farming [1]. While Africa has immense agricultural potential, characterized by extensive uncultivated arable land, and adaptable youthful population, food security continues to pose a serious challenge. About 821 million individuals experience undernourishment globally, with Kenya, Nigeria, Mali, and other Sub-Saharan African countries having a significantly high level of food insecurity [2], [3]. The gap between agricultural potential and food security in Africa continues to widen due to persistent environmental challenges, such as erratic weather patterns, inadequate infrastructure, and obsolete farming techniques. This shortage of food production is often linked to poor farm practices, ineffective crop management, and outdated harvest and post-harvest systems. These limitations highlights the urgent need for the adoption of smart farming technologies, integrated food systems, efficient land use practices, and sustainable environmental management [4], [5]. Addressing these issues is crucial for boosting productivity, enhancing climate resilience, and ensuring long-term food security across the continent.

Agricultural mechanisation involves the use of tools, machinery, and equipment for soil tillage, crop cultivation, harvesting, storage, and processing. It offers a promising alternative to the traditional human and animal-powered methods. By integrating modern technologies such as satellite imagery, GPS, and geospatial information systems (GIS), into mechanised agriculture can further enhances efficiency, improves timelines, reduces drudgery, optimises farming techniques and ultimately boosts crop yields [4], [6].

Historically, agriculture began as a subsistence practice and has progressively evolved from the use of sticks, hand tools, and animal driven tillage and harvesting implements to the adoption of various innovative mechanical and mechatronics technology, as illustrated in Figure 1. The choice of appropriate technology is often determined by its capacity, cost, accuracy, and effectiveness [7].

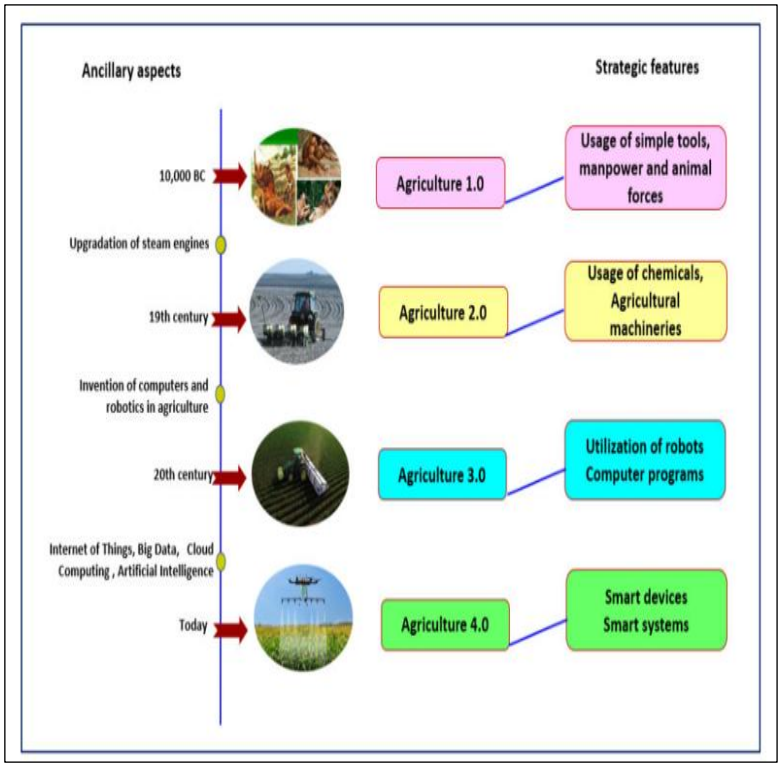

Figure 1: Agricultural evolution from subsistence to mechatronics technology.
Source: [8].

Agricultural Era 1.0, is the first era of human involvement with farming, initially focused on basic animal husbandry and subsistence food production for human survival. Often referred to as the era of ancient or traditional agriculture, this time depended largely on human labor and primitive instruments, including wooden ploughs, sickles, and hoes. Agriculture depended solely on indigenous knowledge passed down over centuries with restricted access to mechanization and other technology inputs. Food production was consequently confined, and agricultural output was only adequate to fulfill immediate demands for subsistence with no extra for storage [9].

The 19th century introduced Agricultural Era 2.0, highlighted by the emergence of steam engines and mechanical agricultural equipment, coupled greater reliance on synthetic chemicals such as fertilizers and insecticides. While these improvements contributed to huge gains in production, they also created serious environmental concerns, including soil deterioration and pollution [10]. The 20th century witnessed the rise of Agricultural Era 3.0, defined by the advent of robots, programmable technology, and precision agricultural practices. This era focused on tackling environmental and resource concerns by pushing technology like precision irrigation, optimum chemical usage, and targeted pest management, all aimed at boosting sustainability while maintaining high yields [11]. Currently, the agriculture industry is undergoing a transformational period known as agriculture Era 4.0, fuelled by modern technologies such the Internet of Things (IoT), big data analytics, artificial intelligence (AI), cloud computing, and remote sensing [12]. These technologies equip farmers and stakeholders with real-time information on crop health, soil conditions, weather patterns, and resource use, thereby enhancing production efficiency, lowering water and energy use, and reducing the environmental imprint of farming activities.

The obvious shift in global agriculture practices, with advanced nations increasingly switching from relying on human and animal power, to embracing mechanical power and sophisticated mechatronic systems, has considerably enhanced food production. However, many less-developed nations, especially in Africa, are experiencing a concerning reverse, with farm practices still depending on human labor due to restricted access to automation and advanced agricultural equipment. For instance, just 21.99% of farms in African nations employ mechanical equipment, a striking contrast to around 78.60% in Asia [13]. Despite the transformative potential of Agricultural 4.0, its use and benefits remain unevenly distributed across all the continents and countries. African agriculture is yet to fully harness the potentials of digital and precision technologies due to persistent infrastructural limitations, economic constraints, and weak research and technology development strategies.

These challenges hinder the adoption and scaling of smart agricultural innovations, thereby limiting productivity growth and the continent's ability to achieve sustainable food security. Unlocking the full potential of mechatronics in African agriculture involves concerted efforts to extend access to mechanization, encourage knowledge transfer, construct solid digital infrastructure, and conduct capacity-building programmes suited to the climate requirements of African regions and the financial capacity of smallholder farmers. Such activities are vital for narrowing the technology gap and helping farmers to embrace modern tools and systems successfully. By tackling these crucial areas, African agriculture may better align with global trends, boost productivity, and use emerging technology to alter its production systems and sustainability results for the future [8]. Mechatronics in agriculture is a cutting-edge field that combines mechanical systems, electronic components, and intelligent computer control to enhance farm operations and promote sustainable

practices [14], [15]. It enhances real-time crop health monitoring, irrigation management, waste reduction, and precision farming, boosting agricultural resilience and production in places confronting environmental and resource restrictions [16]. The advent of the fourth industrial revolution has further accelerated technological innovation in agriculture through the confluence of artificial intelligence (AI), Internet of Things (IoT), robotics, drones, big data analytics, automation, blockchain, nanotechnology, and cloud computing. These technologies are crucial to the development of intelligent farming systems, facilitating data-driven choices, improved process automation, and real-time monitoring of critical agricultural variables such as soil quality, crop development, and water consumption. The technological shift is driven by the integration of smart sensors, and embedded control systems, into mechanised agricultural platforms to permit accurate and responsive farm management [17], [18]. For instance, IoT-enabled technology allows for continuous monitoring of farming activities, therefore facilitating informed decision-making that enhances productivity, conserves natural resources, and decreases environmental damage. These improvements are especially important in Africa, where the use of mechatronic technology would potentially solve critical concerns linked to inefficient land management, low food yields, and susceptibility to climate change.

The increasing corpus of literature shows the transformational potential of mechatronics in agricultural development. As seen in Figure 2, a systematic examination of scholarly articles linked to mechatronics, mechanisation, and precision agriculture from the Web of Science database reveals a considerable rise between 2017 and 2021, showing increased academic and business interest. The peak in citation rates during 2021 shows the usefulness of these technologies in tackling modern agricultural concerns. Although citation rates have fallen significantly in succeeding years, this pattern may indicate a change from conceptual research to the actual application of mechatronic breakthroughs in the field. The expanding research focus on agritronics reflects its potential to greatly increase agricultural efficiency, reinforce food systems, and assist climate-resilient farming in Africa. This research contributes to existing conversation by studying the growth of mechatronic technologies and their essential role in altering agricultural systems toward a more sustainable and productive future.

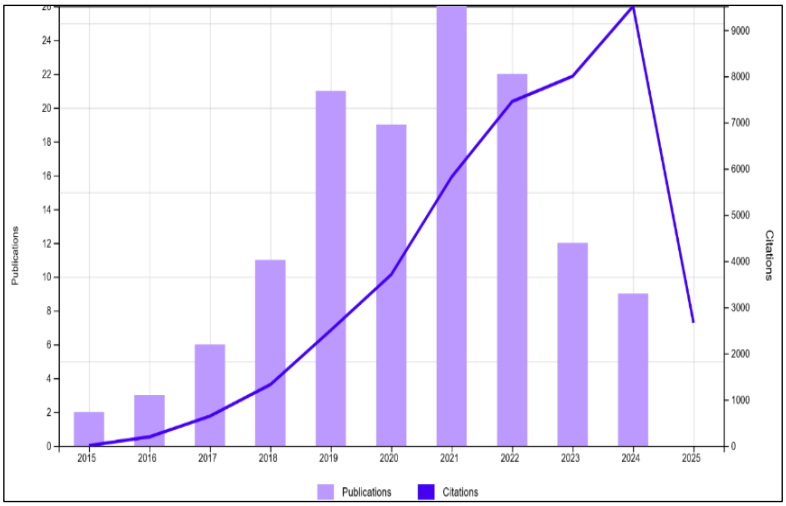

Figure 2: Trends in scholarly output and citations highlighting increasing interest in mechatronics for sustainable agriculture in Africa.
Source: Authors, (2025).

II. MECHATRONICS APPLICATION IN AGRICULTURE

Mechatronics is revolutionising agricultural practices by integrating robotics, automation, sensors, and artificial intelligence to optimize farming practices. These innovations play a major role in increasing agricultural productivity and promoting resources and environmental sustainability [19], [20]. The following is an overview of key innovations in mechatronics and their benefits:

II.1 AGRICULTURAL INTERNET OF THINGS (Ag-IoT)

Internet of things (IoT) has transformed many industries in the last twenty years, with the synchronisation of sensor technology, wireless communication, data analytics, and cloud computing to enhance the collection, processing, and utilisation of agricultural data within Ag-IoT systems. It has been progressively used to monitor essential agricultural characteristics, such as crop health, soil and climatic conditions in real-time. Some of the instruments include soil moisture monitors, temperature sensors, and weather stations [21], [22]. This provides vital data, which is then analysed to facilitate decision-making in irrigation, pest management, and nutrient optimisation [8], [23]. The data-orientated methodology enhances resource utilisation, increases production, and sustainable practices. Researchers are developing innovative methods and equipment using sensors to monitor and communicate crop information at various growth stages, utilising various communication devices and machinery.

This section thoroughly discusses Ag-IoT sensors and its compatible data processing platforms:

Ag-IoT sensors: This sensors are crucial in Ag-IoT systems as they convert physical signals into digital signals, measuring crop, soil, and microclimate parameters, including temperature, light intensity, accelerometers, and soil moisture [24]. Sensors such as photoelectric, electromagnetics, conductivity, and ultrasound, as shown in Figure 3 are widely used to smart agriculture to estimate critical parameters like soil texture, nutrient levels, vegetation, humidity, vapour, air, and temperature. Remote sensing technologies can also be deployed to detect types and varieties of crop, pest and weed infections, and soil, plant, and climatic conditions across different landscapes [25].

Figure 3: Agricultural Internet of Things.
Source: [26]

These environmental and agronomic parameters are continually monitored using sensor-based systems for optimal plant health. Data is captured with the sensor and transmitted to the microcontrollers which trigger action when thresholds are exceeded for the optimal crop requirement. Table 1 presents field parameters, sensor variables, device and application of agricultural IoT use in monitoring crop parameters.

Table 1: Agricultural - IoT for Monitoring Crop Parameters.

Field Parameter	**Sensor Variable**	**Sensor Device**	**Applications in Literature**
Thermal	Heat flux, thermal conductivity	Thermocouples, RTDs, and Thermistors	Impact of Climate Change on Agricultural Ecosystem [27], [28].
Soil Moisture and Humidity	Moisture content Resistance, Conductivity, and Permittivity	Frequency Domain Reflectometry, and Gypsum Block Sensors	Applied in irrigation scheduling, drought stress detection, and water use efficiency studies [29].
Light Intensity	Wavelength of light, Area receiving light, and Quantum	Illuminance sensor, imaging sensors, and thermal imaging camera	Optical Performance of Winter Wheat under Different Irrigation Conditions [30], [31].
Insect wing beat sound	Sound frequency spectrum (wingbeat)	Microphone (electret or MEMS mic) array	Real-time pest monitoring via acoustic classification (e.g. fruit flies); reduces pesticide use [32]
Soil penetration resistance	Tillage force (penetration)	Penetrometer with load cell (hand-held or automated robot probe)	Penetrometer with load cell (hand-held or automated robot probe) [33]
Soil nutrients (pH, EC, NPK)	pH, electrical conductivity (EC)	Soil pH probe (electrode), EC probe	Fertilizer management and nutrient optimization to improve yield [34]
Ambient temperature & humidity	Air temperature (°C), relative humidity (%)	Digital sensor (DHT22, BME280, SHT3x)	Climate monitoring for frost/disease forecasting; greenhouse climate control [8]
Rainfall/ precipitation	Rain amount (mm)	Tipping bucket rain gauge (analog)	Irrigation scheduling and drainage management based on rainfall data [35]
Wind speed	Wind velocity (m/s)	Anemometer (cup or ultrasonic)	Adjust spraying/ dusting operations; protect crops (e.g. windbreak activation) [36]

Source: Authors, (2025).

II.2 COMPATIBLE AG-IOT DATA PROCESSING PLATFORMS

The effective implementation use of Ag-IoT technology depends on the compatibility of sensors with IoT platforms capable of seamless data acquisition, processing, and communication. Identification and choice of suitable platform is vital in ensuring accurate measurements of key field parameters and support real-time responsiveness. These platforms play significant roles in customising Ag-IoT devices to suit diverse agronomic and climatic patterns in Africa. Figure 4 show the flowchart of remote sensing and satellites images methods in smart farming, while the processing platform is discussed as follows:

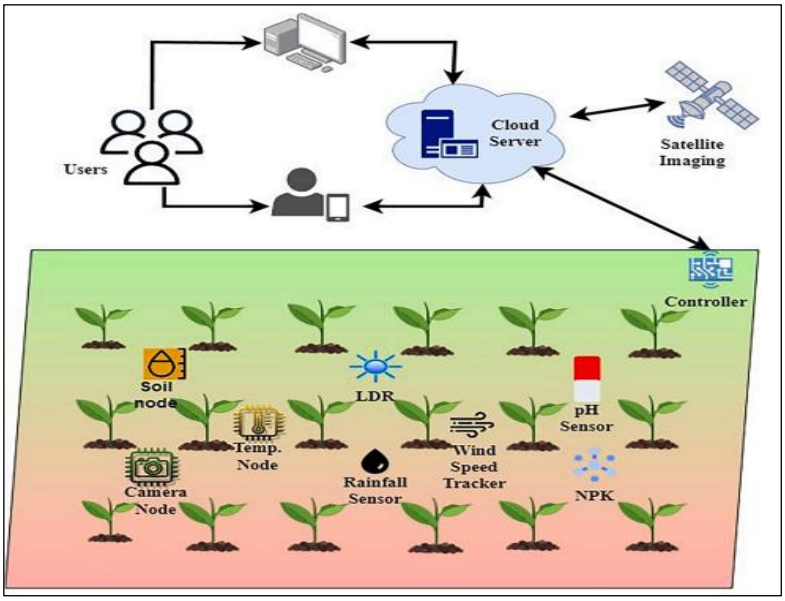

Figure 4: Flowchart of remote sensing and satellites images methods in smart farming.
Source: [8]

- Thermal and Climate Sensors: Microcontrollers like Arduino Uno, ESP32, and Raspberry Pi are used for temperature, humidity, wind speed, and rainfall data acquisition because of their capabilities for both analogue and digital inputs, low energy usage, and compatibility with DHT22, BME280, tipping bucket rain gauges, and anemometers. These platforms are essential for temperature and humidity measurements, which are critical for effective greenhouse management and early disease identification [37].
- Soil Moisture and Nutrient Monitoring: Arduino Mega and NodeMCU ESP8266 are commonly used to connect with capacitive and resistive soil moisture sensors for measuring conductivity, pH, and fertiliser level, along with ion-selective nutrient probes. These microcontrollers provide ample analogue pins and Wi-Fi capabilities for the real-time transmission of soil health information, facilitating precise fertilisation and irrigation practices [38], [39].
- Light Intensity and Optical Sensing: High-data multispectral imaging and chlorophyll assessments are done using Raspberry Pi and Jetson Nano. They offer the necessary processing capabilities for executing image analysis algorithms and can be combined with high-resolution cameras to monitor plant health and identify diseases [40].
- Acoustic Sensing: MEMS microphones are used for pest monitoring acoustic-related applications like wingbeat detection. ESP32, Raspberry Pi Pico, and Raspberry Pi Zero W are the preferred support platforms because they support real-time sound processing and wireless communication while maintaining low power consumption [41].
- Mechanical Sensing: Soil penetration and load cell indices with soil compaction or grain weight are heavy-duty field measurements managed by platforms such as Arduino Uno with HX711 amplifier modules. These systems are dependable and robust for amplifying analogue signals and capturing real-time data from mechanical sensors [42].
- Integrated Systems and Automation: Some extensive smart farming applications required both sensing and actuation; this kind of technology needs platforms like ESP32 and BeagleBone Black. They provide flexibility with GPIOs, support PWM, and come equipped with wireless modules. These are used to control actuators (like irrigation valves, sprayers, and fans) based on input from environmental sensors [43].

III. APPLICATIONS OF MECHATRONICS FOR SUSTAINABLE AGRICULTURAL ECONOMY

The application of mechatronics in agriculture has given leverage for technology-driven crop production. These facilitate a resilient approach during farm survey, land preparation, crop management, harvest, and post-harvest processing stages by enabling automation and data-driven crop tillage, cultivation, harvest, and processing [44].

- Smart land preparation: Smart devices and sensors can be installed on GPS-guided tractors, seeders, and sprayers. Equipping farm machinery with AG-IoT sensors helps mitigate the effect of climate change while improving energy efficiency, reducing greenhouse gas emissions, and preserving soil health [45].
  Combining these advanced technological solutions with context-specific agronomic practices will reduce operational delays and input wastage. These systems will also boost output per hectare, making farms more profitable and reducing dependency on imports [44].
- Post-Harvest Efficiency and Value Addition: Food security and value addition for sustainable farming depend heavily on agro-processing, which transforms agricultural inputs into consumable or intermediate items. However, the industry confronts continuing issues such as labour shortages, uneven product quality, and inefficiencies associated with old processing techniques.
  To address these constraints, robotics and mechatronics have emerged as transformational solutions. These technologies automate essential procedures, improve accuracy, and save operating expenses. Innovations like automated dryers, sorters, and packing systems

not only eliminate post-harvest losses but also greatly increase product quality and uniformity. The integration of mechatronic systems into agro-processing creates new prospects for local value addition, agro-industrial growth, and improved export competitiveness [46].

- Resource optimisation: Smart irrigation, precision fertiliser applications, and climate-responsive greenhouses employ sensors and actuators for administering inputs depending on real-time crop demands. This focused method optimises production per unit of input, consistent with the key principles of sustainable intensification. In particular, vertical farming is predicted to witness a boom in automation, spurred by developments in technology.

  The integration of automation and artificial intelligence (AI) in vertical farming systems boosts efficiency, assures constant plant development, and promotes predictable harvests. This technology-driven strategy not only decreases the danger of human mistakes but also dramatically lowers labour expenses compared to conventional farming techniques, making it a viable model for future agricultural output [47].
- Climate resilience: Mechatronic systems are crucial for improving agricultural adaptability to fluctuations in climate. By consistently tracking weather, soil, and crop conditions, these technologies facilitate prompt and flexible reactions to environmental changes. Automated systems can issue early alerts for drought conditions, pest invasions, and soil decline, aiding proactive decision-making. Climate change, marked by long-term alterations in global weather patterns such as rising temperatures, severe weather occurrences, and changing rainfall patterns, results from both human actions like greenhouse gas emissions and natural phenomena.

  It has a profound effect on ecosystems, biodiversity, public health, and economic stability. The interaction between agriculture and climate change is mutually influential: agriculture not only contributes to climate change but is also significantly affected by its consequences. Incorporating climate-smart technologies such as mechatronics is vital for developing a more sustainable and robust agricultural framework [48].
- Crop Pest and Disease Management: Mechatronic solutions in agriculture, especially with the integration of the Internet of Things, provide a more sustainable and accurate method for managing pests and diseases. The Food and Agriculture Organisation estimated global crop yield lost at about 20 – 40% per year. Although pesticides and agrochemicals have been used to tackle food loss, they pose significant risks to human and animal health and contribute to environmental degradation [49]. IoT devices installed on agricultural robots, wireless sensor networks, and drones have improved the detection and control of crop pests and pathogens. They depend on image detection and processing.

  Remote sensing imagery and in-field sensors continuously gather essential data, including indicators of plant health and pest occurrences, through real-time monitoring, modelling, and forecasting of diseases throughout the growing season. These technologies surpass conventional pest management approaches in terms of both accuracy and effectiveness. Moreover, automated traps enabled by IoT are designed to capture, count, and identify various insect species. The collected data is then sent to cloud-based platforms for thorough analysis. Recent progress in robotics has resulted in the creation of agricultural robots that are fitted with multispectral imaging sensors and precision spraying nozzles. Within IoT management frameworks, these robots can effectively identify and tackle pest infestations, thereby reducing the need for harmful agrochemicals and lessening ecological impact [8], [50].
- Yield Monitoring and Forecasting: Yield monitoring systems deliver immediate insights on crop yield, moisture levels, and quality elements vital for sustainable agricultural strategies. Mechatronics systems for monitoring crop output provide real-time information on essential parameters for forecasting crop maturity, quality, moisture content, and crop yield, as illustrated in Figure 5. Yield forecasting aids farmers in strategic planning, resource allocation, and market preparation by predicting crop quality under various environmental conditions, thereby enhancing crop quality. Evaluating crop maturity by examining factors like fruit size and colouration is crucial for identifying the best time to harvest.

  Precise forecasting of harvest windows leads to enhanced crop quality, increased production, and contributes to market regulation efforts. Having up-to-date information on the ideal harvest period helps farmers enhance their profitability and minimise losses after harvest. Contemporary yield monitors, when integrated into harvesting equipment and linked to mobile apps, showcase real-time harvest data and automatically relay information to cloud-based systems for analysis. Satellite remote sensing technologies are utilised to estimate crop yields over large agricultural areas. In the case of fruit crops, high-resolution RGB satellite images are employed to evaluate traits such as fruit size and colour, supporting predictions of maturation stages, harvest timing, and market readiness [51]. These optical sensors are essential for tracking physiological changes in fruits, like shrinkage during drying, thus aiding in quality control and enhancing post-harvest processing efficiency [8].

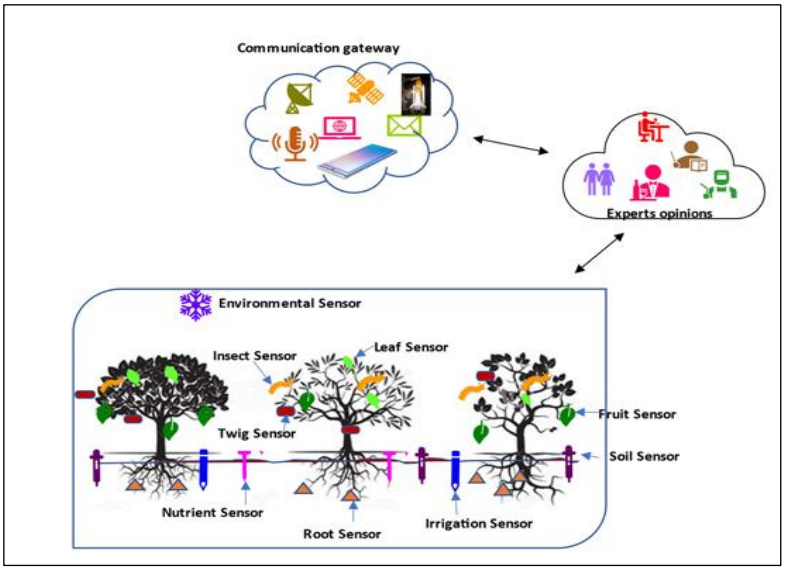

Figure 5: An Internet-of-Things-based network for smart farming.
Source: [8]

IV. CHALLENGES TO ADOPTING MECHATRONICS IN AFRICAN AGRICULTURE

Despite the exciting potential of mechatronic in agriculture (agritronics), many obstacles, including cost and accessibility, infrastructure deficit, skill gaps, and policy and regulatory weaknesses, hinder their widespread implementation in Africa:

- The high initial cost needed for mechatronic equipment such as automated harvesters, irrigation systems, and climate-control devices remains a key obstacle, especially for smallholder farmers who dominate Africa's agricultural landscape. Limited access to finance and funding methods worsens this difficulty [52].
- The shortage of dependable infrastructure, including internet access, energy, and remote road networks, inhibits the implementation and maintenance of smart agricultural systems. In many locations, fundamental infrastructure is either inadequate or altogether nonexistent, hindering the functioning of precision systems [53].
- There is a lack of trained professionals, including engineers, technicians, and agricultural extension workers, who can operate, maintain, and promote the usage of mechatronic systems. This absence of human capital lowers the efficacy and sustainability of technological adoption [53], [54].
- Weak institutional frameworks, limited government investment in agricultural innovation, and the lack of enabling regulations hold down the implementation of mechatronics. Inadequate standards, regulatory backing, and incorporation into national development objectives further impede growth [55].

V. ADVANCING MECHATRONICS DEVELOPMENT IN AFRICA

Africa possesses significant agricultural potential that remains largely untapped, with Nigeria using less than half of 73 million hectares of cultivable land. The continent holds 60% of the world's arable land, yet it is a net importer of food, with 220 million people suffering from undernutrition. Enhancing local engineering and technical skills is essential since agriculture accounts for 24% of Nigeria's GDP [52]. Modern agricultural practices depend on sophisticated mechatronic systems, which highlights the need for local training initiatives to emphasise practical engineering abilities for sustainably revolutionising agriculture and decreasing reliance on foreign technology [14].

V.1 HUMAN RESOURCE DEVELOPMENT

The development of mechatronics in Africa necessitates a strong human resource base, especially in robotics. The continent's large youth demographic and various engineering institutions must be equipped to create mechatronic products. This goal can be accomplished by incorporating agriculture-related modules into educational programmes, like designing farming equipment, to enhance food production without relying on imports. The National Centre for Agricultural Mechanisation (NCAM) in Nigeria not only designs local farming machinery but also conducts training sessions for engineers and farmers [52]. These organisational strategies guarantee that research meets the requirements of farmers and that advancements can transition from laboratories to practical applications in the field by:

- Update engineering programmes to emphasise mechatronic applications within the agricultural sector,
- Broaden the availability of hands-on workshops and internships across the country for apprentices in automation and sensor systems,
- Foster partnerships between the fields of engineering, agriculture, and data science,
- Equip agricultural extension workers with foundational technology skills to support a digitally savvy farming community, and
- Utilise expertise from diaspora professionals and international universities to access the latest developments.

V.2 ACADEMIC AND RESEARCH INSTITUTIONAL SUPPORT

Advancements in mechatronics within Africa necessitate robust institutional backing and well-defined research priorities. It is essential for governments and educational institutions to establish specialised research facilities aimed at addressing agricultural issues. The National Agricultural Technology and Innovation Policy (NATIP) for the years 2022-2027 in Nigeria emphasises the use of knowledge, technology, and innovation to enhance production. Organisations like NCAM, National biotechnology research and development agency (NBRDA), and universities can spearhead research and development focused on adaptive machinery and precision farming technologies [56]. Their research must:

- Concentrate on smart technology solutions tailored for both arable and cash crops,
- Emphasize investigations into sustainable mechanisation and innovations using local materials,
- Leverage intelligent systems, such as robotics, to address issues like rainfall variability and drought conditions.
- Encourage platforms for collaboration to share results and modify technologies accordingly, and
- Boost research and development funding to facilitate the creation of prototypes and conduct field trials.

V.3 DIGITAL INFRASTRUCTURE AND TECHNOLOGY INTERGRATION

Nigeria is encouraging the integration of mechatronics in farming through improvements in its infrastructure and the dissemination of technology. The nation has supported the FAO's Digital Village Initiative, which promotes the establishment of a National Integrated Digital Agriculture Platform that connects farms, markets, research, and extension services. This platform has the capability to compile weather forecasts, soil information, and market pricing, thereby enabling precision agriculture for smallholder farmers [57]. Rural agricultural development strategy should include:

- Investing in broadband and mobile access along with IoT sensors for agriculture in rural areas,
- Digitising the register of farmers and mapping agricultural land for data-driven decision-making in farming,
- Creating local prototyping hubs to foster engineering solutions within communities,
- Encouraging the use of renewable energy via solar-powered agricultural robots,
- Providing funding for demonstration projects to test the deployment of mechatronic tools, and
- Enhancing infrastructure to ensure the fast and equitable spread of technologies in rural regions.

V.4 GOVERNMENT POLICY FRAMEWORK

The Nigerian National Integrated Digital Agriculture Platform (NATIP) seeks to enhance mechatronics by incorporating it into agricultural and industrial strategies. This initiative prioritizes mechanization and the adoption of technology as key national objectives, connecting technological advancement with food security and the creation of jobs. The African Union's Agenda 2063 also highlights the importance of food security and promotes investment in technology. It is essential for national governments to align their policies in science, technology, and agriculture, with NATIP 2022-2027 acting as a guiding framework [53]. Regional frameworks in Africa should promote the use of robotics and automation in agricultural practices and make regulatory support for Agri-Machinery by;

- Developing standards and certification for agri-machinery,
- Simplifying import regulations for local industries,
- Providing quality standards for homegrown machines,
- Reforming of extension services to include technology advisory,
- Revitalizing extension networks for smart agriculture adoption, and
- Monitoring and evaluating for data-driven governance.

V.5 PUBLIC PRIVATE SECTOR FUNDING MECHANISMS

The innovation and scaling in agri-mechatronics are being spearheaded by the public private sector, including startups, cooperatives, and investors. In Nigeria, a wave of new agritech startups is emerging to tackle on-farm issues, with companies like ThriveAgric and Releaf utilizing digital platforms and affordable machinery for financing and processing [58]. Nevertheless, funding presents a significant hurdle, as African agritech startups raised only about US$65 million in 2024, which is considerably less than the capital directed toward fintech [59]. This underscores the necessity for targeted financial support and investment incentives in agri-mechatronics, and commercialization of locally-developed mechatronic solutions by;

- Promoting a dynamic private sector and ensuring access to financial resources,
- Supporting investment initiatives and incentives through venture capital, grants, public-private partnerships, and tax benefits,
- Providing startup support through agritech hubs and accelerator programs,
- Establishing market connections by collaborating with farmer cooperatives and large agribusiness entities,
- Rallying impact investments and donor contributions around agricultural transformation objectives,
- Leveraging funds like USAID's Feed the Future and AfDB's Nigeria Incentive-based Risk Sharing System for Agricultural Lending, and
- Employing blended finance strategies to address early-stage risks in robotics innovation.

VI. CONCLUSIONS

Mechatronics offers a transformative opportunity for improving agriculture and promoting a sustainable economy in Africa. By combining mechanical systems with electronic components and smart control technologies, it enhances productivity, optimizes the use of resources, and reduces post-harvest losses. From precision land preparation that utilizes GPS-guided machinery to sophisticated agro-processing and climate-resilient farming systems, mechatronics supports every step of the agricultural value chain. The flexibility of Ag-IoT platforms like Arduino Uno, ESP32, and Raspberry Pi provides scalable and cost-effective solutions for various farming situations, including those utilized by resource-constrained smallholders.

The widespread adoption of mechatronics in Africa faces challenges such as high initial costs, inadequate infrastructure, skills gaps, and weaknesses in policy and regulation. To tackle these challenges, Africa must enhance local expertise and technical skills, particularly in robotics, by developing human resources, supporting academic and research institutions, improving digital infrastructure and technology integration, and creating favorable government policies. Nigeria is implementing initiatives aimed at equipping local farmers with mechatronic solutions to increase food production without reliance on imports. The policy framework should align with NATIP 2022-2027, and regional strategies should promote the incorporation of robotics and automation in agricultural practices. Additionally, funding from both public and private sectors, including venture capital, grants, and partnerships, is being leveraged to encourage the advancement of agri-mechatronics.

VII. AUTHOR'S CONTRIBUTION

Conceptualization: Thomas Adedayo Ayorinde.
Methodology: Thomas Adedayo Ayorinde.
Investigation: Thomas Adedayo Ayorinde.
Discussion of results: Thomas Adedayo Ayorinde.
Writing – Original Draft: Thomas Adedayo Ayorinde.
Writing – Review and Editing: Tamba Jamiru and Peet F LE Roux.
Resources: Tamba Jamiru and Peet F LE Roux
Supervision: Tamba Jamiru and Peet F LE Roux.
Approval of the final text: Thomas Adedayo Ayorinde

VIII. ACKNOWLEDGMENTS

The authors acknowledge the financial support from Tshwane University of Technology (TUT), Pretoria, South Africa, without which this work would not have been published.

Data Availability: 'The raw/processed Data required to produce these findings cannot be shared at this time due to technical and time limitations'.

IIX. REFERENCES

[1] A. Kamara, A. Conteh, E. R. Rhodes, and R. A. Cooke, "The relevance of smallholder farming to African agricultural growth and development," African Journal of Food, Agriculture, Nutrition and Development, vol. 19, no. 1, pp. 14043-14065, 2019.

[2] P. J. Ericksen, J. S. Ingram, and D. M. Liverman, "Food security and global environmental change: emerging challenges," vol. 12, ed: Elsevier, 2009, pp. 373-377.

[3] L. F. Oliveira, A. P. Moreira, and M. F. Silva, "Advances in agriculture robotics: A state-of-the-art review and challenges ahead," Robotics, vol. 10, no. 2, p. 52, 2021.

[4] K. C. Oni, "Promoting agricultural mechanization in Nigeria through the intervention of Japanese Government," Agricultural Mechanization in Asia, Africa, and Latin America, vol. 44, no. 4, pp. 25-26, 2013.

[5] G. Mrema, J. Kienzle, and J. Mpagalile, "Current status and future prospects of agricultural mechanization in sub-saharan Africa (SSA)," Agricultural Mechanization in Asia, Africa and Latin America, vol. 49, no. 2, pp. 13-30, 2018.

[6] J. Olaoye and A. Rotimi, "Measurement of agricultural mechanization index and analysis of agricultural productivity of farm settlements in Southwest Nigeria," Agricultural Engineering International: CIGR Journal, vol. 12, no. 1, 2010.

[7] L. Clarke and C. Bishop, "Farm power-present and future availability in developing countries," Agricultural Engineering International: CIGR Journal, 2002.

[8] M. Dhanaraju, P. Chenniappan, K. Ramalingam, S. Pazhanivelan, and R. Kaliaperumal, "Smart farming: Internet of Things (IoT)-based sustainable agriculture," Agriculture, vol. 12, no. 10, p. 1745, 2022.

[9] B. Tekinerdogan, "Strategies for technological innovation in agriculture 4.0," Wageningen University: Wageningen, The Netherlands, 2018.

[10] J. Auderset and P. Moser, "Mechanisation and motorisation: Natural resources, knowledge, politics and technology in 19th-and 20th-century agriculture," in Agriculture in Capitalist Europe, 1945–1960: Routledge, 2016, pp. 145-164.

[11] N. Yahya and N. Yahya, "Agricultural 4.0: Its implementation toward future sustainability," Green Urea: For Future Sustainability, pp. 125-145, 2018.

[12] M. A. Dayıoğlu and U. Turker, "Digital transformation for sustainable future-agriculture 4.0: A review," Journal of Agricultural Sciences, vol. 27, no. 4, pp. 373-399, 2021.

[13] N. P. Jellason, E. J. Robinson, and C. C. Ogbaga, "Agriculture 4.0: Is sub-saharan africa ready?," Applied Sciences, vol. 11, no. 12, p. 5750, 2021.

[14] S. Amertet, G. Gebresenbet, H. M. Alwan, and K. O. Vladmirovna, "Assessment of smart mechatronics applications in agriculture: a review," Applied Sciences, vol. 13, no. 12, p. 7315, 2023.

[15] J. Azeta, C. Bolu, F. Alele, E. Daranijo, P. Onyeubani, and A. Abioye, "Application of Mechatronics in Agriculture: A review," in Journal of physics: conference series, 2019, vol. 1378, no. 3, p. 032006: IOP Publishing.

[16] M. De Clercq, A. Vats, and A. Biel, "Agriculture 4.0: The future of farming technology," Proceedings of the world government summit, Dubai, UAE, pp. 11-13, 2018.

[17] N. Reznik et al., "Engineering and Security Management of Technological Transformation Trends of Agrotronics," in Big Data in Finance: Transforming the Financial Landscape: Volume 1: Springer, 2025, pp. 289-298.

[18] G. K. Ontiri and L. L. Amuhaya, "Integration of mechatronic and automation technology in sustainable farming for achieving food security in Kenya," European Journal of Electrical Engineering and Computer Science, vol. 6, no. 1, pp. 66-71, 2022.

[19] N. Chamara, M. D. Islam, G. F. Bai, Y. Shi, and Y. Ge, "Ag-IoT for crop and environment monitoring: Past, present, and future," Agricultural systems, vol. 203, p. 103497, 2022.

[20] M. Dholu and K. Ghodinde, "Internet of things (iot) for precision agriculture application," in 2018 2nd International conference on trends in electronics and informatics (ICOEI), 2018, pp. 339-342: IEEE.

[21] K. Patil and N. Kale, "A model for smart agriculture using IoT," in 2016 international conference on global trends in signal processing, information computing and communication (ICGTSPICC), 2016, pp. 543-545: IEEE.

[22] E. Sisinni, A. Saifullah, S. Han, U. Jennehag, and M. Gidlund, "Industrial internet of things: Challenges, opportunities, and directions," IEEE transactions on industrial informatics, vol. 14, no. 11, pp. 4724-4734, 2018.

[23] X. Shi et al., "State-of-the-art internet of things in protected agriculture," Sensors, vol. 19, no. 8, p. 1833, 2019.

[24] R. M. White, "A sensor classification scheme," IEEE Transactions on ultrasonics, ferroelectrics, and frequency control, vol. 34, no. 2, pp. 124-126, 1987.

[25] F. Chen et al., "Field scale mapping of surface soil clay concentration," Precision Agriculture, vol. 5, pp. 7-26, 2004.

[26] V. Kumar, "A comprehensive review on smart and sustainable agriculture using IoT technologies. Smart Agricultural Technology, 8, 100487," ed, 2024.

[27] M. S. Ayilara et al., "Impact of Climate Change on Agricultural Ecosystem," in Climate Change, Food Security, and Land Management: Strategies for a Sustainable Future: Springer, 2025, pp. 1-24.

[28] L. Huang et al., "Estimation of evapotranspiration using the crop canopy temperature at field to regional scales in large irrigation district," Agricultural and Forest Meteorology, vol. 269, pp. 305-322, 2019.

[29] E. Bwambale, F. K. Abagale, and G. K. Anornu, "Smart irrigation monitoring and control strategies for improving water use efficiency in precision agriculture: A review," Agricultural Water Management, vol. 260, p. 107324, 2022.

[30] M. Zhang, W. Chen, M. Jing, Y. Gao, and Z. Wang, "Canopy Structure, Light Intensity, Temperature and Photosynthetic Performance of Winter Wheat under Different Irrigation Conditions," Plants, vol. 12, no. 19, p. 3482, 2023.

[31] R. A. Slattery and D. R. Ort, "Perspectives on improving light distribution and light use efficiency in crop canopies," Plant Physiology, vol. 185, no. 1, pp. 34-48, 2021.

[32] M. Cardim Ferreira Lima, M. E. Damascena de Almeida Leandro, C. Valero, L. C. Pereira Coronel, and C. O. Gonçalves Bazzo, "Automatic detection and monitoring of insect pests—a review," Agriculture, vol. 10, no. 5, p. 161, 2020.

[33] V. De Cauwer et al., "Development and in-field validation of an autonomous soil mechanical resistance sensor," Sensors (Basel, Switzerland), vol. 25, no. 6, p. 1919, 2025.

[34] F. Silva et al., "Precision Fertilization: A critical review analysis on sensing technologies for nitrogen, phosphorous and potassium quantification," Computers and Electronics in Agriculture, vol. 224, p. 109220, 2024.

[35] A. Kaur, D. P. Bhatt, and L. Raja, "Major Crops Water Requirements and Automated Irrigation Scheduling System," AGRIS on-line Papers in Economics and Informatics, vol. 17, no. 1, pp. 41-50, 2025.

[36] M. S. W. John, "Mackenzie Globular Springtails."

[37] A. F. Suhaimi et al., "IoT based smart agriculture monitoring, automation and intrusion detection system," in Journal of Physics: Conference Series, 2021, vol. 1962, no. 1, p. 012016: IOP Publishing.

[38] E. A. DENEKEW, "DESIGNING SOIL HEALTH MONITORING AND NUTRIENT DETECTION MODEL USING WIRELESS SENSOR NETWORKS," 2022.

[39] B. Kashyap and R. Kumar, "Sensing methodologies in agriculture for soil moisture and nutrient monitoring," IEEE Access, vol. 9, pp. 14095-14121, 2021.

[40] B. G. Ram, P. Oduor, C. Igathinathane, K. Howatt, and X. Sun, "A systematic review of hyperspectral imaging in precision agriculture: Analysis of its current state and future prospects," Computers and Electronics in Agriculture, vol. 222, p. 109037, 2024.

[41] R. D. Martínez, A. Izquierdo, J. J. Villacorta, L. del Val, and L.-A. Basterra, "Acoustic detection and localisation system for Hylotrupes bajulus L. larvae using a MEMS microphone array," Applied Acoustics, vol. 213, p. 109618, 2023.

[42] P. Thomas et al., "Exploring the relationships between penetration resistance, bulk density and water content in cultivated soils," J. Agr. Phy, vol. 20, no. 1, p. 22, 2020.

[43] J. Wahl, "Development and Characterization of an Iot Network for Agricultural Imaging Applications," California Polytechnic State University, 2020.

[44] W. K. Alazzai, B. S. Z. Abood, H. M. Al-Jawahry, and M. K. Obaid, "Precision farming: the power of AI and IoT technologies," in E3S Web of Conferences, 2024, vol. 491, p. 04006: EDP Sciences.

[45] R. U. Modi et al., "Climate-smart technology based farm mechanization for enhanced input use efficiency," Climate Change and Indian Agriculture: Challenges and Adaption Strategies, pp. 325-358, 2020.

[46] V. Singh, D. Borisagar, O. Singh, and S. K. Verma, "Enhancing Agricultural Competitiveness: Harnessing Value Chains and Agro-Processing for Sustainable Growth," in Sustaining the Global Agriculture Supply Chain: IGI Global Scientific Publishing, 2025, pp. 37-72.

[47] K. Sharma, R. Kumar, A. Kumar, S. Balabantaray, and M. Arora, "A digital ecosystem for sustainable fruit supply chain in Uttarakhand: a comprehensive review," Environment, Development and Sustainability, vol. 26, no. 5, pp. 13217-13252, 2024.

[48] C. Parra-López et al., "Integrating digital technologies in agriculture for climate change adaptation and mitigation: State of the art and future perspectives," Computers and Electronics in Agriculture, vol. 226, p. 109412, 2024.

[49] A. Khattab, S. E. Habib, H. Ismail, S. Zayan, Y. Fahmy, and M. M. Khairy, "An IoT-based cognitive monitoring system for early plant disease forecast," Computers and Electronics in Agriculture, vol. 166, p. 105028, 2019.

[50] B. Ramalingam et al., "Remote insects trap monitoring system using deep learning framework and IoT," Sensors, vol. 20, no. 18, p. 5280, 2020.

[51] P. Udomkun, M. Nagle, D. Argyropoulos, B. Mahayothee, and J. Müller, "Multi-sensor approach to improve optical monitoring of papaya shrinkage during drying," Journal of Food Engineering, vol. 189, pp. 82-89, 2016.

[52] O. Ani, K. Chukwuma, G. Okoro, and A. Oyiga, "Applications of Mechatronics and Autonomous Systems in Smart Agriculture: Potentials and Challenges for Nigeria," no. November, 2019.

[53] T. Araoye and S. V. Egoigwe, "INTEGRATING ADVANCED CONTROL STRATEGIES FOR AUTONOMOUS AGRICULTURAL ROBOTICS INTO NIGERIAN EDUCATIONAL REFORMS: CHALLENGES AND OPPORTUNITIES."

[54] S. Mhlongo, K. Mbatha, B. Ramatsetse, and R. Dlamini, "Challenges, opportunities, and prospects of adopting and using smart digital technologies in learning environments: An iterative review," Heliyon, vol. 9, no. 6, 2023.

[55] T. Daum and R. Birner, "The neglected governance challenges of agricultural mechanisation in Africa–insights from Ghana," Food Security, vol. 9, pp. 959-979, 2017.

[56] W. R. Nyemba and K. F. Carter, "Royal Academy of Engineering Interventions," in Doctoral Training in Engineering: Developing Indigenous Capacities and Skills for Economic Growth in Industrialising Countries: Springer, 2024, pp. 41-58.

[57] K. E. Ukhurebor et al., "Precision agriculture: Weather forecasting for future farming," in Ai, edge and iot-based smart agriculture: Elsevier, 2022, pp. 101-121.

[58] A. Elliot, "Agricultural Technology," SMALLHOLDERS, p. 105, 2023.

[59] M. C. Restrepo, D. Jimenez, M. Ouedraogo, T. Talsma, M. Singh, and P. Läderach, "Mapping climate and agronomic digital advisory services landscape of the Transforming Agrifood Systems in West and Central Africa Initiative (TAFS-WCA): A case of Nigeria," 2023.